Post-Polymerization Click Functionalization of Conjugated Polymers

POST-POLYMERIZATION CLICK FUNCTIONALIZATION OF CONJUGATED POLYMERS

BY
VLADIMIR KARDELIS, B.SC.

A THESIS
SUBMITTED TO THE SCHOOL OF GRADUATE STUDIES
OF MCMASTER UNIVERSITY
IN PARTIAL FULFILMENT OF THE REQUIREMENTS
FOR THE DEGREE OF
DOCTOR OF PHILOSOPHY IN CHEMISTRY

PhD of Chemistry (2021) McMaster University
(Chemistry and Chemical Biology) Hamilton, Ontario, Canada

TITLE: Post-Polymerization Click Functionalization of Conjugated Polymers

AUTHOR: Vladimir Kardelis
B.Sc. (Chemistry)
McMaster University, Hamilton, Canada

SUPERVISOR: Professor Alex Adronov

NUMBER OF PAGES: xxviii, 306

Abstract

Conjugated polymers attract significant attention due to their interesting optoelectronic and physical properties. Over the past few decades, tremendous effort has been devoted to expanding the structural diversity and applications of this class of macromolecules. The pursuit of structural variability of conjugated polymers has resulted in a broad range of research to understand their structure-property relationships via functionalization. This functionalization is crucial for tailoring performance in any given application. Thus, the ability to synthesize a library of homologous polymers would prove very useful. Efficiency is of utmost importance when creating a library of homologous conjugated polymers, as the faster a library can by synthesized, the sooner said polymers can be screened for any desirable properties. Such an approach requires a post-polymerization functionalization strategy, whereby a progenitor polymer undergoes efficient reactions at each repeat unit of the backbone.

The work presented in this thesis involves synthesizing a reactive conjugated polymer scaffold, followed by efficiently post-polymerization functionalization via “click” chemistry. Two elegant click reactions are described in this work; the Strain-Promoted Alkyne-Azide Cycloaddition (SPAAC) and Inverse Electron-Demand Diels-Alder (IEDDA). The SPAAC reaction allowed for rapid functionalization of triazole moieties on a dibenzocyclooctyne-containing polymer backbone, creating a small polymer library with a consistent degree of polymerization (DP). Grafting with polystyrene and polyethylene glycol azide-terminated polymers allowed the efficient syntheses of a series of graft-co-polymers with Mn values up to 800 kDa and varying solubilities. Secondly, The IEDDA reaction was applied to a poly(tetrazine-co-fluorene) conjugated polymer, which resulted in the rapid and quantitative functionalization of the polymer backbone with trans-cyclooctene derivatives. These reactive conjugated polymers were explored in a variety of applications, including supramolecular chemistry and gel formation.

Acknowledgements

Not until my 3rd or 4th year of graduate studies did I feel as though I had any momentum building with respect to my research. The first couple of years were mostly comprised of either helping senior graduate students with their projects or pursuing dead-end leads with newly conceived projects. However, these efforts were not in vain as the work I put into setting up any reaction (fruitless or otherwise) helped hone my laboratory skills and improve my critical thinking skills. It was also at this time that I received the most indispensable help from my family, friends, and colleagues.

First and foremost, I would like to thank my supervisor, Dr. Alex Adronov. Taking me on as a fourth-year thesis student was the pivotal leap of faith that made my graduate studies possible. Without his help in the enrollment process, I would have never found an opportunity to pursue some of the most interesting research into carbon nanotubes and soft matter. Over the years, Alex has imparted a tremendous amount of knowledge regarding laboratory techniques, research strategies, and synthetic analysis. This knowledge even included how to put out negligently ignited ether fire (and how to prevent one in the first place). His motivation and passion for research has been a continuous inspiration whenever tackling difficult aspects in any project.

In addition to all the help Alex has provided during my residency at McMaster, he was also able to bring me to the University of Strasbourg, France as a visiting scientist. This was possible through funding from the NSERC CREATE program on the Integrated Development of Extracellular Matrices (IDEM), the International Center for Frontier Research in Chemistry, and the LabEx "Chimie des Systèmes Complexes". It was this

opportunity that allowed me to work under Dr. Jean-François Nierengarten at the University of Strasbourg's European School of Chemistry, Polymers and Materials (ECPM). Dr. Nierengarten was not only an outstanding mentor with respect to our lab work, but also provided indispensable assistance with anything pertaining to living in a foreign country as a student. I am also thankful for Drs. Michel Holler and Uwe Hahn, who provided valuable input on optimizing chemical reactions and for being some of the most approachable and friendly researchers I've ever met. Lastly, Dr. Iwona Nierengarten was always there to brainstorm ideas to further improve our chemistry in addition to aiding with compound characterization.

Thank you to my committee members, Dr. Harald Stöver and Dr. James McNulty for their time, resources, and suggestions. Their brilliant ideas have cultivated my projects in ways that broadened their scientific impact and allowed me to branch out into applications I would not have considered unaccompanied.

Thank you to my first mentor and collaborator, Dr. Ryan Chadwick, whose initial guidance has left me with an indelible mark on the critical thinking portion of my brain. I am also thankful for Dr. Lukas Sadowski, who has never passed up an opportunity to brainstorm new projects with me despite already having five on the docket. In addition, I am thankful for Dr. Stuart McNelles, a bastion of sanity during a time of utter insanity and chemical mischief. To my skillful undergraduate chemical technician, Maria Denk, thank you for handling the grunt work of our ultimate project with the patience of a saint.

Thank you to all my supportive friends throughout grad studies: Dr. Kelvin Li, Dr. James Bod, Dr. Darryl Fong, Dr. Nicole Rice, Dr. Shuai Liang, Christina Shamshoom, Victoria Laval, and everyone else in the Adronov group, past and present. You have all fostered a positive environment that facilitated frequent collaborations, open discussions, and unforgettable karaoke jams.

I would also like to thank the Natural Science and Engineering Research Council of Canada (NSERC) and the Ontario Graduate Scholarships (OGS) program for financial support. Additionally, the NSERC CREATE program on the Integrated Development of Extracellular Matrices (IDEM) was of great help during a large portion of my graduate studies.

To my parents who have always strived to provide for me at any cost, thank you so much. They have made me who I am and for that, I will be eternally grateful. The emotional, physical, and intellectual support provided by them throughout my life as a student has instilled me with compassion and discipline that I can carry forward in future endeavors.

To my best friend, closest confidant, and wife, Sabrina, you have undertaken one of the foolhardiest, yet brave ventures of all time: marrying someone with an unfinished thesis. Despite that, you have showed me nothing but support and compassion even during the most stressful times. By keeping my heart beating, you have, by extension, consented to me finishing my thesis. I couldn’t have done it without you.

Lastly, I need thank my kids, Hailey and Oliver. Thank you for everything that drives you from the moment you wake up to the moment you fall asleep. Spending time with you teaches me more about myself and who I want to be.

List of Abbreviations

AFM	Atomic Force Microscopy
BARAC	Biarylazacyclooctynone
BDT	Benzothiophene
BVE	Butyl Vinyl Ether
CNT	Carbon Nanotube
COSY	Correlation Spectroscopy
CP	Conjugated Polymer
CuAAC	Copper(I)-Catalyzed Alkyne-Azide Cycloaddition
CVD	Chemical Vapour Deposition
Đ	Dispersity
DA	Diels-Alder
DCM	Dichloromethane
DDQ	2,3-dichloro-5,6-dicyano-1,4-benzoquinone
DEPTq	Distortionless Enhancement by Polarisation Transfer with Retention of Quaternaries
DFT	Density Functional Theory
DIBAC	Dibenzoazacyclooctyne
DIBO	Dibenzocyclooctyne
DMF	*N*,*N*-Dimethylformamide
DP	Degrees of Polymerization
DSC	Differential Scanning Calorimetry
EDG	Electron Donating Group
EL	Electroluminescence
EtOAc	Ethyl Acetate
EtOH	Ethanol
ES	Electrochemical Supercapacitor

EWG	Electron Withdrawing Group
FMO	Frontier Molecular Orbital (Theory)
GPC	Gel Permeation Chromatography
HiPCO	High Pressure Carbon Monoxide Disproportionation
HMBC	Heteronuclear Multiple Bond Correlation
HOMO	Highest Occupied Molecular Orbital
HPLC	High-Performance Liquid Chromatography
HSQC`	Heteronuclear Single Quantum Coherence
IEDDA	Inverse Electron Demand Diels-Alder
IR	Infrared
LED	Light-Emitting Diode
LUMO	Lowest Unoccupied Molecular Orbital
M06-2X	Minnesota Functional ’06
MALDI	Matrix-Assisted Laser Desorption/Ionization
M_n	Number-Average Molecular Weight
M_w	Weighted-Average Molecular Weight
MeOH	Methanol
MS	Mass Spectrometry
NBS	*N*-bromosuccinimide
NMR	Nuclear Magnetic Resonance
OFET	Organic Field Effect Transistor
OPV	Organic Photovoltaic
OLED	Organic Light-Emitting Diode
OSC	Organic Solar Cells
PSC	Polymer Solar Cells
PAc	Polyacetylene
PAni	Polyaniline

PAQ	9,10-phenanthrene-quinone
PCBM	[6,6]-phenyl C_{61}-butyric acid methyl ester
PDHT	Poly[3-(3,6-dioxaheptyl)thiophene]
PDI	Polydispersity Index *(See also: Đ)*
PEG	Polyethylene glycol
PM3	Parametric Method 3
PPP	Poly(p-phenylene)
PPV	Poly(phenylene vinylene)
PPy	Polypyrrole
ProDOT	Propylenedioxythiophene
PTh	Polythiophene
RT	Room Temperature
sc-SWNT	Semiconducting Single-Walled Carbon Nanotube
SNP	Semiconducting Nanoparticals
SPAAC	Strain-Promoted Alkyne-Azide Cycloaddition
SWNT	Single-Walled Carbon Nanotube
TCO	trans-Cyclooctene
TFA	Trifluoroacetic Acid
TGA	Thermogravimetric Analysis
THF	Tetrahydrofuran
TLC	Thin-Layer Chromatography
UV	Ultraviolet
UV-Vis-NIR	Ultraviolet Visible-Near Infrared
YM	Young’s Modulu

Contents

List of Tables

List of Figures

List of Schemes

Chapter 1

Overview of Conjugated Polymers

1.1. Introduction to Conjugated Polymers (CPs)

Since the discovery that high electrical conductivity can be induced by doping polyacetylene, conjugated polymers (CPs) have attracted significant attention. Over the past four decades, tremendous effort has been devoted to expanding the structural diversity, synthetic approaches, and applications of this class of macromolecules. In their simplest form, CPs are organic semiconductors comprised of a backbone of alternating single and double bonds. The contiguous sp^2-hybridized centers ensure that any valence electrons occupying the overlapping p_z orbitals are delocalized over the extended length of the polymer chain. In many cases, this resultant extended π-conjugated system leads to interesting opto-electronic properties. The structural variability of conjugated polymers has resulted in a broad range of research to modify their properties and to understand structure-property relationships. Broad classes of CPs include polyacetylene, poly(p-phenylene), poly(p-phenylene vinylene), poly(p-phenylene ethynylene), and poly(fluorene). Introduction of heteroatoms within the backbone structure has expanded the complexity, and the achievable properties of CPs, such as in the cases of polythiophene, polypyrrole, polycarbazole, and polyaniline (Figure 1.1). The preparation of copolymers incorporating the different monomers making up the aforementioned polymers leads to even greater complexity in the available structures, as well as their optoelectronic properties. Mobility of the π-electrons within these structures enables the CPs to behave as both electron transport materials and as chromophores that absorb light in different regions of the electromagnetic spectrum, spanning from the ultraviolet (UV) to the near-infrared (near-IR). Based on these properties, CPs have been incorporated into a variety of devices, including light-emitting diodes (LEDs), field-effect transistors (FETs), organic photovoltaics (OPVs), and energy storage materials (batteries). The processability of CPs enables transformative advances in the performance of these devices, allowing them to be light-weight, flexible, stretchable, and printable. They can adopt form-factors that are not possible with inorganic counterparts, and can be incorporated into materials like textiles, packaging, and a variety of coatings.

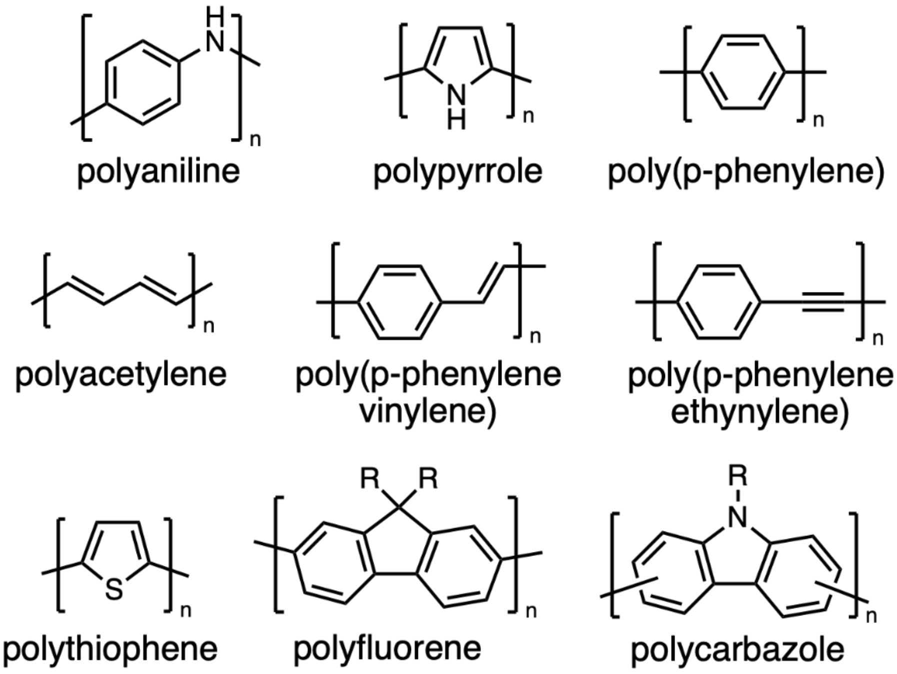

Figure 1.1. Structures of common conjugated polymer classes.

1.2. History of Conjugated Polymers

The earliest reports of conjugated polymers date back to the early 1800's with materials produced from the oxidation of aniline salts with various oxidants.[1] Aniline was treated with copper oxide or chromic acid in the 1830's and 1840's to produce a highly coloured insoluble material. John Lightfoot used oxidized aniline as a dye for textiles, coining the term "aniline black" in the 1860's.[2] Henry Letheby also investigated the oxidation of acidic aniline solutions in the 1860's, and was the first to show that aniline could be electrochemically oxidized, forming a blue coating on the surface of an electrode.[3] This highly insoluble material continued to be investigated, and it wasn't until the early 1910's that its structure was elucidated.[4,5] It took another 50 years for the conductivity of polyaniline to be discovered by Jazefowics and co-workers, who studied pressed pellets of this material and observed conductivities ranging from 10^{-5} to 10 S/cm.[1,6.] These observations placed polyaniline as one of the premier organic conductors to date.

Polypyrrole, another conjugated polymer, was first described by Angeli in 1915, who studied oxidation of pyrrole using hydrogen peroxide and acetic acid.[7] The resulting insoluble product, "pyrrole black", was later prepared with a variety of other oxidizing agents and its chemical structure was first proposed in 1918.[8] The conductivity of polypyrrole was described in 1963 by Donald Weiss, who showed that pellets of the material exhibited conductivities in the range of 0.005-0.09 S/cm.[9] As the purity of polypyrrole and the quality of its films improved, its conductivity was also found to increase, with values of 10-100 S/cm eventually being reported by Arthur Diaz in the 1970s.[6,10]

Perhaps the most significant contribution to the study of conjugated polymers was made by Shirakawa, Heeger, and MacDiarmid in 1977, who went on to share the Nobel Prize in 2000. Their 1977 report described the preparation of highly conductive films of poly(acetylene), where the conductivity was dramatically enhanced via doping with iodine.[11] Building on the work of Natta on the polymerization of acetylene catalyzed by titanium alkoxides and triethylaluminum, which resulted for the first time in the preparation of linear polyacetylene, Hatano and Ikeda optimized polymer crystallinity and developed methods to control cis/trans ratios via temperature modulation.[6,12,13] Shirakawa, a research associate in Ikeda's group, developed a method for creating lustrous, silvery films of all-trans polyacetylene by introducing a large excess of Natta's catalyst.[14–16] This allowed polymerization to occur rapidly at the gas-solvent interface, and along the vessel side-walls, producing the films. Simultaneously, Heeger and MacDiarmid were working at the University of Pennsylvania on films of poly(sulfur nitride), which also had a lustrous golden appearance and were found to increase in conductivity upon reaction with halogens.[11] After a meeting with MacDiarmid in Japan, Shirakawa was invited to visit the University of Pennsylvania to work on polyacetylene in September, 1976. Within two months, Shirakawa showed that the conductivity of trans-polyacetylene could be increased by six orders of magnitude upon exposure to I_2 vapour in a process they referred to as "chemical doping".[17–19] They later showed that the conductivity could be increased even further by treatment with AsF_5, and by switching to cis-polyacetylene.[20] Although this was not the first example of conducting organic polymers, it was certainly the most dramatic, achieving conductivity values that rivaled those of metals. This Nobel Prize-winning work subsequently sparked a broad range of effort, starting with polythiophene in the 1980's, and leading to polyphenylenes, poly(phenylene vinylenes), polyfluorenes, polycarbazoles, and numerous other derivatives.[21–27] Although the full range of derivatives of these basic structures is too broad to enumerate, their development in recent decades has stemmed from device applications, which will be discussed in some detail in section 1.3. Much of the work involved side-chain engineering to render the polymers more processable, or to impart self-assembly properties that modify polymer optoelectronics.[28–31] Modification of backbones has also led to numerous discoveries that enabled control of bandgaps, absorption/emission wavelengths, and conductivity. However, it can be argued that the most important developments of the past 4 decades have revolved around synthetic methodology. A variety of metal-mediated cross-coupling reactions, including Suzuki, Kumada, Sonogashira, Heck, and Stille couplings have enabled the preparation of a wide range of conjugated polymer backbones, and are compatible with many different side-chains.[32–34] More recently, the development of synthetic methods that liberate regioregular polymer structures has had enormous impact on applications such as photovoltaics, where precise polymer structure leads to enhanced interactions with fullerene donors, and increased photovoltaic efficiencies. Furthermore, the discovery that conjugated polymers can be prepared via a pseudo-living chain-growth process has opened the door to structurally well-defined conjugated polymers, and even block copolymers. An even more recent advance in synthetic methodology toward conjugated polymers was the discovery that C-H activation chemistry can be applied to conjugated systems, obviating the need for organometallic functional groups, such as $-B(OR)_3$, $-SnR_3$, -ZnR, or -MgX, on one of the co-monomers undergoing polymerization. The polymerization of one arene monomer bearing a leaving group (I, Br, OTf, etc.) and a second unsubstituted arene using a transition metal catalyst is termed Direct (Hetero)Arylation Polymerization (DHAP), and is rapidly growing in its scope and applications.[35–37]

1.3. Classes of Conjugated Polymers

Conjugated polymers have undergone tremendous expansion in structural diversity over the past 50 years. Beyond the initial discoveries surrounding polyaniline, polypyrrole, and polyacetylene, numerous new conjugated backbone classes have emerged. Among the most widely studied of these structures are polythiophene, poly(p-phenylene), poly(p-phenylene vinylene), polyfluorene, and polycarbazole, whose structures are shown in Figure 1.1. Among these, polythiophene is arguably the most widely studied, and has been investigated for numerous applications. The ability to modify side-chains has enabled modification of solubility, and translated into the possibility of producing high-molecular weight polymer. In addition, extensive investigation of polymerization strategies has enabled the production of regioregular polythiophene, with superior conductivity properties.[38] This material has been incorporated in organic photovoltaics, field-effect transistors, and various sensors, which will be discussed below.

In addition to polythiophene, poly(p-phenylene) (PPP) and poly(phenylene vinylene) (PPV), along with their derivatives, have also received extensive attention.[39–41] Poly(p-phenylenes) are prototypical rigid-rod polymers, typically prepared by poly-Suzuki aryl coupling. They are highly stable, but are completely insoluble if unfunctionalized with alkyl side chains. Introduction of solubilizing chains enabled the investigation of their photophysical properties, which uncovered high quantum yields of fluorescence centered at 460 nm.[42] PPP was the first conjugated polymer to exhibit blue electroluminescence.[43] The chemical structure of PPV is intermediate between that of polyacetylene and polyphenylene, and it is highly stable and crystalline. Introduction of alkyl side-chains on the phenylene units results in soluble structures that have been used as components of light-emitting diodes. In addition, PPV is a good hole transporter, and its derivatives have been incorporated within bulk heterojunction photovoltaic devices in combination with [6,6]-phenyl C_{61}-butyric acid methyl ester (PCBM) as the electron transporter.[44]

Another class of conjugated polymers that has received significant attention is polyfluorene. Derivatives of polyfluorene are especially interesting because they exhibit a rigid biphenyl structure in the monomer, which enhances conjugation and results in a large band-gap that enables efficient fluorescence in the visible range. In addition, facile substitution at the bridging methylene group, position C9, allows introduction of various side-chains that enhance solubility and processability without deleterious effects on conjugation of the backbone.[45] This polymer class has been extensively investigated for application in light emitting diodes, which have become ubiquitous. Many different derivatives of polyfluorene have been prepared and investigated over the past few decades.

Polycarbazoles are another class of conjugated polymers that has attracted widespread attention. Although similar to polyfluorene in structure, polycarbazole has the advantage of being fully aromatic as a result of conjugation of the nitrogen lone pair. It additionally exhibits a bridged biphenyl unit that results in a low band-gap, yet it can also be substituted at the nitrogen to install a variety of side-chains that impart solubility and processability.[46,47] Backbone structure can also be varied through substitution at the 3- and 6- positions, or at the 2- and 7- positions, which leads to different properties and different applications. Poly(3,6-carbazoles) form charge-transfer complexes as a result of the electron-rich character of the carbazole unit, making them useful in xerography.[36] In addition, they are excellent blue emitters and have been investigated in polymer light emitting diodes (PLEDs), as will be discussed below. Although poly(2,7-carbazoles) are more difficult to prepare on account of their meta-substitution pattern, they have longer conjugation length and exhibit intense blue emission. When 2,7-carbazole is copolymerized with other monomers, such as quinoxaline and thiophene, it results in structures with green and red emission, allowing colour tuning throughout the visible spectrum. Interestingly, despite their longer conjugation length, poly(2,7-carbazoles) are less conductive than poly(3,6-carbazoles).[48]

While various other conjugated polymer structures have been investigated, they are too numerous to be comprehensively discussed here. Many excellent reviews of conjugated polymer structures have been published, and are recommended to the interested reader.[32,34,49,50]

1.4. Applications of Conjugated Polymers

Many of the electronic properties of conjugated polymers can be controlled through a process known as doping whereby the backbone of the CP is either oxidized or reduced to promote electron mobility. Before doping, a typical conjugated polymer possesses conductivity consistent with that of insulators or semiconductors (usually in the 10^{-10} to 10^{-5} S/cm range). Upon introducing a dopant, such as I_2 or AsF_5, a CP can be promoted into what is considered the metallic conducting regime (1 to 10^4 S/cm).[50,51] Many conjugated polymers and their derivatives are capable of undergoing doping either via electrochemical p- or n-type redox doping or via photo-doping, effectively generating charge carriers that move along the polymer chains. This process can transform many CPs into materials amenable for use in applications such as light-emitting diodes (LEDs), organic photovoltaic devices (OPVs), super capacitors, and biosensors.[50,52–55]

1.4.1. Organic Light-Emitting Diodes (OLEDs)

Organic Light-Emitting Diodes (OLEDs) are diodes that contain an organic film able to emit light in response to an electric current, a process referred to as electroluminescence (EL). Typically, this consists of one or more organic layer being deposited between two electrodes with at least one of them being composed of transparent indium tin oxide (ITO). With this configuration, an external electrical current can be passed through the organic substrate, resulting in the injection of holes at the anode contact or electrons at the cathode contact. If the respective charge carriers (i.e. holes and electrons) in the organic layer combine to generate an excited state analogous to that of photoluminescence and symmetry-permitted relaxation back to ground-state occurs, then the result is a photon emission (Figure 1.2), the colour of which corresponds to the HOMO/LUMO gap.[56]

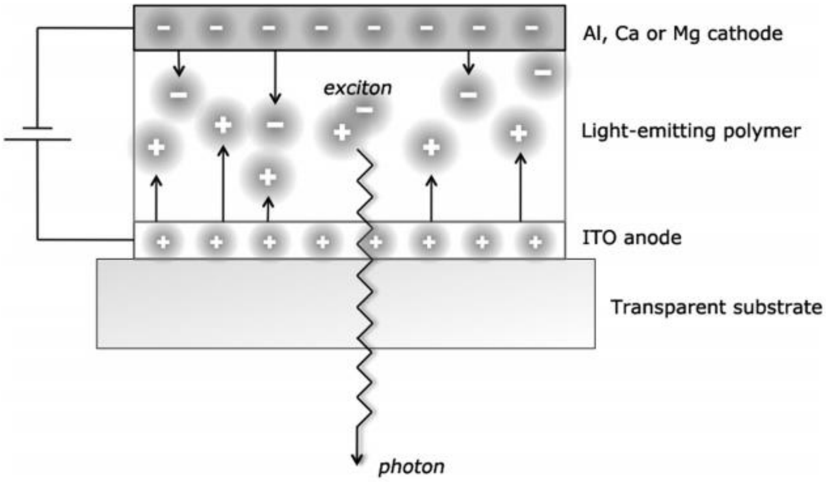

Figure 1.2. Schematic representation of a single-layer electroluminescent (EL) device. The application of a forward bias voltage generates and electron-hole pair. The resultant excited state emits a photon via radiative decay to the ground state. Reproduced with permission.[56] Copyright Chemical Reviews, 2009.

Among the first organic thin film-based LEDs to be developed were by VanSlyke[57] in the late 1980s, which prompted a surge in the development of other organic EL devices, particularly those based on conjugated polymers. Since the first reporting of scalable poly-*para*-phenylene- (PPP) and poly(p-phenylenevinylene) (PPV)-based OLEDs in 1990,[58] a number of other CP classes have been investigated for their use in OLEDs and their applications, including polythiophenes, polyfluorenes, and polycarbazoles.[27,59,60] Much of this research has been focused on designing the appropriate polymer backbone to best suit the specific OLED application. For instance, parameters such as side chain type, average molecular weight, and HOMO/LUMO energy levels need to be taken into consideration when synthesizing conjugated polymers. These factors have a substantial impact on the polymer morphologies and the overall efficiency of the resultant OLEDs.[61]

1.4.2. Supercapacitors

Since the advent of hybrid vehicles, a considerable amount of research has shifted to focus on the development of energy storage devices with high-powered and high-capacity energy resources. Such charge-storing devices come in the form of improved supercapacitors. These devices mirror the function of capacitors, though with much higher capacitance values and lower voltage limits. Filling the gap between rechargeable batteries and electrolytic capacitors, supercapacitors are designed to deliver charge at a significantly faster rate than batteries, in addition to tolerating more charge cycles.[62]

Most electrochemical supercapacitors (ES) can be broken down into the same basic components. Two electrodes are typically found on either side of a separator while being in contact with an electrolyte (Figure 1.3). As charge must be stored at the interface between the conductive electrode and the electrolyte, the electrode's material is fabricated with a high surface area and porosity in mind. When considering materials for electrodes, several classes have been incorporated into ES devices, including high-surface area carbon materials (e.g. activated carbon)[63], metal oxides, and conjugated polymers.[64,65]

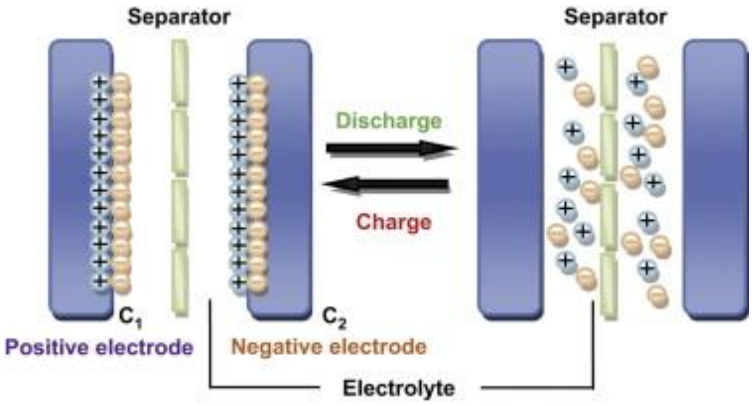

Figure 1.3. Two possible states of a double layer capacitor: Charged (left) and Uncharged (right). Reproduced with permission.[63] Copyright Elsevier, 2013.

Conjugated polymers possess several of the properties that make them suitable for use in ES as the electrode material, including a lower environmental impact, high conductivity (when doped), low cost, and a variable redox potential via chemical modification.[66,67] As such, conjugated polymers provide capacitance via redox reactions, whereby ions are transferred to and from the polymer backbone throughout the entire bulk.[68] This transfer process causes minimal to no change in the polymeric structure and thus, is highly reversible.[69] Several common conjugated polymers have been used in ES applications to date, including polyaniline (PAni), polythiophene (PTh), and Polypyrrole (PPy). PTh, in particular, can be used in both p- and n-doped ES devices. However, these CPs exhibit more optimal conductivity in their oxidized states and thus are typically used as the positive electrode, with other carbon-based materials (e.g. CNTs) being employed for negative electrodes.

1.4.3. Organic Photovoltaic Devices

It has become clear that, among the renewable energy options, which include biomass, geothermal, hydropower, nuclear, solar, and wind, solar energy is the only one that can meet both today's energy demand and all energy needs in the foreseeable future. In fact, the solar radiation striking the Earth's landmass every hour (14 TW) is more than enough to supply the current global energy requirement for an entire year (13 TW). Although current silicon-based photovoltaics, having reached efficiencies of 25%, are capable of sufficient power generation to meet today's needs, their high cost, complex manufacturing protocols and large "footprint", have prevented their infiltration into the energy market beyond the 0.01% level. Based on today's energy requirement to produce 1

m^2 of silicon wafer (1700 kWh/m2), silicon solar cells operating at 15% efficiency require approximately 8 years of operation before they generate an amount of energy equivalent to what was consumed in their manufacture. Besides the large-scale solar power generation panels, inexpensive solar cells are required to meet the needs of niche markets, such as in trickle-charging portable electronic devices (i.e., cell phones, mp3 players, and PDA devices). In these applications, low-cost, light-weight, flexibility, and the ability to operate under low-intensity, diffuse indoor lighting are properties that outweigh the need for high efficiency and longevity (consider the lifetime of most personal electronics). It is therefore clear that alternative and disruptive photovoltaic technologies will be required in order to address both global energy needs, and those of future niche markets.

Organic photovoltaics (OPVs) have attracted significant recent interest. Generally, OPVs are devices that make use of organic films for light absorption, charge transport, and photocurrent generation. These organic films (often composed of conjugated polymers) assist in the absorption of sunlight and the production of electricity via photoinduced charge separation (Figure 1.4). By design, the conjugated polymers used in OPVs are solution processible and can often be printed, removing the need for more expensive photolithographic techniques. Thus, compared to inorganic photovoltaic cells, polymer solar cells (PSC) have numerous advantages including flexibility, lower manufacturing cost, and light weight. Initial organic photovoltaic devices involved the use of P3HT as the light harvesting and electron donating component, in combination with buckminsterfullerene (C60) as the electron acceptor. The near-quantitative photoinduced electron transfer that occurs between P3HT and C60 is responsible for the relatively high power conversion efficiencies (3-5%) that were attained. These bulk heterojunction devices require balanced bicontinuous pathways for both electrons and holes to achieve efficient current generation. Today, the record efficiency for an OPV is approximately 18%, and uses mixtures of complex conjugated polymers in combination with C71 as the electron acceptor.

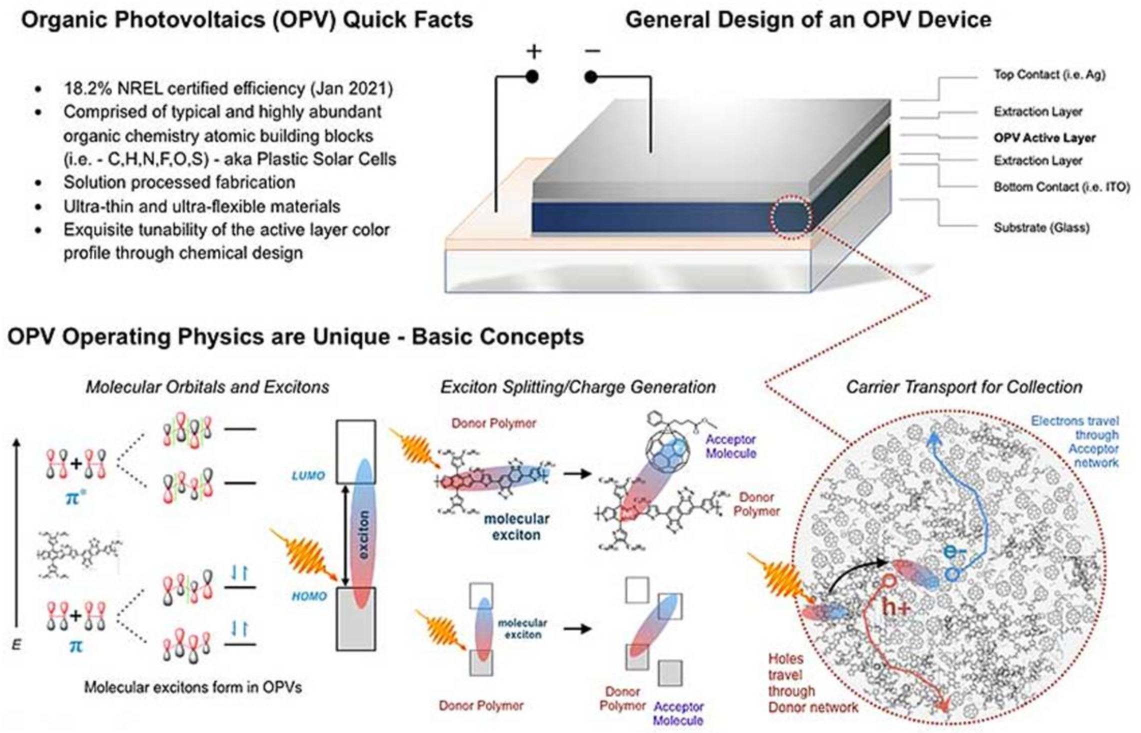

Figure 1.4. The conversion of sunlight to electricity in an organic photovoltaic device (OPV) involves several interacting layers. External electrode layers sandwich an active layer containing charge carriers. Image by Bryon Larson, NREL.

1.4.4. Sensors

Chemical sensors are devices that detect chemical information, such as concentration and pressure of chemical species, and then transduce it into interpretable electrical signals associated with the respective analytes. Several sensor characteristics may be monitored for analyte detection, including conductivity, electric potential, heats, or even optical activity, which vary upon changes to the interacting chemical species.[70] Many current commercially available chemical sensors command the use of inorganic semiconductors with polymers being used in a structural support role, such as the zirconia-based Lambda-probe for detecting oxygen in car exhausts or tin dioxide based carbon monoxide sensors.[71]

Coming into greater prominence commercially, conjugated polymers provide an ideal scaffold for chemosensing materials via both analyte-receptor interactions and nonspecific interactions. As of the 1980s, CPs such as polypyrrole (PPy), polythiophene (PTh) and polyaniline (PAni) have thus far found their use in gas sensors. Coupled with the electron transport and electrical conductivity properties of these CPs, small changes to the backbone structure may often result in observable responses useful in the detection of analytes. Moreover, when compared to their commercially available metal oxide-based chemosensing counterparts, CP-based sensors have shown increased sensitivity.

Many observable physical properties of conducting polymers are affected by their respected levels of doping. As such, these doping levels can be easily modified by chemical reactions with various analytes at low temperatures, and this provides a simple technique to detect the analytes. Many commercially available conducting polymers are doped via redox reactions; therefore, their doping level can be altered by transferring electrons from or to the analytes. For example, redox-active polymers such as PAni react with electron acceptors, such as NO_2 and I_2, altering the doping level in the p-type polymer, thereby enhancing its electrical conductance.

1.5. Conjugated Polymers and Carbon Nanotubes

A great deal of attention has been given to newly uncovered allotropes of carbon, including C_{60} (fullerenes), carbon nanotubes, and graphene, which comprise a large proportion of the nano-materials that are under current investigation. Many studies have particularly focused on the unique properties of single-walled carbon nanotubes (SWNTs), since their discovery.[72,73] Their high electrical and thermal conductivity,[74–76] mechanical strength,[77] aspect ratio,[78] and optical properties[79–81] have enabled investigation of many applications in areas such as sensors,[82–84] field-effect transistors (FETs),[85] flexible electronics,[86,87] organic photovoltaics,[88–90] touch screens,[91] high strength fibers,[92–94] and many other applications.[95] Considering the different nanotube types, it has been found that semiconducting SWNTs (sc-SWNTs) exhibit performance characteristics that are superior to those of traditional silicon-based materials,[85] whereas metallic SWNTs (m-SWNTs) are able to conduct electrons better than typically used metals, like copper.[96] Despite these superior properties, real-world applications and commercialization of carbon nanotubes has not accelerated at the expected pace,[97] particularly where applications require highly pure samples of nanotubes. Considering that all methods for nanotube preparation, which include chemical vapour deposition (CVD),[98] laser ablation,[99] arc-discharge,[100] plasma torch growth,[101] and high-pressure carbon monoxide disproportionation (HiPCO),[102] produce mixtures of both sc-SWNTs and m-SWNTs in a two-to-one ratio. Separation and purification of SWNTs according to their electronic properties has posed a significant challenge.

Recently, several methods for enrichment of electronically-pure SWNTs have been identified. Of these, the first and most widely used was reported by Hersam and co-workers in 2005,[103] and involves density gradient ultracentrifugation. It was found that, when SWNT samples were placed in a density gradient and spun at exceedingly high speeds (250,000 g) for extended periods of time (several days), they could be separated according to the slight differences in density between the different nanotube species. Thus, electronically pure samples of SWNTs could be isolated, enabling their investigation within numerous SWNT-based devices.[95] This breakthrough was followed by other techniques, including electrophoresis,[104] agarose gel filtration,[105] two-phase extraction,[106,107] interactions with single-stranded DNA,[108–110] and size-exclusion chromatography,[111,112] all of which enabled separation of m- and sc-SWNTs. The drawback to all of these techniques, however, is the low yield of purified SWNTs that they produce. Typically, isolation of only microgram quantities of enriched nanotubes has been reported with these methods, and the laborious and expensive nature of the operations makes it difficult to scale them to commercially-viable levels.

Another approach toward nanotube purification that can potentially address the scalability issue involves the use of conjugated polymers (CPs) to selectively disperse specific SWNT types. Early examples of supramolecular interactions between conjugated structures and SWNTs involved small molecules such as pyrene derivatives,[113] which demonstrated that these structures can impart solubility to the SWNT-pyrene complexes. Conjugated polymers, such as poly(phenylene vinylene) (PPV) were also found to produce nanotube dispersions in organic solvents.[114–117] In 2007, a seminal report from Nicholas and co-workers[118] showed that selective dispersions of certain SWNT species could be achieved using standard commercial CPs, such as poly(9,9-di-*n*-octylfluorene) (PFO). Following this report, numerous studies of CP-SWNT interactions have been caried out, and have shown efficient dispersion of sc-SWNTs with purities in excess of 99.9%.[119] It has also been shown that CPs can be removed from the nanotube surface after the purification process, by undergoing conformational changes[117] or backbone depolymerization,[120–122] opening the door to isolation of pure nanotube species. The ability to produce conjugated polymers on large scale makes this approach the most viable for commercial applications.

Although the reports of CP-SWNT complexes have uncovered promising methods for nanotube purification, the underlying principles that dictate the strength and selectivity of nanotube interactions with conjugated polymers remain poorly understood. Rational design of conjugated polymers that can selectively interact with a particular nanotube species remains elusive. This limitation results, in large part, from the synthetic difficulty in producing libraries of conjugated polymers with precise changes to their structure. Even small changes to monomer structure can lead to dramatic differences in polymerization efficiency, which will result in polymers of different molecular weight and dispsersity (Đ), both of which will also influence the efficiency of the interaction with SWNTs. Without control over length and dispersity, any comparisons of homologous polymer structures become flawed. Despite these challenges, the necessity for identification of structure-activity relationships in CP-SWNT interactions remains imperative to the development of a fundamental understanding of the polymer characteristics that drive interaction strength and selectivity. It is therefore necessary to produce polymer libraries where the polymer length and dispersity remain identical, while polymer electronics, sterics, and other structural features can be systematically varied. One approach that can achieve such libraries involves efficient post-polymerization functionalization of a parent conjugated polymer, enabling the preparation of numerous daughter polymers having precise modifications. This approach requires identification of conjugated polymer backbones that are amenable to highly efficient post-polymerization chemistry, allowing quantitative conversion of the parent polymer into daughter structures.

1.6. Post-Polymerization Functionalization of CPs

Functionalization of conjugated polymers is crucial for tailoring their performance in any given application. This can be accomplished by modifying their side-chains or their backbone post-polymerization. There are significantly more reports in the literature of side-chain functionalization than there are of strict backbone functionalization of CPs. This can likely be attributed to greater accessibility of functional groups on the peripherals of CP side-chains compared to any functional handles found in more sterically hindered positions within the backbone. On the same account, while typically offering chemists a greater challenge, backbone functionalization is generally more conducive to imparting significant changes to a CP’s optoelectronic properties.

1.6.1. Side-Chain Functionalization

Side chain selection has a profound impact on the physical properties of a conjugated polymer. Often, the solution-processability of a CP, and therefore its ease of use, is determined by the type of side chain designed. Several classes of side chains have been studied for the purpose of imparting desirable properties to CPs via post-polymerization functionalization, including alkyl, conjugated, and oligoether.

Alkyl chains are among the most commonly used side chains in conjugated polymers. Alkyl chains are typically grouped into two categories: linear and branched alkyl chains. Of the linear alkyl chains, hexyl, octyl, decyl, and dodecyl chains are most common. In recent years, longer side chains, such as tetradecyl and octadecyl, were also introduced in donor−acceptor conjugated polymers. Branched alkyl chains, however, will often impede interchain interdigitation when compared to linear chains. This is likely due to their additional steric bulk. Thus, when comparing side-chain architecture, branched alkyl chains usually impart better solubility relative to linear structures when both chains have identical molecular formula.

The rationale behind grafting on a conjugated side-chain differs completely from that of alkyl side-chains. This is because conjugated side-chains are usually able to affect either the HOMO or LUMO levels of the polymers themselves. This strategy has been best exemplified by Hou and coworkers, utilized conjugated side-chains to generate high-performance polythiophenes, whose absorption profiles could be tuned by regulating the ratio of linear vs. conjugated side-chains.[123] Additionally, a donor/acceptor-type CP could be generated by incorporating an alkyl thienyl group onto a donor unit (such as benzodithiophene – BDT), a modification that further enhanced hole mobility of the polymer.

Oligoether side-chains, in contrast to alkyl chains, have been shown to impart hydrophilicity onto certain CPs without the need for ionic groups. Several oligoether-containing CPs have thus far been reported, including poly(phenylene vinylene), polyfluorene, and propylenedioxythiophene (ProDOT). For example, Roncali and coworkers developed a poly[3-(3,6-dioxaheptyl)thiophene] (PDHT) with oligoether side-chains that no only imparted greater hydrophilicity, but also a 30 nm bathochromic shift in the absorption spectrum compared to its alkyl side-chain analogue. In an effort to impart solution processibility in more environmentally sustainable solvents, Reynolds and coworkers prepared and studied a new dioxythiophene copolymer substituted with oligoether side-chains. These side-chains were shown to impart good CP solubility in more hydrophilic solvents such as acetone, in turn, allowing thin films to be cast and subsequently doped to average film conductivities in excess of 55 ± 3 S/cm.

1.6.2. Backbone Functionalization

Modifying the main chain or backbone of a conjugated polymer typically poses a greater challenge than modifying the side chains alone. However, this type of modification often has a greater impact on the functionalized CP’s optoelectronic and physical properties.[3,4] A few synthetic strategies have already been employed for the derivatization of a conjugated polymer’s backbone post-polymerization. As the π-conjugated backbone of a CP is known to be quite stable, quantitatively functionalizing such a system is particularly challenging.

Prior to the work outlined in this thesis, Dichtel and co-workers reported a $Cu(OTf)_2$-catalyzed benzannulation between the backbone alkynes in a poly(phenylene ethynylene) and an o-(phenylethynyl)-benzaldehyde. This benzannulation reaction was performed in the presence of excess trifluoroacetic acid to quantitatively generate a poly(phenylene) product.[124] Not only does this work outline the synthesis of an otherwise unattainable polyphenylene, but this feat is an example of the first efficient cycloaddition reaction performed on a conjugated polymer backbone.

Additionally, Stevens, Heeney and co-workers reported the quantitative nucleophilic aromatic substitution of an electron-deficient aryl fluoride-containing conjugated polymer with a benzothiadiazole unit using thiols at high temperatures.[125] Despite the harsher reaction conditions, this reaction platform was efficient enough to afford the authors a range of emissive poly(9,9-dioctylfluorene-alt-benzothiadiazole) (F8BT)-based polymers for the creation of mono and multifunctional semiconducting polymer nanoparticles (SPNs). As such, these fluorescent nanoparticles could be functionalized with multiple different groups via orthogonal coupling reactions, leading to the simultaneous coupling of targeting ligands and fluorescent dyes.

Entering the realm of "photoclick" chemistry, Zhang and co-workers reported an elegant bio-orthogonal click reaction between several different electron-rich vinyl ethers and a 9,10-phenanthrene-quinone (PAQ) derivative mediated by visible light.[126] This chemistry was incorporated into a methodology that allowed Fong and coworkers to perform the first such "photoclick" reaction on the backbone of a polyfluorene (PF) containing a 9,10-phenanthrenequinone moiety with relative ease. Coupling with butyl vinyl ethers (BVE), these click reactions could quantitatively produce fully conjugated PF-PAQ-BVE polymers, without the need for catalysts, intense heating, or the generation of by-products. Additionally, this type of backbone "click" reaction has a profound impact on the solubility and optoelectronic properties of the PF-PAQ polymers, producing an increase in fluorescence intensity in the photoclick product.

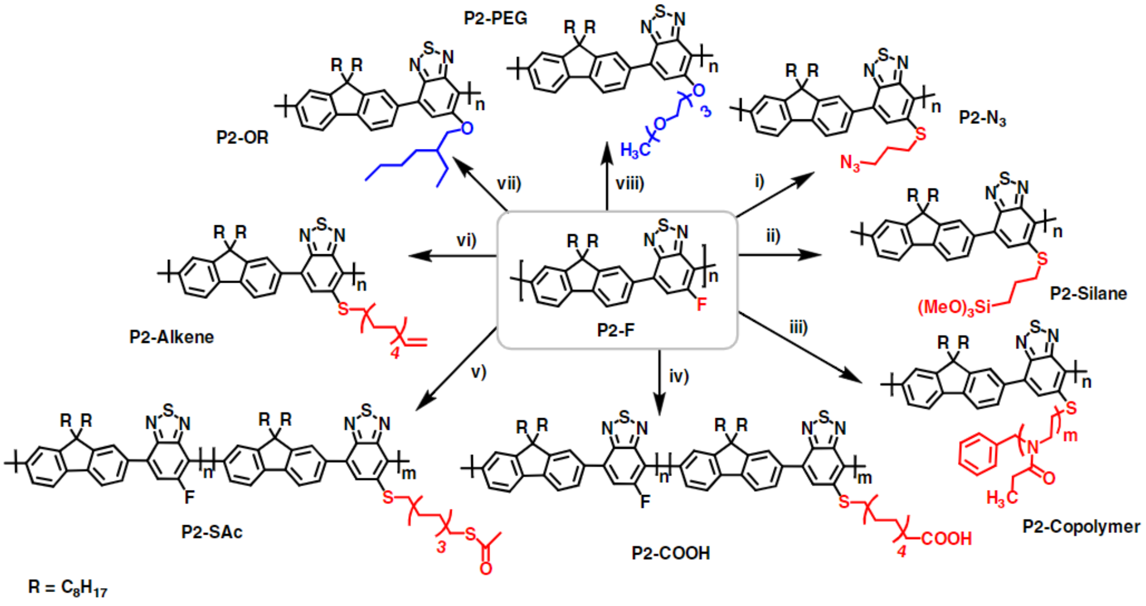

Figure 1.5. Nucleophilic Aromatic Substitution (S$_N$Ar) of polyfluorene P2-F with functionalized alcohols and thiols. Reproduced with permission.[125] Copyright Nature, 2018.

While much of the recent research into post-polymerization click chemistry has yielded promising results, only a handful of "click" reactions have yet to be incorporated for this type of backbone functionalization. As such, there is great capacity for improving these post-polymerization reactions with respect to introducing milder reaction conditions, increasing rates, and minimizing the need for additional catalysts/reagents.

1.7. Click Chemistry

In addition to the aforementioned examples of backbone functionalization, other efficient reactions can be used to modify conjugated polymer backbones. In particular, the field of click chemistry is rapidly growing as a result of numerous clean and fast reactions that have recently been discovered and exploited. First presented in 2001, Kolb, Finn, and Sharpless originally outlined the criteria for the “spring-loaded” reactions they identified as “click” reactions.[127] These reaction criteria include a high product yield, production of only “inoffensive by-products”, the ability to perform the reaction under “simple reaction conditions”, and a relatively large thermodynamic driving force (typically in excess of 20 kJ/mol). The three types of reactions that originally satisfied these criteria were the S_N2 opening of strained rings,[128] 1,3-dipolar cycloadditions,[129] and protecting group reactions on aldehydes and ketones.[130]

A year later, in 2002, Sharpless and coworkers reported the first copper(I)-catalyzed 1,3-dipolar cycloaddition of alkynes with azides. Since its conception, this reaction has received a great deal of attention due to its easily accessible precursors and its applicability toward the synthesis of linear polymers,[131] dendrimers,[132,133] and synthetic hydrogels.[134,135]

The previously studied radical-mediated thiol-ene reaction eventually also fell under the umbrella of click chemistry. The reaction of thiols with alkenes typically exhibits rapid reaction rates and achieves quantitative yields under a variety of solvents and mild conditions. This includes and insensitivity to ambient oxygen and water,[136] which makes thiol-ene click reactions amenable to both materials and biological applications.

Certain ‘click’ reactions are even efficient enough to be viable for the synthesis of step-growth polymers, which can be accomplished via thiol-ene click, copper-catalyzed alkyne-azide cycloaddition, or strain-promoted alkyne-azide cycloaddition (SPAAC). In order to facilitate this, one comonomer is typically bis-functionalized with a ‘clickable’ moiety, such as cyclooctyne, which when paired with a stoichiometric equivalent amount of a bis-azide comonomer, results in polymerization. In the case of (SPAAC), this step-growth polymerization can generate linear chains with degrees of polymerization (DP) in excess of 50 in mild conditions without the production of by-products.[137]

1.7.1. Strain-Promoted Alkyne-Azide Cycloaddition (SPAAC)

Alkyne-Azide ‘Click’ remains an exceptionally popular [3+2] cycloaddition reaction in the fields of materials science, organic chemistry, and biomedical engineering. Whereas classic Huisgen 1,3-dipolar cycloaddition reactions between alkynes and azides required relatively long reaction times at high temperatures, the advent of Cu(I) catalysis has transformed the cycloaddition to allow for shorter reaction times and an overall cleaner reaction/workup (Figure 1.6). However, because Cu-catalyzed alkyne-azide cycloadditions (CuAAC) require the presence of Cu(I), which is cytotoxic, utilizing this type of chemistry for biological applications become less practical, often requiring extra steps to ensure removal of the catalyst.

Addressing the shortcomings of CuAAC, Strain-Promoted Alkyne-Azide Cycloaddition (SPAAC) generates irreversible triazole linkages without the need for catalysts or high temperatures. It accomplishes this transformation by utilizing highly strained cycloalkyne rings, in the place of terminal alkynes. Due to the inherent nature of the rings, a cyclic alkyne moiety cannot adopt an ideal sp-hybridized 180º bond angle, and thus stores internal energy in the form of ring strain, which is inversely proportional to ring size.[138] For cyclooctynes, which happen to be the smallest isolable cyclo-alkyne, this ring strain corresponds to approximately 18 kcal/mol.[139] Conveniently, the reactivity of cyclooctynes, combined with multiple synthetic routes to their preparation, has resulted in the investigation of numerous dibenzoannulated derivatives, such as dibenzocyclooctyne (DIBO), dibenzoazacyclooctyne (DIBAC), and biarylazacyclooctynone (BARAC) for use in SPAAC reactions.

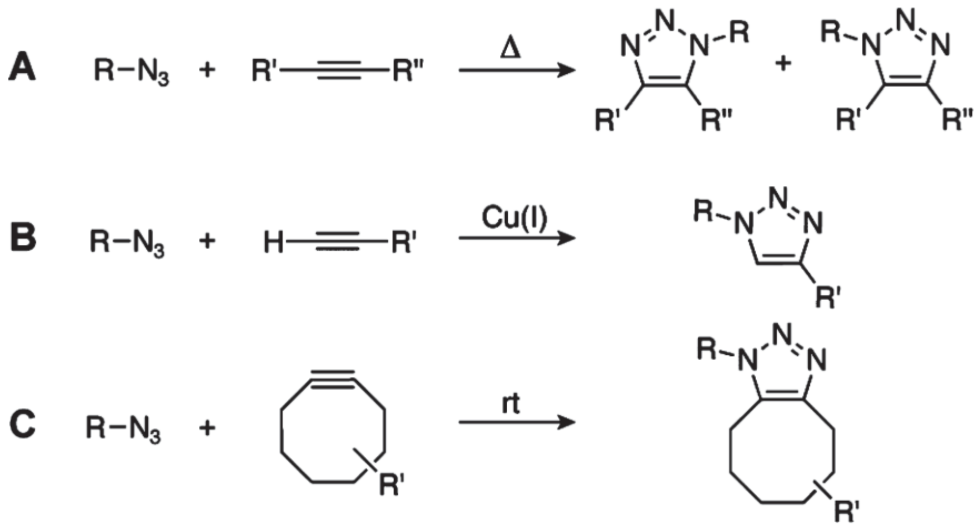

Figure 1.6. 1,3-dipolar cycloaddition of azides and (A) linear alkynes, (B) terminal alkynes with Cu(I) catalysis, and (C) cyclooctynes. Reproduced with permission.[140] Copyright American Chemical Society, 2011.

When undergoing ligation with benzyl azide, the second-order rate constants of these cyclooctynes vary from 0.057 $M^{-1}s^{-1}$ in the case of DIBO up to 0.96 $M^{-1}s^{-1}$ for BARAC. These reaction rates allow for a wide array of applications in biorthogonal chemistry and *in vivo* imaging, in which high reagent concentrations are not possible.[141–143]

Recently, new dibenzocyclooctynes have been synthesizes for the purpose of evaluating their reactivity in SPAAC reactions.[144] This has led to insights into the effect of aryl substituents on alkyne reactivity. In addition to the reactivity enhancement brought on by the increased ring strain from the ketone moiety in *keto*-DIBO, the presence of fluoride and methoxy substituents on the aryl rings also have a dramatic effect on reactivity.

In fact, the increase in alkyne reactivity from the presence of fluoride substitutions on the aryl ring (6.5-fold increase) is comparable to the increase in reactivity from DIBO to DIBAC structures. One such newly synthesized cyclooctyne, keto-FMDIBO, contains both methoxy- and fluoro-substituents and has a second-order rate constant of 3.50 $M^{-1}s^{-1}$ with azides, which makes it one of the most reactive strained cyclooctynes for SPAAC.

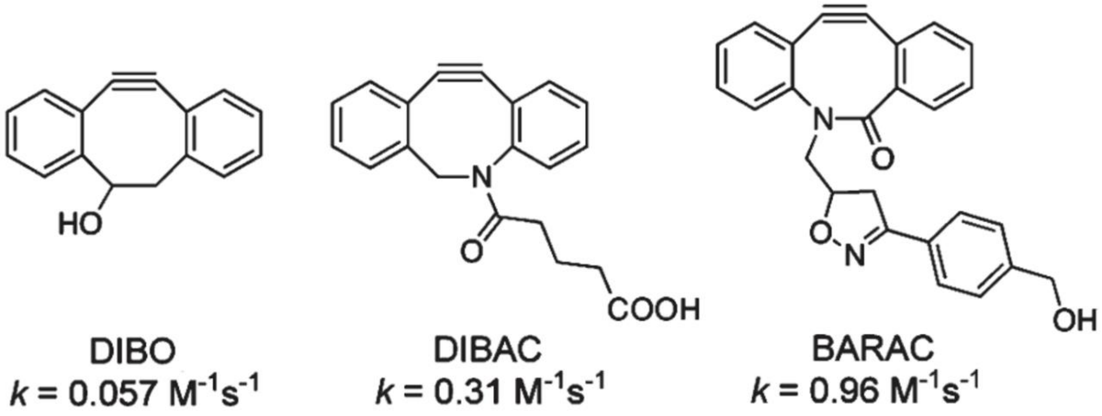

Figure 1.7. SPAAC second-order rate constants of DIBO, DIBAC, and BARAC compounds with benzyl azide in acetonitrile. Reproduced with permission.[140] Copyright American Chemical Society, 2011.

1.7.2. Inverse Electron Demand Diels-Alder (IEDDA)

A click reaction gaining more traction in recent years is the inverse electron demand Diels-Alder addition reaction (IEDDA). Like normal demand Diels-Alder reactions, IEDDA is a concerted [4+2] cycloaddition involving the interaction of a 4π electron system (diene) and a 2π electron system (dienophile) in order to form a 6-membered ring. However, the main distinction between normal and inverse demand Diels Alder reactions lies in the HOMO-LUMO interactions between the diene and dienophile. For a normal demand Diels-Alder reaction, the electron-rich diene (HOMO) reacts with an electron-poor dienophile (LUMO), whereas in a typical inverse demand reaction, the electron-rich dienophile (HOMO) reacts with an electron-poor diene (LUMO). When considering the frontier molecular orbital theory (FMO), the reaction kinetics between the diene and dienophile is determined by the energy gap between their respective HOMOs and LUMOs, that is, reactant pairs with a smaller energy gap would in theory react faster than those with a larger energy gap.

In each case, the energy of the HOMO can be raised with the presence of electron donating groups (EDG), whereas the energy of the LUMO is lowered with any appended electron withdrawing groups (EWG). It is the manipulation of the energy difference between the HOMO and LUMO of the reactants via electronically tuning the reactants by appending different electron withdrawing or electron donating groups which largely determines the kinetics of the reaction (Figure 1.8). As such, 1,2,4,5-tetrazines (also known as s-tetrazines) are typically used as the diene of choice in IEDDA due to their high reaction rates with a large selection of dienophiles, while maintaining bioorthogonality *in vivo*.

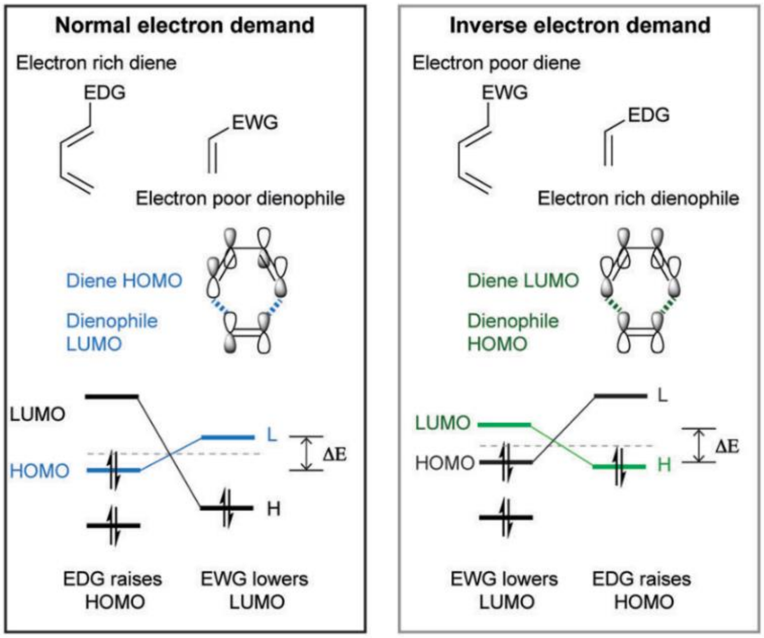

Figure 1.8. Frontier molecular orbital diagrams for normal- (left) and inverse-demand (right) Diels-Alder reactions. Reproduced with permission.[145] Royal Society of Chemistry, 2017.

In addition to electronic effects introduced by various substituents, reaction rates can also be tuned via strain effects on the dienophile. Ring strain, in particular, has a substantial impact on reaction rates by raising the $\text{HOMO}_{\text{dienophile}}$, and the observed rate constant increases with ring strain in the following order: cyclooctene < cyclohexene < cyclopentene < cyclobutene < cyclopropene.[146] An additional effect is observed in the higher reactivity of *trans*- over *cis*-alkenes. For example, the crown-conformation of *trans*-cyclooctene allows it to undergo IEDDA with s-tetrazines at a rate that is 7 orders of magnitude higher than that of its *cis*-cyclooctene counterpart.[147]

Stereochemistry of the dienophile also has a pronounced impact on IEDDA reaction rates. Trans-cyclooctenes containing axial functional groups are more reactive than their corresponding equatorial isomers. This can be seen in the 1.1 kcal/mol (4x) higher reactivity of the axial-functionalized TCO-OR compared to the equatorial analogue. Other functionalized dienophile isomers such as *exo*-norbornene cycloadd to tetrazines approximately 3 times faster than *endo*-norbornene.

The combination of electronic effects imparted by the cycloaddend substituents in addition to the ring strain and stereochemistry of the dienophile allows this system to be tuned to reach reaction rate constants of up to 10^6 $M^{-1}s^{-1}$.[148] These reaction rates are up to 4 orders of magnitude faster than those of CuAAC with a terminal alkyne/azide[149] and up to 6 orders of magnitude faster than SPAAC with a biarylazacyclooctynone/azide (Figure 1.9).[138] Thus, owing to its exceptionally high second order rate constant, IEDDA, particularly via tetrazine ligation, has been increasingly explored for its use in functionalization of proteins and other macromolecules, both biological and non-biological.[150,151]

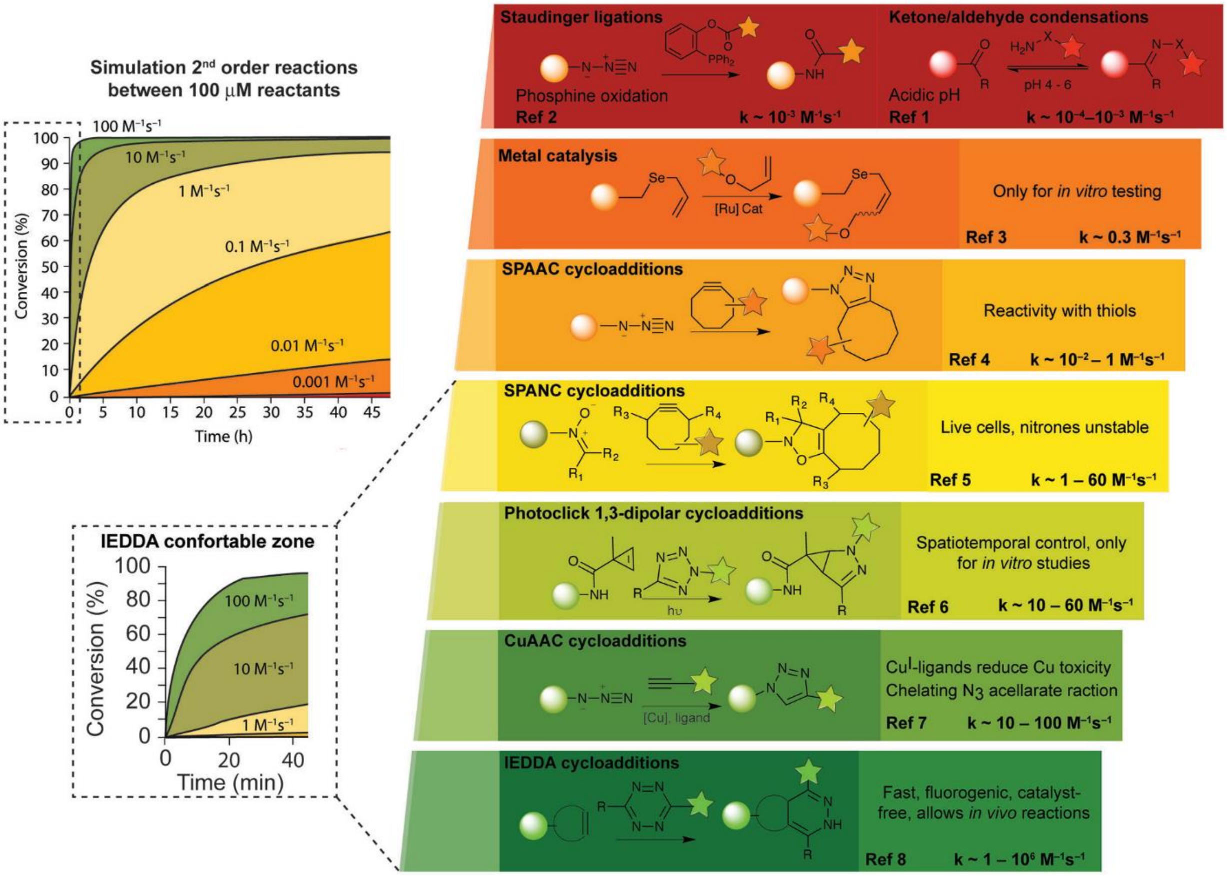

Figure 1.9. Various examples of bioorthogonal "click" reactions ranked by typical second-order rate constants. Reproduced with permission.[145] Royal Society of Chemistry, 2017.

1.8. Thesis Objectives

The central goal of this thesis is to utilize efficient 'click' chemistry for the purpose of functionalizing conjugated polymers in a post-polymerization fashion. In order to accomplish this goal, I focused on three main objectives:

The first of these involved generating a novel reactive polymer that undergoes post-polymerization click at the backbone without significantly changing its conformation. Maintaining the conjugated polymer backbone's planar conformation upon "clicking" is desirable as it maintains any favourable optoelectronic properties brought about by the extended conjugation length of the parent polymer. This objective branches directly off the main goal of my thesis and was the basis behind the projects outlined in chapters 2 and 4, which involve the synthesis of a DIBO-containing polyimine and a *s*-tetrazine-containing polyfluorene, respectively. While both conjugated polymer progenitors undergo quantitative click reactions, the DIBO-containing polyimine produces a slight backbone pucker upon its reaction with azides, thereby altering its conformation significantly. This backbone kink is made evident by both the gel permeation chromatography (GPC) observations, indicating a decrease (~15%) in hydrodynamic volume in addition to computational modeling data that corroborates the conformational change. With the advent of the *s*-tetrazine-containing polyfluorene, this conformational change issue is resolved as the post-click derivatized polymers exhibit a very similar planarity to that of the parent polyfluorene. This improvement also simplifies tracking of reaction progress as the expected increase in the hydrodynamic volume during the post-polymerization coupling reactions can be directly monitored via GPC.

The second objective involved improving the chemical properties of reactive conjugated polymers, including increasing reaction rates and improving stability to acids/bases. The stability and robustness of reactive conjugated polymers is highly desirable property especially when considering one of the primary methods of characterization involves direct comparison of average molecular weight before and after clicking. For example, the earlier DIBO-containing polymers were all synthesized via imine bond formation. While this polymerization is easily reproducible, the resultant polyimine is highly acid-labile and requires careful attention to prevent undesirable hydrolysis during the resultant post-polymerization click reactions. Unlike the DIBO-containing polyimine, the *s*-tetrazine-containing polyfluorene has no labile linkages and is therefore resistant to moderately strong aqueous acidic or basic conditions. In addition to being able to safely store the reactive tetrazine polymer over periods of up to a year without the fear of hydrolysis, it can also be clicked without the need for air- or water-free conditions. The lack of hydrolysable linkages in the resultant "clicked" series also allows the chemist to characterize the polymers without risking their degradation in an NMR tube or GPC vial, which is a valuable attribute to have in a final product, especially when working with milligram quantities of material.

The final objective involved the discovery of new applications for reactive conjugated polymers (e.g., supramolecular chemistry, gel formation). Whenever a novel polymer is designed and synthesized, a considerable amount of foresight must be devoted to its potential applications. While the lion's share of my work went into the synthesis of these polymers and their derivatives, I explored secondary routes to probe which applications these reactive polymers would excel in. This exploration led to the synthesis of supramolecular polymer gels based on the non-covalent interaction of pillar[5]arenes with appropriate guest molecules, both of which were appended to polymeric backbones. These gels were found to be temperature and pH responsive, and could be reversibly hydrolyzed under acidic conditions, leading to a self-healing material.

Ultimately, this thesis should lay the foundation for using reactive conjugated polymers to synthesize libraries of homologous polymers for a variety of applications, including the supramolecular functionalization of single-walled carbon nanotubes.

1.9. References

(1) Rasmussen, S. C. Early History of Conductive Organic Polymers. *Conduct. Polym.* **2018**, 1–22.

(2) Lightfoot, J. *The Chemical History and Progress of Aniline Black*; 1871.

(3) Ateh, D. D.; Navsaria, H. A.; Vadgama, P. Polypyrrole-Based Conducting Polymers and Interactions with Biological Tissues. *J. R. Soc. Interface* **2006**, *3* (11), 741–752.

(4) Green, A. G.; Wolff, S. Anilinschwarz Und Seine Zwischenkörper. *Berichte der Dtsch. Chem. Gesellschaft* **1911**, *44* (3), 2570–2582.

(5) Green, A. G.; Woodhead, A. E. Anilinschwarz Und Seine Zwischenkörper. II. *Berichte der Dtsch. Chem. Gesellschaft* **1912**, *45* (2), 1955–1958.

(6) Rasmussen, S. C. Conjugated and Conducting Organic Polymers: The First 150 Years. *ChemPlusChem*. 2020, pp 1412–1429.

(7) Angeli, A. Pyrrole Black. *Ann. di Chim. Appl.* **1915**, *4*, 228.

(8) Angeli, A.; Pieroni, A. New Mode of Formation of Pyrrole-Black. *Atti Accad. Naz. Lincei* **1918**, *27* (2), 300–304.

(9) Bolto, B. A.; McNeill, R.; Weiss, D. E. Electronic Conduction in Polymers. Iii. Electronic Properties of Polypyrrole. *Aust. J. Chem.* **1963**, *16* (6), 1090–1103.

(10) Rasmussen, S. C. The Path to Conductive Polyacetylene. *Bull. Hist. Chem.* **2014**, *39* (1), 64–72.

(11) Shirakawa, H.; Louis, E. J.; MacDiarmid, A. G.; Chiang, C. K.; Heeger, A. J. Synthesis of Electrically Conducting Organic Polymers: Halogen Derivatives of Polyacetylene, (CH) X . *J. Chem. Soc. Chem. Commun.* **1977**, 578.

(12) Hatano, M. No Title. *Tanso* **1967**, *50*, 26–31.

(13) Ikeda, S. No Title. *H. Soc. Chem. Ind. Japan* **1967**, *70*, 1880–1886.

(14) Shiraka, H.; Ikeda, S. J. Infrared Spectra of Poly(Acetylene). *Polym. J.* **1971**, *2* (2), 231–244.

(15) Ito, T.; Shirakawa, H.; Ikeda, S. Simultaneous polymerization and formation of polyacetylene film on the surface of concentrated soluble ziegler-type catalyst solution. *J Polym Sci Part A-1 Polym Chem* **1974**, *12* (1), 11–20.

(16) Ito, T.; Shirakawa, H.; Ikeda, S. THERMAL CIS - TRANS ISOMERIZATION AND DECOMPOSITION OF POLYACETYLENE. *J Polym Sci Polym Chem Ed* **1975**, *13* (8), 1943–1950.

(17) Chiang, C. K.; Fincher, C. R.; Park, Y. W.; Heeger, A. J.; Shirakawa, H.; Louis, E. J.; Gau, S. C.; MacDiarmid, A. G. Electrical Conductivity in Doped Polyacetylene. *Phys. Rev. Lett.* **1977**, *39* (17), 1098–1101.

(18) Hideki Shirakawa, B.; Louis, E. J.; Macdiarmid, A. G.; W A N K Chiang, C. H.; HEEGERt, A. J. Synthesis of Electrically Conducting Organic Polymers : Halogen Derivatives of Polyacetylene, (CH). **1977**.

(19) MacDiarmid, A. G. “Synthetic Metals”: A Novel Role for Organic Polymers (Nobel Lecture) Copyright((c)) The Nobel Foundation 2001. We Thank the Nobel Foundation, Stockholm, for Permission to Print This Lecture. *Angew. Chem. Int. Ed. Engl.* **2001**, *40* (14), 2581–2590.

(20) Chiang, C. K.; Fincher, C. R.; Park, Y. W.; Heeger, A. J.; Shirakawa, H.; Louis, E. J.; Gau, S. C.; MacDiarmid, A. G. Electrical Conductivity in Doped Polyacetylene. *Phys. Rev. Lett.* **1977**, *39* (17), 1098–1101.

(21) Granier, T.; Thomas, E. L.; Gagnon, D. R.; Karasz, F. E.; Lenz, R. W. Structure Investigation of Poly(P-phenylene Vinylene). *J. Polym. Sci. Part B Polym. Phys.* **1986**, *24* (12), 2793–2804.

(22) Rault-Berthelot, J.; Simonet, J. The Anodic Oxidation of Fluorene and Some of Its Derivatives: Conditions for the Formation of a New Conducting Polymer. *J. Electroanal. Chem. Interfacial Electrochem.* **1985**, *182* (1), 187–192.

(23) Waltman, R. J.; Bargon, J. The Electropolymerization of Polycyclic Hydrocarbons: Substituent Effects and Reactivity/Structure Correlations. *J. Electroanal. Chem. Interfacial Electrochem.* **1985**, *194* (1), 49–62.

(24) Sato, M.; Tanaka, S.; Kaeriyama, K. Soluble Conducting Polythiophenes. *J. Chem. Soc. Chem. Commun.* **1986**, No. 11, 873–874.

(25) Leclerc, M.; Daoust, G. Design of New Conducting 3,4-Disubstituted

Polythiophenes. *J. Chem. Soc. Chem. Commun.* **1990**, No. 3, 273–274.

(26) Yamamoto, T.; Hayashida, N. π-Conjugated Polymers Bearing Electronic and Optical Functionalities. Preparation, Properties and Their Applications. *React. Funct. Polym.* **1998**, *37* (1–3), 1–17.

(27) Grazulevicius, J. V.; Strohriegl, P.; Pielichowski, J.; Pielichowski, K. Carbazole-Containing Polymers: Synthesis, Properties and Applications. *Prog. Polym. Sci.* **2003**, *28* (9), 1297–1353.

(28) Mei, J.; Bao, Z. Side Chain Engineering in Solution-Processable Conjugated Polymers. *Chemistry of Materials*. 2014, pp 604–615.

(29) Zhou, H.; Yang, L.; You, W. Rational Design of High Performance Conjugated Polymers for Organic Solar Cells. *Macromolecules*. American Chemical Society January 24, 2012, pp 607–632.

(30) Giovannitti, A.; Sbircea, D. T.; Inal, S.; Nielsen, C. B.; Bandiello, E.; Hanifi, D. A.; Sessolo, M.; Malliaras, G. G.; McCulloch, I.; Rivnay, J. Controlling the Mode of Operation of Organic Transistors through Side-Chain Engineering. *Proc. Natl. Acad. Sci. U. S. A.* **2016**, *113* (43), 12017–12022.

(31) Root, S. E.; Savagatrup, S.; Printz, A. D.; Rodriquez, D.; Lipomi, D. J. Mechanical Properties of Organic Semiconductors for Stretchable, Highly Flexible, and Mechanically Robust Electronics. *Chemical Reviews*. American Chemical Society May 10, 2017, pp 6467–6499.

(32) Guo, X.; Baumgarten, M.; Müllen, K. Designing π-Conjugated Polymers for Organic Electronics. *Progress in Polymer Science*. Pergamon December 1, 2013, pp 1832–1908.

(33) Rasmussen, S. C. Conjugated and Conducting Organic Polymers: The First 150 Years. *Chempluschem* **2020**, *85* (7), 1412–1429.

(34) Qiu, Z.; Hammer, B. A. G.; Müllen, K. Conjugated Polymers – Problems and Promises. *Progress in Polymer Science*. Elsevier Ltd January 1, 2020, p 101179.

(35) Mercier, L. G.; Leclerc, M. Direct (Hetero)Arylation: A New Tool for Polymer Chemists. *Acc. Chem. Res.* **2013**, *46* (7), 1597–1605.

(36) Morin, J.-F.; Leclerc, M.; Adès, D.; Siove, A. Polycarbazoles: 25 Years of Progress. *Macromol. Rapid Commun.* **2005**, *26*, 761–778.

(37) Leclerc, M.; Brassard, S.; Beaupré, S. Direct (Hetero)Arylation Polymerization:

Toward Defect-Free Conjugated Polymers. *Polym. J.* **2020**, *52* (1), 13–20.

(38) Benanti, T. L.; Kalaydjian, A.; Venkataraman, D. Protocols for Efficient Postpolymerization Functionalization of Regioregular Polythiophenes. *Macromolecules* **2008**, *41* (22), 8312–8315.

(39) Xu, J. M.; Ng, S. C.; Chan, H. S. O. A Series of Thienylene/Phenylene-Based Polymers Functionalized with Electron-Withdrawing or -Donating Groups: Synthesis and Characterization. *Macromolecules* **2001**.

(40) Yamamoto, T.; Morita, A.; Miyazaki, Y.; Maruyama, T. Preparation of π-Conjugated Poly (Thiophene-2, 5-Diyl), Poly (p-Phenylene), and Related Polymers Using Zerovalent Nickel Complexes. Linear Structure and Properties of …. *Macromolecules* **1992**, *25* (4), 1214–1223.

(41) Brédas, J. L.; Elsenbaumer, R. L.; Chance, R. R.; Silbey, R. Electronic Properties of Sulfur Containing Conjugated Polymers. *J. Chem. Phys.* **1983**, *78* (9), 5656–5662.

(42) Scherf, U.; Müllen, K. Oligo- and Poly(Phenylene)S. In *Semiconducting Polymers*; {Hutten, G. H., Van}, P. F., Eds.; 1999; pp 37–62.

(43) Grem, G.; Leditzky, G.; Ullrich, B.; Leising, G. Realization of a Blue-light-emitting Device Using Poly(P-phenylene). *Adv. Mater.* **1992**, *4* (1), 36–37.

(44) Melzer, C.; Koop, E. J.; Mihailetchi, V. D.; Blom, P. W. M. Hole Transport in Poly(Phenylene Vinylene)/Methanofullerene Bulk-Heterojunction Solar Cells. *Adv. Funct. Mater.* **2004**, *14* (9), 865–870.

(45) Leclerc, M. Polyfluorenes: Twenty Years of Progress. *J. Polym. Sci. Part A Polym. Chem.* **2001**, *39*, 2867–2873.

(46) Grazulevicius, J. V.; Strohriegl, P.; Pielichowski, J.; Pielichowski, K. Carbazole-Containing Polymers: Synthesis, Properties and Applications. *Progress in Polymer Science (Oxford)*. Pergamon September 1, 2003, pp 1297–1353.

(47) Li, J.; Grimsdale, A. C. Carbazole-Based Polymers for Organic Photovoltaic Devices. *Chem. Soc. Rev.* **2010**, *39* (7), 2399–2410.

(48) Zotti, G.; Schiavon, G.; Zecchin, S.; Morin, J. F.; Leclerc, M. Electrochemical, Conductive, and Magnetic Properties of 2,7-Carbazole-Based Conjugated Polymers. *Macromolecules* **2002**, *35* (6), 2122–2128.

(49) Swager, T. M. 50th Anniversary Perspective: Conducting/Semiconducting

Conjugated Polymers. A Personal Perspective on the Past and the Future. *Macromolecules*. American Chemical Society July 11, 2017, pp 4867–4886.

(50) Facchetti, A. Π-Conjugated Polymers for Organic Electronics and Photovoltaic Cell Applications†. *Chem. Mater.* **2010**, *23* (3), 733–758.

(51) Gross, M.; Müller, D. C.; Nothofer, H. G.; Scherf, U.; Neher, D.; Bräuchle, C.; Meerholz, K. Improving the Performance of Doped π-Conjugated Polymers for Use in Organic Light-Emitting Diodes. *Nature* **2000**, *405* (6787), 661–665.

(52) Inal, S.; Rivnay, J.; Suiu, A. O.; Malliaras, G. G.; McCulloch, I. Conjugated Polymers in Bioelectronics. *Acc. Chem. Res.* **2018**, *51* (6), 1368–1376.

(53) Babu, S. S.; Praveen, V. K.; Ajayaghosh, A. Functional π-Gelators and Their Applications. *Chem. Rev.* **2014**, *114* (4), 1973–2129.

(54) Murad, A. R.; Iraqi, A.; Aziz, S. B.; Abdullah, S. N.; Brza, M. A. Conducting Polymers for Optoelectronic Devices and Organic Solar Cells: A Review. *Polymers*. MDPI AG November 1, 2020, pp 1–47.

(55) Ates, M.; Karazehir, T.; Sarac, A. S. *Conducting Polymers and Their Applications*; 2012; Vol. 2.

(56) Grimsdale, A. C.; Leok Chan, K.; Martin, R. E.; Jokisz, P. G.; Holmes, A. B. Synthesis of Light-Emitting Conjugated Polymers for Applications in Electroluminescent Devices. *Chem. Rev.* **2009**, *109* (3), 897–1091.

(57) Tang, C. W.; VanSlyke, S. A. Organic Electroluminescent Diodes. *Appl. Phys. Lett.* **1998**, *51* (12), 913.

(58) Burroughes, J. H.; Bradley, D. D. C.; Brown, A. R.; Marks, R. N.; Mackay, K.; Friend, R. H.; Burns, P. L.; Holmes, A. B. Light-Emitting Diodes Based on Conjugated Polymers. *Nature* **1990**, *347* (6293), 539–541.

(59) Perepichka, I. F.; Perepichka, D. F.; Meng, H.; Wudl, F. Light-Emitting Polythiophenes. *Advanced Materials*. October 4, 2005, pp 2281–2305.

(60) Grice, A. W.; Bradley, D. D. C.; Bernius, M. T.; Inbasekaran, M.; Wu, W. W.; Woo, E. P. High Brightness and Efficiency Blue Light-Emitting Polymer Diodes. *Appl. Phys. Lett.* **1998**, *73* (5), 629–631.

(61) Kim, J.-S.; Ho, P. K. H.; Greenham, N. C.; Friend, R. H. Electroluminescence Emission Pattern of Organic Light-Emitting Diodes: Implications for Device Efficiency Calculations. *J. Appl. Phys.* **2000**, *88* (2), 1073.

(62) JR, M.; P, S. Materials Science. Electrochemical Capacitors for Energy Management. *Science* **2008**, *321* (5889), 651–652.

(63) Li, X.; Wei, B. Supercapacitors Based on Nanostructured Carbon. *Nano Energy*. Elsevier March 1, 2013, pp 159–173.

(64) Lewandowski, A.; Zajder, M.; Frackowiak, E.; Béguin, F. Supercapacitor Based on Activated Carbon and Polyethylene Oxide–KOH–H2O Polymer Electrolyte. *Electrochim. Acta* **2001**, *46* (18), 2777–2780.

(65) Fabio, A. Di; Giorgi, A.; Mastragostino, M.; Soavi, F. Carbon-Poly(3-Methylthiophene) Hybrid Supercapacitors. *J. Electrochem. Soc.* **2001**, *148* (8), A845.

(66) Zhou, Y. K.; He, B. L.; Zhou, W. J.; Huang, J.; Li, X. H.; Wu, B.; Li, H. L. Electrochemical Capacitance of Well-Coated Single-Walled Carbon Nanotube with Polyaniline Composites. *Electrochim. Acta* **2004**, *49* (2), 257–262.

(67) Kalakodimi Rajendra Prasad, †,‡; Kazumichi Koga, † and; Norio Miura*, †. Electrochemical Deposition of Nanostructured Indium Oxide: High-Performance Electrode Material for Redox Supercapacitors. *Chem. Mater.* **2004**, *16* (10), 1845–1847.

(68) Sharma, P.; Bhatti, T. S. A Review on Electrochemical Double-Layer Capacitors. *Energy Convers. Manag.* **2010**, *51* (12), 2901–2912.

(69) Conway, B. E. *Electrochemical Supercapacitors*; Springer US, 1999.

(70) Abdul, S.; Judit, T.; Ilona, F.; Nikoletta, M. Functional Thin Films and Nanostructures for Sensors. In *Fundamentals of Nanoparticles: Classifications, Synthesis Methods, Properties and Characterization*; Elsevier, 2018; pp 485–519.

(71) Bai, H.; Shi, G. Gas Sensors Based on Conducting Polymers. *Sensors* **2007**, *7* (3), 267–307.

(72) Iijima, S. Growth of Carbon Nanotubes. *Mater. Sci. Eng. B* **1993**, *19* (1–2), 172–180.

(73) Bethune, D. S.; Klang, C. H.; De Vries, M. S.; Gorman, G.; Savoy, R.; Vazquez, J.; Beyers, R. Cobalt-Catalysed Growth of Carbon Nanotubes with Single-Atomic-Layer Walls. *Nature* **1993**, *363* (6430), 605–607.

(74) Avouris, P. Molecular Electronics with Carbon Nanotubes. *Acc. Chem. Res.* **2002**, *35* (12), 1026–1034.

(75) Avouris, P.; Chen, Z.; Perebeinos, V. Carbon-Based Electronics. *Nature Nanotechnology*. Nature Publishing Group September 30, 2007, pp 605–615.

(76) Han, Z.; Fina, A. Thermal Conductivity of Carbon Nanotubes and Their Polymer Nanocomposites: A Review. *Progress in Polymer Science (Oxford)*. Pergamon July 1, 2011, pp 914–944.

(77) Yu, M. F.; Files, B. S.; Arepalli, S.; Ruoff, R. S. Tensile Loading of Ropes of Single Wall Carbon Nanotubes and Their Mechanical Properties. *Phys. Rev. Lett.* **2000**, *84* (24), 5552–5555.

(78) Terrones, M. Science and Technology of the Twenty-First Century: Synthesis, Properties, and Applications of Carbon Nanotubes. *Annual Review of Materials Research*. Annual Reviews 4139 El Camino Way, P.O. Box 10139, Palo Alto, CA 94303-0139, USA November 28, 2003, pp 419–501.

(79) Kataura, H.; Kumazawa, Y.; Maniwa, Y.; Umezu, I.; Suzuki, S.; Ohtsuka, Y.; Achiba, Y. Optical Properties of Single-Wall Carbon Nanotubes. *Synth. Met.* **1999**, *103* (1–3), 2555–2558.

(80) Weisman, R. B.; Bachilo, S. M. Dependence of Optical Transition Energies on Structure for Single-Walled Carbon Nanotubes in Aqueous Suspension: An Empirical Kataura Plot. *Nano Lett.* **2003**, *3* (9), 1235–1238.

(81) O'Connell, M. J.; Bachilo, S. H.; Huffman, C. B.; Moore, V. C.; Strano, M. S.; Haroz, E. H.; Rialon, K. L.; Boul, P. J.; Noon, W. H.; Kittrell, C.; Ma, J.; Hauge, R. H.; Weisman, R. B.; Smalley, R. E. Band Gap Fluorescence from Individual Single-Walled Carbon Nanotubes. *Science (80-.).* **2002**, *297* (5581), 593–596.

(82) Qi, P.; Vermesh, O.; Grecu, M.; Javey, A.; Wang, Q.; Dai, H.; Peng, S.; Cho, K. J. Toward Large Arrays of Multiplex Functionalized Carbon Nanotube Sensors for Highly Sensitive and Selective Molecular Detection. *Nano Lett.* **2003**, *3* (3), 347–351.

(83) Dionisio, M.; Schnorr, J. M.; Michaelis, V. K.; Griffin, R. G.; Swager, T. M.; Dalcanale, E. Cavitand-Functionalized SWCNTs for N-Methylammonium Detection. *J. Am. Chem. Soc.* **2012**, *134* (15), 6540–6543.

(84) Nigović, B.; Sadiković, M.; Sertić, M. Multi-Walled Carbon Nanotubes/Nafion Composite Film Modified Electrode as a Sensor for Simultaneous Determination of Ondansetron and Morphine. *Talanta* **2014**, *122*, 187–194.

(85) Dürkop, T.; Getty, S. A.; Cobas, E.; Fuhrer, M. S. Extraordinary Mobility in

Semiconducting Carbon Nanotubes. *Nano Lett.* **2004**, *4* (1), 35–39.

(86) Green, A. A.; Hersam, M. C. Colored Semitransparent Conductive Coatings Consisting of Monodisperse Metallic Single-Walled Carbon Nanotubes. *Nano Lett.* **2008**, *8* (5), 1417–1422.

(87) Sun, D. M.; Liu, C.; Ren, W. C.; Cheng, H. M. A Review of Carbon Nanotube- and Graphene-Based Flexible Thin-Film Transistors. *Small*. John Wiley & Sons, Ltd April 22, 2013, pp 1188–1205.

(88) Rowell, M. W.; Topinka, M. A.; McGehee, M. D.; Prall, H. J.; Dennler, G.; Sariciftci, N. S.; Hu, L.; Gruner, G. Organic Solar Cells with Carbon Nanotube Network Electrodes. *Appl. Phys. Lett.* **2006**, *88* (23), 233506.

(89) Bindl, D. J.; Safron, N. S.; Arnold, M. S. Dissociating Excitons Photogenerated in Semiconducting Carbon Nanotubes at Polymeric Photovoltaic Heterojunction Interfaces. *ACS Nano* **2010**, *4* (10), 5657–5664.

(90) Keru, G.; Ndungu, P. G.; Nyamori, V. O. A Review on Carbon Nanotube/Polymer Composites for Organic Solar Cells. *International Journal of Energy Research*. John Wiley & Sons, Ltd October 25, 2014, pp 1635–1653.

(91) Hecht, D. S.; Thomas, D.; Hu, L.; Ladous, C.; Lam, T.; Park, Y.; Irvin, G.; Drzaic, P. Carbon-Nanotube Film on Plastic as Transparent Electrode for Resistive Touch Screens. *J. Soc. Inf. Disp.* **2009**, *17* (11), 941.

(92) Zhan, G. D.; Kuntz, J. D.; Wan, J.; Mukherjee, A. K. Single-Wall Carbon Nanotubes as Attractive Toughening Agents in Alumina-Based Nanocomposites. *Nat. Mater.* **2003**, *2* (1), 38–42.

(93) Liu, L.; Barber, A. H.; Nuriel, S.; Wagner, H. D. Mechanical Properties of Functionalized Single-Walled Carbon-Nanotube/ Poly(Vinyl Alcohol) Nanocomposites. *Adv. Funct. Mater.* **2005**, *15* (6), 975–980.

(94) Coleman, J. N.; Khan, U.; Blau, W. J.; Gun’ko, Y. K. Small but Strong: A Review of the Mechanical Properties of Carbon Nanotube-Polymer Composites. *Carbon*. Pergamon August 1, 2006, pp 1624–1652.

(95) Jariwala, D.; Sangwan, V. K.; Lauhon, L. J.; Marks, T. J.; Hersam, M. C. Carbon Nanomaterials for Electronics, Optoelectronics, Photovoltaics, and Sensing. *Chem. Soc. Rev.* **2013**, *42* (7), 2824–2860.

(96) Hong, S.; Myung, S. Nanotube Electronics: A Flexible Approach to Mobility. *Nature Nanotechnology*. Nature Publishing Group 2007, pp 207–208.

(97) De Volder, M. F. L.; Tawfick, S. H.; Baughman, R. H.; Hart, A. J. Carbon Nanotubes: Present and Future Commercial Applications. *Science*. American Association for the Advancement of Science February 1, 2013, pp 535–539.

(98) Kong, J.; Cassell, A. M.; Dai, H. Chemical Vapor Deposition of Methane for Single-Walled Carbon Nanotubes. *Chem. Phys. Lett.* **1998**, *292* (4–6), 567–574.

(99) Guo, T.; Nikolaev, P.; Thess, A.; Colbert, D. T.; Smalley, R. E. Catalytic Growth of Single-Walled Manotubes by Laser Vaporization. *Chem. Phys. Lett.* **1995**, *243* (1–2), 49–54.

(100) Journet, C.; Maser, W. K.; Bernier, P.; Loiseau, A.; Lamy de la Chapelle, M.; Lefrant, S.; Deniard, P.; Lee, R.; Fischer, J. E. Large-Scale Production of Single-Walled Carbon Nanotubes by the Electric-Arc Technique. *Nature* **1997**, *388* (6644), 756–758.

(101) Kim, K. S.; Cota-Sanchez, G.; Kingston, C. T.; Imris, M.; Simard, B.; Soucy, G. Large-Scale Production of Single-Walled Carbon Nanotubes by Induction Thermal Plasma. *J. Phys. D. Appl. Phys.* **2007**, *40* (8), 2375–2387.

(102) Nikolaev, P.; Bronikowski, M. J.; Bradley, R. K.; Rohmund, F.; Colbert, D. T.; Smith, K. A.; Smalley, R. E. Gas-Phase Catalytic Growth of Single-Walled Carbon Nanotubes from Carbon Monoxide. *Chem. Phys. Lett.* **1999**, *313* (1–2), 91–97.

(103) Arnold, M. S.; Stupp, S. I.; Hersam, M. C. Enrichment of Single-Walled Carbon Nanotubes by Diameter in Density Gradients. *Nano Lett.* **2005**, *5* (4), 713–718.

(104) Tanaka, T.; Jin, H.; Miyata, Y.; Kataura, H. High-Yield Separation of Metallic and Semiconducting Single-Wall Carbon Nanotubes by Agarose Gel Electrophoresis. *Appl. Phys. Express* **2008**, *1* (11), 1140011–1140013.

(105) Liu, H.; Nishide, D.; Tanaka, T.; Kataura, H. Large-Scale Single-Chirality Separation of Single-Wall Carbon Nanotubes by Simple Gel Chromatography. *Nat. Commun.* **2011**, *2* (1), 1–8.

(106) Fagan, J. A.; Khripin, C. Y.; Silvera Batista, C. A.; Simpson, J. R.; Hároz, E. H.; Hight Walker, A. R.; Zheng, M. Isolation of Specific Small-Diameter Single-Wall Carbon Nanotube Species via Aqueous Two-Phase Extraction. *Adv. Mater.* **2014**, *26* (18), 2800–2804.

(107) Khripin, C. Y.; Fagan, J. A.; Zheng, M. Spontaneous Partition of Carbon Nanotubes in Polymer-Modified Aqueous Phases. *J. Am. Chem. Soc.* **2013**, *135* (18), 6822–6825.

(108) Zheng, M.; Jagota, A.; Semke, E. D.; Diner, B. A.; McLean, R. S.; Lustig, S. R.; Richardson, R. E.; Tassi, N. G. DNA-Assisted Dispersion and Separation of Carbon Nanotubes. *Nat. Mater.* **2003**, *2* (5), 338–342.

(109) Tu, X.; Manohar, S.; Jagota, A.; Zheng, M. DNA Sequence Motifs for Structure-Specific Recognition and Separation of Carbon Nanotubes. *Nature* **2009**, *460* (7252), 250–253.

(110) Zheng, M.; Semke, E. D. Enrichment of Single Chirality Carbon Nanotubes. *J. Am. Chem. Soc.* **2007**, *129* (19), 6084–6085.

(111) Flavel, B. S.; Kappes, M. M.; Krupke, R.; Hennrich, F. Separation of Single-Walled Carbon Nanotubes by 1-Dodecanol-Mediated Size-Exclusion Chromatography. *ACS Nano* **2013**, *7* (4), 3557–3564.

(112) Flavel, B. S.; Moore, K. E.; Pfohl, M.; Kappes, M. M.; Hennrich, F. Separation of Single-Walled Carbon Nanotubes with a Gel Permeation Chromatography System. *ACS Nano* **2014**, *8* (2), 1817–1826.

(113) Chen, R. J.; Zhang, Y.; Wang, D.; Dai, H. Noncovalent Sidewall Functionalization of Single-Walled Carbon Nanotubes for Protein Immobilization [11]. *Journal of the American Chemical Society*. American Chemical Society 2001, pp 3838–3839.

(114) Steuerman, D. W.; Star, A.; Narizzano, R.; Choi, H.; Ries, R. S.; Nicolini, C.; Stoddart, J. F.; Heath, J. R. Interactions between Conjugated Polymers and Single-Walled Carbon Nanotubes. *J. Phys. Chem. B* **2002**, *106* (12), 3124–3130.

(115) Samanta, S. K.; Fritsch, M.; Scherf, U.; Gomulya, W.; Bisri, S. Z.; Loi, M. A. Conjugated Polymer-Assisted Dispersion of Single-Wall Carbon Nanotubes: The Power of Polymer Wrapping. *Acc. Chem. Res.* **2014**, *47* (8), 2446–2456.

(116) Wang, H.; Bao, Z. Conjugated Polymer Sorting of Semiconducting Carbon Nanotubes and Their Electronic Applications. *Nano Today*. Elsevier December 1, 2015, pp 737–758.

(117) Lei, T.; Pochorovski, I.; Bao, Z. Separation of Semiconducting Carbon Nanotubes for Flexible and Stretchable Electronics Using Polymer Removable Method. *Acc. Chem. Res.* **2017**, *50* (4), 1096–1104.

(118) Nish, A.; Hwang, J.-Y.; Doig, J.; Nicholas, R. J. Highly Selective Dispersion of Single-Walled Carbon Nanotubes Using Aromatic Polymers. *Nat. Nanotechnol.* **2007**, *2* (10), 640–646.

(119) Brady, G. J.; Joo, Y.; Wu, M. Y.; Shea, M. J.; Gopalan, P.; Arnold, M. S.

Polyfluorene-Sorted, Carbon Nanotube Array Field-Effect Transistors with Increased Current Density and High on/off Ratio. *ACS Nano* **2014**, *8* (11), 11614–11621.

(120) Toshimitsu, F.; Nakashima, N. Semiconducting Single-Walled Carbon Nanotubes Sorting with a Removable Solubilizer Based on Dynamic Supramolecular Coordination Chemistry. *Nat. Commun.* **2014**, *5* (1), 1–9.

(121) Pochorovski, I.; Wang, H.; Feldblyum, J. I.; Zhang, X.; Antaris, A. L.; Bao, Z. H-Bonded Supramolecular Polymer for the Selective Dispersion and Subsequent Release of Large-Diameter Semiconducting Single-Walled Carbon Nanotubes. *J. Am. Chem. Soc.* **2015**, *137* (13), 4328–4331.

(122) Lei, T.; Chen, X.; Pitner, G.; Wong, H.-S. S. P.; Bao, Z. Removable and Recyclable Conjugated Polymers for Highly Selective and High-Yield Dispersion and Release of Low-Cost Carbon Nanotubes. *J. Am. Chem. Soc.* **2016**, *138* (3), 802–805.

(123) McCullough, R. D.; Ewbank, P. C.; Loewe, R. S. Self-Assembly and Disassembly of Regioregular, Water Soluble Polythiophenes: Chemoselective Ionchromatic Sensing in Water. *J. Am. Chem. Soc.* **1997**, *119* (3), 633–634.

(124) Arslan, H.; Saathoff, J. D.; Bunck, D. N.; Clancy, P.; Dichtel, W. R. Highly Efficient Benzannulation of Poly(Phenylene Ethynylene)S. *Angew. Chemie - Int. Ed.* **2012**, *51* (48), 12051–12054.

(125) Creamer, A.; Wood, C. S.; Howes, P. D.; Casey, A.; Cong, S.; Marsh, A. V.; Godin, R.; Panidi, J.; Anthopoulos, T. D.; Burgess, C. H.; Wu, T.; Fei, Z.; Hamilton, I.; McLachlan, M. A.; Stevens, M. M.; Heeney, M. Post-Polymerisation Functionalisation of Conjugated Polymer Backbones and Its Application in Multi-Functional Emissive Nanoparticles. *Nat. Commun.* **2018**, *9* (1).

(126) Li, J.; Kong, H.; Huang, L.; Cheng, B.; Qin, K.; Zheng, M.; Yan, Z.; Zhang, Y. Visible Light-Initiated Bioorthogonal Photoclick Cycloaddition. *J. Am. Chem. Soc.* **2018**, *140* (44), 14542–14546.

(127) Kolb, H. C.; Finn, M. G.; Sharpless, K. B. Click Chemistry: Diverse Chemical Function from a Few Good Reactions. *Angewandte Chemie - International Edition*. 2001, pp 2004–2021.

(128) Caron, M.; Sharpless, K. B. Ti(O-i-Pr)4-Mediated Nucleophilic Openings of 2,3-Epoxy Alcohols. A Mild Procedure for Regioselective Ring-Opening. *J. Org. Chem.* **1985**, *50* (9), 1557–1560.

(129) Huisgen, R. 1,3-Dipolar Cycloadditions. Past and Future. *Angew. Chemie Int. Ed. English* **1963**, *2* (10), 565–598.

(130) Wuts, P. G. M.; Greene, T. W. Protection for the Carbonyl Group. In *Greene's Protective Groups in Organic Synthesis*; Wiley-Interscience, 2006; pp 431–532.

(131) Dirks, A. J.; Van Berkel, S. S.; Hatzakis, N. S.; Opsteen, J. A.; Van Delft, F. L.; Cornelissen, J. J. L. M.; Rowan, A. E.; Van Hest, J. C. M.; Rutjes, F. P. J. T.; Nolte, R. J. M. Preparation of Biohybrid Amphiphiles via the Copper Catalysed Huisgen [3 + 2] Dipolar Cycloaddition Reaction. *Chem. Commun.* **2005**, No. 33, 4172–4174.

(132) Frechet, J. M. J. Supramolecular Chemistry And Self-Assembly Special Feature: Dendrimers and Supramolecular Chemistry. *Proc. Natl. Acad. Sci.* **2002**, *99* (8), 4782–4787.

(133) Hawker, C. J.; Fréchet, J. M. J. Preparation of Polymers with Controlled Molecular Architecture. A New Convergent Approach to Dendritic Macromolecules. *J. Am. Chem. Soc.* **1990**, *112* (21), 7638–7647.

(134) Yigit, S.; Sanyal, R.; Sanyal, A. Fabrication and Functionalization of Hydrogels through "Click" Chemistry. *Chemistry - An Asian Journal*. John Wiley & Sons, Ltd October 2011, pp 2648–2659.

(135) Johnson, J. A.; Finn, M. G.; Koberstein, J. T.; Turro, N. J. Construction of Linear Polymers, Dendrimers, Networks, and Other Polymeric Architectures by Copper-Catalyzed Azide-Alkyne Cycloaddition "Click" Chemistry. *Macromol. Rapid Commun.* **2008**, *29* (12–13), 1052–1072.

(136) Hoyle, C. E.; Bowman, C. N. Thiol-Ene Click Chemistry. *Angew. Chemie Int. Ed.* **2010**, *49* (9), 1540–1573.

(137) McNelles, S. A.; Pantaleo, J. L.; Meichsner, E.; Adronov, A. Strain-Promoted Azide-Alkyne Cycloaddition-Mediated Step-Growth Polymerization. *Macromolecules* **2019**, *52* (19), 7183–7187.

(138) Dommerholt, J.; Rutjes, F. P. J. T.; van Delft, F. L. Strain-Promoted 1,3-Dipolar Cycloaddition of Cycloalkynes and Organic Azides. *Topics in Current Chemistry*. 2016.

(139) Turner, R. B.; Jarrett, A. D.; Goebel, P.; Mallon, B. J. Heats of Hydrogenation. IX. Cyclic Acetylenes and Some Miscellaneous Olefins. *J. Am. Chem. Soc.* **1973**, *95* (3), 790–792.

(140) Sletten, E. M.; Bertozzi, C. R. From Mechanism to Mouse: A Tale of Two Bioorthogonal Reactions. *Acc. Chem. Res.* **2011**, *44* (9), 666–676.

(141) Laughlin, S. T.; Bertozzi, C. R. In Vivo Imaging of Caenorhabditis Elegans Glycans. *ACS Chem. Biol.* **2009**, *4* (12), 1068–1072.

(142) Kim, H. L.; Sachin, K.; Jeong, H. J.; Choi, W.; Lee, H. S.; Kim, D. W. F-18 Labeled RGD Probes Based on Bioorthogonal Strain-Promoted Click Reaction for PET Imaging. *ACS Med. Chem. Lett.* **2015**, *6* (4), 402–407.

(143) Jeong, H. J.; Yoo, R. J.; Kim, J. K.; Kim, M. H.; Park, S. H.; Kim, H.; Lim, J. W.; Do, S. H.; Lee, K. C.; Lee, Y. J.; Kim, D. W. Macrophage Cell Tracking PET Imaging Using Mesoporous Silica Nanoparticles via in Vivo Bioorthogonal F-18 Labeling. *Biomaterials* **2019**, *199*, 32–39.

(144) Terzic, V.; Pousse, G.; Méallet-Renault, R.; Grellier, P.; Dubois, J. Dibenzocyclooctynes: Effect of Aryl Substitution on Their Reactivity toward Strain-Promoted Alkyne-Azide Cycloaddition. *J. Org. Chem.* **2019**, *84* (13), 8542–8551.

(145) Oliveira, B. L.; Guo, Z.; Bernardes, G. J. L. Inverse Electron Demand Diels-Alder Reactions in Chemical Biology. *Chemical Society Reviews*. 2017, pp 4895–4950.

(146) Balcar, J.; Chrisam, G.; Huber, F. X.; Sauer, J. Reaktivität von Stickstoff-Heterocyclen Genenüber Cyclooctin Als Dienophil. *Tetrahedron Lett.* **1983**, *24* (14), 1481–1484.

(147) Thalhammer, F.; Wallfahrer, U.; Sauer, J. Reaktivität Einfacher Offenkettiger Und Cyclischer Dienophile Bei Diels-Alder-Reaktionen Mit Inversem Elektronenbedarf. *Tetrahedron Lett.* **1990**, *31* (47), 6851–6854.

(148) Darko, A.; Wallace, S.; Dmitrenko, O.; Machovina, M. M.; Mehl, R. A.; Chin, J. W.; Fox, J. M. Conformationally Strained Trans-Cyclooctene with Improved Stability and Excellent Reactivity in Tetrazine Ligation. *Chem. Sci.* **2014**, *5* (10), 3770.

(149) Presolski, S. I.; Hong, V.; Cho, S. H.; Finn, M. G. Tailored Ligand Acceleration of the Cu-Catalyzed Azide-Alkyne Cycloaddition Reaction: Practical and Mechanistic Implications. *J. Am. Chem. Soc.* **2010**, *132* (41), 14570–14576.

(150) Oliveira, B. L.; Guo, Z.; Bernardes, G. J. L. Inverse Electron Demand Diels-Alder Reactions in Chemical Biology. *Chemical Society Reviews*. The Royal Society of Chemistry August 14, 2017, pp 4895–4950.

(151) Knall, A. C.; Slugovc, C. Inverse Electron Demand Diels-Alder (IEDDA)-Initiated Conjugation: A (High) Potential Click Chemistry Scheme. *Chem. Soc. Rev.* **2013**, *42* (12), 5131–5142.

Chapter 2

“Click” Functionalization of a Dibenzocyclooctyne-containing Conjugated Polyimine

This chapter has been reprinted with permission from Angewandte Chemie International Edition; Vladimir Kardelis, Ryan C. Chadwick, and Alex Adronov, **2016**, *55*, 945-949, DOI: 10.1002/anie.201508639. Copyright (2016) Wiley-VCH.

Contributions:

Vladimir Kardelis is the first author on this publication and was the primary planner of this study. Vladimir Kardelis was responsible for the synthesis and optimization of all monomer precursor compounds, the cyclooctyne-containing polymer, and all small-molecule azides. Vladimir Kardelis was also responsible for acquiring all AFM images. Ryan C. Chadwick was responsible with assisting the monomer scale-up in addition to the synthesis of the polymeric azides. Vladimir Kardelis and Ryan C. Chadwick carried out the click reactions on the cyclooctyne-containing polymer and the characterization of the compounds thereafter. Additionally, both Vladimir Kardelis and Ryan C. Chadwick carried out computational calculations on the monomer/polymer structures.

Abstract

A conjugated polyphenyl-co-dibenzocyclooctyne Schiff-base polymer, prepared via polycondensation of dibenzocyclooctyne bisamine (DIBO-$(NH_2)_2$) with bis(hexadecyloxy)phenyldialdehyde, is reported. The resulting polymer, having a high molecular weight (M_n > 30 kDa, M_w > 60 kDa), undergoes efficient strain-promoted alkyne-azide cycloaddition reactions with a series of azides. This enables quantitative modification of each repeat unit within the polymer backbone and the rapid synthesis of a conjugated polymer library having widely different substituents, but a consistent degree of polymerization (DP). Kinetic studies show a second order reaction rate constant that is consistent with monomeric dibenzocyclooctynes. Grafting with azide-terminated polystyrene and polyethylene glycol monomethyl ether chains of varying molecular weight resulted in the efficient syntheses of a series of graft copolymers with a conjugated backbone and maximal graft density.

2.1. Introduction

Conjugated polymers have attracted tremendous attention in both academia and industry as a consequence of their unique properties.[1–3] A wide range of conjugated macromolecules have been investigated, including derivatives of polyacetylene,[4,5] polyphenylene,[6] polyarylenevinylene,[7,8] polypyrrole,[9] polythiophene,[10] and polyfluorene backbones,[11,12] as well as numerous more complex structures.[13] This structural variability, combined with post-polymerization modification (i.e., doping), allows manipulation of opto-electronic and physical properties, including absorption/emission wavelengths, band gap, HOMO/LUMO levels, conjugation length, and solubility.[14–18] These parameters have made numerous commercial applications possible, including light-emitting diodes (LEDs),[19–23] field effect transistors (FETs),[24] organic solar cells,[25] and chemical sensors.[26] Conjugated polymers have also been investigated as components in printed electronics.[1] A more recent and rapidly growing area of application involves the selective dispersion of single-walled carbon nanotubes.[27–30] In all of these cases, investigation of structure-activity relationships, where the backbone or side-chain structure of conjugated polymers is varied, requires de novo synthesis of each conjugated polymer. In addition, differences in monomer ratios within iterative syntheses can result in a range of molecular weights, polydispersities, and regiochemistries; all factors that have an effect on polymer properties.[31] In light of these limitations, a method for generation of libraries of conjugated polymers with different backbone structures, but identical degree of polymerization and polydispersity, is desired. Such a method would require modification of the backbone structure post-polymerization in order to maintain constant polymer length. This is challenging, as the post-polymerization modification of conjugated polymer backbones is uncommon, and often suffers from incomplete functionalization.[32] Benzannulations have recently been demonstrated as an efficient method of post-polymerization modification, but generally result in a very specific polymer structure.[33]

We have previously investigated the use of a dibromo derivative of dibenzoazacyclooctyne (DIBAC) for post-polymerization functionalization via strain-promoted azide-alkyne cycloaddition (SPAAC).[34] The strained cyclooctyne within the dibromo-DIBAC structure permitted rapid transformation of the alkynes into conjugated triazoles, thereby altering their electronic and physical properties. Unfortunately, we were unable to introduce the cyclooctyne moiety into the backbone of a polymer, as the metal catalysts used in most cross-coupling polymerizations (Ni, Pd, Cu) rapidly underwent cycloaddition reactions with the strained alkyne of the monomer, rather than the desired oxidative addition at the carbon-halogen bond.[35–37] This led us to explore polymerization methods that do not involve the use of transition metal catalysts, including reactions such as the Wittig, Horner-Wadsworth-Emmons,[38–40] Aza-Wittig,[41,42] and Knoevenagel condensation,[43] as well as Schiff-base formation.[44,45] Many of these methods have been demonstrated to yield high molecular weight polymers, and a wide variety of structural diversity has been explored. Amongst these, Schiff-base formation offers several advantages, as it has been well-explored,[46–48] can produce high molecular weight polymers, and the installation of amine groups is straightforward using Buchwald-Hartwig chemistry.[49]

2.2. Results and Discussion

2.2.1. Preparation of Monomers

The structurally simplest parent structure, dibenzocyclooctyne (DIBO)[50] is ideal as a monomer for conjugated polymer synthesis, as it has a relatively planar, symmetrical structure.[50–54] In our hands, the synthetic approach based on a Wittig-Prévost homologation sequence was found compatible with initial introduction of aryl halides (in this case, iodides), which could subsequently be converted to the required amines in the target monomer **6** (DIBO-$(NH_2)_2$). As illustrated in Scheme 1, starting with dibenzosuberone, standard iodination conditions generated diiodosuberone **1** in modest yield.[55] No ortho/para selectivity of halogenation was observed, and the diortho-, dipara-, and ortho/para derivatives were each isolated in approximately equal amounts. Ring expansion of **1** using the Wittig-Prévost homologation was carried out in good yield to generate the 8-membered cyclooctanone **3**.[56] Subsequently, standard Buchwald-Hartwig amination conditions using benzophenone imine generated the diimine-protected ketone **4** (Scheme 2.1).[49] *In situ* generation of the enol triflate followed by elimination using KHMDS formed the cyclooctyne **5**,[54,57] and finally deprotection under aqueous acidic conditions allowed isolation of monomer **6**. The co-monomer, an alkoxybenzene dialdehyde (**9**), was synthesized from bis(hexadecyloxy)diiodobenzene via a modified Bouveault aldehyde synthesis (Scheme 2.1b).[58,59]

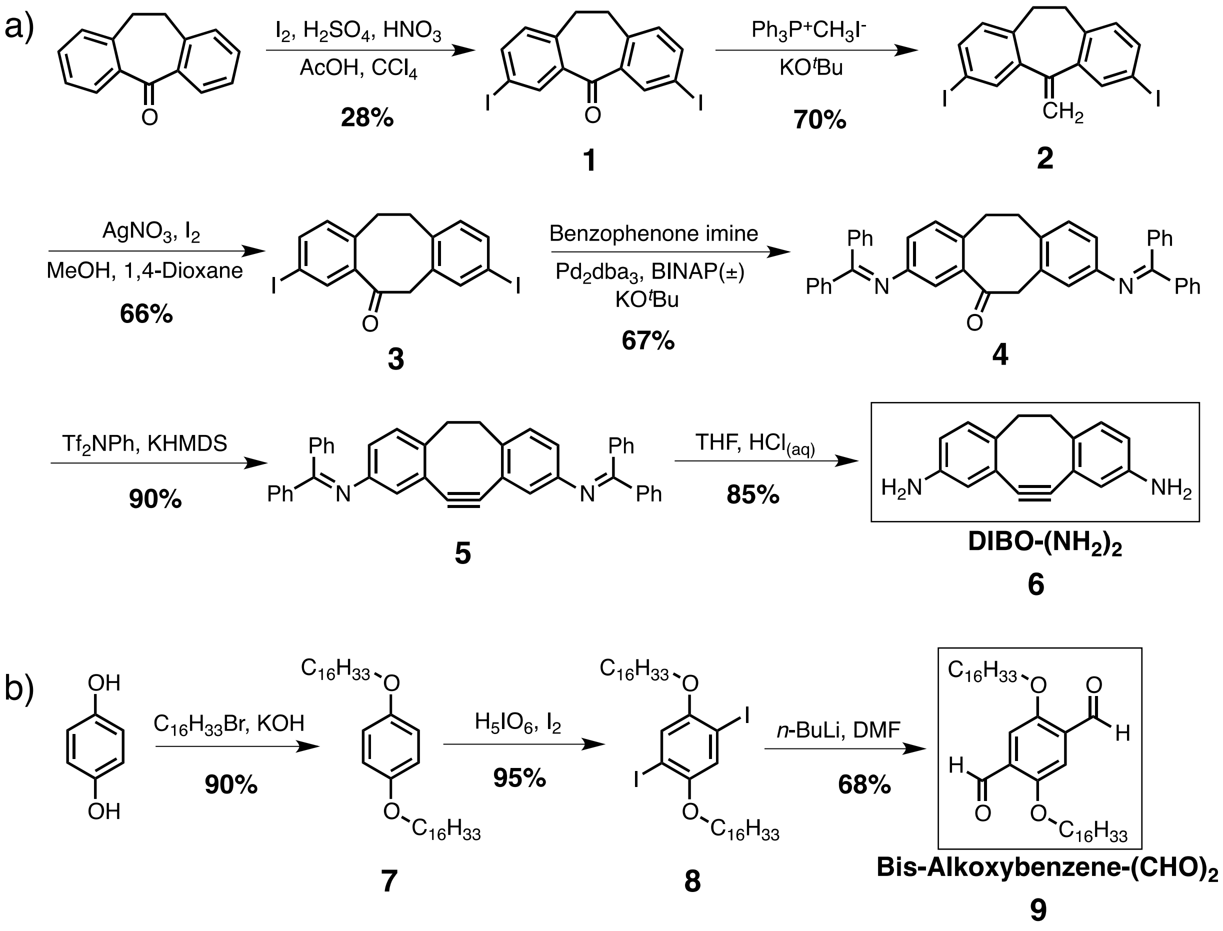

Scheme 2.1. Synthesis of (a) the DIBO-$(NH_2)_2$ monomer (**6**), and (b) the bis(alkoxy)phenyl dialdehyde comonomer (**9**).

2.2.2. Preparation of Dibenzocyclooctyne-Containing Polymer (P0)

Polymerization was performed by heating monomers **6** and **9** in toluene using p-toluenesulfonic acid (PTSA) as a catalyst (Scheme 2.2). This polymerization proceeds rapidly until all of the amines either react or become protonated by the acid catalyst. After this point, the polymerization continues at a much slower rate, as the remaining ammonium ions must undergo deprotonation in order to react. Thus, a degree of molecular weight control can be achieved by varying catalyst amount and stopping the polymerization before oligomer coupling becomes significant. Addition of 2 mol % PTSA resulted in uniform polymerization, producing polymer with molecular weight on the order of 30 kDa within 3-4 hours (**P0**, Table 1). The product polymer **P0** was characterized by ^{1}H- and ^{13}C-NMR, Raman, UV-Vis and fluorescence spectroscopy, as well as gel permeation chromatography (GPC). The presence of alkyne moieties in **P0** was confirmed through observation of the alkyne stretch at 2160 cm^{-1} by Raman spectroscopy, and the position of the bridgehead signals by ^{1}H-NMR (Figure 2.2a and b, respectively). Addition of larger quantities of PTSA resulted in higher polymerization rates, but initial formation of lower molecular weight oligomers. Over the course of several days, these oligomers undergo coupling reactions, resulting in a polymer fraction having much higher molecular weight (>100 kDa). However, a bimodal distribution containing a significant amount of the initially formed oligomers could not be avoided. Thus, best results were achieved when low catalyst loadings were used.

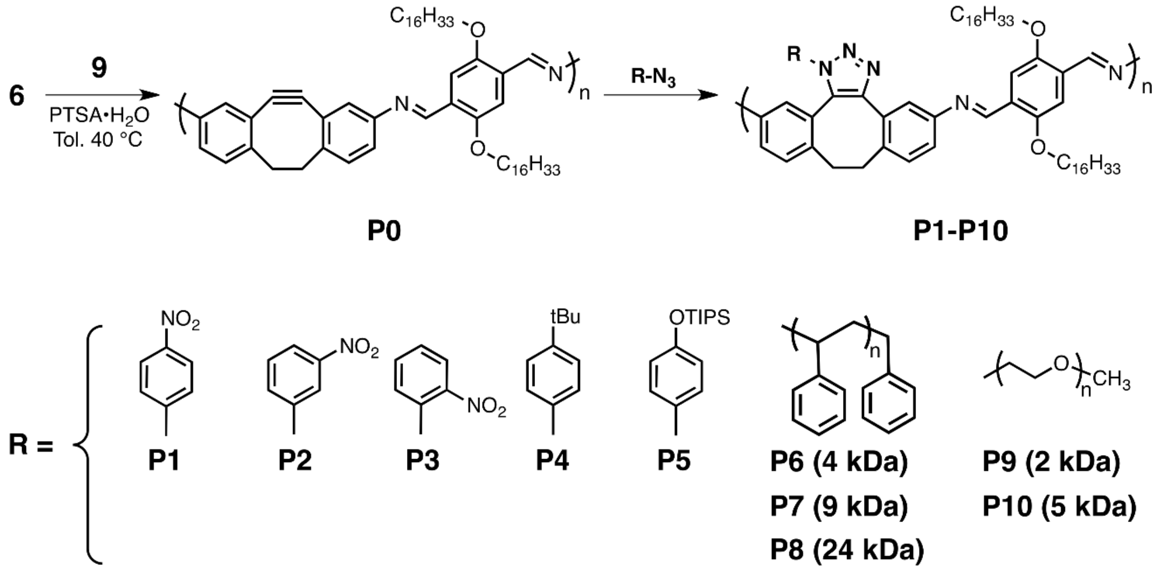

Scheme 2.2. Synthesis of cyclooctyne-containing polymer **P0** and its cycloadducts **P1-P5**.

Table 2.1. Physical and electronic properties of polyimine polymer **P0** and its “clicked” derivatives.

Polymer	**$\lambda_{max,ab}$ (nm)**	**$\lambda_{max,em}$ (nm)**	**M_n (kg/mol)**	**M_w (kg/mol)**	**PDI**
P0	313, 412	545 (weak)	30.8	62.6	2.03
P1	300, 409	-	20.6	44.1	2.15
P2	297, 409	-	19.1	41.3	2.16
P3	298, 409	-	18.9	42.5	2.25
P4	295, 409	-	15.0	38.3	2.55
P5	288, 409	-	24.0	49.5	2.06

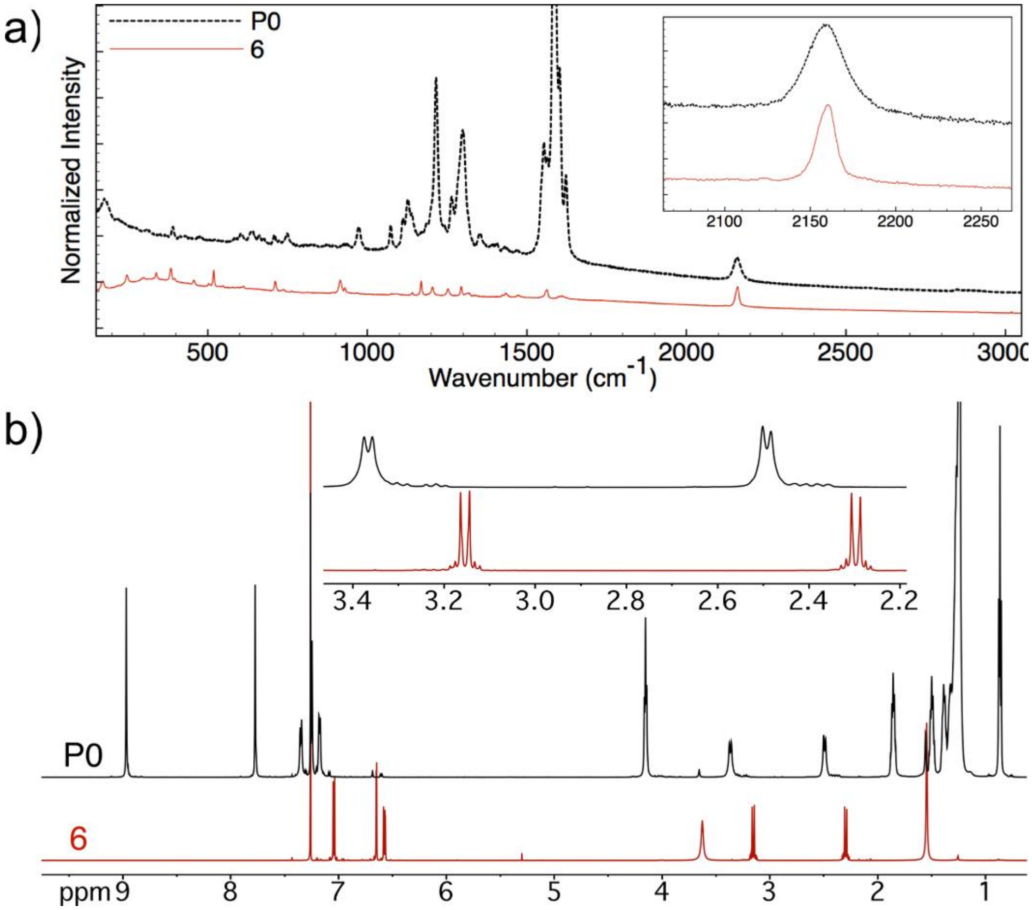

Figure 2.1. a) Raman spectrum of **P0** and **6** using 785 nm excitation, b) ^{1}H NMR spectra of **P0** and **6**. Note the preservation of ethylene bridge proton signals at 2.5 and 3.4 ppm.

2.2.3. Post-Polymerization SPAAC onto Polymer P0

Polymer **P0** was then reacted with a series of aryl azides at room temperature in toluene at an alkyne concentration of ca. 35 mM using a 1.5-fold excess of azide (Scheme 2.2). In all cases, complete functionalization was observed in 30 min, and ^{1}H-NMR showed no trace of unreacted cyclooctyne (see Supporting Information). Varying substituents on the aromatic ring from electron withdrawing (p-, m-, and o-nitro) to electron donating (t-butyl and OTIPS) had no observable effect on the rate of cycloaddition. To our surprise, changing the electron withdrawing/donating nature of the cycloadduct had little effect on the photophysical properties of the polymer backbone, as evidenced by UV-Vis absorption spectroscopy (see Table 2.1 and Figure 2.9). Interestingly, whereas the alkyne-containing polymer was weakly fluorescent, none of the “clicked” derivatives, **P1**-**P5**, exhibited any fluorescence.

GPC data for the “clicked” polymers (Table 2.1) suggested that a decrease in molecular weight occurred upon alkyne-azide cycloaddition. However, ^{1}H-NMR indicated no evidence of backbone degradation, as the amount of residual aldehyde, arising from the end groups, remained constant relative to backbone signals. We hypothesized that the change in apparent molecular weight was possibly due to a change in conformation of the polymer in solution, rather than to chain scission. To investigate this hypothesis, modeling studies using both Density Functional Theory and semi-empirical methods were used to determine any changes in conformation upon cycloaddition. Using DFT (M06 Functional, Pople’s 6-31 basis set),[60,61] we modeled the structure of the DIBO unit, before and after cycloaddition (see Supporting Information). We then constructed oligomers (4 repeat units) using this structure and geometry optimized them using semi-empirical methods (Parametric Method 3).[62] These studies suggest that cycloaddition results in an accordion-like contraction of the polymer chain, which is congruent with the decreased molecular volume exhibited by the “clicked” polymers, as measured by GPC (Figure 2.2).

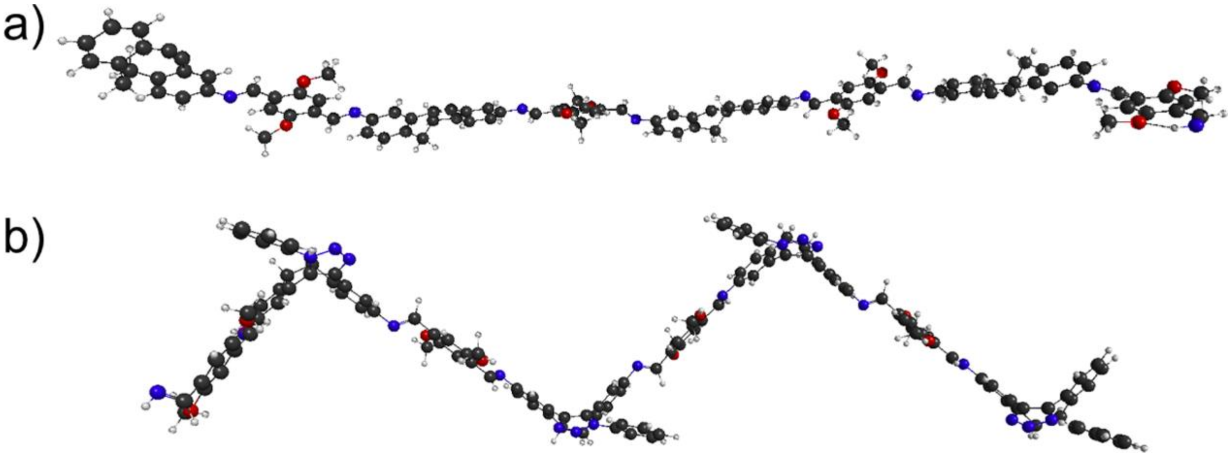

Figure 2.2. Optimized geometry of short polymer chain (PM3), before (a) and after (b) reaction with phenyl azide. Note the accordion-like contraction of the polymer backbone.

2.2.4. Reaction Kinetics of P0

An NMR kinetics study to determine cyclooctyne reactivity within the polymer backbone indicated a 2nd order rate constant of 0.031 $M^{-1}s^{-1}$ with benzyl azide in chloroform (for full details, see Supporting Information).[63] This is slightly lower than the literature value for DIBO derivatives (0.057 $M^{-1}s^{-1}$),[64] but is unsurprising when taking into account the decreased availability and mobility of the cyclooctyne functionality within the polymer chain.

2.2.5. Preparation of Graft-co-Polymers

To further test the cycloaddition, we performed a series of reactions with azide-terminated polymers (Scheme 2, **P6-P10**). Initially we used polystyrene azides having molecular weights of 4, 9, and 24 kDa (Table 2.2).[65,66] Polymer **P0** was stirred with 1.5 equivalents of azide-terminated polymer (per alkyne) at 60 °C for 12 hours in deuterated toluene. Alkyne conversion was found to be quantitative, even when employing 24 kDa polystyrene grafts, as Raman and ^{1}H-NMR spectroscopy showed no evidence of residual alkyne in the high molecular weight products (Figure 2.3a,b, and Table 2.2).

Table 2.2. Graft-co-Polymer Properties (**P6-P10**).

Graft Composition	Graft		Graft-co-Polymer		
	Mn (GPC, kDa)	PDI (GPC)	Mn (GPC, kDa)	Theor. Mn (kDa)	Weight % Graft
N_3-PS-4k (**P6**)	3.9	1.12	140	182	83
N_3-PS-9k (**P7**)	8.7	1.09	270	330	91
N_3-PS-24k (**P8**)	24	1.13	790	980	97
N_3-PEG-OMe-2k (**P9**)	2.0	-	N/A*	106	71
N_3-PEG-OMe-5k (**P10**)	5.0	-	N/A*	220	86

*Values not measured due to poor solubility in THF.

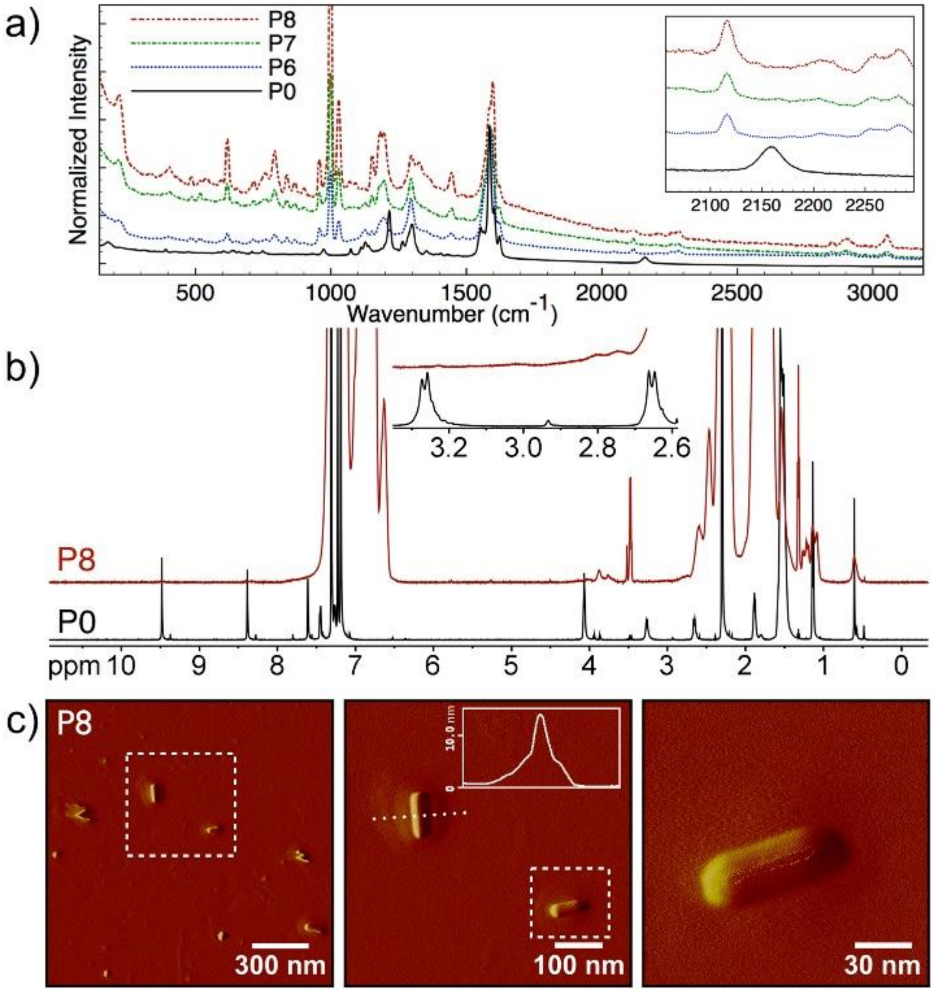

Figure 2.3. a) Raman spectra measured using 785 nm excitation confirming the complete reaction of all alkyne moieties (2160 cm^{-1}, see inset for magnification) of **P0** for each polystyrene graft (**P6**-**P8**). b) ^{1}H-NMR of **P0** and **P8** (24 kDa graft) in toluene-d8 showing the complete disappearance of the ethylene bridge protons (3.27 and 2.66 ppm, magnified in the inset). c) Amplitude mode AFM images showing individual graft-co-polymers for the polystyrene 24k graft (**P8**). Note: dashed boxes represent area of magnification in subsequent image to the right; inset shows the height profile along the indicated dotted line.

The quantitative grafting of polymer chains also provides a method of modifying the polyimine's solution properties. By grafting with azide terminated polyethylene glycol monomethyl ether (N_3-PEG-OMe), we were able to alter the solubility of this polymer. As expected, the starting polyimine and its small molecule cycloadducts (**P0**-**P5**) are highly soluble in non-polar solvents such as chloroform, toluene, and tetrahydrofuran. These structures show only slight solubility in *N*,*N*-dimethylformamide and dimethylsulfoxide, and essentially no solubility in other polar solvents. After grafting with 2 kDa N_3-PEG-OMe, the graft copolymer remained soluble in toluene but also exhibited high solubility in methanol. However, grafting with 5 kDa N_3-PEG-OMe resulted in a graft co-polymer that exhibited marked solubility in water (Figure 2.4d). As in the polystyrene case, ^{1}H-NMR and Raman data show quantitative conversion of the backbone alkynes to the resulting triazole rings (Figure 2.4a,b).

Using tapping-mode atomic force microscopy (AFM), we were able to image individual graft-copolymer structures (Figures 2.3c and 2.4c). Samples for AFM measurements were prepared by spin-coating dilute solutions of the graft copolymers onto freshly cleaved mica. These AFM images show individual graft copolymers on the mica surface, having sizes and aspect ratios that are consistent with the expected features of the graft copolymers. For example, polymer **P8**, which has 24 kDa PS grafts, exhibits a rigid, cylindrical shape having a width on the order of 30 nm, and a length on the order of 80 nm (Figure 2.3c), while polymers **P9** and **P10**, having PEO grafts, exhibit a more spherical shape, with diameter on the order of 20-30 nm (Figure 2.4c). The greater flexibility and lower molecular weight of the PEO grafts allowed the polymer to adopt a more coiled, globular structure, rather than the extended cylindrical shape of **P8**.

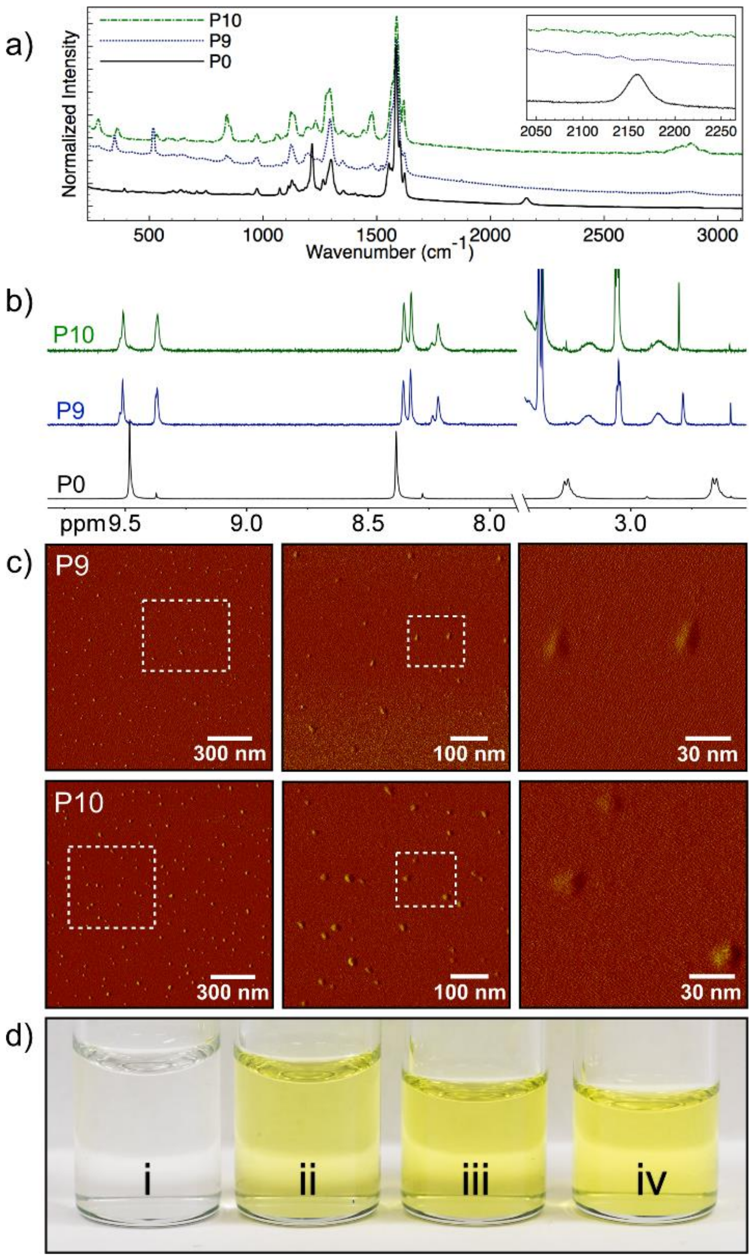

Figure 2.4. a) Raman spectra at a 785 nm excitation confirming the complete reaction of all alkyne groups (2160 cm^{-1}) of **P0** for each PEG-OMe graft (**P9** and **P10**). b) ^{1}H-NMR overlay of **P0** with **P9** and **P10** in toluene d8 showing the complete disappearance of the ethylene bridge protons (3.27 and 2.66 ppm). A shift in the imine protons is also observed (9.5 ppm). c) Amplitude mode AFM images showing individual PEG-OMe graft-co-polymers (**P9** and **P10**). Note: dashed boxes represent area of magnification in subsequent image to the right. d) 2 kDa PEG-OMe graft-co-polymer exhibits no solubility in water (i), but shows solubility in methanol (ii); 5kDa PEG-OMe graft-co-polymer exhibits solubility in both water (iii) and methanol (iv).

2.3. Conclusions

In summary, we demonstrated the synthesis of a high-molecular weight (>30 kDa) polymer containing strained dibenzocyclooctyne moieties. Each cyclooctyne within the polymer backbone reacted with aliphatic and aryl azides at a rate that is consistent with similar small-molecule cyclooctynes. We prepared a library of homologous triazole-containing polymers (**P1-P5**) from the single progenitor poly-alkyne (**P0)** via SPAAC. We also demonstrated the high-efficiency of these reactions though coupling with azide-terminated polystyrene and polyethylene glycol monomethyl ether chains. These polymer grafting reactions were rapid and quantitative, producing samples with compositions containing up to 97% graft in under 12 hours at modest temperatures (60 °C). Further studies investigating more diverse modification of these polymers and their applications are now in progress.

2.4. Supporting Information

2.4.1. General Experimental

All reagents were purchased from commercial chemical suppliers and used without further purification. *N*-Phenyl-bis(trifluoromethanesulfonimide) was synthesized according to a literature procedure[67] Unless otherwise mentioned all reactions were performed under an inert atmosphere. ^{1}H-NMR and ^{13}C-NMR spectra were recorded on Bruker DX500, Avance 600, and Avance 700 MHz spectrometers. High-resolution (HR) electrospray ionization (ESI) MS measurements were carried out on the Micromass Ultima Global instrument (quadrupole time-of-flight). Polymer molecular weights and polydispersity indices (PDI) were analyzed via gel permeation chromatography (GPC) using a Waters 2695 Separations Module, equipped with a Waters 2414 refractive-index detector and a Jordi Fluorinated DVB mixed-bed column. Polystyrene standards were used for calibration, with THF as the eluent at a flow rate of 3.0 mL/min. UV-Vis spectra were measured on a Cary 5000 spectrophotometer, while fluorescence spectra were measured on a Jobin-Yvon SPEX Fluorolog 3.22 equipped with a 450 W Xe lamp, double-excitation and double-emission monochromators, and a digital photon-counting photomultiplier. Raman spectra were collected with a Renishaw InVia Laser Raman spectrometer equipped with a 300 mW Renishaw laser (785 nm, grating 1200 L/mm). Laser intensities of 1-5% were used to collect data. Monomer purities were analyzed via HPLC using a Waters 2695 Separations Module equipped with a Waters 2996 photodiode array. A Phenomenex Luna 3 μ (150 x 4.6 mm) phenyl-hexyl column was used for the 2,5-bis(hexadecyloxy)benzene-1,4-dialdehyde monomer (**9**), while a Phenomenex Gemini-NX 3 μ (100 x 4.6 mm) C18 column was used for the DIBO-diamine monomer (**6**). All other compounds were run using a Phenomenex Kinetex 2.6 μ (100 x 3 mm) C18 column. Atomic force microscopy was carried out by using a Digital Instruments NanoScope IIIa Multimode AFM, with samples prepared by spin coating dilute samples (2500 rpm) onto freshly cleaved mica substrates. The images were recorded with standard (9 nm radius) and ultrasharp (7 nm radius) tips in tapping mode.

Aryl azides were synthesized via literature procedures using Sandmeyer-type diazonium chemistry[68] and 4-triisopropyloxyphenyl azide was prepared via standard silylation conditions from 4-azidophenol.[69] Alkyl and benzyl azides were synthesized by substitution from the respective halides with NaN_3 in DMF. PS azides were synthesized by substitution from their respective bromides[65,70] while PEG-OMe (Aldrich) azides were synthesized by substitution from their respective mesylates.[71] All aryl azides were stored at -20 °C and their purity was re-confirmed by ^{1}H-NMR immediately before use. 1,4-bis(hexadecyloxy)benzene **(7)** and 1,4-diiodo-2,5-bis(hexadecyloxy)benzene **(8)** were synthesized according to modified literature procedures.[72]

2.4.2. Experimental Procedures

General Procedure for Polymer/Azide Cycloaddition

5 mg scale (P1-P5).

A slight excess (1.5 eqv. per alkyne) of a 50 mM solution (150-200 μL) of the respective azide in toluene was added to 5 mg of polymer **P0** in a 1 mL microcentrifuge tube. Upon dissolving, the mixture was stirred at room temperature for 30 min. The toluene was removed by evaporation, and the polymer was triturated with 1 mL of dry ether (to remove excess azide), then dried under vacuum. The polymers were characterized by ^{1}H-NMR, GPC, as well as UV-Vis and Raman spectroscopy. All cycloaddition reactions were performed in ambient atmosphere.

2 mg scale (Graft Polymers P6-P10).

As per previous cycloaddition reactions, 2 mg of polymer **P0** was combined with a slight excess (1.5 eqv. per alkyne) of azide-terminated polymer, 100 μL of toluene-d8 (200 μL in the case of the **N_3-PS-24K**), and a stir bar in a 1-dram screw cap vial. The reaction was stirred at 60 °C for 12 hours and directly monitored via ^{1}H-NMR and GPC by removing aliquots and diluting them with toluene-d8 and THF, respectively. Complete conversion was observed within 1 hour for all except the highest molecular weight PS graft (24 kDa), which required 12 hours for completion. Raman samples were prepared by drop casting 20 μL aliquots from the reaction mixture onto a silicon wafer, and then evaporating most of the residual toluene-d8 under high vacuum for 15 minutes.

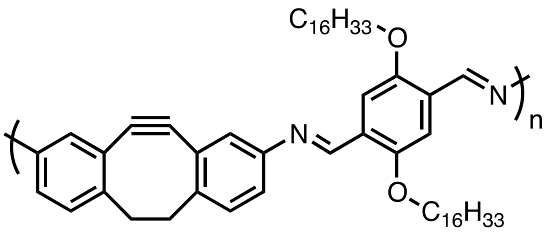

Synthesis of Cyclooctyne-containing polyimine (P0)

Compound **6** (77.8 mg, 0.332 mmol), compound **9** (194 mg, 0.316 mmol), and *p*-toluenesulfonic acid monohydrate (1.2 mg, 2 mol%) were combined in a 3 mL microwave vial containing activated 3Å molecular sieves. The vial was capped with a septum and flushed with N_2, then dichloromethane (0.5 mL) and toluene (1.5 mL) were added via syringe. The polymerization was stirred for 3 hours at 40 °C under N_2 and the extent of reaction was monitored via ^{1}H-NMR and GPC. When the desired molecular weight was achieved, the polymerization mixture was neutralized with the addition of solid MgO. The reaction mixture was filtered and precipitated into 100 mL of cold EtOH to isolate 198 mg (77%) of bright yellow polyimine **P0**. M_n: 30.8 kDa (GPC), M_w: 62.6 kDa (GPC). ^{1}H-NMR (600 MHz; $CDCl_3$): δ 10.53 (s), 8.97 (s, 2H), 7.77 (s, 2H), 7.35 (d, *J* = 7.9, 2H), 7.25 (s, 2H), 7.18 (d, *J* = 7.0, 2H), 4.15 (t, *J* = 6.3, 4H), 3.37 (d, *J* = 10.7, 2H), 2.49 (d, *J* = 10.8, 2H), 1.86 (quintet, *J* = 7.0, 4H), 1.50 (m, 4H), 1.38 (m, 4H), 1.33-1.27 (m, 46H), 0.87 (t, *J* = 7.0, 6H); ^{13}C-NMR (176 MHz; $CDCl_3$): δ 156.28, 156.17, 153.6, 151.65, 151.52, 151.21, 151.05, 145.0, 144.3, 130.17, 130.09, 128.52, 128.48, 128.42, 124.80, 124.68, 124.52, 120.82, 120.68, 118.85, 118.72, 114.63, 114.50, 112.9, 112.0, 111.7, 111.1, 110.7, 69.4, 36.7, 36.3, 35.9, 32.1, 29.87, 29.82, 29.78, 29.55, 29.52, 29.43, 26.3, 22.8, 14.3.

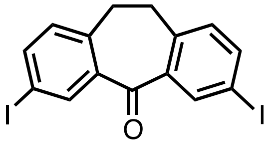

3,7-diiodo-10,11-dihydro-5*H*-dibenzo[*a,d*][7]annulen-5-one (1)[73,74]

Dibenzosuberone (62.40 g, 0.30 mol), I_2 (83.75 g, 0.33 mol), and acetic acid (450 mL) were added to a 1 L, 2-neck round-bottom flask equipped with a condenser and addition funnel, forming a red-violet mixture. A mixture of HNO_3 (24 mL) and H_2SO_4 (60 mL) was then added dropwise to the stirring reaction, followed by CCl_4 (30 mL). The reaction was heated and stirred at reflux for 5 h (R_f:0.4 in 1:4 Et_2O:Hx), then partitioned between water (1 L) and chloroform (1 L) while molten. The aqueous phase was further extracted with $CHCl_3$ (3 × 200 mL). The organic phases were combined and washed with sat. $NaHCO_{3(aq)}$ (3 × 300 mL), sat. $NaSO_{3(aq)}$ (4 × 250 mL), and brine (1 × 300 mL). The organic phase was dried over magnesium sulfate and then filtered and evaporated under reduced pressure to yield a crude reddish solid. The crude material was passed through a silica plug, which was rinsed with 1:1 $CHCl_3$:Hx, then purified via recrystallization from 1:8 1,4-dioxane/ EtOH to yield 38.6 g, 84.0 mmol (28%) of an off-white crystalline solid (**1**). Purity: >97.5% by HPLC; M.W.: 460.05 g/mol; ^{1}H-NMR (700 MHz; $CDCl_3$): δ 8.29 (d, *J* = 1.6, 2H), 7.74 (dd, *J* = 8.0, 1.7, 2H), 6.97 (d, *J* = 8.0, 2H), 3.12 (s, 4H); ^{13}C-NMR (176 MHz; $CDCl_3$): δ 192.5, 141.42, 141.37, 139.7, 139.4, 131.4, 91.8, 34.4; HRMS (ESI+) (m/z) for $C_{15}H_{11}OI_2$ $[M + H]^+$ calculated: 460.8899, found: 460.8919.

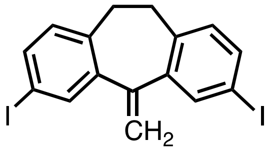

3,7-diiodo-5-methylene-10,11-dihydro-5*H*-dibenzo[*a*,*d*][7]annulene (2)[75]

Methyltriphenylphosphonium iodide (7.90 g, 19.4 mmol) was added to an oven dried 250 mL Schlenk tube. After purging the vessel with N_2, dry THF (30 mL) was added via syringe, creating a milky white suspension. The suspension was then degassed by bubbling N_2 through the stirring mixture for 20 minutes. At 20 °C, KO^{t}Bu (2.18 g, 19.4 mmol) was added as a solid to the stirring suspension, generating the bright yellow methylenetriphenylphosphorane ylide. After allowing the mixture to stir for 15 minutes, compound **1** (6.38 g, 13.9 mmol) was added. The reaction immediately changed from bright yellow to crimson. The reaction was stirred at 40 °C for 12 hours and followed by TLC (R_f:0.5 in 1:4 DCM:Hx) before filtering through a plug of silica gel to remove unreacted ylide/base. The plug was rinsed with dichloromethane to ensure the desired compound was removed from the stationary phase resulting in a crude yellow solid, which was further purified via silica gel column chromatography (1:4 DCM:Hx) to yield 4.45 g (70%) of white powder (**2**). Purity: >98.5% by HPLC; M.W.: 458.08 g/mol; ^{1}H-NMR (700 MHz; $CDCl_3$): δ 7.66 (d, *J* = 1.8, 2H), 7.51 (dd, *J* = 8.0, 1.9, 2H), 6.85 (d, *J* = 8.0, 2H), 5.43 (s, 2H), 3.04 (s, 4H); ^{13}C-NMR (176 MHz; $CDCl_3$): δ 148.9, 142.7, 137.8, 136.84, 136.74, 131.0, 119.1, 91.2, 32.6; HRMS (EI+) (m/z) for $C_{16}H_{12}I_2$ $[M]^+$ calculated: 457.9029, found: 457.9014.

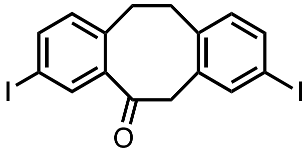

3,8-diiodo-11,12-dihydrodibenzo[*a*,*e*][8]annulen-5(6*H*)-one (3)[75]

Silver nitrate (1.93 g, 11.4 mmol) was ground to a powder using a mortar and pestle, then fully dissolved in refluxing methanol (50 mL) in a 300 mL round bottom flask. I_2 (1.44 g, 5.68 mmol) was added to the stirring solution together with compound **2** (2.55 g, 5.57 mmol), followed immediately by 1,4-dioxane (50 mL). The yellow silver iodide salt could be seen precipitating almost immediately. The reaction mixture was stirred under reflux for 24 hours and monitored by TLC (R_f: 0.2 in 1:3 DCM:Hx) before cooling to room temperature. The silver iodide was filtered and the filtrate evaporated under reduced pressure. The product was purified via silica gel column chromatography (2:3 DCM:Hx) to yield 1.74 g (66%) of a white powder (**3**). Purity: >96% by HPLC; M.W.: 474.07 g/mol; ^{1}H-NMR (700 MHz; $CDCl_3$): δ 7.71 (d, *J* = 1.7, 1H), 7.59 (dd, *J* = 8.0, 1.8, 1H), 7.39 (s, 1H), 7.37 (dd, *J* = 8.1, 1.5, 1H), 6.84 (d, J = 8.0, 1H), 6.73 (d, *J* = 8.0, 1H), 4.05 (s, 2H), 3.20 (m, 4H); ^{13}C-NMR (176 MHz; $CDCl_3$): δ 202.1, 140.8, 140.4, 139.5, 138.1, 137.32, 137.13, 136.98, 135.7, 133.0, 131.9, 92.27, 92.11, 50.9, 34.3, 33.4; HRMS (ESI+) (m/z) for $C_{16}H_{13}OI_2$ $[M + H]^+$ calculated: 474.9056, found: 474.9074.

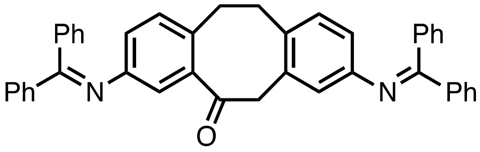

3,8-bis((diphenylmethylene)amino)-11,12-dihydrodibenzo[*a*,*e*][8]annulen-5(6*H*)-one (4)[76]

An oven-dried, 25 mL Schlenk tube was charged with tris(dibenzylideneacetone) dipalladium(0) (Pd_2dba_3) (15.6 mg, 0.017 mmol, 4 mol %) and 2,2'-bis(diphenylphosphino)-1,1'-binaphthyl (BINAP) (±) (31.8 mg, 0.051 mmol, 12 mol %), then further purged with N_2. Dry, degassed toluene (3 mL) was then syringed into the Schlenk tube, followed by the addition of solid potassium *tert*-butoxide (134 mg, 1.19 mmol), then immediately by compound **3** (0.200 g, 0.425 mmol) and benzophenone imine (0.20 mL, 1.19 mmol). The red reaction mixture was stirred at 60 °C under N_2 for 2 days until complete by TLC (R_f: 0.35 in 1:4 EtOAc:Hx). The mixture was filtered through silica gel (eluting with 5:95 EtOAc:DCM). The fractions containing the product were combined, evaporated under reduced pressure, then further purified via gradient elution silica gel column chromatography (1:4 to 1:2 EtOAc:Hx) to yield 165 mg (67%) of a bright yellow solid (**4**). NOTE: Compound **4** is heat sensitive and should not be heated past 60 °C. Purity: >98% by HPLC; M.W.: 580.72 g/mol; ^{1}H-NMR (700 MHz; $CDCl_3$): δ 7.75-7.72 (m, 4H), 7.46 (q, J = 7.2, 2H), 7.39 (q, *J* = 6.2, 4H), 7.34-7.31 (m, 2H), 7.23 (m, 4H), 7.00 (t, *J* = 6.9, 4H), 6.80 (d, *J* = 8.6, 1H), 6.75 (d, *J* = 8.0, 1H), 6.61 (d, *J* = 2.1, 2H), 6.49 (d, *J* = 7.4, 1H), 6.26 (s, 1H), 3.82 (s, 2H), 3.08 (s, 4H); ^{13}C-NMR (176 MHz; $CDCl_3$): δ 204.5, 168.8, 149.6, 139.81, 139.64, 139.1, 136.1, 135.8, 133.8, 133.5, 132.7, 131.2, 130.9, 129.9, 129.61, 129.58, 129.45, 128.88, 128.79, 128.36, 128.33, 128.17, 128.14, 124.2, 123.1, 121.2, 120.5, 51.3, 34.4, 33.3; HRMS (ESI+) (m/z) for $C_{42}H_{32}N_2O$ $[M + H]^+$ calculated: 581.2592, found: 581.2587.

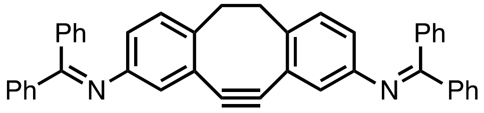

3,8-bis((diphenylmethylene)amino)-11,12-dihydrodibenzo[*a*,*e*][8]annulen-5(6*H*)-yne (5)[57,77]

Compound **4** (80 mg, 0.138 mmol) was added to a nitrogen-filled, flame-dried 25 mL Schlenk tube, followed by further purging with nitrogen gas. Dry THF (1.8 mL) was added via syringe into the Schlenk tube, dissolving the solid. The yellow solution was cooled to -78 °C, at which point *N*-Phenyl-bis(trifluoromethanesulfonimide) (59 mg, 0.165 mmol) was added, followed by potassium bis(trimethylsilyl)amide (0.330 mL, 1 M in THF, 0.330 mmol) over 30 minutes. The reaction mixture was then slowly warmed to 20 °C and stirred for 20 minutes until complete by TLC (R_f:0.45 in 1:4 EtOAc:Hx). The reaction mixture was then evaporated under reduced pressure and purified via silica gel column chromatography (1:5 EtOAc:Hx) to yield 70 mg (90%) of a spongy yellow solid (**5**). NOTE: Compound **5** is mildly heat sensitive and sustained heating should be avoided. Purity: >92% by HPLC; M.W.: 562.70 g/mol; ^{1}H-NMR (700 MHz; $CDCl_3$): δ 7.73 (d, *J* = 7.4, 4H), 7.46 (t, *J* = 7.4, 2H), 7.40 (t, *J* = 7.7, 4H), 7.30-7.25 (m, 6H), 7.12 (d, *J* = 6.7, 4H), 7.01 (d, i = 8.0, 2H), 6.69 (d, *J* = 2.0, 2H), 6.57 (dd, *J* = 8.0, 2.0, 2H), 3.13-3.08 (m, 2H), 2.27-2.21 (m, 2H); ^{13}C-NMR (176 MHz; $CDCl_3$): δ 168.8, 149.7, 148.7, 139.7, 136.1, 130.9, 129.60, 129.47, 129.46, 128.9, 128.33, 128.15, 123.9, 120.4, 118.8, 111.4, 36.2; HRMS (ESI+) (m/z) for $C_{42}H_{30}N_2$ $[M + H]^+$ calculated: 563.2487, found: 563.2473.

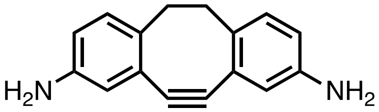

3,8-diamino-11,12-dihydrodibenzo[*a*,*e*][8]annulen-5(6*H*)-yne (DIBO-(NH_2)$_2$) (6)

THF (1 mL) and 2 M $HCl_{(aq)}$ (0.1 mL) were added to a 20 mL round bottom flask containing compound **5** (35 mg, 0.062 mmol). The reaction was stirred at 20 °C, and white precipitate corresponding to the diamine dihydrochloride salt was evolved over 30 minutes (R_f: 0.3 in 1:1 EtOAc:Hx). When TLC showed complete conversion (*ca.* 30 minutes) the reaction mixture was diluted with ethyl acetate (20 mL) and washed with 5% aqueous $NaHCO_3$ (3 x 10 mL) and brine (1 x 15 mL). The organic phase was dried over $MgSO_4$, evaporated under reduced pressure and purified by silica gel column chromatography (1:1 EtOAc:Hx) to yield 12.4 mg (85%) of white powder (**6**), which is prone to oxidation, turning red upon standing for several weeks. Purity: >99% by HPLC; M.W.: 234.30 g/mol; ^{1}H-NMR (600 MHz; $CDCl_3$): δ 7.04 (d, *J* = 8.1, 2H), 6.65 (d, *J* = 2.5, 2H), 6.57 (dd, *J* = 8.0, 2.5, 2H), 3.63 (s, 4H), 3.18-3.13 (m, 2H), 2.33-2.27 (m, 2H); ^{13}C-NMR (176 MHz; $CDCl_3$): δ 144.9, 144.4, 130.0, 124.6, 114.5, 112.9, 111.4, 36.2; HRMS (ESI+) (m/z) for $C_{16}H_{14}N_2$ [M + H]+ calculated: 235.1235, found: 235.1230.

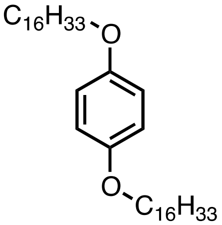

1,4-bis(hexadecyloxy)benzene (7). Prepared according to literature procedures.[72]

M.W.: 558.96 g/mol; ^{1}H-NMR (700 MHz; CDCl$_3$): δ 6.81 (s, 4H), 3.89 (t, *J* = 6.6, 4H), 1.75 (quintet, *J* = 7.3, 4H), 1.43 (quintet, *J* = 7.4, 4H), 1.35-1.33 (m, 4H), 1.29 (m, *J* = 6.7, 44H), 0.88 (t, *J* = 7.1, 6H); ^{13}C-NMR (176 MHz; CDCl$_3$): δ 153.3, 115.5, 68.8, 32.1, 29.86, 29.82, 29.76, 29.75, 29.57, 29.52, 26.2, 22.9, 14.3.

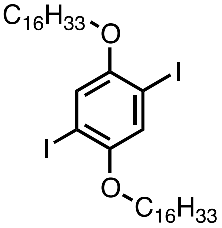

1,4-diiodo-2,5-bis(hexadecyloxy)benzene (8). Prepared according to literature procedures.[72]

M.W.: 810.75 g/mol; ^{1}H-NMR (700 MHz; CDCl$_3$): δ 7.17 (s, 2H), 3.92 (t, *J* = 6.4, 4H), 1.79 (quintet, *J* = 7.2, 4H), 1.49 (quintet, *J* = 7.4, 4H), 1.35 (m, 4H), 1.27 (m, 44H), 0.88 (t, *J* = 7.0, 6H); ^{13}C-NMR (176 MHz; CDCl3): δ 153.0, 122.9, 86.5, 70.5, 32.1, 29.86, 29.83, 29.75, 29.72, 29.53, 29.44, 29.30, 26.2, 22.9, 14.3.

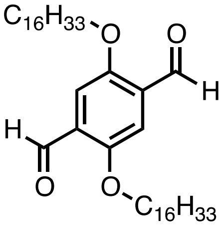

2,5-bis(hexadecyloxy)benzene-1,4-dialdehyde (9)

An oven-dried 250 mL Schlenk tube was charged with the compound **8** (1.622 g, 2.0 mmol). Under N_2, heptane (*ca.* 45 mL) was cannulated into the reaction vessel and the mixture was heated to 40 °C, until compound **8** fully dissolved. At 40 °C, *n*-BuLi (4.8 mL of 2.5 M solution in hexanes, 12 mmol) was added drop-wise via syringe. The reaction mixture was left to stir for 15 minutes at 40 °C, then slowly cooled to room temperature, followed by submersion in an ice bath. At 0 °C, DMF (1.54 mL) was added to the reaction mixture via syringe, which precipitated the LiI salt as a fine white powder. The reaction was slowly warmed to room temperature where it was stirred for a further 30 minutes. TLC showed complete conversion of the starting materials (R_f: 0.65 in 1:1 DCM:Hx). The reaction mixture was diluted with Et_2O (50 mL) washed with 5% LiCl solution in water (2 x 50 mL), then evaporated under reduced pressure and purified by silica gel column chromatography (2:3 DCM:Hx) to yield 836 mg (68%) of a bright yellow powder (**9**). M.W.: 614.98 g/mol; ^{1}H-NMR (700 MHz; $CDCl_3$): δ 10.52 (s, 2H), 7.43 (s, 2H), 4.08 (t, *J* = 6.4, 4H), 1.83 (quintet, *J* = 7.2, 4H), 1.46 (quintet, *J* = 7.4, 4H), 1.35 (quintet, *J* = 6.9, 4H), 1.31-1.26 (m, 44H), 0.88 (t, *J* = 7.0, 6H); ^{13}C-NMR (176 MHz; $CDCl_3$): δ 189.6, 155.4, 129.4, 111.8, 69.4, 32.1, 29.85, 29.82, 29.74, 29.71, 29.52, 29.48, 29.2, 26.2, 22.9, 14.3; HRMS (ESI+) (m/z) for $C_{40}H_{71}0_4$ [M + H]$^+$ calculated: 615.5352, actual: 615.5383.

NMR Data for Azides:

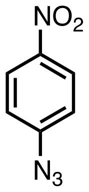

4-Nitrophenylazide (10). Prepared from the corresponding amine according to literature procedures.[68]

75% yield. White powder. ^{1}H-NMR (600 MHz; $CDCl_3$): δ 8.26-8.23 (m, 2H), 7.15-7.13 (m, 2H).

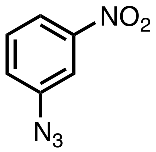

3-Nitrophenylazide (11). Prepared from the corresponding amine according to literature procedures.[68]

91% yield. White powder. ^{1}H-NMR (600 MHz; $CDCl_3$): δ 8.00 (dd, J = 8.2, 1.6, 1H), 7.89 (t, J = 2.2, 1H), 7.54 (t, J = 8.1, 1H), 7.35 (dd, J = 8.0, 1.7, 1H).

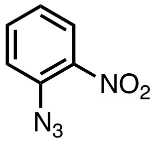

2-Nitrophenylazide (12). Prepared from the corresponding amine according to literature procedures.[68]

67% yield. White powder. ^{1}H-NMR (600 MHz; $CDCl_3$): δ 7.94 (dd, *J* = 8.2, 1.4, 1H), 7.62 (td, *J* = 7.8, 1.2, 1H), 7.34 (dd, *J* = 8.1, 1.0, 1H), 7.26 (td, *J* = 7.8, 1.1, 1H).

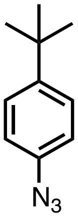

4-tertbutylphenylazide (13). Prepared from the corresponding amine according to literature procedures.[68]

57% yield. Slightly yellow liquid. ^{1}H-NMR (600 MHz; $CDCl_3$): δ 7.38-7.36 (m, 2H), 6.98-6.96 (m, 2H), 1.31 (s, 9H).

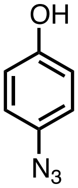

4-azidophenol (14). Prepared from the corresponding amine according to literature procedures. [68]

75% yield. White solid. Oxidizes to dark brown solid. ^{1}H-NMR (600 MHz; DMSO-d6): δ 9.51 (s, 1H), 6.94-6.91 (m, 2H), 6.81-6.78 (m, 2H).

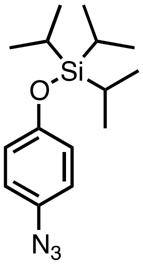

4-triisopropysiloxyphenylazide (14b).[69]

In a 20 mL round bottom flask, compound **14** (100 mg, 0.740 mmol) and imidazole (35 mg, 1.11 mmol) were dissolved in 5 mL of DCM. Under an atmosphere of N_2, triisopropylsilyl chloride (0.190 mL, 0.412 mmol) was added via syringe. The reaction was stirred at 20 °C for 60 minutes (R_f: 0.85 in 1:1 DCM:Hx) then filtered to remove the imidazole hydrochloride salt. The reaction mixture was evaporated under reduced pressure and purified via silica gel column chromatography (1:4 DCM:Hx) to yield 194 mg (90%) of a light yellow liquid (**14b**). M.W.: 291.46; ^{1}H-NMR (600 MHz; $CDCl_3$): δ 6.89-6.85 (m, 4H), 1.24 (septet, *J* = 7.5, 3H), 1.09 (d, *J* = 7.4, 18H).

Polystyrene azides – M_n 4000, 9000, 24,000

White amorphous solids. Prepared according to literature procedures.[65]

Poly(ethylene glycol) methyl ether azide - M_n 2000 (N_3-PEG-OMe-2K). Prepared according to literature procedures.[71]

White waxy solid. ^{1}H-NMR (700 MHz; DMSO-d6): δ 3.51 (m, 183H), 3.24 (s, 3H).

Poly(ethylene glycol) methyl ether azide - M_n 5000 (N_3-PEG-OMe-5K). Prepared according to literature procedures.[71]

White amorphous solid. ^{1}H-NMR (700 MHz; DMSO-d6): δ 3.51 (m, 454H), 3.24 (s, 3H).

2.4.3. Kinetics Studies

Kinetics experiments were performed according to a literature procedure.[78–80] The DIBO-containing polymer was reacted with an equimolar amount (relative to alkyne concentration) of benzyl azide in $CDCl_3$ at concentrations of 12.0-12.3 mM. Hexamethyldisilane was used as an internal standard. The conversion was calculated by ^{1}H-NMR integration ratios relative to the internal standard. All experiments were performed in triplicate. The second order rate constant was calculated by plotting the reciprocal of substrate concentration versus time and fitting the plot to a linear regression.

Sample NMR Overlay:

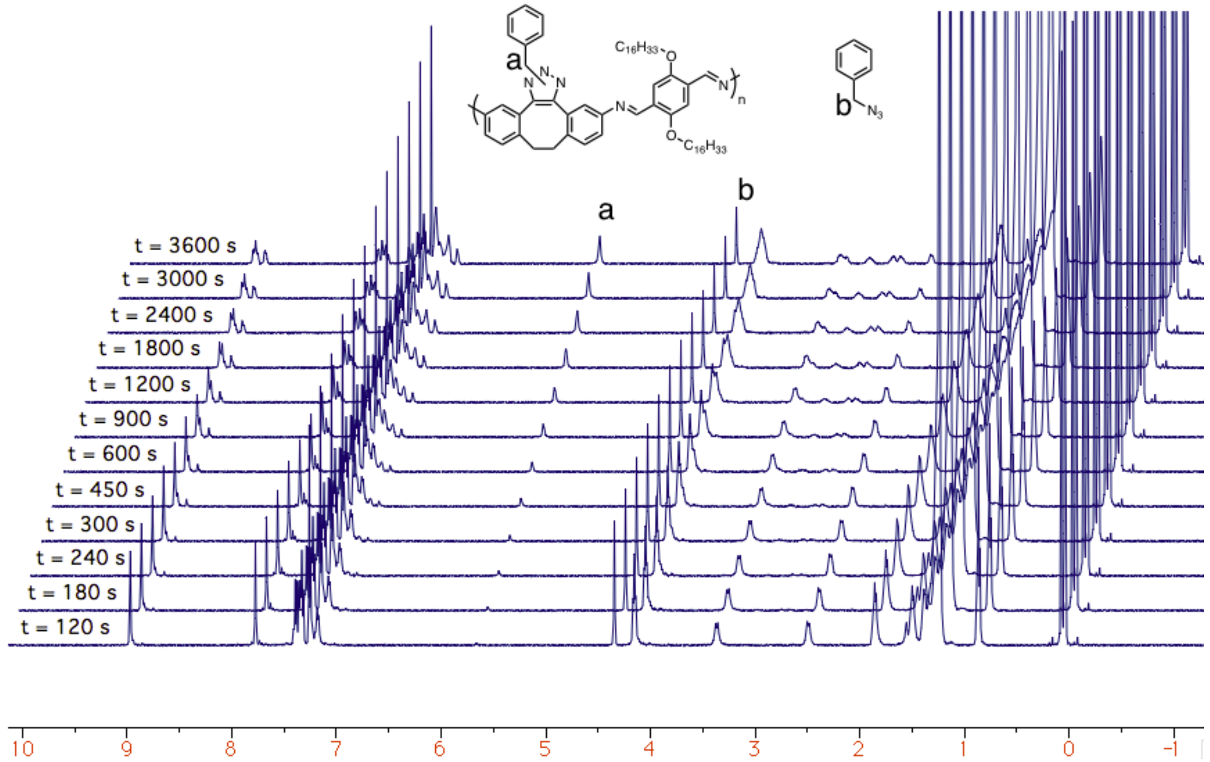

Figure 2.5. ^{1}H-NMR overlay for the reaction of **P0** with benzyl azide.

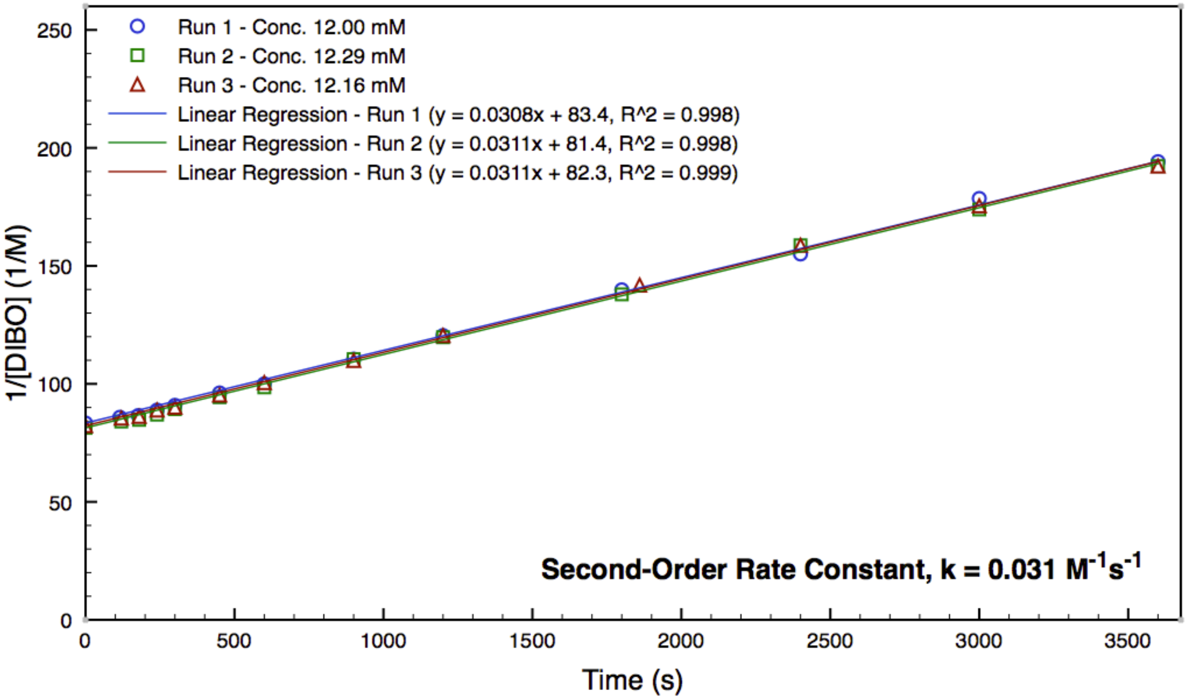

Figure 2.6. Linear regression plot to determine second-order reaction kinetics for **P0** with benzyl azide in $CDCl_3$.

2.4.4. Computational Methods

All calculations were performed using Gamess[81] (1 May 2013 – R1, 64-bit Linux), run in Mac OS X 10.9 on a desktop computer equipped with an Intel i5-3570k processor. The M06 density functional[60] and 6-31G(d) basis set were used for all geometry and frequency calculations on single repeat units. For oligomeric structures the semi-empirical Parameterized Model number 3 (PM3)[62] was used. DFT geometry optimizations were used to calculate the structure of a single repeat unit before and after cycloaddition with phenyl azide. These structures were used as the initial points in a geometry optimization of small oligomers (4 repeat units) using PM3. In all cases alkyl chains were replaced by methyl groups to minimize computational load.

Results of Computations:

Computing the harmonic vibrational frequencies for the single repeat unit, before and after clicking (Figure 2.7), confirmed the structures lie at a minimum rather than a saddle point. The M06 geometries show a dihedral angle of 40° between the alkoxybenzene and DIBO units both before and after clicking with phenyl azide, which suggests the structures may not be fully planar. However, these results do not necessarily describe the repeat units' conformations in solution and the exact dihedral angle in ring-structured polymers can be difficult to calculate.[82] The pucker in the cyclooctyne ring post SPAAC should have far greater influence on the planarity of the resultant triazole-containing polymer. Figure 2.8-c,d shows the oligomer transforming from a relatively planar structure to a more compact, accordion-like structure upon SPAAC.

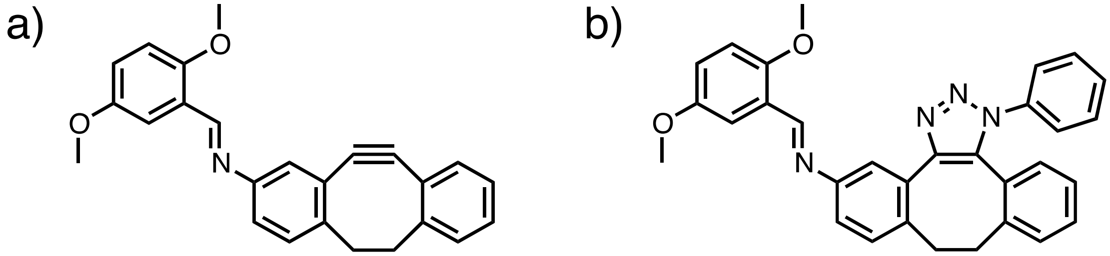

Figure 2.7. 2D structures of single repeat unit before (a) and after (b) cyclooadition with phenyl azide.

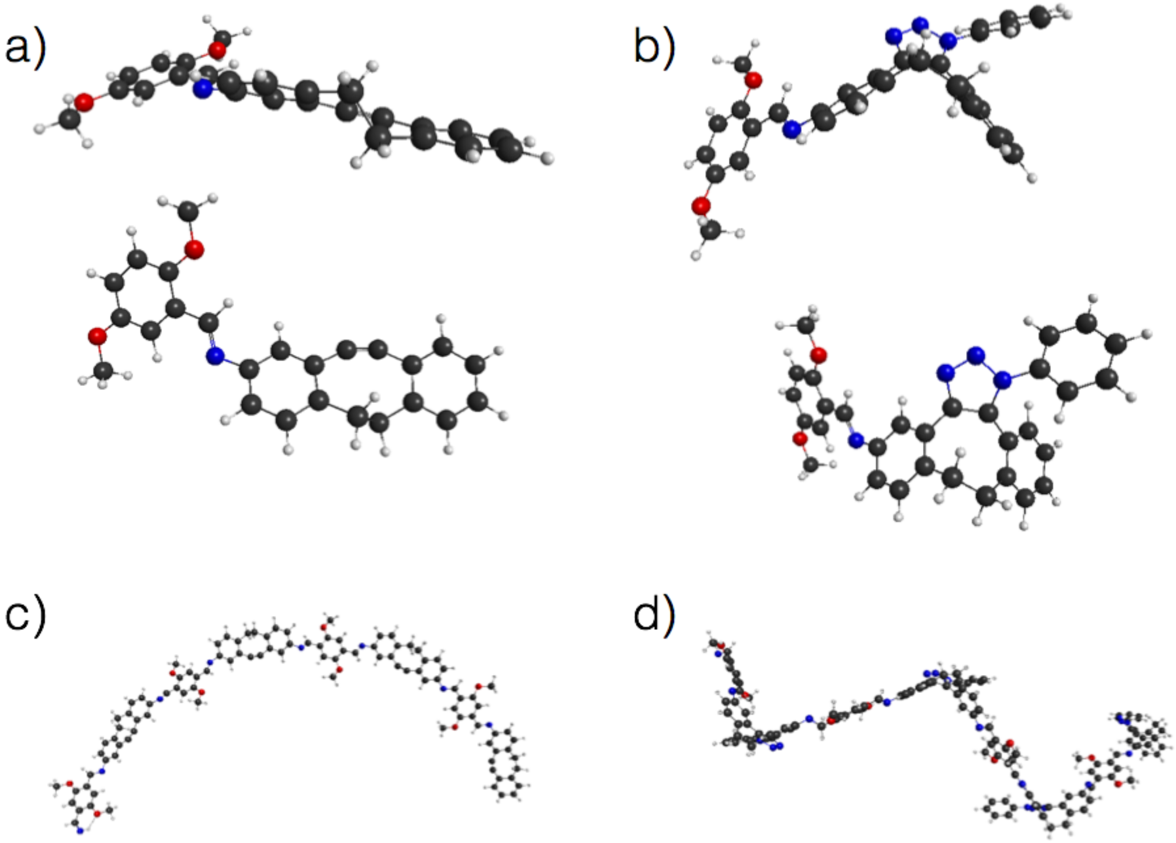

Figure 2.8. M06 equilibrium structure of single repeat unit before (a) and after (b) cycloaddition with phenyl azide. Note: Structures are presented from two orientations. PM3 equilibrium structure of four repeat units before (c) and after (d) cycloaddition.

Coordinates of M06/6-31G(d) stationary point:

Monomer – Before Cycloaddition:

E= -1169.5728748135

ATOM	CHARGE	X	Y	Z
C	6.0	0.4330059183	-2.9584464236	0.4584721926
C	6.0	-0.9117099202	-2.6752162601	0.2425658783
C	6.0	-1.2951770518	-1.3988974766	-0.1472158403
C	6.0	-0.3343013670	-0.4002437034	-0.3145674308
C	6.0	1.0402189179	-0.6724706304	-0.0845532011
C	6.0	1.3937755957	-1.9635371614	0.2934684134
C	6.0	-0.5784741316	0.9263694518	-0.7617827409
C	6.0	-0.2504235390	2.0392524149	-1.1285729258
C	6.0	0.6702653705	3.0293805918	-1.5668677128
C	6.0	1.9833394796	2.5254173679	-1.7557610410
C	6.0	2.2690544888	1.0501629839	-1.6210154704
C	6.0	2.0693599403	0.4253125172	-0.2004452923
C	6.0	0.3849941616	4.3815452244	-1.7514452252
C	6.0	1.3971431801	5.2720297797	-2.1211993649
C	6.0	2.7022359403	4.7875755997	-2.2604530567
C	6.0	2.9795538644	3.4372181796	-2.0954442269
N	7.0	1.1842830258	6.6416313594	-2.3108561891
C	6.0	0.0984133286	7.0351205532	-2.8616172757
C	6.0	-0.2058044117	8.4520798919	-3.0359501409
C	6.0	0.6937089458	9.4211824522	-2.5747311074
C	6.0	0.4218578136	10.7718764433	-2.7330203692
C	6.0	-0.7661883407	11.1598673791	-3.3585378199
C	6.0	-1.6671994906	10.2141688304	-3.8197138928
C	6.0	-1.3969426494	8.8521995183	-3.6642953936
O	8.0	-2.2265449691	7.8634011306	-4.0890955744
O	8.0	1.2316070467	11.7817088204	-2.3204779448
C	6.0	-3.4255694184	8.2303096433	-4.7235534528
C	6.0	2.4336553119	11.4255230193	-1.6854555095
H	1.0	4.0007404028	3.0784298712	-2.2295372040
H	1.0	3.4876609756	5.4955943404	-2.5184649199
H	1.0	-0.6246862779	4.7465134983	-1.5695445285
H	1.0	1.8003665514	1.2305593694	0.4988881103
H	1.0	3.0315898842	0.0287303948	0.1507559960
H	1.0	3.3041581415	0.8728869702	-1.9430936573
H	1.0	1.6335598649	0.5037057164	-2.3336269838
H	1.0	2.4455342537	-2.1927005837	0.4690857119
H	1.0	0.7376693480	-3.9595066968	0.7590935167
H	1.0	-1.6632817826	-3.4512920254	0.3751406329
H	1.0	-2.3424906413	-1.1627389121	-0.3262608507
H	1.0	-0.6514551411	6.3256325727	-3.2429936186
H	1.0	-2.5821412287	10.5474447374	-4.3020462445
H	1.0	-0.9657011061	12.2233505067	-3.4741112053

H	*1.0*	*1.6005141937*	*9.0592439630*	*-2.0962531391*
H	*1.0*	*-3.2379220800*	*8.8046962110*	*-5.6432283616*
H	*1.0*	*-3.9343545048*	*7.2981742964*	*-4.9818170912*
H	*1.0*	*-4.0725465707*	*8.8207919614*	*-4.0573875829*
H	*1.0*	*2.2512311254*	*10.8507694484*	*-0.7646605432*
H	*1.0*	*3.0824655712*	*10.8328771635*	*-2.3483394011*
H	*1.0*	*2.9382287200*	*12.3612198218*	*-1.4313531903*

Monomer – After Cycloaddition:

E= -1565.2522908358

ATOM	*CHARGE*	*X*	*Y*	*Z*
C	*6.0*	*1.0523083811*	*-1.2224382337*	*1.7785630779*
C	*6.0*	*-0.1150348553*	*-1.3392340905*	*1.0311110450*
C	*6.0*	*-0.1040689513*	*-0.9529594586*	*-0.2964443965*
C	*6.0*	*1.0545428568*	*-0.4538370504*	*-0.9177745651*
C	*6.0*	*2.2390003622*	*-0.3363186810*	*-0.1679121576*
C	*6.0*	*2.1964155251*	*-0.7254529310*	*1.1777204322*
C	*6.0*	*0.8854648511*	*-0.0297708702*	*-2.3182765303*
C	*6.0*	*1.0269272687*	*1.2110612479*	*-2.9155799403*
C	*6.0*	*1.7024845054*	*2.3926605744*	*-2.3808456255*
C	*6.0*	*2.9965703364*	*2.2661526757*	*-1.8539480891*
C	*6.0*	*3.7392505313*	*0.9600343085*	*-1.9130481035*
C	*6.0*	*3.6040144743*	*0.0895662409*	*-0.6665610684*
C	*6.0*	*1.0680482097*	*3.6337574997*	*-2.4069406258*
C	*6.0*	*1.6885541787*	*4.7651210967*	*-1.8711865809*
C	*6.0*	*2.9509813702*	*4.6222623500*	*-1.2826102229*
C	*6.0*	*3.5978156848*	*3.3976071808*	*-1.2998375507*
N	*7.0*	*1.0924824411*	*6.0308455004*	*-1.8398207403*
C	*6.0*	*0.3745413425*	*6.4083575633*	*-2.8299040365*
C	*6.0*	*-0.3226038624*	*7.6913225383*	*-2.8268258077*
C	*6.0*	*-0.2244377200*	*8.5367567713*	*-1.7150532483*
C	*6.0*	*-0.8808801371*	*9.7582660058*	*-1.6935427584*
C	*6.0*	*-1.6488384636*	*10.1391082267*	*-2.7972247008*
C	*6.0*	*-1.7575736029*	*9.3141080385*	*-3.9048488723*
C	*6.0*	*-1.0959187522*	*8.0837325028*	*-3.9323725127*
O	*8.0*	*-1.1507708457*	*7.2189112569*	*-4.9777232422*
C	*6.0*	*-1.9077782457*	*7.5847254049*	*-6.1036912344*
H	*1.0*	*-1.5275192324*	*8.5092110283*	*-6.5638446621*
H	*1.0*	*-1.8114293218*	*6.7630641645*	*-6.8177457124*
H	*1.0*	*-2.9702986184*	*7.7197837458*	*-5.8509261485*
O	*8.0*	*-0.8440374064*	*10.6432389852*	*-0.6627414916*
C	*6.0*	*-0.0804296360*	*10.2888177269*	*0.4623986488*
H	*1.0*	*-0.4541043503*	*9.3660362620*	*0.9317789084*
H	*1.0*	*0.9807716764*	*10.1502189017*	*0.2050884235*
H	*1.0*	*-0.1730232523*	*11.1155032939*	*1.1716447068*
H	*1.0*	*0.2568915715*	*5.7926670546*	*-3.7340572929*
H	*1.0*	*-2.3627320838*	*9.6386778393*	*-4.7471482871*

H	1.0	-2.1595305443	11.0995244968	-2.7649474356
H	1.0	0.3863139932	8.1846090061	-0.8871601587
H	1.0	0.0606326007	3.7008991923	-2.8165582947
H	1.0	3.4165343852	5.5027675059	-0.8433020720
H	1.0	4.6025130696	3.3113879681	-0.8818233666
H	1.0	4.0942859789	0.6206690477	0.1648134042
H	1.0	4.2066859304	-0.8218444766	-0.8204970888
H	1.0	4.8122421055	1.1688262878	-2.0371769278
H	1.0	3.4377991915	0.3956708914	-2.8050339973
N	7.0	0.2124764384	-0.7573618311	-3.2622431901
N	7.0	0.4341404107	1.1800867557	-4.1418297108
N	7.0	-0.0470066146	-0.0007298728	-4.3593048099
C	6.0	-0.1489231360	-2.1310340509	-3.2740505056
C	6.0	0.7201295926	-3.0890021406	-2.7587155557
C	6.0	0.3498581371	-4.4272315160	-2.7872210008
C	6.0	-0.8699876564	-4.8070288747	-3.3388243214
C	6.0	-1.7240156577	-3.8419460024	-3.8635373929
C	6.0	-1.3714883770	-2.4987016392	-3.8288162473
H	1.0	1.6785127727	-2.7833099451	-2.3431389125
H	1.0	-2.0223820862	-1.7276952280	-4.2337371659
H	1.0	-2.6774980510	-4.1339814414	-4.2993300730
H	1.0	-1.1533496256	-5.8574819507	-3.3631805648
H	1.0	1.0259507058	-5.1782893937	-2.3834903977
H	1.0	-1.0195218900	-1.0186471964	-0.8832279390
H	1.0	3.1107671160	-0.6337755250	1.7655249486
H	1.0	1.0696183136	-1.5100584301	2.8283055506
H	1.0	-1.0311287717	-1.7160881376	1.4813753106

Coordinates PM3 stationary point:

Oligomer – Before Cycloaddition:

E= -632.5412045710

ATOM	CHARGE	X	Y	Z
C	6.0	14.4021240518	32.7841415087	-1.5683919578
C	6.0	14.5581753379	31.4347355344	-1.8639268091
C	6.0	13.4899897104	30.7028174317	-2.3731059948
C	6.0	12.2666896835	31.3348220593	-2.5764657512
C	6.0	12.0863437270	32.7034194954	-2.2612025294
C	6.0	13.1760237865	33.4146908200	-1.7636725002
C	6.0	11.1243633865	30.7325354749	-3.1490105036
C	6.0	10.0227258819	30.7398841171	-3.6272822836
C	6.0	8.8339756735	31.3638281031	-4.0669920463
C	6.0	8.9158609559	32.7776611069	-4.0974440505
C	6.0	10.2124462399	33.4930070005	-3.8326862277
C	6.0	10.7437628151	33.3693118498	-2.3935859079
C	6.0	7.6555956498	30.7015260519	-4.3869337404

C	*6.0*	*6.5225015866*	*31.4520111034*	*-4.7270741744*
C	*6.0*	*6.5823272531*	*32.8504679183*	*-4.7446612046*
C	*6.0*	*7.7726899382*	*33.4998958069*	*-4.4338804242*
N	*7.0*	*5.2611406611*	*30.8570790554*	*-5.0497567379*
C	*6.0*	*5.1013491953*	*29.5706902819*	*-5.1120925965*
C	*6.0*	*3.7858820358*	*29.0053765343*	*-5.4293679325*
C	*6.0*	*2.7315399127*	*29.8331819063*	*-5.8133373426*
C	*6.0*	*1.4700063456*	*29.3042915112*	*-6.0976883102*
C	*6.0*	*1.2316972128*	*27.9178389704*	*-6.0073996881*
C	*6.0*	*2.2898505861*	*27.0839511996*	*-5.6389808337*
C	*6.0*	*3.5515240738*	*27.6132882198*	*-5.3522943366*
C	*6.0*	*-0.1026081501*	*27.3810879350*	*-6.2870442998*
O	*8.0*	*4.6343041033*	*26.8497885747*	*-4.9563034047*
O	*8.0*	*0.4205499448*	*30.0939709023*	*-6.5443988180*
C	*6.0*	*4.5096429226*	*25.4510013432*	*-5.0334851052*
C	*6.0*	*0.4424391008*	*31.4420917858*	*-6.1362401788*
N	*7.0*	*-0.3080912255*	*26.1070164114*	*-6.4244619397*
H	*1.0*	*0.1669151783*	*31.5358818387*	*-5.0803639830*
H	*1.0*	*1.4191036698*	*31.9217665372*	*-6.3006332013*
H	*1.0*	*-0.3204679385*	*31.8985101274*	*-6.7711199120*
H	*1.0*	*4.2801202079*	*25.1048894317*	*-6.0478284801*
H	*1.0*	*3.7626315904*	*25.0624856310*	*-4.3313731450*
H	*1.0*	*5.5084131266*	*25.1174148857*	*-4.7385044389*
H	*1.0*	*-0.9370452050*	*28.1050741326*	*-6.3817101580*
H	*1.0*	*5.9460136489*	*28.8806762993*	*-4.9202566752*
H	*1.0*	*5.6938999618*	*33.4384907802*	*-5.0048676481*
H	*1.0*	*7.8092394273*	*34.5957196889*	*-4.4585757917*
H	*1.0*	*7.6029359333*	*29.6019398803*	*-4.3695351759*
H	*1.0*	*13.6064366595*	*29.6420674107*	*-2.6173723669*
H	*1.0*	*15.2483591237*	*33.3571304234*	*-1.1750167798*
H	*1.0*	*13.0682534270*	*34.4775140514*	*-1.5169239966*
H	*1.0*	*10.0197401203*	*32.8079774706*	*-1.7683955018*
H	*1.0*	*10.7953847488*	*34.3819237523*	*-1.9454127307*
H	*1.0*	*10.0900094493*	*34.5676027001*	*-4.0759821930*
H	*1.0*	*10.9677781939*	*33.1134885758*	*-4.5506937252*
C	*6.0*	*-2.7265383825*	*26.4247414762*	*-6.9099801783*
C	*6.0*	*-1.6173075132*	*25.5941867504*	*-6.7077748333*
C	*6.0*	*-1.7546457218*	*24.2024513435*	*-6.7959251995*
C	*6.0*	*-3.0067489711*	*23.6695128437*	*-7.0884278587*
C	*6.0*	*-4.1370810527*	*24.5001766489*	*-7.2848436025*
C	*6.0*	*-3.9717302192*	*25.8804918084*	*-7.1943477994*
C	*6.0*	*-3.2826903069*	*22.2962852842*	*-7.2837908987*
C	*6.0*	*-3.9643441178*	*21.3680909750*	*-7.6269384198*
C	*6.0*	*-5.1308252775*	*20.7802051455*	*-8.1687630016*
C	*6.0*	*-6.0159239458*	*21.7230109612*	*-8.7448873945*
C	*6.0*	*-5.6456557578*	*23.1743370738*	*-8.8732670294*
C	*6.0*	*-5.5019910050*	*23.9231595784*	*-7.5371075839*
C	*6.0*	*-5.4503495624*	*19.4264712502*	*-8.1096111426*
C	*6.0*	*-6.6796022984*	*19.0007487262*	*-8.6259287133*
C	*6.0*	*-7.5678130277*	*19.9232944419*	*-9.1945565389*
C	*6.0*	*-7.2347089050*	*21.2708507005*	*-9.2463970413*
N	*7.0*	*-7.0975353417*	*17.6345636405*	*-8.6608165662*
C	*6.0*	*-6.8971562523*	*16.7891662260*	*-7.7012786208*
C	*6.0*	*-7.4726155302*	*15.4397456720*	*-7.8007537335*

C	6.0	-8.4706768235	15.1675031754	-8.7403159801
C	6.0	-9.0876778336	13.9162682306	-8.7860825491
C	6.0	-8.7208210362	12.8983339496	-7.8777385631
C	6.0	-7.7005062157	13.1558618226	-6.9659357523
C	6.0	-7.0768490401	14.4087035667	-6.9261511456
C	6.0	-9.4338850429	11.6145625728	-7.8965275692
O	8.0	-6.0145807093	14.6859655729	-6.0806537492
O	8.0	-10.1151460210	13.5995034054	-9.6582932003
C	6.0	-5.9443972965	13.9232288093	-4.8980646482
C	6.0	-10.3228201535	14.4600715167	-10.7515811023
N	7.0	-9.5441522522	10.8977997394	-6.8240183551
H	1.0	-10.6908099399	15.4442175240	-10.4379234500
H	1.0	-9.4248342486	14.5812463336	-11.3681364052
H	1.0	-11.0990325680	13.9331154257	-11.3132291012
H	1.0	-6.0743927364	12.8451186039	-5.0760659226
H	1.0	-4.9354648830	14.1329551991	-4.5350207141
H	1.0	-6.6904203526	14.2616803519	-4.1710260017
H	1.0	-9.9004685844	11.3139146538	-8.8501607173
H	1.0	-6.3350093674	17.0408356386	-6.7868640847
H	1.0	-8.5296176149	19.5874593098	-9.6008279804
H	1.0	-7.9378656409	21.9831157147	-9.6945003747
H	1.0	-4.7429446532	18.7174732038	-7.6636183759
H	1.0	-0.8942158685	23.5396824255	-6.6465655227
H	1.0	-2.6048230327	27.5176420087	-6.8406400193
H	1.0	-4.8300141896	26.5459045075	-7.3454460144
H	1.0	-5.7540780521	23.2497256019	-6.6926257767
H	1.0	-6.2551484727	24.7356389171	-7.4990811612
H	1.0	-6.4054358867	23.6914171382	-9.4931495023
H	1.0	-4.7014214797	23.2402506739	-9.4515454644
C	6.0	-11.7084212575	9.7927054747	-7.1670562361
C	6.0	-10.3558051603	9.7152186133	-6.8144795452
C	6.0	-9.8023486040	8.5053635544	-6.3799001444
C	6.0	-10.6212816723	7.3812114444	-6.3191721065
C	6.0	-11.9962631333	7.4485723179	-6.6523098031
C	6.0	-12.5187041894	8.6675335860	-7.0767707000
C	6.0	-10.1897681821	6.0717126125	-6.0038719236
C	6.0	-10.3190147735	4.8788003336	-5.9378629668
C	6.0	-11.0165848547	3.6616827095	-6.1165199224
C	6.0	-12.2150118715	3.8041468500	-6.8564011697
C	6.0	-12.5947233330	5.1093479511	-7.4981354670
C	6.0	-12.8967185648	6.2527481727	-6.5146374743
C	6.0	-10.6301077394	2.4311383591	-5.5928967952
C	6.0	-11.4529323363	1.3191799941	-5.8060482398
C	6.0	-12.6501294150	1.4477263151	-6.5211687742
C	6.0	-13.0239802395	2.6835207660	-7.0342353760
N	7.0	-11.0992670483	-0.0011926347	-5.3877507899
C	6.0	-10.6804711298	-0.2888498725	-4.1974006277
C	6.0	-10.4009226925	-1.6899966997	-3.8485595406
C	6.0	-10.8188583178	-2.7221411307	-4.6915602577
C	6.0	-10.5945676557	-4.0576578362	-4.3511192863
C	6.0	-9.9451889370	-4.3892200512	-3.1438692866
C	6.0	-9.5196642332	-3.3626540785	-2.3030474506
C	6.0	-9.7371461900	-2.0241871467	-2.6485240529
C	6.0	-9.7218745661	-5.7995735231	-2.7957614212

O	*8.0*	*-9.3089246425*	*-0.9536045097*	*-1.8847738820*
O	*8.0*	*-11.0065440300*	*-5.1338477420*	*-5.1180979967*
C	*6.0*	*-8.8695647153*	*-1.2236735572*	*-0.5761556733*
C	*6.0*	*-11.4820375324*	*-4.8630786842*	*-6.4136817361*
N	*7.0*	*-9.7959990915*	*-6.1928954264*	*-1.5653503752*
H	*1.0*	*-12.4219381108*	*-4.2987398155*	*-6.3996327280*
H	*1.0*	*-10.7445497191*	*-4.3379254634*	*-7.0315425225*
H	*1.0*	*-11.6563922491*	*-5.8681771259*	*-6.8075470606*
H	*1.0*	*-7.9390958931*	*-1.8034466650*	*-0.5648261428*
H	*1.0*	*-9.6299373106*	*-1.7328151655*	*0.0270439087*
H	*1.0*	*-8.6875733852*	*-0.2189770213*	*-0.1847572090*
H	*1.0*	*-9.5152583174*	*-6.4906039286*	*-3.6309902205*
H	*1.0*	*-10.5385911170*	*0.4777010293*	*-3.4181809071*
H	*1.0*	*-13.2960142277*	*0.5764177112*	*-6.6826893801*
H	*1.0*	*-13.9620650746*	*2.7721339075*	*-7.5952269725*
H	*1.0*	*-9.6943177681*	*2.3459342424*	*-5.0283748187*
H	*1.0*	*-8.7448912159*	*8.4312529452*	*-6.1027627767*
H	*1.0*	*-12.1390972460*	*10.7414093659*	*-7.5102423970*
H	*1.0*	*-13.5796382707*	*8.7448327837*	*-7.3428359623*
H	*1.0*	*-12.8313195547*	*5.8860264514*	*-5.4700001655*
H	*1.0*	*-13.9500093836*	*6.5714979221*	*-6.6478022225*
H	*1.0*	*-13.4799638455*	*4.9527529069*	*-8.1467956317*
H	*1.0*	*-11.7760553205*	*5.4044108012*	*-8.1859361923*
C	*6.0*	*-10.3228883461*	*-8.5836433681*	*-1.9020825308*
C	*6.0*	*-9.6486437741*	*-7.5726947718*	*-1.2079001434*
C	*6.0*	*-8.8628063472*	*-7.8829968131*	*-0.0910142622*
C	*6.0*	*-8.7612220655*	*-9.2121720236*	*0.3064475237*
C	*6.0*	*-9.4523457815*	*-10.2447742833*	*-0.3735358158*
C	*6.0*	*-10.2252581159*	*-9.9052482678*	*-1.4811297576*
C	*6.0*	*-7.9434055480*	*-9.6852561118*	*1.3576555925*
C	*6.0*	*-7.3996336723*	*-10.5403605587*	*2.0024864091*
C	*6.0*	*-7.0596590549*	*-11.8760729882*	*2.3149829375*
C	*6.0*	*-7.4555863967*	*-12.8050875135*	*1.3217570613*
C	*6.0*	*-8.0382092381*	*-12.3520118364*	*0.0113148679*
C	*6.0*	*-9.4130152190*	*-11.6680474166*	*0.1112400491*
C	*6.0*	*-6.4458843666*	*-12.2880633970*	*3.4928228281*
C	*6.0*	*-6.2410546432*	*-13.6579628311*	*3.7036244692*
C	*6.0*	*-6.6414531363*	*-14.5896988805*	*2.7398338724*
C	*6.0*	*-7.2397086764*	*-14.1602042731*	*1.5600061253*
N	*7.0*	*-5.5545791237*	*-14.0431412983*	*4.8993607870*
C	*6.0*	*-5.8996305171*	*-15.0798423797*	*5.5929588350*
C	*6.0*	*-5.1490162030*	*-15.4425083990*	*6.8028420352*
C	*6.0*	*-4.4671032953*	*-14.4753100759*	*7.5410277833*
C	*6.0*	*-3.7697623194*	*-14.8247855575*	*8.7021874184*
C	*6.0*	*-3.7364824925*	*-16.1633242317*	*9.1478944261*
C	*6.0*	*-4.4134413544*	*-17.1286133407*	*8.4024482909*
C	*6.0*	*-5.1144754051*	*-16.7803337828*	*7.2458548608*
C	*6.0*	*-3.0229921996*	*-16.6088284318*	*10.3547206468*
O	*8.0*	*-5.7436635706*	*-17.7165392518*	*6.4403388540*
O	*8.0*	*-3.0929564455*	*-13.9173261830*	*9.4989973604*
C	*6.0*	*-6.1442366933*	*-18.9106237198*	*7.0708576531*
C	*6.0*	*-2.9500533976*	*-12.6010554182*	*9.0216068058*
N	*7.0*	*-2.3495954303*	*-15.8754455040*	*11.1643271085*
H	*1.0*	*-2.4322547478*	*-12.5595083703*	*8.0565964479*

H	*1.0*	*-3.9128133010*	*-12.0819408895*	*8.9502076044*
H	*1.0*	*-2.3343072348*	*-12.1441740768*	*9.8014700064*
H	*1.0*	*-6.3797452839*	*-19.5627435032*	*6.2265212775*
H	*1.0*	*-5.3502504724*	*-19.3534845357*	*7.6907694955*
H	*1.0*	*-7.0346855341*	*-18.7471973856*	*7.6874223672*
H	*1.0*	*-3.0665260678*	*-17.6823536962*	*10.5930841590*
H	*1.0*	*-6.7467454783*	*-15.7298449082*	*5.3151510245*
H	*1.0*	*-6.4779612972*	*-15.6627065716*	*2.8993208548*
H	*1.0*	*-7.5382694286*	*-14.9008346502*	*0.8084332189*
H	*1.0*	*-6.1370843938*	*-11.5474682213*	*4.2395877427*
H	*1.0*	*-8.3289514619*	*-7.1014686541*	*0.4615650148*
H	*1.0*	*-10.9410919714*	*-8.3417325000*	*-2.7755747653*
H	*1.0*	*-10.7688989902*	*-10.6851535671*	*-2.0276054781*
H	*1.0*	*-9.7707845061*	*-11.6842075689*	*1.1609318139*
H	*1.0*	*-10.1512419384*	*-12.2666296429*	*-0.4593664531*
H	*1.0*	*-8.1218057694*	*-13.2227072533*	*-0.6696905492*
H	*1.0*	*-7.3085028250*	*-11.6704854379*	*-0.4715939067*
H	*1.0*	*-4.3953731906*	*-18.1840441925*	*8.7213232399*
H	*1.0*	*-4.4849123609*	*-13.4342865374*	*7.1893799035*
H	*1.0*	*-9.0177744971*	*-3.6268455668*	*-1.3624618265*
H	*1.0*	*-11.3321869374*	*-2.4663136764*	*-5.6296015506*
H	*1.0*	*-8.7722989500*	*15.9604992892*	*-9.4399070735*
H	*1.0*	*-7.3828093349*	*12.3743680418*	*-6.2556860934*
H	*1.0*	*2.1081997132*	*26.0016618933*	*-5.5773674958*
H	*1.0*	*2.8832983763*	*30.9234526802*	*-5.8949757132*
H	*1.0*	*15.5241848804*	*30.9462228139*	*-1.6997072350*
H	*1.0*	*-2.3066305853*	*-14.9035312169*	*10.9511691924*

Oligomer – After Cycloaddition:

E= -819.8792503438

ATOM	*CHARGE*	*X*	*Y*	*Z*
C	*6.0*	*-1.0221585668*	*0.3327853682*	*-1.7961336657*
C	*6.0*	*-2.0122027317*	*0.4528001667*	*-2.7670927044*
C	*6.0*	*-1.7752264437*	*1.2278883173*	*-3.8895965838*
C	*6.0*	*-0.5480009565*	*1.8878015132*	*-4.0719703533*
C	*6.0*	*0.4527211529*	*1.7740326674*	*-3.0986427230*
C	*6.0*	*0.1862900337*	*0.9871278593*	*-1.9645845621*
C	*6.0*	*-0.4537722416*	*2.7274120448*	*-5.2621918987*
C	*6.0*	*-0.3140337938*	*4.1122352902*	*-5.3462238791*
C	*6.0*	*0.0371681675*	*5.0363010881*	*-4.2781608315*
C	*6.0*	*1.1959634507*	*4.7714612146*	*-3.5305370674*
C	*6.0*	*2.0961963013*	*3.6389902694*	*-3.9051239509*
C	*6.0*	*1.8349582963*	*2.3529351197*	*-3.1403244696*
C	*6.0*	*-0.7474778120*	*6.1509986059*	*-3.9940645036*
C	*6.0*	*-0.3926050688*	*6.9905104515*	*-2.9310944762*
C	*6.0*	*0.7385846446*	*6.7075765910*	*-2.1549938023*
C	*6.0*	*1.5271771825*	*5.6070585528*	*-2.4642074010*
N	*7.0*	*-1.1397057868*	*8.1542984717*	*-2.5640537875*

C	*6.0*	*-2.1068037408*	*8.6229144782*	*-3.2911186960*
C	*6.0*	*-2.8306116369*	*9.8251714589*	*-2.8595079584*
C	*6.0*	*-2.4359995328*	*10.5119170625*	*-1.7098183141*
C	*6.0*	*-3.1269600946*	*11.6499080826*	*-1.2838875523*
C	*6.0*	*-4.2336858386*	*12.1214917554*	*-2.0094621867*
C	*6.0*	*-4.6350953594*	*11.4451898604*	*-3.1589664272*
C	*6.0*	*-3.9436373506*	*10.3065663026*	*-3.5863218339*
C	*6.0*	*-5.0211933716*	*13.2794818319*	*-1.5449268285*
O	*8.0*	*-4.2827496309*	*9.5727891124*	*-4.7076783443*
O	*8.0*	*-2.8348748568*	*12.3396739431*	*-0.1192095906*
C	*6.0*	*-5.3402849195*	*10.0445158649*	*-5.5046722879*
C	*6.0*	*-1.5438247123*	*12.1704629262*	*0.4124474933*
N	*7.0*	*-4.5850052871*	*14.4804835327*	*-1.7124468943*
N	*7.0*	*-0.6747699240*	*2.3261176770*	*-6.5945431922*
N	*7.0*	*-0.6747562166*	*3.4327445318*	*-7.4086353742*
N	*7.0*	*-0.4754838081*	*4.4690950029*	*-6.6936541171*
H	*1.0*	*-1.3928952278*	*11.1605391981*	*0.8125063055*
H	*1.0*	*-0.7564821322*	*12.3984949857*	*-0.3148726388*
H	*1.0*	*-1.5307017662*	*12.9006853609*	*1.2258750768*
H	*1.0*	*-5.1437664831*	*11.0413758414*	*-5.9159356125*
H	*1.0*	*-6.2965315683*	*10.0468299985*	*-4.9683984076*
H	*1.0*	*-5.3654507552*	*9.3048652415*	*-6.3098720001*
H	*1.0*	*-5.9709328394*	*13.0362445769*	*-1.0403233951*
H	*1.0*	*-2.4057000189*	*8.1272363062*	*-4.2342418557*
H	*1.0*	*1.0086706178*	*7.3547301818*	*-1.3120266819*
H	*1.0*	*2.4222758755*	*5.3938880987*	*-1.8685689119*
H	*1.0*	*-1.6343803481*	*6.3850834680*	*-4.6029804255*
H	*1.0*	*-2.5642779989*	*1.3303134517*	*-4.6438409952*
H	*1.0*	*-1.1995700671*	*-0.2735876869*	*-0.9017542296*
H	*1.0*	*0.9565947447*	*0.8888223840*	*-1.1889149317*
H	*1.0*	*2.1717401087*	*2.5116082426*	*-2.0926426254*
H	*1.0*	*2.4969779533*	*1.5616478310*	*-3.5511732234*
H	*1.0*	*3.1487422604*	*3.9413999613*	*-3.7218737788*
H	*1.0*	*2.0387080231*	*3.4527295926*	*-4.9968137616*
C	*6.0*	*-4.7803311350*	*16.2762152715*	*-0.0777918413*
C	*6.0*	*-5.2993696484*	*15.6133625147*	*-1.1966906181*
C	*6.0*	*-6.4472835375*	*16.0958042649*	*-1.8173190659*
C	*6.0*	*-7.1285702219*	*17.2137711609*	*-1.3037002935*
C	*6.0*	*-6.6573994135*	*17.8411343873*	*-0.1434049065*
C	*6.0*	*-5.4624838324*	*17.3663202542*	*0.4288034148*
C	*6.0*	*-8.3036599189*	*17.6195195713*	*-2.0704847363*
C	*6.0*	*-8.6700033109*	*18.8497571908*	*-2.6144990784*
C	*6.0*	*-8.0460916828*	*20.1495894627*	*-2.4134621123*
C	*6.0*	*-7.8954598305*	*20.6118684102*	*-1.0978723982*
C	*6.0*	*-8.3901545702*	*19.7976604991*	*0.0523232609*
C	*6.0*	*-7.2993988774*	*18.9347732419*	*0.6585875936*
C	*6.0*	*-7.5789003531*	*20.9090755731*	*-3.4847523025*
C	*6.0*	*-6.9654403630*	*22.1431138927*	*-3.2412638141*
C	*6.0*	*-6.8136772199*	*22.6101650347*	*-1.9289169172*
C	*6.0*	*-7.2777730626*	*21.8424793972*	*-0.8697541579*
N	*7.0*	*-6.4550586143*	*22.9853435409*	*-4.2797148312*
C	*6.0*	*-6.5854239663*	*22.6944237831*	*-5.5365849233*
C	*6.0*	*-6.0101945446*	*23.5765991412*	*-6.5583618782*
C	*6.0*	*-4.9915242232*	*24.4690117063*	*-6.2244971530*

C	6.0	-4.3943152253	25.2673339250	-7.2052780376
C	6.0	-4.8077670499	25.1750903920	-8.5437511237
C	6.0	-5.8417586124	24.3046929289	-8.8832161167
C	6.0	-6.4467962543	23.5140403076	-7.9013410667
C	6.0	-4.1212991768	25.9243171880	-9.6122423851
O	8.0	-7.4882334310	22.6378392398	-8.1429987553
O	8.0	-3.3279708183	26.1151004986	-6.9522131659
C	6.0	-7.9047196555	22.4679851363	-9.4749446398
C	6.0	-3.2545551035	26.6502313588	-5.6521161122
N	7.0	-4.3442106505	27.1803996599	-9.7932070878
N	7.0	-9.2585354724	16.6834153169	-2.5139439448
N	7.0	-10.1348035233	17.2412657797	-3.2503078819
N	7.0	-9.8324082841	18.5740793130	-3.3603237161
H	1.0	-4.1732105606	27.1727261894	-5.3631036665
H	1.0	-3.0199464437	25.8820463848	-4.9048697928
H	1.0	-2.4258787486	27.3578802645	-5.7378198980
H	1.0	-8.6963395742	21.7204290181	-9.3726240473
H	1.0	-8.3136555345	23.3899502572	-9.9045876411
H	1.0	-7.1047949354	22.0827393186	-10.1177963704
H	1.0	-3.4053418828	25.3380854965	-10.2114444749
H	1.0	-7.1098995119	21.7762832279	-5.8651611914
H	1.0	-6.3296368335	23.5754263196	-1.7364357660
H	1.0	-7.1544781106	22.2010321595	0.1591694032
H	1.0	-7.6863495310	20.5532272875	-4.5215771782
H	1.0	-6.8361115285	15.5900754503	-2.7107926599
H	1.0	-3.8559887985	15.9320436235	0.4004432795
H	1.0	-5.0598818678	17.8680421978	1.3181236121
H	1.0	-7.7133725019	18.4486365126	1.5675289654
H	1.0	-6.4969723977	19.6151147608	1.0185068461
H	1.0	-8.7776790402	20.4788953795	0.8386190478
H	1.0	-9.2580297024	19.1761474242	-0.2458756640
C	6.0	-2.5390682840	28.7139758527	-10.3760352927
C	6.0	-3.6231657672	27.9272459028	-10.7840644832
C	6.0	-4.0309385058	27.9171704310	-12.1203742447
C	6.0	-3.3100009925	28.6598479654	-13.0560671102
C	6.0	-2.1957976399	29.4155378006	-12.6653133197
C	6.0	-1.8341228108	29.4507918249	-11.3180371178
C	6.0	-3.7033521938	28.6974717607	-14.4567944633
C	6.0	-3.9953693263	29.8137810446	-15.2376415035
C	6.0	-4.1464177559	31.2196638644	-14.8723243041
C	6.0	-3.1859509744	31.9866207412	-14.2009239603
C	6.0	-1.7832403538	31.6088614359	-13.8270705153
C	6.0	-1.3888192338	30.1510658307	-13.6846908035
C	6.0	-5.3766547612	31.7970657163	-15.2302945945
C	6.0	-5.6602100025	33.1251206011	-14.9211956842
C	6.0	-4.7184242552	33.8887905028	-14.2174061039
C	6.0	-3.5085005332	33.3168101094	-13.8746432046
N	7.0	-6.8950301288	33.7744379553	-15.2346507771
C	6.0	-7.5914079487	33.5186181905	-16.2948576068
C	6.0	-8.8172993342	34.2918970363	-16.5473522419
C	6.0	-8.8790880006	35.6351020990	-16.1779479553
C	6.0	-10.0271665456	36.3898444341	-16.4369398126
C	6.0	-11.1333359077	35.8007804895	-17.0729075236
C	6.0	-11.0827797533	34.4568690177	-17.4353321958

C	6.0	-9.9336272432	33.7022210723	-17.1772002316
C	6.0	-12.3728727572	36.5632292169	-17.3159865856
O	8.0	-9.7970721159	32.3594164863	-17.4769431965
O	8.0	-10.1901829502	37.7114323311	-16.0587812663
C	6.0	-10.8400755542	31.7407718318	-18.1877170504
C	6.0	-9.0256458881	38.4328703984	-15.7416118037
N	7.0	-12.4428435318	37.3899806729	-18.3019441762
N	7.0	-3.8221267617	27.6071616800	-15.3398855225
N	7.0	-4.1646162133	28.0704402994	-16.5854165609
N	7.0	-4.2719077584	29.3380601063	-16.5341509686
H	1.0	-8.5656599046	38.0836140101	-14.8094514973
H	1.0	-8.2839147049	38.4122910585	-16.5481391801
H	1.0	-9.4113952548	39.4473528468	-15.6099034506
H	1.0	-11.0153646109	32.2042518353	-19.1654170150
H	1.0	-11.7754258376	31.7180418908	-17.6162677765
H	1.0	-10.4570796431	30.7246509361	-18.3170457639
H	1.0	-13.1924588633	36.3866809241	-16.6004712943
H	1.0	-7.3153567592	32.7522177392	-17.0384235065
H	1.0	-4.9314018602	34.9307000249	-13.9507976312
H	1.0	-2.7712648767	33.9293992160	-13.3398465261
H	1.0	-6.1200361093	31.1872804802	-15.7621028300
H	1.0	-4.9056534702	27.3365613542	-12.4356061327
H	1.0	-2.2376672071	28.7443247484	-9.3221251419
H	1.0	-0.9781110351	30.0602906286	-11.0050966559
H	1.0	-0.3176770432	30.1064125230	-13.3957693975
H	1.0	-1.4439221727	29.6392093063	-14.6666935802
H	1.0	-1.1216102964	32.0712487380	-14.5898626334
H	1.0	-1.5365016312	32.1143728674	-12.8677131950
C	6.0	-13.5564883236	39.5513166693	-18.1770514454
C	6.0	-13.6067895071	38.1971445489	-18.5274869527
C	6.0	-14.7398041766	37.6636286854	-19.1482471470
C	6.0	-15.8367957825	38.4911213840	-19.3846671989
C	6.0	-15.8173667541	39.8356598678	-18.9865964440
C	6.0	-14.6632392203	40.3587106126	-18.4036050464
C	6.0	-17.0362582362	37.9779890660	-20.0286174367
C	6.0	-17.7240513456	38.4935820707	-21.1265927854
C	6.0	-17.3251557547	39.5245894841	-22.0809689805
C	6.0	-16.9695158023	40.8383909907	-21.7480437559
C	6.0	-17.0513495385	41.5100822937	-20.4101024682
C	6.0	-17.0363932411	40.6856638440	-19.1371547552
C	6.0	-17.2547821222	39.1062386843	-23.4191549094
C	6.0	-16.8544892081	39.9781879756	-24.4295340009
C	6.0	-16.4722712886	41.2856761441	-24.1010458299
C	6.0	-16.5315597891	41.6893610293	-22.7800905668
N	7.0	-16.8307237982	39.6215828568	-25.8163461948
C	6.0	-17.1876938963	38.4434431807	-26.2248505247
C	6.0	-17.1990931992	38.1252508554	-27.6565556626
C	6.0	-16.3915760988	38.8324479061	-28.5486519162
C	6.0	-16.4080508558	38.5284562211	-29.9127444696
C	6.0	-17.2391240320	37.5060080880	-30.4042032028
C	6.0	-18.0477183862	36.7971617393	-29.5202611247
C	6.0	-18.0319352507	37.0996110789	-28.1548186785
C	6.0	-17.2438513632	37.1621742399	-31.8398289825
O	8.0	-18.8157265732	36.4621367259	-27.2101098715

O	*8.0*	*-15.6115392339*	*39.1527157109*	*-30.8583685822*
C	*6.0*	*-19.5889569296*	*35.3674372734*	*-27.6340667829*
C	*6.0*	*-15.0803575345*	*40.4086941769*	*-30.5127216349*
N	*7.0*	*-18.2816010350*	*37.4154426254*	*-32.5510145066*
N	*7.0*	*-17.7630694101*	*36.8733152657*	*-19.5569807899*
N	*7.0*	*-18.8131896337*	*36.6975201841*	*-20.2572023564*
N	*7.0*	*-18.8553280964*	*37.6575055653*	*-21.2357113402*
H	*1.0*	*-14.3236131704*	*40.3335313140*	*-29.7227347085*
H	*1.0*	*-15.8547395301*	*41.1239151755*	*-30.2130311196*
H	*1.0*	*-14.6127591413*	*40.7272430071*	*-31.4482161605*
H	*1.0*	*-20.3499440767*	*35.6534661372*	*-28.3696217679*
H	*1.0*	*-20.0693511121*	*35.0543851075*	*-26.7025004675*
H	*1.0*	*-18.9753645657*	*34.5521306303*	*-28.0342031919*
H	*1.0*	*-16.3149664084*	*36.7045602822*	*-32.2181952942*
H	*1.0*	*-17.5039312307*	*37.6579760277*	*-25.5103769502*
H	*1.0*	*-16.1336911135*	*41.9802356747*	*-24.8791449330*
H	*1.0*	*-16.2276535044*	*42.7144839334*	*-22.5306702038*
H	*1.0*	*-17.5297878190*	*38.0739351673*	*-23.6955774583*
H	*1.0*	*-14.7782601821*	*36.6077889016*	*-19.4407804650*
H	*1.0*	*-12.6568735641*	*39.9751452482*	*-17.7157343953*
H	*1.0*	*-14.6351950465*	*41.4150211799*	*-18.1122851462*
H	*1.0*	*-17.9511201712*	*40.0626438781*	*-19.0701651858*
H	*1.0*	*-17.0987012559*	*41.3808299294*	*-18.2735267788*
H	*1.0*	*-17.9822608151*	*42.1158371630*	*-20.4225210187*
H	*1.0*	*-16.2166980768*	*42.2418663760*	*-20.3430635883*
H	*1.0*	*-18.6995974985*	*36.0099756247*	*-29.9189111753*
H	*1.0*	*-15.7506963445*	*39.6385565733*	*-28.1650906482*
H	*1.0*	*-11.9574694273*	*34.0098075030*	*-17.9234307760*
H	*1.0*	*-8.0151863426*	*36.0891206687*	*-15.6734846969*
H	*1.0*	*-4.6503311864*	*24.5377999880*	*-5.1810200516*
H	*1.0*	*-6.1676800624*	*24.2584048634*	*-9.9295358578*
H	*1.0*	*-5.4962676667*	*11.8299264157*	*-3.7191127944*
H	*1.0*	*-1.5772008208*	*10.1408520490*	*-1.1318256244*
H	*1.0*	*-2.9732280961*	*-0.0565031725*	*-2.6419501337*
C	*6.0*	*-0.7706605407*	*0.9814177781*	*-7.1205548402*
C	*6.0*	*0.0149283033*	*-0.0372941643*	*-6.5686393359*
C	*6.0*	*-0.0700395297*	*-1.3229651079*	*-7.0880167321*
C	*6.0*	*-0.9227820585*	*-1.5953626965*	*-8.1531509800*
C	*6.0*	*-1.6975714306*	*-0.5790500284*	*-8.7015394578*
C	*6.0*	*-1.6301397833*	*0.7130169694*	*-8.1917605925*
H	*1.0*	*-2.2387313624*	*1.5064871555*	*-8.6437098870*
H	*1.0*	*-2.3665934296*	*-0.7941963536*	*-9.5417828498*
H	*1.0*	*-0.9849168811*	*-2.6109477848*	*-8.5581761705*
H	*1.0*	*0.5371000719*	*-2.1242133848*	*-6.6532984851*
H	*1.0*	*0.6824200547*	*0.1677409457*	*-5.7208223017*
C	*6.0*	*-10.6805217465*	*19.4948060231*	*-4.0876408909*
C	*6.0*	*-11.2378382309*	*19.1006163930*	*-5.3094452052*
C	*6.0*	*-12.0676007296*	*19.9816309605*	*-5.9939747899*
C	*6.0*	*-12.3400855456*	*21.2422290446*	*-5.4737467500*
C	*6.0*	*-11.7847641951*	*21.6282531100*	*-4.2579137189*
C	*6.0*	*-10.9576189180*	*20.7594483420*	*-3.5568450100*
H	*1.0*	*-12.0001636630*	*22.6205873028*	*-3.8472279318*
H	*1.0*	*-12.9906033238*	*21.9320105914*	*-6.0217388604*
H	*1.0*	*-12.5059979887*	*19.6779101209*	*-6.9508404164*

H	*1.0*	*-11.0390653961*	*18.1064124122*	*-5.7295603834*
H	*1.0*	*-10.5202737716*	*21.0728897368*	*-2.5995608622*
C	*6.0*	*-3.5516966268*	*26.2091543267*	*-15.0801945885*
C	*6.0*	*-2.4544242074*	*25.8467385689*	*-14.2905999060*
C	*6.0*	*-2.1956856196*	*24.5021321714*	*-14.0556546001*
C	*6.0*	*-3.0150509610*	*23.5224972616*	*-14.6077121717*
C	*6.0*	*-4.0990811528*	*23.8869509853*	*-15.3989747044*
C	*6.0*	*-4.3768211227*	*25.2279493158*	*-15.6409157034*
H	*1.0*	*-4.7367420644*	*23.1144320907*	*-15.8421836093*
H	*1.0*	*-5.2255222250*	*25.4989032358*	*-16.2814996636*
H	*1.0*	*-1.8057929484*	*26.6149235363*	*-13.8482587995*
H	*1.0*	*-1.3391752595*	*24.2153812074*	*-13.4360129707*
H	*1.0*	*-2.8024174412*	*22.4641004078*	*-14.4232230520*
C	*6.0*	*-19.9484062947*	*37.7427998625*	*-22.1815144833*
C	*6.0*	*-20.4524064923*	*36.5750033785*	*-22.7649497211*
C	*6.0*	*-21.5097940371*	*36.6662327737*	*-23.6632513627*
C	*6.0*	*-22.0622283239*	*37.9030138195*	*-23.9784243243*
C	*6.0*	*-21.5600908997*	*39.0603297226*	*-23.3914788554*
C	*6.0*	*-20.5057105717*	*38.9889007578*	*-22.4893264996*
H	*1.0*	*-22.8922269112*	*37.9666610207*	*-24.6900324183*
H	*1.0*	*-21.9062310354*	*35.7556281342*	*-24.1254086088*
H	*1.0*	*-20.0352951738*	*35.5910889614*	*-22.5160600785*
H	*1.0*	*-20.1087341762*	*39.9070170226*	*-22.0375118657*
H	*1.0*	*-21.9945625623*	*40.0341683831*	*-23.6412285943*
H	*1.0*	*-18.2281379250*	*37.1740025042*	*-33.5070457959*

Gamess File Headers:

Monomers:

```
$BASIS GBASIS=N31 NGAUSS=6 NDFUNC=1 $END
$CONTRL SCFTYP=RHF RUNTYP=OPTIMIZE DFTTYP=m06 $END
$STATPT OPTTOL=0.0005 NSTEP=25 $END
$contrl nzvar=1 $end
$zmat dlc=.t. auto=.t. $end
$SYSTEM mwords=100 $END
$scf dirscf =.t. $end
```

Oligomers:

```
$BASIS GBASIS=PM3 $END
$CONTRL SCFTYP=RHF RUNTYP=OPTIMIZE $END
$STATPT OPTTOL=0.0001 NSTEP=500 $END
$SYSTEM mwords=100 $END
```

2.4.5. UV-Vis Spectrum

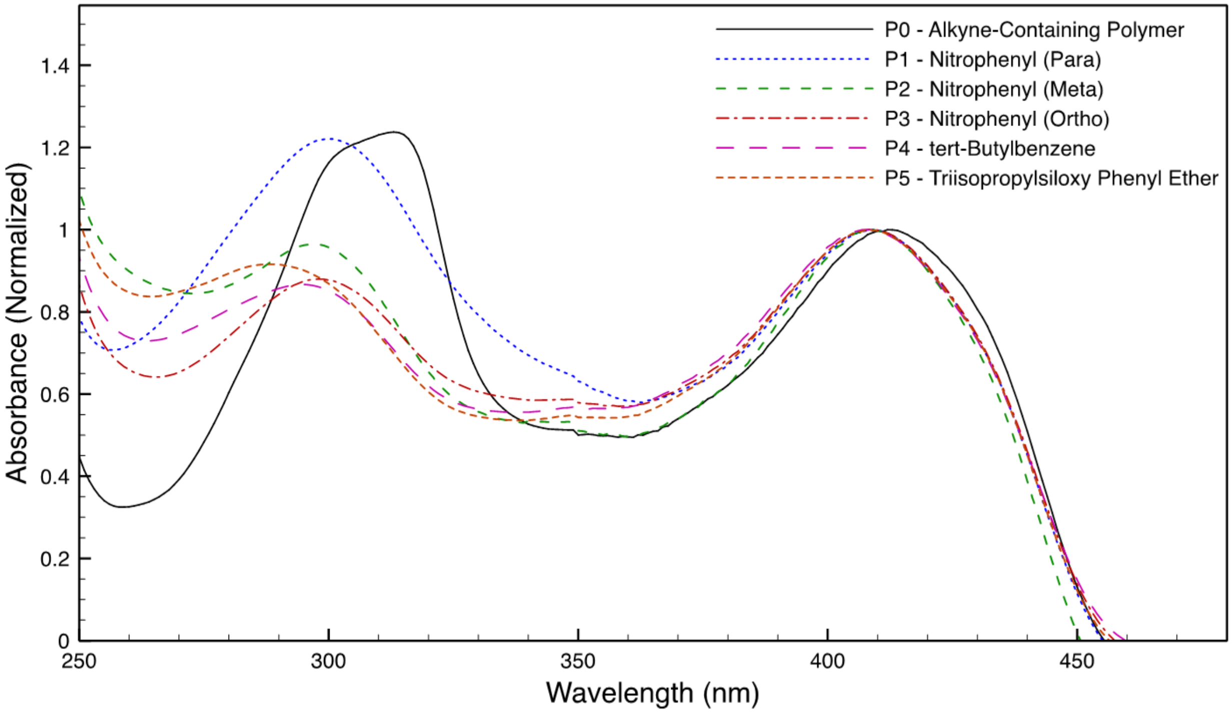

Figure 2.9. UV-Vis absorption spectra of **P0** to **P5** in THF, normalized to the absorption maxima at ca. 410 nm.

2.4.6. NMR Spectra

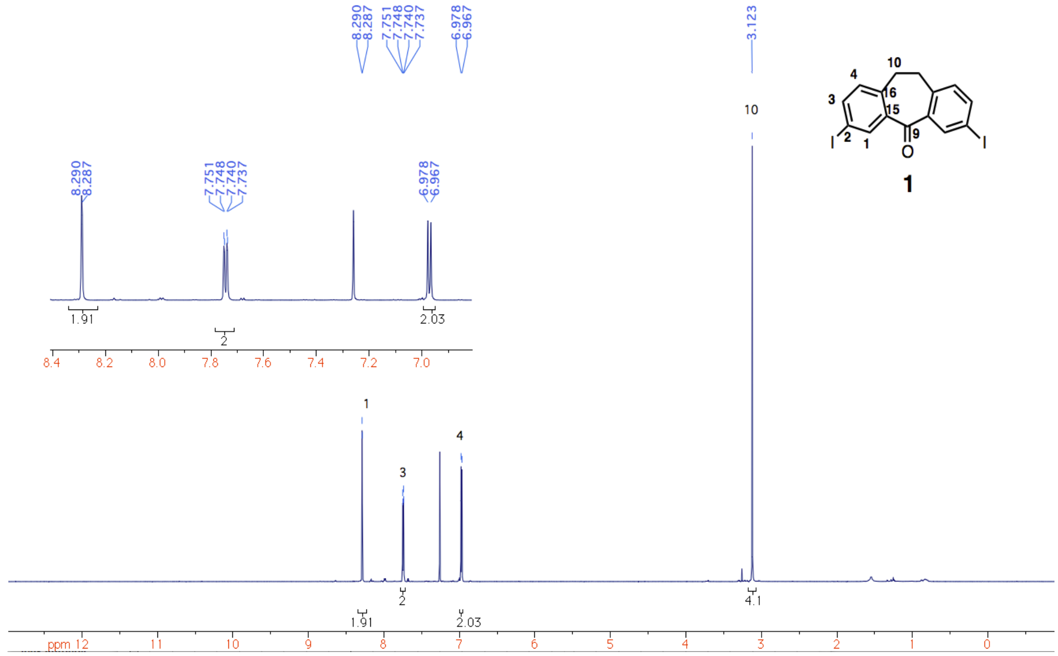

Figure 2.10. ^{1}H-NMR spectrum of **1** in $CDCl_3$.

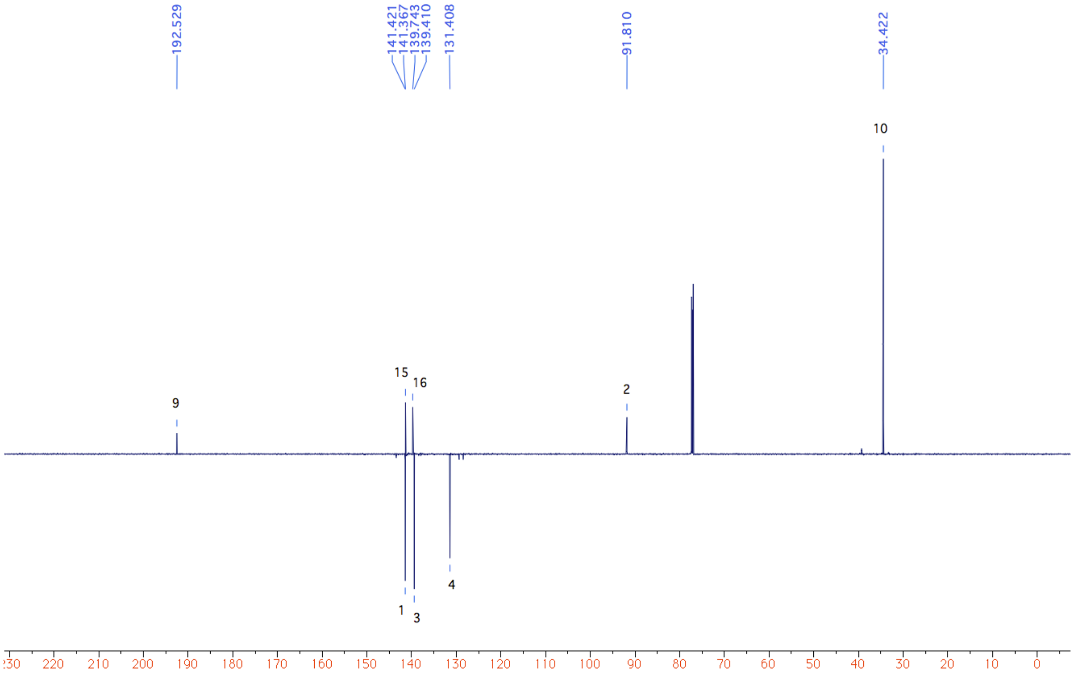

Figure 2.11. DEPTq spectrum of **1** in $CDCl_3$.

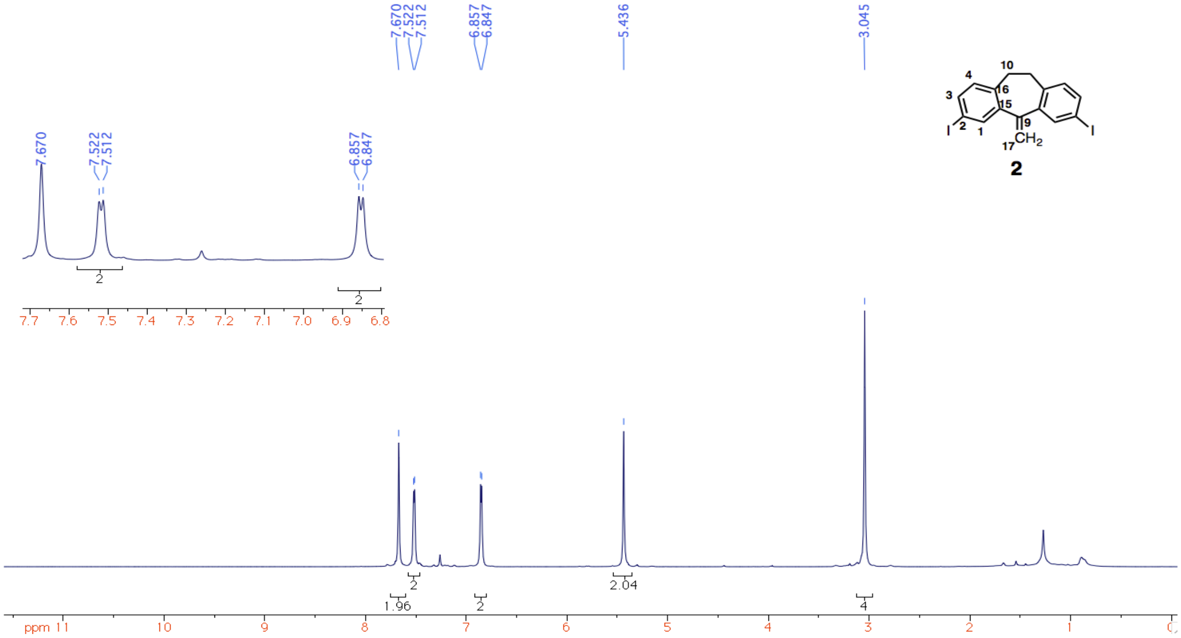

Figure 2.12. ^{1}H-NMR spectrum of **2** in $CDCl_3$.

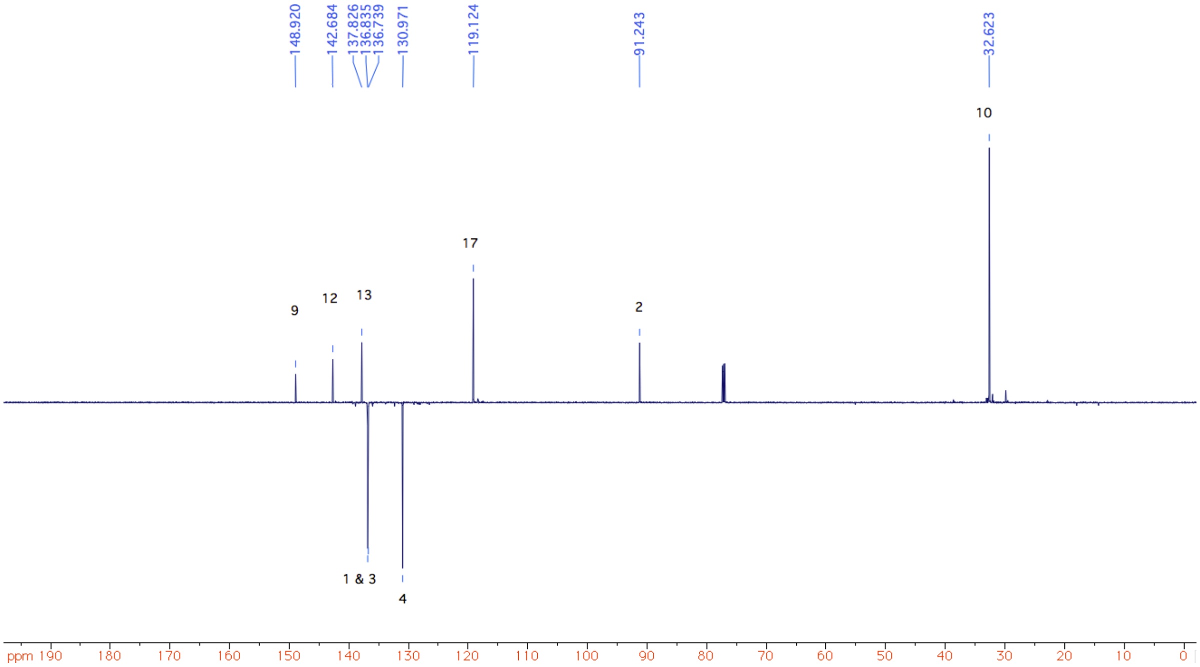

Figure 2.13. DEPTq spectrum of **2** in $CDCl_3$.

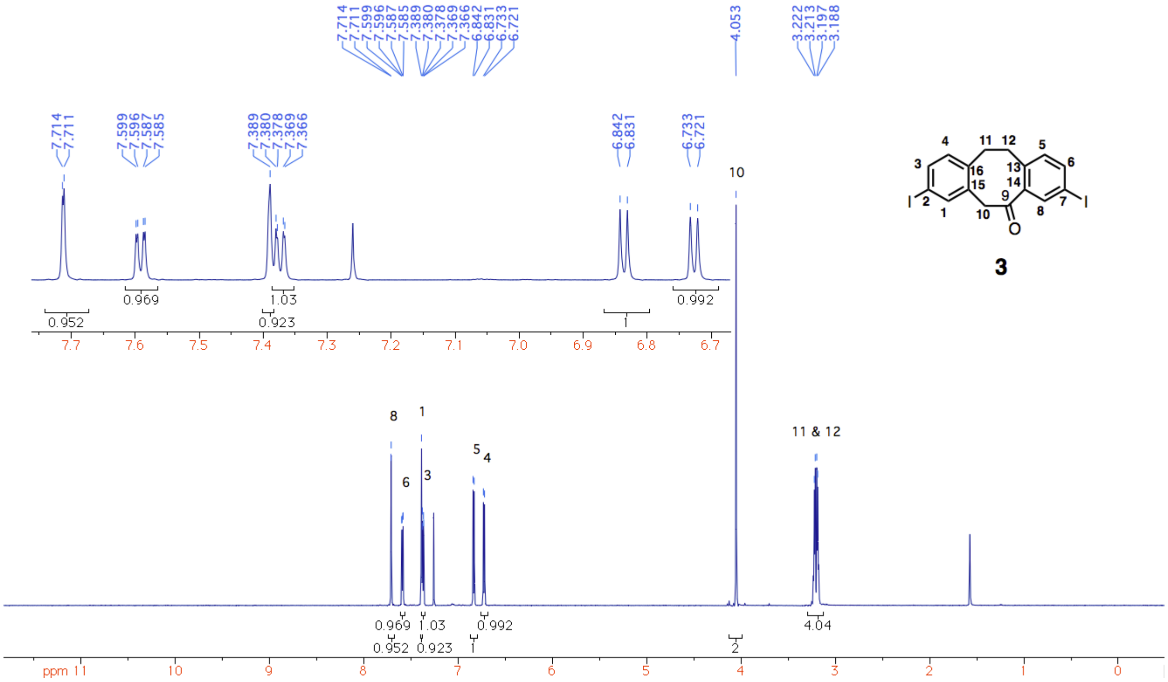

Figure 2.14. ^{1}H-NMR spectrum of **3** in $CDCl_3$.

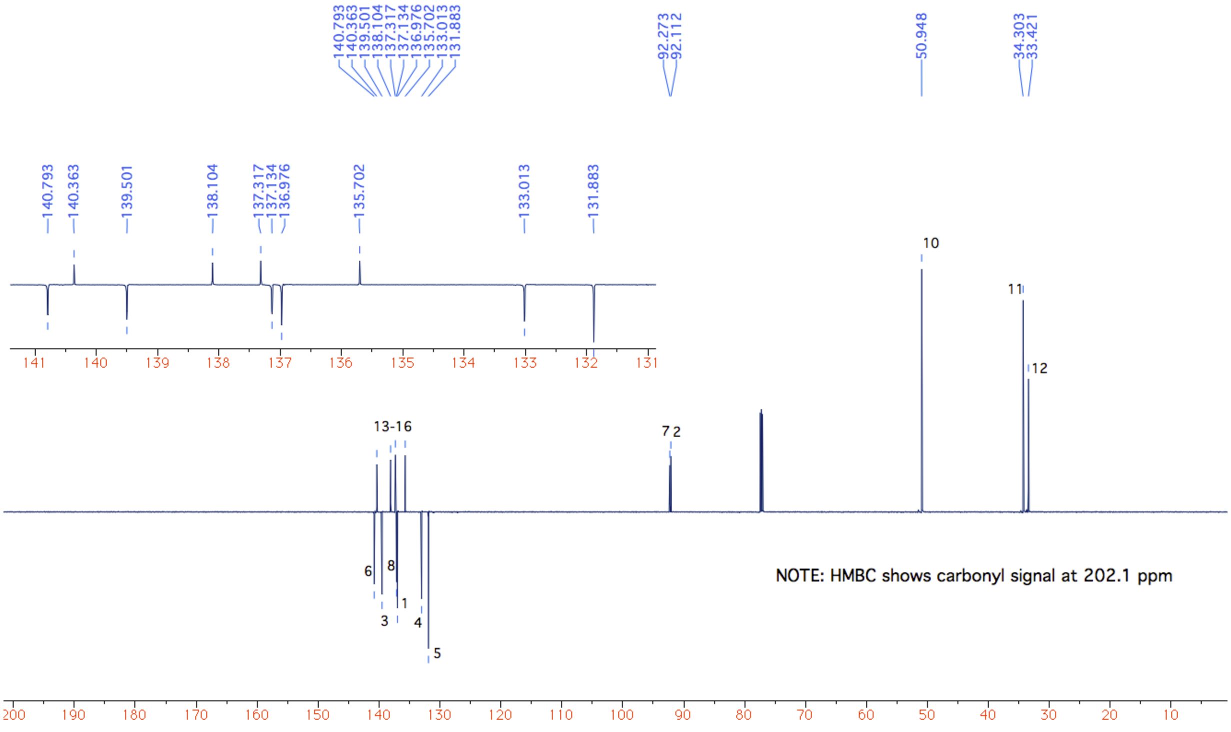

Figure 2.15. DEPTq spectrum of **3** in $CDCl_3$.

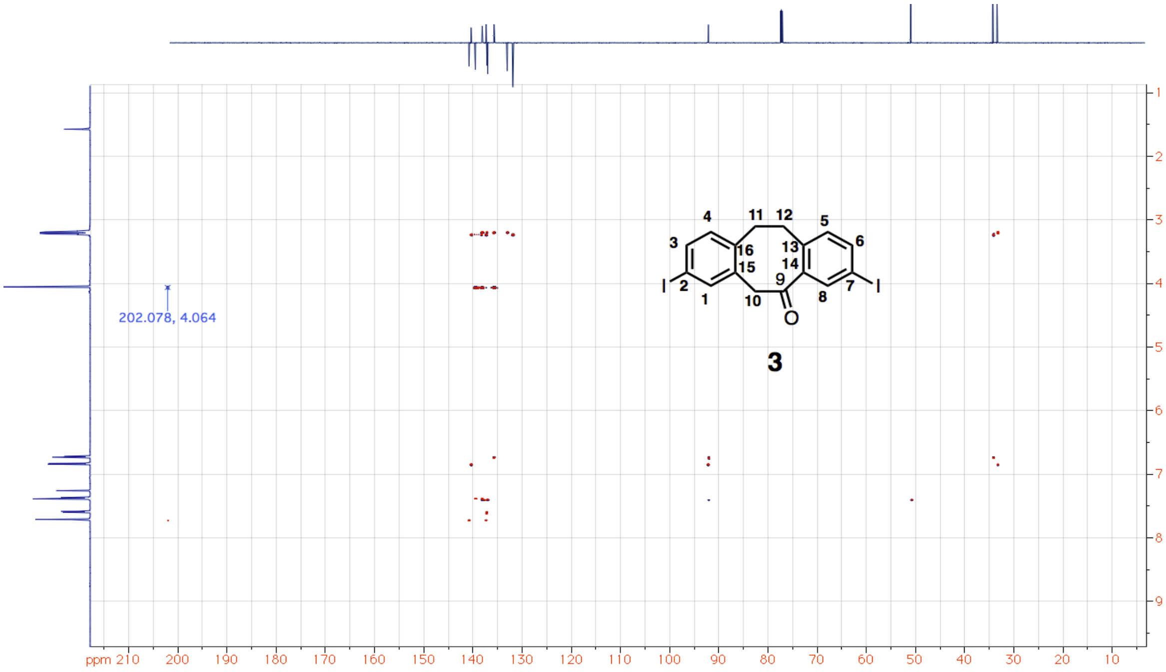

Figure 2.16. HMBC spectrum of **3** in $CDCl_3$.

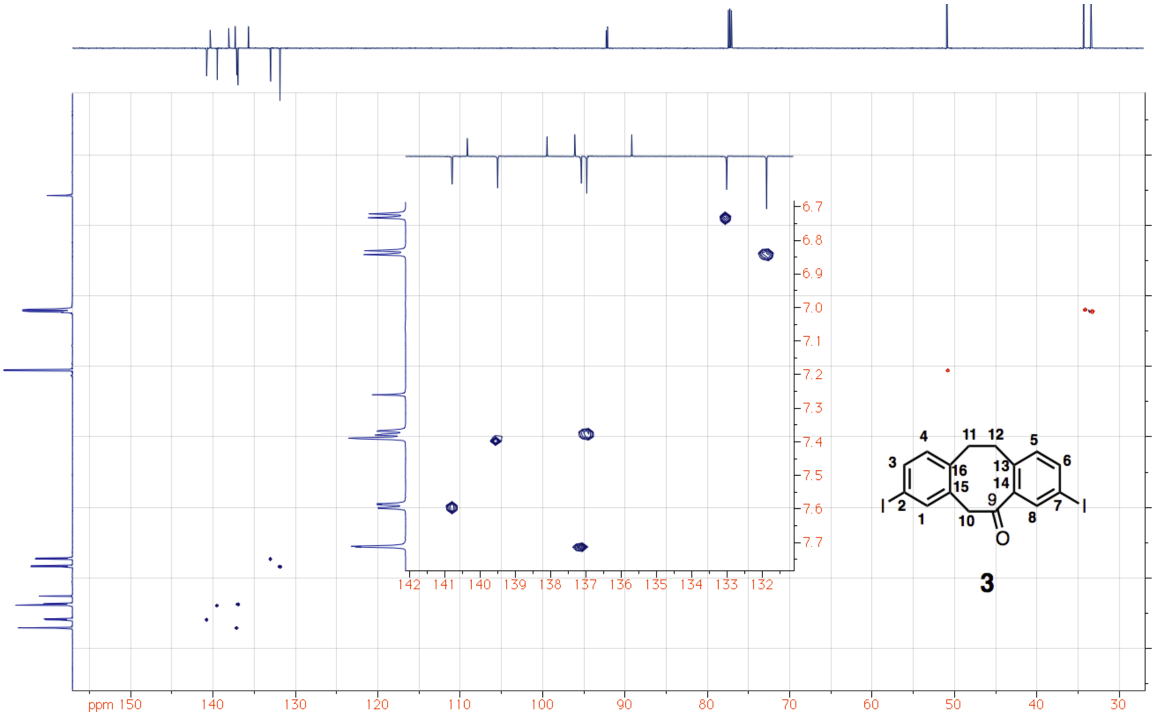

Figure 2.17. HSQC spectrum of **3** in $CDCl_3$.

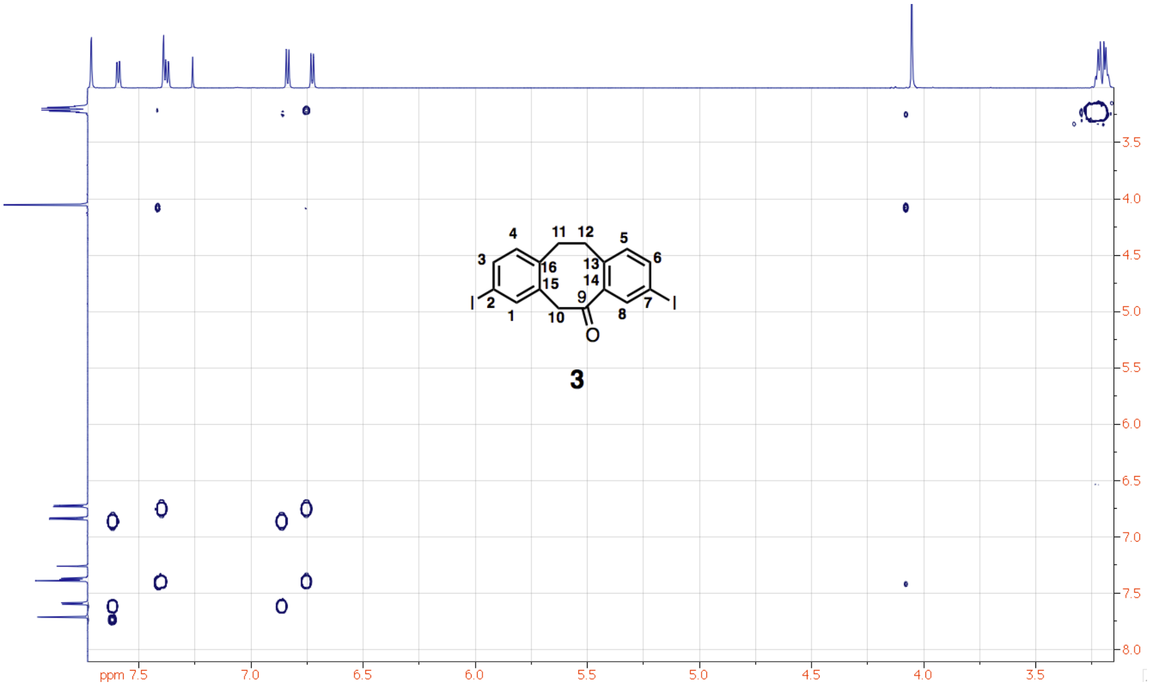

Figure 2.18. COSY spectrum of **3** in $CDCl_3$.

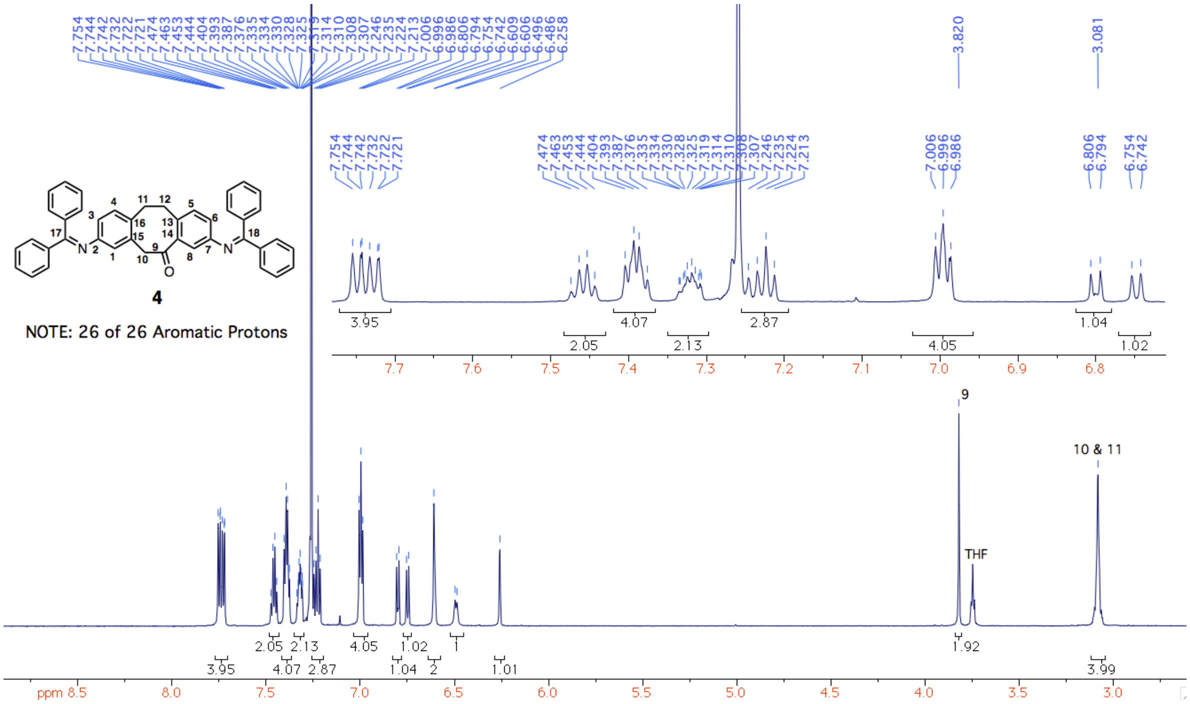

NOTE: 26 of 26 Aromatic Protons

Figure 2.19. ^{1}H-NMR spectrum of **4** in $CDCl_3$.

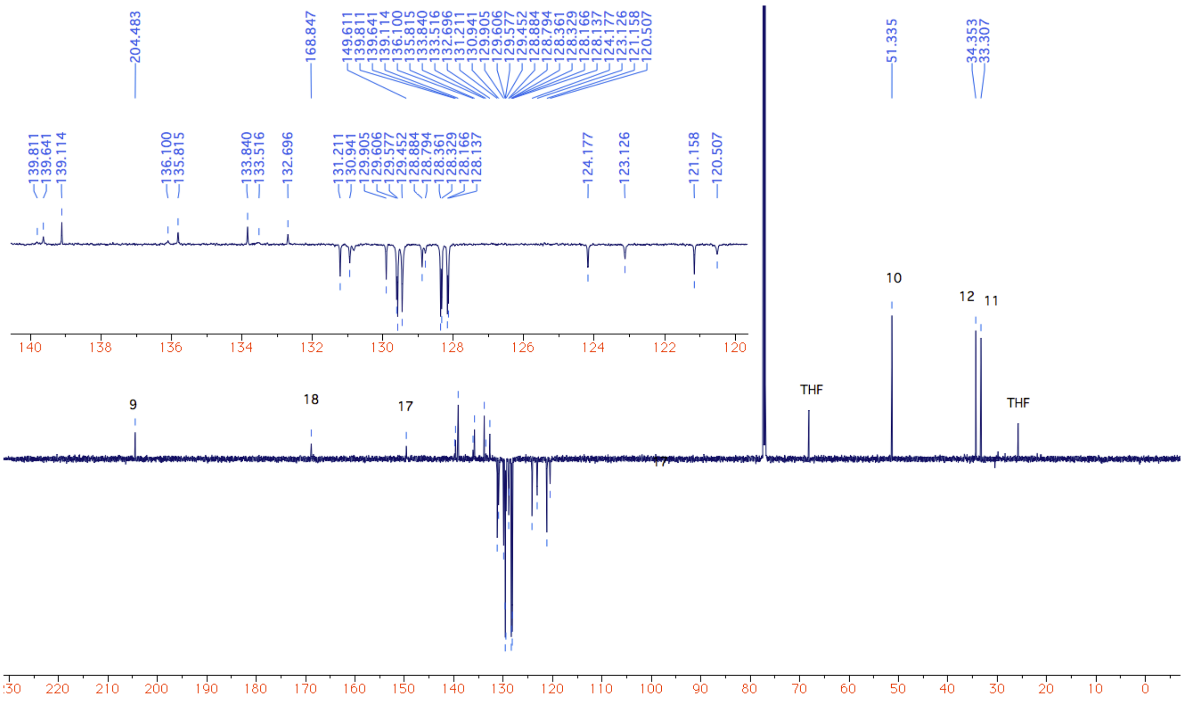

Figure 2.20. DEPTq spectrum of **4** in $CDCl_3$.

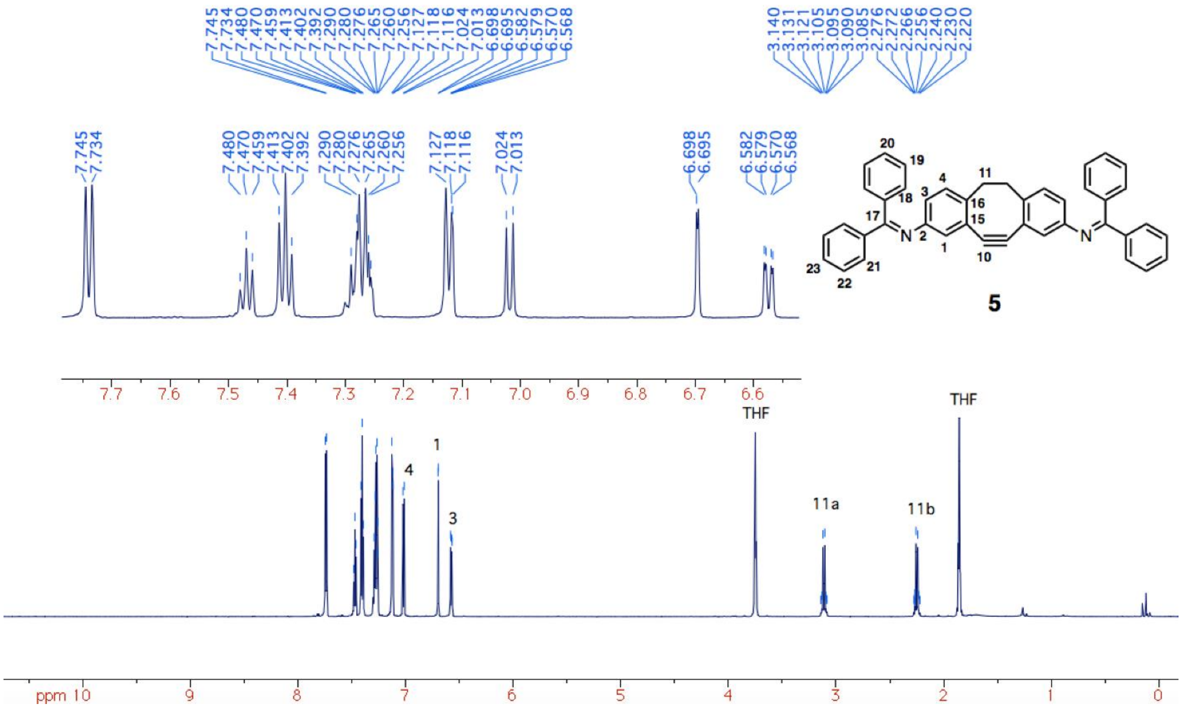

Figure 2.21. ^{1}H-NMR spectrum of **5** in $CDCl_3$.

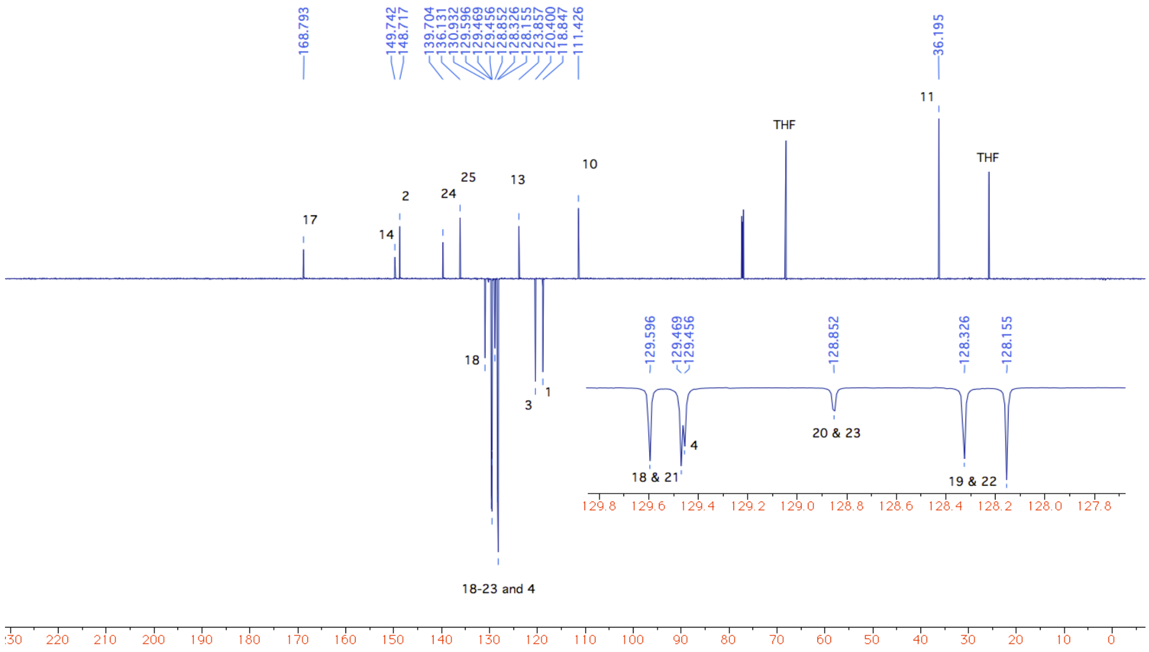

Figure 2.22. DEPTq spectrum of **5** in $CDCl_3$

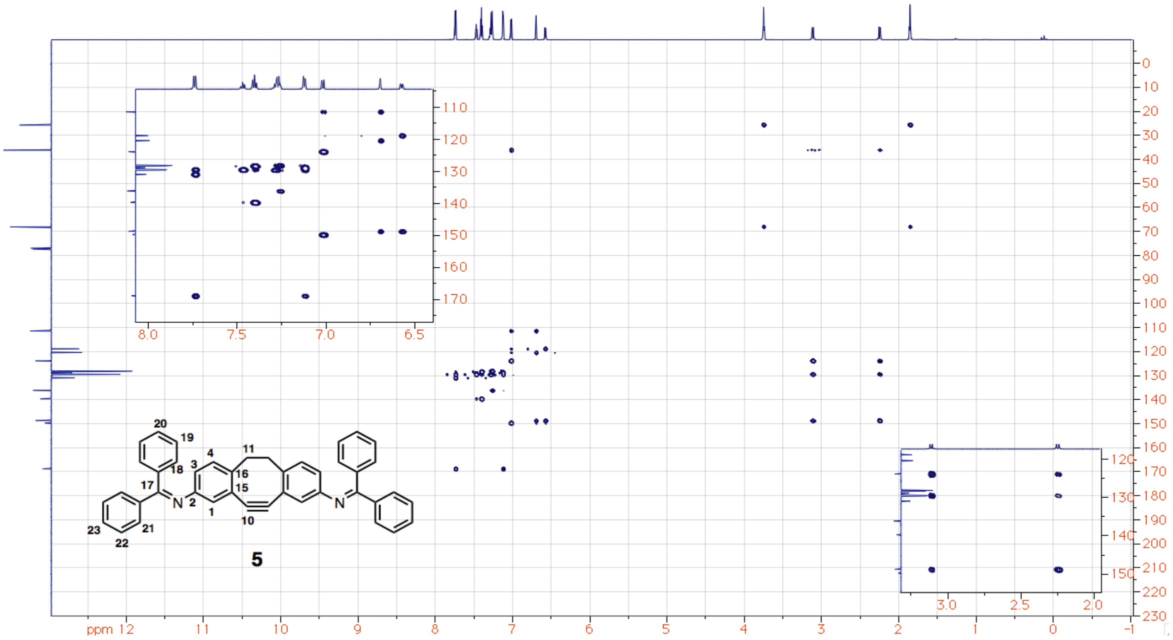

Figure 2.23. HMBC spectrum of **5** in $CDCl_3$.

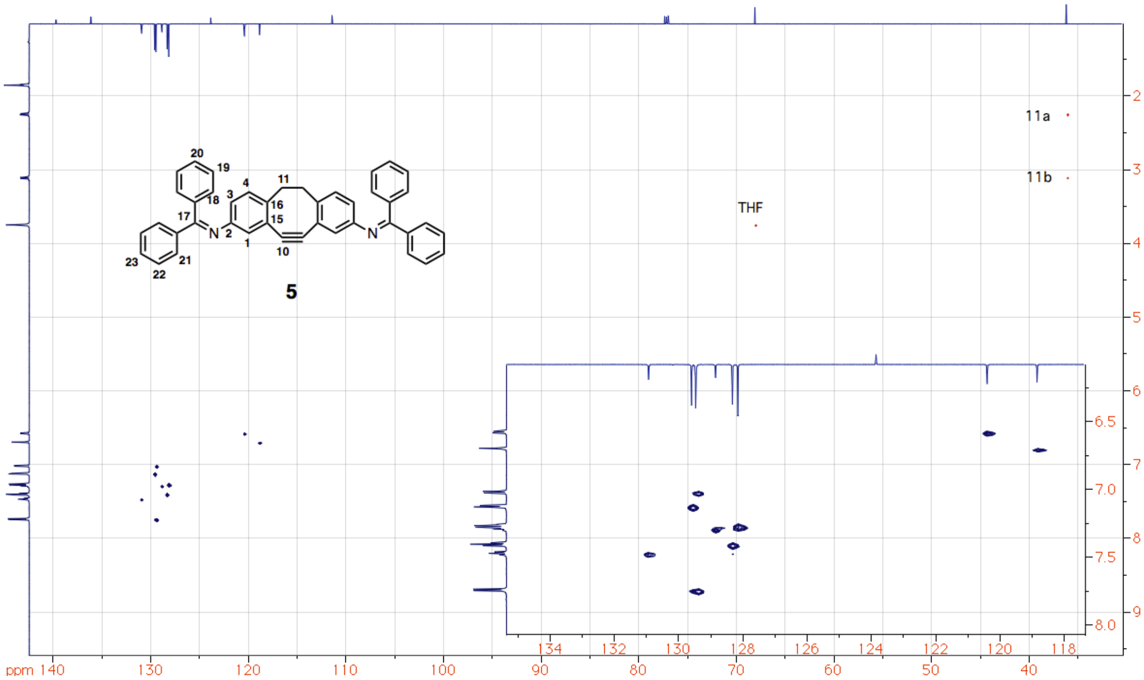

Figure 2.24. HSQC spectrum of **5** in $CDCl_3$.

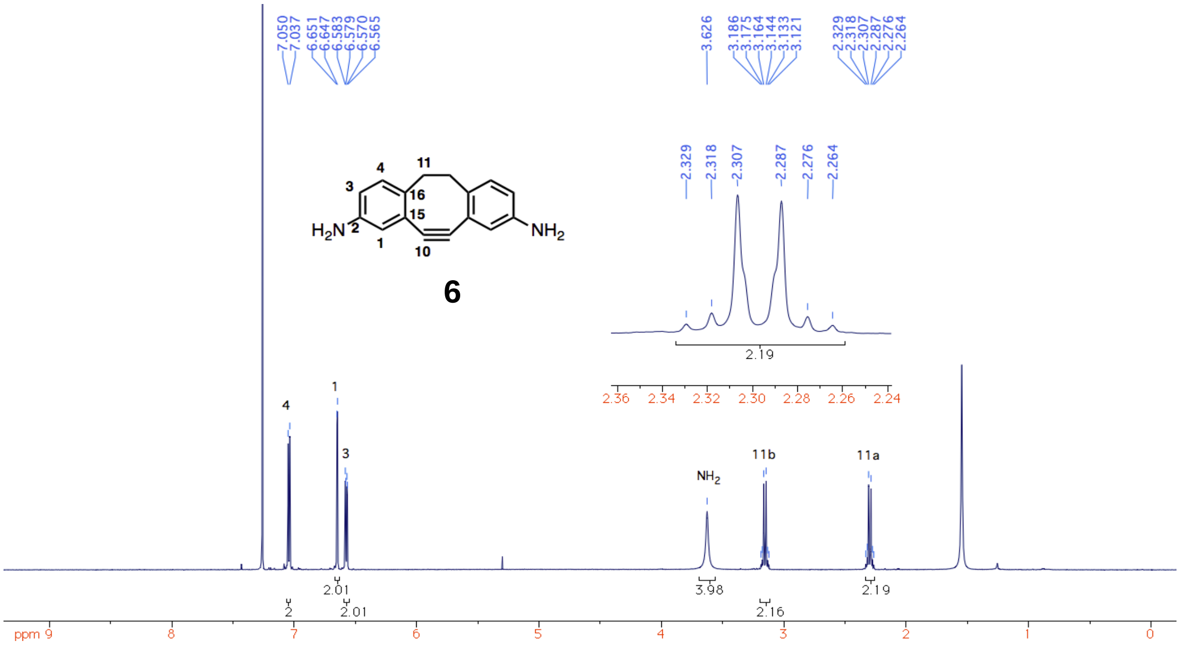

Figure 2.25. ^{1}H-NMR spectrum of **6** in CDCl$_3$.

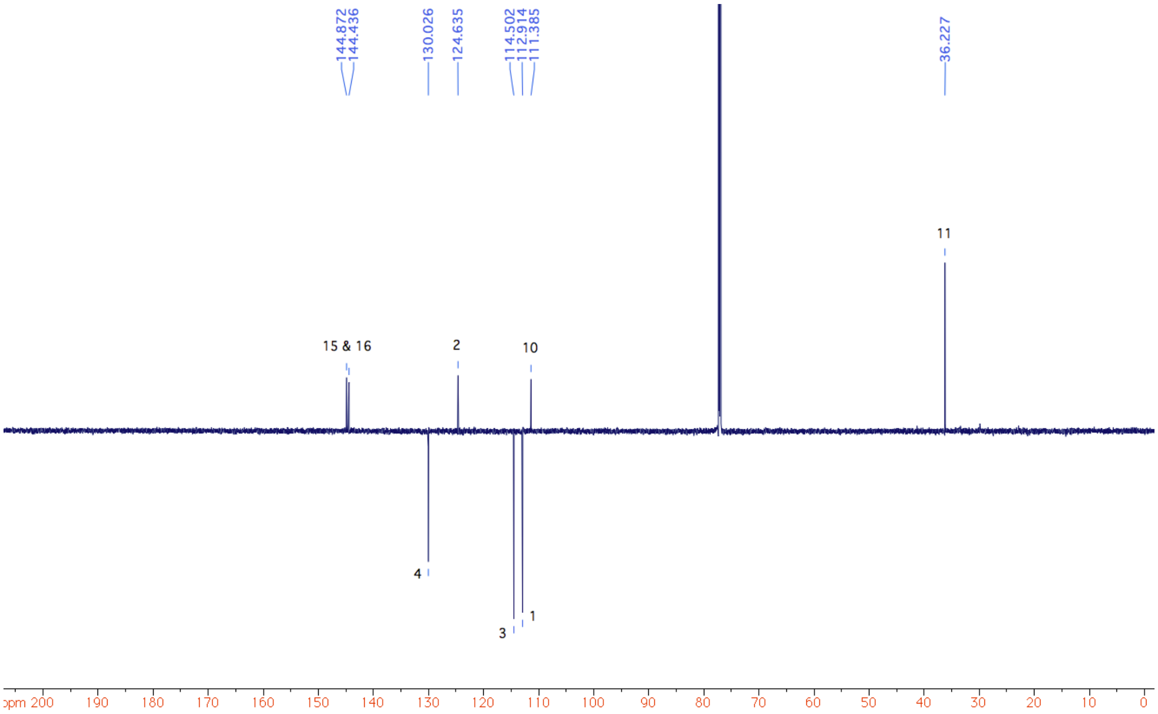

Figure 2.26. DEPTq spectrum of **6** in CDCl$_3$.

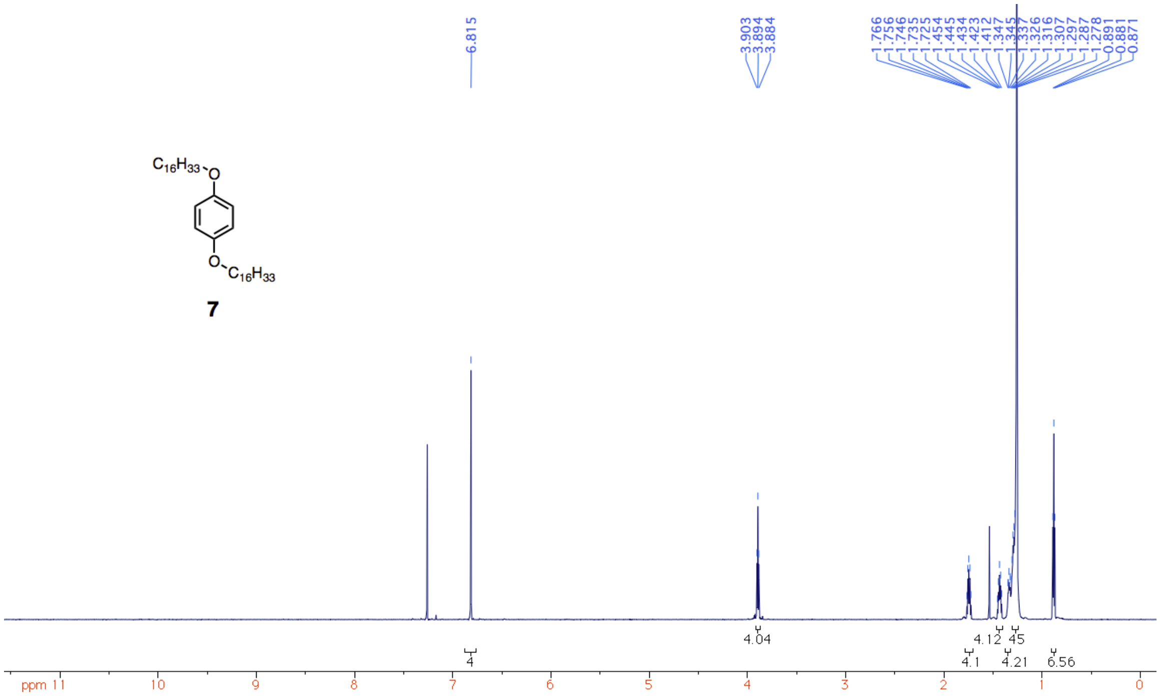

Figure 2.27. ^{1}H-NMR spectrum of **7** in $CDCl_3$.

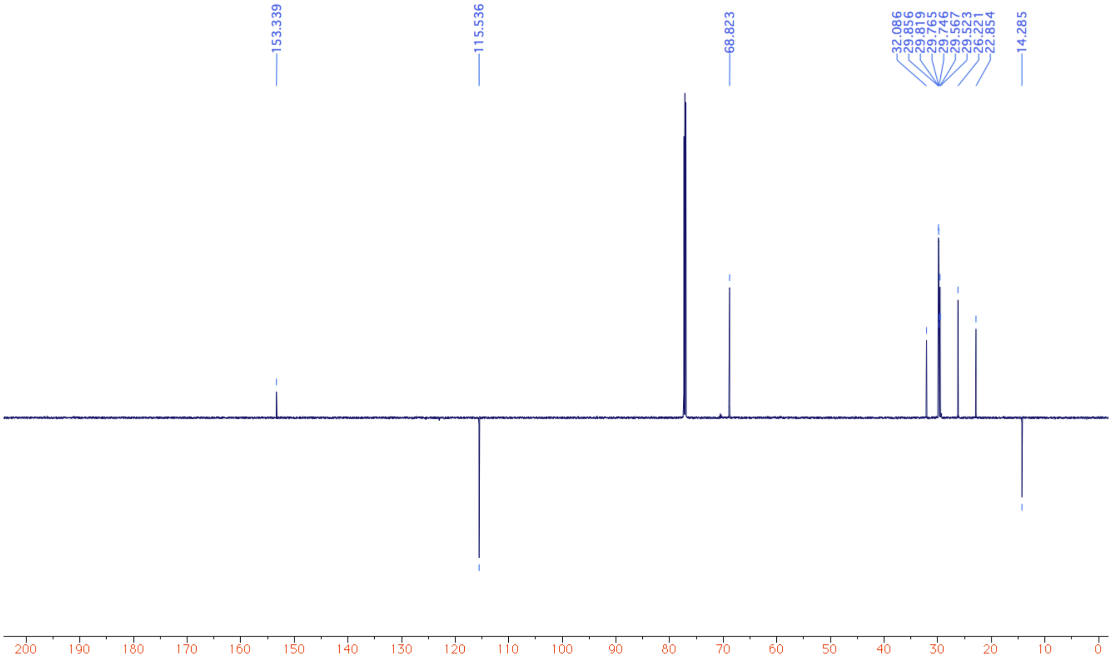

Figure 2.28. DEPTq spectrum of **7** in $CDCl_3$.

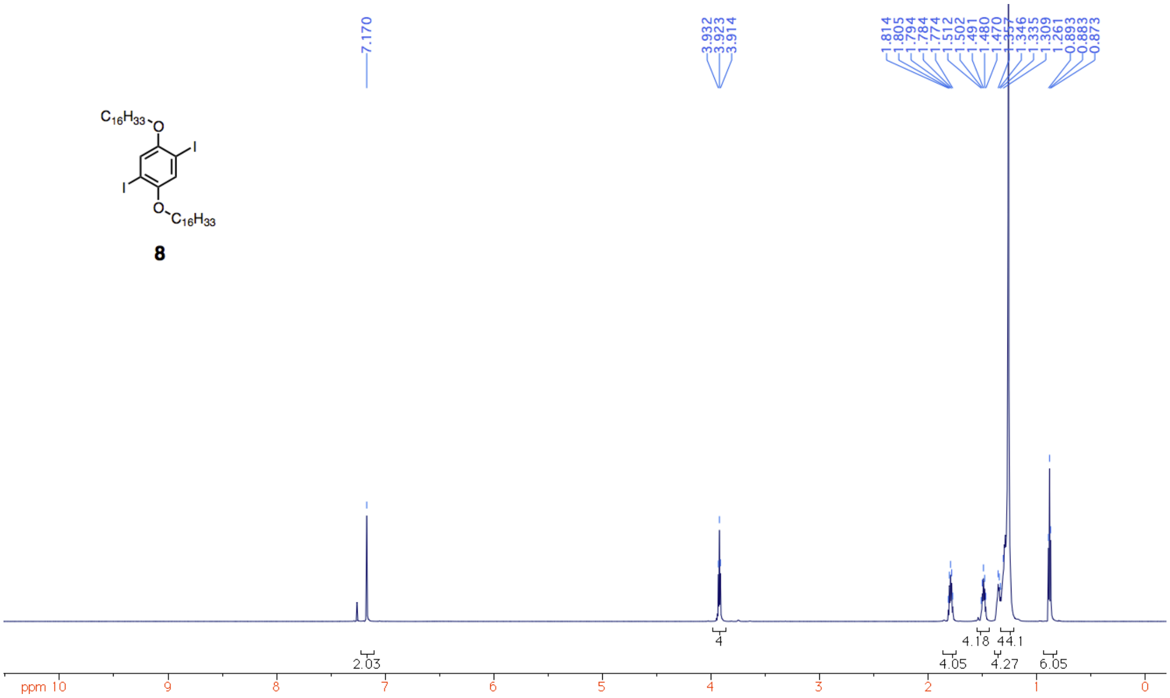

Figure 2.29. ^{1}H-NMR spectrum of **8** in $CDCl_3$.

Figure 2.30. DEPTq spectrum of **8** in $CDCl_3$.

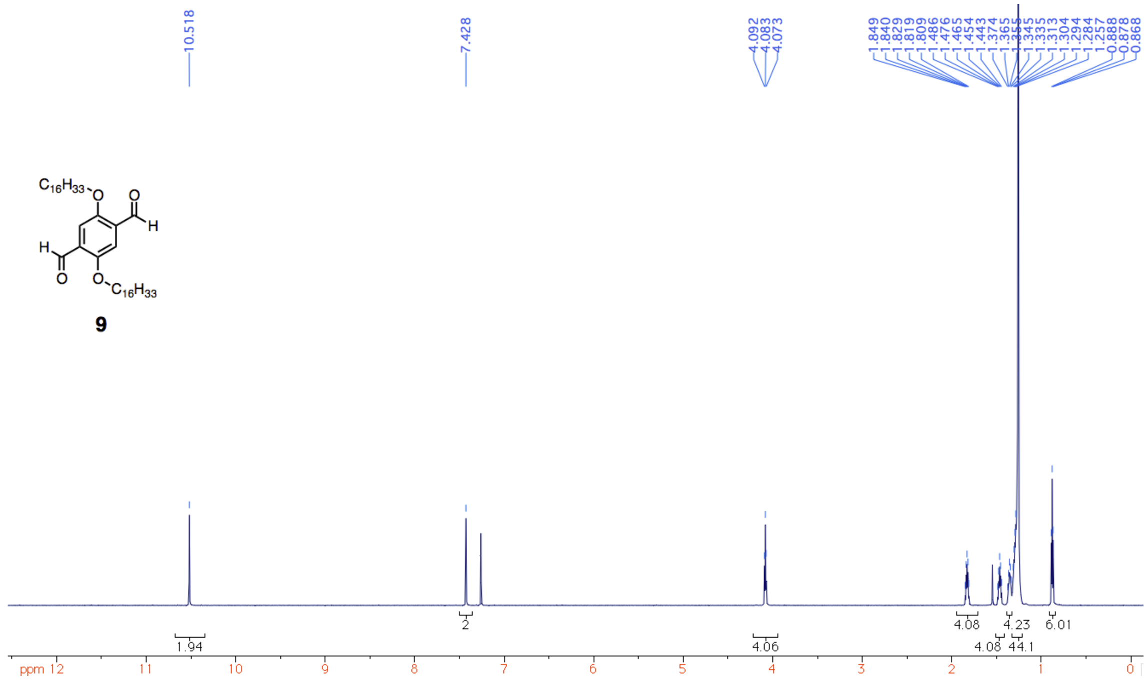

9

Figure 2.31. ^{1}H-NMR spectrum of **9** in $CDCl_3$.

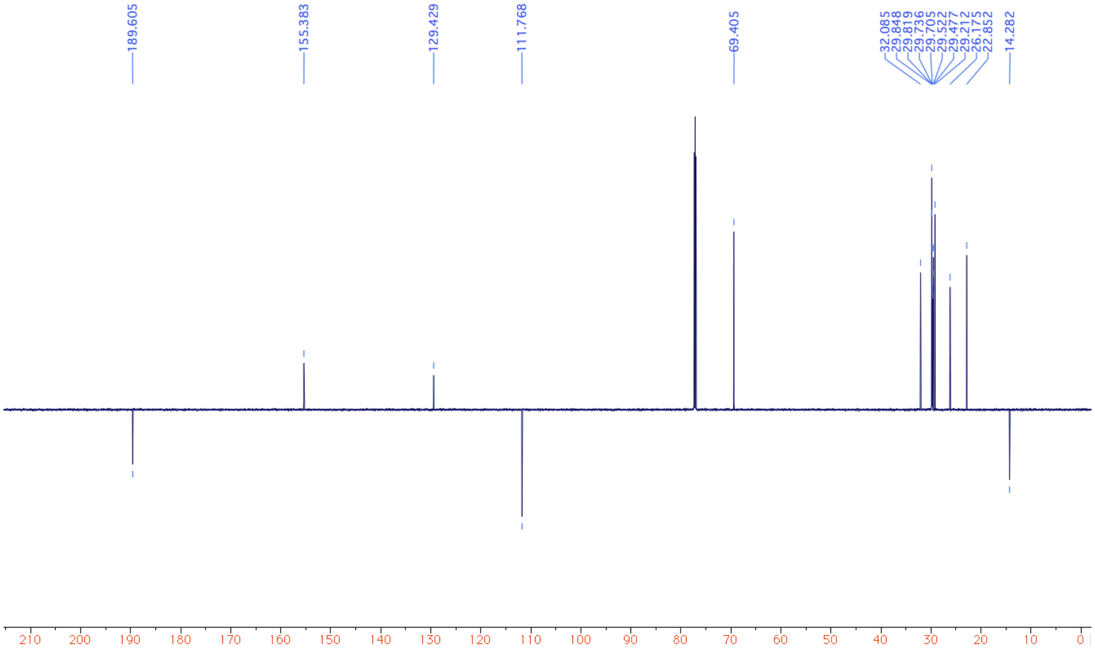

Figure 2.32. DEPTq spectrum of **9** in $CDCl_3$.

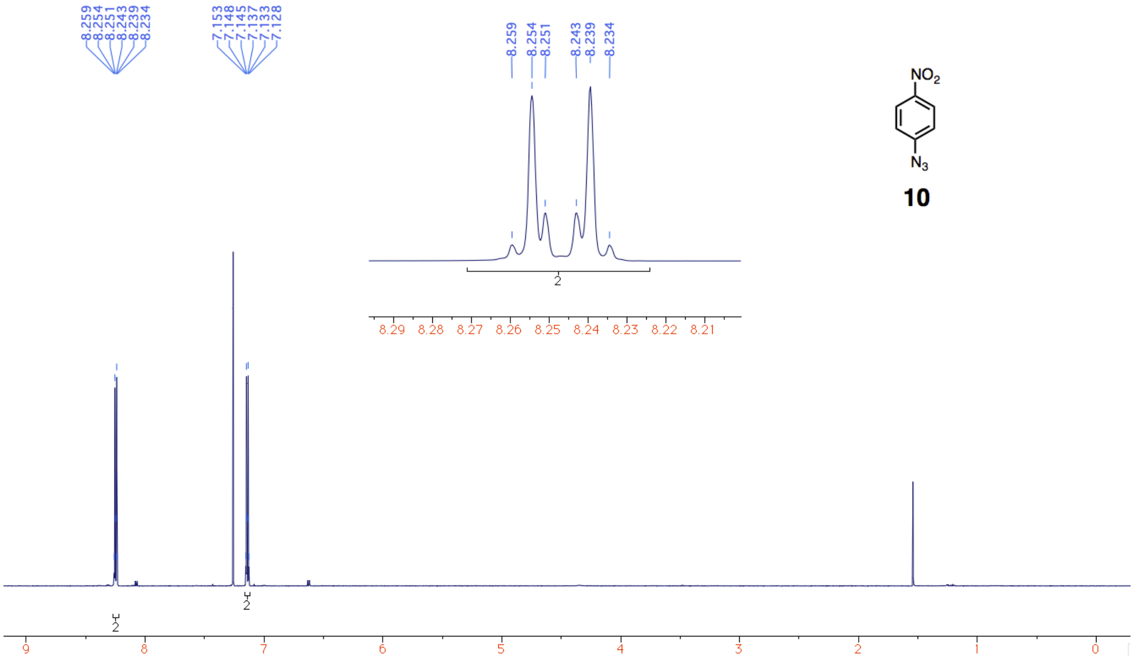

Figure 2.33. ^{1}H-NMR spectrum of **10** in CDCl$_3$.

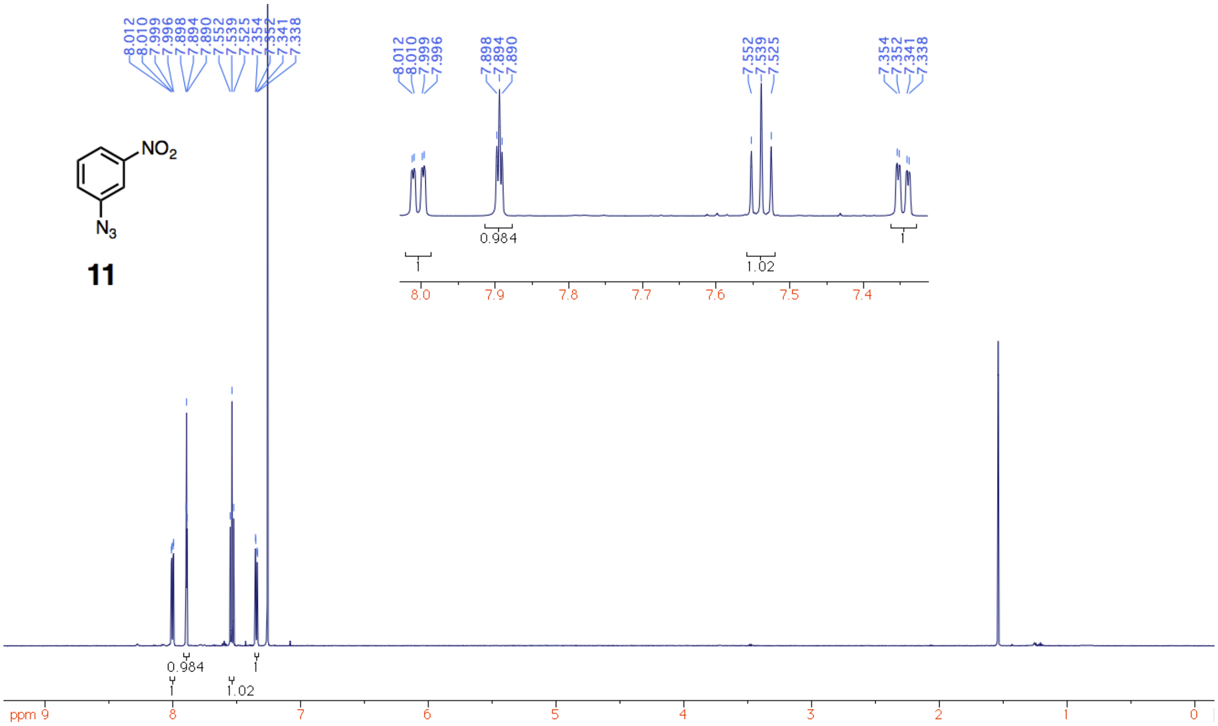

Figure 2.34. ^{1}H-NMR spectrum of **11** in CDCl$_3$.

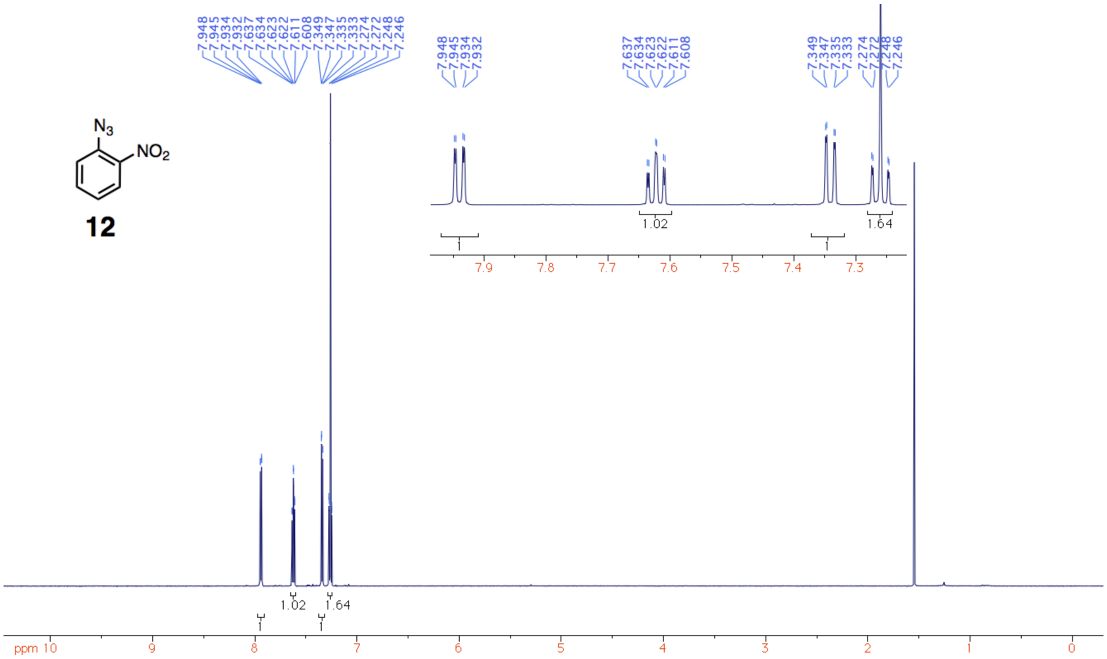

Figure 2.35. ^{1}H-NMR spectrum of **12** in CDCl$_3$.

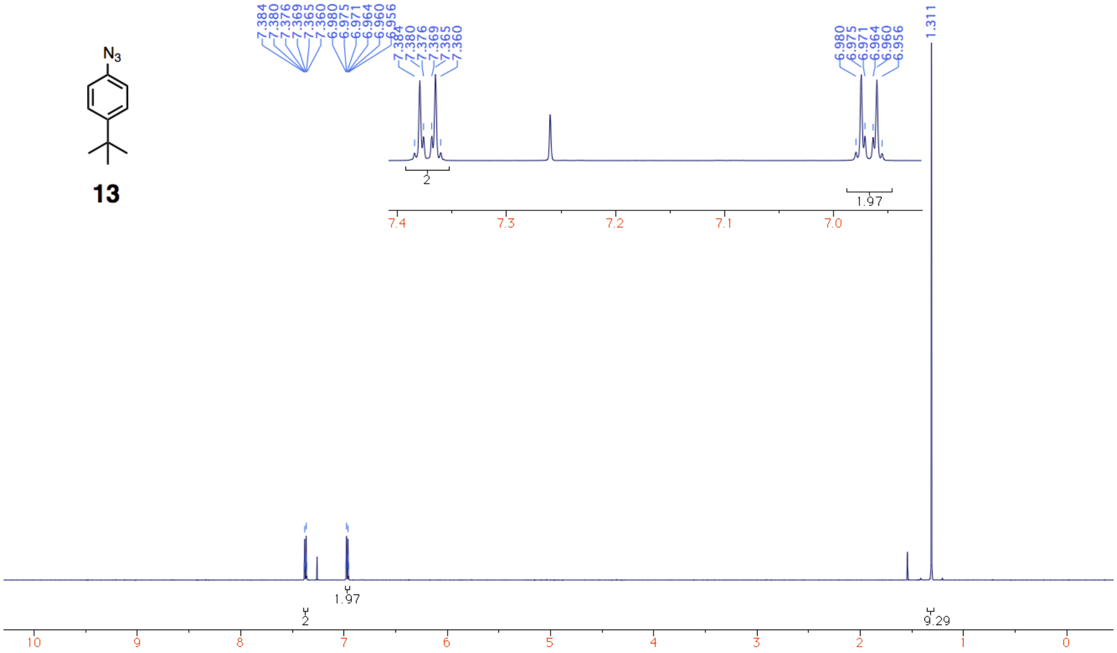

Figure 2.36. ^{1}H-NMR spectrum of **13** in CDCl$_3$.

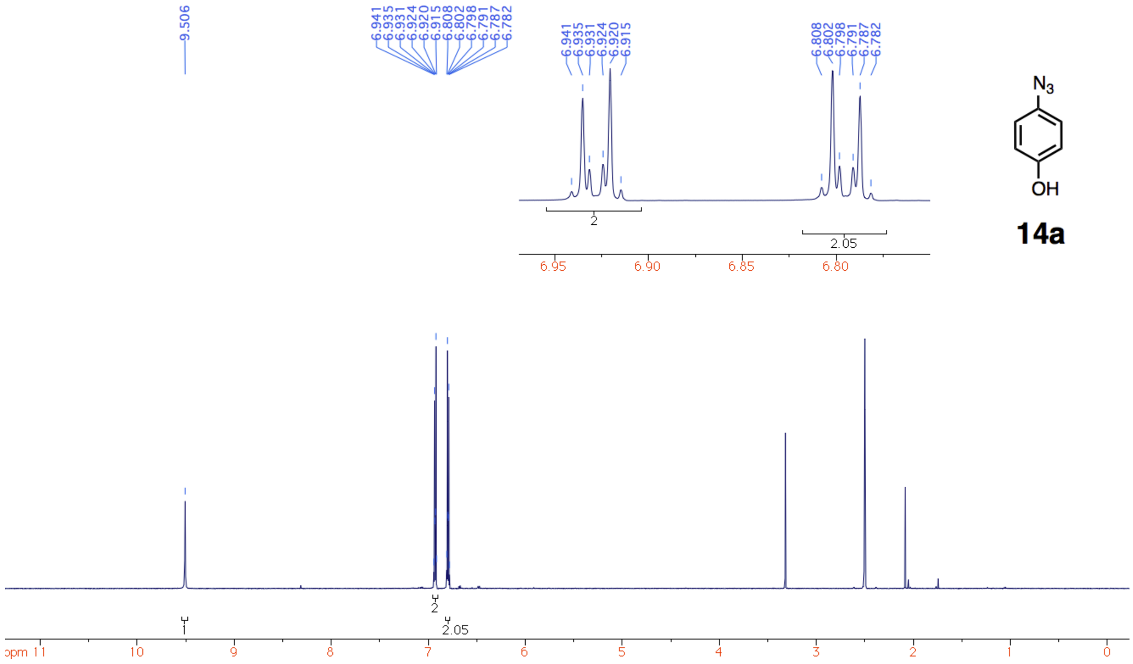

Figure 2.37. ^{1}H-NMR spectrum of **14a** in DMSO-d6.

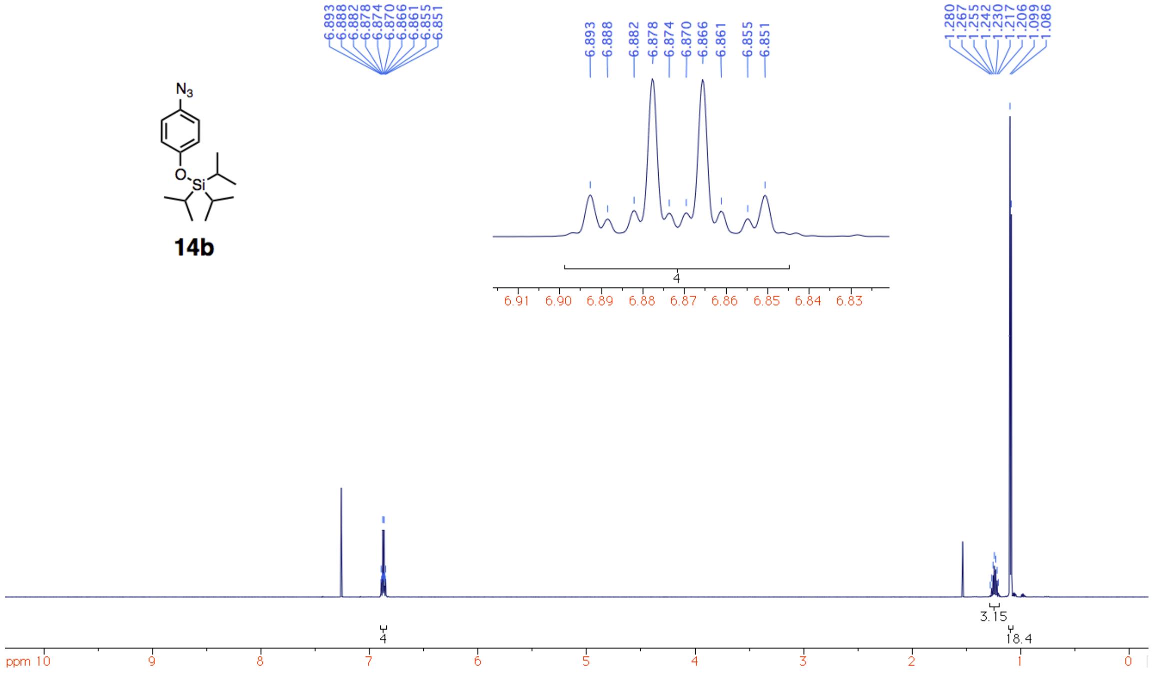

Figure 2.38. ^{1}H-NMR spectrum of **14b** in $CDCl_3$.

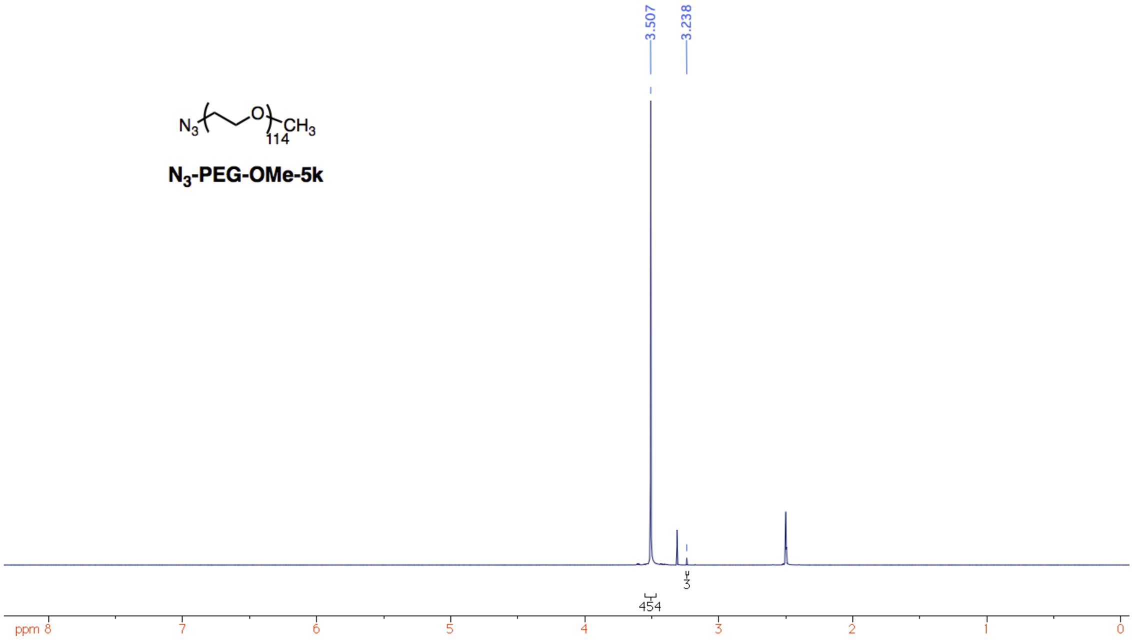

Figure 2.39. ^{1}H-NMR spectrum of **N_3-PEG-OMe-5K** in DMSO-d6.

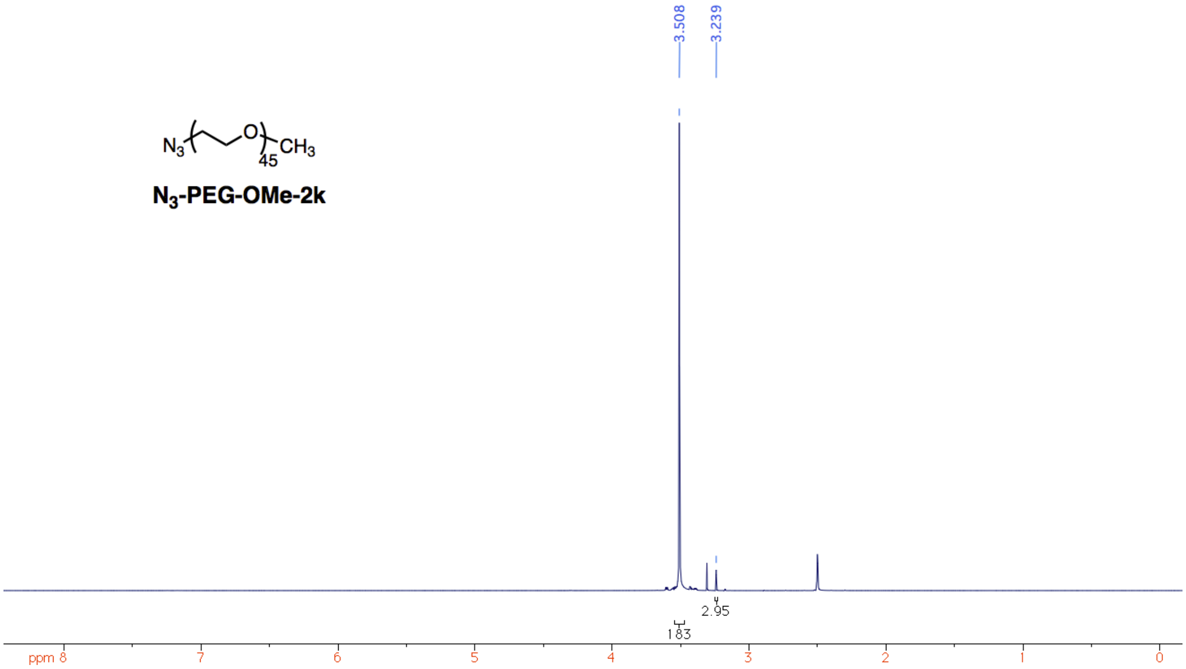

Figure 2.40. ^{1}H-NMR spectrum of **N_3-PEG-OMe-2K** in DMSO-d6.

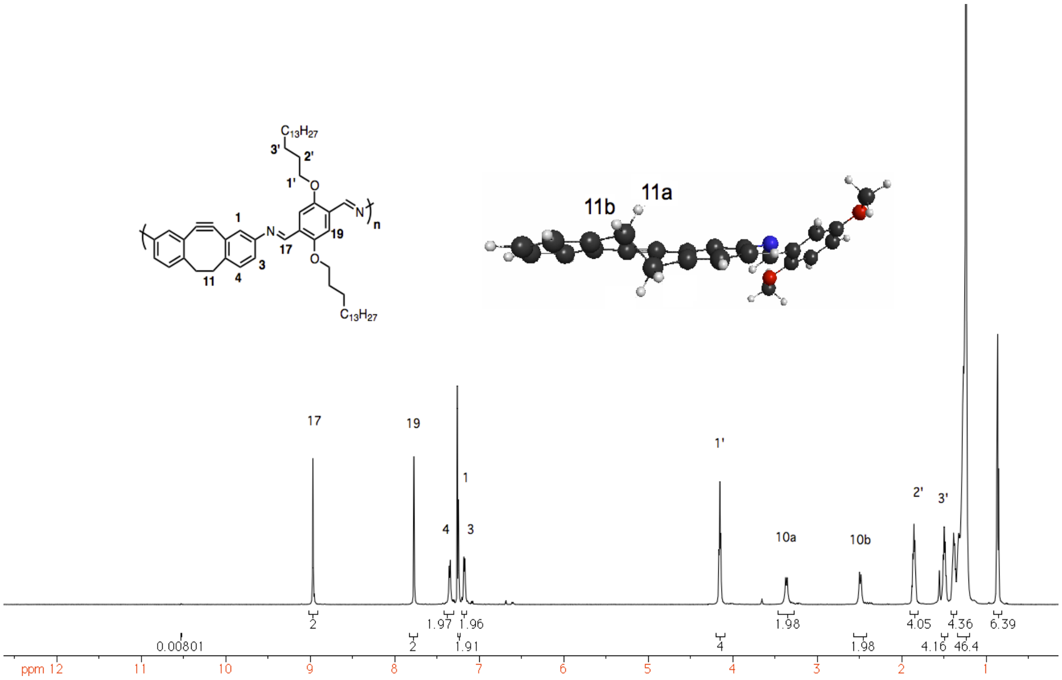

Figure 2.41. ^{1}H-NMR spectrum of **P0** (alkyne-containing polymer) in CDCl$_3$.

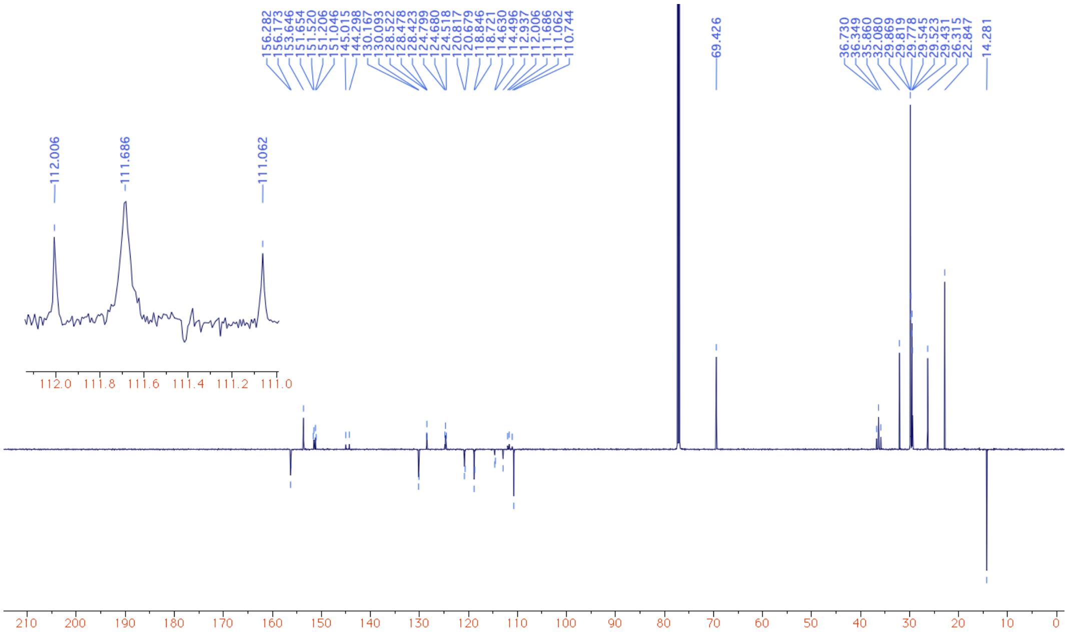

Figure 2.42. DEPTq spectrum of **P0** (alkyne-containing polymer) in CDCl$_3$.

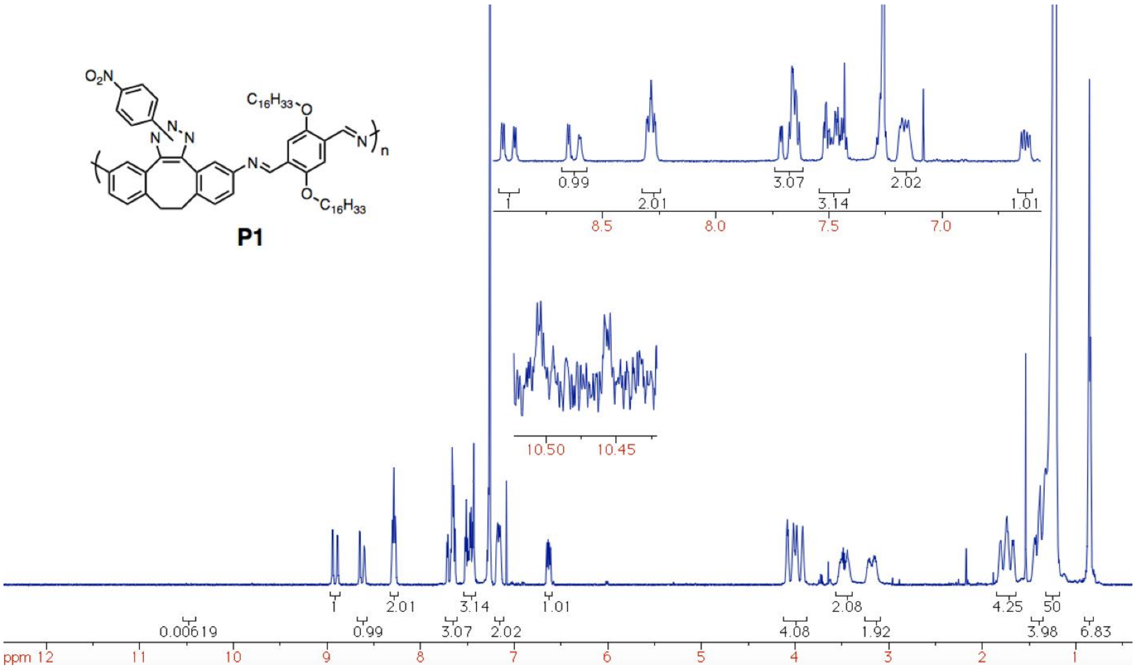

Figure 2.43. ^{1}H-NMR spectrum of **P1** (para-nitrophenyl derivative) in $CDCl_3$.

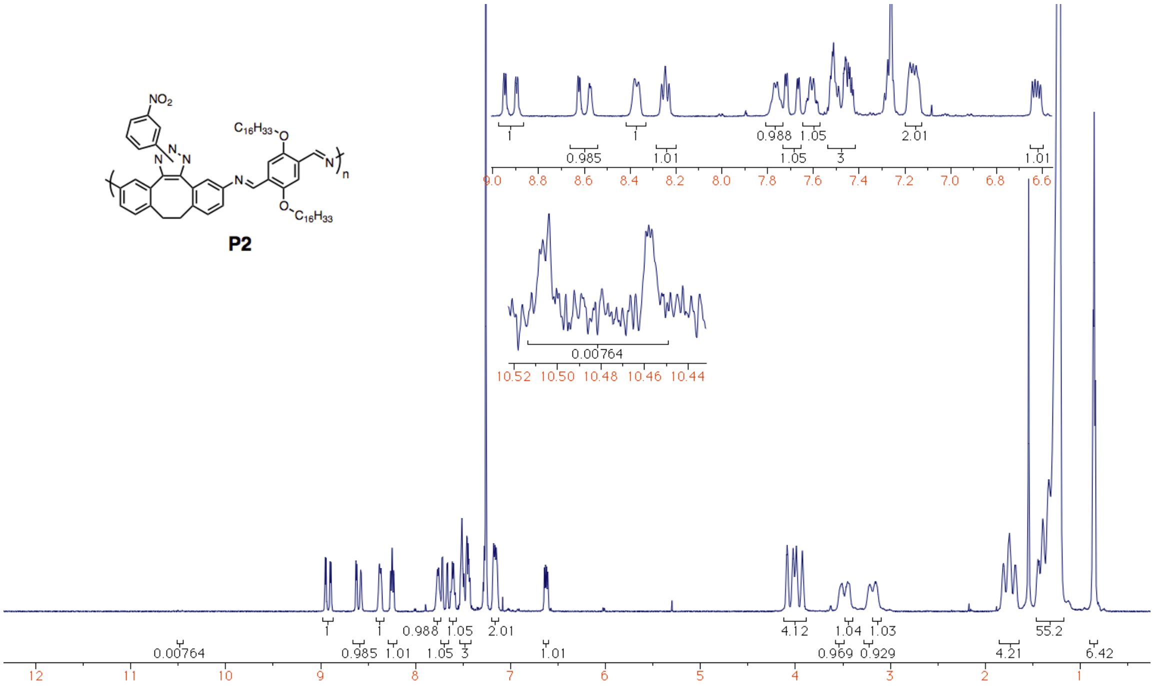

Figure 2.44. ^{1}H-NMR spectrum of **P2** (meta-nitrophenyl derivative) in $CDCl_3$.

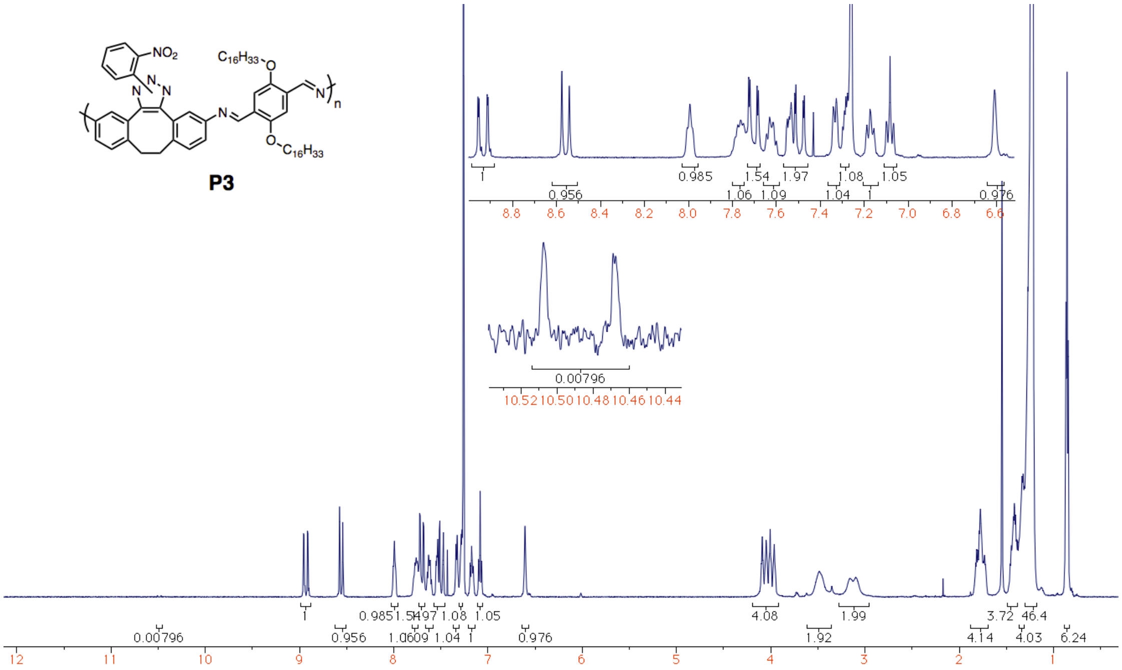

Figure 2.45. ^{1}H-NMR spectrum of **P3** (ortho-nitrophenyl derivative) in CDCl$_3$.

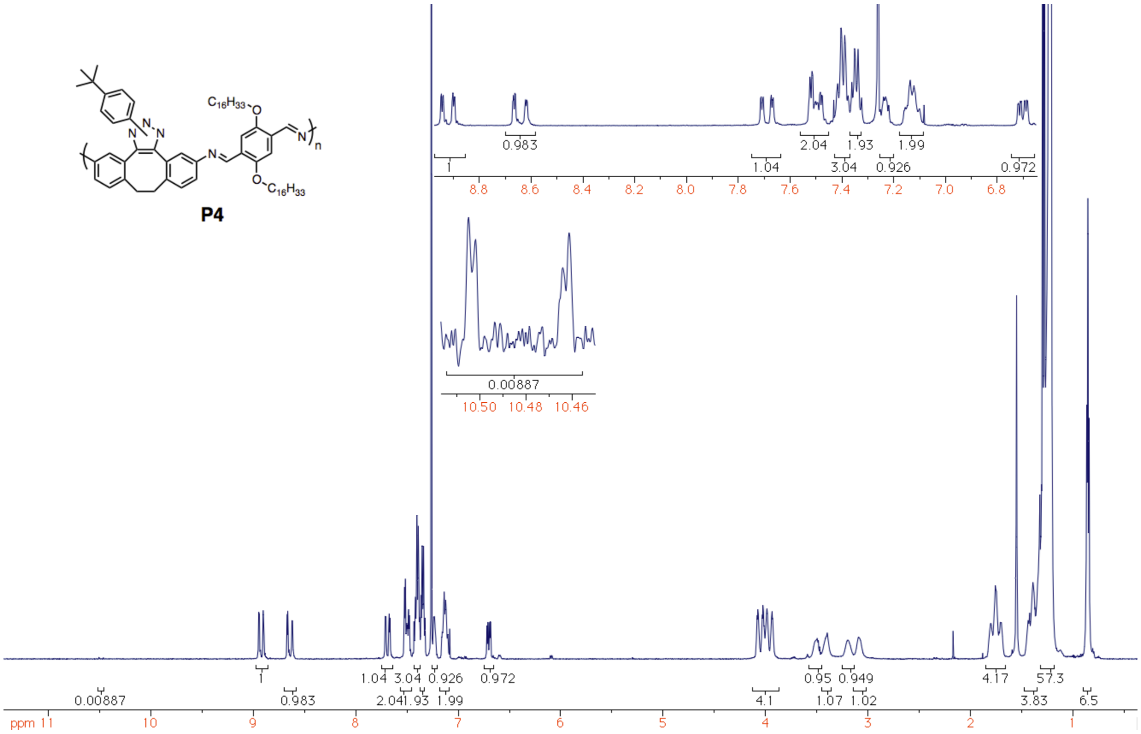

Figure 2.46. ^{1}H-NMR spectrum of **P4** (tert-butylbenzene derivative) in CDCl$_3$.

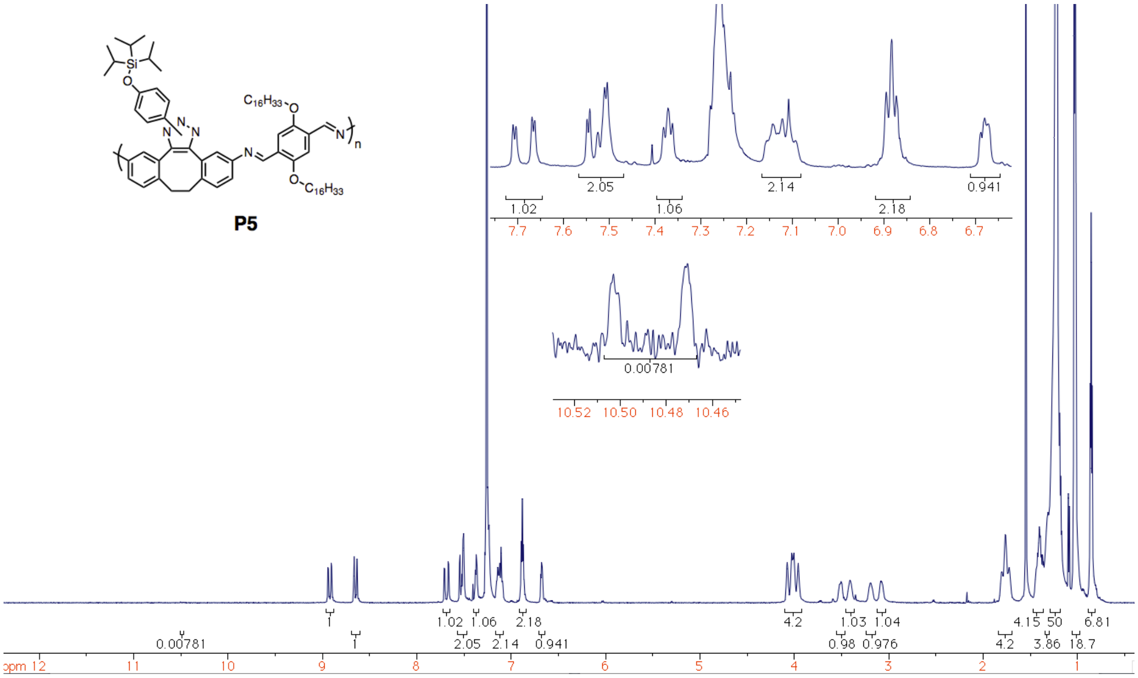

Figure 2.47. ^{1}H-NMR spectrum of **P5** (triisopropylsiloxy-benzene derivative) in $CDCl_3$.

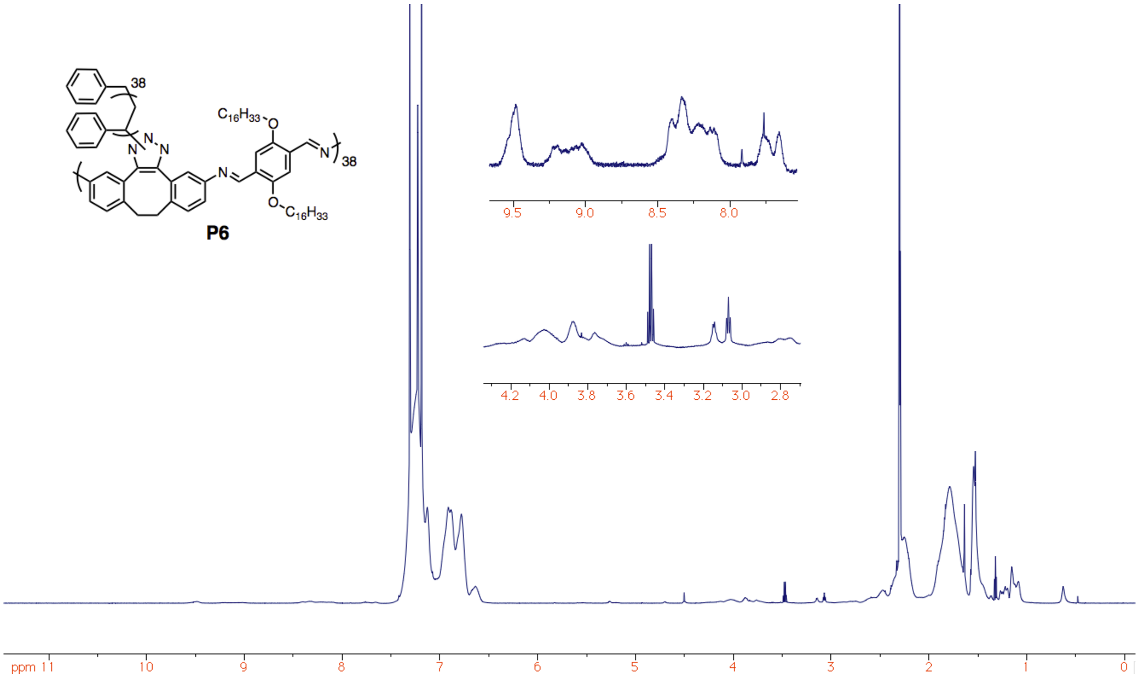

Figure 2.48. ^{1}H-NMR spectrum of **P6** (PS-4K graft) in toluene-d8.

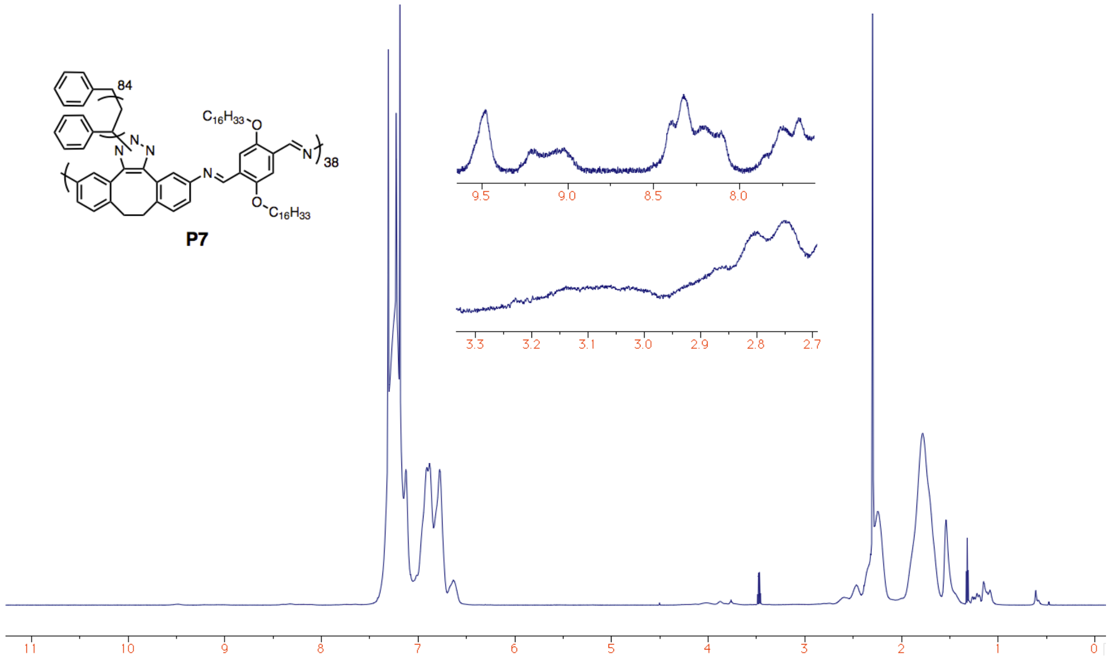

Figure 2.49. ^{1}H-NMR spectrum of **P7** (PS-9K graft) in toluene-d8.

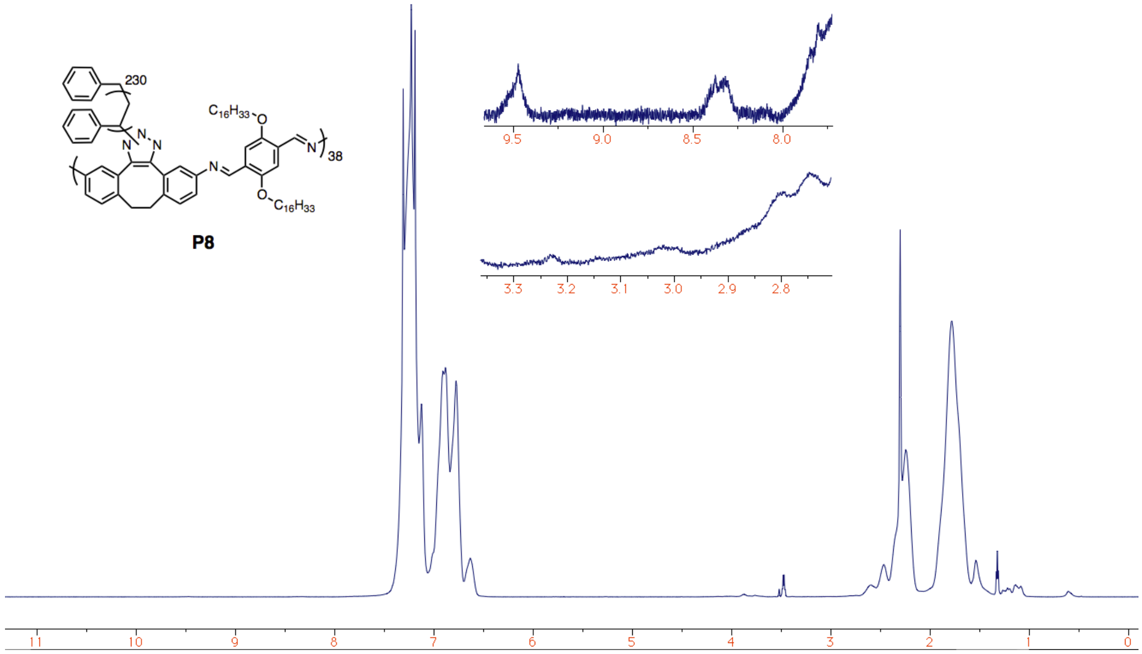

Figure 2.50. ^{1}H-NMR spectrum of **P8** (PS-24K graft) in toluene-d8.

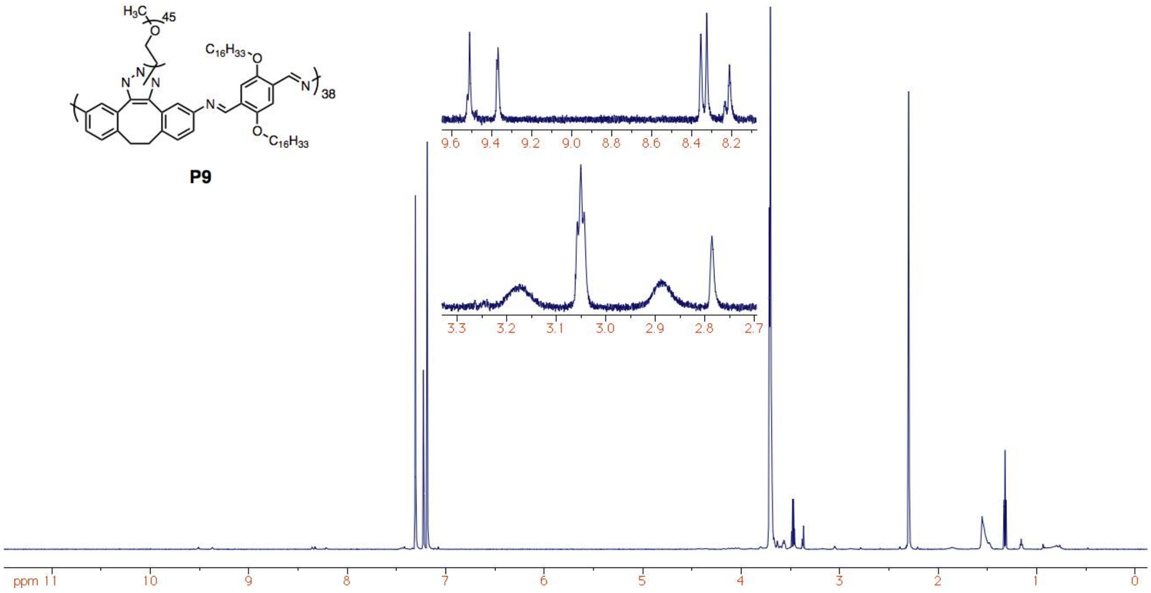

Figure 2.51. ^{1}H-NMR spectrum of **P9** (PEG-OMe-2K graft) in toluene-d8.

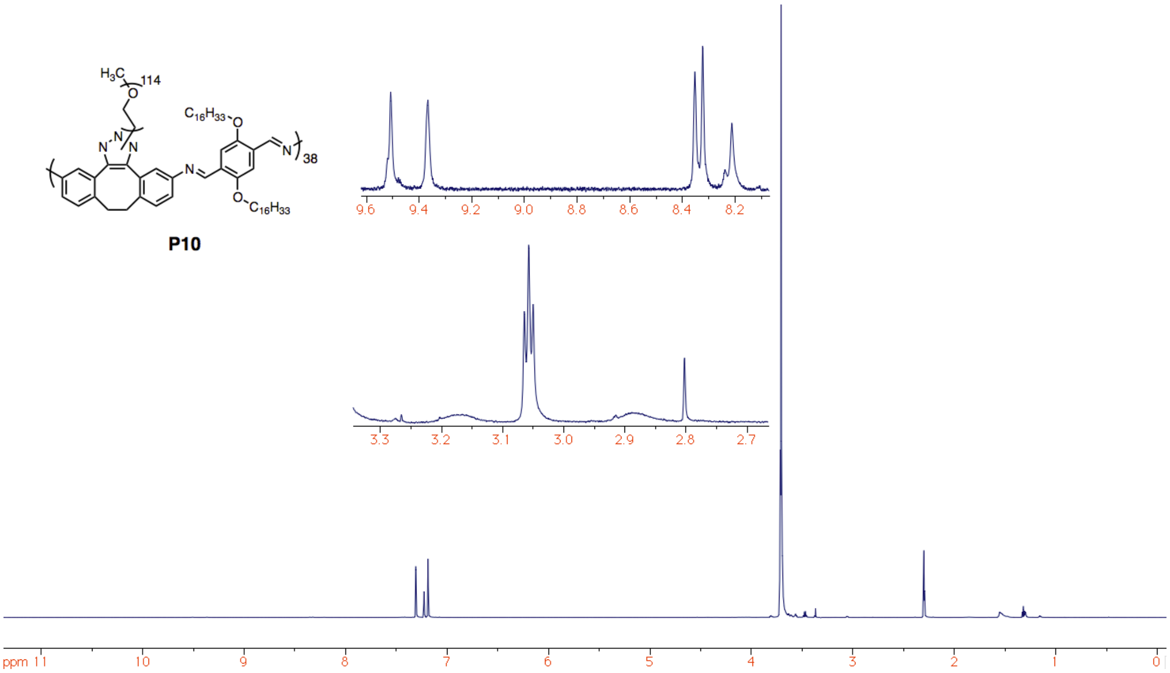

Figure 2.52. ^{1}H-NMR spectrum of **P10** (PEG-OMe-2K graft) in toluene-d8.

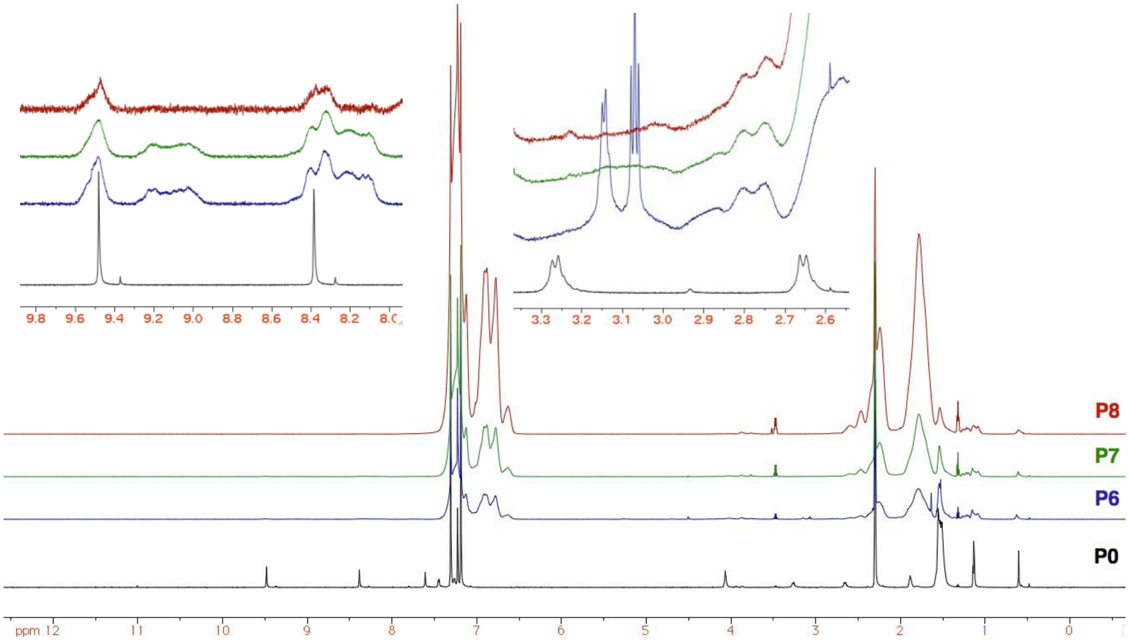

Figure 2.53. ^{1}H-NMR spectrum overlay of **P0** (alkyne-containing polymer) with **P6-P8** (polystyrene graft copolymers) in toluene-d8.

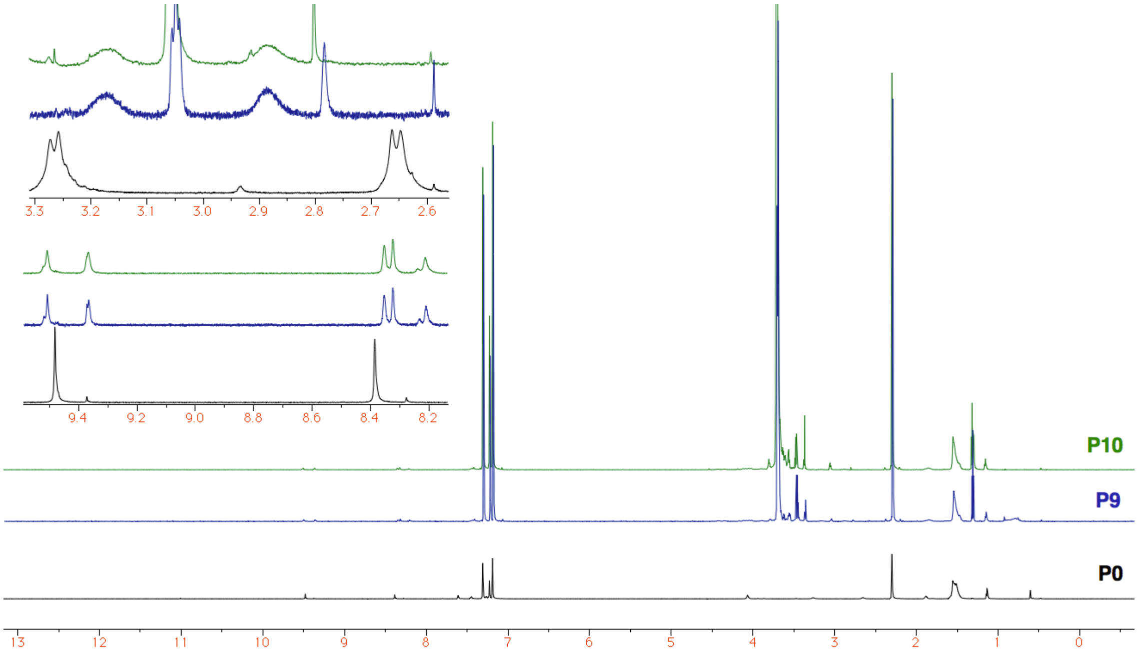

Figure 2.54. ^{1}H-NMR spectrum overlay of **P0** (alkyne-containing polymer) with **P9** and **P10** (polyethylene glycol monomethyl ether grafts) in toluene-d8.

2.4.7. HPLC Traces

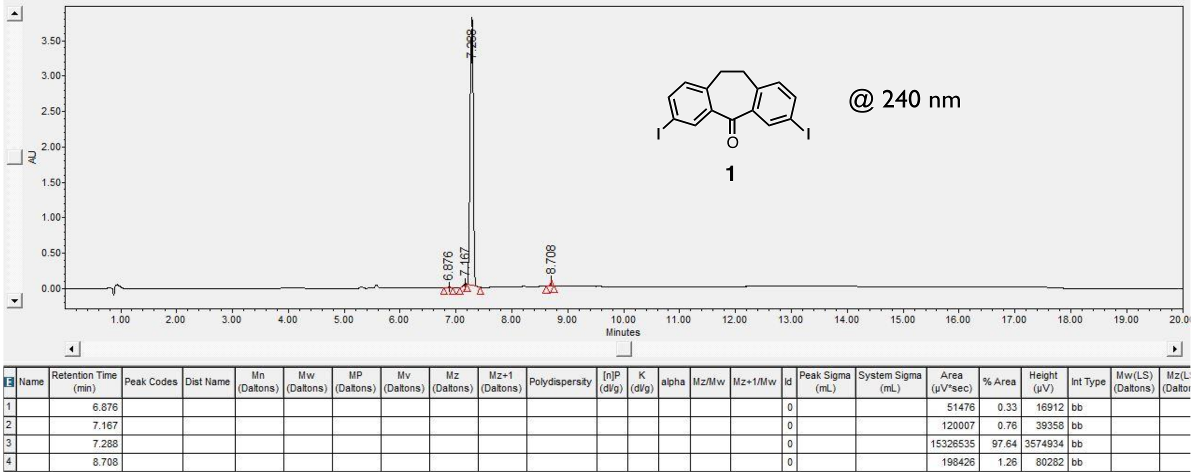

E	Name	Retention Time (min)	Peak Codes	Dist Name	Mn (Daltons)	Mw (Daltons)	MP (Daltons)	Mv (Daltons)	Mz (Daltons)	Mz+1 (Daltons)	Polydispersity	[n]P (dl/g)	K (dl/g)	alpha	Mz/Mw	Mz+1/Mw	Id	Peak Sigma (mL)	System Sigma (mL)	Area (µV*sec)	% Area	Height (µV)	Int Type	Mw(LS) (Daltons)	Mz(L (Dalto
1		6.876															0			51476	0.33	16912	bb		
2		7.167															0			120007	0.76	39358	bb		
3		7.288															0			15326535	97.64	3574934	bb		
4		8.708															0			198426	1.26	80282	bb		

Figure 2.55. HPLC trace of **1** at 240 nm.

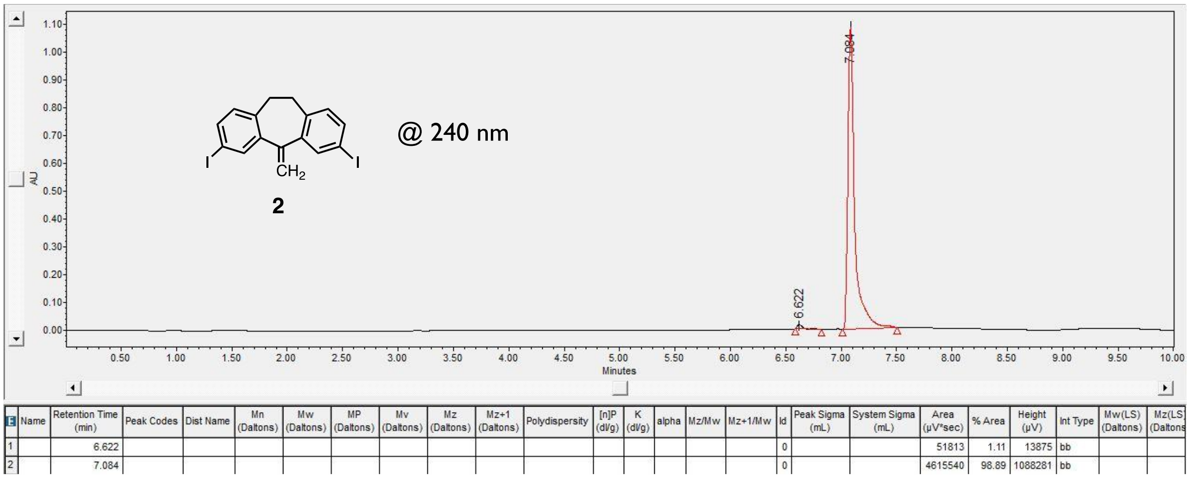

E	Name	Retention Time (min)	Peak Codes	Dist Name	Mn (Daltons)	Mw (Daltons)	MP (Daltons)	Mv (Daltons)	Mz (Daltons)	Mz+1 (Daltons)	Polydispersity	[n]P (dl/g)	K (dl/g)	alpha	Mz/Mw	Mz+1/Mw	Id	Peak Sigma (mL)	System Sigma (mL)	Area (µV*sec)	% Area	Height (µV)	Int Type	Mw(LS) (Daltons)	Mz(LS (Daltons
1		6.622															0			51813	1.11	13875	bb		
2		7.084															0			4615540	98.89	1088281	bb		

Figure 2.56. HPLC trace of **2** at 240 nm.

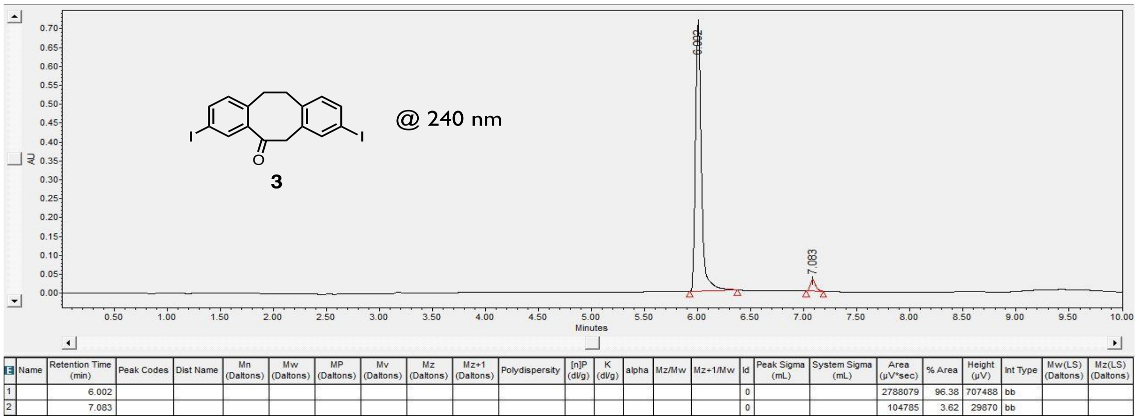

	Name	Retention Time (min)	Peak Codes	Dist Name	Mn (Daltons)	Mw (Daltons)	MP (Daltons)	Mv (Daltons)	Mz (Daltons)	Mz+1 (Daltons)	Polydispersity	[n]P (dl/g)	K (dl/g)	alpha	Mz/Mw	Mz+1/Mw	Id	Peak Sigma (mL)	System Sigma (mL)	Area (µV*sec)	% Area	Height (µV)	Int Type	Mw(LS) (Daltons)	Mz(LS) (Daltons)
1		6.002															0			2788079	96.38	707488	bb		
2		7.083															0			104785	3.62	29870	bb		

Figure 2.57. HPLC trace of **3** at 240 nm.

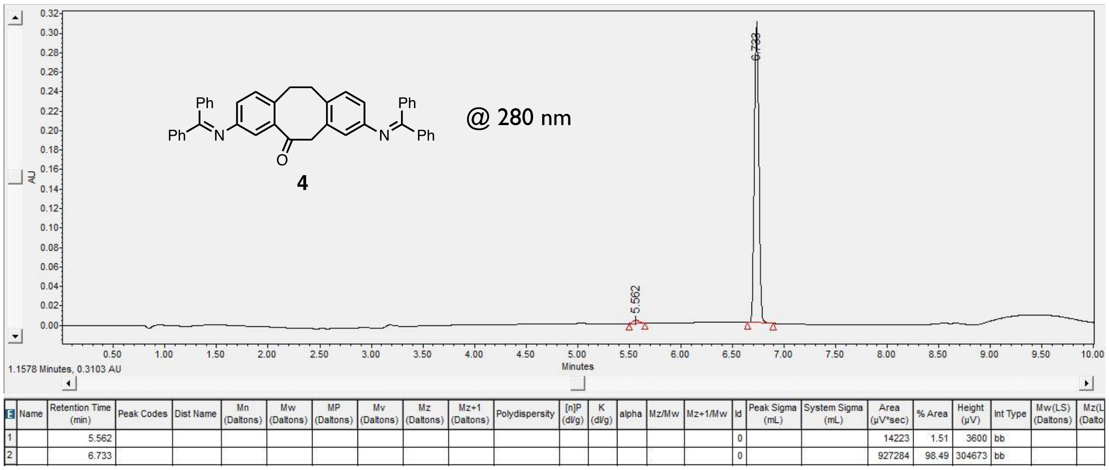

	Name	Retention Time (min)	Peak Codes	Dist Name	Mn (Daltons)	Mw (Daltons)	MP (Daltons)	Mv (Daltons)	Mz (Daltons)	Mz+1 (Daltons)	Polydispersity	[n]P (dl/g)	K (dl/g)	alpha	Mz/Mw	Mz+1/Mw	Id	Peak Sigma (mL)	System Sigma (mL)	Area (µV*sec)	% Area	Height (µV)	Int Type	Mw(LS) (Daltons)	Mz(L (Dalto
1		5.562															0			14223	1.51	3600	bb		
2		6.733															0			927284	98.49	304673	bb		

Figure 2.58. HPLC trace of **4** at 280 nm.

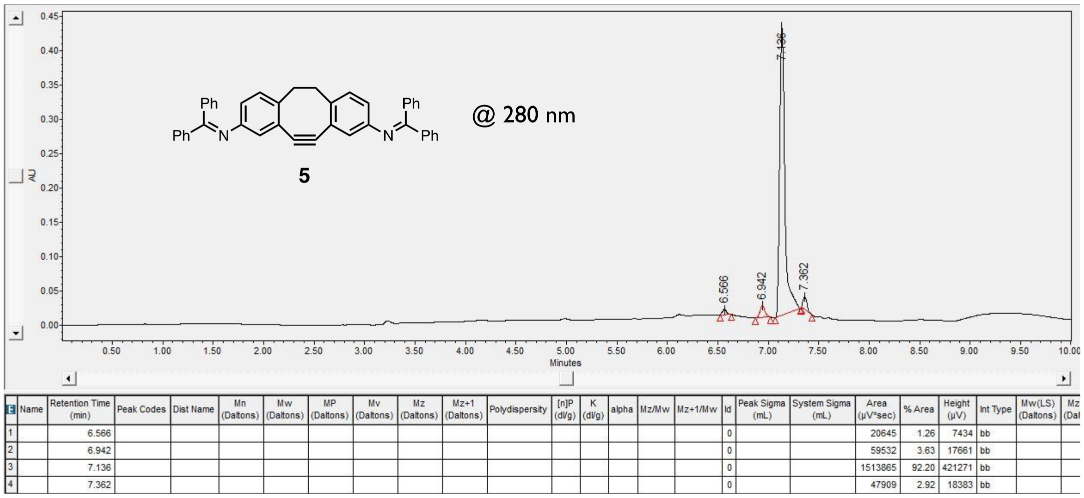

	Name	Retention Time (min)	Peak Codes	Dist Name	Mn (Daltons)	Mw (Daltons)	MP (Daltons)	Mv (Daltons)	Mz (Daltons)	Mz+1 (Daltons)	Polydispersity	[n]P (dl/g)	K (dl/g)	alpha	Mz/Mw	Mz+1/Mw	Id	Peak Sigma (mL)	System Sigma (mL)	Area (µV*sec)	% Area	Height (µV)	Int Type	Mw(LS) (Daltons)	Mz (Dal
1		6.566															0			20645	1.26	7434	bb		
2		6.942															0			59532	3.63	17661	bb		
3		7.136															0			1513865	92.20	421271	bb		
4		7.362															0			47909	2.92	18383	bb		

Figure 2.59. HPLC trace of **5** at 280 nm.

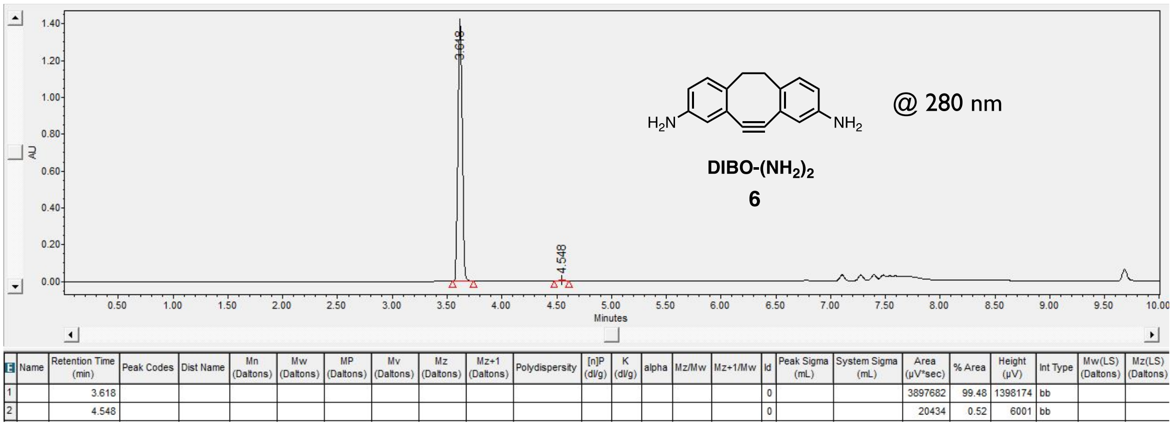

E	Name	Retention Time (min)	Peak Codes	Dist Name	Mn (Daltons)	Mw (Daltons)	MP (Daltons)	Mv (Daltons)	Mz (Daltons)	Mz+1 (Daltons)	Polydispersity	[n]P (dl/g)	K (dl/g)	alpha	Mz/Mw	Mz+1/Mw	Id	Peak Sigma (mL)	System Sigma (mL)	Area (µV*sec)	% Area	Height (µV)	Int Type	Mw(LS) (Daltons)	Mz(LS) (Daltons)
1		3.618															0			3897682	99.48	1398174	bb		
2		4.548															0			20434	0.52	6001	bb		

Figure 2.60. HPLC trace of **6** at 280 nm.

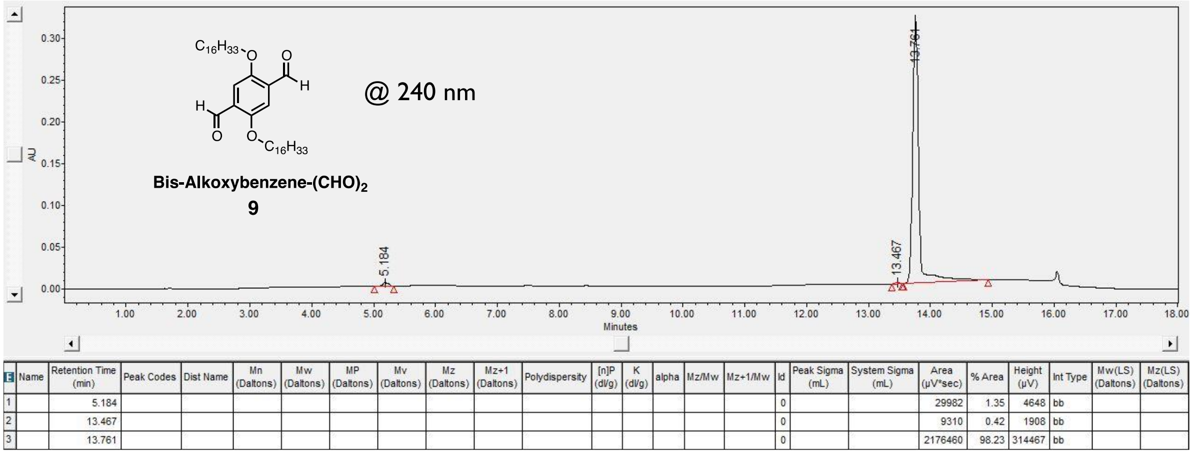

E	Name	Retention Time (min)	Peak Codes	Dist Name	Mn (Daltons)	Mw (Daltons)	MP (Daltons)	Mv (Daltons)	Mz (Daltons)	Mz+1 (Daltons)	Polydispersity	[n]P (dl/g)	K (dl/g)	alpha	Mz/Mw	Mz+1/Mw	Id	Peak Sigma (mL)	System Sigma (mL)	Area (µV*sec)	% Area	Height (µV)	Int Type	Mw(LS) (Daltons)	Mz(LS) (Daltons)
1		5.184															0			29982	1.35	4648	bb		
2		13.467															0			9310	0.42	1908	bb		
3		13.761															0			2176460	98.23	314467	bb		

Figure 2.61. HPLC trace of **9** at 240 nm.

2.4.8. Raman Spectra

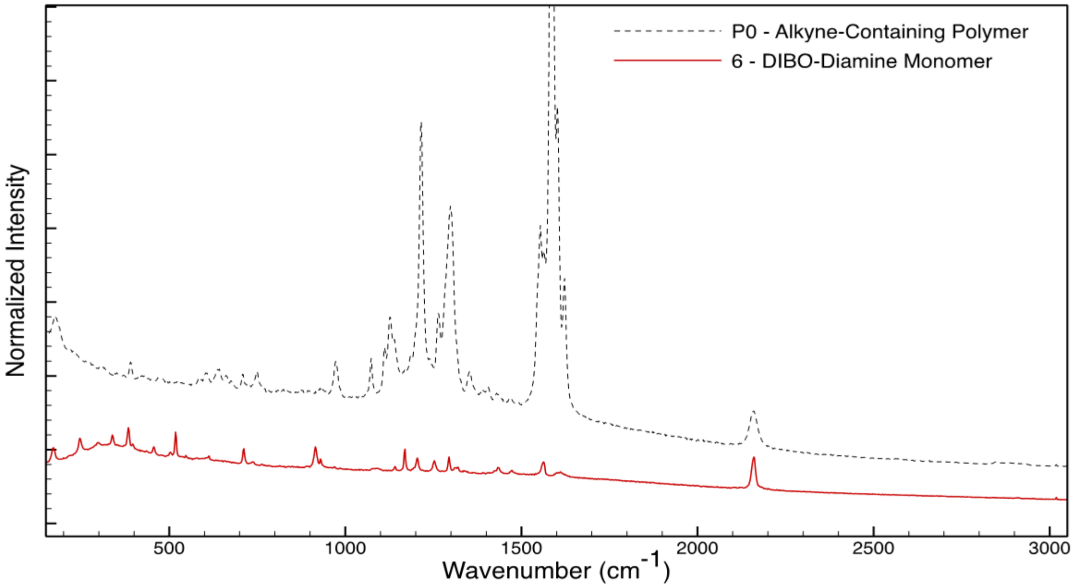

Figure 2.62. Raman spectrum overlay of compound **6** with **P0** at a 785 nm excitation. The internal alkyne stretch is observed at 2160 cm^{-1}.

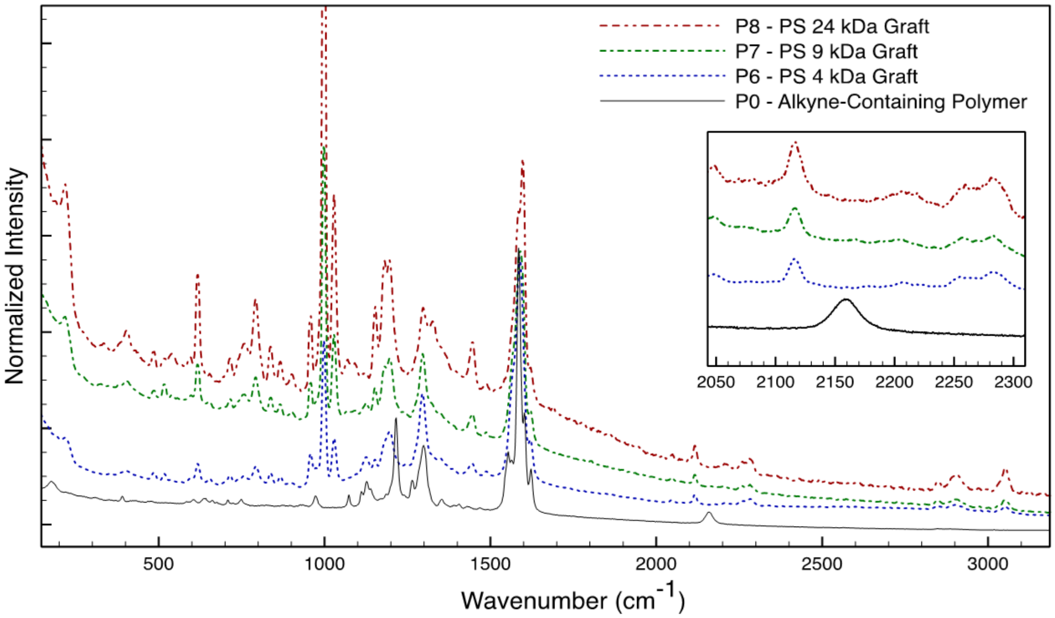

Figure 2.63. Raman spectrum overlay of **P0** with **P6-P8** at a 785 nm excitation. The internal alkyne stretch is observed at 2160 cm^{-1} in **P0**, but not in the graft polymers (**P6-P8**). The peaks observed from 2100 cm^{-1} to 2300 cm^{-1} are associated with toluene d8.

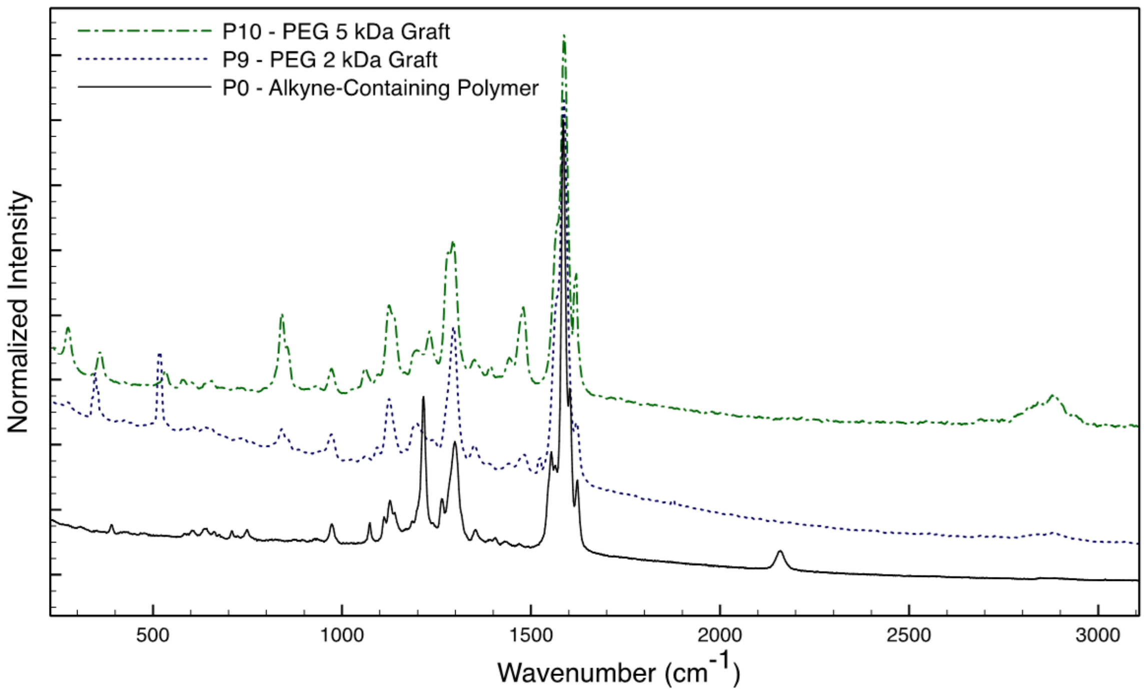

Figure 2.64. Raman spectrum overlay of **P0** with **P9** and **P10** at a 785 nm excitation.

2.4.9. GPC Traces

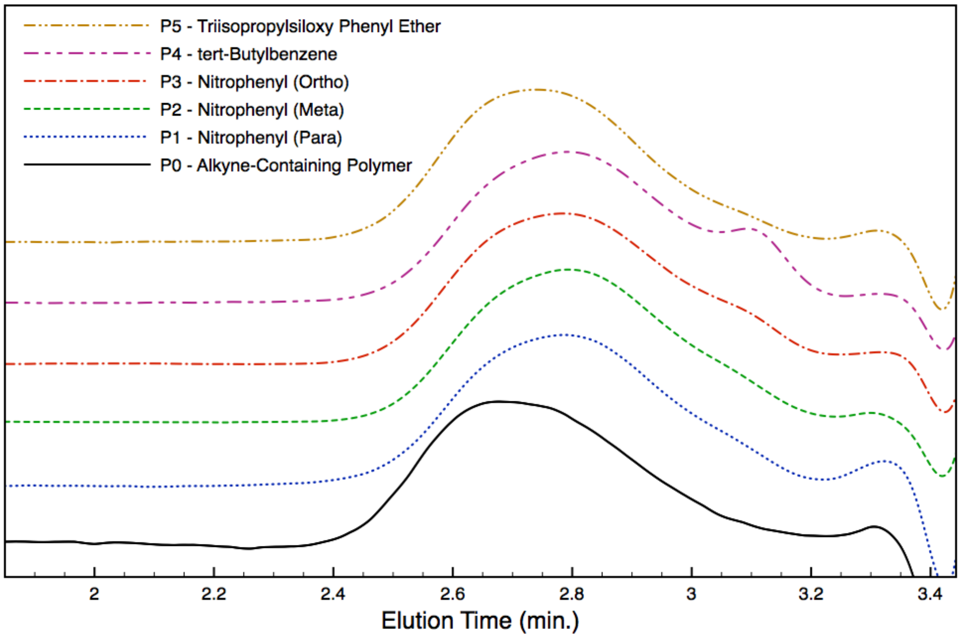

Figure 2.65. GPC trace overlay of **P0** with **P1-P5**.

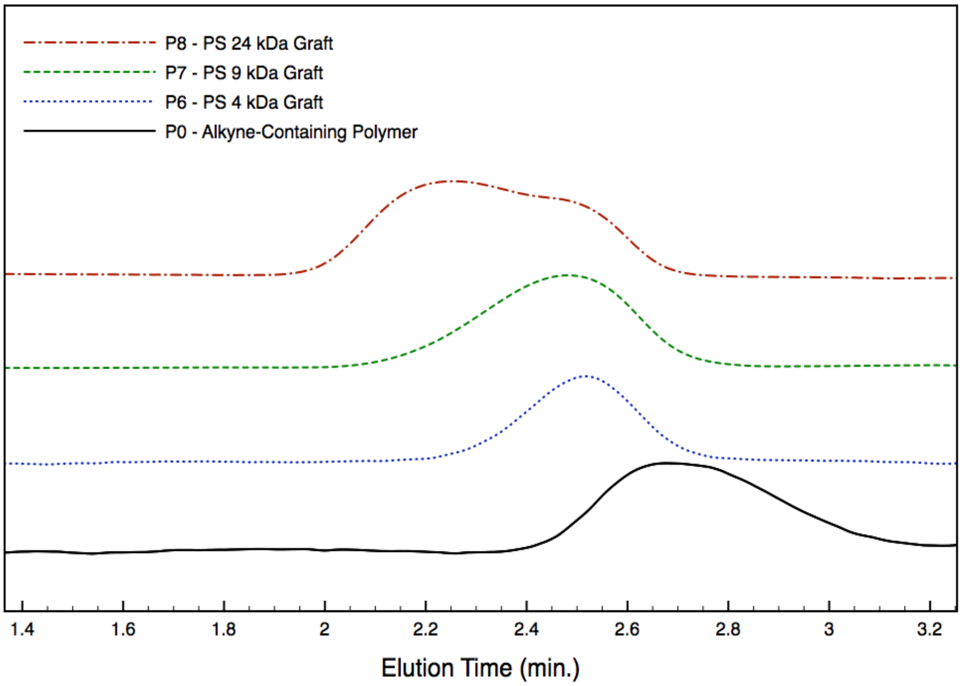

Figure 2.66. GPC trace overlay of **P0** with **P6-P8.**

2.5. References:

(1) Facchetti, A. Pi-Conjugated Polymers for Organic Electronics and Photovoltaic Cell Applications. *Chem. Mater.* **2011**, *23* (3), 733–758.

(2) *Conjugated Polymer Processing and Applications*, 3rd ed.; Skotheim, T. A., Reynolds, J. R., Eds.; CRC Press: Boca Rat, 2007.

(3) *Conjugated Polymers: Theory, Synthesis, Properties, and Characterization*, 3rd ed.; Skotheim, T. A., Reynolds, J., Eds.; CRC Press: Boca Raton, 2006.

(4) Shirakawa, H.; Louis, E. J.; MacDiarmid, A. G.; Chiang, C. K.; Heeger, A. J. Synthesis of Electrically Conducting Organic Polymers: Halogen Derivatives of Polyacetylene, (CH) X. *J. Chem. Soc. Chem. Commun.* **1977**, No. 16, 578.

(5) Chiang, C. K.; Fincher, C. R.; Park, Y. W.; Heeger, A. J.; Shirakawa, H.; Louis, E. J.; Gau, S. C.; MacDiarmid, A. G. Electrical Conductivity in Doped Polyacetylene. *Phys. Rev. Lett.* **1977**, *39* (17), 1098–1101.

(6) Rehahn, M.; Schlüter, A.-D.; Wegner, G.; Feast, W. J. Soluble Poly(Para-Phenylene)s. 2. Improved Synthesis of Poly(Para-2,5-Di-n-Hexylphenylene) via Pd-Catalysed Coupling of 4-Bromo-2,5-Di-n-Hexylbenzeneboronic Acid. *Polymer (Guildf).* **1989**, *30* (6), 1060–1062.

(7) Burroughes, J. H.; Bradley, D. D. C.; Brown, A. R.; Marks, R. N.; Mackay, K.; Friend, R. H.; Burns, P. L.; Holmes, A. B. Light-Emitting Diodes Based on Conjugated Polymers. *Nature* **1990**, *347* (6293), 539–541.

(8) Wessling, R. A.; Zimmermann, R. G. No Title. U.S. Pat. 3,401,152, 1972.

(9) McNeill, R.; Siudak, R.; Wardlaw, J.; Weiss, D. Electronic Conduction in Polymers. I. The Chemical Structure of Polypyrrole. *Aust. J. Chem.* **1963**, *16* (6), 1056.

(10) Yamamoto, T.; Sanechika, K.; Yamamoto, A. Preparation of Thermostable and Electric-Conducting Poly(2,5-Thienylene). *J. Polym. Sci. Polym. Lett. Ed.* **1980**, *18* (1), 9–12.

(11) Leclerc, M. Polyfluorenes: Twenty Years of Progress. *J. Polym. Sci. Part A Polym. Chem.* **2001**, *39* (17), 2867–2873. https://doi.org/10.1002/pola.1266.

(12) Prey, V. V.; Schindlbauer, H.; Cmelka, D. Versuche Zur Polymerisation von Fluoren. *Angew. Makromol. Chemie* **1973**, *28* (1), 137–143.

(13) Beaujuge, P. M.; Reynolds, J. R. Color Control in Pi-Conjugated Organic Polymers for Use in Electrochromic Devices. *Chem. Rev.* **2010**, *110* (1), 268–320.

(14) *Design and Synthesis of Conjugated Polymers*; Leclerc, M., Morin, J.-F., Eds.; Wiley-VCH Verlag GmbH & Co.: Weinheim, 2010.

(15) Zalar, P.; Henson, Z. B.; Welch, G. C.; Bazan, G. C.; Nguyen, T.-Q. Color Tuning in Polymer Light-Emitting Diodes with Lewis Acids. *Angew. Chemie Int. Ed. English* **2012**,

(16) Welch, G. C.; Bazan, G. C. Lewis Acid Adducts of Narrow Band Gap Conjugated Polymers. *J. Am. Chem. Soc.* **2011**, *133* (12), 4632–4644.

(17) van Haare, J. A. E. H.; Havinga, E. E.; van Dongen, J. L. J.; Janssen, R. A. J.; Cornil, J.; Brédas, J.-L. Redox States of Long Oligothiophenes: Two Polarons on a Single Chain. *Chem. - A Eur. J.* **1998**, *4* (8), 1509–1522.

(18) Sirringhaus, H.; Brown, P. J.; Friend, R. H.; Nielsen, M. M.; Bechgaard, K.; Langeveld-Voss, B. M. W.; Spiering, A. J. H.; Janssen, R. A. J.; Meijer, E. W.; Herwig, P.; de Leeuw, D. M. Two-Dimensional Charge Transport in Self-Organized, High-Mobility Conjugated Polymers. *Nature* **1999**, *401* (6754), 685–688.

(19) Morin, J.-F.; Leclerc, M. 2,7-Carbazole-Based Conjugated Polymers for Blue, Green, and Red Light Emission. *Macromolecules* **2002**, *35* (22), 8413–8417.

(20) Donat-Bouillud, A.; Lévesque, I.; Tao, Y.; D'Iorio, M.; Beaupré, S.; Blondin, P.; Ranger, M.; Bouchard, J.; Leclerc, M. Light-Emitting Diodes from Fluorene-Based π-Conjugated Polymers. *Chem. Mater.* **2000**, *12* (8), 1931–1936.

(21) Beaupré, S.; Boudreault, P.-L. T.; Leclerc, M. Solar-Energy Production and Energy-Efficient Lighting: Photovoltaic Devices and White-Light-Emitting Diodes Using Poly(2,7-Fluorene), Poly(2,7-Carbazole), and Poly(2,7-Dibenzosilole) Derivatives. *Adv. Mater.* **2010**, *22*, E6--E27.

(22) Blouin, N.; Leclerc, M. Poly(2,7-Carbazole)s: Structure-Property Relationships. *Acc. Chem. Res.* **2008**, *41* (July), 1110–1119.

(23) Perepichka, I. F.; Perepichka, D. F.; Meng, H.; Wudl, F. Light-Emitting Polythiophenes. *Adv. Mater.* **2005**, *17* (19), 2281–2305.

(24) Sirringhaus, H. Integrated Optoelectronic Devices Based on Conjugated Polymers. *Science (80-.).* **1998**, *280* (5370), 1741–1744.

(25) Heeger, A. J. Semiconducting Polymers: The Third Generation. *Chem. Soc. Rev.* **2010**, *39* (7), 2354–2371.

(26) Tyler McQuade, D.; Pullen, A. E.; Swager, T. M. Conjugated Polymer-Based Chemical Sensors. *Chem. Rev.* **2000**, *100* (7), 2537–2574.

(27) Hirsch, A. Functionalization of Single-Walled Carbon Nanotubes. *Angew. Chemie - Int. Ed.* **2002**, *41* (11), 1853–1859.

(28) Star, A.; Liu, Y.; Grant, K.; Ridvan, L.; Stoddart, J. F.; Steuerman, D. W.; Diehl, M. R.; Boukai, A.; Heath, J. R. Noncovalent Side-Wall Functionalization of Single-Walled Carbon Nanotubes. *Macromolecules* **2003**, *36* (3), 553–560.

(29) Rice, N. A.; Soper, K.; Zhou, N.; Merschrod, E.; Zhao, Y. Dispersing As-Prepared Single-Walled Carbon Nanotube Powders with Linear Conjugated Polymers. *Chem. Commun. (Camb).* **2006**, No. 47, 4937–4939.

(30) Rice, N. A.; Adronov, A. Selective Interactions of a High-Molecular-Weight Polycarbazole with Different Commercial Nanotube Samples. *J. Polym. Sci. Part A Polym. Chem.* **2014**, *52* (19), 2738–2747.

(31) Yang, X.; Loos, J. Toward High-Performance Polymer Solar Cells: The Importance of Morphology Control. *Macromolecules* **2007**, *40* (5), 1353–1362.

(32) Yuan, Y.; Michinobu, T.; Ashizawa, M.; Mori, T. Microwave-Assisted TCNE/TCNQ Addition to Poly(Thienyleneethynylene) Derivative for Construction of Donor-Acceptor Chromophores. *J. Polym. Sci. Part A Polym. Chem.* **2011**, *49* (4), 1013–1020.

(33) Arslan, H.; Saathoff, J. D.; Bunck, D. N.; Clancy, P.; Dichtel, W. R. Highly Efficient Benzannulation of Poly(Phenylene Ethynylene)S. *Angew. Chemie - Int. Ed.* **2012**, *51* (48), 12051–12054.

(34) Chadwick, R. C.; Kardelis, V.; Liogier, S.; Adronov, A. Synthesis of Conjugated Polymers Containing DIBAC-Derived Triazole Monomers. *Macromolecules* **2013**, *46* (24), 9593–9598.

(35) Wittig, G.; Fischer, S. Reaktionen von Cyclooctin Mit Übergangsmetall-Derivaten. *Chem. Ber.* **1972**, *105* (11), 3542–3552.

(36) Bennett, M. A.; Schwemlein, H. P. Metal Complexes of Small Cycloalkynes and Arynes. *Angew. Chemie Int. Ed. English* **1989**, *28* (10), 1296–1320.

(37) Gröger, G.; Behrens, U.; Olbrich, F. Monomeric and Dimeric Cyclooctyne-Stabilized Complexes of Copper(I) 1. *Organometallics* **2000**, *19* (17), 3354–3360.

(38) Lapitskii, G. A.; Makin, S. M.; Berlin, A. A. Study of the Structure and Certain Properties of Conjugated Polymers Obtained by Wittig's Reaction. *Polym. Sci. U.S.S.R.* **1967**, *9* (6), 1423–1430.

(39) Laughlin, B. J.; Smith, R. C. Gilch and Horner−Wittig Routes to Poly(p - Phenylenevinylene) Derivatives Incorporating Monoalkyl Defect-Free 9,9-Dialkyl-1,4-Fluorenylene Units. *Macromolecules* **2010**, *43* (8), 3744–3749.

(40) Egbe, D. A. M.; Tillmann, H.; Birckner, E.; Klemm, E. Synthesis and Properties of Novel Well-Defined Alternating PPE/PPV Copolymers. *Macromol. Chem. Phys.* **2001**, *202* (13), 2712–2726.

(41) Miyake, J.; Tsuji, Y.; Nagai, A.; Chujo, Y. Aza-Wittig Polymerization: Kinetic Study and Efficient End Functionalization of Poly(Azomethine)S. *Macromolecules* **2009**, *42* (10), 3463–3468.

(42) Miyake, J.; Chujo, Y. Aza-Wittig Polymerization: A Simple Method for the Synthesis of Regioregular Poly(Azomethine)S. *Macromolecules* **2008**, *41* (24), 9677–9682.

(43) Kim, S.; Lim, C.-K.; Na, J.; Lee, Y.-D.; Kim, K.; Choi, K.; Leary, J. F.; Kwon, I. C. Conjugated Polymer Nanoparticles for Biomedical in Vivo Imaging. *Chem. Commun.* **2010**, *46* (10), 1617–1619.

(44) Hodgkin, J. H.; Heller, J. Synthesis of Conjugated Schiff-Base Polymers. *J. Polym. Sci. Part C Polym. Symp.* **2007**, *29* (1), 37–46.

(45) Yang, C.-J.; Jenekhe, S. A. Conjugated Aromatic Polyimines. 2. Synthesis, Structure, and Properties of New Aromatic Polyazomethines. *Macromolecules* **1995**, *28* (4), 1180–1196.

(46) Marvel, C. S.; Tarkoy, N. Heat Stability Studies on Chelates from Schiff Bases of Salicylaldehyde Derivatives'. *JACS* **1958**, *80*, 832–835.

(47) Goodwin, H. A.; Bailar, J. C. Coördination Compounds Derived from Polymeric Schiff's Bases. *JACS* **1961**, *83*, 2467–2471.

(48) Iwan, A.; Sek, D. Processible Polyazomethines and Polyketanils: From Aerospace to Light-Emitting Diodes and Other Advanced Applications. *Prog. Polym. Sci.* **2008**, *33* (3), 289–345.

(49) Wolfe, J. P.; Åhman, J.; Sadighi, J. P.; Singer, R. A.; Buchwald, S. L. An Ammonia Equivalent for the Palladium-Catalyzed Amination of Aryl Halides and Triflates. *Tetrahedron Lett.* **1997**, *38* (36), 6367–6370.

(50) Seitz, G.; Pohl, L.; Pohlke, R. 5,6-Didehydro-11,12-Dihydrodibenzo[a,e]-Cyclooctene. *Angew. Chemie Int. Ed. English* **1969**, *8* (6), 447–448.

(51) Mbua, N. E.; Guo, J.; Wolfert, M. A.; Steet, R.; Boons, G.-J. Strain-Promoted Alkyne-Azide Cycloadditions (SPAAC) Reveal New Features of Glycoconjugate Biosynthesis. *Chembiochem* **2011**, *12* (12), 1912–1921.

(52) Meier, H.; Gugel, H. Synthese des 5,6-Didehydro-11,12-dihydro-dibenzo-[a,e]cyclooctens - eines hochgespannten Cycloalkyns. *Synthesis (Stuttg).* **1976**, *1976* (05), 338–339.

(53) Kornmayer, S.; Rominger, F.; Gleiter, R. Synthesis of 11,12-Didehydrodibenzo[a,e]Cycloocten-5(6H)-One: A Strained Eight-Membered Alkyne. *Synthesis (Stuttg).* **2009**, *2009* (15), 2547–2552.

(54) Bühl, H.; Gugel, H.; Kolshorn, H.; Meier, H. Eine verbesserte Cyclooctyn-Synthese. *Synthesis (Stuttg).* **1978**, *1978* (07), 536–537.

(55) Lešetický, L.; Smrček, S.; Sváta, V.; Podlahová, J.; Podlaha, J.; Císařová, I. The Synthesis and X-Ray Structure of 3,7-Diiododibenzosuberone. Synthesis of 3,7-Diiodoamitriptyline. *Collect. Czechoslov. Chem. Commun.* **1990**, *55* (11), 2677–2684.

(56) Hossini, M. S.; McCulloug, K. J.; McKay, R.; Proctor, G. R. Ring-Expansion by a Wittig-Prévost Sequence. *Tetrahedron Lett.* **1986**, *27* (32), 3783–3786.

(57) McKay, C. S.; Moran, J.; Pezacki, J. P. Nitrones as Dipoles for Rapid Strain-Promoted 1,3-Dipolar Cycloadditions with Cyclooctynes. *Chem. Commun.* **2010**, *46* (6), 931–933.

(58) Bouveault, L. No Title. *Bull. Soc. Chim. Fr.* **1904**, *31*, 1306–1322.

(59) Braude, E. A.; Evans, E. A. Alkenylution with Lithium Alkenyls. Part XI.* A New Synthesis of Ethylenic Aldehydes. *J. Chem. Soc.* **1955**, 3334–3337.

(60) Zhao, Y.; Truhlar, D. G. The M06 Suite of Density Functionals for Main Group Thermochemistry, Thermochemical Kinetics, Noncovalent Interactions, Excited States, and Transition Elements: Two New Functionals and Systematic Testing of Four M06-Class Functionals and 12 Other Function. *Theor. Chem. Acc.* **2007**, *120* (1–3), 215–241.

(61) Hehre, W. J.; Ditchfield, R.; Pople, J. a. Self—Consistent Molecular Orbital Methods. XII. Further Extensions of Gaussian—Type Basis Sets for Use in Molecular Orbital Studies of Organic Molecules. *J. Chem. Phys.* **1972**, *56*, 2257–2261.

(62) Stewart, J. J. P. Optimization of Parameters for Semiempirical Methods I. Method. *J. Comput. Chem.* **1989**, *10* (2), 209–220.

(63) Sletten, E. M.; Bertozzi, C. R. From Mechanism to Mouse: A Tale of Two Bioorthogonal Reactions. *Acc. Chem. Res.* **2011**, *44* (9), 666–676.

(64) Gordon, C. G.; MacKey, J. L.; Jewett, J. C.; Sletten, E. M.; Houk, K. N.; Bertozzi, C. R. Reactivity of Biarylazacyclooctynones in Copper-Free Click Chemistry. *J. Am. Chem. Soc.* **2012**, *134*, 9199–9208.

(65) Chadwick, R. C.; Khan, U.; Coleman, J. N.; Adronov, A. Polymer Grafting to Single-Walled Carbon Nanotubes: Effect of Chain Length on Solubility, Graft

Density and Mechanical Properties of Macroscopic Structures. *Small* **2013**, *9* (4), 552–560.

(66) Li, H.; Cheng, F.; Duft, A. M.; Adronov, A. Functionalization of Single-Walled Carbon Nanotubes with Well-Defined Polystyrene by "Click" Coupling. *J. Am. Chem. Soc.* **2005**, *127* (23), 14518–14524.

(67) Greenfield, A.; Grosanu, C. Convenient Synthesis of Primary Sulfonamides. *Tetrahedron Lett.* **2008**, *49*, 6300–6303.

(68) Kwok, S. W.; Fotsing, J. R.; Fraser, R. J.; Rodionov, V. O.; Fokin, V. V. Transition-Metal-Free Catalytic Synthesis of 1,5-Diaryl-1,2,3-Triazoles. *Org. Lett.* **2010**, *12* (19), 4217–4219.

(69) Wuts, P. G. M.; Greene, T. W. *Greene's Protective Groups In Organic Synthesis*, 4th ed.; John Wiley & Sons, Inc., 2006.

(70) Jakubowski, W.; Min, K.; Matyjaszewski, K. Activators Regenerated by Electron Transfer for Atom Transfer Radical Polymerization of Styrene. *Macromolecules* **2006**, *39* (I), 39–45.

(71) Harris, J. M.; Struck, E. C.; Case, M. G.; Paley, M. S.; Yalpani, M.; Van Alstine, J. M.; Brooks, D. E. Synthesis and Characterization of Poly(Ethylene Glycol) Derivatives. *J. Polym. Sci. Polym. Chem. Ed.* **1984**, *22* (2), 341–352.

(72) Weder, C.; Wrighton, M. S. Efficient Solid-State Photoluminescence in New Poly (2, 5-Dialkoxy-p-Phenyleneethynylene) S. *Macromolecules* **1996**, *29* (15), 5157–5165.

(73) Chadwick, R. C.; Kardelis, V.; Lim, P.; Adronov, A. Metal-Free Reduction of Secondary and Tertiary N-Phenyl Amides by Tris(Pentafluorophenyl)Boron-Catalyzed Hydrosilylation. *J. Org. Chem.* **2014**, *79* (16), 7728–7733.

(74) Lešetický, L.; Smrček, S.; Sváta, V.; Podlahová, J.; Podlaha, J.; Císařová, I. No Title. *Collect. Czech. Chem. Commun.* **1990**, *55*, 2677–2684.

(75) Hossini, M. S.; McCulloug, K. J.; McKay, R.; Proctor, G. R. Ring-Expansion by a Wittig-Prevost Sequence. *Tetrahedron Lett.* **1986**, *27* (32), 3783–3786.

(76) Wolfe, J. P.; Åhman, J.; Sadighi, J. P.; Singer, R. A. An Ammonia Equivalent for the Palladium-Catalyzed Amination of Aryl Halides and Triflates. *Tetrahedron Lett.* **1997**, *38* (36), 6367–6370.

(77) Buhl, H.; Gugle, H.; Kolshorn, H.; Meier, H. Eine Verbesserte Cyclooctyn-Synthese. *Synthesis (Stuttg).* **1978**, *07*, 536–567.

(78) Chadwick, R. C.; Van Gyzen, S.; Liogier, S.; Adronov, A. Scalable Synthesis of

Strained Cyclooctyne Derivatives. *Synthesis (Stuttg).* **2014**, *46* (05), 669–677.

(79) Starke, F.; Walther, M.; Pietzsch, H. J. A Novel Dibenzoazacyclooctyne Precursor in Regioselective Copper-Free Click Chemistry. An Innovative 3-Step Synthesis. *ARKIVOC* **2010**, *xi*, 350–359.

(80) Jewett, J. C.; Sletten, E. M.; Bertozzi, C. R. Rapid Cu-Free Click Chemistry with Readily Synthesized Biarylazacyclooctynones. *J. Am. Chem. Soc.* **2010**, *132* (11), 3688–3690.

(81) Schmidt, M. W.; Baldridge, K. K.; Boatz, J. A.; Elbert, S. T.; Gordon, M. S.; Jensen, J. H.; Koseki, S.; Matsunaga, N.; Nguyen, K. A.; Su, S.; Windus, T. L.; Dupuis, M.; Montgomery, J. A. General Atomic and Molecular Electronic Structure System. *J. Comput. Chem.* **1993**, *14* (11), 1347–1363.

(82) Dávila, L. Y. A.; Caldas, M. J. Applicability of MNDO Techniques AM1 and PM3 to Ring-Structured Polymers. *J. Comput. Chem.* **2002**, *23* (12), 1135–1142.

Chapter 3

Supramolecular Organogels Prepared from Pillar[5]arene-Functionalized Conjugated Polymers

This chapter has been reprinted with permission from Macromolecules; Vladimir Kardelis, Kelvin Li, Iwona Nierengarten, Michel Holler, Jean-François Nierengarten, and Alex Adronov, **2017**, *50*, 9144-9150, DOI: 10.1021/acs.macromol.7b02399. Copyright (2017) American Chemical Society.

Contributions:

Vladimir Kardelis primarily planned this study. Vladimir Kardelis synthesized all monomeric/polymeric compounds and prepared/characterized the resultant organogels. Mechanical testing of all organogels was also performed by Vladimir Kardelis. Kelvin Li assisted in scaling up synthesis of the monomeric and pillar[5]arene compounds. Iwona Nierengarten performed the ^{1}H-NMR titration experiments for characterizing the host-guest complexes. Michel Holler assisted in the design and synthesis of the pillar[5]arene and cyano-alkyl compounds.

Abstract

Supramolecular polymeric networks are capable of producing gels that exhibit stimulus responsive, self-healing properties, and are useful in a variety of applications. In this work, a pillar[5]arene derivative bearing a single azide functionality was prepared, and coupled via strain-promoted azide-alkyne cycloaddition chemistry to a conjugated polyimine consisting of dibenzocyclooctyne units in its backbone. The resulting polypillar[5]arene structure was found to form inclusion complexes with cyanoalkanes, and produced organogels when mixed with cyanoalkyl-functionalized polymers. The resulting gels could be hydrolyzed by exposure to acid, and could subsequently be re-generated by dehydration. In addition, these organogels exhibited self-healing behavior if severed and re-connected.

3.1. Introduction

Three-dimensional polymer networks are composed of an interpenetrating assembly of crosslinked macromolecules. Depending on the solvent in which they are prepared, these 3D networks can form organogels[1] or hydrogels,[2] each having its own properties and applications, which include super-absorbent materials,[3,4] scaffolds for cell and tissue culture,[5,6] wound dressings,[7] storage and controlled release systems,[8] and many others.[9–11] The nature of crosslinks in these systems dictates many of their properties, and can be covalent[12,13] or supramolecular.[14] In the latter case, non-covalent, reversible crosslinks impart tunability of function and enable the networks to exhibit stimuli-responsive behavior,[15–17] shear-thinning properties,[18] and self-healing capability.[19,20] These supramolecular crosslinks can be composed of hydrogen-bonding partners,[21,22] π-π interactions,[23,24] Van der Waals interactions,[25] and host-guest complexation,[26,27] each of which allows spontaneous gelation to occur. The use of host-guest complexation in the formation of polymer networks has received significant attention, with numerous host structures having been investigated.[28,29] Amongst these, cyclodextrins,[30] calixarenes,[31] and cucurbiturils[32,33] have been most extensively studied. A recent addition to the collection of supramolecular hosts is the macrocycle composed of 1,4-disubstituted hydroquinone subunits connected via methylene bridges in their 2 and 5 positions, also known as the pillar[5]arene.[34] This new class of macrocycles has attracted significant attention as a result of its high-yielding, one-step synthesis,[35,36] its well-defined cylindrical shape,[37] and the rich host-guest chemistry that it exhibits.[38–40] Indeed, it has been shown that pillar[5]arenes can serve as hosts for viologens,[41–43] alkylated pyridines,[44] alkylamines,[45] nitrile-terminated alkanes,[46] and other electron deficient small molecules.[47] In addition, pillar[5]arenes can easily be modified to introduce functional groups that allow their conjugation to a variety of other structures. For example, the synthesis of mono-functionalized pillar[5]arenes has recently been reported,[48] and has allowed for the preparation of a self-complementary structure that assembles into a linear polymer.[49] The introduction of pillar[5]arenes within conjugated structures has also received recent attention, with a polymerizable derivative having been introduced into the backbone of a poly(phenylene ethynylene) structure.[50] Although several examples of conjugated polymers bearing pillar[5]arenes in their backbone have recently been reported, their incorporation as side-chains via flexible linkers has received little attention.[51] Considering their ability to form inclusion complexes with electron-deficient guests, pillar[5]arenes should serve as ideal components of supramolecular polymer networks. While supramolecular gels produced from pillar[5]arene small molecules have been prepared,[52–55] to our knowledge, only one example of a polymeric gel in which pillar[5]arene structures take part in gel crosslinking has been described so far.[56] This supramolecular gel obtained from a dicationic bis(pyridinium) guest and a methacrylate copolymer with pillar[5]arene pendant groups is, however, only responsive to temperature changes.

Recently, we developed a conjugated polyimine containing dibenzocyclooctyne (DIBO) in its backbone structure, and demonstrated its strain-promoted reactivity toward a variety of azide-functionalized small molecules and polymers.[57] It was found that this poly(DIBO) (**P1**, Figure 3.1) reacted with all tested azides in quantitative fashion under mild conditions, with each cyclooctyne along the polymer backbone undergoing strain-promoted azide-alkyne cycloaddition (SPAAC). This enabled the preparation of a library of conjugated polymers, all having the same average length, but differing in side-chain structure. In the present work, we set out to decorate poly(DIBO) with azide-functionalized pillar[5]arene structures to produce a conjugated polymer bearing pillar[5]arene side-chains. Pillar[5]arene-decorated **P2** can serve as a multifunctional host polymer that, when mixed with an appropriate guest-decorated polymer, can form a supramolecular network structure based on the formation of inclusion complexes between pillar[5]arenes and the guests. Specifically, we show that cyanoalkanes can serve as guest molecules to produce 3D network structures in organic solvent, resulting in organogel formation. Furthermore, we show that these supramolecular organogels are pH and moisture-sensitive. The gels can be reversibly degraded *via* acid-catalyzed hydrolysis, and re-constituted by dehydration with appropriate drying agents. Finally, the self-healing properties of these gels have also been demonstrated.

3.2. Results and Discussion

3.2.1. Preparation of Azide-Derivatized Pillar[5]arene

We recently reported the preparation of a dibenzocyclooctyne diamine (DIBO-$(NH_2)_2$) that could be co-polymerized with a dialdehyde via Schiff-base formation to produce a polyimine structure containing DIBO repeat units (**P1**, Figure 3.1).[58] This polyimine is highly reactive toward a variety of azide derivatives, enabling quantitative formation of multiple functional polymers and graft copolymers using post-polymerization functionalization via SPAAC, all starting with the same **P1** structure.

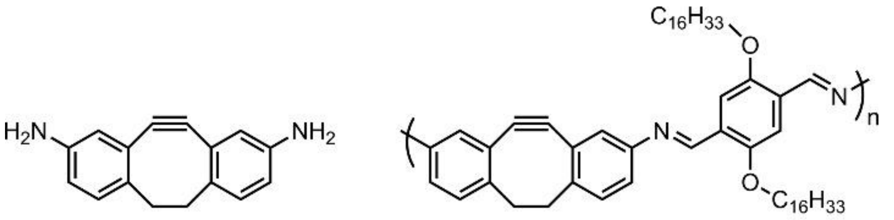

DIBO-$(NH_2)_2$ Poly(DIBO) **P1**

Figure 3.1. Chemical structures of DIBO-$(NH_2)_2$ and the poly(DIBO) **P1.**

In order to derivatize poly(DIBO) **P1** with pillar[5]arene side-chains, a pillar[5]arene derivative bearing a single azide functionality had to be prepared. Monofunctionalization of pillar[5]arene has previously been carried out by one of two approaches,[38,59] including (i) co-cyclization of a monofunctional hydroquinone with 1,4-dialkoxybenezene,[49,60] or (ii) statistical mono-deprotection of a pre-formed alkylated pillar[5]arene.[48,61] In our hands, the mono-deprotection route resulted in better yields, as chromatographic separation of the product from by-products was more efficient using this approach. Thus, following literature procedures, the ethoxy derivative of pillar[5]arene **1** (Scheme 3.1) was prepared in 60% yield via reaction of *p*-diethoxybenzene with paraformaldehyde in the presence of BF_3•OEt_2.[48] Mono-dealkylation of **1** was accomplished using a stoichiometric amount of BBr_3 to afford the mono-hydroxylated derivative **2** in 28% yield. This was followed by alkylation with 1,6-dibromohexane under standard Williamson ether synthesis conditions, forming the bromohexyl ether derivative in 77% yield. Near-quantitative reaction with sodium azide produced the desired monofunctionalized derivative **4** (Scheme 3.1).

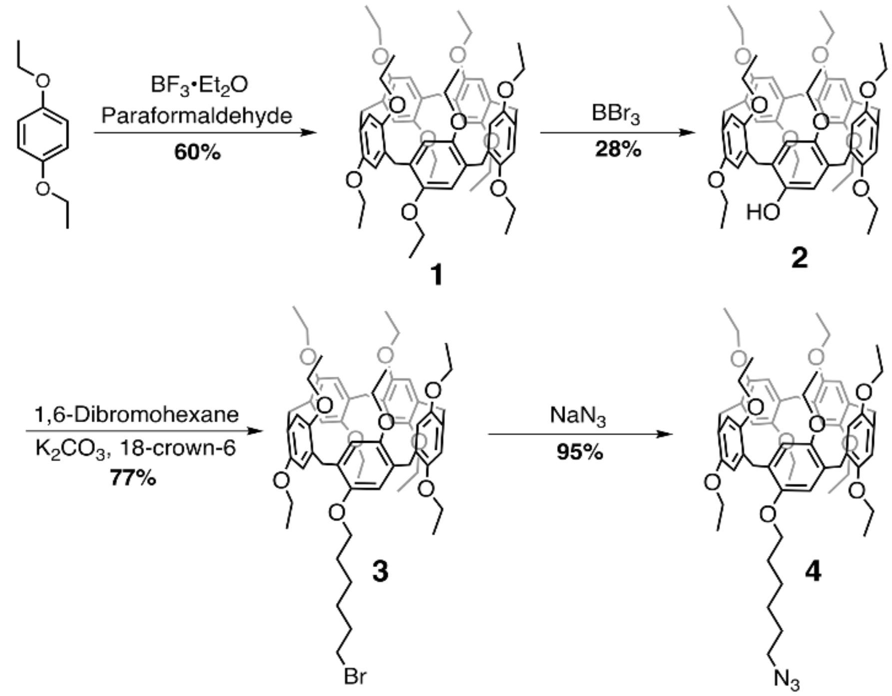

Scheme 3.1. Synthesis of the mono-azide derivative of pillar[5]arene.

3.2.2. Preparation of Polypillar[5]arene (P2)

With the desired azide-derivatized pillar[5]arene in hand, SPAAC coupling with polymer **P1** was carried out by mixing a small excess of pillar[5]arene azide **4** with **P1** (1.1 equiv. of pillar[5]arene relative to each cyclooctyne repeat unit) in dichloromethane and stirring at room temperature for 30 min (Scheme 3.2). Analysis of the reaction mixture by thin layer chromatography indicated that near complete disappearance of **4** occurred within the first 5 minutes. Upon completion of the reaction, precipitation of the reaction mixture into methanol resulted in a yellow solid that was easily isolated by filtration. Characterization of the resulting “polypillar[5]arene” **P2** by ^{1}H NMR (in $CDCl_3$) indicated a quantitative shift of the signals corresponding to the bridge methylene protons in the cyclooctyne repeat units upon conversion from **P1** to **P2** (Figure 3.2A). In addition, Raman spectroscopy showed a complete disappearance of the signal at 2160 cm^{-1} corresponding to the alkyne stretch (Figure 3.2B). Together, this data indicated quantitative conversion from **P1** to **P2** via SPAAC.

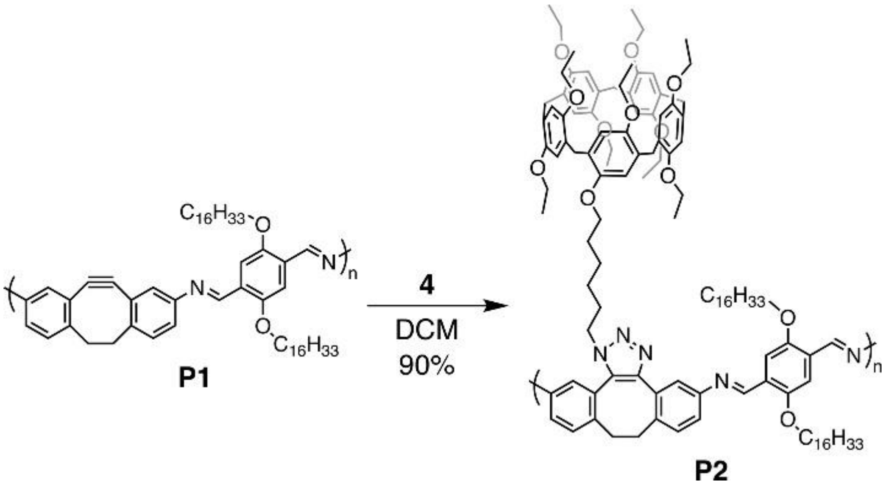

Scheme 3.2. SPAAC coupling of pillar[5]arene azide **4** to **P1**, generating polypillar[5]arene **P2**.

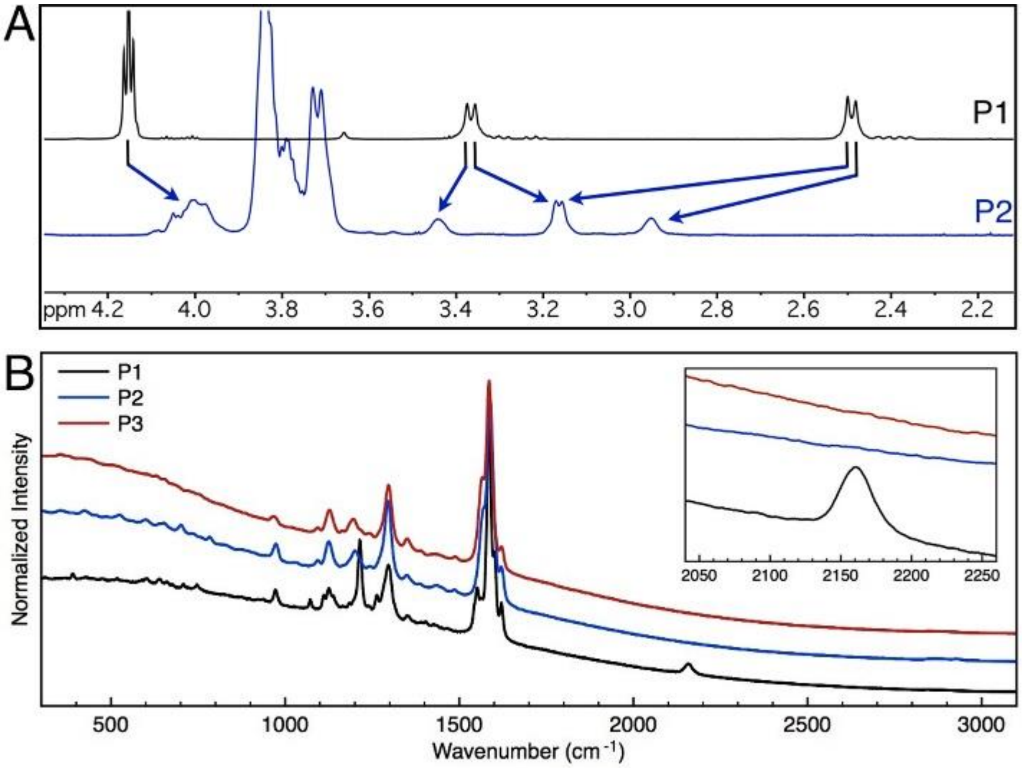

Figure 3.2. (A) ^{1}H NMR spectra of pre-clicked **P1** and post-clicked **P2** ($CDCl_3$; 700 MHz); (B) Raman spectra for **P1**-**P3** (785 nm excitation), with inset showing the region in which the alkyne stretch (2160 cm^{-1}) appears in **P1**, and is undetectable in **P2** and **P3**.

3.2.3. Host-Guest Chemistry of Polypillar[5]arene (P2)

Pillar[5]arene is known to form inclusion complexes with alkyl nitriles, such as 1,6-dicyanohexane.[62,63] To probe the ability of polypillar[5]arene **P2** to form similar inclusion complexes, we first investigated the host-guest chemistry of the monomeric model compound **5** produced by reacting DIBO-(NH_2)$_2$ with pillar[5]arene azide **4** (Scheme 3.3). Titration of **5** with 1,6-dicyanohexane was carried out and monitored by ^{1}H NMR spectroscopy in $CDCl_3$ at 25°C. Continuous changes were observed for all the signals of **5** upon successive additions of the guest. Curve-fitting analysis of the complexation-induced changes in chemical shift allowed calculation of the association constant (K_a) for the 1:1 inclusion complex (Figure 3.12). Based on this data, a $\log K_a$ value of 3.2(1) was found. Control titrations performed with 1,6-dicyanohexane and pillar[5]arene derivatives **1** and **3** gave similar results (Table 3.1 and Figures 3.10, 3.11). The same titration was then carried out using polypillar[5]arene **P2** as the host structure. Complexation-induced changes in chemical shifts were monitored to calculate the K_a value. Interestingly, the observed binding isotherm has a sigmoidal shape, indicating a cooperative binding behavior, where initial guest-binding results in an additional recognition motif such that subsequent guests bind more strongly (Figure 3.13). Curve-fitting analysis of the experimental data gave the stepwise association constants $\log K_1 = 3.1(1)$ and $\log K_2 = 5.2(2)$. The allosteric cooperative factor (α),[64,65] calculated as K_2/K_1, reveals a value of 125, indicating a strong positive cooperativity in the system. The observed behavior is most likely due to intramolecular dipole-dipole interactions between the CN groups of guest molecules associated to pillar[5]arene subunits of the same polymer backbone.[63] Such cooperative effects may play an important role in the formation of supramolecular gels and contribute to their overall stability.

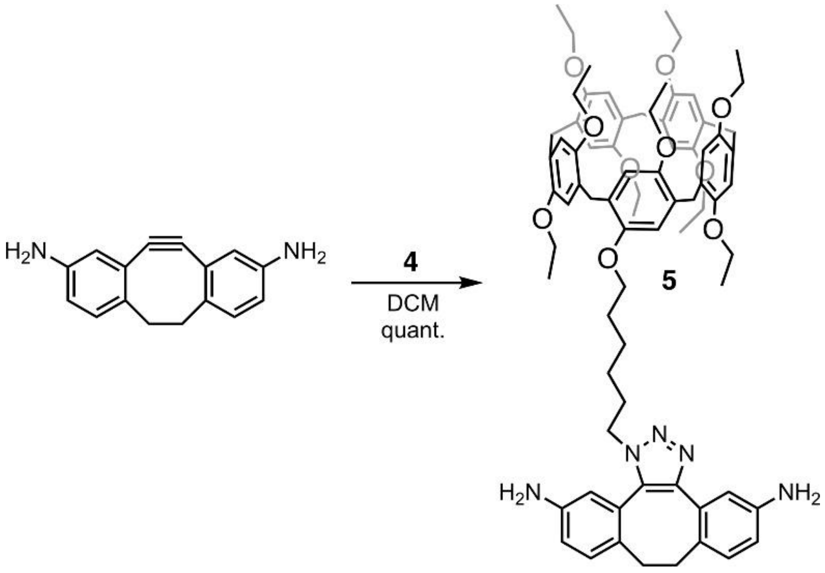

Scheme 3.3. Synthesis of model pillar[5]arene conjugate with DIBO-$(NH_2)_2$.

3.2.4. Preparation of Polymeric Gels

We next set out to determine whether polypillar[5]arene **P2** could function as a supramolecular crosslinker in the formation of polymeric gels. To test this, the hydroxyl end groups of polyethylene glycol having an average molecular weight of 600 g/mol (PEG_{600}) were alkylated via treatment with excess 1,6-dibromohexane, followed by reaction with KCN to install nitrile end groups, producing a bifunctional guest molecule for the polypillar[5]arene (Scheme 3.4). ^{1}H NMR binding studies with model pillar[5]arene derivatives **1** and **5** are consistent with the formation of 2:1 host-guest complexes, thus showing that compound **6** may be an effective cross-linking host for the formation of supramolecular networks with **P2** (Figures 3.16 to 3.19). Binding studies were also carried out with polypillar[5]arene **P2** and **6**, however quantitative analysis to determine the association constant could not be achieved due to aggregation phenomena. Nevertheless, these data indicated the formation of host-guest complexes between **6** and the pillar[5]arene subunits of polymer **P2**.

Network formation between polypillar[5]arene **P2** and bis(cyanohexyl)PEG$_{600}$ (**6**) was attempted by mixing the two components in a 1:1 molar ratio of pillar[5]arene units relative to cyanohexyl end-groups of **6** in chloroform. It was found that gelation occurred over the course of 4 h, but only at total polymer concentrations of 50 mM or higher. At lower concentrations, the association constant between cyanohexyl guests and the pillar[5]arene hosts is not large enough to result in sufficient complexation to produce a gel. Furthermore, the gels formed from these two components were very soft, and tended to lose their rigidity on standing over the course of several hours. This likely occurs due to hydrolysis of imine linkages, as the hydrophilic PEG$_{600}$ may retain significant amounts of water within the organogel.

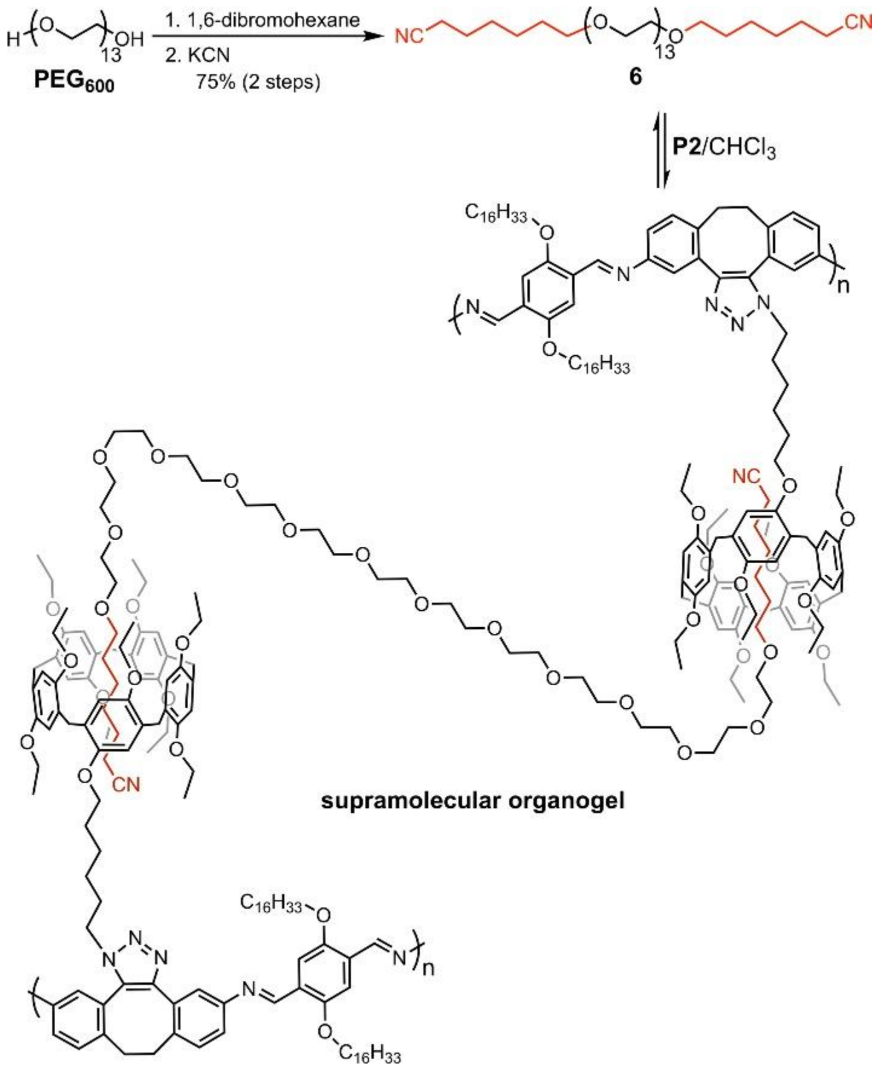

Scheme 3.4. Preparation of cyanohexyl-terminated PEG_{600} and its use in supramolecular organogel formation.

To increase the rigidity and stability of the supramolecular pillar[5]arene-based gels, we again used the DIBO polymer **P1** in a reaction with 11-azidoundecanenitrile (**7**), which was prepared by sequentially treating 1,10-dibromodecane with KCN and sodium azide. SPAAC coupling of **7** with **P1** proceeded smoothly at room temperature over 30 min to produce the cyanoalkane-decorated **P3** (Scheme 3.5). The ability of **P3** to form inclusion complexes with pillar[5]arene derivatives was first evidenced by ^{1}H NMR binding studies with model compound **1** in $CDCl_3$ at 25°C (Figure 3.20). Quantitative analysis gave a $\log K_a$ value of 1.8(2). NMR spectra were also recorded for mixtures of polymers **P2** and **P3**. Whereas the observed changes in chemical shifts for the signals of both polymers were consistent with the formation of host-guest complexes, treatment of the data to derive a K_a value was prohibited by the formation of aggregates, resulting in substantial broadening of the observed signals.

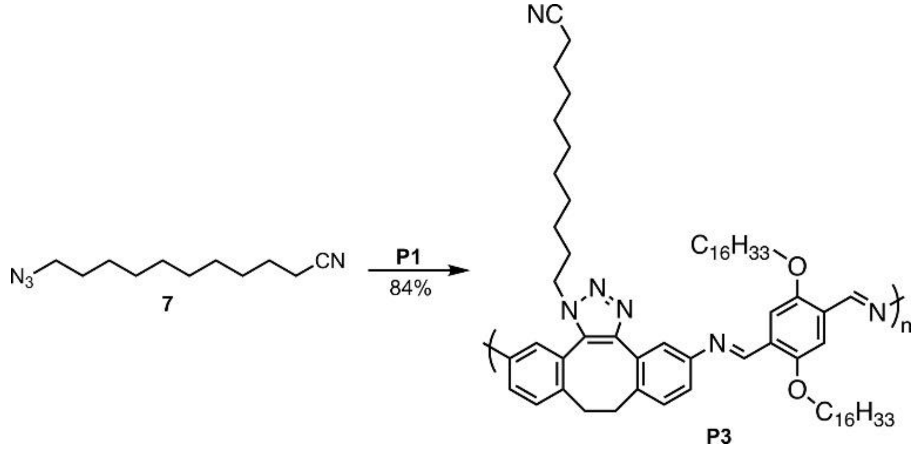

Scheme 3.5. Preparation of cyanoalkyl-functionalized polymer **P3**.

Combination of equimolar ratios of polypillar[5]arene **P2** and polycyanoalkyl **P3** in chloroform at a concentration of 50 mM resulted in gelation upon standing for 4 h. The resulting yellow gel was found to be stiffer and more stable than the PEG-based **P2-6** gel, with no observable degradation over time. Although the gel stability of the **P2-P3** gel was higher than that of the **P2-6** gel, the imine linkages that form the backbone of both **P2** and **P3** are hydrolytically unstable. Treatment of the **P2-P3** gel with trifluoroacetic acid (TFA) vapors, by placing the vial containing the gel into a secondary container to which was added a drop of TFA prior to sealing its lid, resulted in a transition from the yellow gel to a red liquid over the course of 1 hour (Figure 3.3). Interestingly, dehydration of the red liquid by simply placing the vial in another secondary container charged with activated 3 Å molecular sieves resulted in reversion of the red liquid into a red gel (Figure 3.4). The red color arises from protonation of the imines and formation of quaternary iminium salts in the polymer backbone. This process can be followed by ^{1}H NMR ($CDCl_3$), which clearly shows the appearance of aldehyde protons at 10.5 ppm upon degradation of the gel and their disappearance after dehydration (Figure 3.8). Thus, the reversible hydrolysis of the polyimine backbone enables reversible degradation of the gel, and the degradation-reformation process can be cycled multiple times (this was done in triplicate with no observable differences from one cycle to the next). Furthermore, the red gel can be reverted back to the original yellow gel structure upon exposure to vapors of triethylamine (or other volatile bases). It should be noted that reformation of the gel is not complete, as the ratio of imine to aldehyde protons does not revert to its starting value. This indicates that polymer chains formed upon dehydration do not recover the original average length of polymers prior to hydrolysis.

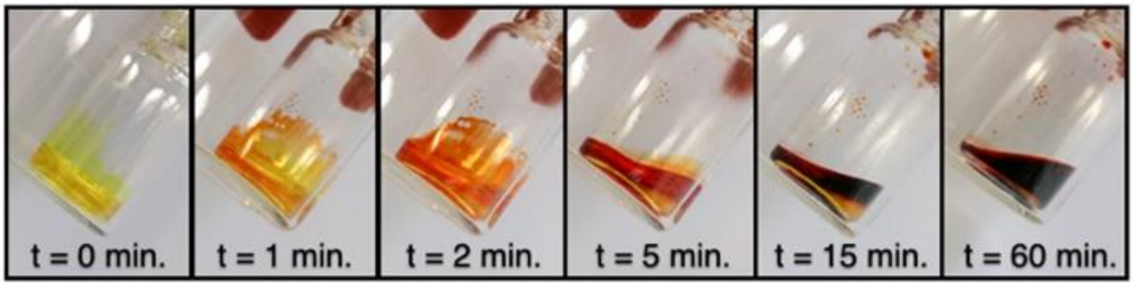

Figure 3.3. Degradation of supramolecular organogel by exposure to acid vapor over the course of 60 minutes.

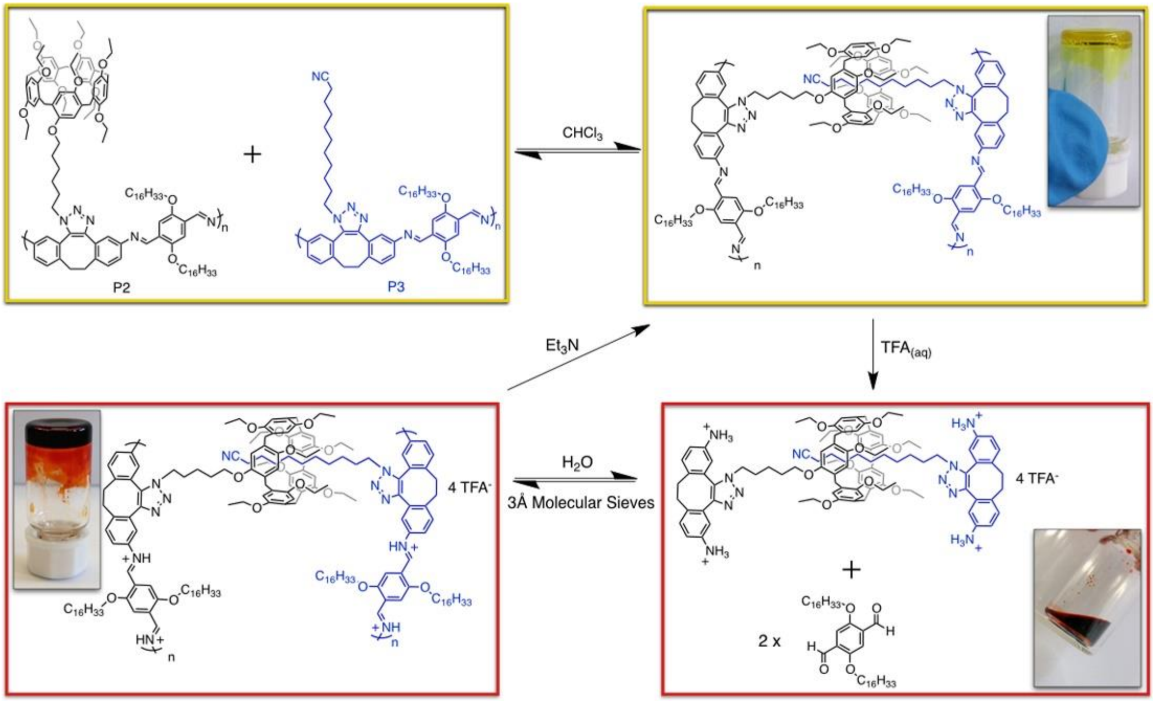

Figure 3.4. The supramolecular gel formation, degradation, and re-fromation cycle. **P2** and **P3** form a yellow organogel in the presence of chloroform. The imine linkages can be hydrolyzed with trifluoroacetic acid (TFA), resulting in a red, degraded gel. The gel can then be regenerated upon exposure to 3Å molecular sieves, followed by addition of triethylamine. This degradation/regeneration cycle can be repeated multiple times.

It is interesting to note that the degradation/reformation of the **P2-P3** gel results in the formation of a new polymer system as the pillar[5]arene and cyanoalkane monomers scramble, forming random copolymers of these components after gel reformation. The effect of the degradation/reformation process and monomer scrambling on the stiffness of the gel was determined by performing mechanical strength measurements on a freshly made **P2-P3** gel, as well as a regenerated (1 cycle) **P2-P3** gel at a 25 wt% concentration in the non-volatile solvent, 1,2-dichlorobenzene (see Supporting Information). The force-deformation curves from these measurements are depicted in Figure 3.5. The regenerated gel was found to exhibit a much lower Young's modulus (YM) value (YM = 0.1 ± .01 kPa) than the original, freshly made gel (YM = 2.0 ± 0.2 kPa). The cause of the decrease in mechanical stiffness could be either the scrambling of monomers into random copolymers after the degradation/reformation process, or a decrease in polymer molecular weight, caused by incomplete repolymerization, as evidenced by the incomplete reformation of the imine signal in the ^{1}H NMR spectrum of this material. To determine which factor is responsible for the diminished mechanical properties, we synthesized a random copolymer containing the pillar[5]arene- and cyanoalkyl-functionalized monomers. This random polyimine was prepared by reacting equimolar ratios of azides **4** and **7** with poly(DIBO) **P1** (Scheme 3.6). By introducing an equal amount of host and guest moieties on the same polymer chain, **P4**, this polymer undergoes self-gelation upon addition of solvent. The force-deformation curve from the random copolymer showed a Young's modulus of 2.7 ± 0.2 kPa, which is slightly higher than the original gel formed from the homopolymers, **P2-P3**. It seems that the random copolymers are able to self-associate more effectively, resulting in a higher number of crosslinks, and therefore a stiffer gel. Thus, we can confirm that the decreased Young's modulus of the reformed gel is caused by the lower degree of polymerization of the component polymers, rather than scrambling of the monomer units in the product.

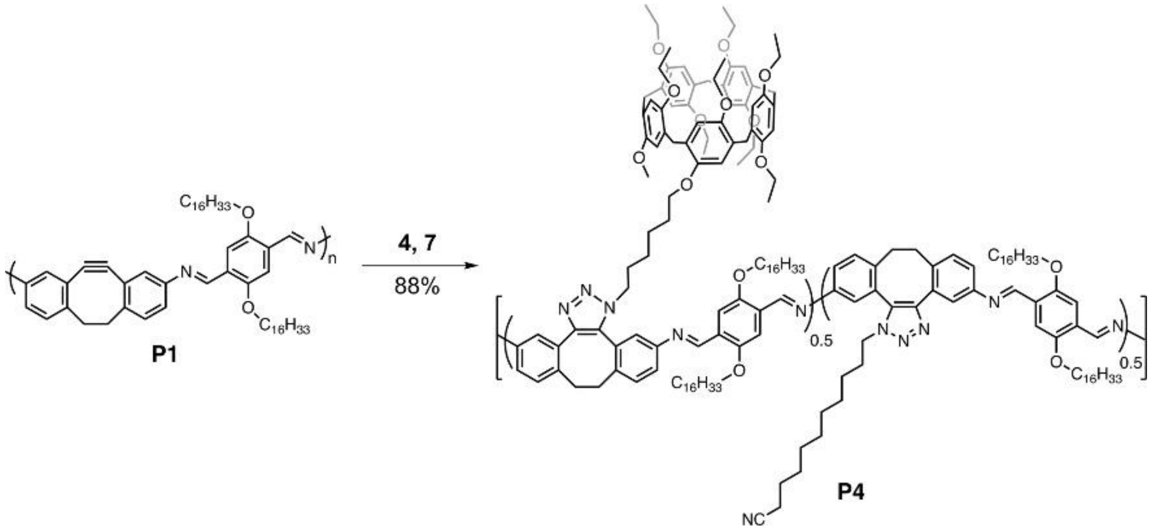

Scheme 3.6. Preparation of pillar[5]arene-co-cyanoalkane random polymer **P4.**

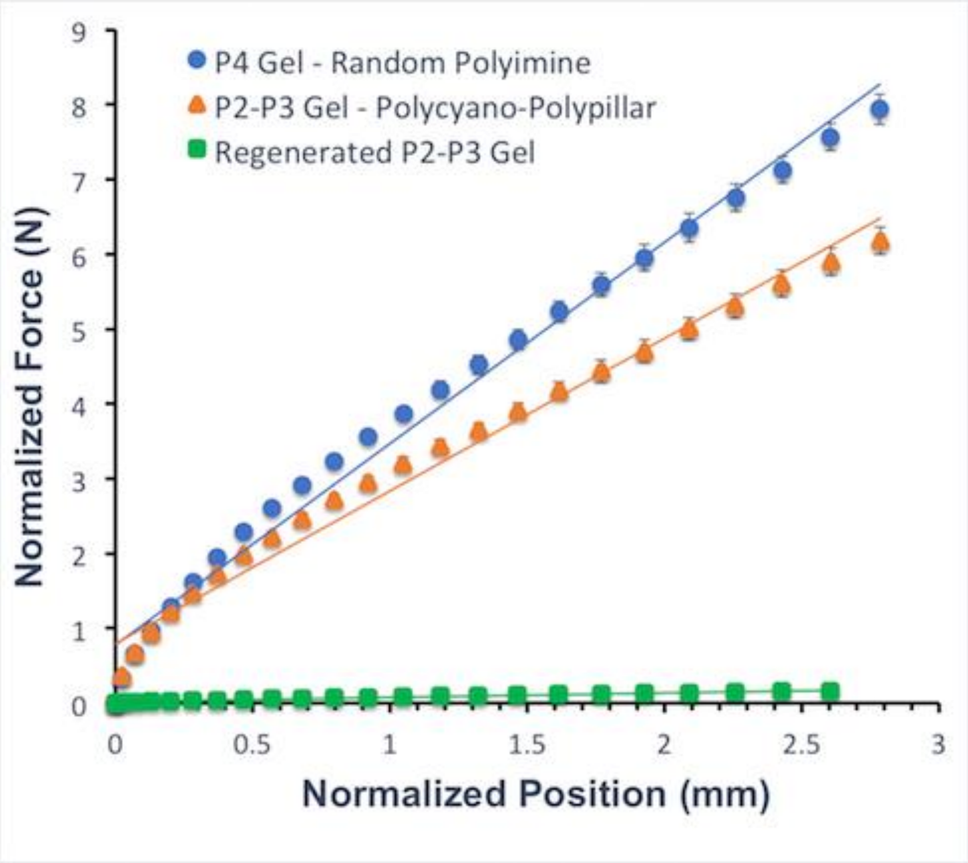

Figure 3.5. Applied force vs. deformation depth curves for the **P2-P3**, **P4**, and regenerated **P2-P3** gels.

Considering that gelation of **P2-P3** mixtures results from reversible, supramolecular interactions of pillar[5]arene units with alkyl nitrile side-chains, the resulting gel should exhibit self-healing properties if the gel is damaged.[66,67] To test this, we prepared a sample of the gel and severed it with a blade into two pieces of roughly equal size (Figure 3.6a and b). The two pieces were then brought in contact with minimal force (by hand, Figure 3.6c) and left undisturbed for 10 minutes. After this time, the two pieces could not be pulled apart at the interface of the cut when pulled with tweezers (Figure 3.6d). If pulled apart to the point of breaking, the gel broke in areas that were different from the site of the cut.

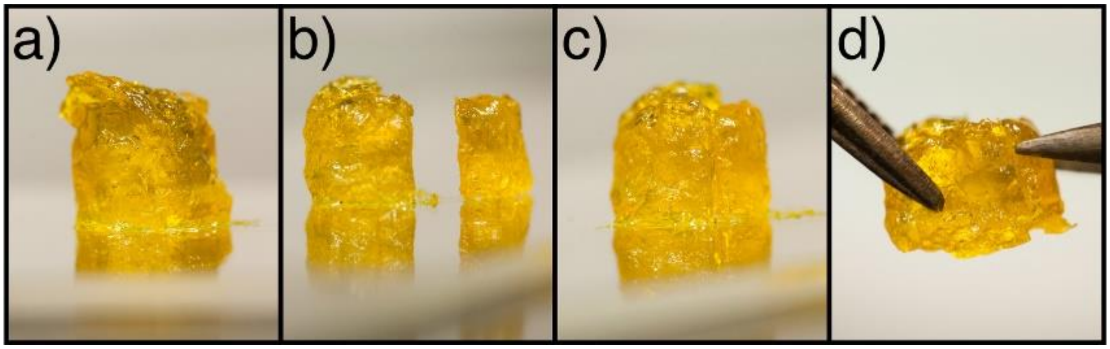

Figure 3.6. Successive photographs of a sample of **P2-P3** gel as prepared (a), after being cut (b), after severed pieces were reattached (c), and during an attempt to pull the severed pieces apart (d).

3.3. Conclusions

Functionalization of poly(DIBO) with a mono-azide derivative of pillar[5]arene was accomplished by SPAAC. The resulting polypillar[5]arene structure undergoes host-guest chemistry with dicyanohexane, as well as with cyanohexane-terminated PEG chains. Organogel formation was observed when the polypillar[5]arene was mixed with cyanohexane-terminated PEG_{600}, but this gel was relatively weak and unstable. Reaction of poly(DIBO) with 11-azidoundecanenitrile produced a polymeric guest that assembles with polypillar[5]arene and results in a more highly crosslinked, stiffer gel that does not degrade over time. Acid-catalyzed hydrolysis of the gel can be carried out by exposure to acid vapor, leading to cleavage of the imine linkages. However, the gel can be re-formed via dehydration with molecular sieves. The stiffness of the gel was found to decrease upon hydrolysis and reformation, which was caused by incomplete re-polymerization of the polymer chains upon dehydration. In addition, this gel exhibits self-healing properties if severed and re-attached.

3.4. Supporting Information

3.4.1. General Experimental

All reagents were purchased from commercial chemical suppliers and used without further purification. Unless otherwise mentioned all reactions were performed under an inert atmosphere. ^{1}H-NMR and ^{13}C-NMR spectra were recorded on Bruker AC 400, Avance 600 and Avance 700 MHz spectrometers. High-resolution (HR) electrospray ionization (ESI) MS measurements were carried out on the Micromass Ultima Global instrument (quadrupole time-of-flight). Polymer molecular weights and polydispersity indices (PDI) were analyzed via gel permeation chromatography (GPC) using a Waters 2695 Separations Module, equipped with a Waters 2414 refractive-index detector, and a Jordi Fluorinated DVB 10^4 Å column. Polystyrene standards were used for calibration, with THF as the eluent at a flow rate of 2.0 mL/min. Raman spectra were collected with a Renishaw InVia Laser Raman spectrometer equipped with a 300 mW Renishaw laser (785 nm, grating 1200 L/mm). Laser intensities of 1-5% were used to collect data. Infrared spectra were collected with a Thermo Scientific Nicolet 6700 spectrometer equipped with a Smart ITX ATR sample analyzer. Melting points were obtained using a Digimelt MPA160 melting point apparatus.

3.4.2. Experimental Procedures

Synthesis of Compounds 1-8:

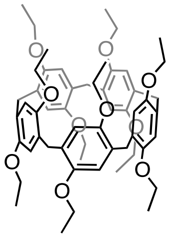

1

Compound 1 (1,4-bis(ethoxy)pillar[5]arene) was synthesized according to literature procedures.[68,39]

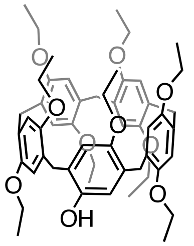

2

Compound 2 (Mono-*O*-de-ethylated pillar[5]arene)[69]

Under argon, a boron tribromide solution (1 M in dichloromethane, 0.20 mL, 0.20 mmol) was added dropwise to a solution of compound **1** (200 mg, 0.22 mmol) in dichloromethane (24 mL) at rt. The resulting mixture was stirred at rt for 60 min then quenched with distilled water (10 mL). The organic phase was dried with $MgSO_4$, filtered, and concentrated. Column chromatography (SiO_2, EtOAc:Cyclohexane 1:5) yielded **2** (54 mg, 28%) as a colorless solid. M.W.: 863.09 g/mol; ^{1}H-NMR (400 MHz; $CDCl_3$): δ 6.90 (s, 1H), 6.78 (s, 1H), 6.70 (s, 1H), 6.69 (s, 1H) 6.64 (m, 3H), 6.55 (m, 3H), 6.49 (s, 1H), 4.03 (q, J = 7.0 Hz, 2H), 3.92-3.72 (m, 24H), 3.64 (q, J = 7.0 Hz, 2H), 1.44-1.35 (m, 10H), 1.24-1.07 (m, 16H), 1.03 (t, J = 7.0 Hz, 3H); HRMS (ESI+) (m/z) for $C_{53}H_{70}NO_{10}$ $[M\text{-}NH_4]^+$ calculated: 880.5000, found: 880.4979.

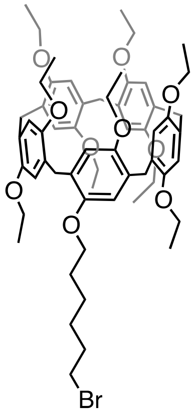

3

Compound 3 (Mono-*O*-alkylated pillar[5]arene bromide)[70]

A mixture of **2** (200 mg, 0.23 mmol), 1,6-dibromohexane (566 mg, 2.32 mmol), K_2CO_3 (321 mg, 2.32 mmol) and 18-crown-6 (6 mg, 0.023 mmol) in acetone (2 mL) was stirred at 50 °C for 24 h. The resulting mixture was cooled to rt, filtered and concentrated. Column chromatography (SiO_2, EtOAc:Cyclohexane 1:20 to 1:10) yielded **3** (184 mg, 77%) as a colorless solid. M.W.: 1026.14 g/mol; mp = 195-197 °C; ^1H-NMR (400 MHz; CD_2Cl_2): δ 6.89-6.86 (broad, 9H), 6.84 (s, 1H), 3.97-3.87 (m, 20H), 3.72 (s, 10H), 3.45 (t, J = 7.0 Hz, 2H), 1.95-1.81 (m, 4H), 1.62-1.53 (m, 4H), 1.44 (t, J = 7.0 Hz, 27H); HRMS (ESI+) (m/z) for $C_{59}H_{81}BrNO_{10}$ $[M\text{-}NH_4]^+$ calculated: 1042.5044, found: 1042.5044.

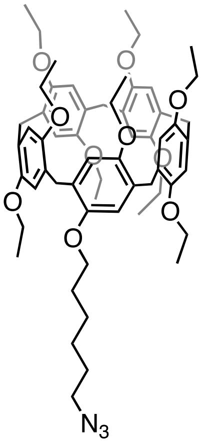

4

Compound 4 (Mono-*O*-alkylated pillar[5]arene azide)

A solution of **3** (50 mg, 0.048 mmol) and sodium azide (31 mg, 0.48 mmol) in *N*,*N*-dimethylformamide (0.5 mL) and tetrahydrofuran (0.5 ml) was stirred at 40 °C for 16 h. The resulting mixture was diluted with diethyl ether (20 mL), washed with water (3 x 20 mL), dried with magnesium sulfate, and concentrated. Column chromatography (SiO_2, EtOAc:Cyclohexane 1:9) yielded **4** (45 mg, 95%) as a colorless solid. M.W.: 988.26 g/mol; mp = 175-177 °C; ^{1}H-NMR (400 MHz; CD_2Cl_2): δ 6.88-6.86 (broad, 9H), 6.84 (s, 1H), 3.96-3.86 (m, 20H), 3.72 (s, 10H), 3.29 (t, J = 7.0 Hz, 2H), 1.85 (m, 2H), 1.66 (m, 2H), 1.60-1.54 (m, 2H), 1.49-1.46 (m, 2H), 1.44 (t, J = 7.0 Hz, 27H); HRMS (ESI+) (m/z) for $C_{59}H_{81}N_4O_{10}$ [M-NH$_4$]$^+$ calculated: 1005.5947, found: 1005.5948.

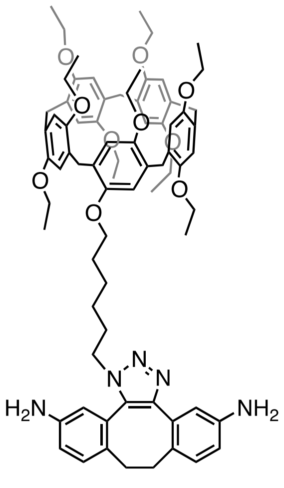

5

Compound 5 (Pillar[5]arene-DIBO-(NH$_2$)$_2$ conjugate)

A solution of compound **4** (20.0 mg, 20.2 μmol) and DIBO-(NH$_2$)$_2$ (synthesized as previously described[5], 4.3 mg, 18.4 μmol) in dichloromethane (0.2 mL) was stirred at 40 °C for 60 min. The reaction mixture was purified by column chromatography (SiO$_2$, EtOAc:Cyclohexane 1:1 to 9:1) to yield **5** (23 mg, 100%) as a colorless solid. M.W.: 1222.55 g/mol; mp = 113-117 °C; ^{1}H-NMR (700 MHz; CDCl$_3$): δ 7.09 (d, J = 8.5 Hz, 1H), 6.93 (d, J = 8.5 Hz, 1H), 6.83 (d, J = 2.5, 1H), 6.77 (s, 1H), 6.73 (d, J = 5.0 Hz, 2H), 6.71 (d, J = 7.0 Hz, 4H), 6.69 (s, 1H), 6.67 (s, 1H), 6.65-6.63 (m, 2H), 6.56 (dd, J = 8.0 Hz, 2.5 Hz, 1H), 6.43 (d, J = 2.5 Hz, 1H), 4.44 (dt, J = 14.0 Hz, 7.0 Hz, 1H), 4.34 (dt, J = 14.0 Hz, 7.0 Hz, 1H), 3.84-3.75 (m, 30H), 3.60 (s, 4H), 3.22-3.19 (m, 1H), 2.96-2.90 (m, 2H), 2.76-2.72 (m, 1H), 1.90-1.86 (m, 1H), 1.86-1.82 (m, 1H), 1.73-1.68 (m, 2H), 1.49-1.43 (m, 2H), 1.37 (dt, J = 14.5 Hz, 8.0 Hz, 2H), 1.27-1.23 (m, 21H), 1.21-1.18 (m, 6H); ^{13}C-NMR (176 MHz; CDCl$_3$): δ 150.17, 150.07, 150.02, 149.97, 149.86, 146.9, 144.8, 144.3, 134.0, 132.0, 131.2, 130.8, 128.78, 128.69, 128.52, 128.45, 128.1, 127.4, 118.0, 117.0, 115.67, 115.55, 115.43, 115.32, 115.16, 115.00, 114.83, 68.6, 63.99, 63.93, 63.88, 63.78, 48.4, 36.1, 32.4, 30.5, 30.23, 30.18, 29.98, 29.92, 29.78, 29.4, 26.4, 25.9, 15.25, 15.19, 15.09; HRMS (ESI+) (m/z) for $C_{75}H_{91}N_5O_{10}$ $[M-H]^+$ calculated: 1222.6839, found: 1222.6837.

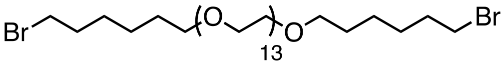

6a

Compound 6a (Bis(6-bromohexyl)polyethylene glycol 600)[71]

A suspension of sodium hydride (60% oil dispersion, 670 mg, 16.7 mmol), 1,6-dibromohexane (4.07 g, 16.7 mmol), and polyethylene glycol 600 g/mol (1.00 g, 1.67 mmol) in dry tetrahydrofuran (4 mL) was stirred for 16 h at rt. The mixture was filtered, concentrated, and purified via column chromatography (SiO_2, MeOH:DCM 1:9) to yield **6a**, (1.45 g, 92%) as a colorless oil. M.W.: 916.81 g/mol. ^{1}H-NMR (600 MHz; $CDCl_3$): δ 3.66-3.62 (m, 55H), 3.58-3.57 (m, 4H), 3.45 (t, J = 6.5 Hz, 4H), 3.40 (t, J = 6.5 Hz, 4H), 1.88-1.84 (m, 4H), 1.62-1.57 (m, 4H), 1.48-1.43 (m, 4H), 1.39-1.35 (m, 4H).

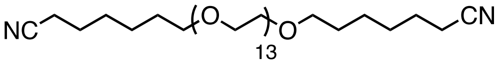

6

Compound 6 (Bis(6-cyanohexyl)polyethylene glycol 600)

A solution of compound **6a** (300 mg, 0.319 mmol) and potassium cyanide (207 mg, 3.19 mmol) in *N*,*N*-dimethylformamide (0.5 mL) was stirred at 50 °C for 16 h. The resulting mixture was concentrated and purified via column chromatography (SiO_2, MeOH:DCM 1:9) to yield **6** (219 mg, 81%) as a light brown oil. M.W.: 809.04 g/mol. ^{1}H-NMR (600 MHz; $CDCl_3$): δ 3.63-3.61 (m, 53H), 3.57-3.55 (m, 4H), 3.44 (t, J = 7.0 Hz, 4H), 2.32 (t, J = 7.0 Hz, 4H), 1.67-1.63 (m, 4H), 1.60-1.56 (m, 4H), 1.48-1.43 (m, 4H), 1.39-1.35 (m, 4H). HRMS (ESI+) (m/z) for $C_{40}H_{80}N_3O_{14}$ $[M-NH_4]^+$ calculated: 831.5189, found: 831.5195.

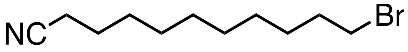

7a

Compound 7a (11-Bromoundecanenitrile)[72]

A solution of 1,10-dibromodecane (1.00 g, 3.33 mmol) and potassium cyanide (217 mg, 3.33 mmol) in *N*,*N*-dimethylformamide (10 mL) was stirred for 16 h at 50 °C. The resulting mixture was cooled to rt, diluted with diethyl ether (50 mL), washed with water (3 x 30 mL), dried over magnesium sulfate, and concentrated. Column chromatography (SiO_2, DCM:Cyclohexane 1:1) yielded **7a** (126 mg, 15%) as a colorless oil. M.W.: 246.19. ^{1}H-NMR (400 MHz; $CDCl_3$): δ 3.41 (t, J = 7.0 Hz, 2H), 2.33 (t, J = 7.0 Hz, 2H), 1.85 (q, J = 7.0 Hz, 2H), 1.66 (q, J = 7.0 Hz, 2H), 1.46-1.39 (m, 4H), 1.30 (s, 8H).

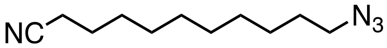

7

Compound 7 (11-Azidoundecanenitrile)

A solution of compound **7a** (85 mg, 0.345 mmol) and sodium azide (112 mg, 1.73 mmol) in *N*,*N*-dimethylformamide (0.5 mL) was stirred at 50 °C for 16 h. The resulting mixture was cooled to rt, diluted with diethyl ether (10 mL), washed with water (3 x 10 mL), dried over magnesium sulfate, and concentrated. Column chromatography (SiO_2, DCM:Cyclohexane 1:1) yielded **7** (68 mg, 95%) as a light yellow oil. M.W.: 208.30. ^{1}H-NMR (400 MHz; $CDCl_3$): δ 3.26 (t, J = 7.0 Hz, 2H), 2.34 (t, J = 7.0 Hz, 2H), 1.70-1.56 (m, 4H), 1.46-1.43 (m, 2H), 1.38-1.30 (m, 10H). Compound **7** could not be observed via mass spectrometry; thus, for further characterization compound **8** (**azidoundecanenitrile-DIBO-(NH_2)$_2$ conjugate)** was synthesized.

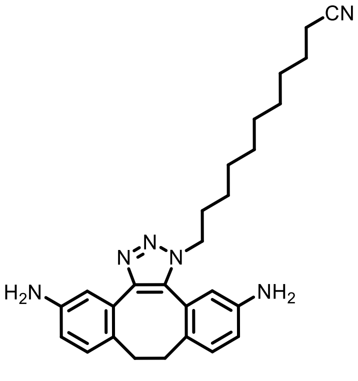

8

Compound 8 (Azidoundecanenitrile-DIBO-(NH_2)$_2$ conjugate)

Synthesized as reported for compound **5.** Yield = 92%. Beige solid. M.W.: 442.61. ^{1}H NMR (700 MHz; $CDCl_3$): δ 7.11 (d, J = 8.0 Hz, 1H), 6.92 (d, J = 8.0 Hz, 1H), 6.83 (d, J = 2.0 Hz, 1H), 6.67 (dd, J = 8.0 Hz, 2.0 Hz, 1H), 6.56 (dd, J = 8.0 Hz, 2.0 Hz, 1H), 6.44 (d, J = 2.0 Hz, 1H), 4.42 (dt, J = 14.0 Hz, 7.0 Hz, 1H), 4.31 (dt, J = 14.0 Hz, 7.0 Hz, 1H), 3.21-3.19 (m, 1H), 2.93 (q, J = 8.0 Hz, 2H), 2.77-2.74 (m, 2H), 2.32 (t, J = 7.0 Hz, 2H), 1.83 (dd, J = 14.0 Hz, 7. Hz, 1H), 1.76 (dd, J = 14.0 Hz, 7.0 Hz, 1H), 1.63 (dt, J = 15.0 Hz, 7.5 Hz, 2H), 1.41 (dt, J = 15.0 Hz, 7.5 Hz, 2H), 1.31-1.15 (m, 10H). HRMS (ESI+) (m/z) for $C_{27}H_{35}N_6$ $[M-H]^+$ calculated: 443.2923, found: 443.2905.

Synthesis of Polymeric Compounds P1-P3:

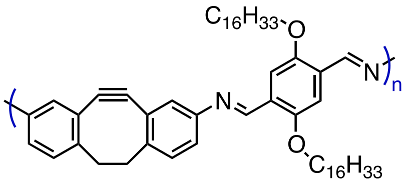

P1

Synthesis of Cyclooctyne-Containing Polyimine P1

Polyimine **P1** was synthesized as previously described.[73]

Yield: 80%. Bright yellow solid. M_n:29.3 kDa (GPC), M_w:58.8 kDa (GPC). ^{1}H-NMR (600 MHz; $CDCl_3$): δ 10.53 (s), 8.97 (s, 2H), 7.77 (s, 2H), 7.35 (d, J = 8.0 Hz, 2H), 7.25 (s, 2H), 7.18 (d, J = 7.0 Hz, 2H), 4.15 (t, J = 6.5 Hz, 4H), 3.37 (d, J = 10.5 Hz, 2H), 2.49 (d, J = 10.5 Hz, 2H), 1.86 (m, 4H), 1.50 (m, 4H), 1.38 (m, 4H), 1.33-1.27 (m, 46H), 0.87 (t, J = 7.0 Hz, 6H); ^{13}C-NMR (176 MHz; $CDCl_3$): δ 156.28, 156.17, 153.6, 151.65, 151.52, 151.21, 151.05, 145.0, 144.3, 130.17, 130.09, 128.52, 128.48, 128.42, 124.80, 124.68, 124.52, 120.82, 120.68, 118.85, 118.72, 114.63, 114.50, 112.9, 112.0, 111.7, 111.1, 110.7, 69.4, 36.7, 36.3, 35.9, 32.1, 29.87, 29.82, 29.78, 29.55, 29.52, 29.43, 26.3, 22.8, 14.3.

General Procedure for Polymer/Azide Cycloaddition (P2 and P3)

A slight excess of the azide **4** or **7** (1.1 eq per alkyne) and the cyclooctyne-containing polymer **P1** were dissolved in dry dichloromethane (50 mM azide concentration). The resultant solution was stirred for 60 min before precipitating in dry diethyl ether at rt to remove excess azide. The solids were filtered and dried.

Procedure for P4

50 mM stock solutions of azides **4** and **7** in dichloromethane were created in separate vials. 0.6 eq (per alkyne) of each azide was simultaneously pipetted into a 1 mL screw cap vial containing **P1.** The resulting mixture was stirred for 60 min at rt and monitored by ^{1}H-NMR spectroscopy for completion. The yellow solution was precipitated into dry diethyl ether at rt to remove excess azide. The solid was filtered and dried.

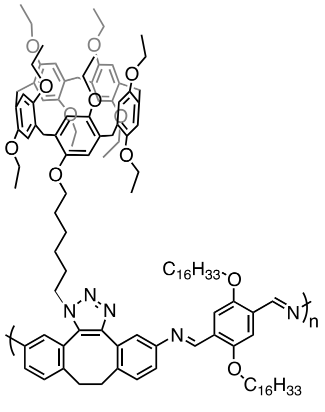

P2

Pillar[5]arene-containing polyimine (P2)

Yield: 90%. Bright yellow powder. M_n:25.1 kDa (GPC), M_w:50.8 kDa (GPC); ^{1}H-NMR (700 MHz; CDCl$_3$): δ 10.51 (s), 8.92-8.88 (m, 2H), 7.74-7.69 (m, 2H), 7.46-7.40 (m, 2H), 7.23-7.20 (m, 2H), 7.13-7.08 (m, 2H), 6.78-6.69 (m, 10H), 4.50-4.42 (m, 2H), 4.10-3.95 (m, 4H), 3.84-3.79 (m, 20H), 3.73-3.70 (m, 10H), 3.44 (s, 1H), 3.16 (d, J = 10.0 Hz, 2H), 2.95 (s, 1H), 1.91 (s, 2H), 1.77 (s, 1H), 1.69 (s, 5H), 1.34-1.26 (m, 30H), 1.25-0.78 (m, 54H).

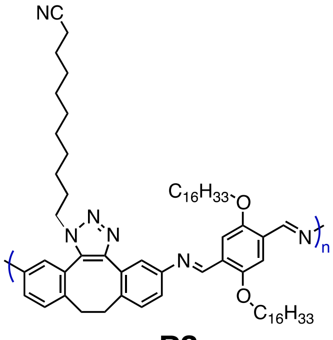

P3

Alkylcyano-containing polyimine (P3)

Yield: 84%. Dark yellow waxy solid. M_n:20.3 kDa (GPC), M_w:33.7 kDa (GPC); ^{1}H-NMR (700 MHz; $CDCl_3$): δ 10.50 (s), 8.90 (d, J = 16.0 Hz, 2H), 7.72-7.66 (m, 2H), 7.44 (s, 1H), 7.41 (s, 1H), 7.22-7.20 (m, 2H), 7.12 (s, 1H), 7.07 (s, 1H), 4.51 (s, 1H), 4.42 (s, 1H), 4.06 (s, 4H), 3.43 (s, 1H), 3.16 (d, J = 10.5 Hz, 2H), 2.96 (s, 1H), 2.30 (s, 2H), 1.84 (s, 1H), 1.79 (s, 5H), 1.61 (t, J = 7.5 Hz, 2H), 1.42 (s, 6H), 1.24 (s, 60H), 0.86 (t, J = 7.0 Hz, 6H).

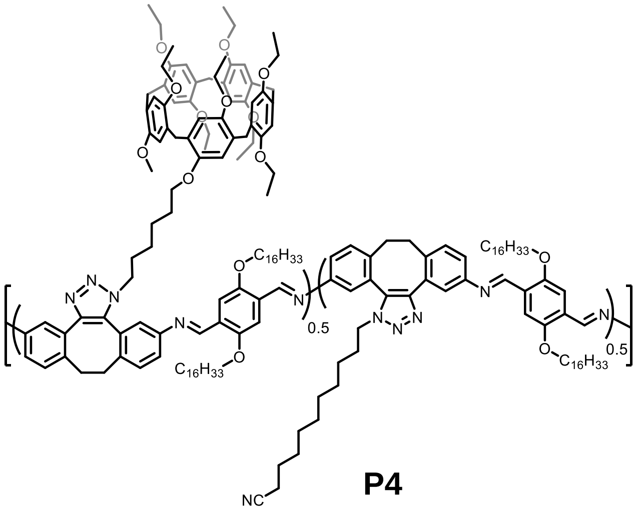

P4

Random Polyimine (P4)

Yield: 88%. Bright yellow powder. M_n:24.9 kDa (GPC), M_w:51.6 kDa (GPC); ^{1}H-NMR (700 MHz; $CDCl_3$): δ 10.50 (s), 8.90 (m, 2H), 7.69 (m, 2H), 7.45-7.40 (m, 2H), 7.22 (s, 2H), 7.10 (d, 2H), 6.79 (s, 5H), 4.65-4.35 (m, 2H), 4.06 (s, 5H), 3.85 (s, 9H), 3.72 (s, 4H), 3.44 (s, 1H), 3.16 (s, 2H), 2.95 (s, 1H), 1.88 (s, 2H), 1.75 (s, 6H), 1.45-1.05 (m, 70H), 0.85 (s, 6H).

General Procedures for Gel Formation/Hydrolysis/Reformation:

Synthesis of Supramolecular Organogels

To form the **P2-6** (PEG) organogel, **P2** (25.6 mg, 14.2 mmol) was combined with bis(6-cyanohexyl)polyethylene glycol 600 **6** (5.68 mg, 7.1 mmol) in a 2 mL screw-cap vial. The two components were dissolved in 190 µL of chloroform, resulting in a yellow organogel in approximately 30 min.

To form the **P2-P3** (zipper gel), **P2** (25.6 mg, 14.2 mmol) was combined with **P3** (14.9 mg, 14.2 mmol) in a 2 mL screw-cap vial. The polymers were dissolved in 190 µL of chloroform, resulting in a yellow organogel in approximately 5-10 min. Organogels were also formed in dichloromethane, toluene, and 1,2-dichlorobenzene.

Hydrolysis of Supramolecular Gel

Trifluoroacetic acid (5 µL) was added to an empty 20 mL vial. The unlidded 2 mL vial containing the organogel was placed into the larger vial containing the trifluoroacetic acid, allowing the acidic vapours to hydrolyze the gel. Full hydrolysis was complete after approximately 1 hour at room temperature for both the **P2-6** and **P2-P3** gels (Figure 3.7).

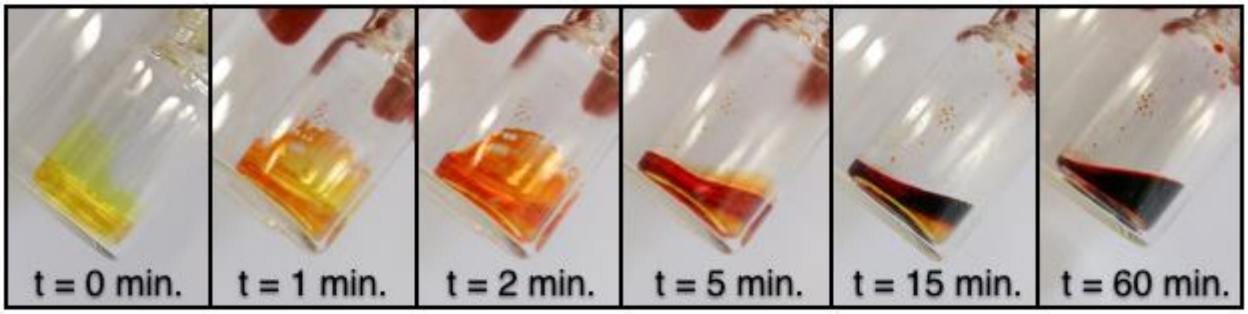

Figure 3.7. Degradation of the ‘zipper gel’ in the presence of TFA vapour.

Reformation of Gel

The supramolecular organogels were reformed with the addition of 3Å molecular sieves to remove water from the hydrolyzed gel. The sieves are added to a separate 20 mL vial, within which the smaller gel-containing vial is sealed (as with the hydrolysis). After 12-16 h at room temperature the gel recovers much of its original viscosity, now with a dark red color as the equilibrium is driven towards the formation of polyimine. This process results in the evaporation of approximately half of the 190 µL of chloroform; therefore, another 100 µL is added to the gel as it's drying to retain the volume of the original gel. Triethylamine (10 µL) can also be added to the external vial to regenerate the free base of the polyimine over a period of 24 h.

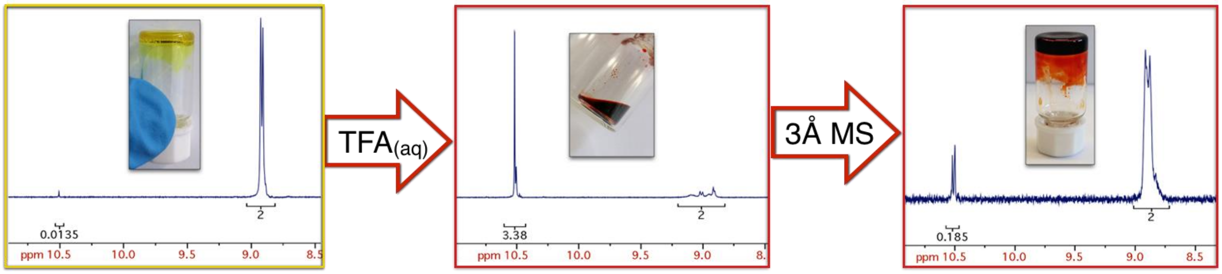

Figure 3.8. Relative intensities of the aldehyde end group signal @10.5 ppm compared to the backbone imine signal @8.9 ppm before gel degradation with TFA and after regeneration with 3Å molecular sieves.

Self-Healing Procedure

For self-healing tests, the **P2-P3** (zipper gel) was formed at a concentration of 30% w/w in toluene by dissolving **P2** (18.9 mg, 10.5 mmol) and **P3** (11.1 mg, 10.5 mmol) in toluene (80 µL) inside a modified 1 mL polypropylene syringe (Figure S3). The mixture was briefly mixed with a small spatula and allowed to gel for 10 min before extruding it onto a glass slide. The gel was then cut in half and separated using a precision knife. The two separated halves were gently recombined at the cut site and allowed to sit for another 10 min before pulling them apart with tweezers.

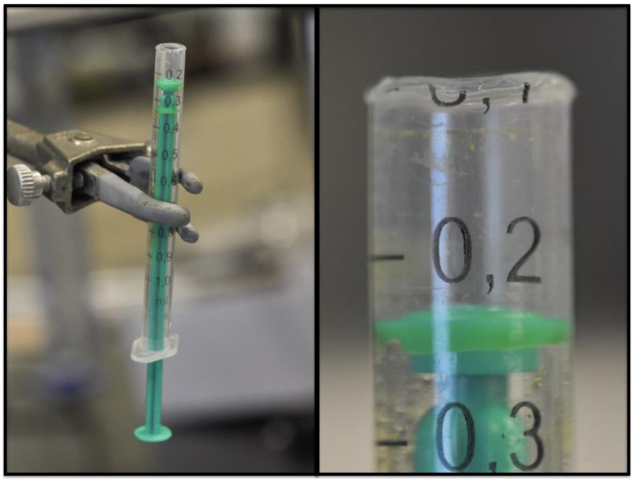

Figure 3.9. Modified 1 mL polypropylene syringe used for forming and extruding organogel **P2-P3** for self-healing. The tip of the syringe was removed using precision knife, which allows the gels to be extruded in a cylindrical shape.

3.4.3. Binding Studies

All the ^1H NMR titration experiments were performed on a Bruker AC 300 at 25(1)°C, in $CDCl_3$ purchased from Sigma Aldrich Chemical Company. The appropriate amount of a stock solution of 1,6-dicyanohexane or **6** ($CDCl_3$, 70 mM) was added to solution of the host (**1**, **3**, **5** or **P2**) in $CDCl_3$. The association constants (K_a) for the 1:1 complexes [1,6-dicyanohexane $\subset$ **1**], [1,6-dicyanohexane $\subset$ **3**] and [1,6-dicyanohexane $\subset$ **5**] were determined based on the complexation-induced changes in chemical shifts of the signals from hosts. In the particular case of **P2**, the titration of multitopic receptor **P2** by an increasing amount of 1,6-dicyanohexane resulted in the formation of different supramolecular species. The stepwise association constants were determined for HG ($\log K_1 = 3.1$) and H_2G_2 ($\log K_2 = 5.2$) complexes. Titrations of **6** with **1** or **6** with **5** led to the determination of two binding constants, K_1 for the 1:1 complex and K_2 for the 2:1 complex.

Finally, for the titration of **1** with **P3**, the appropriate amount of guest **P3** stock solution ($CDCl_3$, 72 mM) was added to a solution of **1** in $CDCl_3$. Under such conditions, compound **P3** is present in a large excess relative to **1** so that complexes involving more than one host molecule can be neglected. This allowed to calculate the association constant for a 1:1 complex. All the calculations were done using the nonlinear least-square regression analysis program HypNMR.[74]

Table 3.1. Values of the association constants ($\log K_a$ and $\log \beta_a$) calculated for the host-guest complexes.

Host	$NC{-}(CH)_6{-}CN$	$NC{-}(CH)_6{-}O{-}(CH_2O)_{13}{-}(CH_2)_6{-}CN$ **(6)**	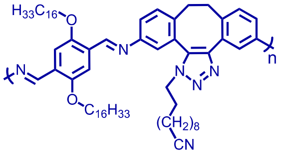 **(P3)**
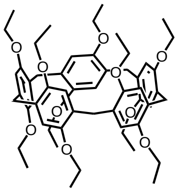 **(1)**	$\log K_{HG} = 2.9(1)$	$\log K_{HG} = 2.2(1)$ $\log \beta_{H2G} = 3.8(*)$	$\log K_{HG} = 1.8(2)$
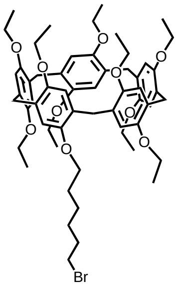	$\log K_{HG} = 3.0(1)$	-----	------

(3)			
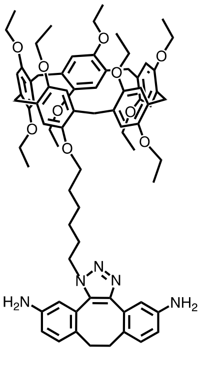 **(5)**	$\log K_{HG} = 3.2(1)$	$\log K_{HG} = 2.1(2)$ $\log \beta_{H2G} = 3.6(*)$	------
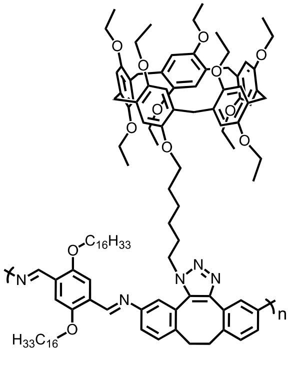 **(P2)**	$\log K_{HG} = 3.1(1)$ $\log \beta_{H2G2} = 8.3(2)$	(**)	(**)

(*) The values of $\log K_{H2G}$ were estimated by manual fitting. The program calculates $\log K_{H2G}$ with high error as this complex H_2G is present in very small amount (less that 5 %), additionally the guest tends to aggregate in solution at higher concentrations.

(**) The quantitative evaluation of the association constants was not possible due to aggregation in solution.

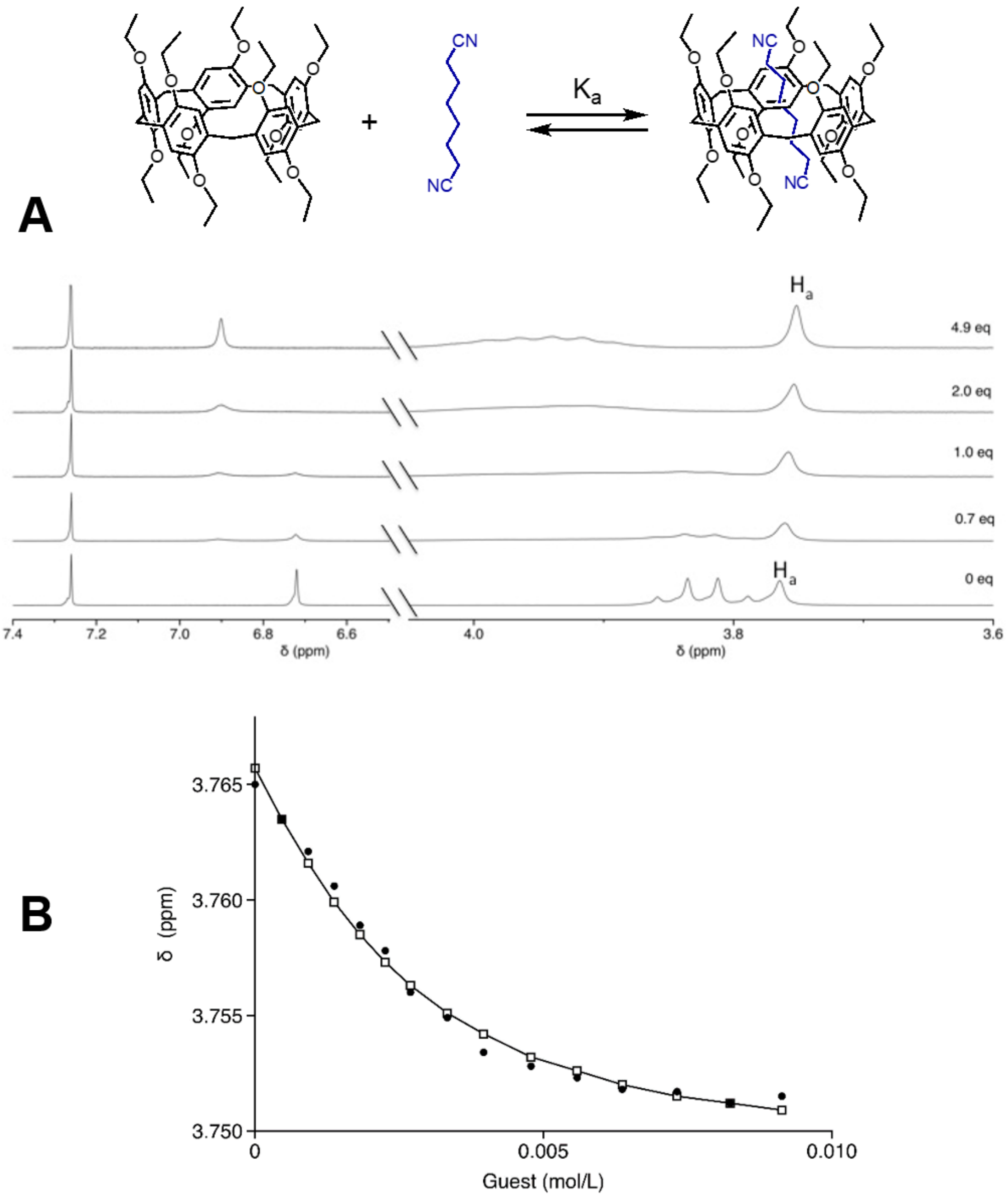

Figure 3.10. (A) Partial ^{1}H NMR spectra (300 MHz, CDCl$_3$, 298K) recorded upon successive additions of 1,6-dicyanohexane to a solution of host **1** (2.13 mM); (B) Chemical shifts of H$_a$ (**1**, calculated: □, experimental: ●) as a function of guest concentration (H$_a$: pillar[5]arene methylene group).

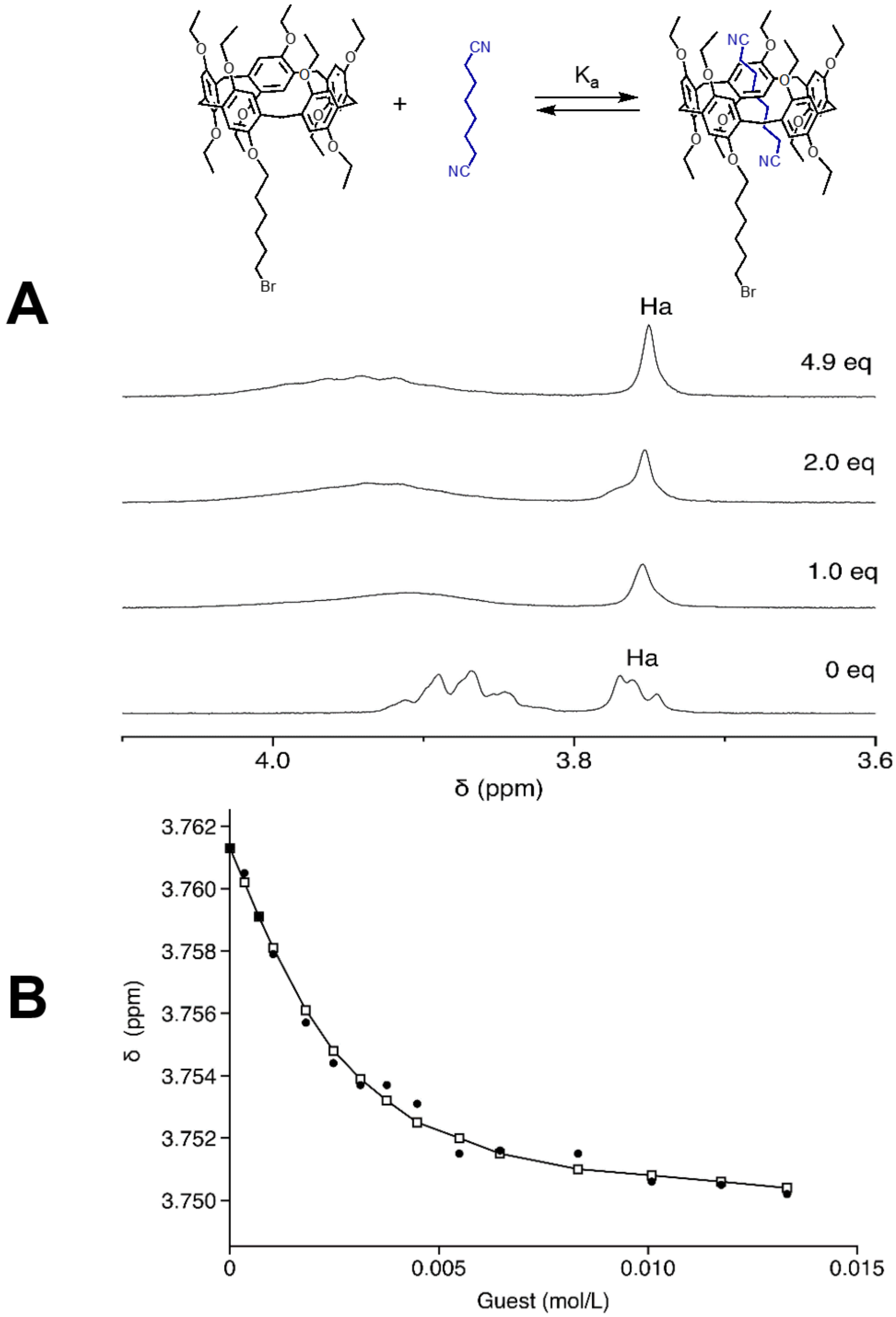

Figure 3.11. (A) Partial ^{1}H NMR spectra (300 MHz, CDCl$_3$, 298K) recorded upon successive additions of 1,6-dicyanohexane to a solution of host **3** (2.4 mM); (B) Chemical shifts of H$_a$ (**3**, calculated: □, experimental: ●) as a function of guest concentration (H$_a$: pillar[5]arene methylene group).

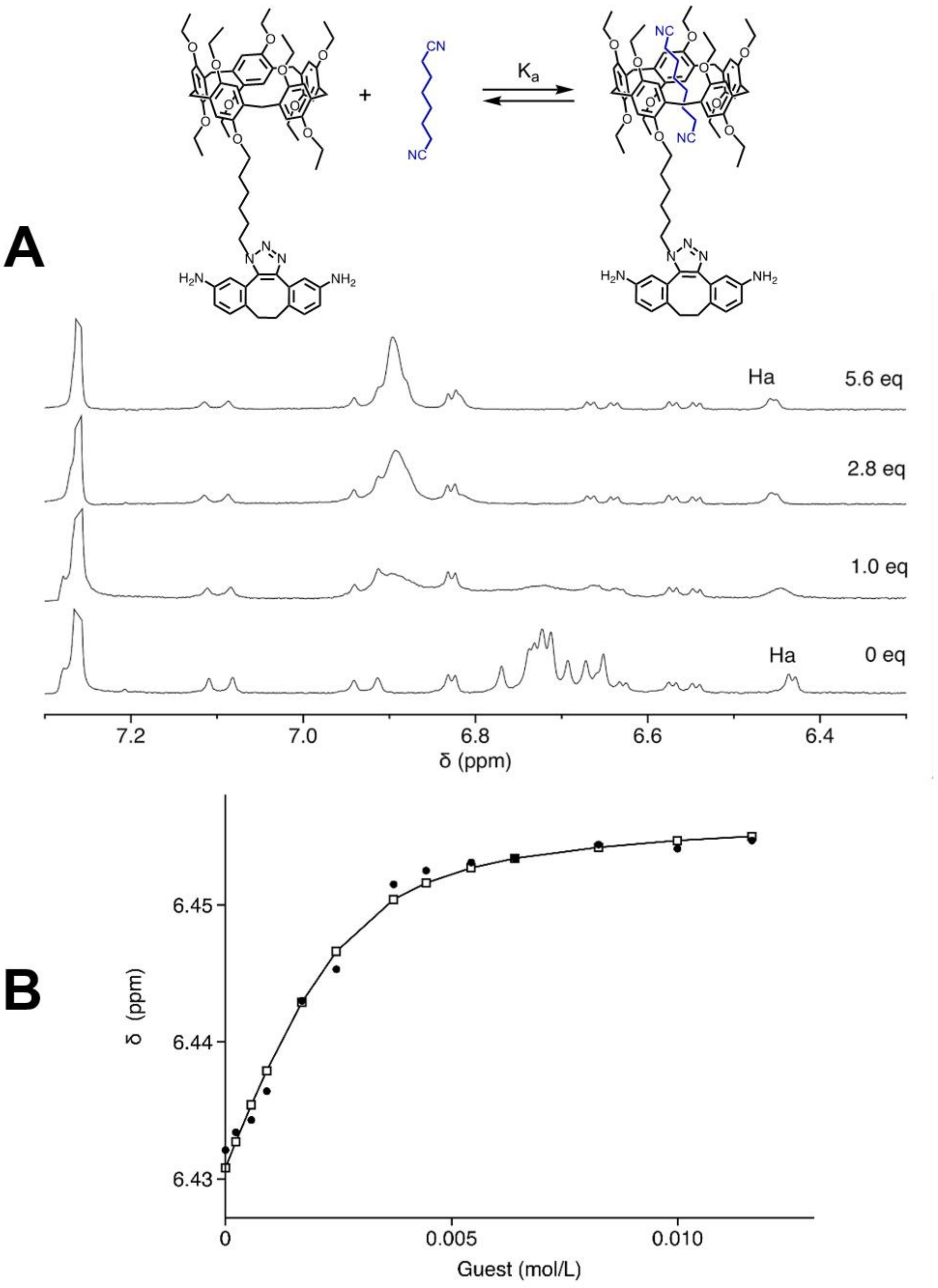

Figure 3.12. (A) Partial ^{1}H NMR spectra (300 MHz, $CDCl_3$, 298K) recorded upon successive additions of 1,6-dicyanohexane to a solution of compound **5** (2.5 mM); (B) Chemical shifts of H_a (**5**, calculated: □, experimental: ●) as a function of guest concentration (H_a: pillar[5]arene aromatic proton).

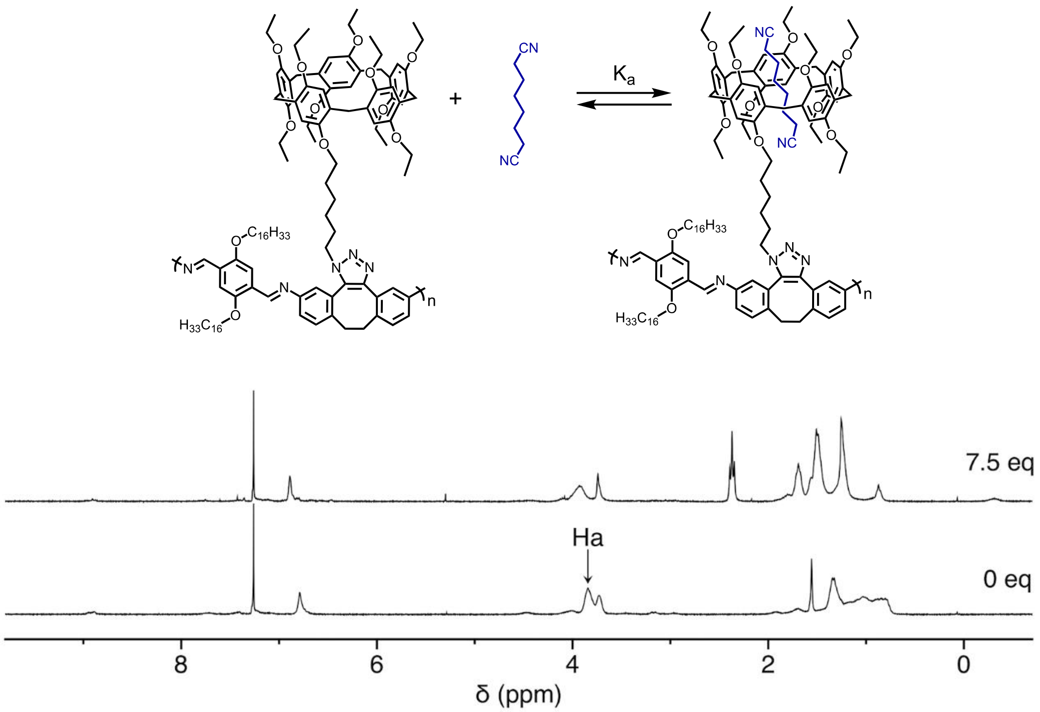

Figure 3.13. ^{1}H NMR spectra (300 MHz, $CDCl_3$, 298K) recorded upon successive additions of 1,6-dicyanohexane to a solution of polymer **P2** (concentration in pillar[5]arene: 2.48 mM).

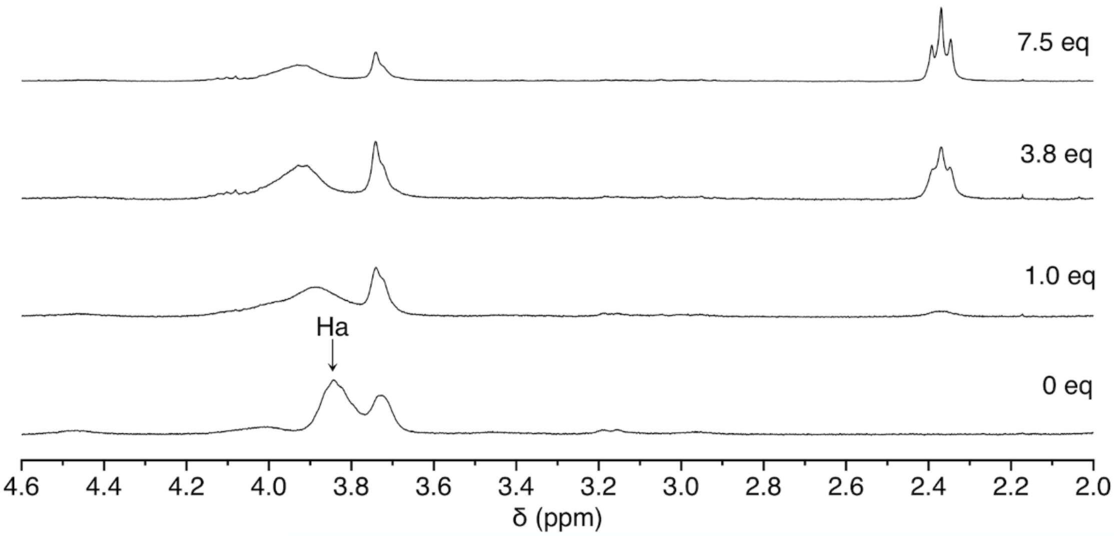

Figure 3.14. Partial ^{1}H NMR spectra (300 MHz, $CDCl_3$, 298K) recorded upon successive additions of 1,6-dicyanohexane to a solution of polymer **P2** (concentration in pillar[5]arene: 2.48 mM)

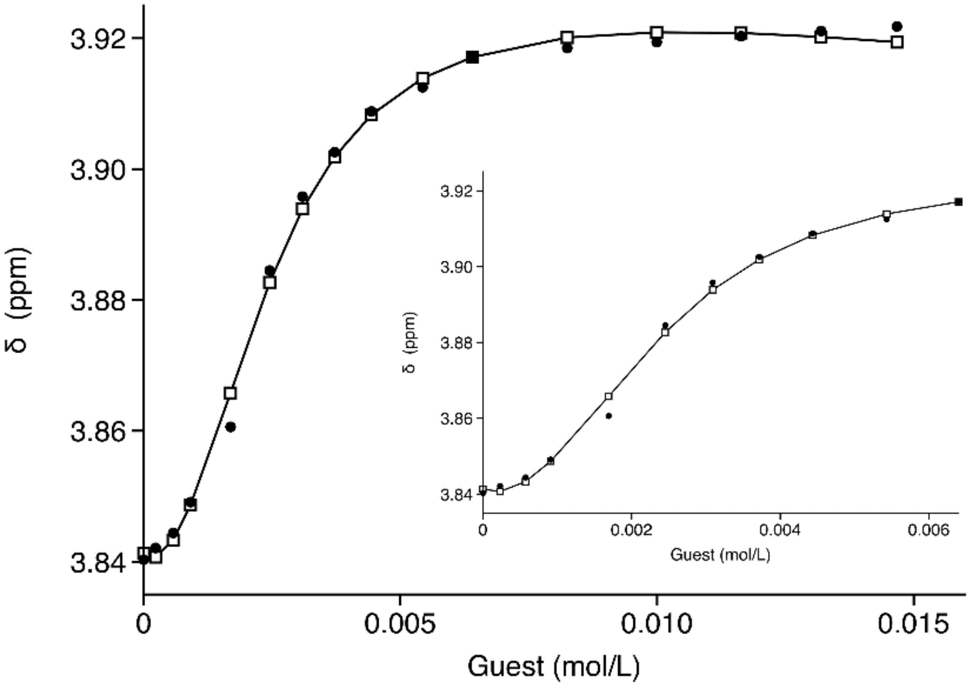

Figure 3.15. Chemical shifts of H_a (**P2**, calculated: □, experimental: ●) as a function of guest concentration. Inset: detailed view of the initial part of the titration (H_a: pillar[5]arene OCH_2).

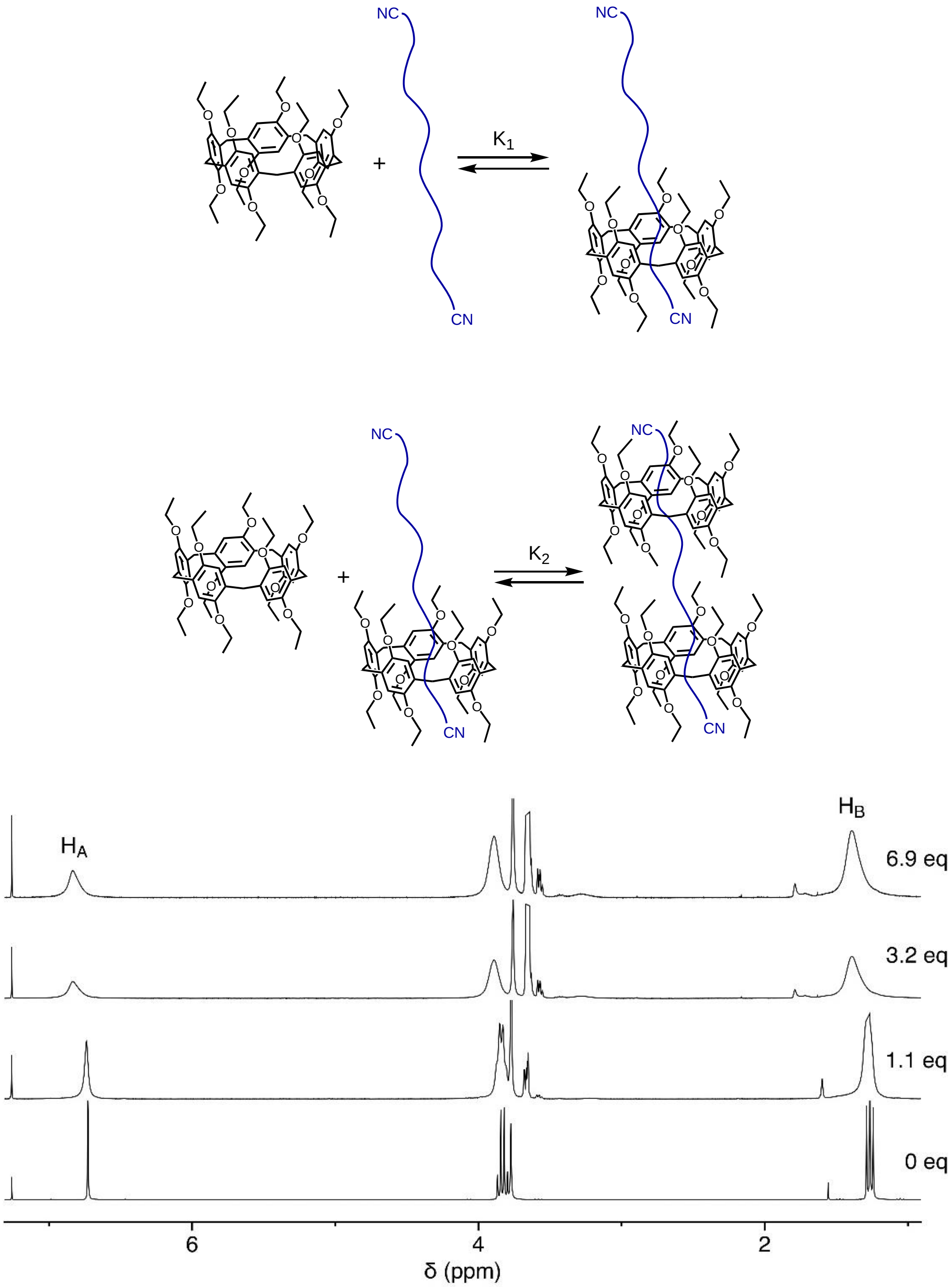

Figure 3.16. Partial ^{1}H NMR spectra (300 MHz, $CDCl_3$, 298K) recorded upon successive additions of guest **6** to a solution of compound **1** (2.47 mM).

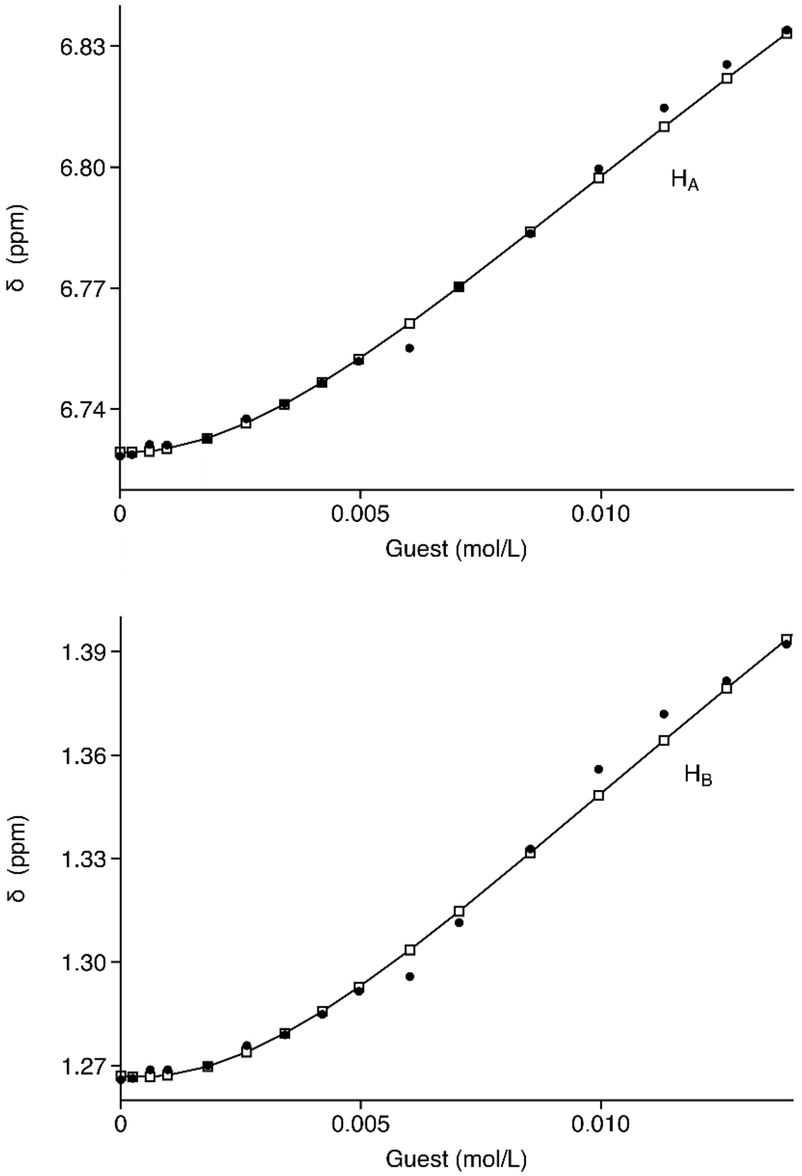

Figure 3.17. Chemical shifts of H_A and H_B (**1**, calculated: □, experimental: ●) as a function of guest concentration. The stability constants were calculated by considering simultaneously the changes in chemical shifts of H_A and H_B (H_A: pillar[5]arene aromatic proton; H_B: pillar[5]arene $OCH_2\underline{CH_3}$).

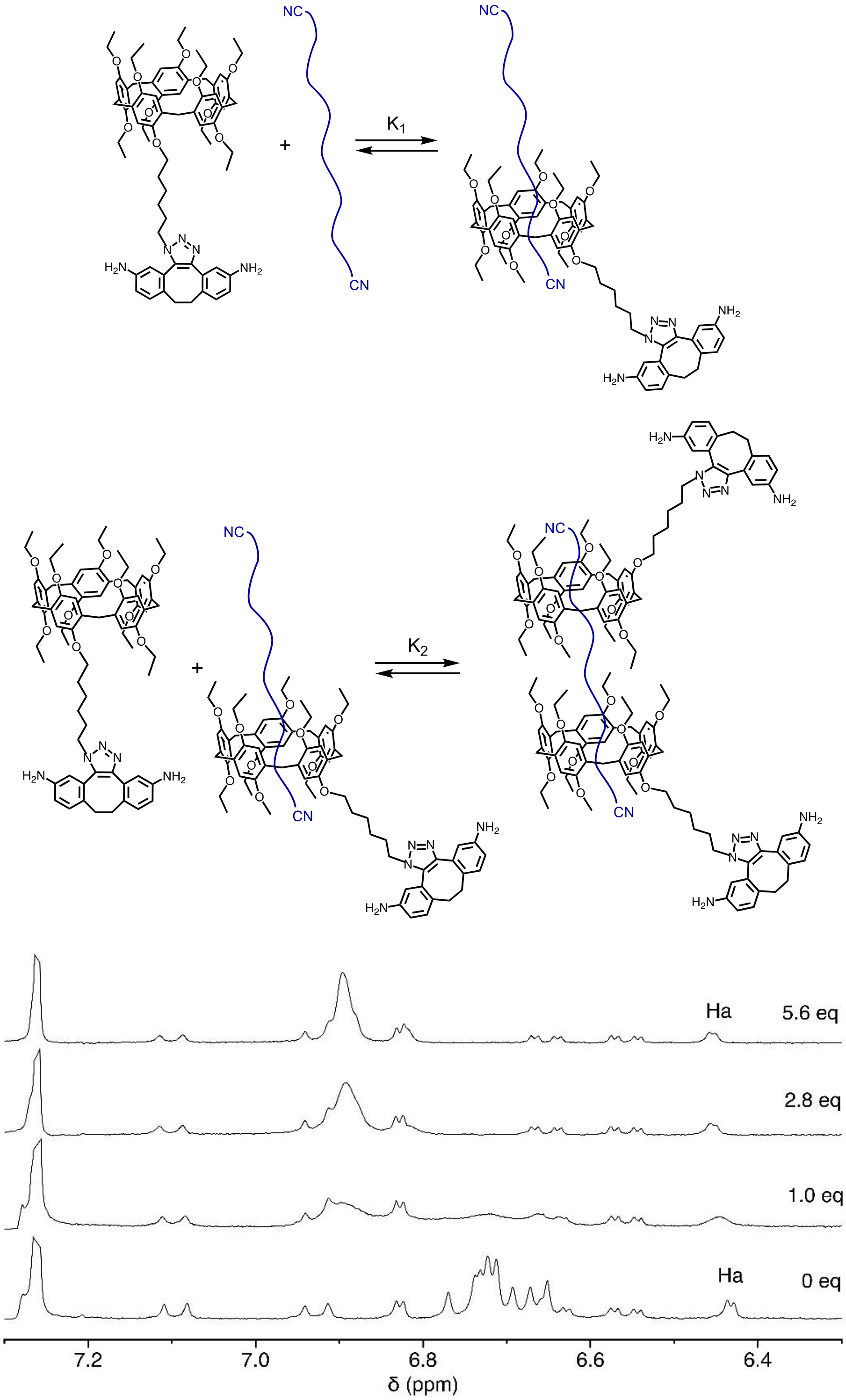

Figure 3.18. Partial ^{1}H NMR spectra (300 MHz, $CDCl_3$, 298K) recorded upon successive additions of guest **6** to a solution of compound **5** (2.45 mM).

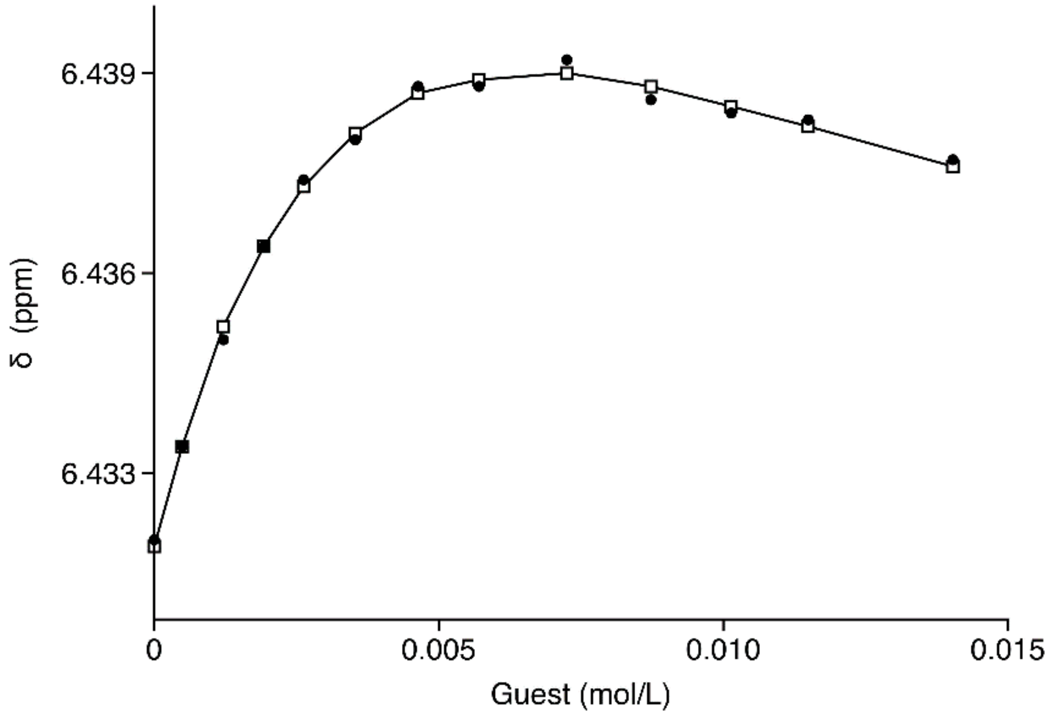

Figure 3.19. Chemical shifts of H_a (**5**, calculated: □, experimental: ●) as a function of guest concentration (H_a: pillar[5]arene aromatic proton).

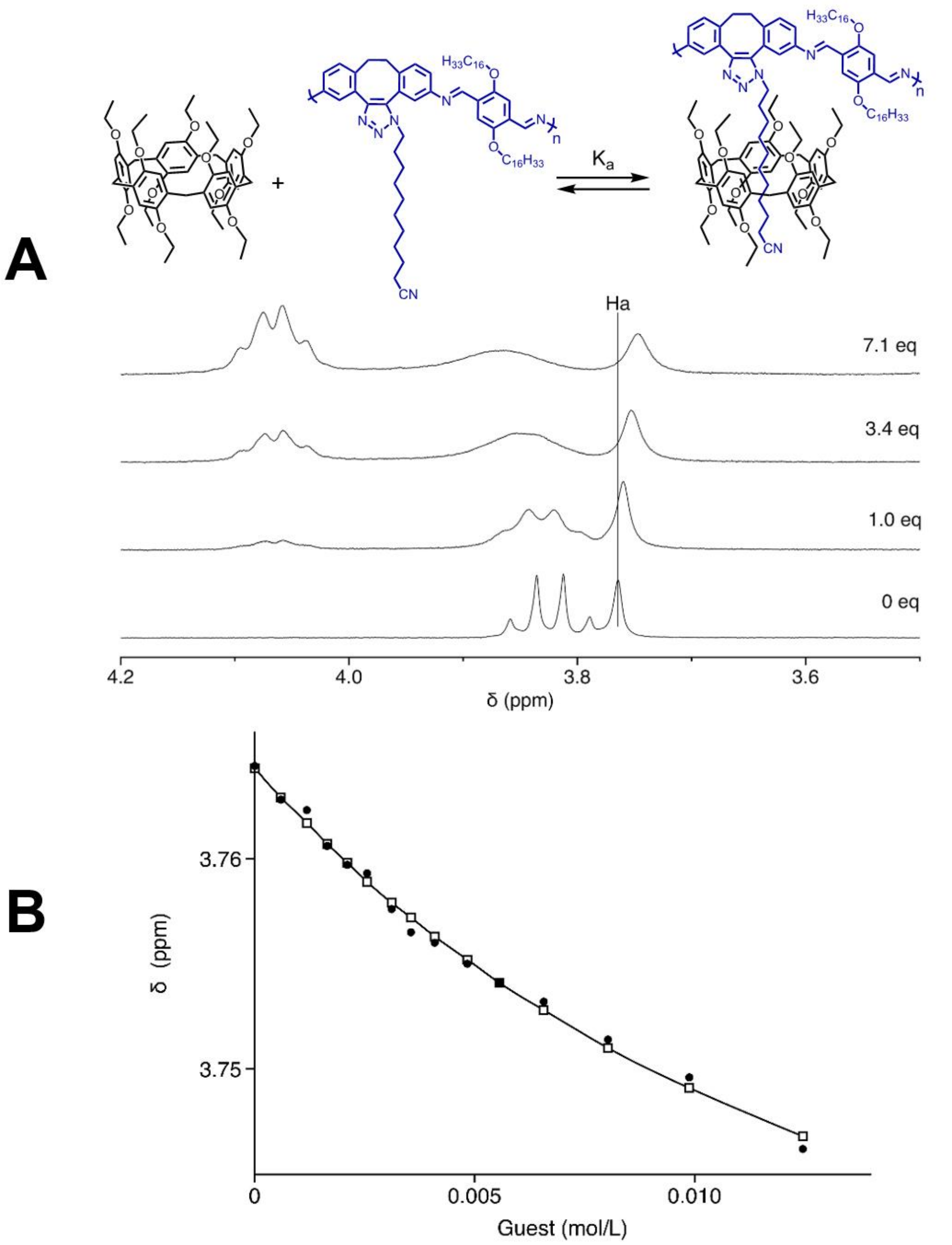

Figure 3.20. (A) Partial ^{1}H NMR spectra (300 MHz, CDCl$_3$, 298K) recorded upon successive additions of guest **P3** to a solution of compound **1** (2.1 mM); (B) Chemical shifts of H$_a$ (**1**, calculated: □, experimental ●) as a function of guest concentration (H$_a$: pillar[5]arene methylene group).

3.4.4. Mechanical Testing of Organogels

Mechanical properties of the organogels were determined, as previously described by our group,[75] using a home-built apparatus that measures the contact mechanics between a glass hemisphere and an elastic organogel. This relationship can be described by the Hertzian theory as

$$F = \frac{4ER^{1/2}}{3(1-\nu^2)}d^{3/2} \tag{1}$$

where F is the force, d is the deformation, R is the radius of the glass hemispherical indenter, ν is the Poisson's ratio and E is the Young's modulus of the elastic substrate.[76] Each organogel was investigated using a compression method with a hemispherical indenter consisting of a glass melting point tube (VWR) with a hemispherical end (r = 0.83 mm) attached to a force transducer (Transducer Techniques, GSO series, 10 g full scale). The vertical position of the glass indenter was controlled with a servo motor, which contacts and indents the gel at a constant speed. The force transducer is then able to measure the force applied by the gel relative to time and vertical position of the indenter. This was repeated in triplicate at different positions for each gel. The Young's modulus (YM) was obtained using the equation described by the Hertzian theory, rearranged to isolate YM as the slope, when plotting the measured force (F) as a function of deformation (d). The Poisson's ratio is assumed to be $\nu = 0.45$ based on polymer gels having similar mechanical properties to elastic, rubber-like materials.[77,78]

The Young's Modulus for both the **P2-P3** gel and **P4** gel was measured at a concentration of 25% w/w in 1,2-dichlorobenzene. 1,2-dichlorobenzene was chosen as due to its relatively low volatility at room temperature. The **P2-P3** gel was formed by dissolving **P2** (18.9 mg, 10.5 mmol) and **P3** (11.1 mg, 10.5 mmol) in 1,2-dichlorobenzene (70 μL) inside a microcentrifuge tube. The **P4** gel was formed by dissolving **P4** (30.0 mg) in 1,2-dichlorobenzene (70 μL) The mixture was briefly mixed with a small spatula and allowed to gel for 10 min before proceeding to mechanical testing. After testing the **P2-P3** gel, it was hydrolyzed and reformed according to the procedure described above, then retested.

3.4.5. NMR Spectra

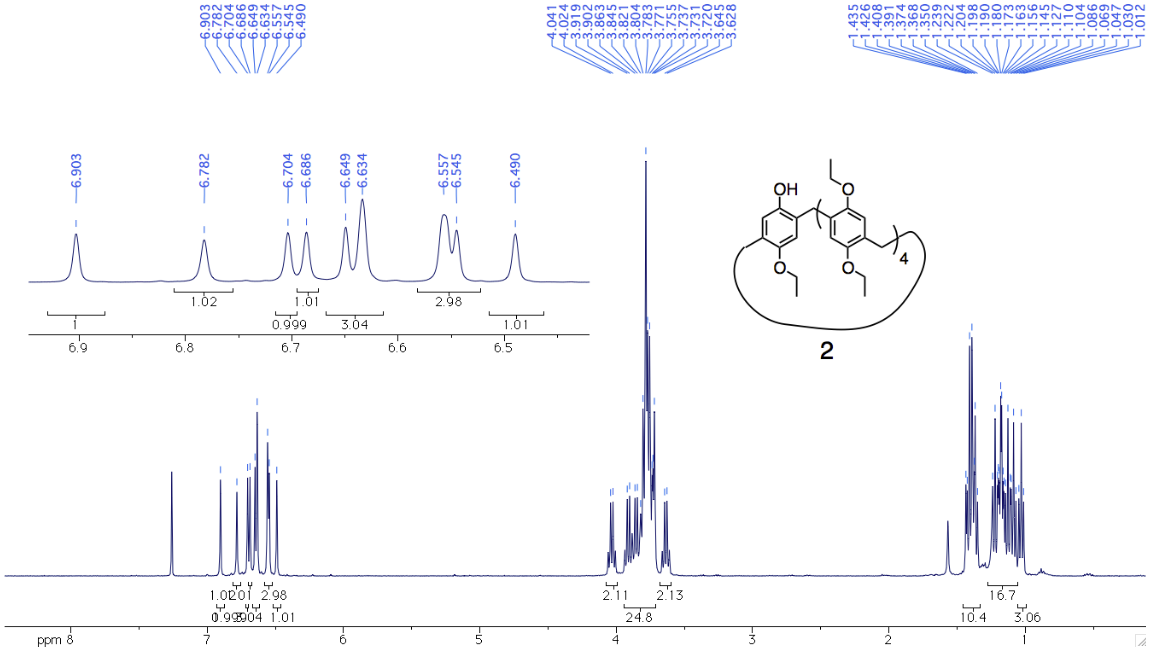

Figure 3.21. ^{1}H-NMR spectrum of **2** in $CDCl_3$.

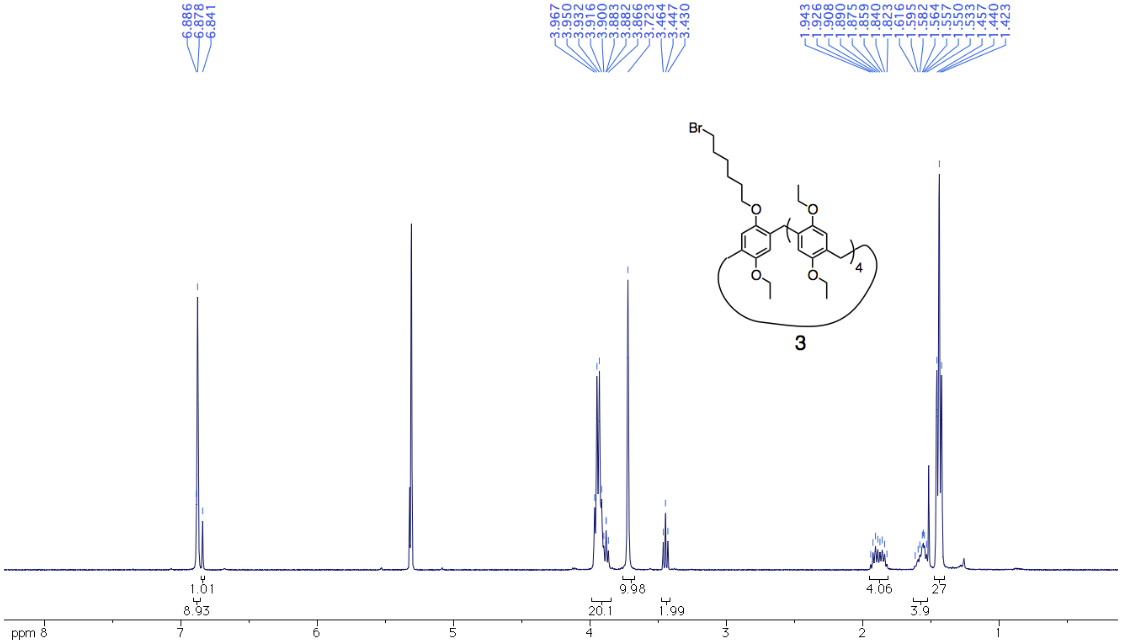

Figure 3.22. ^{1}H-NMR spectrum of **3** in CD_2Cl_2.

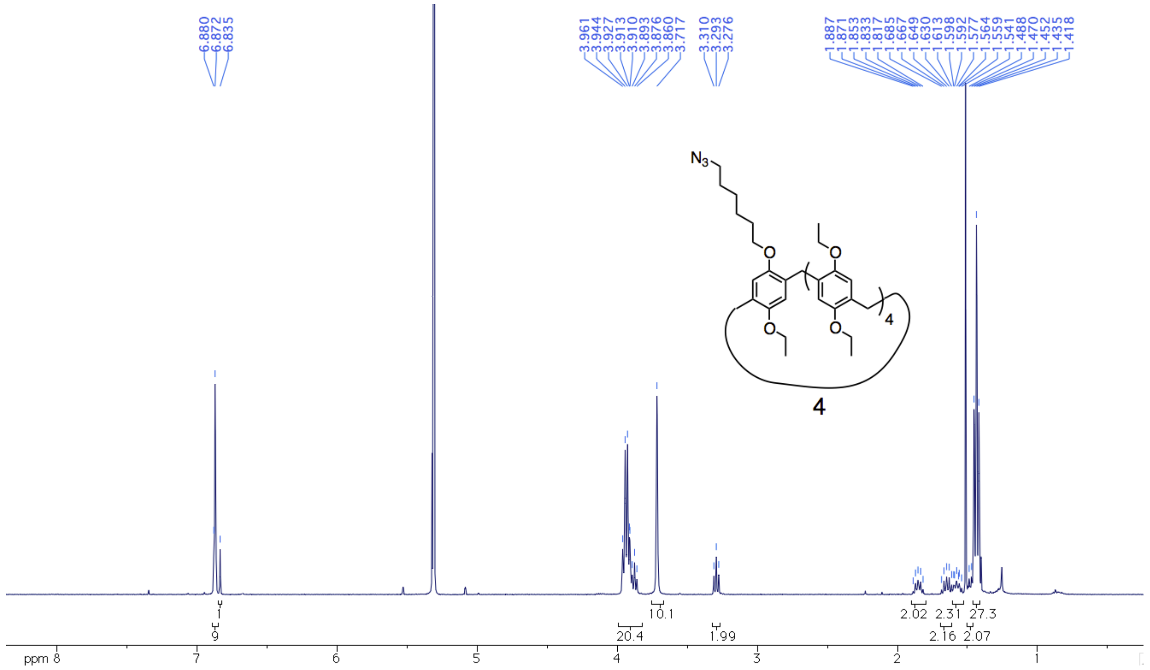

Figure 3.23. ^{1}H-NMR spectrum of **4** in CD_2Cl_2.

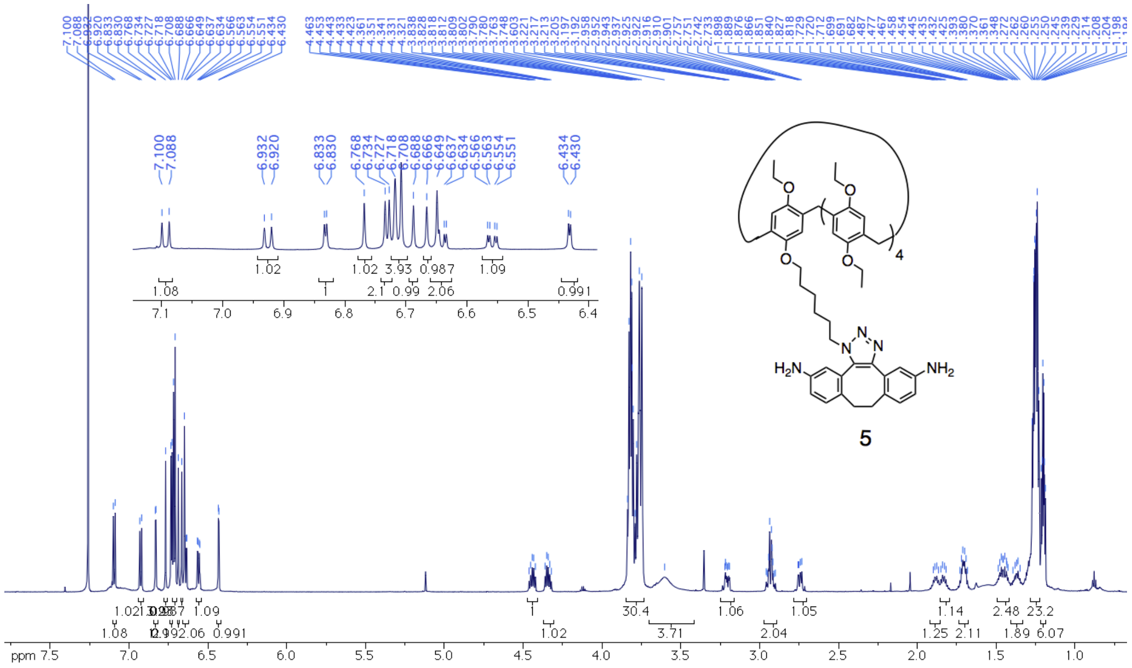

Figure 3.24. ^{1}H-NMR spectrum of **5** in $CDCl_3$.

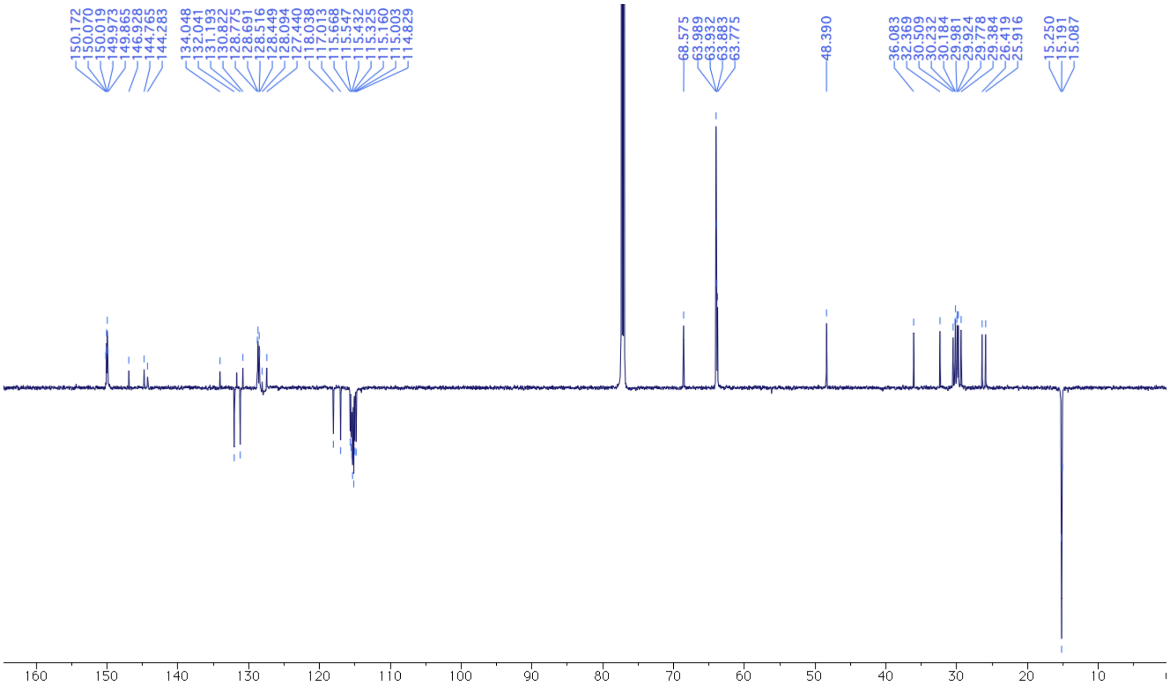

Figure 3.25. DEPTq ^{13}C-NMR spectrum of **5** in CDCl$_3$.

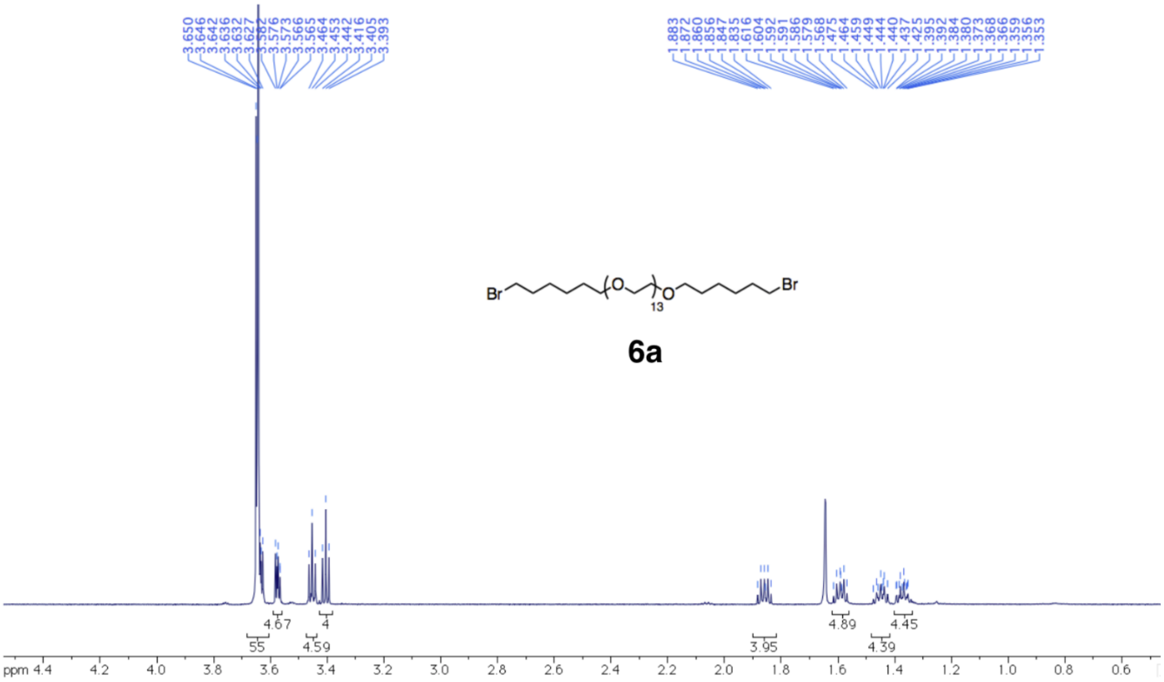

Figure 3.26. ^{1}H-NMR spectrum of **6a** in CDCl$_3$.

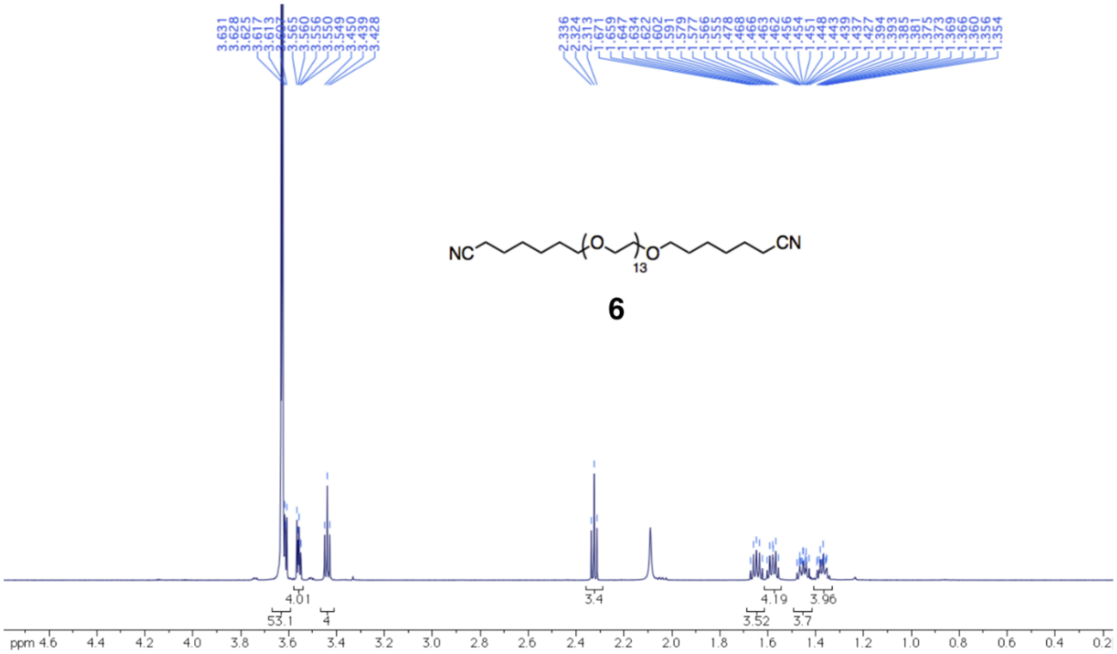

Figure 3.27. ^{1}H-NMR spectrum of **6** in $CDCl_3$.

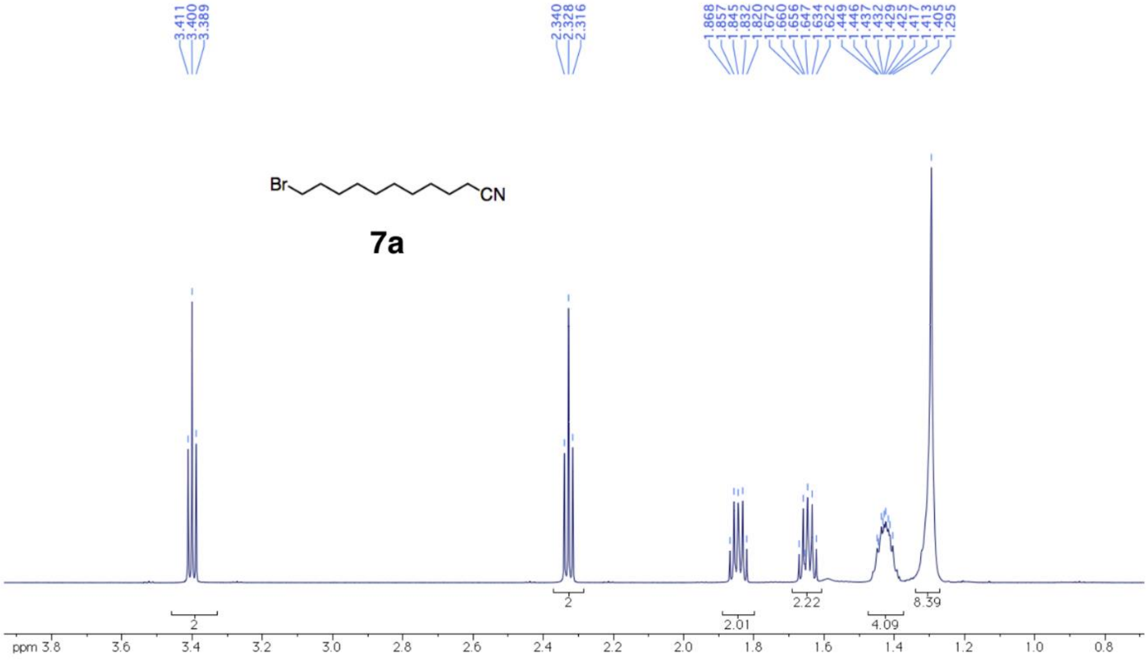

Figure 3.28. ^{1}H-NMR spectrum of **7a** in $CDCl_3$.

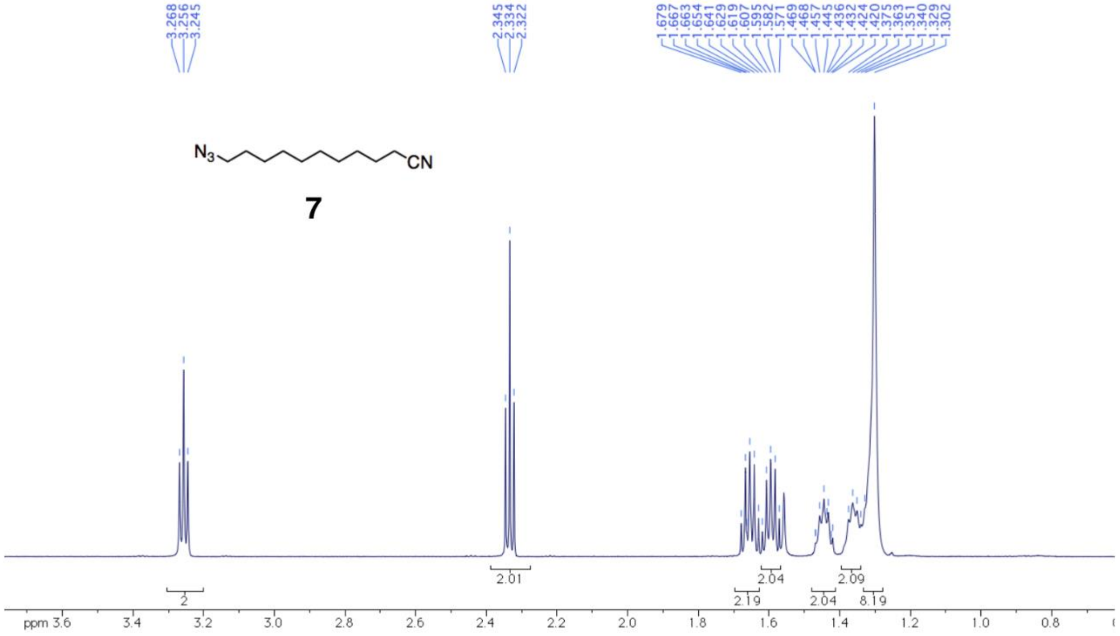

Figure 3.29. ^{1}H-NMR spectrum of **7** in $CDCl_3$.

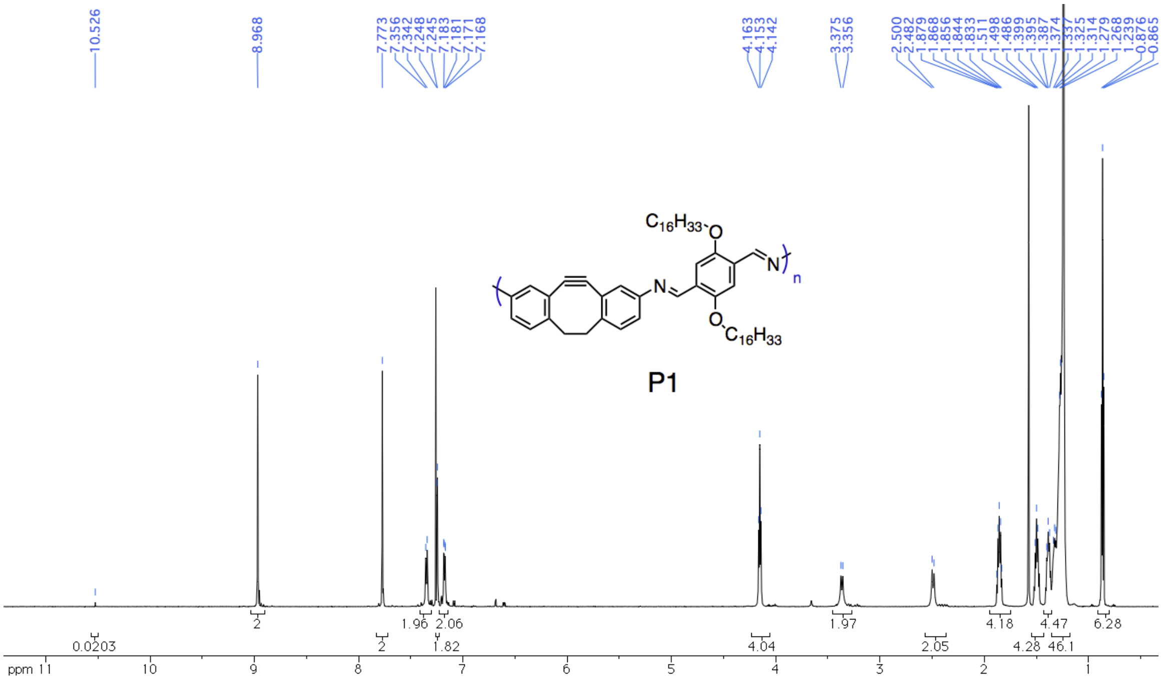

Figure 3.30. ^{1}H-NMR spectrum of **P1** in $CDCl_3$.

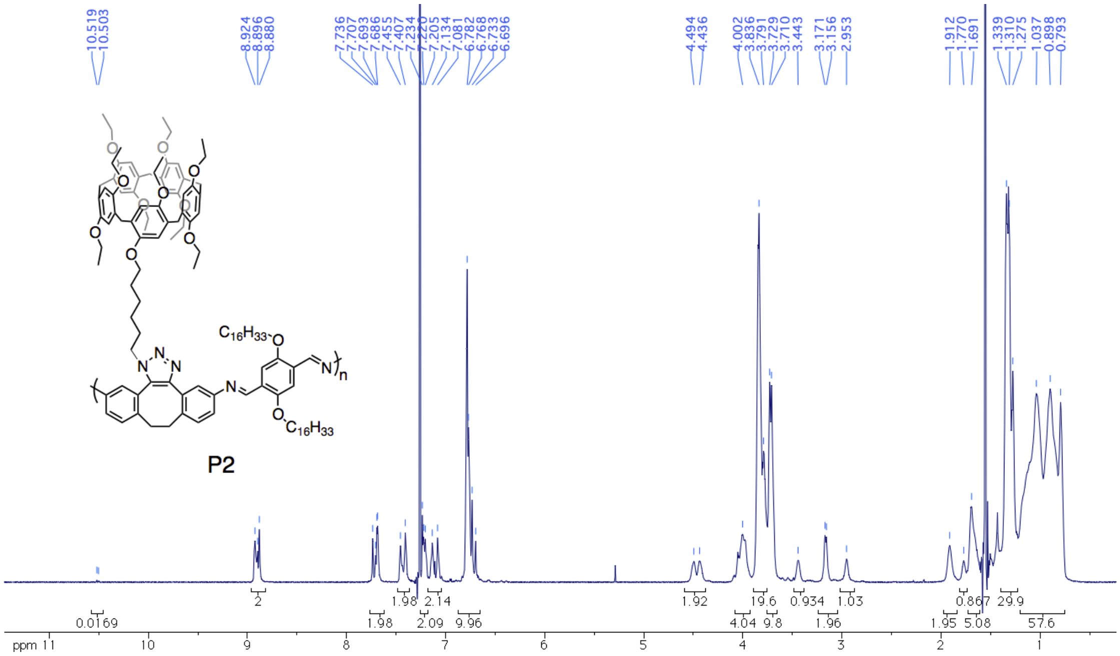

Figure 3.31. ^{1}H-NMR spectrum of **P2** in $CDCl_3$.

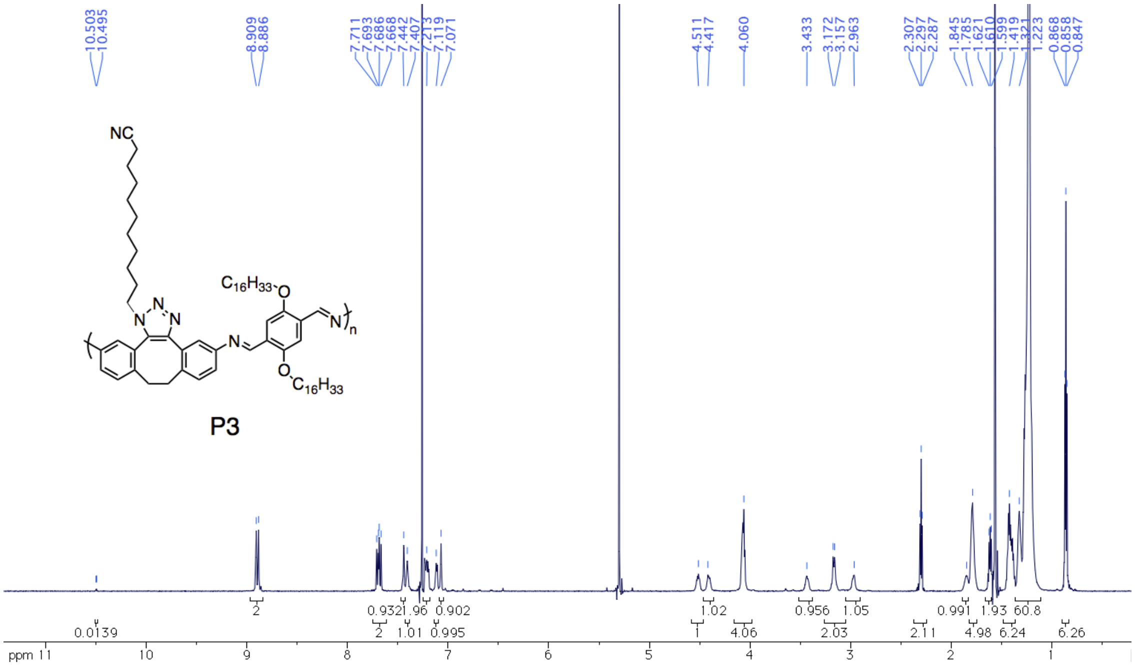

Figure 3.32. ^{1}H-NMR spectrum of **P3** in $CDCl_3$.

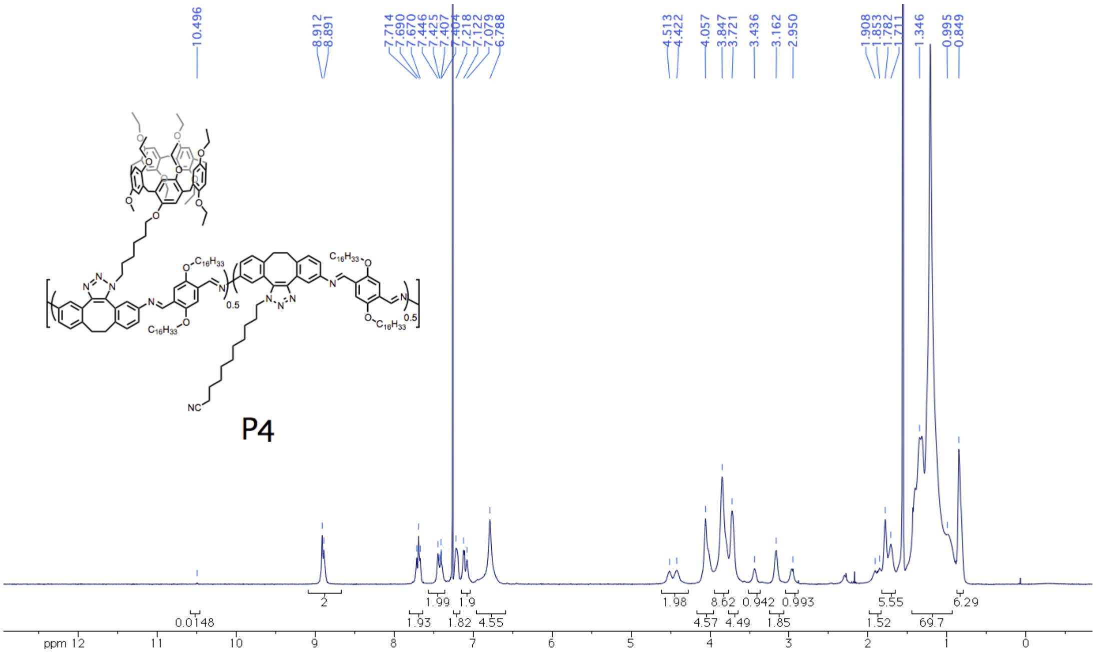

Figure 3.33. ^{1}H-NMR spectrum of **P4** in CDCl$_3$.

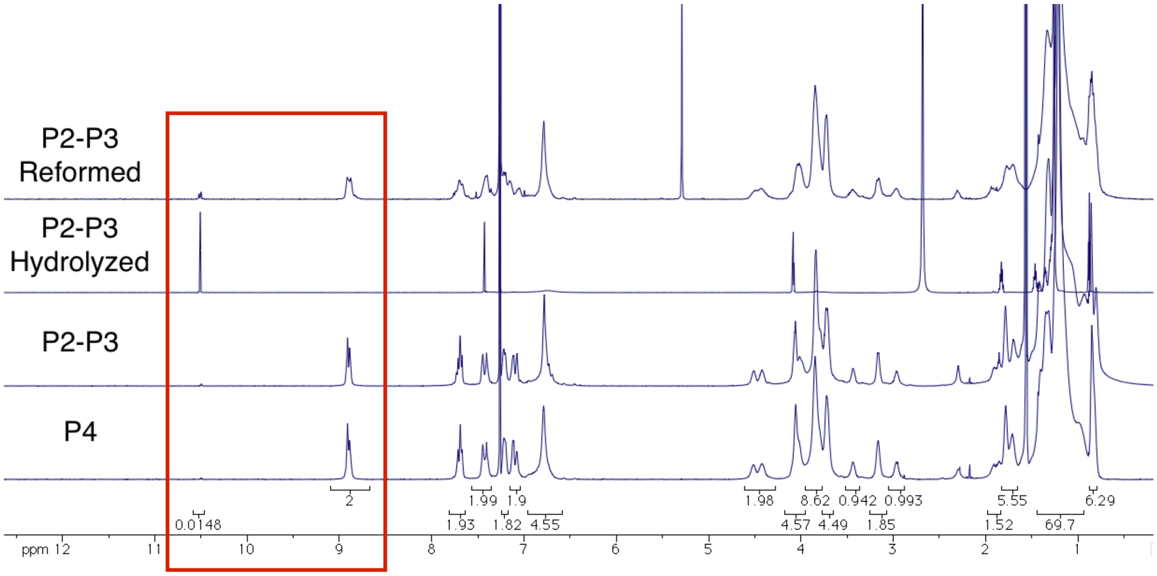

Figure 3.34. ^{1}H-NMR spectrum overlay of **P4, P2-P3** gel**,** hydrolyzed **P2-P3** gel, and the reformed **P2-P3** gel in CDCl$_3$.

3.4.6. Infrared Spectra

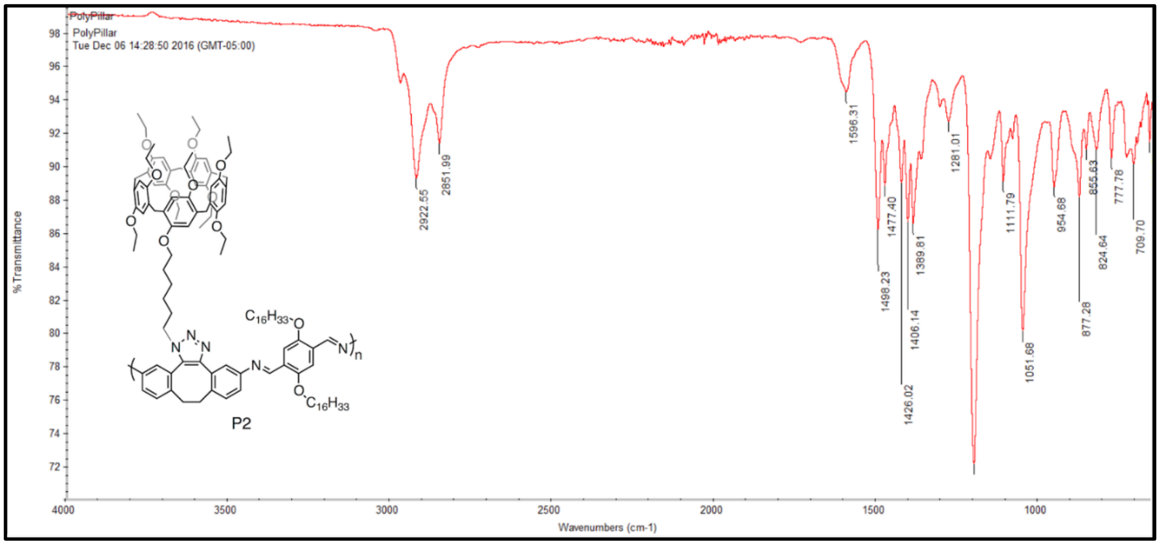

Figure 3.35. Infrared spectrum of **P2.**

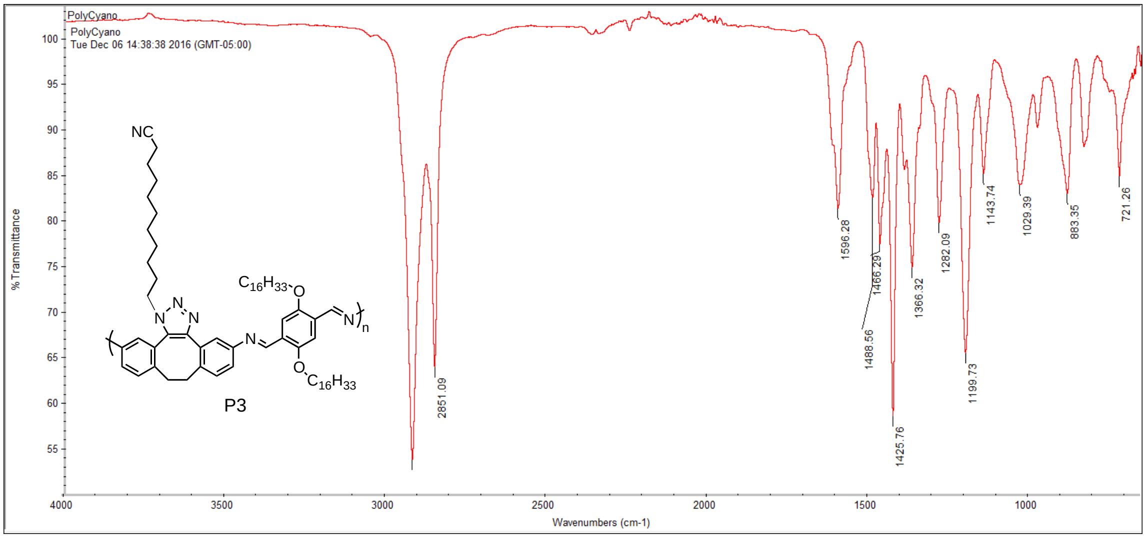

Figure 3.36. Infrared spectrum of **P3.**

3.4.7. GPC Traces

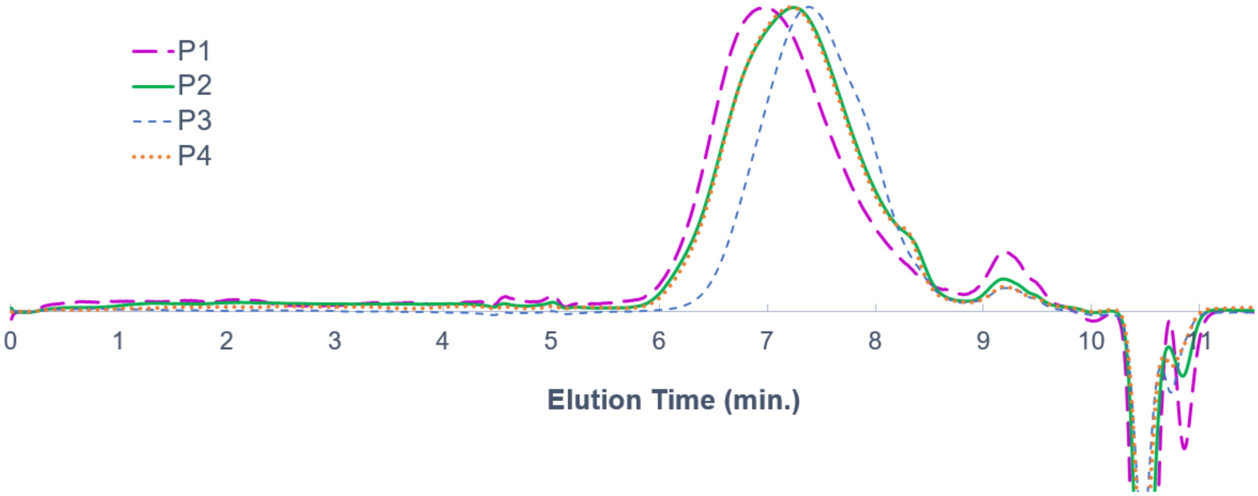

Figure 3.37. GPC trace overlay of **P1** through **P4.**

3.5. References

(1) Suzuki, M.; Hanabusa, K. Polymer Organogelators That Make Supramolecular Organogels through Physical Cross-Linking and Self-Assembly. **2010**, 455–463.

(2) Appel, E. A.; del Barrio, J.; Loh, X. J.; Scherman, O. A. Supramolecular Polymeric Hydrogels. *Chem. Soc. Rev.* **2012**, *41* (18), 6195–6214.

(3) Chen, J.; Park, H.; Park, K. Synthesis of Superporous Hydrogels: Hydrogels with Fast Swelling and Superabsorbent Properties. *J. Biomed. Mater. Res.* **1998**, *44* (1), 53–62.

(4) Wang, W.; Wang, A. Synthesis and Swelling Properties of PH-Sensitive Semi-IPN Superabsorbent Hydrogels Based on Sodium Alginate-g-Poly(Sodium Acrylate) and Polyvinylpyrrolidone. *Carbohydr. Polym.* **2010**, *80* (4), 1028–1036.

(5) Shin, H.; Jo, S.; Mikos, A. G. Biomimetic Materials for Tissue Engineering. *Biomaterials* **2003**, *24* (24), 4353–4364.

(6) Bryant, S. J.; Anseth, K. S. Controlling the Spatial Distribution of ECM Components in Degradable PEG Hydrogels for Tissue Engineering Cartilage. *J. Biomed. Mater. Res. A* **2003**, *64* (1), 70–79.

(7) Boateng, J. S.; Matthews, K. H.; Stevens, H. N. E.; Eccleston, G. M. Wound Healing Dressings and Drug Delivery Systems: A Review. *J. Pharm. Sci.* **2008**, *97* (8), 2892–2923.

(8) Hoare, T. R.; Kohane, D. S. Hydrogels in Drug Delivery: Progress and Challenges. *Polymer (Guildf).* **2008**, *49* (8), 1993–2007.

(9) Perale, G.; Rossi, F.; Sundstrom, E.; Bacchiega, S.; Masi, M.; Forloni, G.; Veglianese, P. Hydrogels in Spinal Cord Injury Repair Strategies. *ACS Chem. Neurosci.* **2011**, *2* (7), 336–345.

(10) Sun, J.-Y.; Zhao, X.; Illeperuma, W. R. K.; Chaudhuri, O.; Oh, K. H.; Mooney, D. J.; Vlassak, J. J.; Suo, Z. Highly Stretchable and Tough Hydrogels. *Nature* **2012**, *489* (7414), 133–136.

(11) Buenger, D.; Topuz, F.; Groll, J. Hydrogels in Sensing Applications. *Prog. Polym. Sci.* **2012**, *37* (12), 1678–1719.

(12) Patenaude, M.; Smeets, N. M. B.; Hoare, T. Designing Injectable , Covalently Cross-Linked Hydrogels for Biomedical Applications. 598–617.

(13) Kloxin, C. J.; Bowman, C. N. Covalent Adaptable Networks: Smart, Reconfigurable and Responsive Network Systems. *Chem. Soc. Rev.* **2013**, *42* (17), 7161–7173.

(14) Kajita, T.; Noro, A.; Matsushita, Y. Design and Properties of Supramolecular Elastomers. *Polym. (United Kingdom)* **2017**.

(15) Yan, X.; Wang, F.; Zheng, B.; Huang, F. Stimuli-Responsive Supramolecular Polymeric Materials. *Chem. Soc. Rev.* **2012**, *41* (18), 6042–6065.

(16) Ma, X.; Tian, H. Stimuli-Responsive Supramolecular Polymers in Aqueous Solution. *Acc. Chem. Res.* **2014**, *47* (7), 1971–1981.

(17) Wang, M.; Sayed, S. M.; Guo, L. X.; Lin, B. P.; Zhang, X. Q.; Sun, Y.; Yang, H. Multi-Stimuli Responsive Carbon Nanotube Incorporated Polysiloxane Azobenzene Liquid Crystalline Elastomer Composites. *Macromolecules* **2016**, *49* (2), 663–671.

(18) Rodell, C. B.; MacArthur, J. W.; Dorsey, S. M.; Wade, R. J.; Wang, L. L.; Woo, Y. J.; Burdick, J. A. Shear-Thinning Supramolecular Hydrogels with Secondary Autonomous Covalent Crosslinking to Modulate Viscoelastic Properties In Vivo. *Adv. Funct. Mater.* **2015**, *25* (4), 636–644.

(19) Wei, Z.; Yang, J. H.; Zhou, J.; Xu, F.; Zrínyi, M.; Dussault, P. H.; Osada, Y.; Chen, Y. M. Self-Healing Gels Based on Constitutional Dynamic Chemistry and Their Potential Applications. *Chem. Soc. Rev.* **2014**, *43*, 8114–8131.

(20) Yang, Y.; Urban, M. W. Self-Healing Polymeric Materials. *Chem. Soc. Rev.* **2013**, *42* (17), 7446–7467.

(21) Yu, X.; Cao, X.; Chen, L.; Lan, H.; Liu, B.; Yi, T. Thixotropic and Self-Healing Triggered Reversible Rheology Switching in a Peptide-Based Organogel with a Cross-Linked Nano-Ring Pattern. *Soft Matter* **2012**, *8* (12), 3329.

(22) Nanda, J.; Biswas, A.; Banerjee, A. Single Amino Acid Based Thixotropic Hydrogel Formation and PH-Dependent Morphological Change of Gel Nanofibers. *Soft Matter* **2013**, *9* (16), 4198.

(23) Babu, S. S.; Praveen, V. K.; Ajayaghosh, A. Functional π-Gelators and Their Applications. *Chem. Rev.* **2014**, *114* (4), 1973–2129.

(24) Ghosh, S.; Praveen, V. K.; Ajayaghosh, A. The Chemistry and Applications of π-Gels. *Annu. Rev. Mater. Res.* **2016**, *46* (1), 235–262.

(25) Wu, Y.; Wu, S.; Tian, X.; Wang, X.; Wu, W.; Zou, G.; Zhang, Q. Photoinduced Reversible Gel–Sol Transitions of Dicholesterol-Linked Azobenzene Derivatives through Breaking and Reforming of van Der Waals Interactions. *Soft Matter* **2011**, *7* (2), 716–721.

(26) Zhang, M.; Xu, D.; Yan, X.; Chen, J.; Dong, S.; Zheng, B.; Huang, F. Self-Healing Supramolecular Gels Formed by Crown Ether Based Host-Guest Interactions. *Angew. Chemie* **2012**, *124* (28), 7117–7121.

(27) Miyamae, K.; Nakahata, M.; Takashima, Y.; Harada, A. Self-Healing, Expansion-Contraction, and Shape-Memory Properties of a Preorganized Supramolecular Hydrogel through Host-Guest Interactions. *Angew. Chemie - Int. Ed.* **2015**, *54* (31), 8984–8987.

(28) Voorhaar, L.; Hoogenboom, R. Chem Soc Rev Supramolecular Polymer Networks : Hydrogels And. *Chem. Soc. Rev.* **2016**, *45* (2014), 4013–4031.

(29) Wei, P.; Yan, X.; Huang, F. Supramolecular Polymers Constructed by Orthogonal Self-Assembly Based on Host–Guest and Metal–Ligand Interactions. *Chem. Soc. Rev.* **2015**, *44* (3), 815–832.

(30) Chen, G.; Jiang, M. Cyclodextrin-Based Inclusion Complexation Bridging Supramolecular Chemistry and Macromolecular Self-Assembly. *Chem. Soc. Rev.* **2011**, *40* (5), 2254–2266.

(31) Guo, D. S.; Liu, Y. Calixarene-Based Supramolecular Polymerization in Solution. *Chemical Society Reviews*. 2012, pp 5907–5921.

(32) Kim, K. Mechanically Interlocked Molecules Incorporating Cucurbituril and Their Supramolecular Assemblies. *Chem. Soc. Rev.* **2002**, *31* (2), 96–107.

(33) Kim, K.; Selvapalam, N.; Ko, Y. H.; Park, K. M.; Kim, D.; Kim, J. Functionalized Cucurbiturils and Their Applications. *Chem. Soc. Rev.* **2007**, *36* (2), 267–279.

(34) Ogoshi, T.; Yamagishi, T. A.; Nakamoto, Y. Pillar-Shaped Macrocyclic Hosts

Pillar[n]Arenes: New Key Players for Supramolecular Chemistry. *Chem. Rev.* **2016**, *116* (14), 7937–8002.

(35) Ogoshi, T.; Kanai, S.; Fujinami, S.; Yamagishi, T. A.; Nakamoto, Y. Para-Bridged Symmetrical Pillar[5]Arenes: Their Lewis Acid Catalyzed Synthesis and Host-Guest Property. *J. Am. Chem. Soc.* **2008**, *130* (15), 5022–5023.

(36) Holler, M.; Allenbach, N.; Sonet, J.; Nierengarten, J.-F. The High Yielding Synthesis of Pillar[5]Arenes under Friedel–Crafts Conditions Explained by Dynamic Covalent Bond Formation. *Chem. Commun.* **2012**, *48* (20), 2576–2578.

(37) Ogoshi, T.; Ueshima, N.; Akutsu, T.; Yamafuji, D.; Furuta, T.; Sakakibara, F.; Yamagishi, T.-A. The Template Effect of Solvents on High Yield Synthesis, Co-Cyclization of Pillar[6]Arenes and Interconversion between Pillar[5]- and Pillar[6]Arenes. *Chem. Commun.* **2014**, *50*, 5774–5777.

(38) Ogoshi, T.; Yamagishi, T. Pillararenes: Versatile Synthetic Receptors for Supramolecular Chemistry. *European J. Org. Chem.* **2013**, *2013* (15), 2961–2975.

(39) Milev, R.; Lopez-Pacheco, A.; Nierengarten, I.; Trinh, T. M. N.; Holler, M.; Deschenaux, R.; Nierengarten, J.-F. Preparation of Pillar[5]Arene-Based [2]Rotaxanes from Acyl Chlorides and Amines. *European J. Org. Chem.* **2015**, *2015* (3), 479–485.

(40) Nierengarten, I.; Guerra, S.; Ben Aziza, H.; Holler, M.; Abidi, R.; Barberá, J.; Deschenaux, R.; Nierengarten, J. F. Piling Up Pillar[5]Arenes to Self-Assemble Nanotubes. *Chem. - A Eur. J.* **2016**, *22* (18), 6185–6189.

(41) Strutt, Nathan L(1) Zhang, Y.; Shi, B.; Li, H.; Qu, W.; Gao, G.; Lin, Q.; Yao, H.; Wei, T. Polym. Chem. 2014, 5 (16), 4722.; Zhang, H.; Giesener, M. A.; Lei, J.; Stoddart, J. F. A Self-Complexing and Self-Assembling Pillar[5]Arene. *Chem. Commun. (Camb).* **2012**, *48* (11), 1647–1649.

(42) Wang, Q.; Cheng, M.; Zhao, Y.; Wu, L.; Jiang, J.; Wang, L.; Pan, Y. A Pillar[5]Arene-Fused Cryptand: From Orthogonal Self-Assembly to Supramolecular Polymer. *Chem. Commun.* **2015**, *51* (17), 3623–3626.

(43) Kakuta, T.; Yamagishi, T.; Ogoshi, T. Supramolecular Chemistry of Pillar[n]Arenes Functionalised by a Copper-Catalysed Alkyne–Azide Cycloaddition “Click” Reaction. *Chem. Commun.* **2017**, *53* (38), 5250–5266.

(44) Ogoshi, T.; Kayama, H.; Yamafuji, D.; Aoki, T.; Yamagishi, T. Supramolecular Polymers with Alternating Pillar[5]Arene and Pillar[6]Arene Units from a Highly Selective Multiple Host–Guest Complexation System and Monofunctionalized Pillar[6]Arene. *Chem. Sci.* **2012**, *3* (11), 3221.

(45) Strutt, N. L.; Forgan, R. S.; Spruell, J. M.; Botros, Y. Y.; Stoddart, J. F. Monofunctionalized Pillar[5]Arene as a Host for Alkanediamines. *J. Am. Chem. Soc.* **2011**, *133* (15), 5668–5671.

(46) Shu, X.; Chen, S.; Li, J.; Chen, Z.; Weng, L.; Jia, X.; Li, C. Highly Effective Binding of Neutral Dinitriles by Simple Pillar[5]Arenes. *Chem. Commun.* **2012**, *48* (24), 2967.

(47) Yu, G.; Zhang, Z.; He, J.; Abliz, Z.; Huang, F. Cavity-Extended Pillar[5]Arenes: Syntheses and Host-Guest Complexation with Paraquat and Bispyridinium Derivatives. *European J. Org. Chem.* **2012**, No. 30, 5902–5907.

(48) Ogoshi, T.; Demachi, K.; Kitajima, K.; Yamagishi, T.-A. Monofunctionalized Pillar[5]Arenes: Synthesis and Supramolecular Structure. *Chem. Commun. (Camb).* **2011**, *47* (25), 7164–7166.

(49) Strutt, Nathan L(1) Zhang, Y.; Shi, B.; Li, H.; Qu, W.; Gao, G.; Lin, Q.; Yao, H.; Wei, T. Polym. Chem. 2014, 5 (16), 4722.; Zhang, H.; Giesener, M. A.; Lei, J.; Stoddart, J. F. A Self-Complexing and Self-Assembling Pillar[5]Arene. *Chem. Commun. (Camb).* **2012**, *48* (11), 1647–1649.

(50) Ma, Y.; Chen, L.; Li, C.; Mullen, K. A Fishing Rod-like Conjugated Polymer Bearing Pillar[5]Arenes. *Chem. Commun.* **2016**, *52*, 6662–6664.

(51) Sun, S.; Hu, X.-Y.; Chen, D.; Shi, J.; Dong, Y.; Lin, C.; Pan, Y.; Wang, L. Pillar[5]Arene-Based Side-Chain Polypseudorotaxanes as an Anion-Responsive Fluorescent Sensor. *Polym. Chem.* **2013**, *4* (7), 2224.

(52) Strutt, N. L.; Zhang, H.; Giesener, M. A.; Lei, J.; Stoddart, J. F. A Self-Complexing and Self-Assembling Pillar[5]Arene. *Chem. Commun.* **2012**, *48* (11), 1647–1649.

(53) Zhang, Y.; Shi, B.; Li, H.; Qu, W.; Gao, G.; Lin, Q.; Yao, H.; Wei, T.; Huang, F.; Yu, Y.; Gibson, H. W.; Huang, F. Copillar[5]Arene-Based Supramolecular Polymer Gels. *Polym. Chem.* **2014**, *5* (16), 4722.

(54) Li, Z. Y.; Zhang, Y.; Zhang, C. W.; Chen, L. J.; Wang, C.; Tan, H.; Yu, Y.; Li, X.; Yang, H. B. Cross-Linked Supramolecular Polymer Gels Constructed from Discrete Multi-Pillar[5]Arene Metallacycles and Their Multiple Stimuli-Responsive Behavior. *J. Am. Chem. Soc.* **2014**, *136* (24), 8577–8589.

(55) Lin, Q.; Mao, P.-P.; Fan, Y.-Q.; Liu, L.; Liu, J.; Zhang, Y.-M.; Yao, H.; Wei, T.-B.; Li, C.; Jia, D. Z. A Novel Supramolecular Polymer Gel Based on Naphthalimide Functionalized-Pillar[5]Arene for the Fluorescence Detection of Hg 2+ and I − and Recyclable Removal of Hg 2+ via Cation–π Interactions. *Soft Matter* **2017**, *112*, 199–204.

(56) Chang, J.; Zhao, Q.; Kang, L.; Li, H.; Xie, M.; Liao, X. Multiresponsive Supramolecular Gel Based on Pillararene-Containing Polymers. *Macromolecules* **2016**, *49* (7), 2814–2820.

(57) Kardelis, V.; Chadwick, R. C.; Adronov, A. Click Functionalization of a Dibenzocyclooctyne-Containing Conjugated Polyimine. *Angew. Chem. Int. Ed. Engl.* **2016**, *55* (3), 945–949.

(58) Kardelis, V.; Chadwick, R. C.; Adronov, A. Click Functionalization of a Dibenzocyclooctyne-Containing Conjugated Polyimine. *Angew. Chem. Int. Ed. Engl.* **2016**, *55* (3), 945–949.

(59) Strutt, N. L.; Zhang, H.; Schneebeli, S. T.; Stoddart, J. F. Functionalizing Pillar[n]Arenes. *Acc. Chem. Res.* **2014**, *47* (8), 2631–2642.

(60) Strutt, N. L.; Forgan, R. S.; Spruell, J. M.; Botros, Y. Y.; Stoddart, J. F. Monofunctionalized Pillar [5] Arene as a Host for Alkanediamines. *J. Am. Chem. Soc.* **2011**, *70* (15), 5668–5671.

(61) Ogoshi, T.; Demachi, K.; Kitajima, K.; Yamagishi, T.-A. Selective Complexation of N-Alkanes with Pillar[5]Arene Dimers in Organic Media. *Chem. Commun. (Camb).* **2011**, *47*, 10290–10292.

(62) Shu, X.; Chen, S.; Li, J.; Chen, Z.; Weng, L.; Jia, X.; Li, C. Highly Effective Binding of Neutral Dinitriles by Simple Pillar[5]Arenes. *Chem. Commun.* **2012**, *48* (24), 2967.

(63) Nierengarten, I.; Guerra, S.; Ben Aziza, H.; Holler, M.; Abidi, R.; Barberá, J.; Deschenaux, R.; Nierengarten, J. F. Piling Up Pillar[5]Arenes to Self-Assemble

Nanotubes. *Chem. - A Eur. J.* **2016**, *22* (18), 6185–6189.

(64) Moreira, L.; Calbo, J.; Aragó, J.; Illescas, B. M.; Nierengarten, I.; Delavaux-Nicot, B.; Ortí, E.; Martín, N.; Nierengarten, J. F. Conjugated Porphyrin Dimers: Cooperative Effects and Electronic Communication in Supramolecular Ensembles with C60. *J. Am. Chem. Soc.* **2016**, *138* (47), 15359–15367.

(65) Elhabiri, M.; Trabolsi, A.; Cardinali, F.; Hahn, U.; Albrecht-Gary, A. M.; Nierengarten, J. F. Cooperative Recognition of C60-Ammonium Substrates by a Ditopic Oligophenylenevinylene/Crown Ether Host. *Chem. - A Eur. J.* **2005**, *11* (16), 4793–4798.

(66) Bhattacharjee, S.; Bhattacharya, S. Phthalate Mediated Hydrogelation of a Pyrene Based System: A Novel Scaffold for Shape-Persistent, Self-Healing Luminescent Soft Material. *J. Mater. Chem. A* **2014**, *2* (42), 17889–17898.

(67) Wang, Q.; Mynar, J. L.; Yoshida, M.; Lee, E.; Lee, M.; Okuro, K.; Kinbara, K.; Aida, T. High-Water-Content Mouldable Hydrogels by Mixing Clay and a Dendritic Molecular Binder. *Nature* **2010**, *463* (7279), 339–343.

(68) Ogoshi, T.; Kitajima, K.; Aoki, T.; Fujinami, S.; Yamagishi, T.; Nakamoto, Y. Synthesis and Conformational Characteristics of Alkyl-Substituted Pillar[5]Arenes. *J. Org. Chem.* **2010**, *75* (10), 3268–3273.

(69) Ogoshi, T.; Demachi, K.; Kitajima, K.; Yamagishi, T.-A. Monofunctionalized Pillar[5]Arenes: Synthesis and Supramolecular Structurew. *Chem. Commun. Chem. Commun* **2011**, *47* (47), 7164–7166.

(70) Ogoshi, T.; Kayama, H.; Yamafuji, D.; Aoki, T.; Yamagishi, T. Supramolecular Polymers with Alternating Pillar[5]Arene and Pillar[6]Arene Units from a Highly Selective Multiple Host–Guest Complexation System and Monofunctionalized Pillar[6]Arene. *Chem. Sci.* **2012**, *3* (11), 3221.

(71) Edition, I.; Chemistry, P. Macrocycles , Derivatives of Nitrogen Containing Heterocycles 2 .Synthesis and Electrochemical Properties of Diindolizinadiquinoxalinacyclooxaalkaphanes. *Russ. Chem. Bull. Int. Ed. Izv. Akad. Nauk. Seriya Khimicheskaya* **2009**, *58* (7), 1484–1492.

(72) Zhang, Y.; Gilliam, A.; Maitra, R.; Damaj, M. I.; Tajuba, J. M.; Seltzman, H. H.; Thomas, B. F. Synthesis and Biological Evaluation of Bivalent Ligands for the

Cannabinoid 1 Receptor. *J. Med. Chem.* **2010**, *53* (19), 7048–7060.

(73) Kardelis, V.; Chadwick, R. C.; Adronov, A. Click Functionalization of a Dibenzocyclooctyne-Containing Conjugated Polyimine. *Angew. Chemie - Int. Ed.* **2016**, *55* (3), 945–949.

(74) Frassineti, C.; Ghelli, S.; Gans, P.; Sabatini, A.; Moruzzi, M. S.; Vacca, A. Nuclear Magnetic Resonance as a Tool for Determining Protonation Constants of Natural Polyprotic Bases in Solution. *Anal. Biochem.* **1995**, *231* (2), 374–382.

(75) Hodgson, S. M.; Bakaic, E.; Stewart, S. A.; Hoare, T.; Adronov, A. Properties of Poly(Ethylene Glycol) Hydrogels Cross-Linked via Strain-Promoted Alkyne-Azide Cycloaddition (SPAAC). *Biomacromolecules* **2016**, *17* (3), 1093–1100.

(76) Long, R.; Hall, M. S.; Wu, M.; Hui, C.-Y. Effects of Gel Thickness on Microscopic Indentation Measurements of Gel Modulus. *Biophys. J.* **2011**, *101*, 643–650.

(77) Takigawa, T.; Morino, Y.; Urayama, K.; Masuda, T. Poisson's Ratio of Polyacrylamide (PAAm) Gels. *Polym. Gels Networks* **1996**, *4* (1), 1–5.

(78) Anseth, K. S.; Bowman, C. N.; Brannon-Peppas, L. Mechanical Properties of Hydrogels and Their Experimental Determination. *Biomaterials*. January 1996, pp 1647–1657.

Chapter 4

Click-Functionalization of a Poly(Tetrazine)-co-Fluorene-Conjugated Polymer with a Series of *trans*-Cyclooctene Derivatives

This chapter has been reprinted with permission from Angewandte Chemie International Edition; Vladimir Kardelis, Maria M. Denk, and Alex Adronov, **2021,** *60*, 2980-2986, DOI: 10.1002/anie.202010795. Copyright (2021) Wiley-VCH.

Contributions:

Vladimir Kardelis primarily planned this study. Vladimir Kardelis synthesized/designed all monomeric/polymeric compounds and prepared/characterized the resultant polymeric series. All *trans*-Cyclooctene derivatives were also prepared and characterized by Vladimir Kardelis. Vladimir Kardelis also carried out all computational calculations on the monomer/polymer structures. Maria M. Denk assisted in scaling up synthesis of the monomers and *trans*-Cyclooctene derivatives.

Abstract

A soluble poly(tetrazine) polymer was prepared via Suzuki polycondensation of 3,6-bis(5-bromofuran-2-yl)-1,2,4,5-tetrazine and a fluorene diboronate derivative. This poly(tetrazine) was shown to undergo efficient and quantitative post-polymerization inverse electron demand Diels-Alder “click” reactions with a variety of trans-cyclooctene (TCO) derivatives. The resulting polymers were oxidized to convert dihydropyridazine rings into the more stable and conjugated pyridazines. It was found that the absorption spectra of the product polymers, both before and after oxidation, underwent hypsochromic shifts that correlated with steric hindrance of the appended side-chains. In addition, they exhibited significantly enhanced fluorescence intensity relative to the original poly(tetrazine). While gel permeation chromatography indicated that the product polymers, especially after oxidation, exhibited longer retention times, NMR end-group analysis showed that the polymers retained relatively constant degrees of polymerization. Graft copolymers were easily prepared via reaction with TCO-functionalized poly(ethylene glycol), PEG_{5k}, chains. In addition, a cross-linked foam was produced by reacting the poly(tetrazine) with a bis-TCO crosslinker.

4.1. Introduction

Since their discovery, conjugated polymers have played an increasingly important role in numerous disruptive technologies. The wide array of structures that constitute the polymer backbone allows their optimization for applications that include lighting and displays,[1] energy generation and storage,[2,3] sensors,[4,5] field-effect transistors,[6,7] as well as information storage and computing.[8] A variety of conjugated polymer properties can be modified by varying polymer structure, including bandgap, HOMO and LUMO levels, extinction coefficient, quantum yield, conductivity, and solubility.[9–14] However, modification of polymer properties typically requires the preparation of new polymer structures, which are prepared via de novo synthesis incorporating new monomers.[12] When developing polymers for new applications, it is often necessary to prepare libraries of homologous polymers that exhibit only small changes from one to another. Such small changes are difficult to achieve when carrying out polymerizations with different monomers, as control over molecular weight and dispersity in conjugated polymers remains a challenge in all but a few specialized polymerization methods.[15–21] These factors greatly impact the resultant polymer morphologies and other physical properties, such as solubility. Thus, post-polymerization functionalization has been widely considered. Although modification of a pre-formed conjugated polymer can be routinely achieved through the chemistry of side-chains, quantitative changes to the conjugated backbone are much more difficult. Only a few examples of efficient modification of a conjugated polymer backbone have been published, including $Cu(OTf)_2$-catalyzed benzannulation of phenylene ethynylenes,[22] and nucleophilic aromatic substitution on aryl fluoride derivatives of benzothiadiazole monomer units.[23]

In previous work, we have shown that post-polymerization functionalization of a dibenzocyclooctyne (DIBO)-containing conjugated polymer is possible via strain-promoted alkyne-azide cycloaddition (SPAAC).[24–26] Not only is SPAAC functionalization rapid (2nd order rate constant of 0.031 $M^{-1}s^{-1}$), but the reaction was shown to be efficient enough to quantitatively functionalize the polymer backbone with 24 kDa polystyrene azide, resulting in a graft copolymer having a number average molecular weight (M_n) exceeding 800 kDa.[24] Though a versatile polymer, the DIBO-containing polyimine is plagued with poor hydrolytic stability,[27] and the multi-step synthesis to the monomer is prohibitive to its applications (six steps; overall yield of 7%). In addition, classic metal-mediated cross-coupling conditions cannot be used to polymerize the cyclooctyne monomer, as it rapidly generates metallocycles with the strained triple bond. Furthermore, upon SPAAC coupling with azide derivatives, we found that the polymer backbone adopts a severely kinked conformation, which detracts from any favourable optoelectronic properties that the parent polymer exhibits.

Rather than working with strained cyclooctynes as the reactive moiety, which precludes classic transition metal-catalyzed cross coupling polymerizations, we decided to introduce the *s*-tetrazine moiety into the polymer backbone. 1,2,4,5-Tetrazines undergo inverse-electron-demand Diels-Alder (IEDDA) reactions with various cyclooctenes, cyclooctynes, and norbornenes with 2nd order rate constants ranging from 1 to 10^6 $M^{-1}s^{-1}$.[28] In addition to their fast reaction rates and bioorthogonal reactivity, 1,2,4,5-tetrazines are relatively simple to synthesize, often in 1-2 steps from commercially available starting materials. Furthermore, they tolerate Suzuki conditions, which facilitate the formation of high molecular weight conjugated polymers. Herein, we describe a convenient method for synthesizing a conjugated *s*-tetrazine-containing polymer and its resultant series of cycloadduct polymers via post-polymerization IEDDA chemistry.

4.2. Results and Discussion

4.2.1. Preparation of *s*-Tetrazine-Containing Polymer (P1)

The tetrazine monomer **2** was synthesized according to a literature procedure,[29] wherein commercially available 2-furonitrile undergoes a modified Pinner reaction with hydrazine hydrate followed by an oxidation with isoamyl nitrite to generate the *s*-tetrazine **1** (Scheme 4.1a). This tetrazine was then doubly brominated using *N*-bromosuccinimide to yield the desired *s*-tetrazine-Br_2 monomer **2** in a modest 31% yield over the two steps. Monomer **2** was readily copolymerized with a previously synthesized fluorene bis(pinacolato)boronate ester comonomer **3**[30] via Suzuki polycondensation under mild conditions (50 °C for 15 minutes) to yield the progenitor *s*-tetrazine-containing polymer **P1** (Scheme 4.1b). The Suzuki reaction produced a polymer with a number average molecular weight of 38.8 kDa and a dispersity (Đ) of 1.6, as determined by gel permeation chromatography (GPC). To provide a functional NMR handle that could be used to corroborate the GPC data for **P1** and all subsequent cycloadduct polymers, growing polymer chains were end-capped by adding *p*-anisole pinacolato boronate ester **4** and allowing the mixture to stir for 30 min. Anisole was used because the phenyl methoxy group provides a distinct ^{1}H-NMR resonance at ~3.85 ppm, which does not overlap with any other signals corresponding to the polymer chain (See Supporting Information, Figure 4.31). Based on the integration of this signal, the degree of polymerization (DP) for **P1** was found to be 44, which corresponds to an M_n (NMR) of 36.3 kDa, in excellent agreement with the GPC data. The reactive, conjugated polymer **P1** was further characterized via UV-Vis, and infrared (IR) spectroscopy, as well as by thermogravimetric analysis (TGA), with details provided in the Supporting Information. The TGA thermogram of this polymer showed two distinct decompositions, including a 7% mass loss at ~280 °C corresponding to the loss of N_2, and a 78% mass loss at ~400 °C corresponding to the loss of the hexadecyl side-chains of the fluorenyl monomer (Figure 4.67).

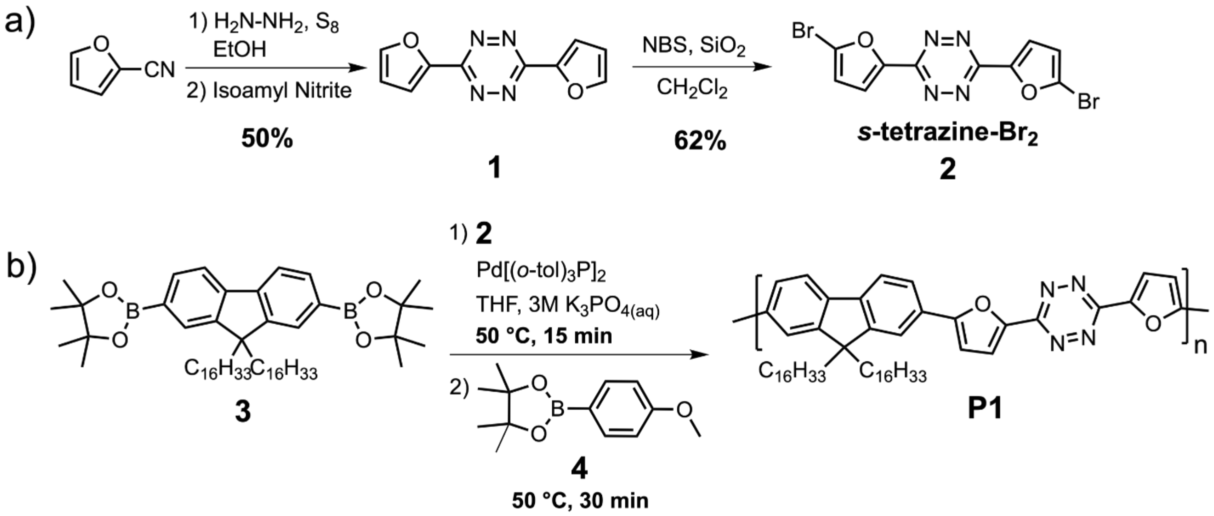

Scheme 4.1. Synthesis of the s-tetrazine-Br$_2$ monomer (a), and synthesis of the s-tetrazine containing polymer **P1** (b).

4.2.2. Preparation of TCO-derivatives

Having prepared the reactive polymer **P1**, we set out to investigate its ability to undergo inverse electron demand Diels-Alder (IEDDA) reactions with a small library of *trans* cyclooctene (TCO) derivatives. This began with the preparation of *rel*-(1*R*, 4*E*, p*R*)-Cyclooct-4-enol (**5**) from the corresponding (Z)-cyclooct-4-enol following the procedure of Fox and co-workers.[31] The TCO derivatives were synthesized via activation of **5** using nitrophenyl chloroformate to form carbonate **6**, followed by the substitution of the activated enol with a series of amines to yield carbamates **7a**-**7f** (Scheme 4.2). Aliphatic and benzylic amines were used due to their relatively high nucleophilicity, allowing the reactions to be performed at room temperature, thereby minimizing the risk of thermal reisomerization to the (*Z*)-cyclooctenol. All coupling reactions with the small molecule derivatives proceeded to high conversion, allowing isolation of the desired products (**7a-e**) in excellent yield (~90%) after chromatographic purification. In addition, a 5 kDa α-methoxy ω-amino poly(ethylene glycol) (PEG-NH_2) was appended in order to investigate the formation of a graft copolymer via IEDDA. The resulting PEG-TCO derivative (**7f**) was isolated in 74% yield after precipitation.

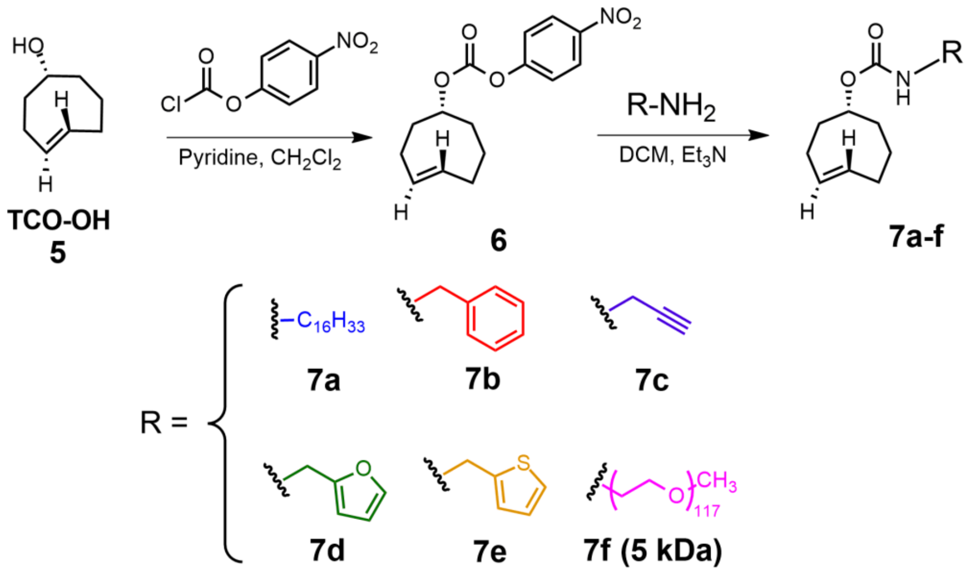

Scheme 4.2. Preparation of a library of trans-cyclooctene (TCO) derivatives.

4.2.3. Post-Polymerization IEDDA onto P1

The IEDDA reactions between **P1** and the TCO derivatives **5** and **7a-e** were carried out by combining a small excess (1.5 equiv. per polymer repeat unit) of each derivative with **P1** in tetrahydrofuran at room temperature (Scheme 4.3). Upon mixing, effervescence was immediately observed as a result of N_2 evolution, providing visual confirmation that the reaction was occurring. Stirring the reaction mixture at room temperature for 30 minutes resulted in a visible increase in solution viscosity, and quantitative conversion of the tetrazines to the cycloadducts. This could be easily confirmed by the complete disappearance of signals at 7.05 and 7.90 ppm in the NMR spectrum, which correspond to the furyl protons that are adjacent to the tetrazine groups in **P1** (Figure 4.1a). It should be noted that, because the TCO derivatives are not symmetrical about the C_2 axis, each of the dihydropyridazine subunits within the products (**P2**, **P2a-f**) is formed as a mixture of two regioisomers (Scheme 4.3b), which considerably complicates the ^{1}H-NMR spectra associated with these products. It should also be noted that IEDDA of trans-cyclooctenes onto *s*-tetrazines yields 4,5-dihydropyridazines, which readily tautomerize into 1,4-dihydropyridazines as evident by the presence of an N-H resonance between 8 and 9 ppm in the ^{1}H-NMR spectra (see spectrum for P2a in Figure 4.1a, as well as additional ^{1}H-NMR spectra in the Supporting Information, Figures 4.31-4.37). In addition to NMR analysis, IR corroborated the introduction of the TCO derivatives on the polymer backbone with the strong carbonyl stretch of the primary carbamates observed at 1708-1722 cm^{-1} for each of the products (see Supporting Information, Figures 4.77-4.84). The molecular weight of each of the functionalized product polymers was measured by both GPC and NMR, with observed values provided in Table 1. In most cases, the apparent number average molecular weight (M_n) observed by GPC was in good agreement with the corresponding value from NMR, both of which indicated a small increase in molecular weight as a result of the side chains that were appended via the IEDDA reactions. In the case of **P2**, the significant decrease in apparent molecular weight from the GPC measurement was likely caused by interactions between the hydroxyl groups in this product with the stationary phase of the GPC columns, which delays its elution and results in an observed M_n value that is lower than the actual value. Additionally, reaction progress could be monitored by UV-Vis spectroscopy, where the strong absorption of **P1**, centered around 460 nm, undergoes a significant hypsochromic shift to 400 nm in **P2**. The extent of this shift for each of the polymers, including **P2a-e**, is given in Table 2, and correlates well with steric hindrance from the appended side-chain, which would result in a twisting of the polymer backbone and decreased conjugation length. In addition, while the unreacted polytetrazine **P1** exhibited only very weak fluorescence, the cycloadduct dihydropyridazine polymers (**P2**, **P2a-e**) exhibited much stronger fluorescence, with a broad emission band centered around 510 nm (Supporting Information, Figures 4.59-4.64). In fact, the onset of fluorescence could be observed by carrying out the reaction while irradiating the reaction vessel with UV light at 365 nm (video 1, Supporting Information).

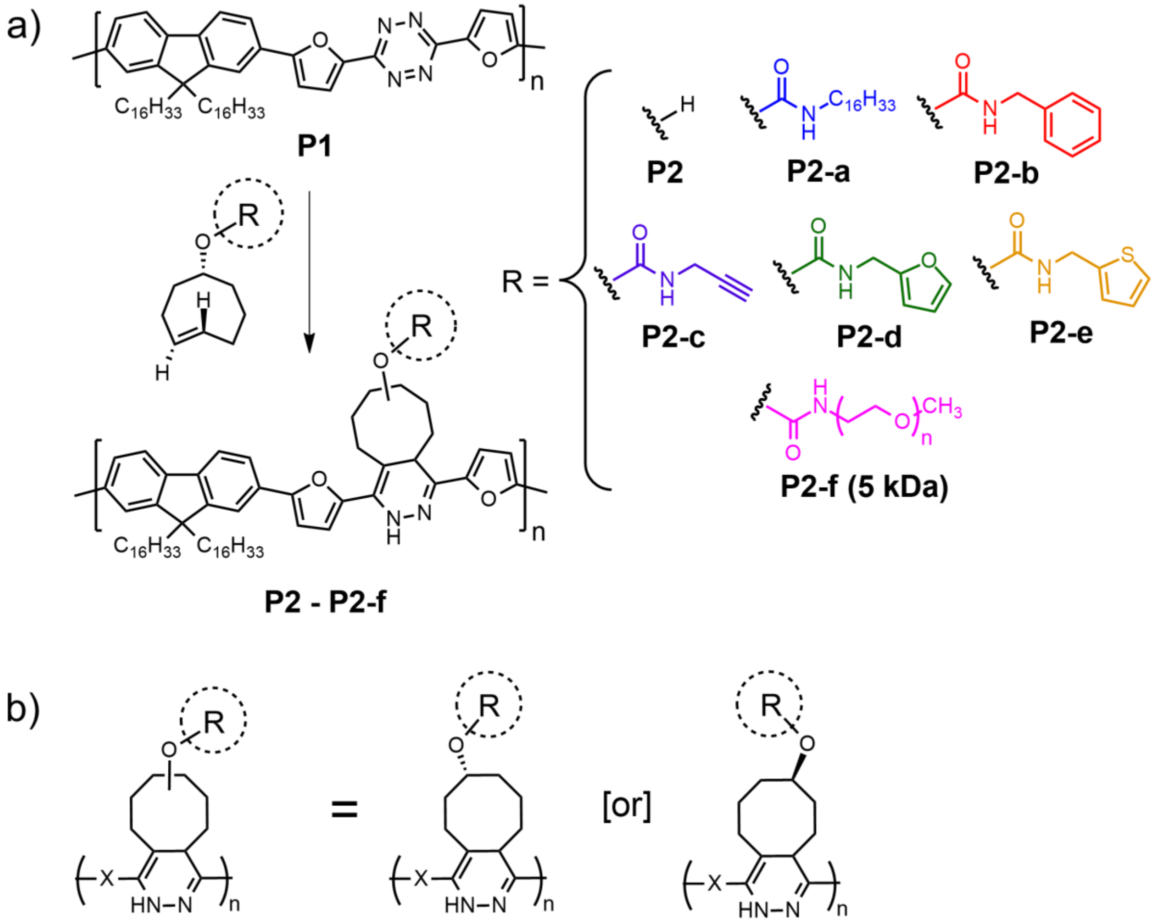

Scheme 4.3. Inverse Electron Demand Diels Alder (IEDDA) reaction to functionalize polymer **P1** with TCO derivatives (a). Illustration of the two regioisomers that are possible at each clicked repeat unit (b).

4.2.4. Reaction Kinetics of P1 with TCO-OH (5)

To determine the rate of the reaction between the poly(tetrazine) **P1** and TCO-OH (**5**), a kinetics study was performed. The reaction was carried out in a quartz cuvette with equimolar concentrations of both **P1** and **5** (0.242 mM), and reaction progress was monitored by measuring the absorption of the reaction mixture at 500 nm over the course of 90 min. The starting polymer, **P1**, exhibits a strong absorption at this wavelength, while the product, **P2**, exhibits negligible absorption (Figure 4.1b). The kinetics study was performed in triplicate, and resulted in an average second order rate constant of 1.25 ± 0.07 M^{-1} s^{-1} (see Supporting Information). Although a modest rate constant for typical tetrazine ligations with trans-cyclooctenes, the IEDDA on **P1** is two orders of magnitude faster than strain-promoted alkyne-azide cylooaddition (SPAAC) reactions that we have previously carried out on polymeric substrates.[32]

4.2.5. Oxidation of poly(1,4-dihydropyridazines)

Considering the goal of producing a set of homologous conjugated polymers, it was necessary to oxidize the dihydropyridazine rings in **P2**, and **P2a-e** in order to aromatize them into pyridazines. This was accomplished by treating each of the polymers with 2,3-dichloro-5,6-dicyano-1,4-benzoquinone (DDQ) in THF at room temperature for 1 h, resulting in polymers **P3, P3a – P3e**. Upon oxidation, ^{1}H-NMR showed a clean disappearance of the N-H resonance corresponding to the dihydropyridazine between 8 and 9 ppm (Figure 4.1a), indicating that the oxidation was effective. The IR spectra of the product polymers did not change appreciably upon oxidation (Figures 4.31-4.37), but the absorption spectrum of each polymer underwent a bathochromic shift, ranging from 16 to

38 nm (Table 4.2 and Figures 4.52-4.57). This indicates that the formation of pyridazine rings results in increased conjugation along the polymer backbone. In all cases, fluorescence of the oxidized polymers slightly increased in intensity, and spectra exhibited small changes to fine structure (see Supporting Information, Figures 4.59-4.64). The changes in absorption and emission spectra for **P3** relative to the original polymer **P1** are illustrated in Figure 4.2, which shows the significant hypsochromic shift in the absorption spectrum, and the increase in fluorescence intensity.

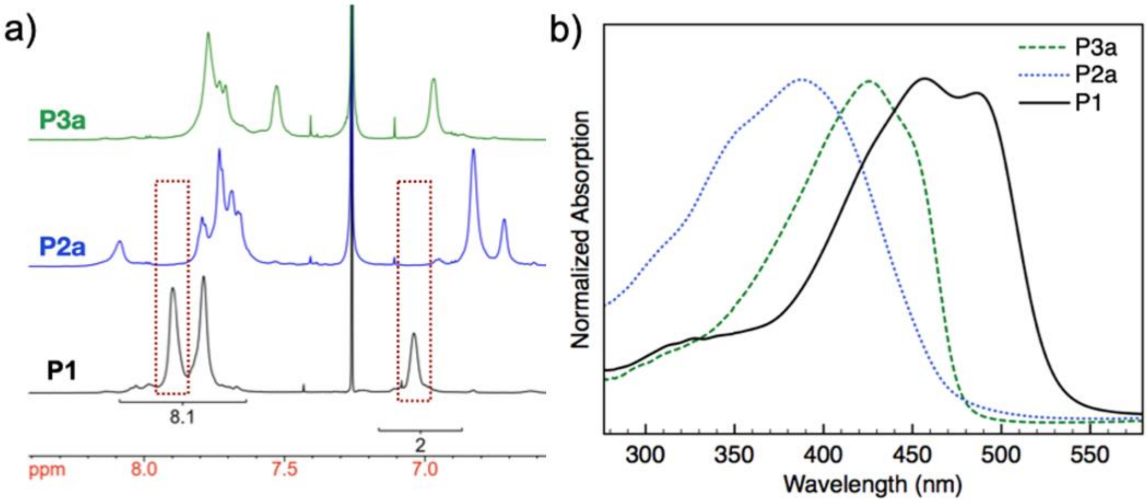

Figure 4.1. (a) NMR data illustrating the sequential transformation of **P1** upon clicking and oxidation. (b) UV-Vis absorption data for **P1** (black), **P2-a** (blue), and **P3-a** (green), illustrating the effect of breaking conjugation (hypsochromic shift) upon click coupling, followed by reformation of conjugated structures upon oxidation (bathochromic shift).

Interestingly, upon oxidation of the dihydropyridazine backbone to yield the poly(pyridazines) **P3**, **P3a-e**, the observed GPC molecular weights decrease, while the NMR molecular weights remain relatively unchanged. The largest decrease was for **P3,** which can again be explained by the presence of hydroxyl groups along the polymer backbone that interact with the stationary phase of the column. The lower than expected GPC values for **P3a-e** indicate that these structures must either adopt a more compact conformation in solution than the **P2** series, or that the formation of the pyridazine rings also results in enhanced interaction with the stationary phase, causing delayed elution. Chain scission as a result of the oxidation process was ruled out by ^{1}H-NMR end-group analysis (see Figures 4.39-4.44), which indicated that the molecular weights were not significantly changed upon oxidation (Table 4.1). TGA analysis of the product polymers was also carried out under Ar atmosphere to determine their thermal decomposition patterns and temperatures (see Supporting Information, Figures 4.66-4.72). In all cases, two distinct decompositions were observed, which correspond to the loss of the Diels-Alder adducts at 200-300 °C (4-23% mass loss, depending on the molecular weight of the TCO derivative), followed by the loss of the hexadecyl side-chains of the fluorenyl units at ~400 °C (50-61% mass loss).

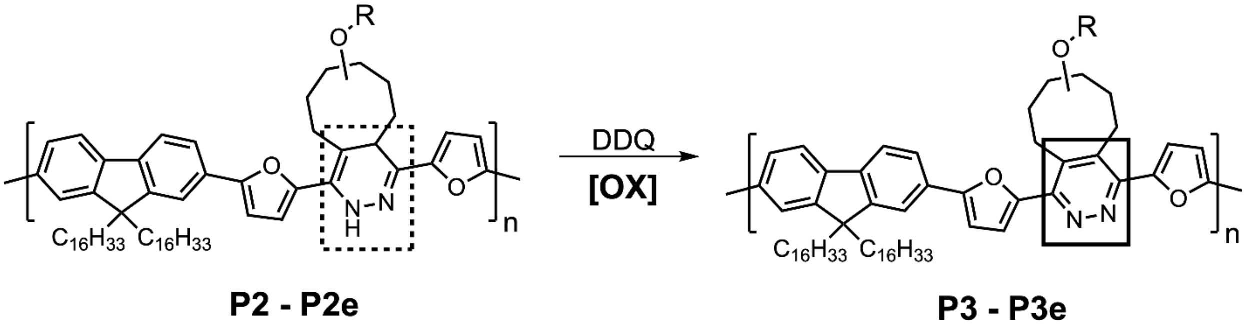

Scheme 4.4. Oxidation of the clicked poly(1,4-dihydropyridazine) series.

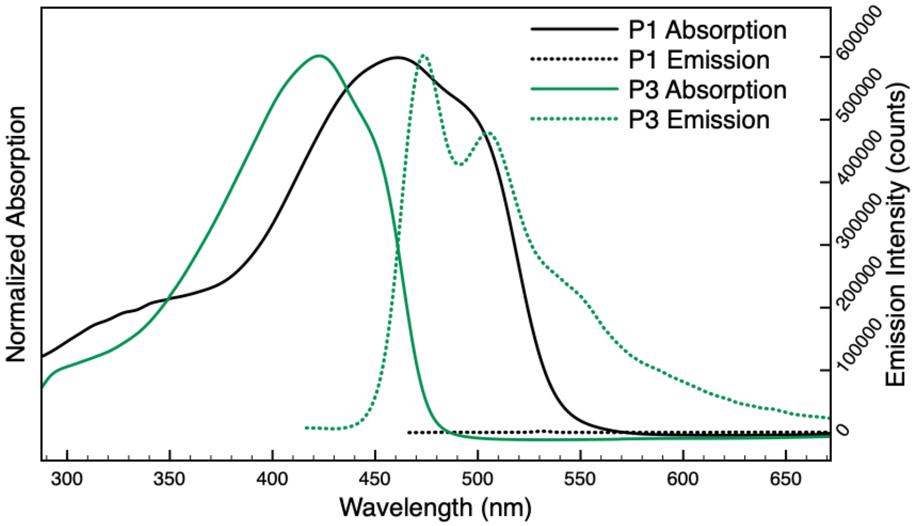

Figure 4.2. Overlay of absorption and emission spectra comparing **P1** and **P3**.

4.2.6. Analysis of Polymer Geometry – DFT Calculations

In order to probe the effect of backbone functionalization via IEDDA on the overall structure of the polymer, we carried out modeling studies using semi-empirical methods (Parametric Method 3). This involved construction of three separate oligomers (3 repeat units each) corresponding to the structures prior to functionalization, post functionalization with **5**, and after oxidation of the dihydropyridazines with DDQ, followed by geometry optimization of each structure. As shown in Figure 3, the geometry of starting polymer **P1** is planar, as would be expected from its conjugated structure. Upon IEDDA with **5**, the geometry retains much of its planarity, with only slight perturbations caused by the introduction of cyclooctyl rings and the decreased conjugation that results from formation of the dihydropyridazines. After oxidation, the calculations indicate that the **P3** polymer backbone adopts a slightly puckered structure relative to the planarity of **P1**, but overall remains relatively planar. This puckering in **P2** and **P3** is likely caused by steric interactions between the cyclooctyl ring and the neighbouring furans, which changes the angle between the two ring structures away from planarity. To corroborate this, we carried out additional DFT geometry optimizations on truncated model compounds and found that the coplanar rings on either side of the tetrazine unit adopt a ~30° angle in the puckered dihydropyridazine structure, but only a 4° upon oxidation to the more planar pyridazine (Figure 4.8). These slight changes between **P1**, **P2**, and **P3** might also explain some of the differences in apparent hydrodynamic diameter that contribute to the changes in molecular weight values observed from GPC.

Table 4.1. GPC and NMR molecular weights for polymers produced.

Polymer	NMR		GPC		
	M_n (kDa)	**DP**	**M_n (kDa)**	**M_w (kDa)**	**Đ**
P1	36.3	44	38.8	63.7	1.64
P2	36.0	39	12.2	15.0	1.23
P2a	53.3	45	46.8	67.8	1.45
P2b	45.9	44	40.9	71.8	1.76
P2c	45.0	45	39.3	82.5	2.10
P2d	46.5	44	38.4	79.6	2.07
P2e	47.2	44	33.5	53.4	1.60
P3	36.8	40	12.9	22.6	1.76
P3a	51.0	43	24.6	45.4	1.84
P3b	47.5	45	14.1	24.2	1.72
P3c	41.8	42	16.4	28.8	1.76
P3d	45.9	44	25.5	45.4	2.08
P3e	56.6	44	17.8	33.1	1.86

Table 4.2. Absorption spectrum λ_{max} values and resultant hypsochromic and bathochromic shifts produced upon cycloaddition and oxidation of the polymers, respectively.

Polymer	**λ_{max} (nm)**	**Polymer**	**λ_{max} (nm)**	**Shift (nm)**	**Polymer**	**λ_{max} (nm)**	**Shift (nm)**
P1	457	**P2**	400	-57	**P3**	423	+23
		P2a	388	-69	**P3a**	426	+38
		P2b	402	-55	**P3b**	424	+22
		P2c	412	-45	**P3c**	428	+16
		P2d	404	-53	**P3d**	428	+24
		P2e	405	-52	**P3e**	427	+22

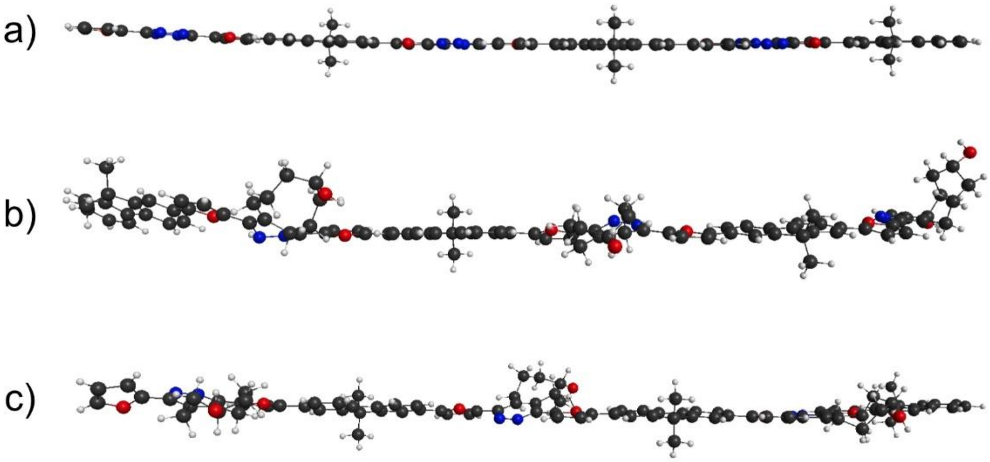

Figure 4.3. Optimized geometry (PM3) of trimers **P1** (a), **P2** (b), and **P3** (c). Note the minimal amount of puckering in the backbones of **P2** and **P3** upon undergoing IEDDA. Alkyl chains were replaced with methyl groups to ease computational loads.

4.2.7. Post-Polymerization IEDDA of 5 kDa PEG onto P1

To further test the efficiency of the IEDDA cycloaddition reaction in functionalizing the polymer backbone, a 5 kDa poly(ethylene glycol)-TCO derivative **7f** was grafted onto **P1**. Reaction with **7f** was found to be significantly slower than with the small molecule derivatives, requiring slight heating and a longer reaction time. Thus, a small excess (1.2 eq.) of **7f** was stirred with **P1** at 40 °C for 8 hours, which resulted in quantitative functionalization of the backbone. Dialysis in water over 72 h using a 50 kDa molecular weight cutoff dialysis membrane allowed for the removal of the excess PEG-TCO carbamate from the reaction mixture, leaving behind the pure dihydropyridazine graft copolymer **P2f**. Figure 4 shows the ^{1}H-NMR spectrum of **P2f** overlaid with the starting polymer **P1**. The aromatic region displays a similar shifting of the furyl proton resonances as observed in the small molecule cycloadditions. Additionally, a large resonance corresponding to the methylene protons of the PEG chains is observed at 3.7 ppm, indicating the presence of the graft on the **P1** backbone. Consistent with the small molecule click reactions, an hypsochromic shift is observed in the polymer UV-Vis spectrum, though the shift is much larger in the case of **P2f**, amounting to over 110 nm (Figure 4.58). This large blue-shift is likely caused by a significant twisting of the polymer backbone away from conjugation in order to accommodate all of the appended PEG chains. The molecular weight of PEG graft poly(1,4-dihydropyridazine) **P2f** could not be accurately measured by GPC due to interactions between the PEG grafts and the column stationary phase, leading to extensive retention on the column. Additionally, the functional methoxy end-group handle could not be accurately integrated via ^{1}H-NMR due to overlap of the signals with those of the PEG methylene units. As a result, only a theoretical molecular weight is listed in the Supporting Information. Thermogravimetric analysis of **P2f** showed a single, large mass loss at approximately 400 °C, which corresponds to the decomposition of the grafted PEG chains that make up nearly 90% of the mass of **P2f**.

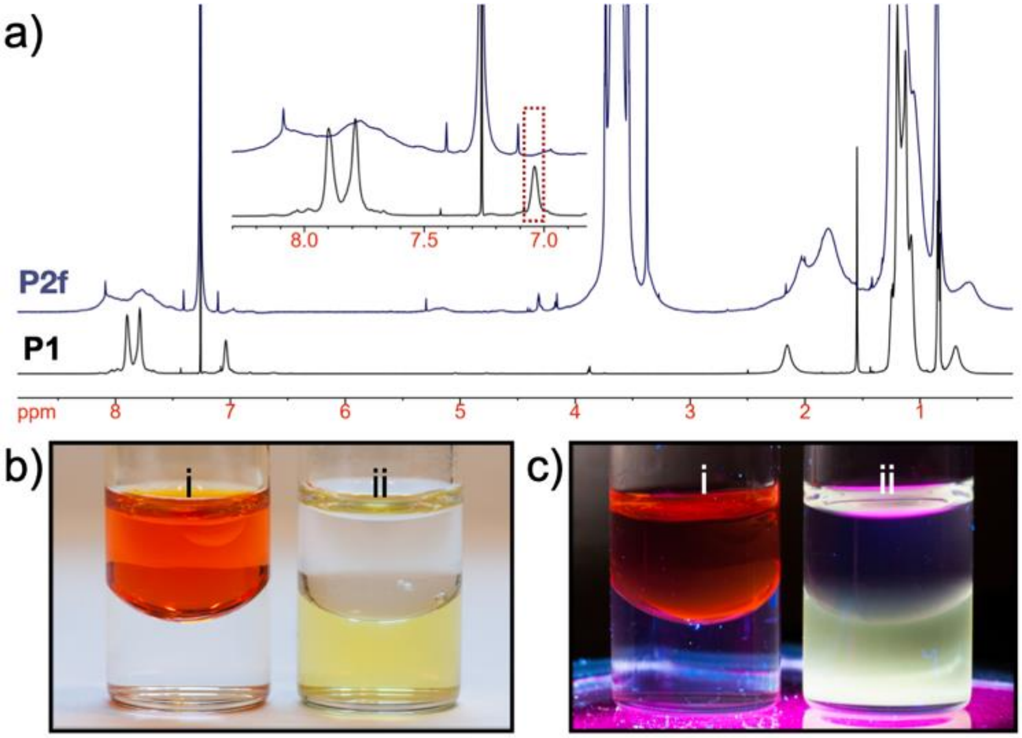

Figure 4.4. (a) 1H-NMR spectra of **P1** and **P2f**, illustrating the shift of furyl aromatic signals and the appearance of PEG signals upon click coupling. (b) Photograph of the biphasic mixtures of water and toluene where **P1** remains in the organic phase (i), while **P2f** dissolves in the aqueous phase (ii). (c) Photograph of the same two mixtures under UV light irradiation (365 nm), showing that **P1** is not appreciably fluorescent, while **P2f** exhibits strong emission.

The PEG-grafted **P2f** was found to exhibit a significant solubility change relative to the parent polymer, **P1**. While **P1** is soluble in organic solvents, such as chloroform, dichloromethane, tetrahydrofuran, and toluene, **P2f** exhibits solubility in more polar organics (tetrahydrofuran, alcohols) and was even soluble in water. Figure 4.4(b) illustrates this difference, showing that **P1** remains in the organic phase of a biphasic mixture of toluene and water, while **P2f** prefers the aqueous phase. When irradiated with a hand-held UV lamp at 365 nm, only the graft copolymer exhibits fluorescence, with a λ_{em} at ~475 nm

(Figure 4.4(c); see Supporting Information, Figure 4.65, for the complete emission spectrum).

4.2.8. Crosslinking of P1 with bis-TCO carbamate derivative (8)

In addition to the grafting of poly(ethylene glycol) onto the backbone of **P1**, it is also possible to carry out a crosslinking reaction. Reaction of the nitrophenyl carbonate **6** with 1,4-diaminobutane resulted in the difunctional crosslinker **8** (Figure 4.5), which could be subsequently used to carry out IEDDA chemistry to crosslink polymer **P1**. The crosslinking chemistry occurs rapidly over the course of several minutes, liberating a crosslinked network polymer (see Supporting Information, Video 2, for a video of the process). The N_2 gas evolved from this reaction acts as a blowing agent, resulting in an intractable red foam as the product. The foam was treated with DDQ to oxidize any dihydropyridazines and isolate the crosslinked **P4** (Figure 5). The spongy red solid was found to exhibit fluorescence when irradiated with a hand-held UV lamp at 365 nm.

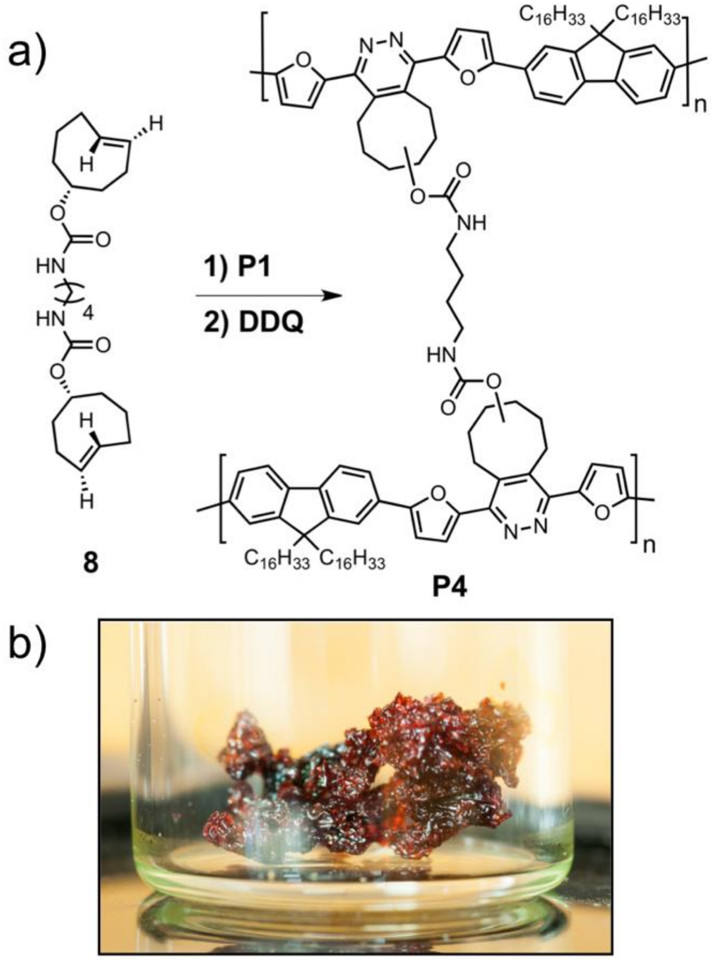

Figure 4.5. (a) Use of the bis-TCO crosslinker **8** to crosslink **P1** and produce the network polymer **P4**. (b) Photograph of the crosslinked foam.

4.3. Conclusions

We have demonstrated the synthesis of a high molecular weight conjugated polymer containing reactive *s*-tetrazine moieties within the backbone. Functionalization of the progenitor poly(tetrazine) **P1** was conducted via IEDDA using a series of TCO derivatives to generate a small library of dihydropyridazine polymers (**P2**, **P2a-e**) which were further oxidized to produce the corresponding conjugated poly(pyridazines) (**P3**, **P3a-e**). The product polymers, both before and after oxidation, exhibited substantial hypsochromic shifts in absorption, and increased emission intensity, relative to **P1**. Molecular modeling studies showed that, upon undergoing the "click" reaction, the pyridazine rings along the polymer backbone do not exhibit a significant change in conformation, remaining relatively planar. NMR analysis indicated that the "click" reaction did not alter the average degree of polymerization of the polymers. Additionally, IEDDA 'click' reactions on the backbone of **P1** occur at rates comparable to those of small molecule *s*-tetrazines with TCO. The high efficiency of the IEDDA reaction was demonstrated by grafting a 5 kDa poly(ethylene glycol)-TCO chain, a reaction that resulted in quantitative functionalization over 8 hours at 40 °C. Finally, the **P1** backbone can be rapidly crosslinked with a difunctional TCO resulting in the generation of a foam-like material.

4.4. Supporting Information

4.4.1. General Experimental

Unless otherwise specified, all reagents were purchased from commercial chemical suppliers and used without further purification. Small molecule amines were purchased from Sigma-Aldrich, while α-methoxy ω-amino PEG-5 kDa was purchased from Polymer Source, Inc. Unless otherwise mentioned all reactions were performed under an inert atmosphere. Flash chromatography was performed using an IntelliFlash 280 system from Analogix. Unless otherwise noted, compounds were monitored using a variable wavelength detector at 254 nm. Columns were prepared in Biotage® SNAP KP-Sil cartridges using 40 – 63 µm silica or 25 – 40 µm silica purchased from Silicycle. Dialysis was performed in distilled water using the Spectra/Por® Biotech CE Trial Kit membrane (MWCO: 50 kDa).

^{1}H-NMR and ^{13}C-NMR spectra were recorded on the Avance 600 MHz and Avance 700 MHz spectrometers. All chemical shifts are reported in ppm. High-resolution (HR) electrospray ionization (ESI) MS measurements were carried out on the Micromass Ultima Global instrument (quadrupole time-of-flight). MALDI spectra were collected on a Bruker UltraFlextreme spectrometer in positive ion mode using dithranol as matrix. Polymer molecular weights and polydispersity indices (Đ) were analyzed via gel permeation chromatography (GPC) using a Waters 2695 Separations Module, equipped with a Waters 2414 refractive-index detector, and a Jordi Fluorinated DVB mixed-bed column. Polystyrene standards were used for calibration, with THF as the eluent at a flow rate of 2.0 mL/min. UV-Vis spectra were measured on a Cary 5000 spectrophotometer, while fluorescence spectra were measured on a Jobin-Yvon SPEX Fluorolog 3.22 equipped with a 450 W Xe lamp, double-excitation and double-emission monochromators, and a digital photon-counting photomultiplier. Raman spectra were collected with a Renishaw InVia Laser Raman spectrometer equipped with a 300 mW Renishaw laser (785 nm, grating 1200 L/mm). Sample were prepared via spin-coating the polymer solutions onto a silicon wafer, which diminished the film thickness and background fluorescence. Laser intensities of 1-5% were used to collect data. Infrared spectra were recorded using a Thermo Scientific Nicolet 6700 FT-IR spectrometer equipped with a Smart iTX attenuated total reflectance (ATR) sample analyzer. Polymer solutions in dichloromethane were drop-casted onto the ATR crystal and allowed to dry before collecting the data. Thermogravimetric analysis was performed on a Mettler Toledo TGA-DSC 3+ System. All samples were heated at 10 °C/min between temperatures of 30 °C to 800 °C under argon.

4.4.2. Experimental Procedures

(*Z*)-Cyclooct-4-enol was synthesized according to a literature procedure.[33]

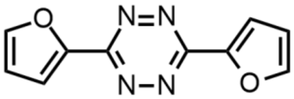

3,6-di(furan-2-yl)-1,2,4,5-tetrazine (1)[29]

Sulfur (594 mg, 8.90 mmol) and hydrazine hydrate (2.88 mL, 59.3 mmol) were sequentially added to a stirring solution of 2-furonitrile (1.38 g, 14.8 mmol) in anhydrous ethanol (10 mL) in a 25 mL round bottom flask. The reaction was heated to reflux and stirred for 3 h before cooling to rt and filtering the precipitate. The filtered yellow-orange solid was rinsed with cold ethanol (30 mL), then redissolved in ethanol:chloroform (5:10 mL). Isoamyl nitrite (10 mL) was added to the solution and the reaction mixture was refluxed overnight before evaporating under a flow of N_2. Silica gel column chromatography (1:1 $CHCl_3$:Hx to $CHCl_3$) yielded **1** (803 mg, 50%) as a bright red, crystalline solid. M.W.: 214.18 g/mol; ^{1}H-NMR (600 MHz; $CDCl_3$): δ 7.81 (d, *J* = 1.0 Hz, 1H), 7.67 (d, *J* = 3.5 Hz, 1H), 6.72 (dd, *J* = 3.5, 1.7 Hz, 1H).

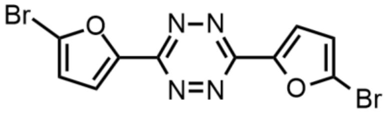

3,6-bis(5-bromofuran-2-yl)-1,2,4,5-tetrazine (2)[29]

A mixture of compound **1** (2.8 mmol, 600 mg), *N*-bromosuccinimide (5.88 mmol, 1.05 g), and silica gel (150 mg) in dichloromethane (12 mL) was stirred at room temperature for 16 h and then at reflux for another 6 h. The reaction mixture was then cooled to 0 °C and filtered. The solid was rinsed with isopropanol (15 mL), dried and recrystallized from toluene (80 mL) to yield **2** (643 mg, 62%) as a deep red, crystalline solid. M.W.: 371.97 g/mol; ^{1}H-NMR (600 MHz; $CDCl_3$): δ 7.61 (d, *J* = 3.6 Hz, 2H), 6.66 (d, *J* = 3.6 Hz, 2H).

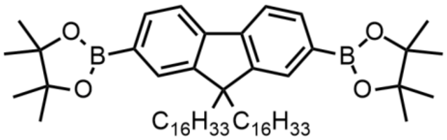

2,2'-(9,9-dihexadecyl-9H-fluorene-2,7-diyl)bis(4,4,5,5-tetramethyl-1,3,2-dioxaborolane) (3)

Synthesized according to a literature procedure.[30] M.W.: 866.99 g/mol; ^{1}H-NMR (600 MHz; $CDCl_3$): δ 7.80 (d, *J* = 7.5 Hz, 2H), 7.74 (s, 2H), 7.71 (d, *J* = 7.5 Hz, 2H), 1.99 (dt, *J* = 7.9, 4.1 Hz, 4H), 1.29-1.10 (m, 40H), 1.05-0.99 (m, 12H), 0.87 (t, *J* = 7.0 Hz, 6H), 0.60-0.49 (m, 4H).

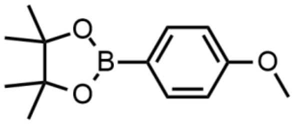

2-(4-methoxyphenyl)-4,4,5,5-tetramethyl-1,3,2-dioxaborolane (4)[34]

A mixture of 4-bromoanisole (1.00g, 5.35 mmol), bis(pinacolato)boron (1.49 g, 5.88 mmol), and potassium acetate (787 mg, 8.02 mmol) in DMSO (10 mL) was degassed in a 20 mL schlenk tube via freeze-pump-thaw. After the addition of [1,1'-Bis(diphenylphosphino)ferrocene] dichloropalladium(II) (130 mg, 0.160 mmol) the reaction mixture was stirred for at 70 °C 6 h under nitrogen. The resultant mixture was cooled to room temperature, then partitioned between water (40 mL) and diethyl ether (40 mL). The organic phase was washed with water (2 x 20 mL), dried with magnesium sulfate, filtered, and concentrated. Column chromatography (1:4 EtOAc:Hx) yielded **4** (1.02 g, 81%) as a clear oil. M.W.: 234.10 g/mol; ^{1}H-NMR (600 MHz; $CDCl_3$): δ 7.75 (d, *J* = 8.6 Hz, 2H), 6.89 (d, *J* = 8.6 Hz, 2H), 3.83 (s, 3H), 1.33 (s, 12H).

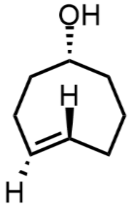

***rel*-(1*R*, 4*E*, p*R*)-Cyclooct-4-enol (5)**[31]

(*Z*)-Cyclooct-4-enol (2.00 g, 15.85 mmol) and methyl benzoate (2.158 g, 15.85 mmol) were dissolved in 9:1 ether:hexanes (200 mL) in a 500 mL quartz flask. The flask was placed in a photoreactor and connected to a fluid metering pump and a 25 g Biotage® cartridge via PTFE tubing. The bottom of column was packed with silica gel (13 g) while the top was filled with $AgNO_3$-impregnated silica gel. After flushing the column with 9:1 Et_2O:Hx (200 mL), the pump, followed by the UV lamp were turned on. After carrying out the photoisomerization for 16 h, the column was flushed with additional 9:1 Et_2O:Hx (200 mL), then dried by a flow of N_2. The contents of the column were emptied into an Erlenmeyer flask (500 mL) then partitioned with dichloromethane (200 mL) and ammonium hydroxide (200 mL). The mixture was vigorously stirred for 30 min, filtered, then the filtrate was transferred into a separatory funnel. The mixture was separated and the ammonium hydroxide layer was further washed dichloromethane (2 x 100 mL). The organic layers were combined, washed with water (100 mL), dried with magnesium sulfate, filtered, and concentrated. The two diastereomers of (*E*)-Cyclooct-4-enol were separated via column chromatography (R_fs = 0.2 (major) and 0.4 (minor) in 1:4 EtOAc:Hx) run with 5 CVs at 1:9 EtOAc:Hx, then a 10 CV ramp from 1:9 to 1:3 EtOAc:Hx, followed by 5 CVs at 1:3 EtOAc:Hx. Separation yielded **5** (665 mg, 33%) as a colorless oil. M.W.: 126.20 g/mol; ^{1}H-NMR (700 MHz; $CDCl_3$): δ 5.57 (m, 1H), 5.38 (m, 1H), 3.46 (td, *J* = 6.1, 2.9 Hz, 1H), 2.38-2.25 (m, 3H), 1.98-1.90 (m, 4H), 1.70-1.56 (m, 3H), 1.30 (s, 1H).

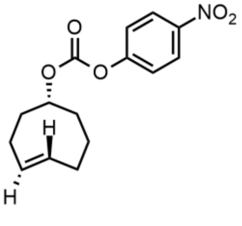

(1*R*, 4*E*)-cyclooct-4-en-1-yl (4-nitrophenyl) carbonate (6)[35]

A solution of 4-nitrophenyl chloroformate (264 mg, 1.31 mmol) in dichloromethane (4 mL) was added to a solution of compound **5** (150 mg, 1.19 mmol) and pyridine (250 µL, 2.97 mmol) in dichloromethane (20 mL) via syringe at room temperature. Another 0.2 eq of 4-nitrophenyl chloroformate was added to the reaction mixture at 60 min and the reaction was stirred at room temperature for another 20 h. The reaction mixture was worked up by adding ammonium hydroxide (20 mL) to the schlenk tube, turning the biphasic mixture yellow. The mixture was transferred to a separatory funnel and the organic phase washed water (20 mL), followed by brine (20 mL). The organic phase was dried with magnesium sulfate, filtered, and concentrated. Silica gel column chromatography (1:19 to 1:9 EtOAc:Hx) yielded **6** (255 mg, 74%) as a white solid. M.W.: 291.30 g/mol; ^{1}H-NMR (600 MHz; $CDCl_3$): δ 8.27 (d, *J* = 9.0 Hz, 2H), 7.36 (d, *J* = 9.0 Hz, 2H), 5.66-5.59 (m, 1H), 5.54-5.48 (m, 1H), 4.46-4.41 (m, 1H), 2.45-2.37 (m, 3H), 2.20-2.11 (m, 2H), 2.05-1.95 (m, 2H), 1.91-1.85 (m, 1H), 1.79-1.70 (m, 2H).

General Procedure for Substitution of Compound 6 with Aliphatic Amines (7a-7e)[35]

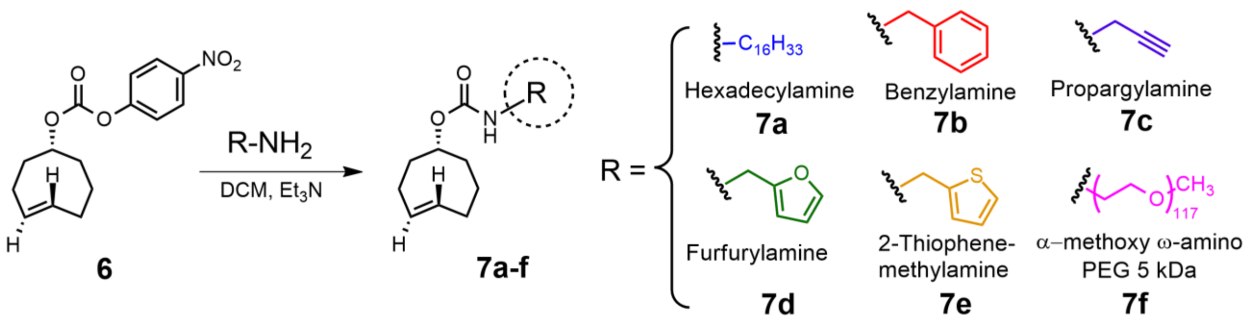

A solution of compound **6** (50 mg, 0.172 mmol) in dichloromethane (0.2 mL) was added to a solution of the respective amine (0.257 mmol) and triethylamine (71.8 µL, 0.515 mmol) in dichloromethane (0.2 mL) via syringe into a 2 mL microwave vial. The reaction mixture was covered in aluminum foil and stirred at rt for 12 h before evaporating under a flow of N_2. The residue was purified via silica gel column chromatography. All substituted products were stored at -18 °C until ready for use.

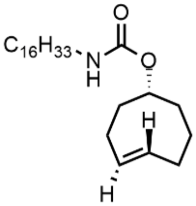

(1*R*, 4*E*)-cyclooct-4-en-1-yl hexadecylcarbamate (7a)

Purification via column chromatography (1:5 to 2:3 Et_2O:Hx) yielded **7a** (61 mg, 90%) as a white, crystalline solid. M.W.: 393.65 g/mol; ^{1}H-NMR (600 MHz; $CDCl_3$): δ 5.63 (m, *J* = 12.4, 6.1 Hz, 2H), 4.52 (s, 1H), 4.34 (s, 1H), 3.13 (t, *J* = 6.7 Hz, 2H), 2.38-2.32 (m, 3H), 2.01 (d, *J* = 12.3 Hz, 1H), 1.95-1.90 (m, 3H), 1.71-1.66 (m, 2H), 1.56-1.53 (m, 1H), 1.46 (s, 2H), 1.31-1.25 (m, 27H), 0.88 (t, *J* = 7.0 Hz, 3H); ^{13}C-NMR (151 MHz; $CDCl_3$): δ 156.3, 134.9, 133.0, 80.3, 41.2, 41.0, 38.7, 34.3, 32.6, 31.9, 31.0, 30.1, 29.70, 29.59, 29.38, 29.30, 26.8, 22.7, 14.1; HRMS (ESI+) (m/z) for $C_{25}H_{47}NO_2$ $[M+H]^+$ calculated: 394.3680, found: 394.3674.

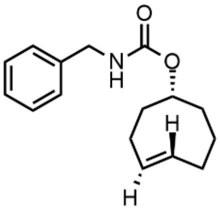

(1*R*, 4*E*)-cyclooct-4-en-1-yl benzylcarbamate (7b)

Purification via column chromatography (1:5 to 1:1 Et_2O:Hx) yielded **7b** (39 mg, 88%) as a white, crystalline solid. M.W.: 259.34 g/mol; ^{1}H-NMR (700 MHz; $CDCl_3$): δ 7.33 (t, *J* = 7.5 Hz, 2H), 7.28-7.26 (m, 3H), 5.60-5.49 (m, 2H), 4.87 (s, 1H), 4.45-4.28 (m, *J* = 5.3 Hz, 3H), 2.39-2.33 (m, 3H), 2.03 (d, *J* = 12.5 Hz, 1H), 1.96-1.91 (m, 3H), 1.78-1.73 (m, 2H), 1.56-1.53 (m, 1H); ^{13}C-NMR (176 MHz; $CDCl_3$): δ 156.4, 138.8, 135.1, 133.1, 128.8, 127.64, 127.56, 80.9, 45.2, 41.3, 38.8, 34.4, 32.7, 31.1; HRMS (ESI+) (m/z) for $C_{16}H_{21}NO_2$ $[M+Na]^+$ calculated: 282.1465, found: 282.1464.

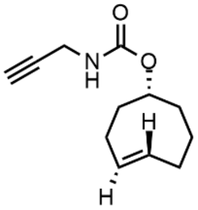

(1*R*, 4*E*)-cyclooct-4-en-1-yl prop-2-yn-1-ylcarbamate (7c)

Purification via column chromatography (1:5 to 2:3 Et_2O:Hx) yielded **7c** (31 mg, 88%) as a white, waxy solid. M.W.: 207.27 g/mol; ^{1}H-NMR (600 MHz; $CDCl_3$): δ 5.59-5.47 (m, 2H), 4.74 (s, 1H), 4.40-4.33 (m, 1H), 3.95 (s, 2H), 2.38-2.32 (m, 3H), 2.22 (s, 1H), 2.02 (d, *J* = 11.5 Hz, 1H), 1.96-1.90 (m, 3H), 1.78-1.71 (m, 2H), 1.60-1.51 (m, 1H); ^{13}C-NMR (176 MHz; $CDCl_3$): δ 155.8, 135.0, 133.1, 81.3, 80.0, 71.5, 41.2, 38.8, 34.4, 32.6, 31.1, 30.8; HRMS (ESI+) (m/z) for $C_{12}H_{17}NO_2$ $[M+Na]^+$ calculated: 230.1151, found: 230.1154.

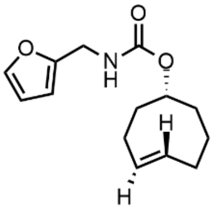

(1*R*, 4*E*)-cyclooct-4-en-1-yl (furan-2-ylmethyl)carbamate (7d)

Purification via column chromatography (1:5 to 2:3 Et_2O:Hx) yielded **7d** (36 mg, 84%) as a colorless oil. M.W.: 249.31 g/mol; ^{1}H-NMR (600 MHz; $CDCl_3$): δ 7.34 (s, 1H), 6.30 (d, *J* = 1.8 Hz, 1H), 6.20 (s, 1H), 5.59-5.47 (m, 2H), 4.89 (s, 1H), 4.40-4.22 (m, 3H), 2.38-2.32 (m, 3H), 2.02 (d, *J* = 12.1 Hz, 1H), 1.97-1.88 (m, 3H), 1.80-1.69 (m, 2H), 1.59-1.50 (m, 1H); ^{13}C-NMR (176 MHz; $CDCl_3$): δ 156.1, 151.9, 142.3, 135.1, 133.1, 110.5, 107.2, 81.0, 41.3, 38.8, 38.1, 34.4, 32.7, 31.1; HRMS (ESI+) (m/z) for $C_{14}H_{19}NO_3$ $[M+H]^+$ calculated: 250.1438, found: 250.1435.

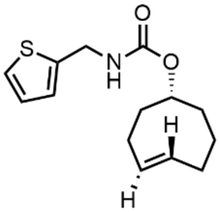

(1*R*, 4*E*)-cyclooct-4-en-1-yl (thiophen-2-ylmethyl)carbamate (7e)

Purification via column chromatography (1:5 to 1:1 Et_2O:Hx) yielded **7e** (41 mg, 90%) as a white solid. M.W.: 265.37 g/mol; ^{1}H-NMR (700 MHz; $CDCl_3$): δ 7.26-7.21 (m, 2H), 6.93 (dd, *J* = 10.8, 7.5 Hz, 2H), 5.62-5.49 (m, 2H), 4.90 (s, 1H), 4.53-4.44 (m, 2H), 4.44-4.39 (m, 1H), 2.39-2.32 (m, 3H), 2.03 (d, *J* = 9.5 Hz, 1H), 2.00-1.91 (m, 3H), 1.80-1.73 (m, 2H), 1.54 (s, 1H); ^{13}C-NMR (151 MHz; $CDCl_3$): δ 156.0, 141.7, 135.1, 133.1, 127.0, 125.8, 125.2, 81.1, 41.3, 39.9, 38.8, 34.4, 32.6, 31.1; HRMS (ESI+) (m/z) for $C_{14}H_{19}NO_2S$ $[M+Na]^+$ calculated: 288.1029, found: 288.1032.

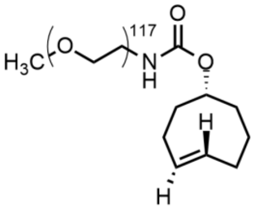

(1*R*, 4*E*)-cyclooct-4-en-1-yl poly(ethylene glycol)-5 kDa-carbamate (7f)

A solution of compound **6** (26.2 mg, 90 µmol) in dichloromethane (0.2 mL) was added to a solution of α-methoxy ω-amino poly(ethylene glycol) - 5kDa (250 mg, 50 µmol) and triethylamine (63 µL, 0.454 mmol) in dichloromethane (0.5 mL) via syringe into a 2 mL microwave vial. The reaction mixture was covered in aluminum foil and stirred at rt for 24 h before evaporating under a flow of N_2. The residue was redissolved in dichloromethane (0.6 mL) and precipitated into cold methanol (40 mL). Filtration of the precipitate yielded **7f** (204 mg, 74%) as a white, amorphous solid. M.W.: 5000 g/mol ;^{1}H-NMR (600 MHz; $CDCl_3$): δ 5.58-5.46 (m, 2H), 5.13 (s, 1H), 4.37-4.28 (m, 1H), 3.63 (s, 1H), 3.37 (s, 3H), 3.33 (d, *J* = 4.6 Hz, 2H), 2.37-2.30 (m, 3H), 1.99 (s, 6H), 1.95-1.86 (m, 3H), 1.78-1.67 (m, 2H), 1.57-1.48 (m, 1H). See MALDI-TOFs (Figures S3-S5).

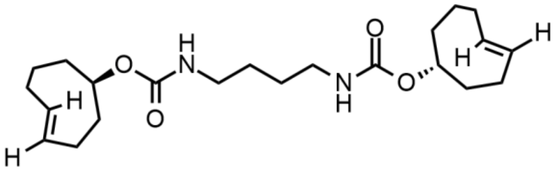

bis((1*R*, 4*E*)-cyclooct-4-en-1-yl) butane-1,4-diyldicarbamate (8)

A solution of compound **6** (40 mg, 0.137 mmol) in dichloromethane (0.2 mL) was added to a solution of 1,4-diaminobutane (6.6 µL, 66 µmol) and triethylamine (39 µL, 0.275 mmol) in dichloromethane (0.2 mL) via syringe into a 2 mL microwave vial. The reaction mixture was covered in aluminum foil and stirred at rt for 12 h before evaporating under a flow of N_2. Purification of the residue via column chromatography (1:2 to 2:1 Et_2O:Hx) yielded **8** (22 mg, 86%) as a white, amorphous solid. M.W.: 392.53 g/mol; ^{1}H-NMR (700 MHz; $CDCl_3$): δ 5.59-5.48 (m, 4H), 4.59 (s, 2H), 4.32 (s, 2H), 3.15 (s, 4H), 2.37-2.32 (m, 6H), 2.00 (d, *J* = 11.8 Hz, 2H), 1.95-1.90 (m, 6H), 1.78-1.69 (m, 4H), 1.55-1.49 (m, 6H); ^{13}C-NMR (176 MHz; $CDCl_3$): δ 156.4, 135.1, 133.1, 80.6, 41.3, 40.7, 38.8, 34.4, 32.7, 31.1, 27.5; HRMS (ESI+) (m/z) for $C_{22}H_{36}N_2O_4$ $[M+Na]^+$ calculated: 415.2567, found: 415.2562.

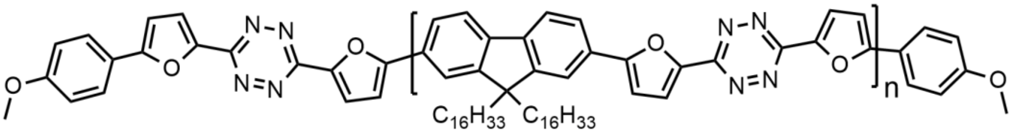

Synthesis of s-tetrazine-containing polymer - Poly[(9,9-dihexadecyl-9H-fluorenene)-*alt*-(3,6-bis(furan-2-yl)-*s*-tetrazine)] (P1)

A mixture of compound **2** (400 mg, 1.08 mmol) and compound **3** (876 mg, 1.01 mmol) in tetrahydrofuran (10 mL) and 3M potassium phosphate (10 mL) was degassed in a 100 mL schlenk tube via freeze-pump-thaw (three cycles). Palladium was then added to the frozen mixture under N_2. The resulting mixture was warmed to 50 °C and stirred for 15 min before adding a degassed solution of compound **4** (50.3 mg, 0.215 mmol) in tetrahydrofuran (1 mL) via syringe. The reaction mixture was stirred for another 30 min, then cooled to room temperature, filtered through neutral alumina, and precipitated into 1:1 EtOH:THF (100 mL). The precipitate was filtered, yielding **P1** (480 mg, 74%) as a deep red amorphous solid. M_n:36.3 kDa (NMR), M_n:38.8 kDa (GPC), M_w:63.7 kDa (GPC); ^{1}H-NMR (600 MHz; $CDCl_3$): δ 8.03-7.67 (m, 8H), 7.04 (s, 2H), 3.87 (s,), 2.15 (s, 4H), 1.25-1.08 (m, 54H), 0.84 (t, *J* = 4.9 Hz, 6H), 0.69 (s, 4H).

General Procedures for IEDDA Reactions on P1

P2:

An excess (1.5 eqv. per polymer repeat unit) of a solution of compound **5** (6.9 mg, 54.5 µmol) in tetrahydrofuran (0.5 mL) was added to a solution of **P1** (30 mg, 36.3 µmol - repeat unit basis) in tetrahydrofuran (0.5 mL) in a microwave vial. Upon mixing, the resultant effervescent mixture was stirred at rt for 30 min. The highly viscous reaction mixture was diluted with tetrahydrofuran (1 mL) before precipitating into cold ethanol (20 mL). Filtration followed by drying of the precipitate under reduced pressure yielded **P2 (**28 mg, 82%) as an orange solid.

P2a to P2e:

A slight excess (1.5 eqv. per polymer repeat unit) of a solution of the respective carbamate (54.5 µmol) in tetrahydrofuran (0.5 mL) was added to a solution of **P1** (30 mg, 36.3 µmol - repeat unit basis) in tetrahydrofuran (0.5 mL) in a microwave vial. The resultant effervescent mixture was stirred at rt for 30 min before precipitating into cold ethanol (15 mL). Filtration followed by drying of the precipitate under reduced pressure yielded dihydropyridazine polymers **P2(a-e)**. The polymers were characterized by ^{1}H-NMR, GPC, UV-Vis, IR, and Raman spectroscopy.

Polymer Graft P2f:

A slight excess (1.2 eqv. per polymer repeat unit) of a solution of compound **7f** (116 mg, 21.8 µmol) in tetrahydrofuran (1 mL) was added to a solution of **P1** (15 mg, 18.1 µmol - repeat unit basis) in tetrahydrofuran (0.2 mL) in a microwave vial. The resultant effervescent mixture was stirred at 40 °C for 8 h before evaporating under a flow of N_2.

The residue was redissolved in distilled water (5 mL) and dialysed for 72 h to ensure full removal of excess carbamate. Lyophilization of the dialysed solution yielded **P2f (**92 mg, 84%) as a bright yellow solid.

General Procedures for Oxidation of Polydihydropyridazines P2x:

2,3-dichloro-5,6-dicyano-1,4-benzoquinone (8.1 mg, 35.8 µmol) was added to a solution of the respective polydihydropyridazine **P2x** (24.0 µmol - repeat unit basis) in tetrahydrofuran (0.5 mL) in a small screw-cap vial. The reaction mixture was stirred at rt for 60 minutes before precipitating in cold ethanol (10 mL). Filtration onto paper followed by drying of the precipitate under reduced pressure yielded pyridazine polymers **P3, P3(a-e)**. The polymers were characterized by ^{1}H-NMR, GPC, UV-Vis, IR, and Raman spectroscopy.

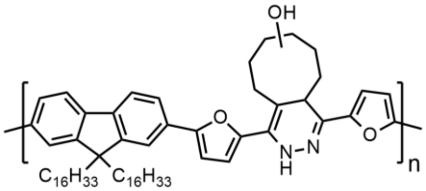

Poly[(9,9-dihexadecyl-9H-fluorenene)-*alt*-(3,6-bis(furan-2-yl)-cycloocta-1,4-dihydropyridazin-8-ol)] (P2)

Yield: 82%. Orange solid. M_n:36.0 kDa (NMR), M_n:12.2 kDa (GPC), M_w:15.0 kDa (GPC); ^{1}H-NMR (700 MHz; $CDCl_3$): δ 8.12-8.05 (m, 1H), 7.78-7.52 (m, 6H), 6.95-6.61 (m, 4H), 5.41-5.16 (m,), 4.20 (s, 1H), 3.85 (s,), 3.68 (s, 1H), 3.42-3.02 (m, 1H), 2.23 (s, 1H), 2.09 (s, 6H), 1.86 (s, 4H), 1.29-1.01 (m, 62H), 0.88-0.81 (m, 16H), 0.65 (s, 4H).

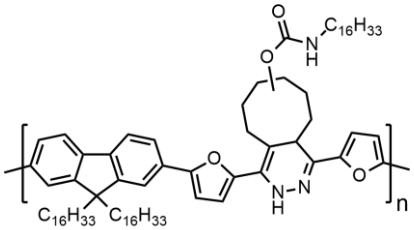

Poly[(9,9-dihexadecyl-9H-fluorenene)-*alt*-(3,6-bis(furan-2-yl)-1,4-dihydropyridazine)]-*graft*-hexadecyl carbamate (P2a)

M_n:53.3 kDa (NMR), M_n:46.8 kDa (GPC), M_w:67.8 kDa (GPC); ^{1}H-NMR (700 MHz; $CDCl_3$): δ 8.09 (s, 1H), 7.79-7.66 (m, 6H), 6.98-6.65 (m, 4H), 5.08 (s, 1H), 4.62 (s, 1H), 3.85 (s,), 3.65 (s, 1H), 3.30-3.00 (m, 3H), 2.27 (s, 1H), 2.09 (s, 6H), 1.95-1.71 (m, 4H), 1.50 (s, 3H), 1.25-1.08 (m, 86H), 0.86 (dt, *J* = 15.3, 7.3 Hz, 12H), 0.64 (s, 4H).

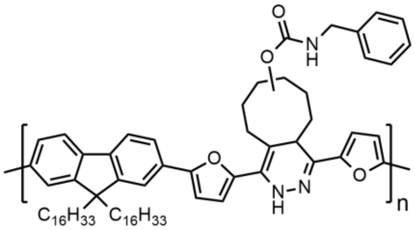

Poly[(9,9-dihexadecyl-9H-fluorenene)-*alt*-(3,6-bis(furan-2-yl)-1,4-dihydropyridazine)]-*graft*-benzyl carbamate (P2b)

M_n:45.9 kDa (NMR), M_n:40.9 kDa (GPC), M_w:71.8 kDa (GPC); ^{1}H-NMR (700 MHz; $CDCl_3$): δ 8.10 (s, 1H), 7.79-7.64 (m, 6H), 7.37-7.29 (m, 5H), 6.83-6.71 (m, 4H), 5.14 (s, 1H), 5.03-4.91 (m, 1H), 4.40 (s, 2H), 3.83 (s,), 3.73-3.60 (m, 1H), 3.24-3.06 (m, 1H), 2.30 (s, 1H), 2.22-2.02 (m, 6H), 1.96-1.72 (m, 4H), 1.64 (s, 1H), 1.30-0.98 (m, 54H), 0.85 (t, *J* = 6.8 Hz, 6H), 0.64 (s, 4H).

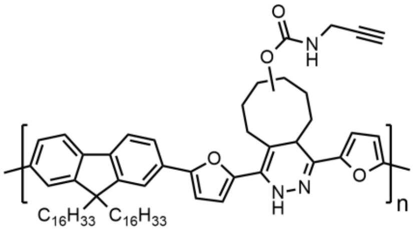

Poly[(9,9-dihexadecyl-9H-fluorenene)-*alt*-(3,6-bis(furan-2-yl)-1,4-dihydropyridazine)]-*graft*-propargyl carbamate (P2c)

M_n:45.0 kDa (NMR), M_n:39.3 kDa (GPC), M_w:82.5 kDa (GPC); ^{1}H-NMR (700 MHz; $CDCl_3$): δ 8.10 (s, 1H), 7.79-7.66 (m, 6H), 7.00-6.78 (m, 3H), 6.71 (s, 1H), 5.13 (s, 1H), 4.86-4.82 (m, 1H), 4.02 (s, 2H), 3.86-3.85 (m,), 3.65 (s, 1H), 3.28-3.00 (m, 1H), 2.27 (s, 1H), 2.10 (s, 6H), 1.98-1.75 (m, 4H), 1.31-0.98 (m, 56H), 0.85 (t, *J* = 6.6 Hz, 6H), 0.65 (s, 4H).

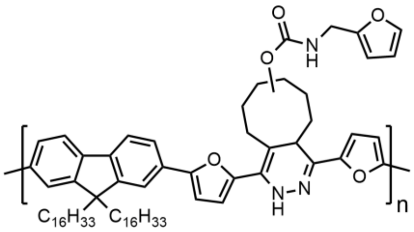

Poly[(9,9-dihexadecyl-9H-fluorenene)-*alt*-(3,6-bis(furan-2-yl)-1,4-dihydropyridazine)]-*graft*-furyl carbamate (P2d)

M_n:46.5 kDa (NMR), M_n:38.4 kDa (GPC), M_w:79.6 kDa (GPC); ^{1}H-NMR (700 MHz; $CDCl_3$): δ 8.12 (s, 1H), 7.80-7.53 (m, 6H), 7.37 (s, 1H), 6.98-6.60 (m, 4H), 6.35-6.27 (m, 1H), 6.25-6.23 (m, 1H), 5.13-4.95 (m, 2H), 4.39 (s, 2H), 3.87-3.84 (m,), 3.64 (s, 1H), 3.26-3.06 (m, 1H), 2.29 (s, 1H), 2.09 (s, 6H), 1.96-1.72 (m, 4H), 1.25-1.07 (m, 58H), 0.84 (t, *J* = 6.3 Hz, 6H), 0.64 (s, 4H).

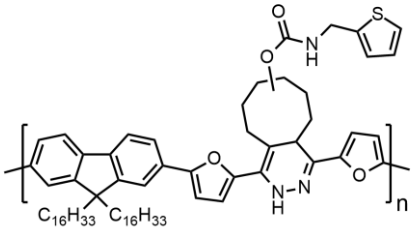

Poly[(9,9-dihexadecyl-9H-fluorenene)-*alt*-(3,6-bis(furan-2-yl)-1,4-dihydropyridazine)]-*graft*-thiophenyl carbamate (P2e)

M_n:47.2 kDa (NMR), M_n:33.5 kDa (GPC), M_w:53.4 kDa (GPC); ^{1}H-NMR (700 MHz; $CDCl_3$): δ 8.09 (s, 1H), 7.83-7.63 (m, 6H), 7.24 (s, 1H), 7.00-6.93 (m, 2H), 6.90-6.70 (m, 3H), 5.40-4.98 (m, 2H), 4.56 (s, 2H), 3.84 (d, *J* = 14.4 Hz,), 3.75-3.66 (m, 1H), 3.35-3.05 (m, 1H), 2.48-2.22 (m, 2H), 2.20-2.01 (m, 6H), 1.96-1.72 (m, 3H), 1.64 (s, 1H), 1.26-1.07 (m, 54H), 0.85 (t, *J* = 6.1 Hz, 6H), 0.64 (s, 4H).

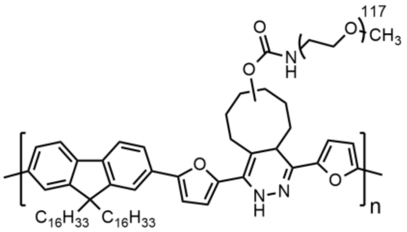

Poly[(9,9-dihexadecyl-9H-fluorenene)-*alt*-(3,6-bis(furan-2-yl)-1,4-dihydropyridazine)]-*graft*-poly(ethylene glycol) methyl ether (P2f)

M_n:256.4 kDa (theoretical), acquisition of this data by NMR and GPC was not possible due to signal overalap in NMR and interactions with column stationary phase in GPC; ^{1}H-NMR (700 MHz; $CDCl_3$): δ 8.09-7.61 (m, 5H), 6.97-6.81 (m, 1H), 5.21-4.65 (m,), 3.74-3.54 (m, 1H), 3.38 (s, 4H), 2.03-1.80 (m, 18H), 1.25-1.06 (m, 66H), 0.85 (s, 9H), 0.57 (s, 4H).

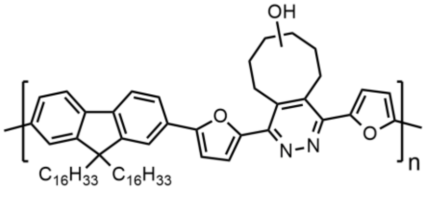

Poly[(9,9-dihexadecyl-9H-fluorenene)-*alt*-(3,6-bis(furan-2-yl)-cycloocta-pyridazin-8-ol)] P3

M_n:36.8 kDa (NMR), M_n:12.9 kDa (GPC), M_w:22.6 kDa (GPC); ^{1}H-NMR (700 MHz; $CDCl_3$): δ 8.13-7.52 (m, 7H), 6.96-6.59 (m, 3H), 4.72-4.55 (m, 1H), 4.35-4.00 (m, 1H), 3.85 (s,), 3.64-3.28 (m, 1H), 2.64-2.45 (m, 1H), 2.24-1.76 (m, 10H), 1.49 (s, 2H), 1.29-1.00 (m, 71H), 0.89-0.81 (m, 24H), 0.65 (s, 4H).

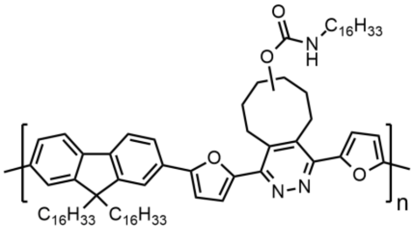

Poly[(9,9-dihexadecyl-9H-fluorenene)-*alt*-(3,6-bis(furan-2-yl)-pyridazine)]-*graft*-hexadecyl carbamate (P3a)

M_n:51.0 kDa (NMR), M_n:24.6 kDa (GPC), M_w:45.4 kDa (GPC); ^{1}H-NMR (700 MHz; $CDCl_3$): δ 7.77-7.68 (m, 6H), 7.53 (s, 2H), 6.97 (s, 2H), 5.38-4.89 (m, 1H), 4.76-4.46 (m, 1H), 3.87 (s,), 3.55-3.28 (m, 2H), 3.19 (s, 2H), 2.57 (s, 1H), 2.31 (s, 2H), 2.08 (s, 4H), 1.89 (s, 1H), 1.70-1.55 (m, 4H), 1.51 (s, 3H), 1.28-1.07 (m, 90H), 0.85 (t, *J* = 6.6 Hz, 12H), 0.71 (s, 4H).

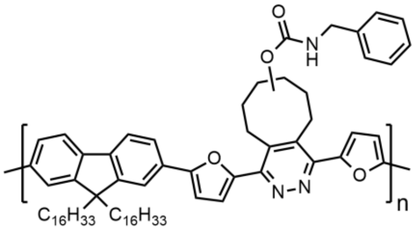

Poly[(9,9-dihexadecyl-9H-fluorenene)-*alt*-(3,6-bis(furan-2-yl)-pyridazine)]-*graft*-benzyl carbamate (P3b)

M_n:47.5 kDa (NMR), M_n:14.1 kDa (GPC), M_w:24.2 kDa (GPC); ^{1}H-NMR (700 MHz; $CDCl_3$): δ 7.76-7.52 (m, 8H), 7.30 (s, 5H), 6.97-6.87 (m, 2H), 5.38-4.92 (m, 2H), 4.39 (s, 2H), 3.86 (s,), 3.61-3.11 (m, 2H), 2.59-2.31 (m, 3H), 2.06-1.85 (m, 7H), 1.61 (m, 4H), 1.25-1.07 (m, 60H), 0.85-0.79 (m, 9H), 0.70 (s, 4H).

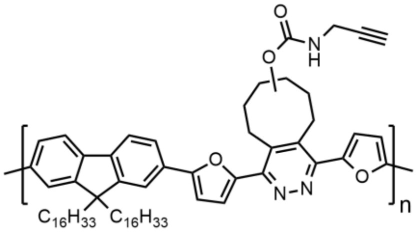

Poly[(9,9-dihexadecyl-9H-fluorenene)-*alt*-(3,6-bis(furan-2-yl)-pyridazine)]-*graft*-propargyl carbamate (P3c)

M_n:41.8 kDa (NMR), M_n:16.4 kDa (GPC), M_w:28.8 kDa (GPC); ^{1}H-NMR (700 MHz; $CDCl_3$): δ 7.77-7.53 (m, 6H), 7.21 (s, 1H), 6.96 (d, *J* = 15.9 Hz, 3H), 5.38-4.92 (m, 2H), 4.56 (s, 2H), 3.86 (s,), 3.58-3.22 (m, 2H), 2.60 (s, 1H), 2.34 (s, 2H), 2.07-1.58 (m, 8H), 1.25-1.07 (m, 48H), 0.84 (s, 6H), 0.70 (s, 4H).

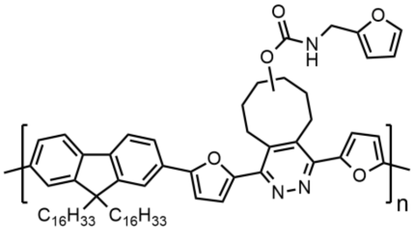

Poly[(9,9-dihexadecyl-9H-fluorenene)-*alt*-(3,6-bis(furan-2-yl)-pyridazine)]-*graft*-furyl carbamate (P3d)

M_n:45.9 kDa (NMR), M_n:25.5 kDa (GPC), M_w:45.4 kDa (GPC); ^{1}H-NMR (600 MHz; $CDCl_3$): δ 7.86-7.64 (m, 6H), 7.53 (s, 2H), 7.36 (s, 1H), 6.97 (s, 2H), 6.35-6.20 (m, 2H), 5.15-4.70 (m, 2H), 4.39 (s, 2H), 3.87 (s,), 3.55-3.24 (m, 2H), 2.59 (s, 1H), 2.34 (s, 2H), 2.07 (s, 4H), 1.96-1.60 (m, 4H), 1.25-1.07 (m, 57H), 0.84 (t, *J* = 6.3 Hz, 6H), 0.70 (s, 4H).

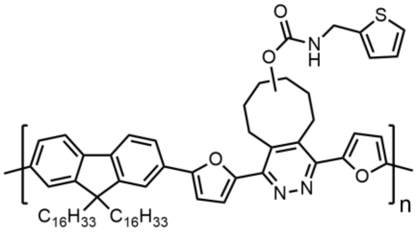

Poly[(9,9-dihexadecyl-9H-fluorenene)-*alt*-(3,6-bis(furan-2-yl)-pyridazine)]-*graft*-thiophenyl carbamate (P3e)

M_n:56.6 kDa (NMR), M_n:17.8 kDa (GPC), M_w:33.1 kDa (GPC); ^{1}H-NMR (700 MHz; $CDCl_3$): δ 7.77-7.53 (m, 8H), 7.21 (s, 1H), 6.97 (s, 4H), 5.38-4.99 (m, 2H), 4.56 (s, 2H), 3.86 (s,), 3.59-3.20 (m, 2H), 2.60 (s, 1H), 2.34 (s, 2H), 2.07 (s, 4H), 1.91-1.58 (m, 4H), 1.25-1.07 (m, 54H), 0.84 (t, *J* = 5.5 Hz, 8H), 0.70 (s, 4H).

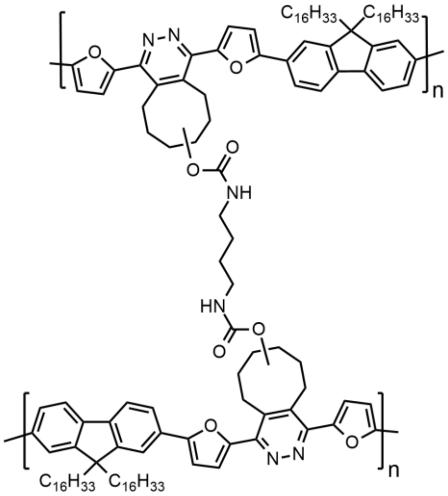

Crosslinked Network P4:

A solution of compound **8** (6.7 mg, 17.0 µmol) in tetrahydrofuran (0.1 mL) was added to a solution of **P1** (28 mg, 34.0 µmol - repeat unit basis) in tetrahydrofuran (0.2 mL) in a small screw-cap vial. The reaction mixture was briefly stirred via syringe needle and allowed to sit for 5 min. as N_2 evolution was observed. Drying of the resultant crosslinked foam under reduced pressure yielded **P4a** as a red solid. Oxidation of the dihydropyridazine network **P4a** was performed by stirring the network solid in a solution of 2,3-dichloro-5,6-dicyano-1,4-benzoquinone (10.6 mg, 46.8 µmol) in tetrahydrofuran (1 mL) at rt for 60 minutes. The reaction mixture was decanted and the solid rinsed 3 times with excess tetrahydrofuran to yield the pyridazine network **P4** as a red solid.

4.4.3. Kinetics Study

Kinetics measurements were performed using the Cary 5000 spectrophotometer equipped with a temperature-controlled multicell holder at 30 °C. The reaction kinetics were monitored using the Cary WinUV Kinetics software package. The IEDDA click reaction on the polymer was performed in a 1 mm path length quartz cuvette using an equimolar mixture of compound **5** and **P1** at a concentration of 0.242 mM for each reactant (repeat unit basis for **P1**). Measurements were performed in triplicate in dichloromethane.

The Kinetics software plotted the absorbance of the reaction mixture at 500 nm vs time. Due to the blue shift of the UV-Vis spectrum of the reaction mixture upon quantitative cycloaddition, absorbance measurements at 500 nm directly correlated with concentration of the two reactants at any given time. Second order rate constants *k*, calculated by the Cary WinUV Kinetics software, were found to be 1.17 $M^{-1}s^{-1}$, 1.30 $M^{-1}s^{-1}$, and 1.28 $M^{-1}s^{-1}$ for the three runs, respectively.

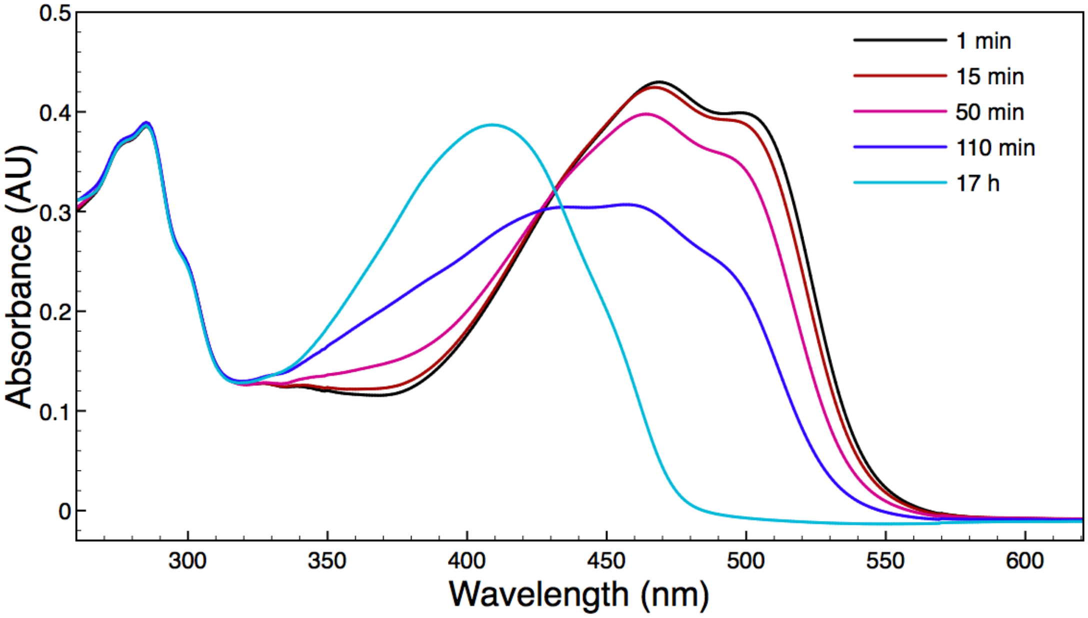

Figure 4.6. Monitoring reaction of **P1** (0.01 mg/mL) with 2 eq. (per repeat unit) of compound **5** (3.1 µg/mL) via UV-Vis.

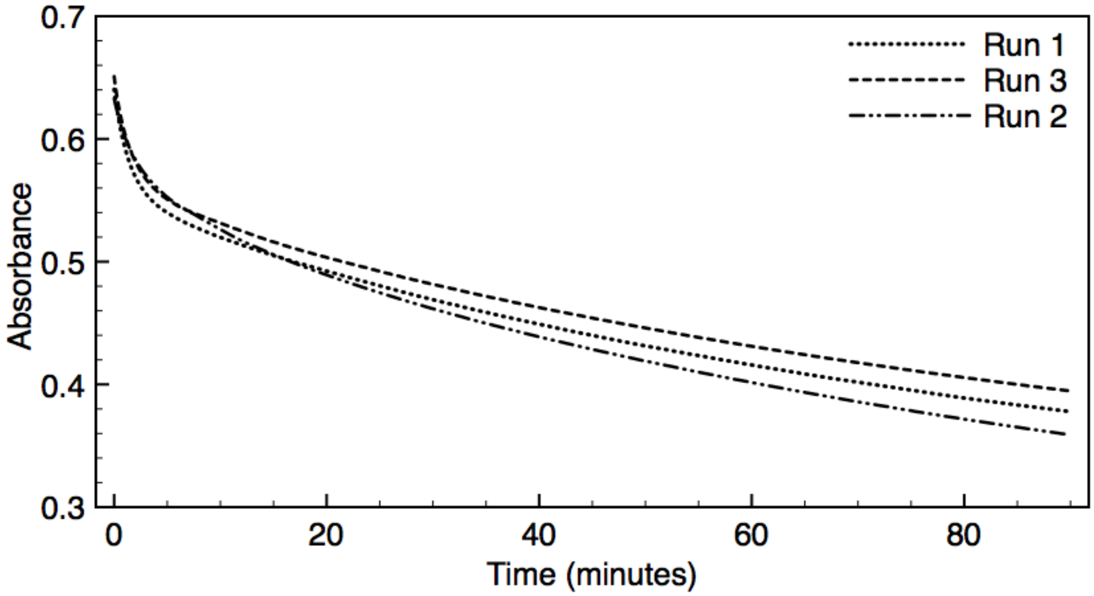

Figure 4.7. Overlay of three kinetics runs, monitoring reaction of equimolar **P1** and compound **5** (0.242 mM concentration) via UV-Vis. Reaction was monitored at 500 nm. Solvent is dichloromethane.

4.4.4. Computational Methods

All calculations were performed using Gamess[36] (1 May 2013 – R1, 64-bit Linux), run in Mac OSX 10.9 on a desktop computer equipped with an Intel i5-3570 processor. For oligomeric structures (3 repeat units) the semi-empirical Parameterized Model number 3[37] (PM3) was used for geometry optimization. In these calculations, alkyl chains were replaced with methyl groups to ease computational loads.

In order to observe finer details of any torsion and dihedral angles imparted onto the polymer backbone by the click and subsequent oxidation reactions, more intensive DFT geometry optimizations were performed on the individual repeat unit of **P1**, **P2**, and **P3**. These calculations utilized the M06-2X functional and an ample basis set of 6-311G+(d,p). This time, all alkyl chains were replaced with hydrogen atoms to ease computational loads.

Gamess File Headers:

Oligomers (PM3):

```
 $CONTRL SCFTYP=RHF RUNTYP=OPTIMIZE MAXIT=50 $END
 $BASIS GBASIS=PM3 $END
 $STATPT OPTTOL=0.0005 NSTEP=500 $END
 $SYSTEM mwords=100 $END
 $SCF DIRSCF=.TRUE. $END
```

Repeat Units (M06):

```
$CONTRL SCFTYP=RHF RUNTYP=OPTIMIZE DFTTYP=M06-2X MAXIT=100
$END
$BASIS GBASIS=N311 NGAUSS=6 NDFUNC=1 NPFUNC=1 DIFFSP=.TRUE. $END
$STATPT OPTTOL=0.0005 NSTEP=50 $END
$CONTRL NZVAR=1 $END
$ZMAT DLC=.TRUE. AUTO=.TRUE. $END
$SYSTEM mwords=150 $END
$SCF DIRSCF=.TRUE. $END
```

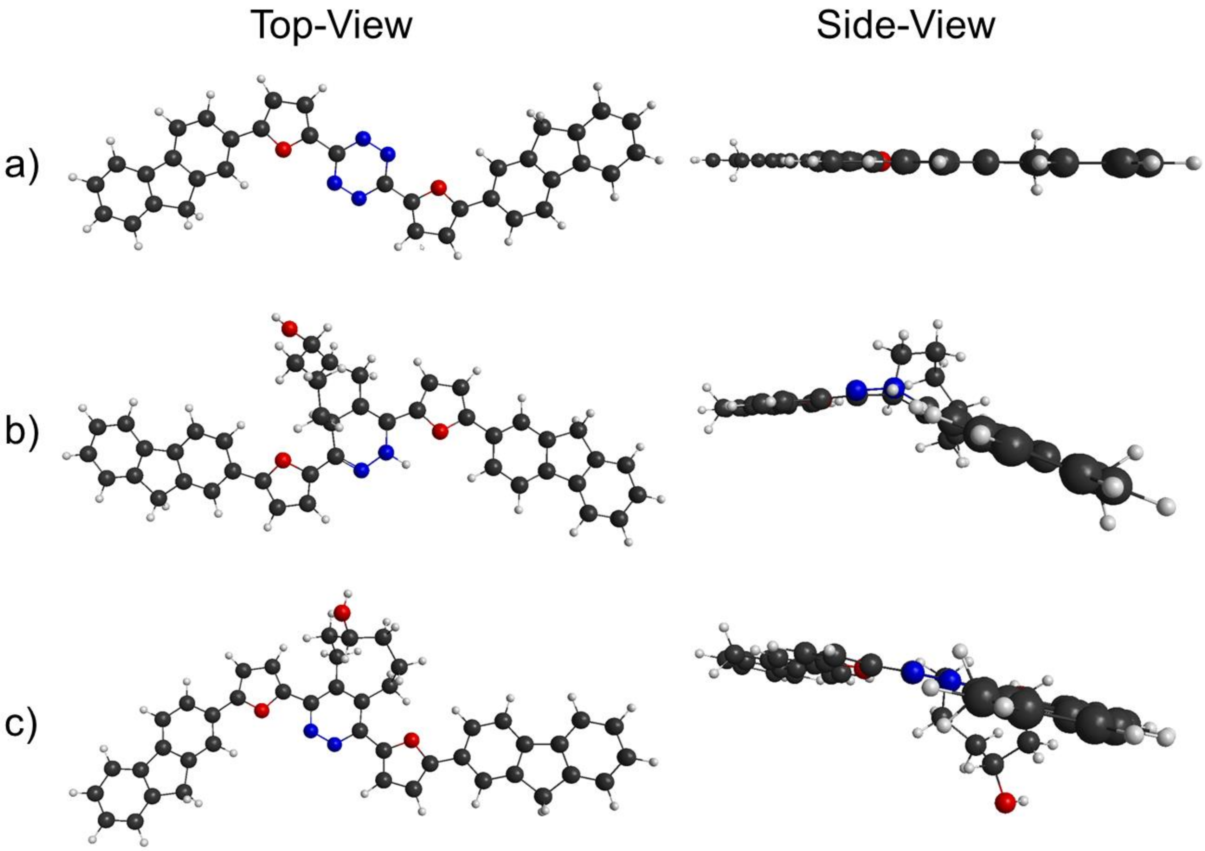

Figure 4.8. Optimized geometries (M06-2X) of **P1** (a), **P2** (b), and **P3** (c) repeat units. As observed in the side-views, P2 and P3 display pucker angles of 30º and 4° from linear, respectively, as the dihydropyridazine units re-aromatize to pyridazines.

Coordinates of PM3 stationary point calculations:

Oligomer – P1:

ATOM	*CHARGE*	*X*	*Y*	*Z*
C	6.0	2.0969533395	25.3425672008	-3.8994873702
C	6.0	4.2341389453	26.5381779360	-4.7952363856
C	6.0	6.1915171234	24.8547155398	-4.4790474334
C	6.0	5.1283194882	22.7267140023	-3.4062688874
O	8.0	2.6897981764	23.0724015772	-3.0837493531
C	6.0	6.4673793231	20.3995164484	-2.7106796486
N	7.0	8.9933193591	20.1694045149	-3.0980923733
N	7.0	10.1975283475	18.0503413813	-2.4655065989
C	6.0	8.9193365867	16.0867082102	-1.4232660249
N	7.0	6.3937178041	16.3173303697	-1.0352863824
N	7.0	5.1896788910	18.4362234280	-1.6676075951
C	6.0	10.2535776203	13.7544272934	-0.7366907791
C	6.0	9.1823864442	11.6258777354	0.3244092603
C	6.0	11.1277648623	9.9273542231	0.6309417128
C	6.0	13.2815233650	11.1224547322	-0.2633144191
O	8.0	12.6898690555	13.4023335474	-1.0635755804
H	1.0	10.9632075232	8.0482862899	1.4150646141
C	6.0	15.8773076735	10.0787212747	-0.3510732940
H	1.0	7.2184131224	11.3384504126	0.8162860377
H	1.0	0.2097973792	26.1274270953	-3.8616172614
H	1.0	4.3482217032	28.4194190540	-5.5867292183
H	1.0	8.1537707946	25.1494749994	-4.9734375463
C	6.0	16.4069789706	7.6072620389	0.5123236125
C	6.0	18.8860160076	6.7039730168	0.3833309166
C	6.0	20.8017635222	8.2002580539	-0.5708484264
C	6.0	20.3462828673	10.6446375162	-1.4353413740
C	6.0	17.8677938509	11.5802597500	-1.3220334038
C	6.0	19.8774985416	4.1469091938	1.1825716259
C	6.0	22.6450589424	4.4258705441	0.5318633792
C	6.0	23.1421702607	6.7827934877	-0.4766266886
C	6.0	24.5802706346	2.6534965402	0.8344274071
C	6.0	27.0638808085	3.3012190197	0.0950721144
C	6.0	27.5329107987	5.7276649825	-0.9305010764
C	6.0	25.5676335659	7.4838062401	-1.2221424880
C	6.0	19.5063941521	3.7199822986	4.0299162579
C	6.0	18.6470790537	2.0165266015	-0.3586699925
H	1.0	17.4621263731	3.6646889162	4.5049744739
H	1.0	20.4018597086	5.2692174579	5.1306627484
H	1.0	20.3726823394	1.9007997820	4.6197942249
H	1.0	16.5852746175	1.9263299801	0.0268719035
H	1.0	18.9241506780	2.3397642317	-2.4159390863
H	1.0	19.4954715359	0.1624408459	0.1416916546
H	1.0	17.5038137284	13.4784895047	-1.9940766568
H	1.0	21.8604069177	11.7996191427	-2.1800634885
H	1.0	14.9436129602	6.3982909410	1.2652660351
H	1.0	25.9356388048	9.3345471807	-2.0098369715
H	1.0	29.4211628001	6.2628353822	-1.5096831943
H	1.0	24.1403046302	0.8229756677	1.6252966303
C	6.0	62.9191070626	-11.8133952451	-1.8024962361
C	6.0	65.0977721538	-10.5963928118	-2.6015857673
C	6.0	67.0084174082	-12.3513813366	-2.4249152847
C	6.0	65.8931389248	-14.5340904414	-1.5327189541
O	8.0	63.4638583730	-14.1594522644	-1.1787921739
C	6.0	67.1796832745	-16.9415824525	-1.0419949096
N	7.0	65.8609379939	-18.9638349238	-0.1768216607
N	7.0	67.0212675449	-21.1554068435	0.2622183781
C	6.0	69.5423320879	-21.4011468110	-0.1475687024
N	7.0	70.8605860397	-19.3783652164	-1.0105309719
N	7.0	69.7003698722	-17.1879649268	-1.4507993326
C	6.0	70.8343755402	-23.8089600755	0.3248816918
C	6.0	69.7309456387	-26.0101507005	1.1865589477
C	6.0	71.6529103518	-27.7573157597	1.3390409376
C	6.0	73.8246590459	-26.5153500460	0.5596612485
O	8.0	73.2654702289	-24.1650033488	-0.0304056911
H	1.0	71.4626527393	-29.6975163285	1.9494413289
C	6.0	76.4089349232	-27.5753918389	0.3834065056
H	1.0	67.7621157211	-26.3129792900	1.6488426161

Oligomer – P2:

ATOM	*CHARGE*	*X*	*Y*	*Z*
C	6.0	-18.5974161431	-24.7614380039	18.5359323592
C	6.0	-17.2485534499	-24.4432478312	18.4320159866
C	6.0	-16.8384848705	-23.2246835310	17.8859297259
C	6.0	-17.8111395285	-22.3408074503	17.4505949559
C	6.0	-19.1841496180	-22.6621877198	17.5580671898
C	6.0	-19.5817803946	-23.8704164667	18.0987325974
C	6.0	-17.6913816535	-21.0139124753	16.8506430694
C	6.0	-18.9906133975	-20.5194670691	16.5908812907
C	6.0	-20.0432012278	-21.5298774363	17.0196757463
C	6.0	-16.5734482067	-20.2579004642	16.5425321431
C	6.0	-16.7532565357	-18.9934581073	15.9793434789
C	6.0	-18.0347986503	-18.4940077102	15.7282231764
C	6.0	-19.1691175841	-19.2714547599	16.0309145744
C	6.0	-20.8751385189	-21.9925141462	15.8312910903
C	6.0	-20.9371220245	-20.9588806285	18.1126604831
C	6.0	-18.2446535584	-17.1588934401	15.1902193935
C	6.0	-19.3993066351	-16.4177368779	15.0459788531
C	6.0	-19.0060270119	-15.1396202458	14.5341709039
C	6.0	-17.6326602554	-15.1632132569	14.3828760045
O	8.0	-17.1529489554	-16.4149933577	14.7719977112
C	6.0	-16.6467580890	-14.1665338373	13.9713102475
N	7.0	-15.2708164449	-14.4775444634	14.3217185508
N	7.0	-14.3063521902	-13.9770013937	13.4718470500
C	6.0	-14.4711035753	-12.7955852433	12.9234349450
C	6.0	-15.7334665937	-12.0031028296	13.2315200706
C	6.0	-16.9070778088	-12.9553523918	13.3847715522
C	6.0	-13.3447926538	-12.3951715288	12.0817192185
C	6.0	-12.2749270329	-13.1618700109	11.6522775181
C	6.0	-11.4511982972	-12.3106758446	10.8485680614
C	6.0	-12.0621722873	-11.0720187547	10.8279756890
O	8.0	-13.2148961388	-11.1006501087	11.6001220471
C	6.0	-15.9239103828	-10.7780371252	12.3479071153
C	6.0	-16.2079397201	-11.0670916188	10.8810078308
C	6.0	-17.5465072695	-10.5128556269	10.3761487801
C	6.0	-18.7456844119	-11.2926324376	10.9233936310
C	6.0	-18.8359074091	-11.3610116398	12.4411982885
C	6.0	-18.3319206420	-12.6633849409	13.0366717538
O	8.0	-17.7486505084	-9.1428024831	10.6785540837
C	6.0	-11.7083893637	-9.8488083499	10.1248053887
C	6.0	-12.5561842690	-8.7367056648	10.0997769587
C	6.0	-12.2091162052	-7.5825995364	9.3941330175
C	6.0	-11.0066450086	-7.5560587594	8.7071951929
C	6.0	-10.1467153207	-8.6789942286	8.7275670055
C	6.0	-10.4840030081	-9.8163056859	9.4313336580
C	6.0	-10.3864913959	-6.5135311510	7.8900462326
C	6.0	-9.1473640996	-6.9994262277	7.4108334503
C	6.0	-8.8992611911	-8.4164178189	7.9004256595
C	6.0	-10.8138265059	-5.2382205453	7.5590345897
C	6.0	-9.9944403394	-4.4392547004	6.7581381128
C	6.0	-8.7635209668	-4.9114651536	6.2921291596
C	6.0	-8.3393085355	-6.2140250017	6.6154428056
C	6.0	-7.6456601839	-8.4861198601	8.7622347928
C	6.0	-8.8052700991	-9.3889462028	6.7321899706
C	6.0	-7.8638734939	-4.0781727554	5.5087224182
C	6.0	-6.5258633464	-4.2407946741	5.2024308308
C	6.0	-6.1252650124	-3.0747413501	4.4748810228
C	6.0	-7.2437662432	-2.2687290371	4.3713984112
O	8.0	-8.3269609248	-2.8807361024	4.9844202280
C	6.0	-7.4080636136	-0.9684507929	3.7303132471
N	7.0	-6.6112859505	-0.8083158978	2.5263182519
N	7.0	-6.2974902721	0.4696653862	2.1133886589
C	6.0	-7.0602356309	1.4811860251	2.4392663737
C	6.0	-8.2583081591	1.3334607006	3.3440598554
C	6.0	-8.2194886326	0.0416184483	4.1224723459
C	6.0	-6.7775400829	2.8126178860	1.9166708086
C	6.0	-7.4867575746	3.9935565670	2.0477222863
C	6.0	-6.7777183035	4.9807274086	1.2938639555

H	1.0	65.3009554920	-8.6670203728	-3.2410501443
H	1.0	68.9780599079	-12.0668075001	-2.8953058776
C	6.0	76.9147956728	-30.1183394088	1.0263668757
C	6.0	79.3882013264	-31.0268818691	0.8267551196
C	6.0	81.3185375256	-29.4661949704	0.0138327942
C	6.0	80.8853178429	-26.9524814615	-0.6342676305
C	6.0	78.4147467783	-26.0108876936	-0.4460320249
C	6.0	80.3597850457	-33.6517868551	1.4045577376
C	6.0	83.1329201382	-33.3353333412	0.7957825107
C	6.0	83.6496468122	-30.8997600019	-0.0057258697
C	6.0	85.0633697209	-35.1340690226	0.9565037059
C	6.0	87.5306148677	-34.4184864829	0.2895249186
C	6.0	88.0398393297	-31.9362936035	-0.5238698383
C	6.0	86.0866185487	-30.1481592848	-0.6775234584
C	6.0	79.9696322183	-34.3236600328	4.2014466858
C	6.0	79.1260396401	-35.6313504163	-0.3234266028
H	1.0	77.9222652887	-34.4076583529	4.6587792721
H	1.0	80.8219931250	-36.1930147744	4.6338726835
H	1.0	80.8674977268	-32.8824416110	5.4384424201
H	1.0	77.0614951012	-35.7418426948	0.0416873553
H	1.0	79.9613741157	-37.5271424244	0.0173287873
H	1.0	79.4169440586	-35.1311588446	-2.3430523549
H	1.0	78.0693048678	-24.0574212483	-0.9480377335
H	1.0	82.4112337834	-25.7481779868	-1.2686108501
H	1.0	75.4381259915	-31.3753473413	1.6667005267
H	1.0	86.4699683626	-28.2391014003	-1.3015298768
H	1.0	89.9475933033	-31.4039577927	-1.0334155536
H	1.0	84.6695886196	-37.0407269552	1.5818329325
C	6.0	29.1793156682	1.4883670852	0.3676083964
C	6.0	29.0538189653	-0.9555399457	1.3046857192
C	6.0	31.4740666269	-1.8989289533	1.1810976396
C	6.0	32.9365822605	0.0156847257	0.1814703866
O	8.0	31.5242577491	2.0047158141	-0.2831754393
C	6.0	35.6630789156	-0.0993239979	-0.3130142126
N	7.0	36.9988695246	-2.2321821312	0.1862702906
N	7.0	39.4729176850	-2.3296541977	-0.2704197888
C	6.0	40.7004458921	-0.2970838225	-1.2381295699
N	7.0	39.3653733790	1.8369837354	-1.7351464019
N	7.0	36.8900968967	1.9329251238	-1.2827082059
C	6.0	43.4259787869	-0.4177050323	-1.7359211896
C	6.0	44.9044248106	1.5088139204	-2.6883619847
C	6.0	47.3169434929	0.5476236940	-2.8368377555
C	6.0	47.1694125850	-1.9193946857	-1.9657496642
O	8.0	44.8209934083	-2.4302254147	-1.3247357119
H	1.0	48.9656538281	1.5498209743	-3.5079172483
C	6.0	49.2630966986	-3.7656758730	-1.7585979014
H	1.0	44.3027927479	3.3913400521	-3.2135546312
H	1.0	27.4133856299	-1.9566789795	1.9970813211
H	1.0	32.0913834153	-3.7625389279	1.7534956413
C	6.0	51.7585365571	-3.1168006606	-2.4558312019
C	6.0	53.6683125376	-4.9284431705	-2.2311994737
C	6.0	53.1338413365	-7.3251826407	-1.3424235472
C	6.0	50.6966806274	-8.0265544411	-0.6373478839
C	6.0	48.7575572023	-6.2307289377	-0.8489027082
C	6.0	56.4423546985	-4.6579477926	-2.8579082003
C	6.0	57.3922821580	-7.2684341693	-2.1911372828
C	6.0	55.4513068015	-8.7824637334	-1.3198980134
C	6.0	59.8562580789	-8.2041886839	-2.3677699708
C	6.0	60.3430703906	-10.7294106240	-1.6457245682
C	6.0	58.3267894535	-12.2488070100	-0.7597454361
C	6.0	55.8649867175	-11.2781114618	-0.5913708506
C	6.0	56.8302398548	-4.0894615237	-5.6782297506
C	6.0	57.6990035831	-2.6294403284	-1.2046247281
H	1.0	55.9939227217	-2.2289884943	-6.1752087882
H	1.0	58.8768697913	-4.0405743124	-6.1438204395
H	1.0	55.9156313740	-5.5655264927	-6.8607257875
H	1.0	57.4095920481	-3.0549877235	0.8322164277
H	1.0	59.7633402521	-2.5508088300	-1.5789794463
H	1.0	56.8801286209	-0.7392608064	-1.6102166169
H	1.0	46.8594786258	-6.7678457552	-0.3046805210
H	1.0	50.2994413275	-9.9085703468	0.0564272180
H	1.0	52.2257335131	-1.2570079325	-3.1580533789
H	1.0	54.3307181881	-12.4472660332	0.0870218817
H	1.0	58.6576237822	-14.1882894829	-0.1972684959
H	1.0	61.3395984930	-6.9810446411	-3.0558381002
H	1.0	89.0495010276	-35.7833410775	0.4015289779

C	6.0	-5.6819755221	4.3442272980	0.7372086225
O	8.0	-5.6622460787	3.0128433180	1.1213109395
C	6.0	-9.5602058580	1.4290770092	2.5229687881
C	6.0	-10.5063097733	2.4813139224	3.0791861075
C	6.0	-10.7640965753	2.3366752996	4.5885902748
C	6.0	-11.4596939438	1.0226965839	4.9842345556
C	6.0	-10.5831675219	-0.2203894259	4.8784104558
C	6.0	-9.1294826055	-0.0061431610	5.3080874168
O	8.0	-11.4743469857	3.4516834206	5.0813744864
C	6.0	-4.6395816259	4.8301146000	-0.1542270846
C	6.0	-3.6545218629	3.9718424075	-0.6549672079
C	6.0	-2.6762862368	4.4363572484	-1.5345712829
C	6.0	-2.6950925364	5.7700621246	-1.9049538532
C	6.0	-3.6818829227	6.6465521695	-1.3976652572
C	6.0	-4.6495404074	6.1877789170	-0.5265935465
C	6.0	-1.8176492071	6.5229096937	-2.7969378543
C	6.0	-2.2601708298	7.8652518246	-2.8362035332
C	6.0	-3.4856278293	8.0489408664	-1.9538645717
C	6.0	-0.7169766898	6.1194976680	-3.5336046465
C	6.0	-0.0442236139	7.0674491813	-4.3051188165
C	6.0	-0.4676230308	8.4002344971	-4.3394925602
C	6.0	-1.5954001653	8.8033385285	-3.5998374921
C	6.0	-4.6898444549	8.4834962347	-2.7785775926
C	6.0	-3.2089509644	9.0467925687	-0.8374828142
C	6.0	0.2469728031	9.4030634721	-5.1143966773
C	6.0	0.1045716086	10.7745346227	-5.1879544520
C	6.0	1.1091249129	11.2434053726	-6.0950886173
C	6.0	1.8126762760	10.1369831474	-6.5288594413
O	8.0	1.2833701789	8.9923909946	-5.9374098161
C	6.0	2.9524952561	9.9667856037	-7.4253574097
N	7.0	3.4712117237	8.6119999553	-7.5136000720
N	7.0	4.7362909524	8.4170657598	-8.0198391437
C	6.0	5.3162026359	9.3152141007	-8.7735119280
C	6.0	4.7067709085	10.6634306726	-9.0647952493
C	6.0	3.4989697153	10.9381239759	-8.2017142622
C	6.0	6.6204989187	8.9575750574	-9.3185378853
C	6.0	7.2503983170	7.7363484651	-9.4463139844
C	6.0	8.5199262343	7.9949897753	-10.0699428178
C	6.0	8.5819324542	9.3508951639	-10.2767396714
O	8.0	7.4394308806	9.9646857624	-9.8247657351
C	6.0	4.3972751887	10.8185409832	-10.5636997239
C	6.0	3.0362986048	10.2840417386	-10.9872446535
C	6.0	2.0654776846	11.3743289076	-11.4806733409
C	6.0	2.1213453747	12.6710980330	-10.6581855042
C	6.0	1.7677749421	12.4787019007	-9.1903421041
C	6.0	2.9873627494	12.3399367242	-8.2787031119
O	8.0	2.3376640184	11.7651336580	-12.8178818690
H	1.0	-18.8966727387	-25.7234505793	18.9650294295
H	1.0	-16.4951230501	-25.1563039647	18.7827690620
H	1.0	-15.7764230235	-22.9717223757	17.8056324416
H	1.0	-20.6447249511	-24.1221060907	18.1793199886
H	1.0	-15.5681089275	-20.6442919803	16.7408313660
H	1.0	-15.8692937061	-18.3919173824	15.7388827007
H	1.0	-20.1796757829	-18.8936681171	15.8323014437
H	1.0	-20.2440994653	-22.4049586280	15.0343836276
H	1.0	-21.4490542143	-21.1586497308	15.4055771122
H	1.0	-21.5866599686	-22.7733445578	16.1316165522
H	1.0	-20.3508848299	-20.6228952331	18.9771084718
H	1.0	-21.6521081782	-21.7131782469	18.4675300200
H	1.0	-21.5100589162	-20.0984634791	17.7424056986
H	1.0	-20.4172764385	-16.7196321799	15.2807462850
H	1.0	-19.6887972701	-14.3116067508	14.3401382525
H	1.0	-15.0769683321	-15.4457110940	14.4546813090
H	1.0	-15.5738775189	-11.5926243788	14.2679900381
H	1.0	-12.0824487785	-14.2094786875	11.8742967680
H	1.0	-10.5301470881	-12.6047747461	10.3508362714
H	1.0	-16.7217793072	-10.1427381292	12.7927510590
H	1.0	-15.0157292612	-10.1425402124	12.4310217238
H	1.0	-16.1863539147	-12.1583884134	10.6908857094
H	1.0	-15.3907744586	-10.6421114028	10.2607324090
H	1.0	-17.5585377402	-10.5986623682	9.2598769464
H	1.0	-18.7183935016	-12.3158067164	10.4950128760
H	1.0	-19.6743238226	-10.8312719169	10.5300828504
H	1.0	-18.3694221757	-10.4761911702	12.9198221575
H	1.0	-19.9093526572	-11.2881760316	12.7169827907
H	1.0	-18.6671601245	-13.4915623611	12.3710878349

H	1.0	-18.9039993891	-12.7899801423	13.9872091131
H	1.0	-16.9119076203	-8.7117483256	10.5655971958
H	1.0	-13.5124664237	-8.7654455864	10.6373337373
H	1.0	-12.8766096560	-6.7146182855	9.3807111620
H	1.0	-9.8068288324	-10.6795994959	9.4457984096
H	1.0	-11.7748259987	-4.8611849845	7.9244807678
H	1.0	-10.3257341467	-3.4243715027	6.5039445542
H	1.0	-7.3798781365	-6.6003354557	6.2495666578
H	1.0	-7.7009976647	-7.7918616071	9.6100181849
H	1.0	-6.7526855490	-8.2286484575	8.1771676270
H	1.0	-7.5041643387	-9.4969823700	9.1671395834
H	1.0	-9.7015951538	-9.3472956822	6.1009380168
H	1.0	-8.6957052915	-10.4216729986	7.0893306032
H	1.0	-7.9391479737	-9.1574807704	6.0980395726
H	1.0	-5.8821454104	-5.0785805929	5.4613932788
H	1.0	-5.1230961562	-2.8873541861	4.0960982395
H	1.0	-5.7809662647	-1.3601734836	2.5121527858
H	1.0	-8.2365118963	2.1751936748	4.0921183263
H	1.0	-8.4248025143	4.1396028442	2.5922938328
H	1.0	-7.0601447221	6.0253642758	1.1907019664
H	1.0	-10.0662183799	0.4382800357	2.4945747424
H	1.0	-9.3323904752	1.6765132954	1.4669174514
H	1.0	-11.4616481934	2.4542266346	2.5193311658
H	1.0	-10.0633151615	3.4888348399	2.8877564568
H	1.0	-9.7847622742	2.4213446938	5.1366304128
H	1.0	-12.3674485877	0.8782701394	4.3641751853
H	1.0	-11.8243596072	1.1210337543	6.0273737062
H	1.0	-10.6080207379	-0.5961328312	3.8303727164
H	1.0	-11.0333763072	-1.0285267630	5.4886500229
H	1.0	-8.8180138234	-0.7944285750	6.0194628743
H	1.0	-9.0331381134	0.9495894016	5.8737484283
H	1.0	-12.3311482493	3.4423958938	4.6721590637
H	1.0	-3.6398985660	2.9155494064	-0.3616514170
H	1.0	-1.9101221768	3.7595695775	-1.9273431398
H	1.0	-5.4118393107	6.8724164099	-0.1349839459
H	1.0	-0.3807268068	5.0775492024	-3.5084197423
H	1.0	0.8293417723	6.7493933502	-4.8857501258
H	1.0	-1.9409572404	9.8441110143	-3.6241419458
H	1.0	-4.9006955027	7.7729047507	-3.5875605904
H	1.0	-4.5180926806	9.4674440737	-3.2350010213
H	1.0	-5.5892920336	8.5538045069	-2.1526830328
H	1.0	-2.3434171001	8.7463130117	-0.2341280561
H	1.0	-4.0723486533	9.1314908091	-0.1641630839
H	1.0	-3.0009704864	10.0447571688	-1.2461286214
H	1.0	-0.6177062382	11.3972878509	-4.6660092055
H	1.0	1.2761203245	12.2842694134	-6.3767276653
H	1.0	3.3968776959	8.0825337132	-6.6723546564
H	1.0	5.4820843475	11.4288971711	-8.7979809007
H	1.0	6.8751016131	6.7629553644	-9.1390256695
H	1.0	9.2684701870	7.2494409868	-10.3221085864
H	1.0	9.3200651539	10.0179518149	-10.7115188869
H	1.0	5.1965733743	10.3258267010	-11.1507206506
H	1.0	4.4672568893	11.9008322575	-10.8215746709
H	1.0	2.5498809524	9.7479264760	-10.1471205765
H	1.0	3.1662148092	9.5175789267	-11.7785949796
H	1.0	1.0265388700	10.9602231029	-11.4482817105
H	1.0	1.4272420947	13.4081747160	-11.1091061032
H	1.0	3.1374948186	13.1182435469	-10.7559135551
H	1.0	1.0963056249	11.6061846032	-9.0590854331
H	1.0	1.1821297271	13.3555843427	-8.8487767611
H	1.0	2.7245476141	12.6938755494	-7.2567563540
H	1.0	3.7956939192	13.0212108568	-8.6179749609
H	1.0	2.3891585101	10.9696425522	-13.3305309074

Oligomer – P3:

ATOM	*CHARGE*	*X*	*Y*	*Z*
C	6.0	0.9032670357	12.6327378168	-0.5761123827
C	6.0	1.5093490097	13.2511592533	0.4898585027
C	6.0	2.5957495971	12.3965564998	0.8936691434
C	6.0	2.5730405587	11.3179192048	0.0401832889

O	8.0	1.5322503938	11.4469499771	-0.8713495523
C	6.0	3.3994851681	10.1106866803	-0.0330244091
N	7.0	2.9147806650	9.0319304456	0.6606163910
N	7.0	3.5502579399	7.9254598934	0.6901923530
C	6.0	4.7488449314	7.7733423980	0.0337457856
C	6.0	5.3091975482	8.8266908723	-0.7145376017
C	6.0	4.6068106185	10.0481442780	-0.7543774930
C	6.0	5.3387364831	6.4440327188	0.1665374428
C	6.0	4.7992717644	5.1774774411	0.0826483173
C	6.0	5.8862591450	4.2580798826	0.2744634912
C	6.0	7.0204384921	5.0214720022	0.4689307939
O	8.0	6.6958407466	6.3656289229	0.4383189319
H	1.0	5.8146474541	3.1737135871	0.2539518534
C	6.0	8.4242279397	4.6820808576	0.6372418407
H	1.0	3.7607068869	4.9102532588	-0.0964239520
H	1.0	0.0561289705	12.8747844314	-1.2108981772
H	1.0	1.2368809120	14.1939489835	0.9550500034
H	1.0	3.2790556833	12.5792821489	1.7182930483
C	6.0	8.7565488672	3.4010304588	1.1092496048
C	6.0	10.0910111119	3.0716598520	1.2346493539
C	6.0	11.0996500052	4.0038625026	0.8976878117
C	6.0	10.7725387566	5.2689763152	0.4386912405
C	6.0	9.4248029091	5.6040276567	0.3078792505
C	6.0	10.7054383627	1.7637380039	1.7058925718
C	6.0	12.1911595070	2.0579384992	1.5782982851
C	6.0	12.4011732124	3.3762939525	1.1113995842
C	6.0	13.2594798305	1.2261461924	1.8415633273
C	6.0	14.5620911131	1.7151182188	1.6333388631
C	6.0	14.7650339221	3.0234929465	1.1856424029
C	6.0	13.6826938168	3.8641980058	0.9205414198
C	6.0	10.3290271060	1.4741394388	3.1528431199
C	6.0	10.2963214102	0.6094111815	0.8009360868
H	1.0	9.2452617464	1.3292217078	3.2547481554
H	1.0	10.8269222836	0.5638570072	3.5125121568
H	1.0	10.6195412615	2.2979376099	3.8166907252
H	1.0	9.2118966512	0.4419408342	0.8446221599
H	1.0	10.5620738395	0.8047762915	-0.2454069939
H	1.0	10.7940569344	-0.3215083641	1.1036243331
H	1.0	9.1562186502	6.6087739759	-0.0662943643
H	1.0	11.5565906869	5.9884559704	0.1796262793
H	1.0	7.9732686987	2.6787734069	1.3692597433
H	1.0	13.8431396929	4.8879712294	0.5662478662
H	1.0	15.7832100060	3.4020013114	1.0372838049
H	1.0	13.0937015427	0.2026375552	2.1992776642
C	6.0	33.9876358186	-4.3676902186	1.0071234757
C	6.0	35.0860269440	-3.6492751342	1.4410216770
C	6.0	36.1974261515	-4.5539043024	1.4269091893
C	6.0	35.7114238569	-5.7676357744	0.9811805291
O	8.0	34.3559257805	-5.6696664682	0.7157465544
C	6.0	36.3311406642	-7.0779453041	0.8111713603
N	7.0	35.5772226577	-8.1449620396	1.2503824366
N	7.0	36.0130066805	-9.3360586336	1.1797440341
C	6.0	37.2571071714	-9.6305831291	0.6564446533
C	6.0	38.0901525370	-8.6070680950	0.1638882656
C	6.0	37.6013696082	-7.2833787713	0.2516637402
C	6.0	37.5427625969	-11.0593883275	0.6681820968
C	6.0	36.6951802879	-12.1399100126	0.8214873970
C	6.0	37.5128593992	-13.3153813797	0.7631498156
C	6.0	38.8139268588	-12.8879273107	0.5816260697
O	8.0	38.8521518310	-11.5020822490	0.5220048434
H	1.0	37.1575011434	-14.3393321572	0.8507572986

C	6.0	40.0623368169	-13.6210192694	0.4521619060
H	1.0	35.6168074762	-12.1172356259	0.9656450006
H	1.0	35.1159781699	-2.6071619196	1.7481159655
H	1.0	37.2235877999	-4.3252806502	1.7253578563
C	6.0	40.0074473054	-15.0244074376	0.3666794812
C	6.0	41.1883199927	-15.7279026451	0.2479283798
C	6.0	42.4302168349	-15.0526820185	0.2147916150
C	6.0	42.4877828631	-13.6719775939	0.2966345151
C	6.0	41.2942903860	-12.9593962828	0.4145158727
C	6.0	41.3933343596	-17.2304045464	0.1372013743
C	6.0	42.9069911734	-17.3299570898	0.0416812240
C	6.0	43.4948791681	-16.0446833792	0.0885359046
C	6.0	43.6968584312	-18.4578417391	-0.0763413644
C	6.0	45.0835944097	-18.2961577869	-0.1472744692
C	6.0	45.6595576927	-17.0322352984	-0.1006571821
C	6.0	44.8684619610	-15.8872591607	0.0181578202
C	6.0	40.7299291427	-17.7803165725	-1.1184530167
C	6.0	40.8754140334	-17.9458757046	1.3775459665
H	1.0	41.0934554498	-17.2727280265	-2.0205962925
H	1.0	40.9359719409	-18.8528661050	-1.2327633948
H	1.0	39.6405395003	-17.6481911791	-1.0769062919
H	1.0	39.7894415192	-17.8184682150	1.4794287487
H	1.0	41.0856708858	-19.0223936091	1.3253028476
H	1.0	41.3440201155	-17.5582424858	2.2906324958
H	1.0	41.3361342649	-11.8650706387	0.4777075061
H	1.0	43.4507921952	-13.1513575664	0.2694645418
H	1.0	39.0464598503	-15.5527128165	0.3926357476
H	1.0	45.3197117144	-14.8905273361	0.0551369748
H	1.0	46.7482724972	-16.9299801145	-0.1576470270
H	1.0	43.2434961435	-19.4541789948	-0.1130523952
C	6.0	15.6773119774	0.8172597807	1.8883933112
C	6.0	15.7603399805	-0.3325331006	2.6517166978
C	6.0	17.0892466460	-0.8391276087	2.4823965165
C	6.0	17.7348425859	0.0354857114	1.6326075034
O	8.0	16.8897633723	1.0672173410	1.2638962448
C	6.0	19.1069205958	0.0275052475	1.1357460680
N	7.0	19.8544246439	1.1642787465	1.3528737231
N	7.0	21.0780026426	1.2281422836	1.0087358527
C	6.0	21.7294706708	0.1578142786	0.4267273247
C	6.0	21.0376177166	-1.0306985111	0.1552386434
C	6.0	19.6673370966	-1.0844248020	0.4948885576
C	6.0	23.1310083009	0.4143796235	0.1132612666
C	6.0	23.7667254151	1.5264880267	-0.3997553315
C	6.0	25.1633977835	1.2017478643	-0.4719794621
C	6.0	25.2957849607	-0.0867150936	0.0062589082
O	8.0	24.0577234988	-0.5803173210	0.3844048550
H	1.0	25.9508211291	1.8546463429	-0.8397031917
C	6.0	26.4415848379	-0.9707515007	0.1516771139
H	1.0	23.3147308073	2.4711700298	-0.6920307898
H	1.0	14.9820558503	-0.7780071833	3.2661025366
H	1.0	17.5081594839	-1.7478253901	2.9204520083
C	6.0	27.7321079269	-0.4145773492	0.2002578973
C	6.0	28.8120985848	-1.2646065636	0.3369694152
C	6.0	28.6200615562	-2.6627035860	0.4208951419
C	6.0	27.3511723289	-3.2133742911	0.3682512328
C	6.0	26.2606883795	-2.3558289193	0.2335927163
C	6.0	30.2928506571	-0.9257411719	0.4265874119
C	6.0	30.9201322106	-2.3039026585	0.5763825257
C	6.0	29.9218327959	-3.3047851785	0.5666835442
C	6.0	32.2516921259	-2.6431830279	0.7127505831
C	6.0	32.5896108123	-4.0023438505	0.8409834607

C	6.0	31.5957803860	-4.9868165140	0.8287103024
C	6.0	30.2516813683	-4.6433325900	0.6899013877
C	6.0	30.7743568498	-0.2425273415	-0.8461875988
C	6.0	30.5805454294	-0.0599046130	1.6457304065
H	1.0	30.2720722524	0.7238557887	-0.9867560455
H	1.0	31.8562043116	-0.0581459672	-0.8068101535
H	1.0	30.5727089845	-0.8559031644	-1.7332449988
H	1.0	30.2373851487	-0.5405229890	2.5704204502
H	1.0	31.6575586948	0.1288788966	1.7470779538
H	1.0	30.0736105780	0.9110354558	1.5659772347
H	1.0	25.2508647349	-2.7856185057	0.1940212417
H	1.0	27.2094770973	-4.2974083066	0.4323260873
H	1.0	27.8773831539	0.6705014266	0.1353351992
H	1.0	29.4736521019	-5.4140028673	0.6820721758
H	1.0	31.8641767118	-6.0448575886	0.9343687734
H	1.0	33.0281886499	-1.8689440459	0.7223364961
H	1.0	45.7227777840	-19.1803675077	-0.2408620768
C	6.0	6.6040266873	8.6163876592	-1.4328309534
C	6.0	7.7960682235	8.9497837760	-0.5355150824
C	6.0	8.4098548908	10.3426220981	-0.7415452334
C	6.0	7.3668137663	11.4692720054	-0.6322765698
C	6.0	6.4425171347	11.5659394095	-1.8387594908
C	6.0	4.9825094576	11.2605512517	-1.5493897601
O	8.0	9.1777009391	10.4155143707	-1.9201680392
C	6.0	18.8230140730	-2.2617250661	0.1237388676
C	6.0	18.7799817427	-3.3516945321	1.1861875295
C	6.0	19.9762104339	-4.3210560676	1.1589946682
C	6.0	21.2911386658	-3.6486374011	1.6005199646
C	6.0	22.2428808766	-3.2223474412	0.4958825611
C	6.0	21.6827220203	-2.2091073892	-0.4976307233
O	8.0	20.0708644358	-4.9947020242	-0.0732095668
H	1.0	19.7563863473	-5.1671040262	1.8517649861
H	1.0	21.0497356770	-2.7742489772	2.2387861386
H	1.0	21.8379773372	-4.3515444410	2.2604645127
H	1.0	23.1574380426	-2.8113054204	0.9723713603
H	1.0	22.5878382252	-4.1115720367	-0.0715148561
H	1.0	22.4912280493	-1.8721262684	-1.1769145060
H	1.0	20.9330409435	-2.7149157780	-1.1562647357
H	1.0	17.7909159297	-1.9093105789	-0.0789025608
H	1.0	19.1935983340	-2.6924232901	-0.8384667171
H	1.0	17.8519426708	-3.9410256432	1.0375727361
H	1.0	18.6760090000	-2.8932073007	2.1959875789
H	1.0	4.5522746852	12.1499029802	-1.0368481137
H	1.0	4.4398864510	11.1822252953	-2.5153483271
H	1.0	6.4898447624	12.5910648258	-2.2589730565
H	1.0	6.8138865885	10.9108753621	-2.6637365908
H	1.0	6.7822200936	11.3220709776	0.2970349690
H	1.0	7.8976331620	12.4326399068	-0.5006982022
H	1.0	9.1968177943	10.4977339283	0.0341793337
H	1.0	8.5844627889	8.1709133339	-0.6726862019
H	1.0	7.4986115010	8.8653527046	0.5297629864
H	1.0	6.6694996175	7.5601473709	-1.7671117609
H	1.0	6.6227425387	9.2032013911	-2.3764601140
C	6.0	39.3835773243	-8.9882991271	-0.4889966041
C	6.0	40.5946882106	-8.0724309486	-0.4248808353
C	6.0	41.0121169284	-7.6350362892	0.9834424462
C	6.0	40.0122032632	-6.7040474078	1.6911886452
C	6.0	39.3913212316	-5.6186836148	0.8281098100
C	6.0	38.4012260414	-6.1172626424	-0.2250391164
O	8.0	42.2789849692	-7.0151077462	0.8187667461
H	1.0	39.2111503745	-7.3275255078	2.1386709880

H	1.0	40.5154007814	-6.2210608336	2.5553861731
H	1.0	41.1491209711	-8.5461064015	1.6194939877
H	1.0	40.4551783737	-7.1806632831	-1.0746526928
H	1.0	41.4411749062	-8.6228028768	-0.8900374501
H	1.0	39.6988288167	-9.9839965768	-0.0876159104
H	1.0	39.1436772911	-9.1613310766	-1.5599793159
H	1.0	37.7238309945	-5.2845174949	-0.5111193190
H	1.0	38.9273363388	-6.3895185725	-1.1659550136
H	1.0	38.8571665405	-4.9023264625	1.4954504529
H	1.0	40.1865399520	-5.0318885185	0.3281564166
H	1.0	8.5646121075	10.4156971928	-2.6502266575
H	1.0	20.1755415202	-4.3170128928	-0.7411203904
H	1.0	42.5522436165	-6.7182538208	1.6762956685

Coordinates of M06-2X stationary point calculations:

Repeat Unit – P1:

ATOM	*CHARGE*	*X*	*Y*	*Z*
C	6.0	-4.6301781192	-1.5035443590	1.7875350164
C	6.0	-3.3694239519	-3.7144557774	1.0796574638
C	6.0	-0.8124743275	-3.6582111621	0.4482217904
C	6.0	0.4609277271	-1.3544002565	0.5369181440
C	6.0	-0.8048163479	0.8701949881	1.2483356336
C	6.0	-3.3519628725	0.8048908331	1.8756899501
C	6.0	3.1052576604	-0.7198004373	-0.0136597112
C	6.0	3.4457639323	1.8877067669	0.3626977068
C	6.0	0.9901674208	3.0967484969	1.1923792514
C	6.0	5.1238805185	-2.2270307981	-0.7864982300
C	6.0	7.4680336454	-1.1088378175	-1.1758294250
C	6.0	7.8183208982	1.4961639980	-0.8023543652
C	6.0	5.7800873184	3.0067764769	-0.0242140332
H	1.0	0.3667637284	4.5430310949	-0.1523999526
H	1.0	1.1722848183	3.9741572836	3.0594247693
C	6.0	18.2531792252	18.8934490573	-0.3518430399
C	6.0	15.9575404610	19.8455646923	0.3948709346
C	6.0	14.2530605079	17.7715934944	0.4583540395
C	6.0	15.6260130056	15.7002974494	-0.2532601668
O	8.0	18.0492269728	16.3709536567	-0.7456905072
C	6.0	14.9370935511	13.0661650372	-0.5446591002
N	7.0	12.5181440646	12.4626724501	-0.0427113298
N	7.0	11.8401313892	10.1122275336	-0.2870418778
C	6.0	13.6172635363	8.4492197055	-1.0275228649
N	7.0	16.0362570254	9.0526854591	-1.5292838140
N	7.0	16.7142552030	11.4031460666	-1.2850131654
C	6.0	12.9280909106	5.8152409661	-1.3197108137
C	6.0	14.3013332942	3.7437592773	-2.0302227315
C	6.0	12.5962534069	1.6702254580	-1.9691618612
C	6.0	10.2999785723	2.6227673189	-1.2249421929
O	8.0	10.5041529459	5.1450930147	-0.8301932977
C	6.0	33.1768812286	23.0232358392	-3.3912844885
C	6.0	31.9167585427	25.2339859873	-2.6817764920
C	6.0	29.3610018107	25.1771121856	-2.0456078587
C	6.0	28.0881440195	22.8729001003	-2.1311989038
C	6.0	29.3532632064	20.6484767470	-2.8442447697
C	6.0	31.8992206786	20.7143744589	-3.4763271825
C	6.0	25.4450003500	22.2376894445	-1.5756540178
C	6.0	25.1045969115	19.6299938739	-1.9506483474
C	6.0	27.5590508128	18.4214094948	-2.7843541787
C	6.0	23.4272860937	23.7445679236	-0.7997444505
C	6.0	21.0841098096	22.6258278715	-0.4061343019
C	6.0	20.7339033251	20.0206289209	-0.7783500984

Repeat Unit – P2:

ATOM	*CHARGE*	*X*	*Y*	*Z*
C	6.0	5.1504636689	10.5076527286	-1.6040845452
C	6.0	6.3293526990	9.8443264470	-1.9439328381
C	6.0	6.5372347322	8.5241774227	-1.5580718841
C	6.0	5.5471291768	7.8758572537	-0.8257418266
C	6.0	4.3592469120	8.5444556560	-0.4831245591
C	6.0	4.1576910443	9.8590794341	-0.8704115229
C	6.0	5.4863503242	6.5192892239	-0.2907944098
C	6.0	4.2614593073	6.3558241933	0.3804107978
C	6.0	3.4600562452	7.6284990262	0.3046016134
C	6.0	6.3942112618	5.4663999487	-0.3500344961
C	6.0	6.0755207450	4.2617659894	0.2597156171
C	6.0	4.8550644898	4.0895152788	0.9324728826
C	6.0	3.9441781060	5.1577089991	0.9869077651
H	1.0	3.2313905132	8.0319118645	1.3029800151
H	1.0	2.4896062498	7.4749332531	-0.1921766898
C	6.0	3.7343617656	-13.3010488203	5.6569641042
C	6.0	3.0675570971	-12.2337171296	6.2582815675
C	6.0	3.3555027632	-10.9222725368	5.8952245613
C	6.0	4.3219895697	-10.6938857286	4.9201431652
C	6.0	4.9938726948	-11.7692530316	4.3143255594
C	6.0	4.7027919517	-13.0733686271	4.6800025500
C	6.0	4.8261426078	-9.4502988356	4.3462568309
C	6.0	5.8072692801	-9.7631373473	3.3883198933
C	6.0	5.9825279071	-11.2561503850	3.3008716630
C	6.0	4.4962857386	-8.1224191243	4.5976210132
C	6.0	5.1454947590	-7.1182646531	3.8938377399
C	6.0	6.1262936927	-7.4207365426	2.9365150463
C	6.0	6.4529829320	-8.7644567046	2.6889353735
H	1.0	5.7729518332	-11.6368717187	2.2895089832
H	1.0	7.0128024194	-11.5643527922	3.5358831154
C	6.0	4.5293270812	2.8289837635	1.5669078044
C	6.0	3.4306527909	2.3729789932	2.2497821697
C	6.0	3.7039517199	1.0367168825	2.6264580018
C	6.0	4.9570255505	0.7499148795	2.1572195602
O	8.0	5.4629301773	1.8387979014	1.5111025349
C	6.0	5.8000019768	-0.4227418888	2.2340209826
C	6.0	7.1441085386	-0.4302265506	1.5499698058
C	6.0	7.4434936003	-1.8329855229	1.0926026474
C	6.0	6.9771574808	-2.8339459721	1.8782894353
N	7.0	6.1553104024	-2.5172812654	2.9745637411
N	7.0	5.3715035704	-1.4049529712	2.9540240690
C	6.0	7.2097077660	-4.2530764966	1.6912822863
C	6.0	8.0277086844	-5.0196985683	0.9015665319

C	6.0	22.7712563223	18.5103922209	-1.5594518927
H	1.0	28.1852965936	16.9757067315	-1.4402711959
H	1.0	27.3738312828	17.5433818578	-4.6508050460
H	1.0	-4.3934896068	-5.4907274813	1.0219441657
H	1.0	0.1616673930	-5.3796345406	-0.1009689791
H	1.0	4.8831086775	-4.2433576096	-1.0831985879
H	1.0	9.0514532601	-2.2664312686	-1.7776465078
H	1.0	6.0574925661	5.0195538435	0.2626562497
H	1.0	-4.3407185031	2.5179638178	2.4270576151
H	1.0	-6.6214572991	-1.5835104759	2.2728618411
H	1.0	13.0146463471	-0.2751808091	-2.4180941097
H	1.0	16.2804420915	3.7449905311	-2.5264228389
H	1.0	12.2744841048	17.7699880473	0.9566776943
H	1.0	15.5391241553	21.7909952683	0.8436812288
H	1.0	19.5013731192	23.7831538430	0.1979819808
H	1.0	22.4939408155	16.4974688863	-1.8453955061
H	1.0	23.6679887880	25.7610492081	-0.5040373462
H	1.0	28.3873283089	26.8984184306	-1.4951958733
H	1.0	32.9403528837	27.0106070777	-2.6265534911
H	1.0	35.1672275485	23.1036748737	-3.8803399261
H	1.0	32.8874948949	19.0014395470	-4.0289860013

C	6.0	7.7639394661	-6.3732679365	1.2297760884
C	6.0	6.8031082528	-6.3702077272	2.2028785676
O	8.0	6.4632146098	-5.0809487771	2.4851924574
C	6.0	8.2160669124	0.1239890011	2.5029503802
C	6.0	9.6237053318	0.0889516314	1.9217223187
C	6.0	9.7626645066	0.7991936690	0.5699005307
C	6.0	9.8486612962	-0.1032462004	-0.6598419805
C	6.0	8.6108843086	-0.9071919201	-1.0416661667
C	6.0	8.2574389644	-2.0951546294	-0.1467957866
O	8.0	10.1240553198	0.6822233530	-1.8073282494
H	1.0	10.8857535963	1.2429628969	-1.6082855692
H	1.0	2.3141445802	-12.4294960126	7.0194788862
H	1.0	2.8321441045	-10.0912720790	6.3676151871
H	1.0	3.4962747835	-14.3212073571	5.9533718840
H	1.0	5.2214027349	-13.9105696323	4.2127906595
H	1.0	3.7378235315	-7.8650005096	5.3363750911
H	1.0	4.8927767933	-6.0773487842	4.0819348338
H	1.0	7.2136330590	-9.0124003390	1.9480320056
H	1.0	8.2339167943	-7.2455350477	0.7919302722
H	1.0	8.7435011439	-4.6648397495	0.1741326567
H	1.0	7.0884539517	0.2400035411	0.6818551249
H	1.0	5.6714146825	-3.2984587375	3.3974363772
H	1.0	2.5246551415	2.9321462759	2.4509683259
H	1.0	3.0699682906	0.3502891359	3.1728031638
H	1.0	2.9941701813	5.0364738130	1.5084366042
H	1.0	6.7758930487	3.4300582814	0.2190714049
H	1.0	7.3461561086	5.5781972262	-0.8684589980
H	1.0	7.4596624643	8.0096026600	-1.8261553056
H	1.0	7.0943728695	10.3653743928	-2.5173485172
H	1.0	5.0043222680	11.5409377532	-1.9144291553
H	1.0	3.2378951585	10.3812278392	-0.6065713825
H	1.0	9.2073032121	-2.5879049116	0.1352761337
H	1.0	7.7305111694	-2.8432575052	-0.7625065429
H	1.0	8.8300900973	-1.2994685724	-2.0441988247
H	1.0	7.7604226765	-0.2231065813	-1.1788891741
H	1.0	10.6732987775	-0.8284364147	-0.4864317985
H	1.0	8.9429897787	1.5209765954	0.4161143301
H	1.0	10.6862903921	1.4014230088	0.5763939838
H	1.0	9.9601564658	-0.9567766725	1.8323946311
H	1.0	10.3040618675	0.5489647770	2.6513073789
H	1.0	7.9467974008	1.1625775086	2.7563358814
H	1.0	8.1861443265	-0.4523587140	3.4399768049

Repeat Unit – P3:

ATOM	*CHARGE*	*X*	*Y*	*Z*
C	6.0	-2.3734561053	0.7153582557	-0.1654061487
C	6.0	-2.0864085791	-0.5230250347	-0.7455569896
C	6.0	-0.7702611724	-0.9658602850	-0.8610301455
C	6.0	0.2550705780	-0.1495394424	-0.3864985530
C	6.0	-0.0330627013	1.0971755159	0.1976352962
C	6.0	-1.3463662833	1.5334493013	0.3100831546
C	6.0	1.7117956920	-0.3451045517	-0.3709099638
C	6.0	2.3088574501	0.7826749920	0.2226861138
C	6.0	1.2469662571	1.7846180816	0.6290123436
C	6.0	2.5032350526	-1.3992437987	-0.8228239184
C	6.0	3.8840015274	-1.3187170518	-0.6784620522
C	6.0	4.4862378717	-0.1956669295	-0.0871047744
C	6.0	3.6826798585	0.8627829943	0.3662704927
H	1.0	1.3813401869	2.7397455008	0.1109102881
H	1.0	1.2598339925	1.9627294511	1.7092185339
C	6.0	20.8885473555	-0.3329143370	3.1545074669

C	6.0	21.4216150378	-1.5163566499	2.6369761043
C	6.0	20.6118400442	-2.4209775868	1.9530650464
C	6.0	19.2594269325	-2.1227551865	1.7949729076
C	6.0	18.7216838474	-0.9315903488	2.3156932399
C	6.0	19.5335488923	-0.0339478408	2.9962759450
C	6.0	18.1796804285	-2.8689380501	1.1332465960
C	6.0	16.9872335759	-2.1324567976	1.2516689626
C	6.0	17.2396206451	-0.8463039654	2.0112275135
C	6.0	18.1848114798	-4.0945098917	0.4676124810
C	6.0	16.9976153367	-4.5716628502	-0.0730932459
C	6.0	15.8046408044	-3.8401813189	0.0426048879
C	6.0	15.8022512442	-2.6070052430	0.7130505977
H	1.0	16.6445731604	-0.8032851944	2.9291566882
H	1.0	17.0071139473	0.0300607392	1.3976707589
C	6.0	5.9348336807	-0.1222476501	0.0594794660
C	6.0	6.7934194251	0.8066138730	0.5824568171
C	6.0	8.1088952761	0.2803119608	0.4313910309
C	6.0	7.9728166487	-0.9341700794	-0.1816374985
O	8.0	6.6504950461	-1.1828453567	-0.4044850484
C	6.0	8.9912103994	-1.9197731205	-0.5511837349
C	6.0	8.7915537725	-3.1275184651	-1.2524044375
C	6.0	9.9082396912	-3.9488597057	-1.4138720604
C	6.0	11.1365688940	-3.5015378862	-0.8807587356
N	7.0	11.2435126013	-2.3180165848	-0.2508066186
N	7.0	10.2011888643	-1.5560491812	-0.0893351194
C	6.0	12.4083271064	-4.2282179058	-0.9696273525
C	6.0	12.8531686072	-5.4113186552	-1.5085779040
C	6.0	14.2480168302	-5.4969949855	-1.2272685622
C	6.0	14.5705969857	-4.3626578743	-0.5336003018
O	8.0	13.4633519593	-3.6009845811	-0.3803411880
C	6.0	7.4434037114	-3.5487555727	-1.7844254673
C	6.0	6.6786473327	-4.5459635332	-0.8971274069
C	6.0	7.1277282585	-6.0171555588	-0.7782542480
C	6.0	8.4951452182	-6.3309111074	-0.1452630006
C	6.0	9.6532802635	-6.4519286672	-1.1436046992
C	6.0	9.7612998660	-5.2692216592	-2.1128769420
O	8.0	8.4281487877	-7.5402508803	0.6026594628
H	1.0	8.1466303168	-8.2491506937	0.0150759168
H	1.0	22.4774407493	-1.7316631268	2.7699429406
H	1.0	21.0301530566	-3.3401514839	1.5521429818
H	1.0	21.5352010337	0.3596846560	3.6844750152
H	1.0	19.1237088069	0.8878631438	3.4007564561
H	1.0	19.0992846156	-4.6727139623	0.3696206245
H	1.0	16.9930698518	-5.5252630750	-0.5928978039
H	1.0	14.8767114747	-2.0451508843	0.7997389647
H	1.0	14.9149838535	-6.2986326246	-1.5055884903
H	1.0	12.2813474647	-6.1504457862	-2.0427904375
H	1.0	6.5213380293	1.7519034977	1.0273719655
H	1.0	9.0458328124	0.7224236365	0.7309883777
H	1.0	4.1373174118	1.7368728366	0.8257147082
H	1.0	4.5137348779	-2.1320535113	-1.0241453318
H	1.0	2.0545554356	-2.2754674491	-1.2822287254
H	1.0	-0.5512675681	-1.9294581591	-1.3127221682
H	1.0	-2.8982700449	-1.1452324761	-1.1094559113
H	1.0	-3.4052083015	1.0432077310	-0.0842277414
H	1.0	-1.5749424392	2.4957889993	0.7605523994
H	1.0	10.5580259611	-5.4118823550	-2.8479585181
H	1.0	8.8511525349	-5.2701500896	-2.7138682518
H	1.0	10.5712892229	-6.5944304447	-0.5676103722
H	1.0	9.4945399425	-7.3629715706	-1.7367878645
H	1.0	8.7149970529	-5.5538243334	0.5953806220
H	1.0	7.0190846967	-6.5461075442	-1.7365061709
H	1.0	6.3961610334	-6.4614447475	-0.0941914730
H	1.0	5.6515576068	-4.5759941325	-1.2776208611
H	1.0	6.6207853308	-4.1197685264	0.1116835764
H	1.0	6.8106750399	-2.6655190350	-1.8647451088

H	1.0	7.5070302607	-3.8914198871	-2.8220761031

4.4.5. MALDI Spectra

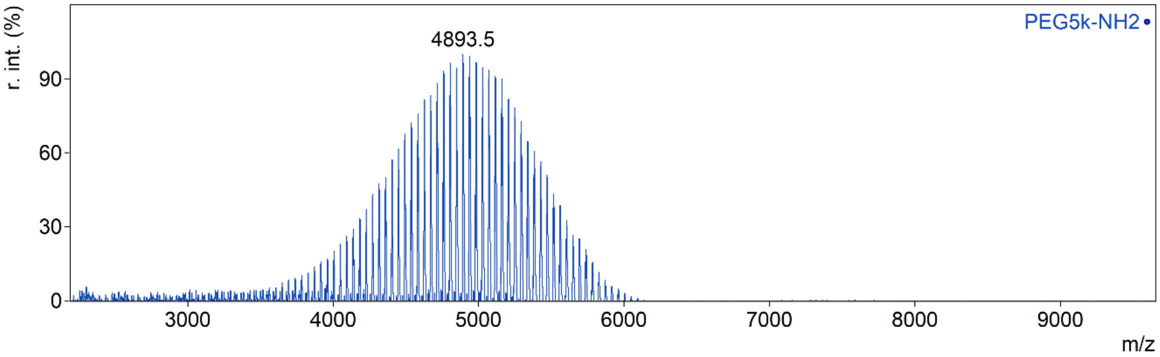

Figure 4.9. MALDI-TOF spectrum of α-methoxy ω-amino poly(ethylene glycol) - 5kDa.

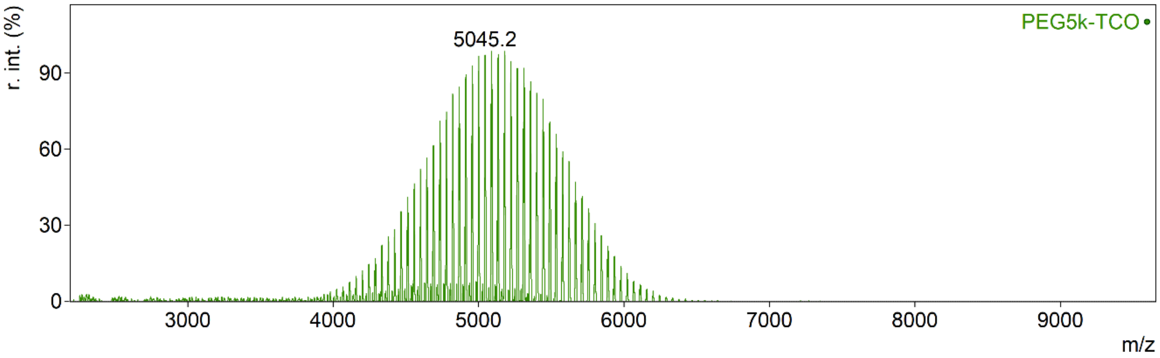

Figure 4.10. MALDI-TOF spectrum of **7f**.

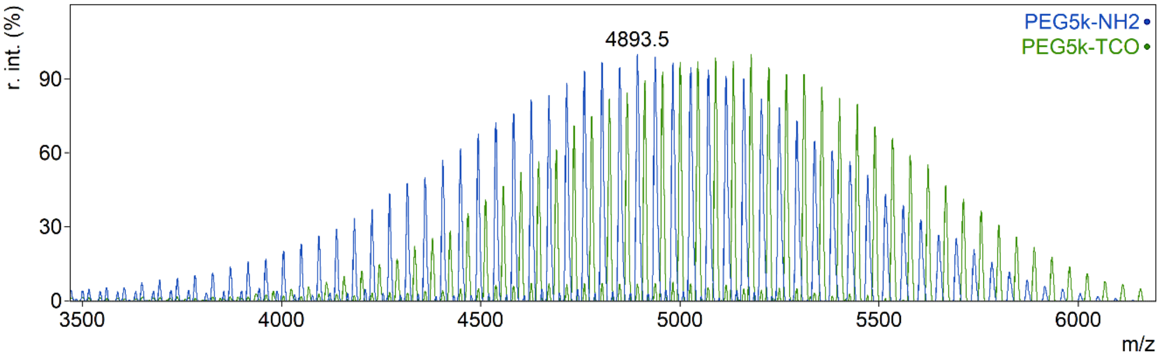

Figure 4.11. MALDI-TOF spectrum overlay of **7f** with α-methoxy ω-amino poly(ethylene glycol) - 5kDa

4.4.6. NMR Spectra

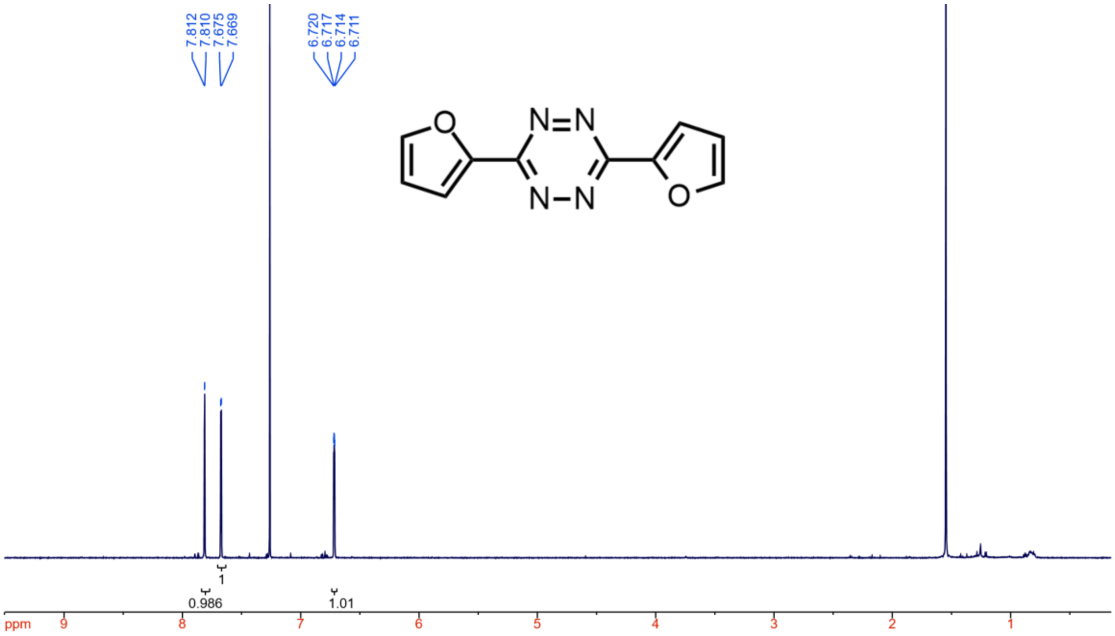

Figure 4.12. ^{1}H-NMR spectrum of **1** in CDCl$_3$.

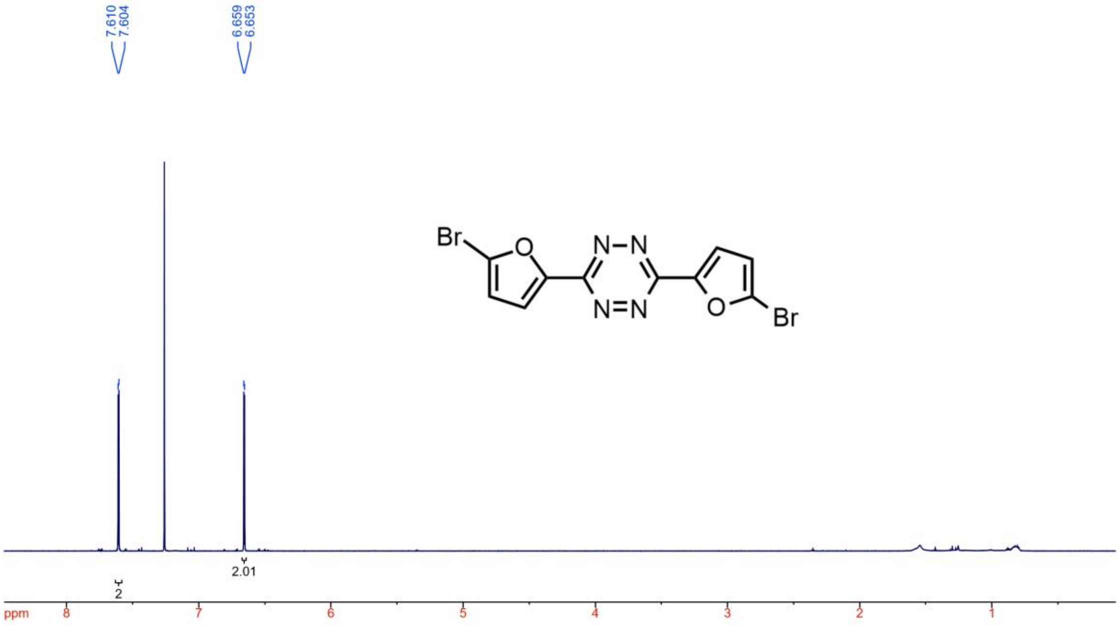

Figure 4.13. ^{1}H-NMR spectrum of **2** in CDCl$_3$.

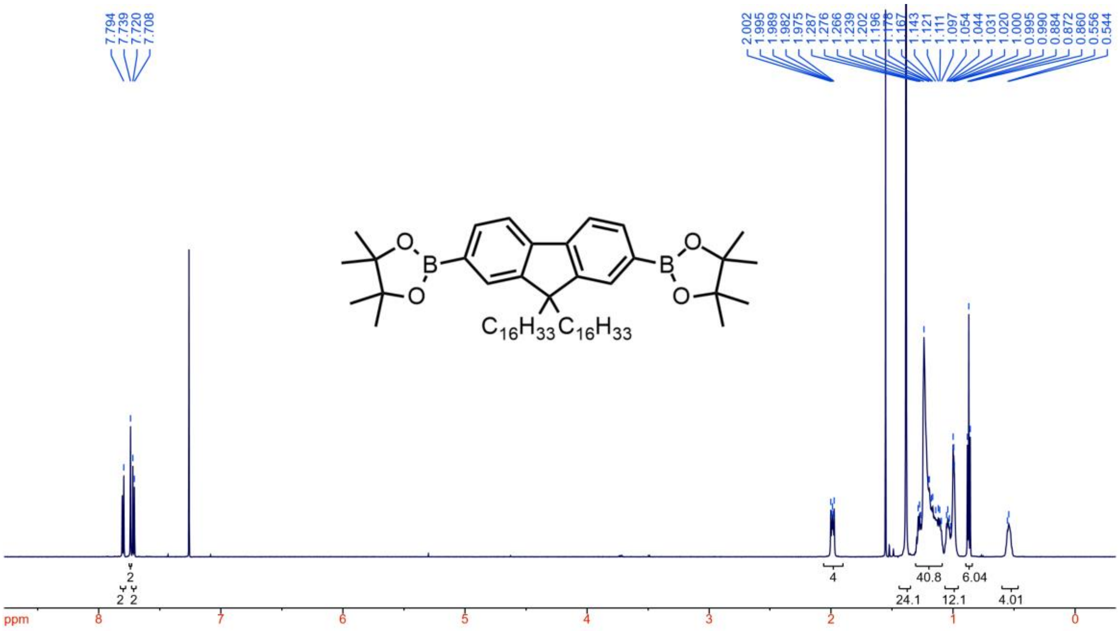

Figure 4.14. ^{1}H-NMR spectrum of **3** in $CDCl_3$.

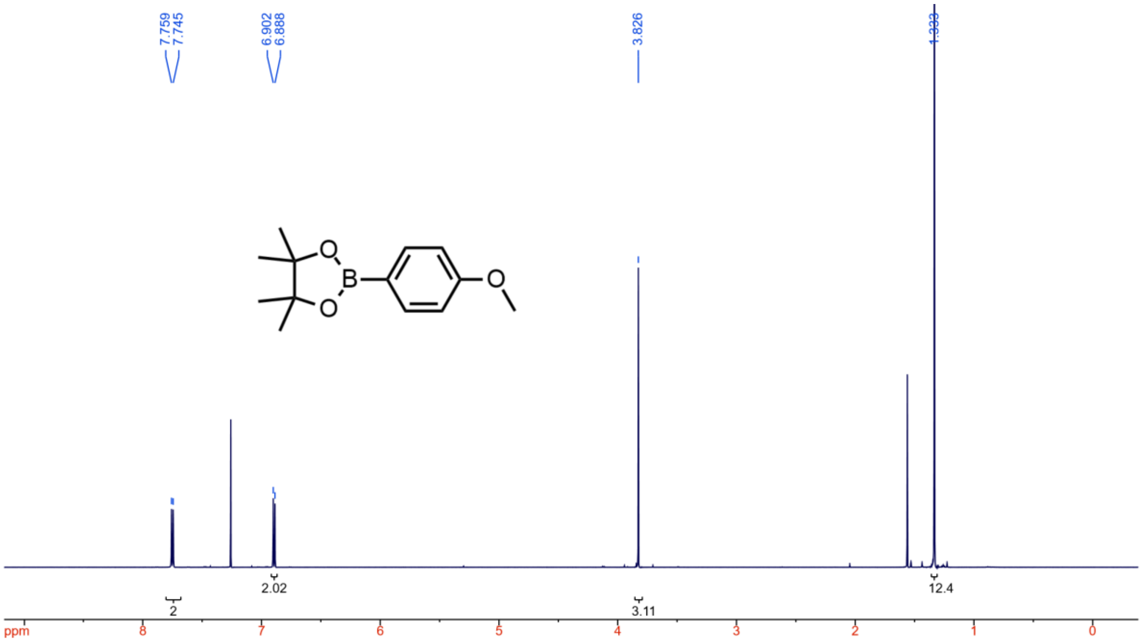

Figure 4.15. ^{1}H-NMR spectrum of **4** in $CDCl_3$.

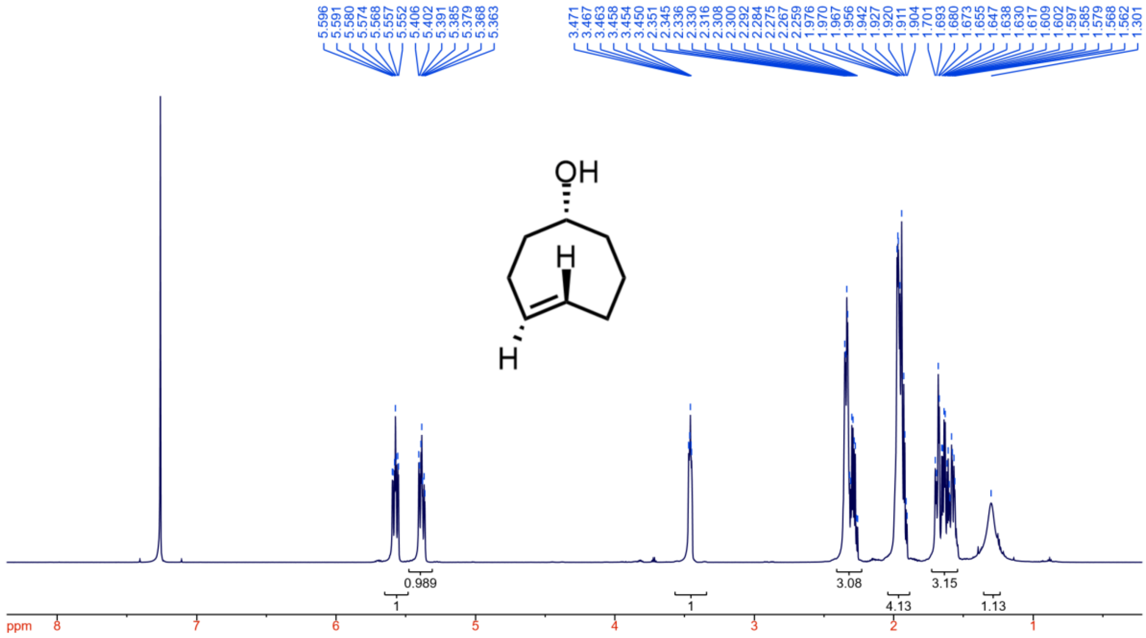

Figure 4.16. ^{1}H-NMR spectrum of **5** in $CDCl_3$.

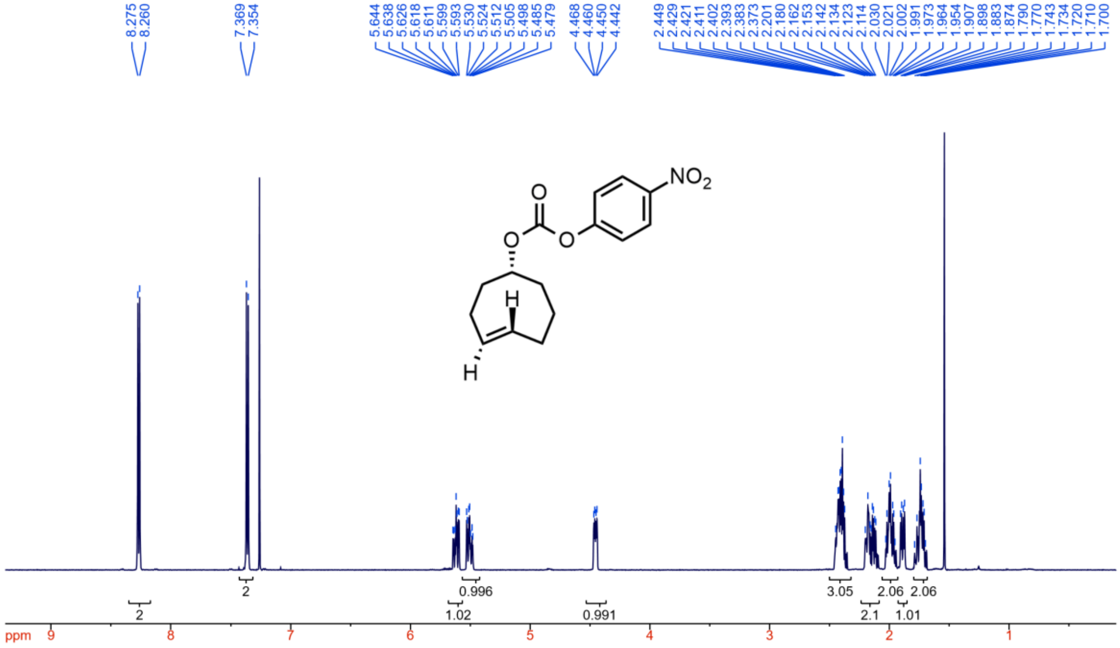

Figure 4.17. ^{1}H-NMR spectrum of **6** in $CDCl_3$.

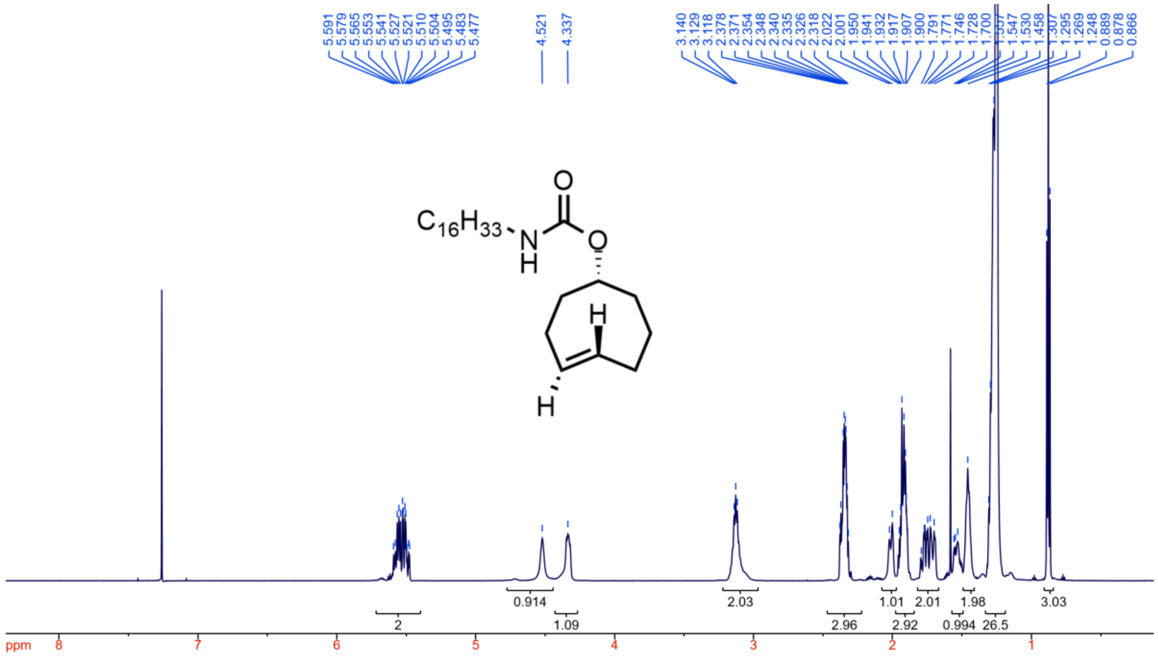

Figure 4.18. ^{1}H-NMR spectrum of **7a** in $CDCl_3$.

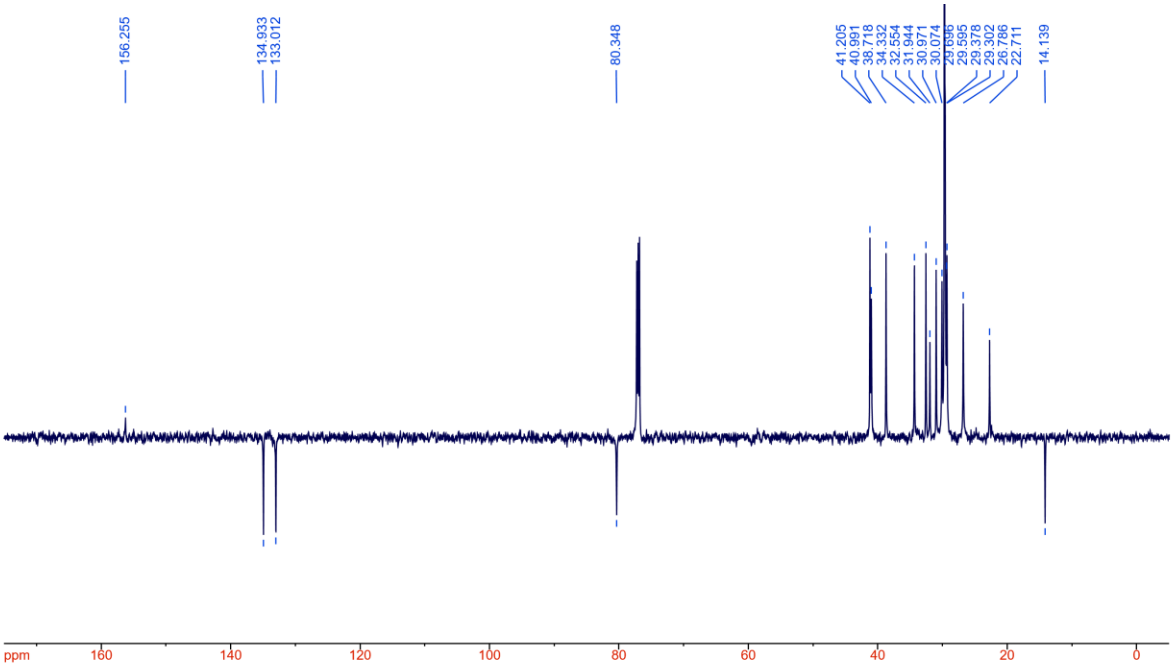

Figure 4.19. DEPTq spectrum of **P2** in $CDCl_3$.

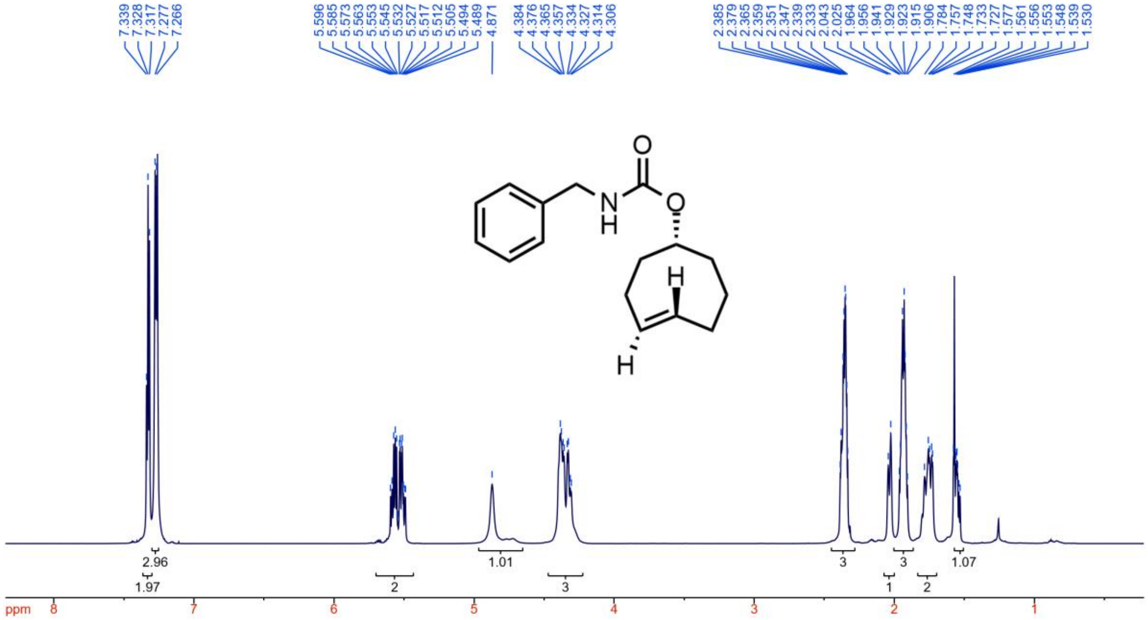

Figure 4.20. ^{1}H-NMR spectrum of **7b** in $CDCl_3$.

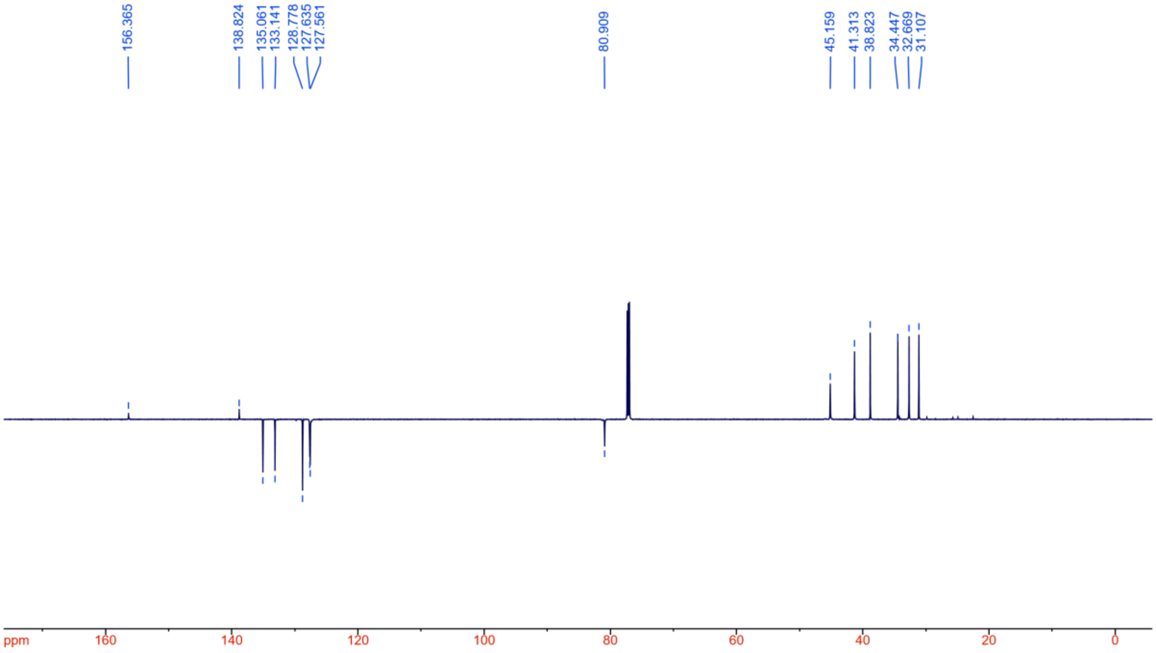

Figure 4.21. DEPTq spectrum of **7b** in $CDCl_3$.

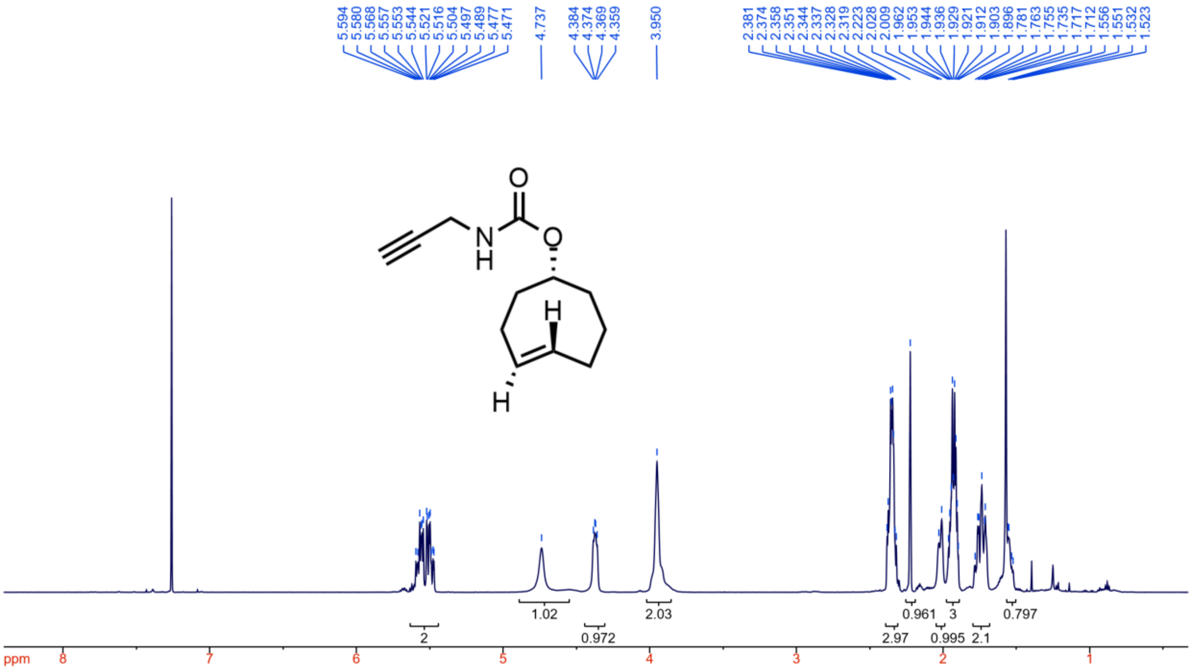

Figure 4.22. ^{1}H-NMR spectrum of **7c** in $CDCl_3$.

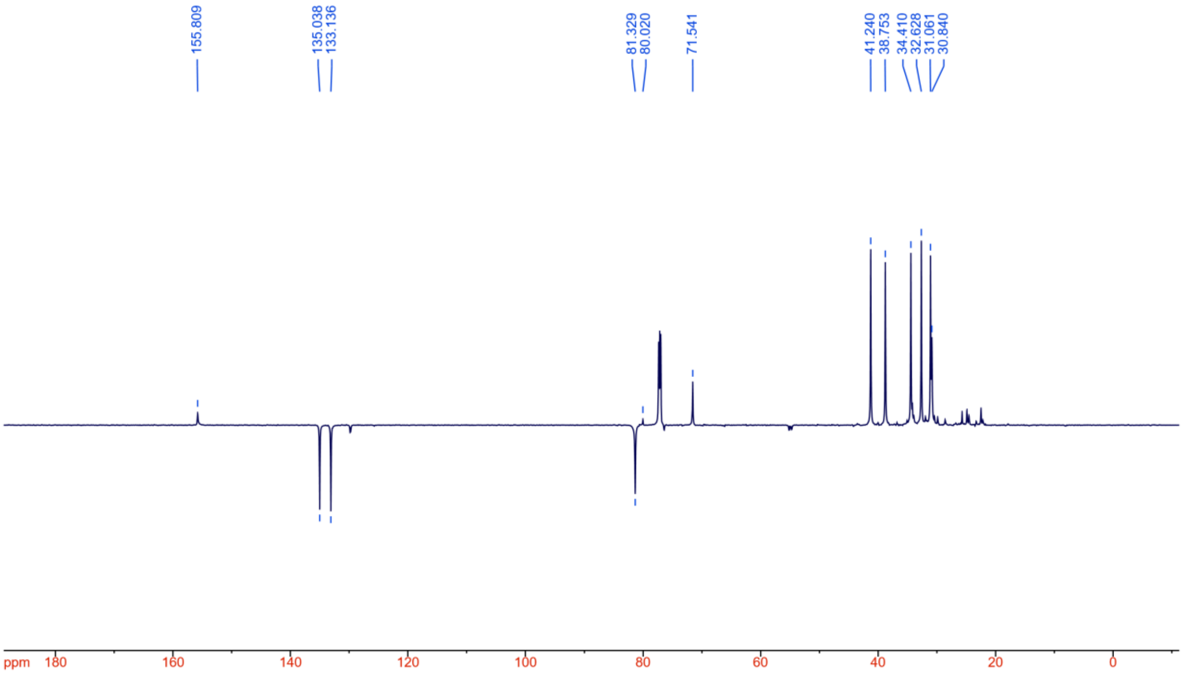

Figure 4.23. DEPTq spectrum of **7c** in $CDCl_3$.

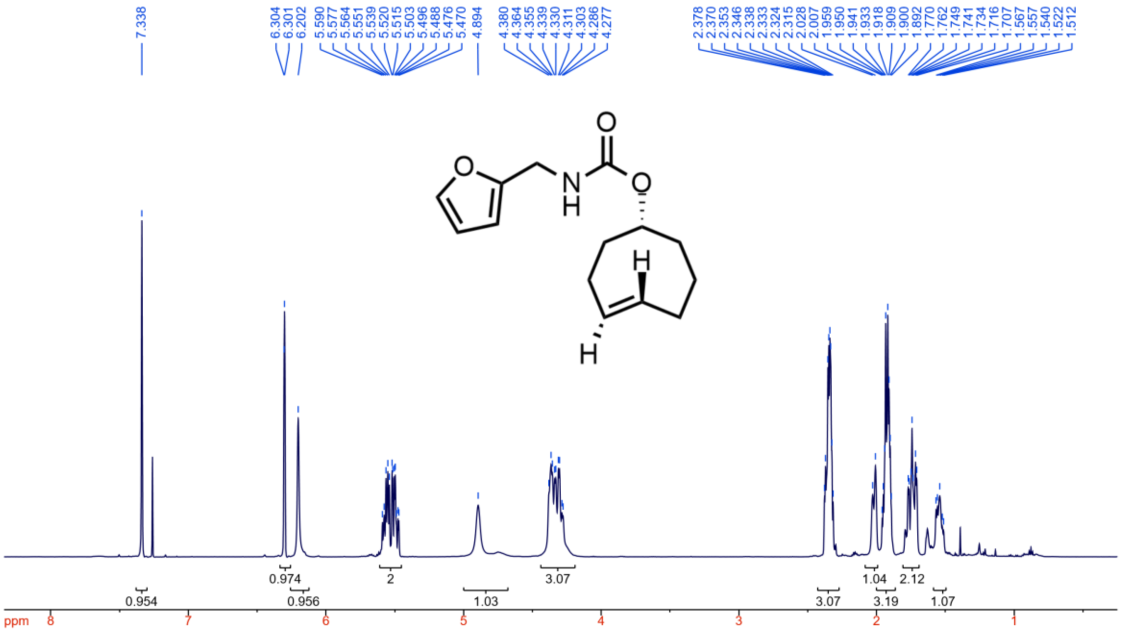

Figure 4.24. ^{1}H-NMR spectrum of **7d** in $CDCl_3$.

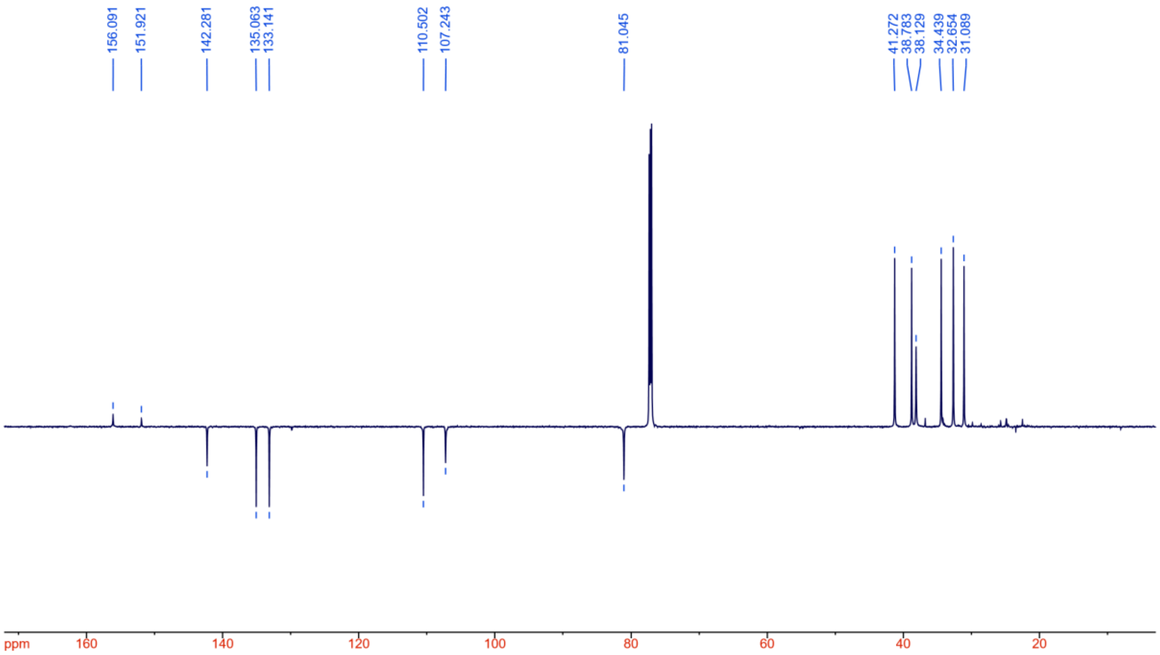

Figure 4.25. DEPTq spectrum of **7d** in $CDCl_3$.

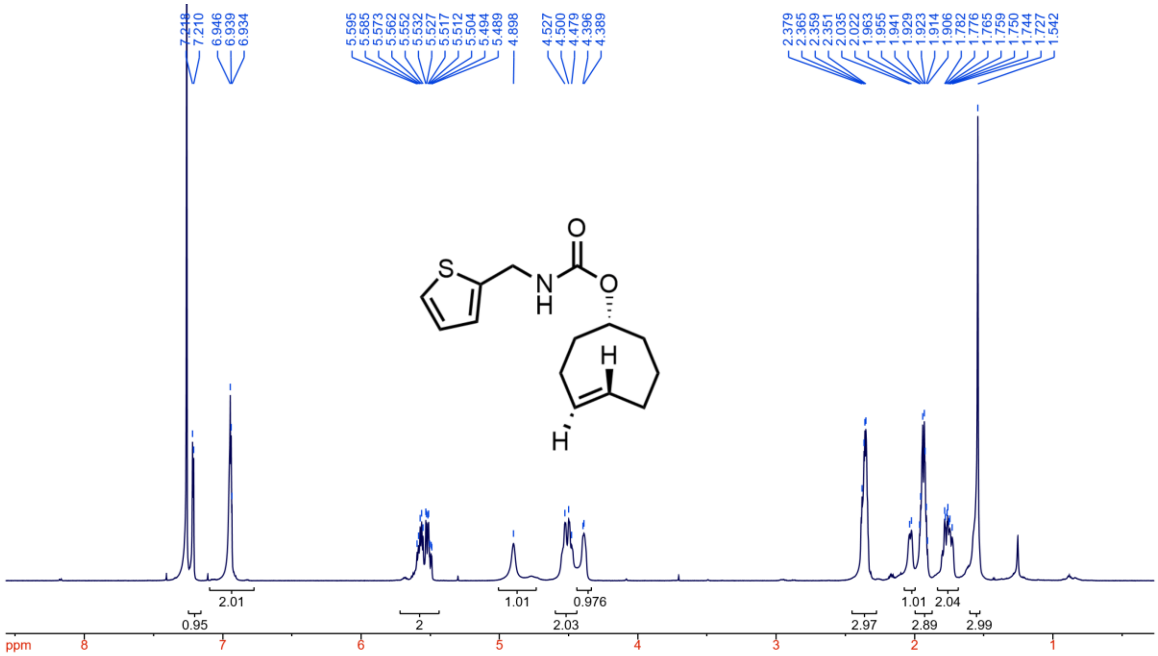

Figure 4.26. ^{1}H-NMR spectrum of **7e** in $CDCl_3$.

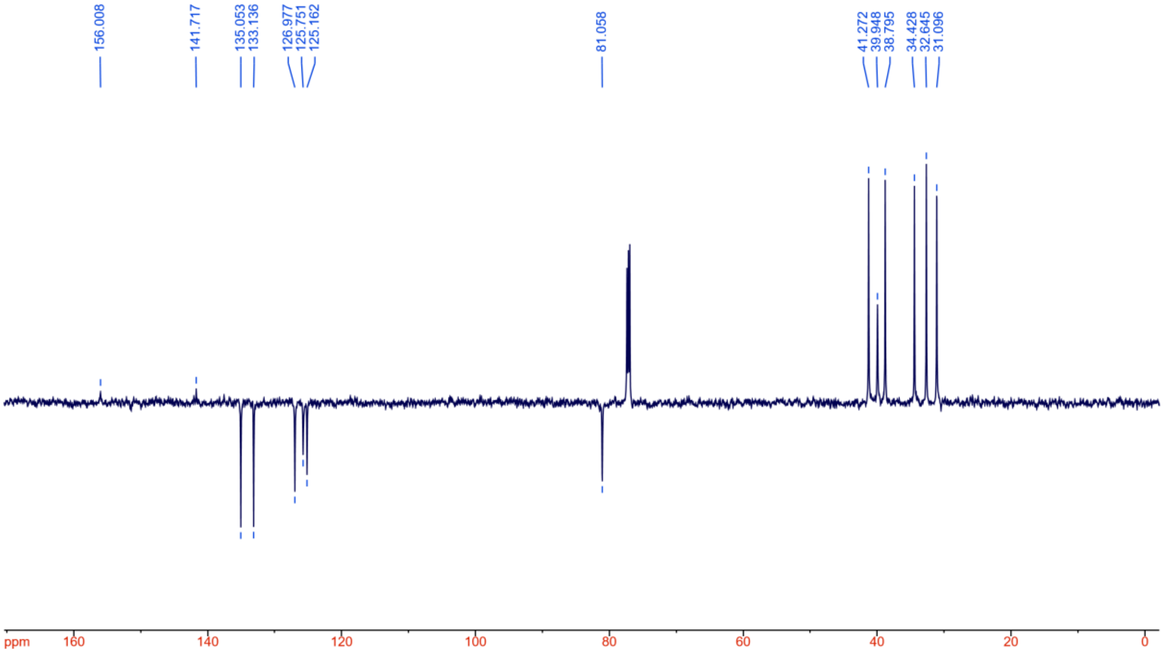

Figure 4.27. DEPTq spectrum of **7e** in $CDCl_3$.

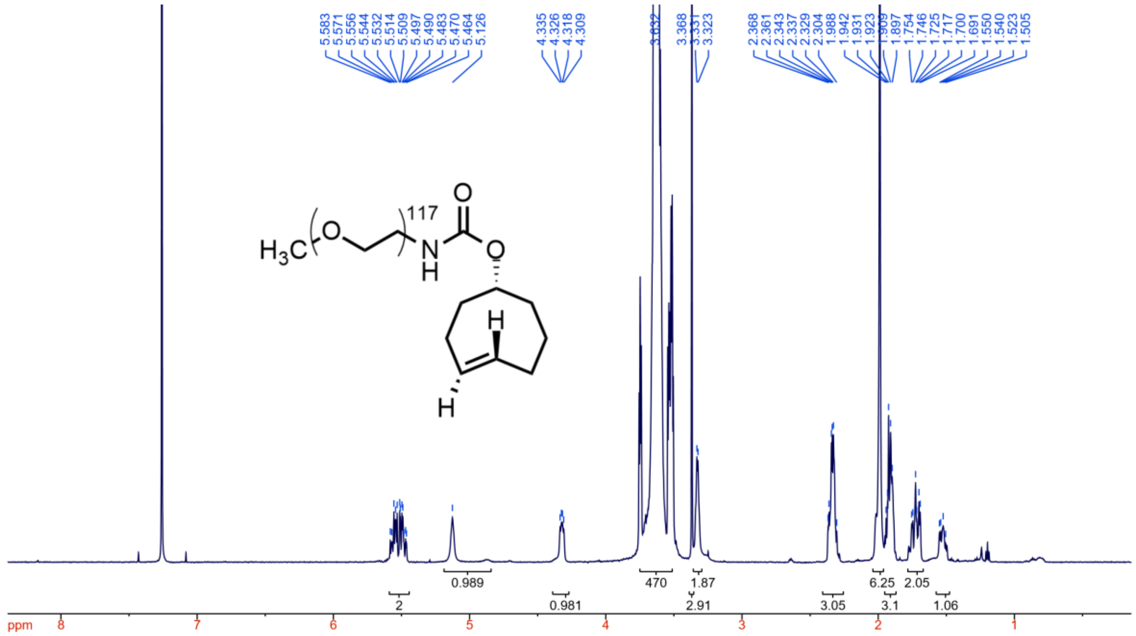

Figure 4.28. ^{1}H-NMR spectrum of **7f** in $CDCl_3$.

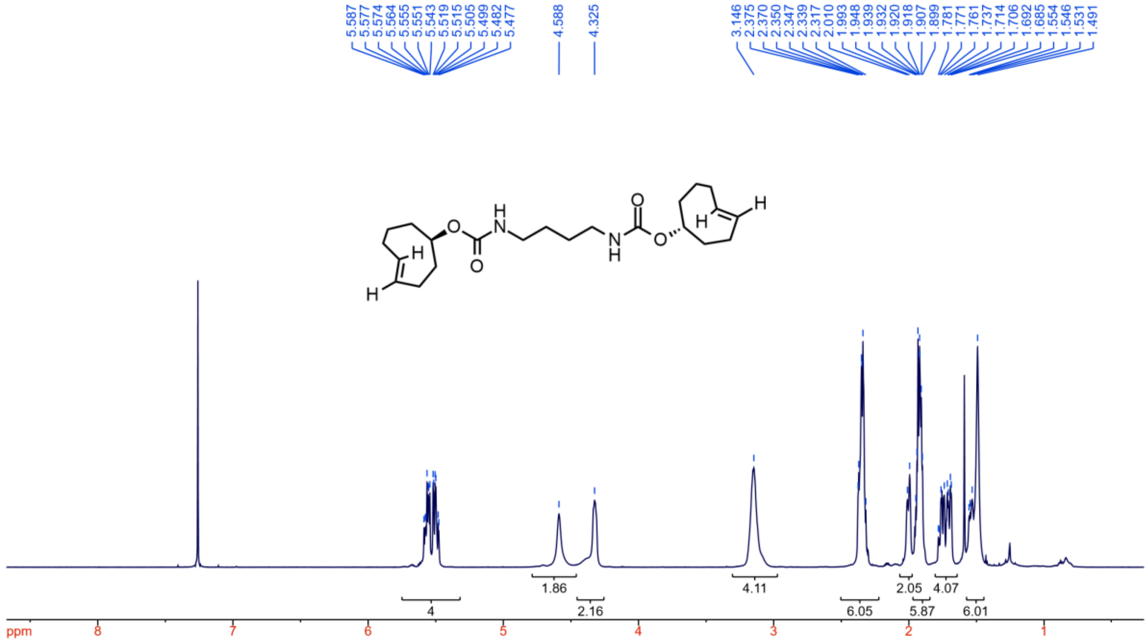

Figure 4.29. ^{1}H-NMR spectrum of **8** in $CDCl_3$.

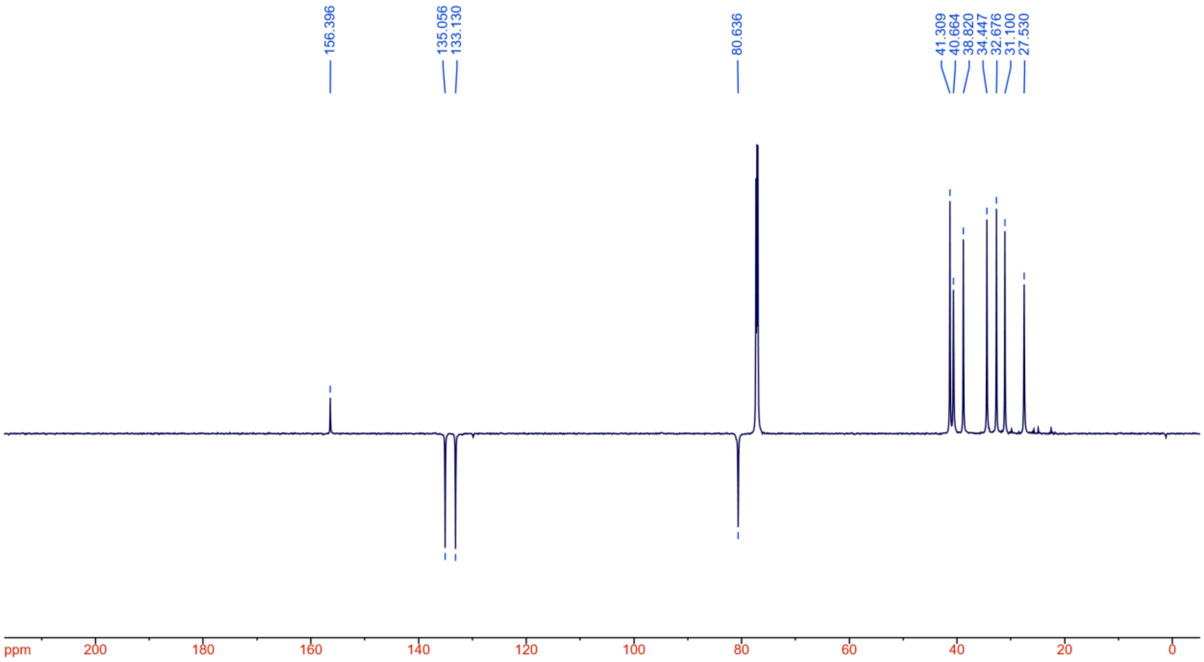

Figure 4.30. DEPTq spectrum of **8** in $CDCl_3$.

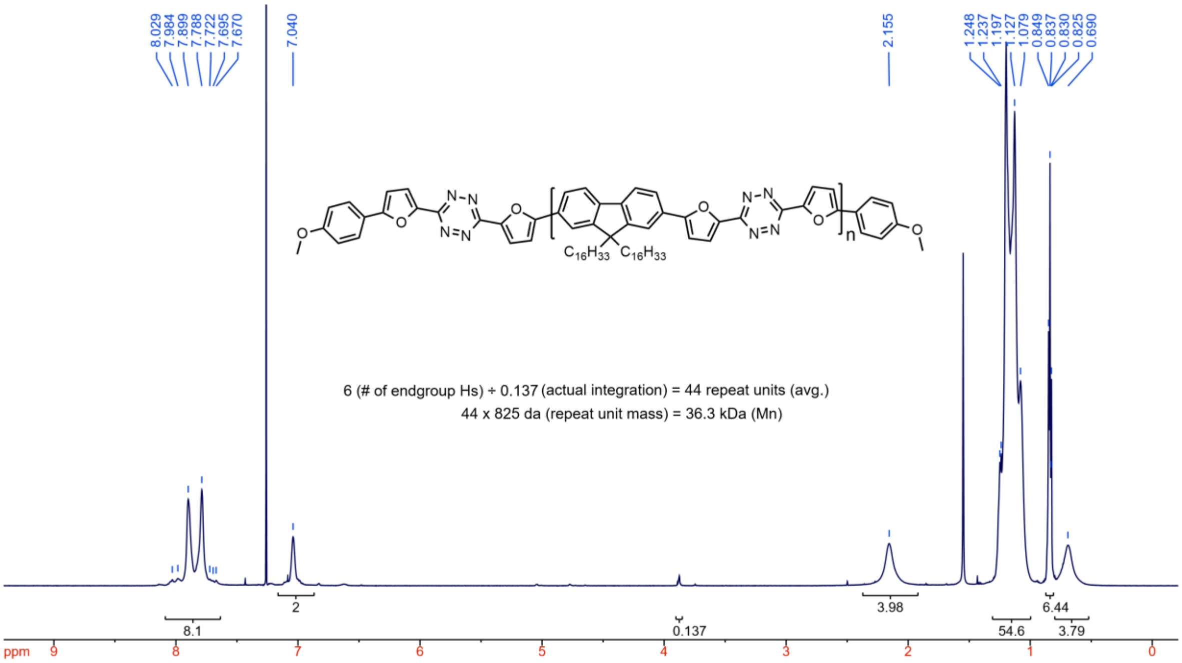

6 (# of endgroup Hs) ÷ 0.137 (actual integration) = 44 repeat units (avg.)

44 x 825 da (repeat unit mass) = 36.3 kDa (Mn)

Figure 4.31. ^{1}H-NMR spectrum of **P1** in $CDCl_3$.

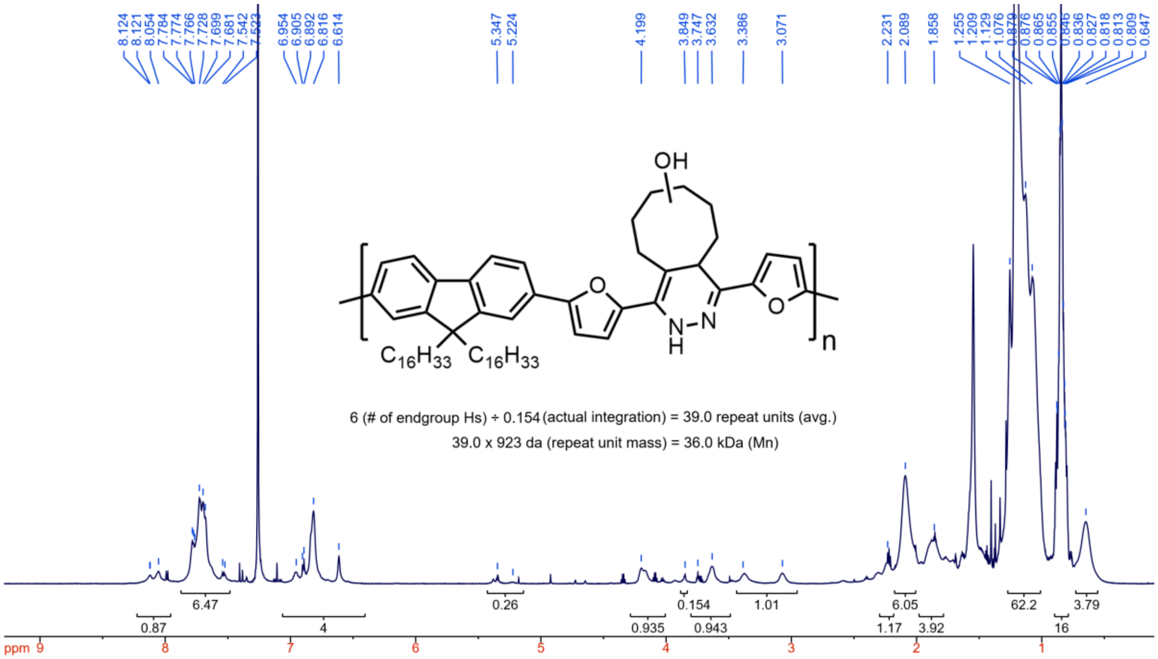

6 (# of endgroup Hs) ÷ 0.154 (actual integration) = 39.0 repeat units (avg.)
39.0 x 923 da (repeat unit mass) = 36.0 kDa (Mn)

Figure 4.32. ^{1}H-NMR spectrum of **P2** in $CDCl_3$.

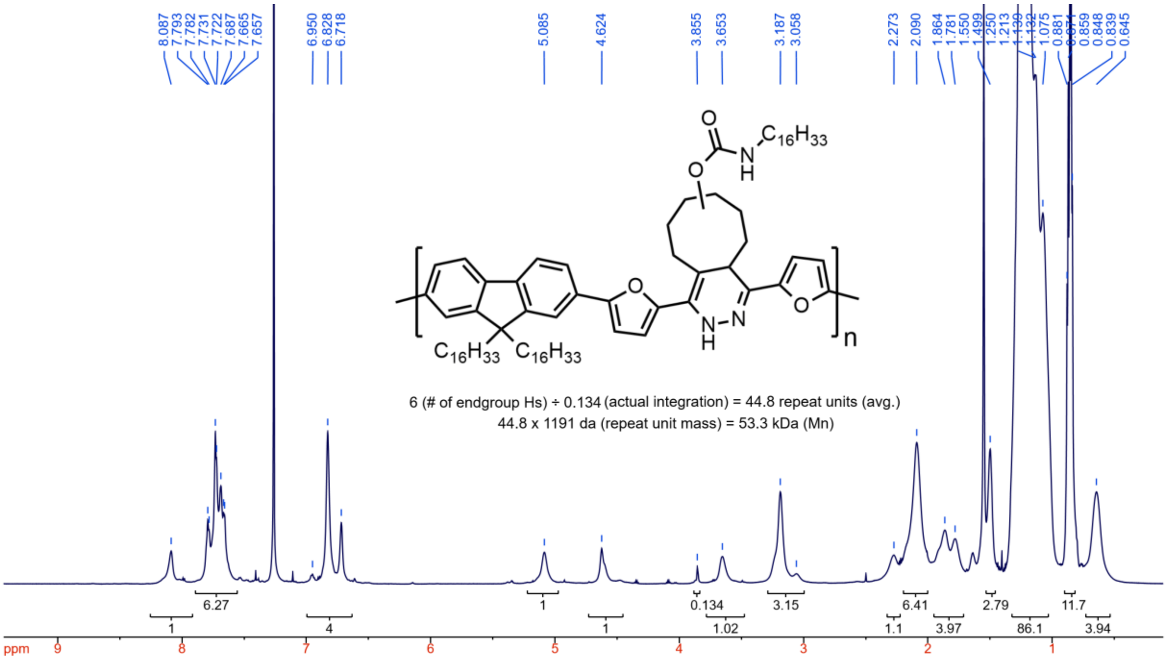

6 (# of endgroup Hs) ÷ 0.134 (actual integration) = 44.8 repeat units (avg.)
44.8 x 1191 da (repeat unit mass) = 53.3 kDa (Mn)

Figure 4.33. ^{1}H-NMR spectrum of **P2a** in $CDCl_3$.

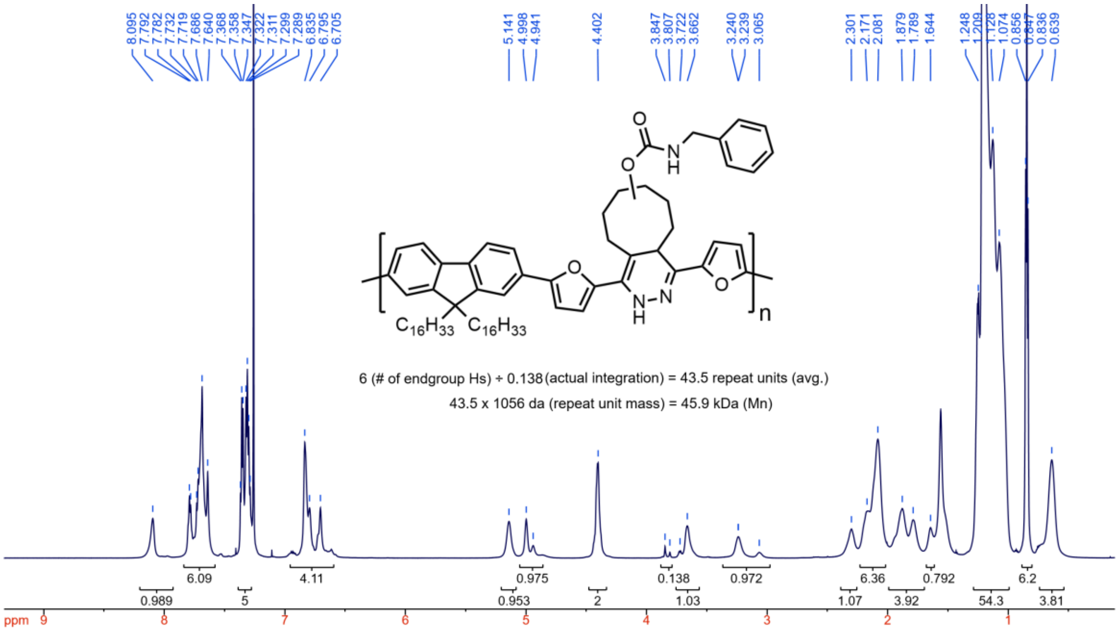

Figure 4.34. ^{1}H-NMR spectrum of **P2b** in $CDCl_3$.

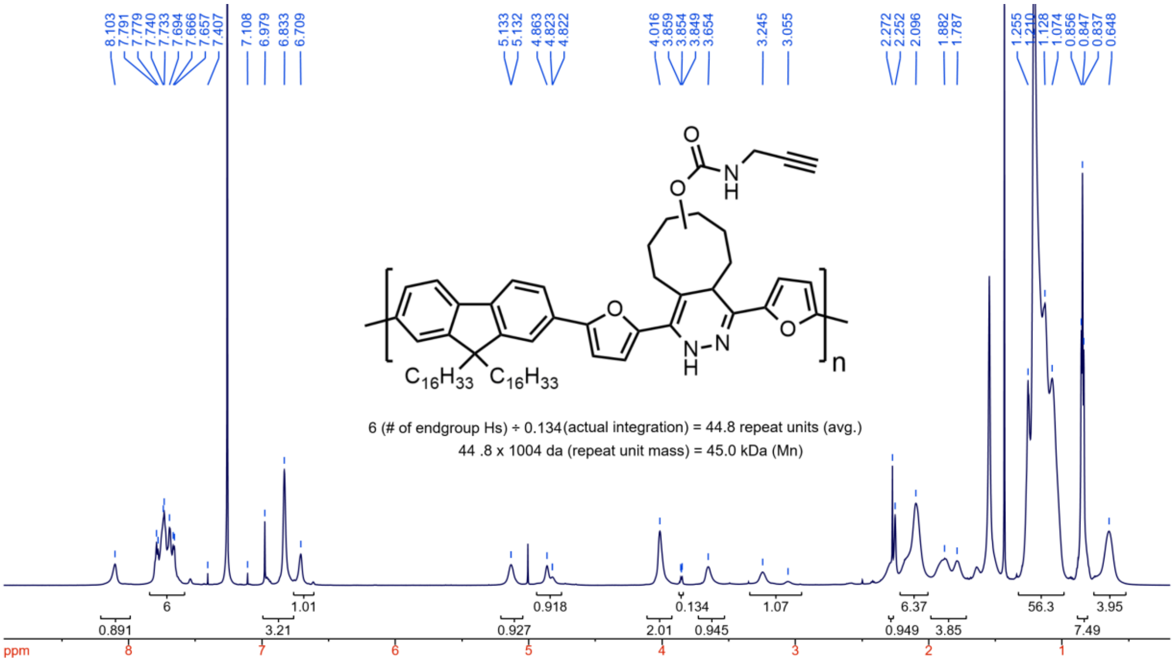

Figure 4.35. ^{1}H-NMR spectrum of **P2c** in $CDCl_3$.

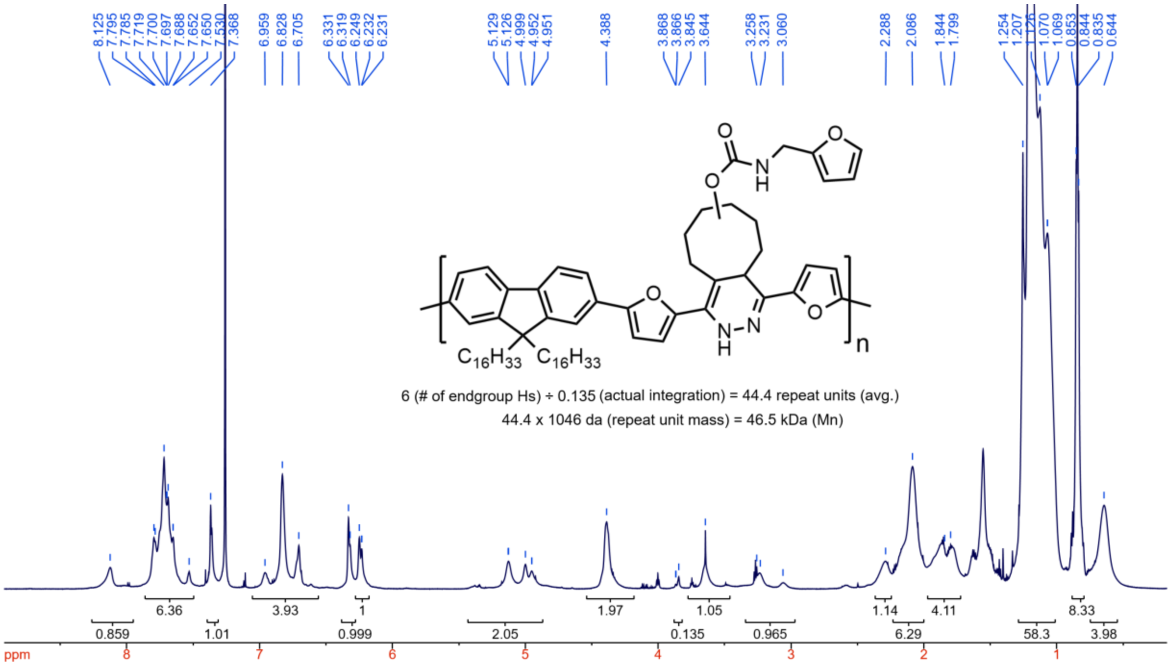

6 (# of endgroup Hs) ÷ 0.135 (actual integration) = 44.4 repeat units (avg.)
44.4 x 1046 da (repeat unit mass) = 46.5 kDa (Mn)

Figure 4.36. ^{1}H-NMR spectrum of **P2d** in $CDCl_3$.

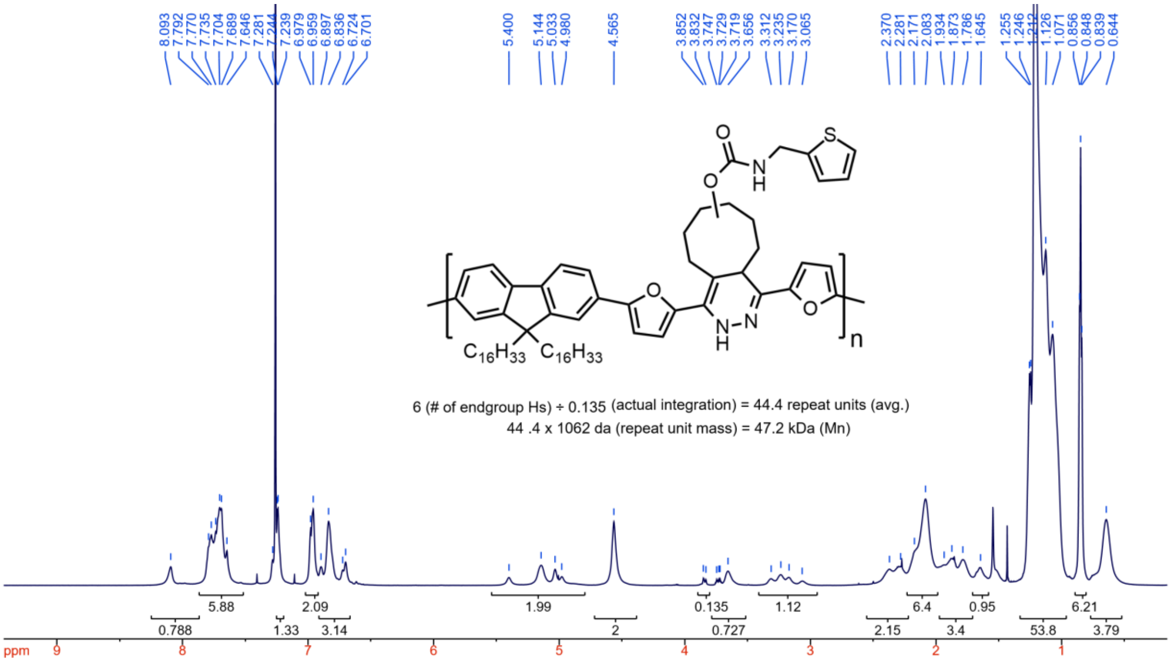

6 (# of endgroup Hs) ÷ 0.135 (actual integration) = 44.4 repeat units (avg.)
44 .4 x 1062 da (repeat unit mass) = 47.2 kDa (Mn)

Figure 4.37. ^{1}H-NMR spectrum of **P2e** in $CDCl_3$.

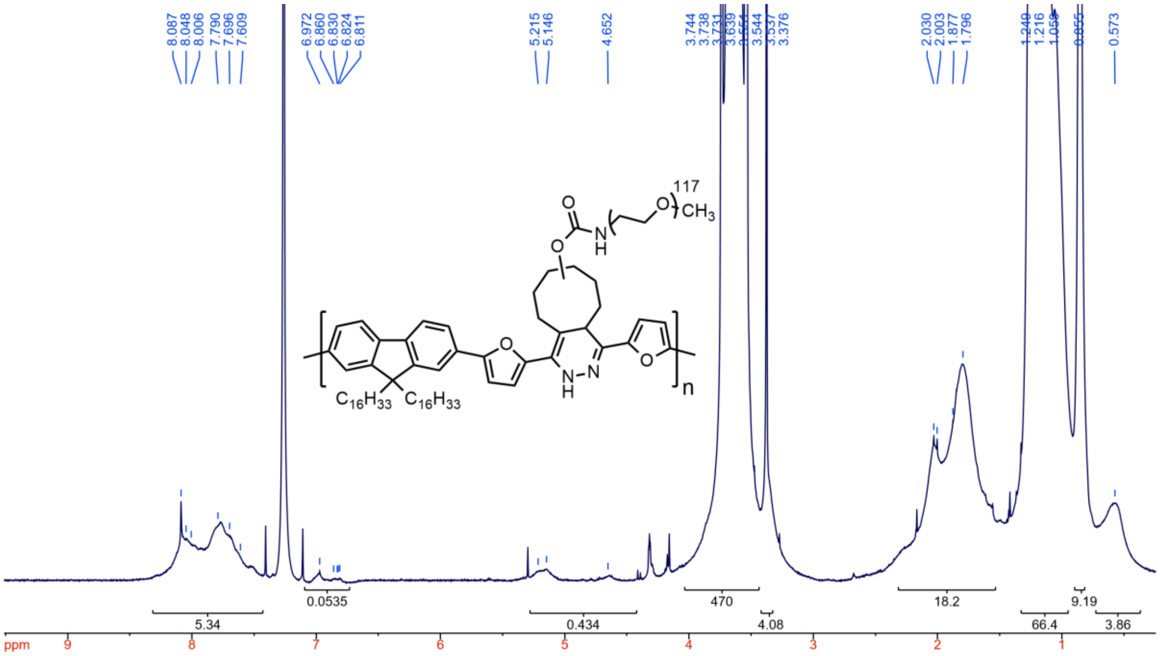

Figure 4.38. ^{1}H-NMR spectrum of **P2f** in $CDCl_3$.

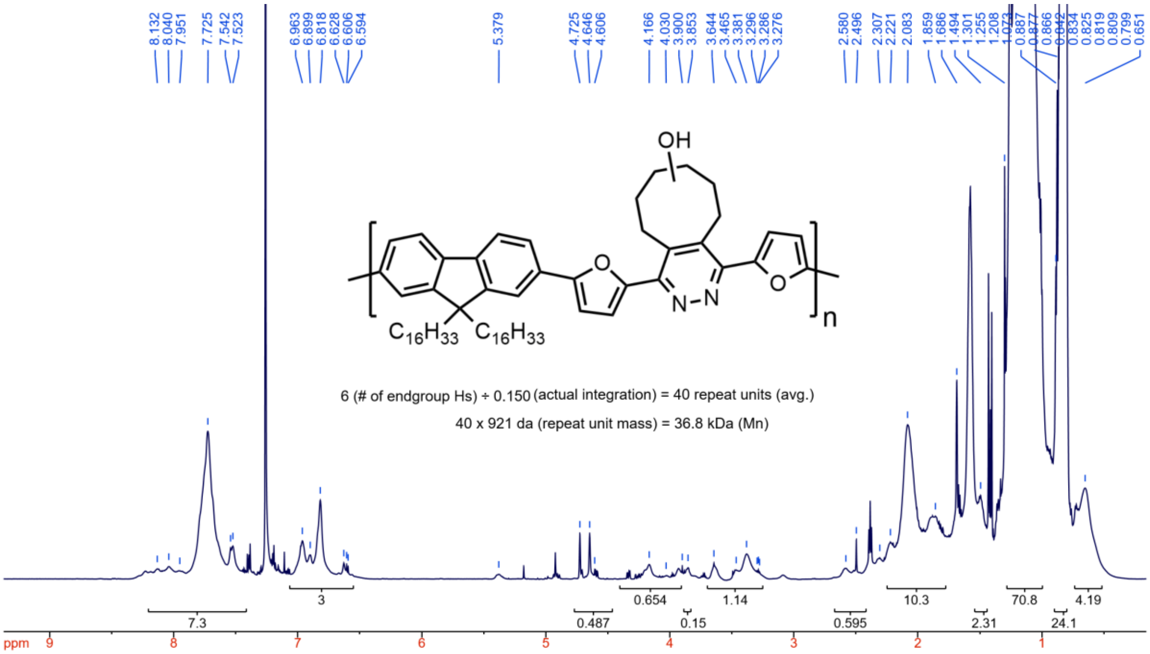

6 (# of endgroup Hs) ÷ 0.150 (actual integration) = 40 repeat units (avg.)

40 x 921 da (repeat unit mass) = 36.8 kDa (Mn)

Figure 4.39. ^{1}H-NMR spectrum of **P3** in $CDCl_3$.

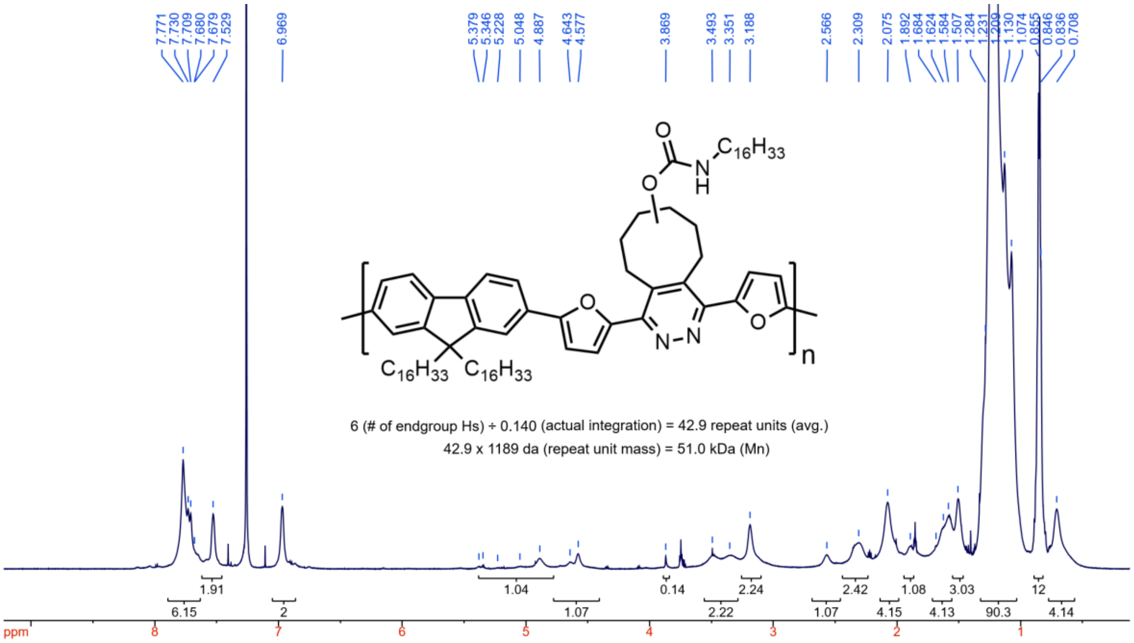

6 (# of endgroup Hs) ÷ 0.140 (actual integration) = 42.9 repeat units (avg.)
42.9 x 1189 da (repeat unit mass) = 51.0 kDa (Mn)

Figure 4.40. ^{1}H-NMR spectrum of **P3a** in $CDCl_3$.

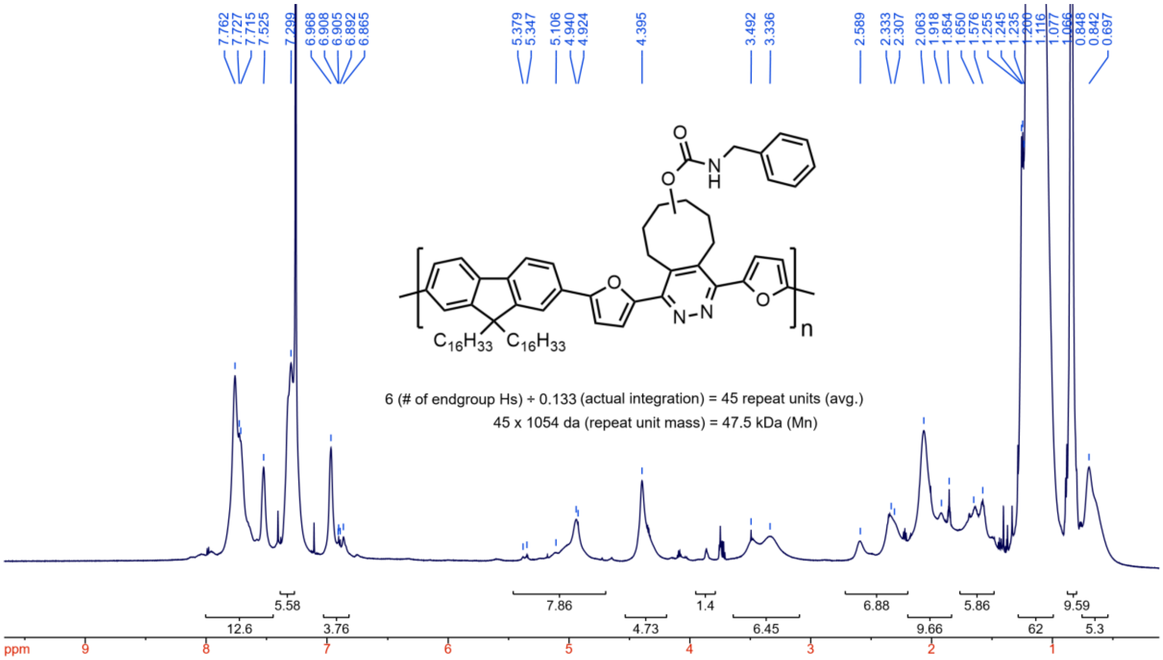

6 (# of endgroup Hs) ÷ 0.133 (actual integration) = 45 repeat units (avg.)
45 x 1054 da (repeat unit mass) = 47.5 kDa (Mn)

Figure 4.41. ^{1}H-NMR spectrum of **P3b** in $CDCl_3$.

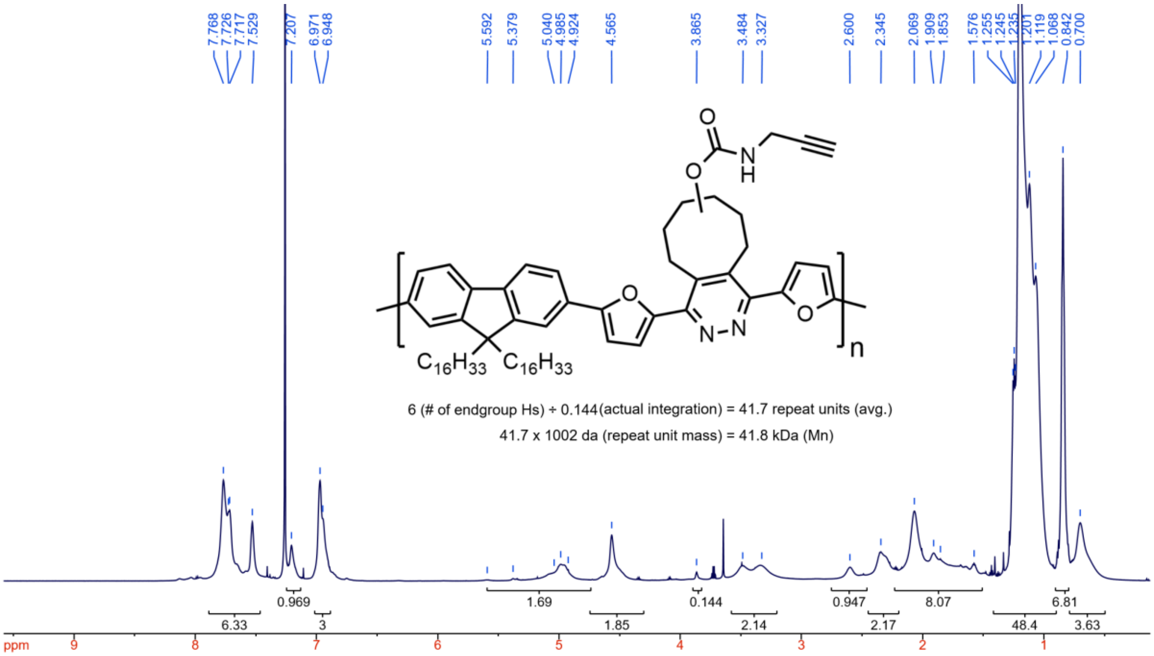

6 (# of endgroup Hs) ÷ 0.144(actual integration) = 41.7 repeat units (avg.)

41.7 x 1002 da (repeat unit mass) = 41.8 kDa (Mn)

Figure 4.42. ^{1}H-NMR spectrum of **P3c** in $CDCl_3$.

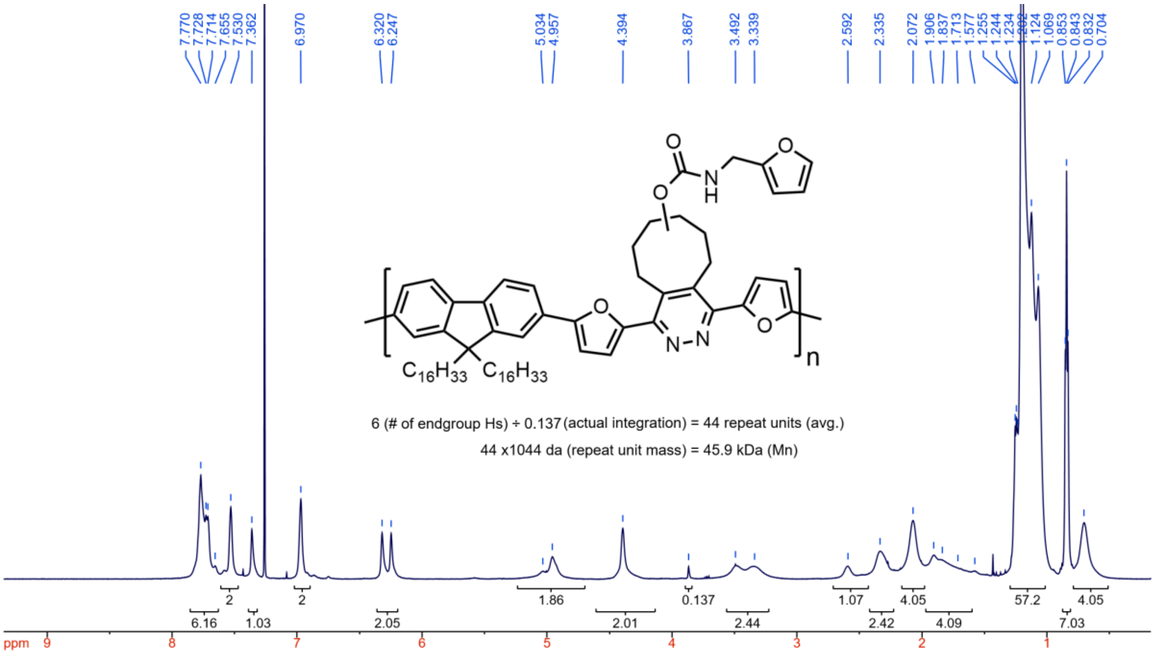

6 (# of endgroup Hs) ÷ 0.137(actual integration) = 44 repeat units (avg.)

44 x1044 da (repeat unit mass) = 45.9 kDa (Mn)

Figure 4.43. ^{1}H-NMR spectrum of **P3d** in $CDCl_3$.

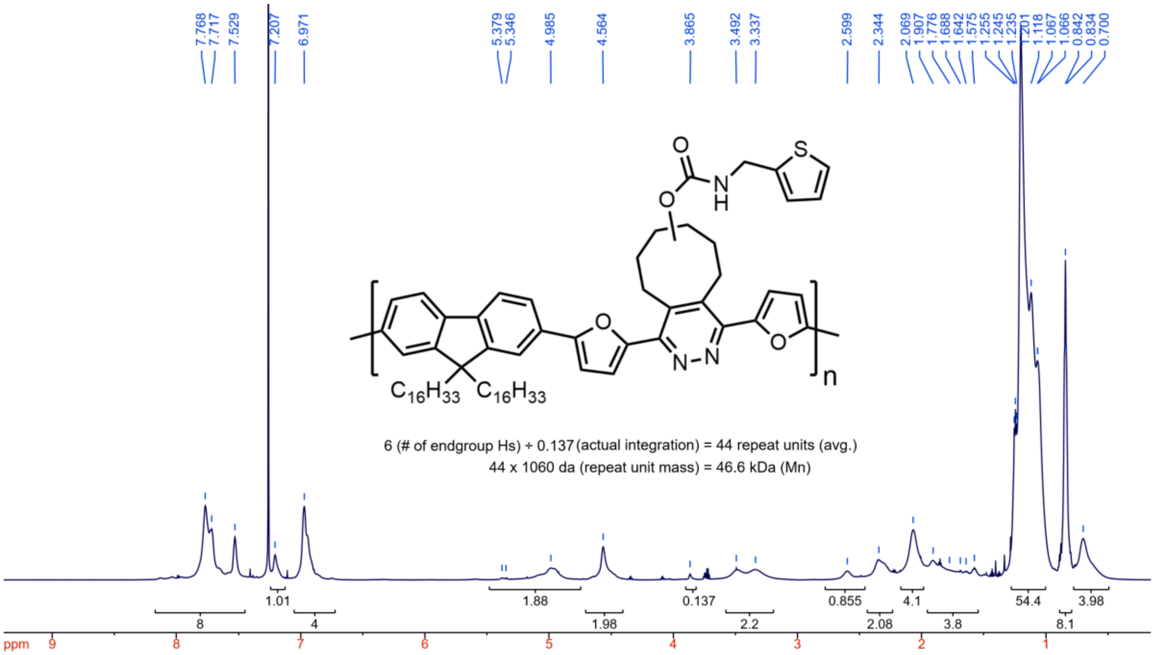

6 (# of endgroup Hs) ÷ 0.137 (actual integration) = 44 repeat units (avg.)
44 x 1060 da (repeat unit mass) = 46.6 kDa (Mn)

Figure 4.44. ^{1}H-NMR spectrum of **P3e** in $CDCl_3$.

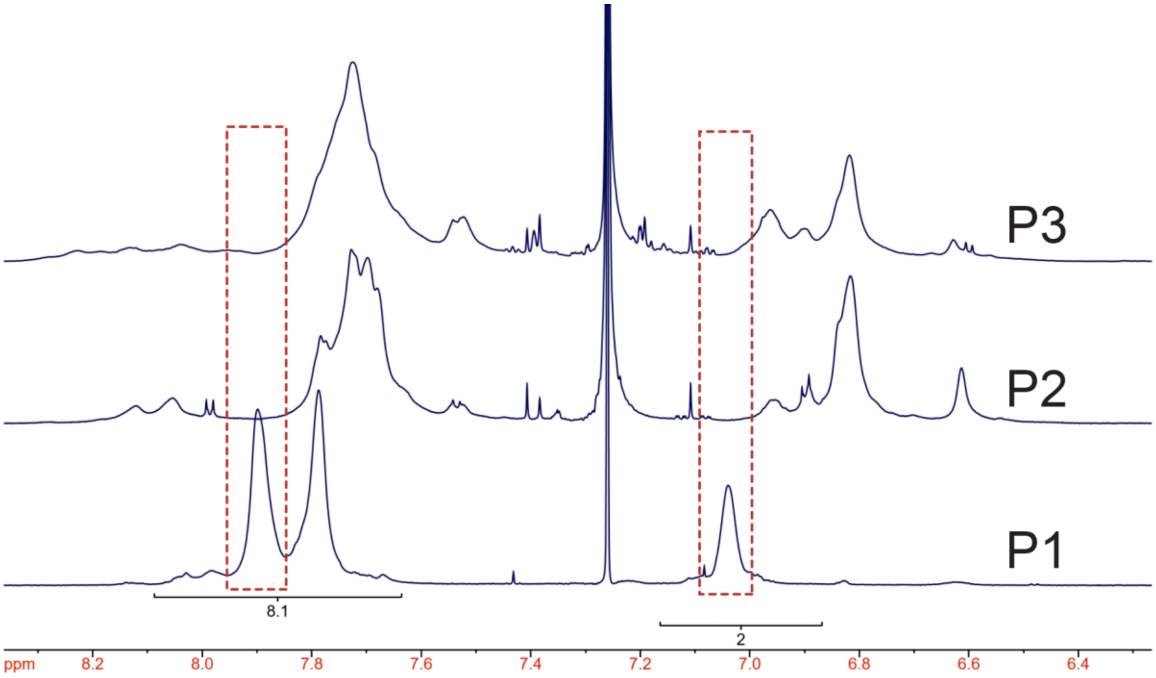

Figure 4.45. ^{1}H-NMR overlay of **P1**, **P2**, and **P3** in $CDCl_3$.

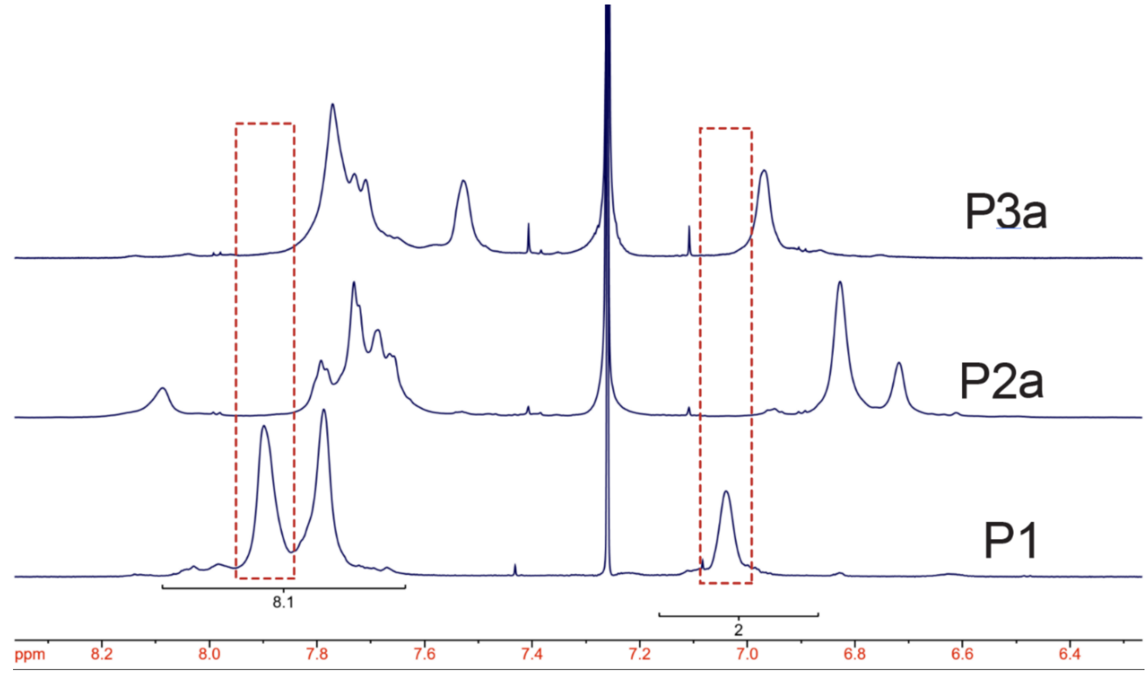

Figure 4.46. ^{1}H-NMR overlay of **P1**, **P2a**, and **P3a** in $CDCl_3$.

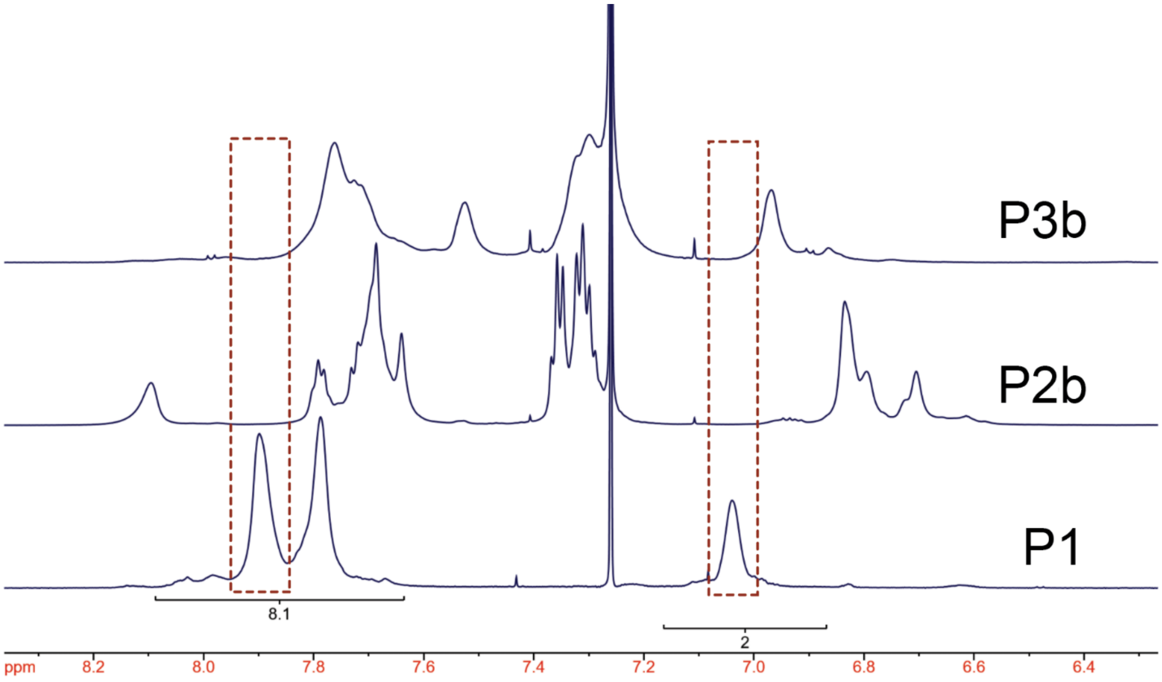

Figure 4.47. ^{1}H-NMR overlay of **P1, P2b**, and **P3b** in $CDCl_3$.

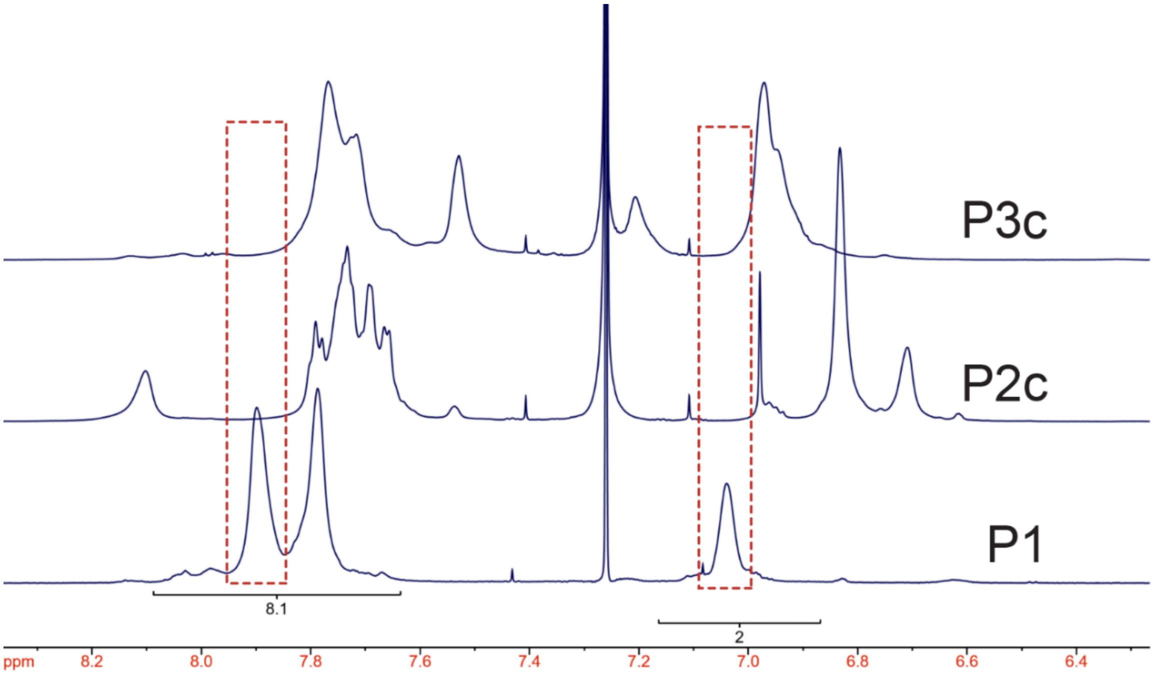

Figure 4.48. ^{1}H-NMR overlay of **P1**, **P2c**, and **P3c** in $CDCl_3$.

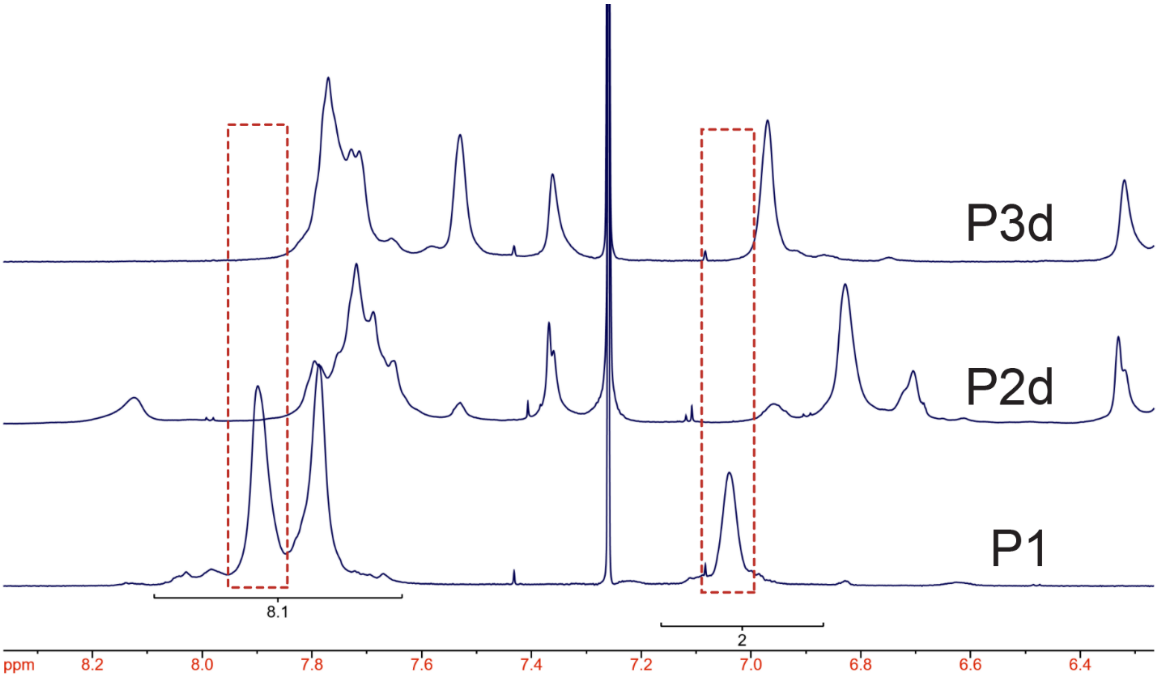

Figure 4.49. ^{1}H-NMR overlay of **P1**, **P2d**, and **P3d** in $CDCl_3$.

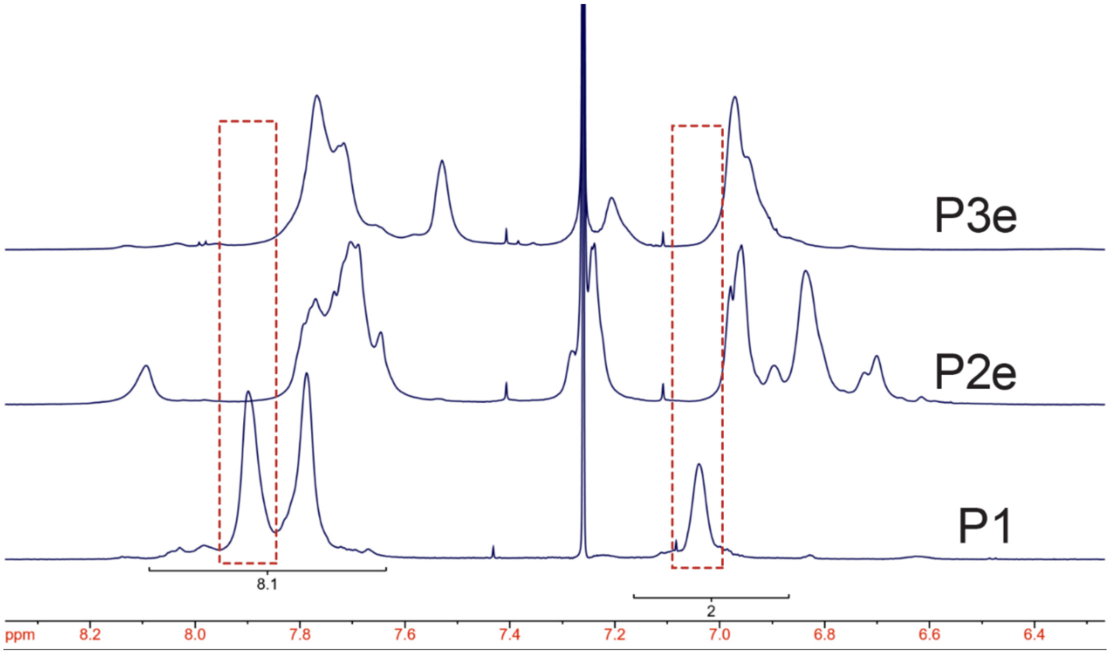

Figure 4.50. ^{1}H-NMR overlay of **P1**, **P2e**, and **P3e** in CDCl$_3$.

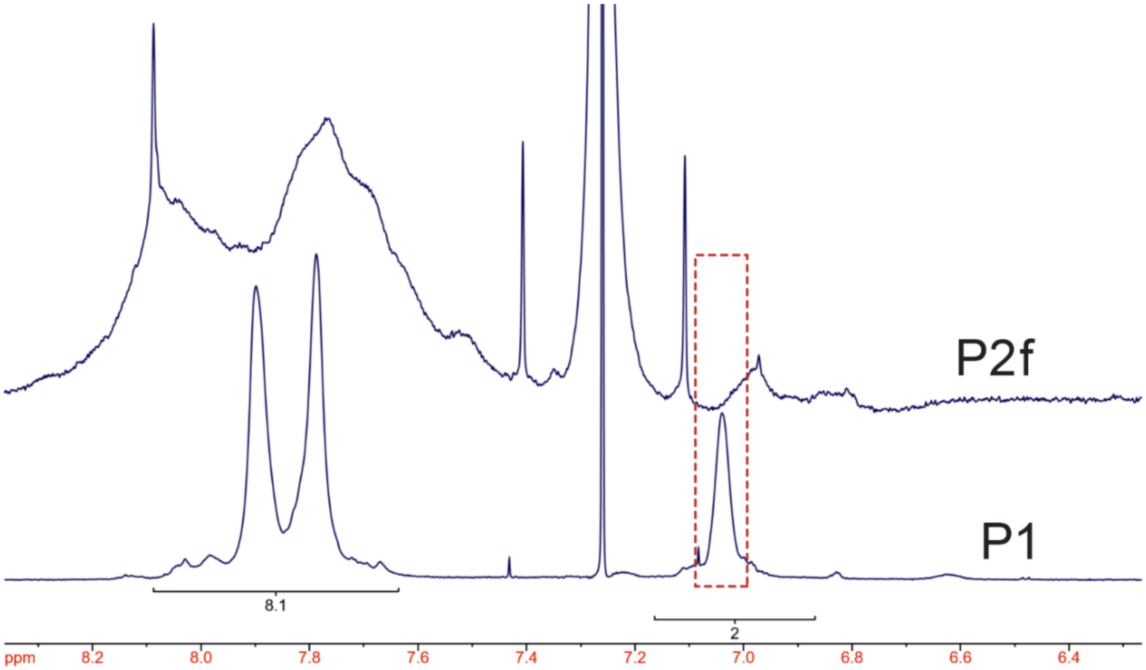

Figure 4.51. ^{1}H-NMR overlay of **P1** and **P2f** in CDCl$_3$.

4.4.7. UV-Vis Spectra

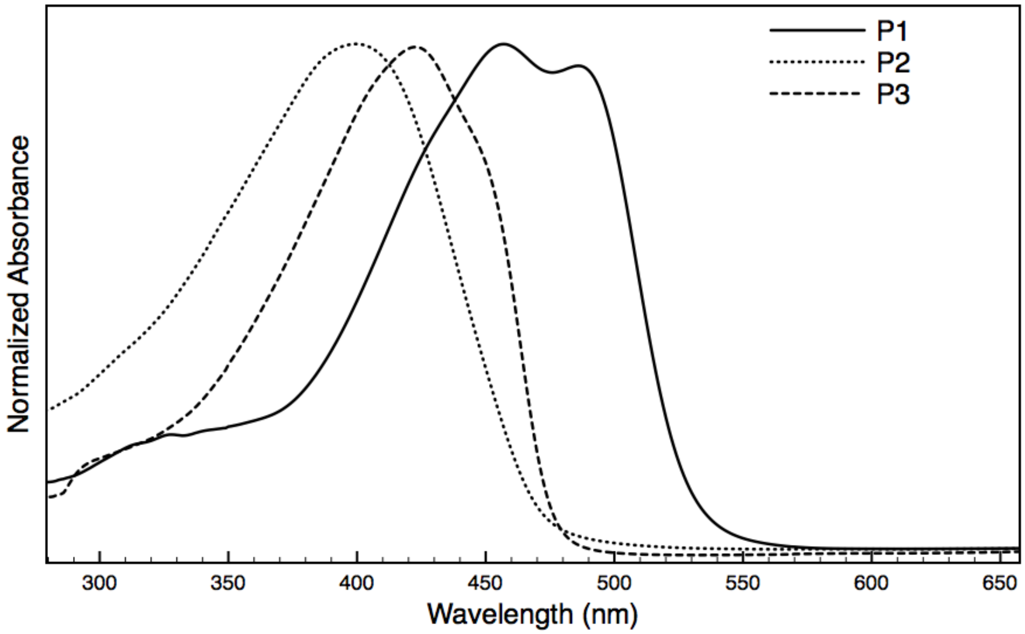

Figure 4.52. UV-Vis spectrum overlay of **P1**, **P2**, and **P3** in THF.

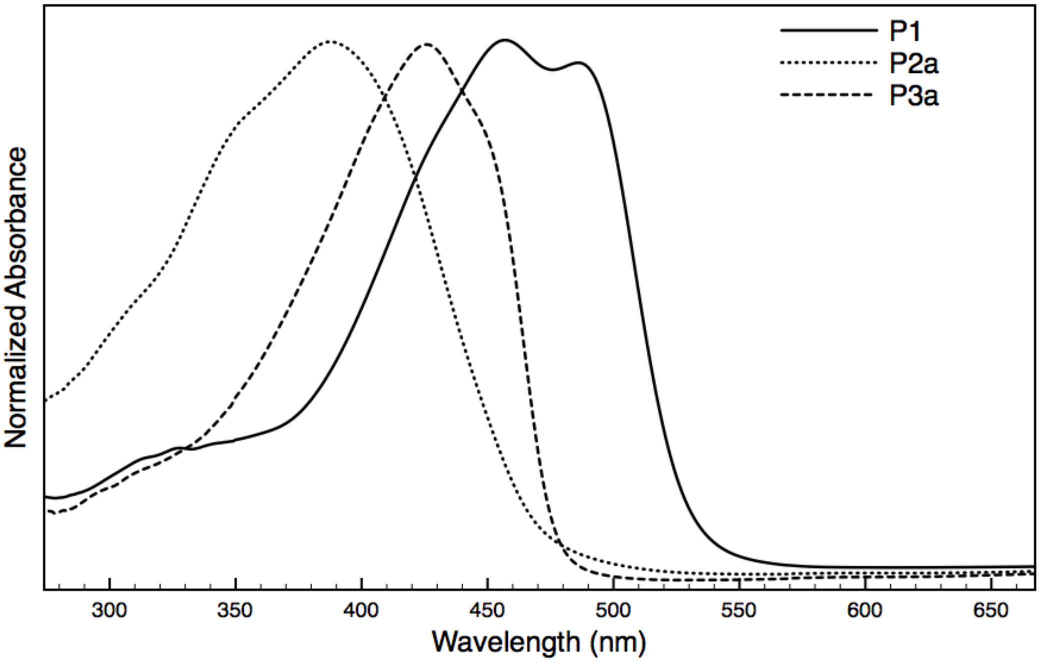

Figure 4.53. UV-Vis spectrum overlay of **P1**, **P2a**, and **P3a** in THF.

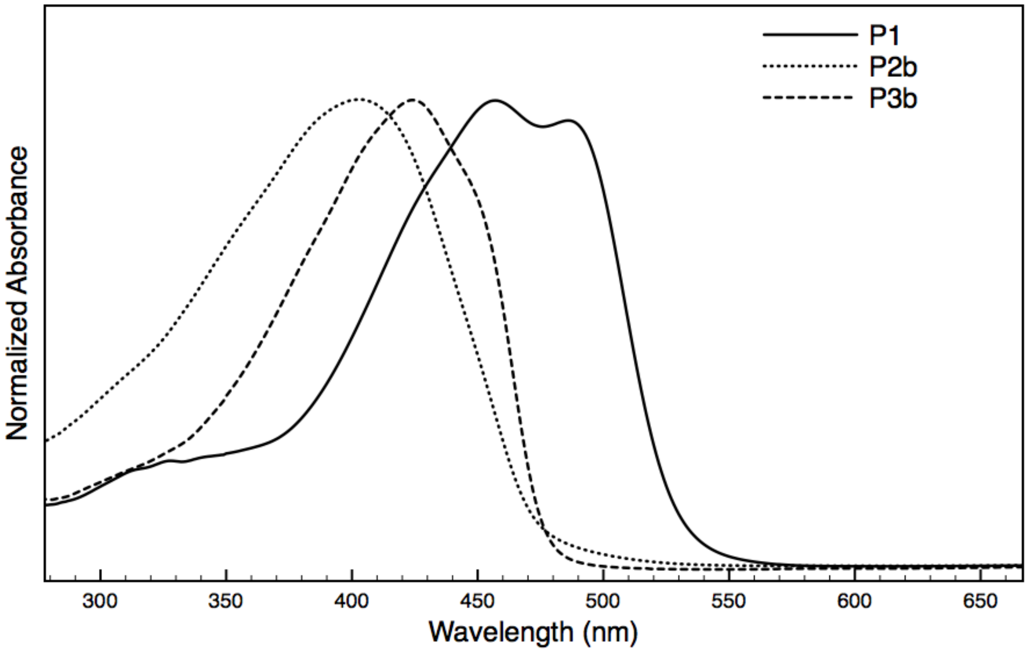

Figure 4.54. UV-Vis spectrum overlay of **P1**, **P2b**, and **P3b** in THF.

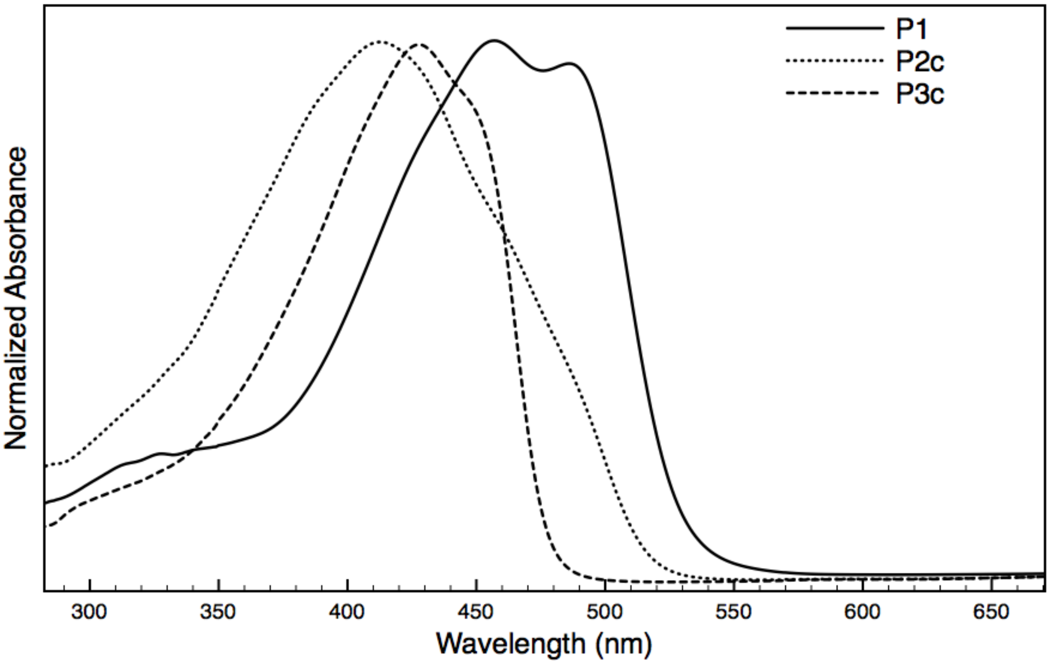

Figure 4.55. UV-Vis spectrum overlay of **P1**, **P2c**, and **P3c** in THF.

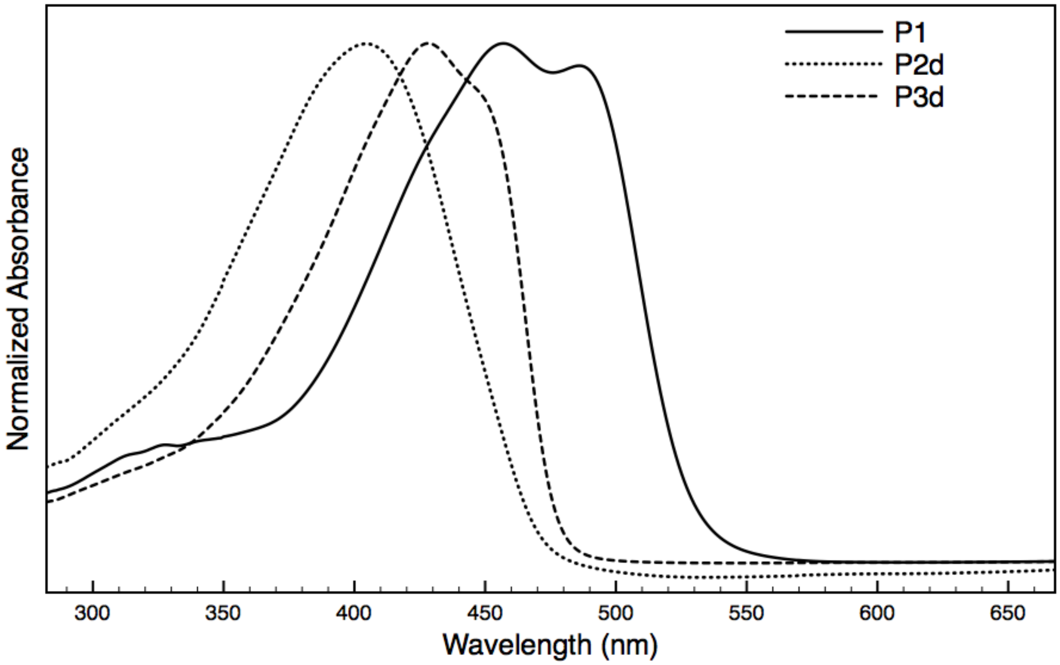

Figure 4.56. UV-Vis spectrum overlay of **P1**, **P2d**, and **P3d** in THF.

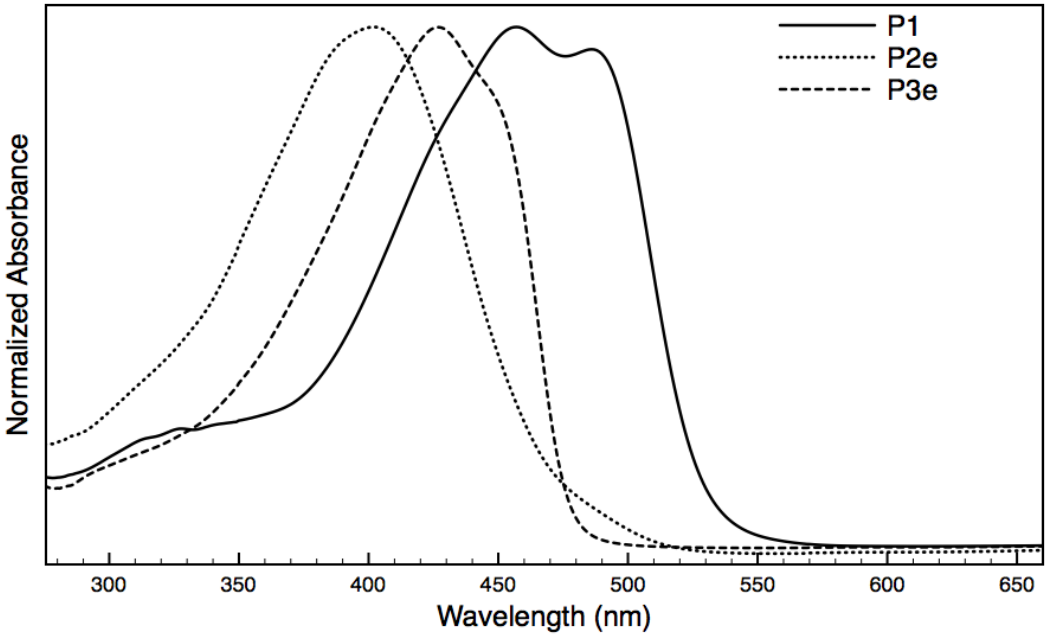

Figure 4.57. UV-Vis spectrum overlay of **P1**, **P2e**, and **P3e** in THF.

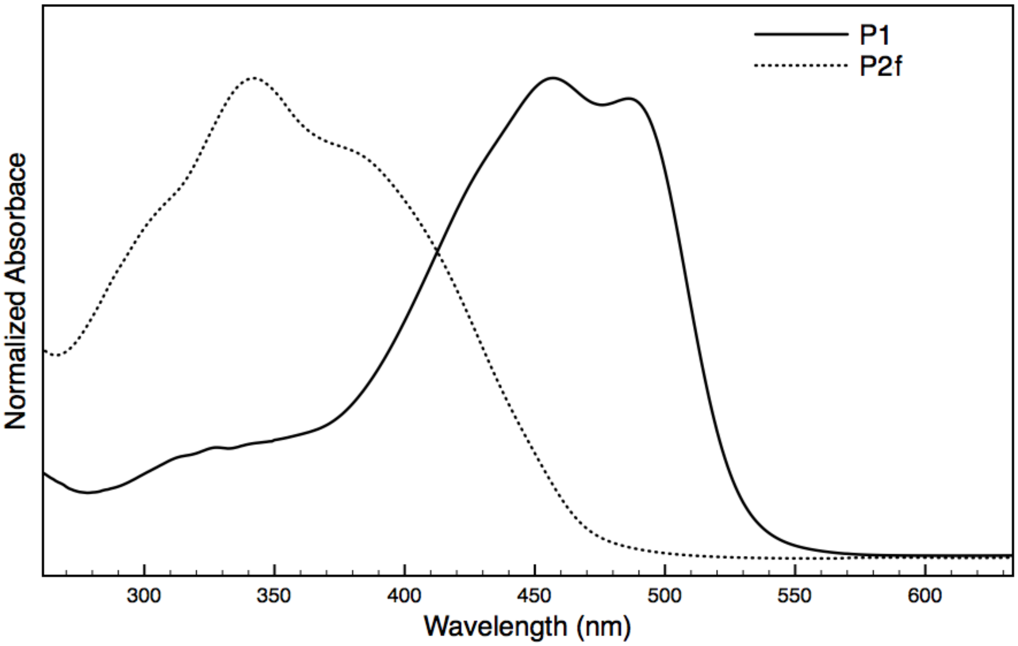

Figure 4.58. UV-Vis spectrum overlay of **P1**, and **P2f** in THF.

4.4.8. Fluorescence Spectra

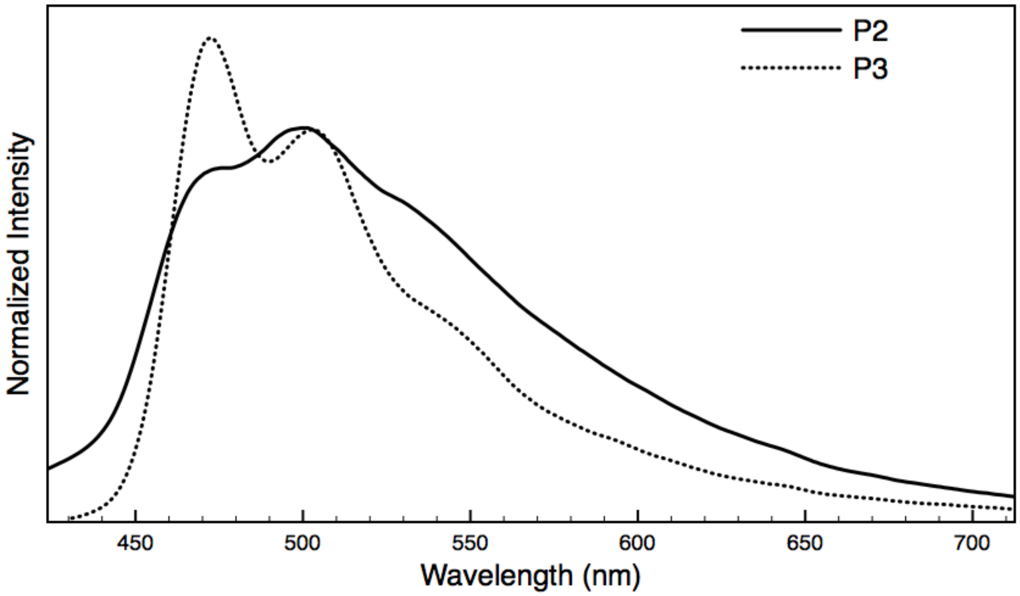

Figure 4.59. Fluorescence spectrum overlay of **P2** and **P3** in THF. Excitation at 400 nm and 420 nm, respectively.

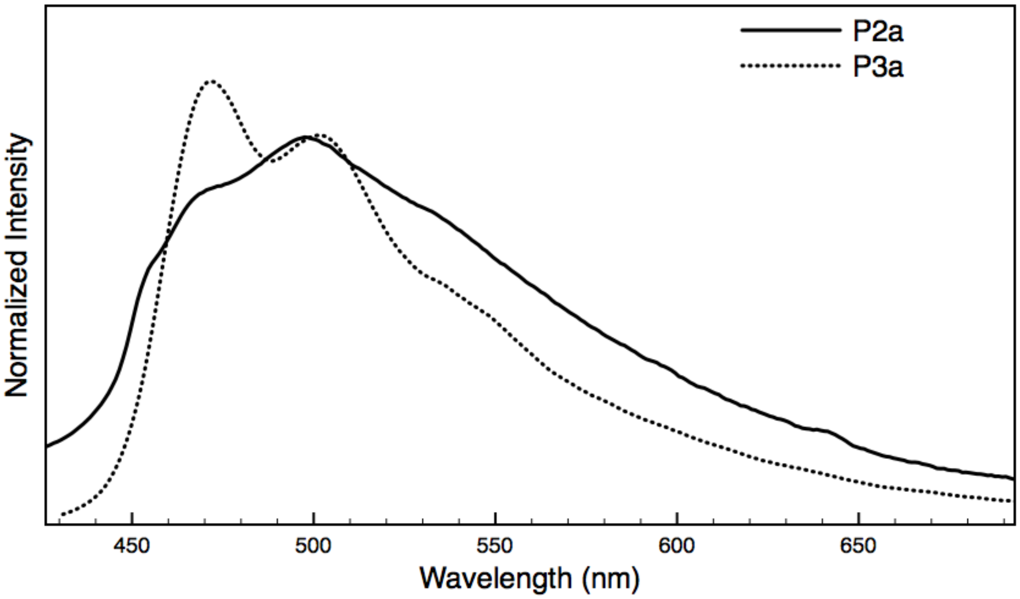

Figure 4.60. Fluorescence spectrum overlay of **P2a** and **P3a** in THF. Excitation at 400 nm and 420 nm, respectively.

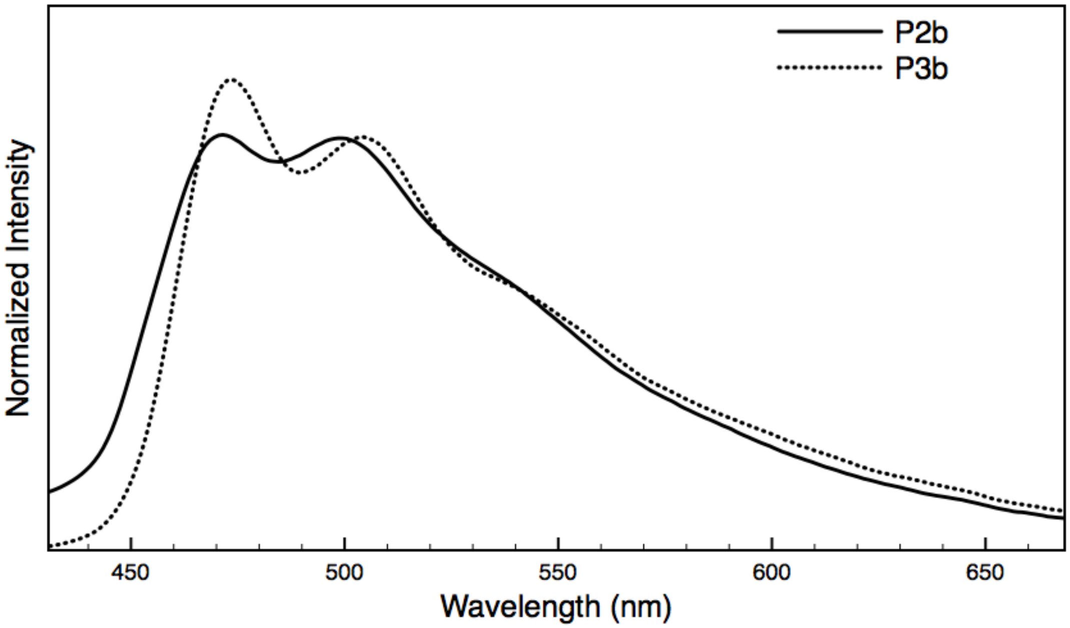

Figure 4.61. Fluorescence spectrum overlay of **P2b** and **P3b** in THF. Excitation at 400 nm and 420 nm, respectively.

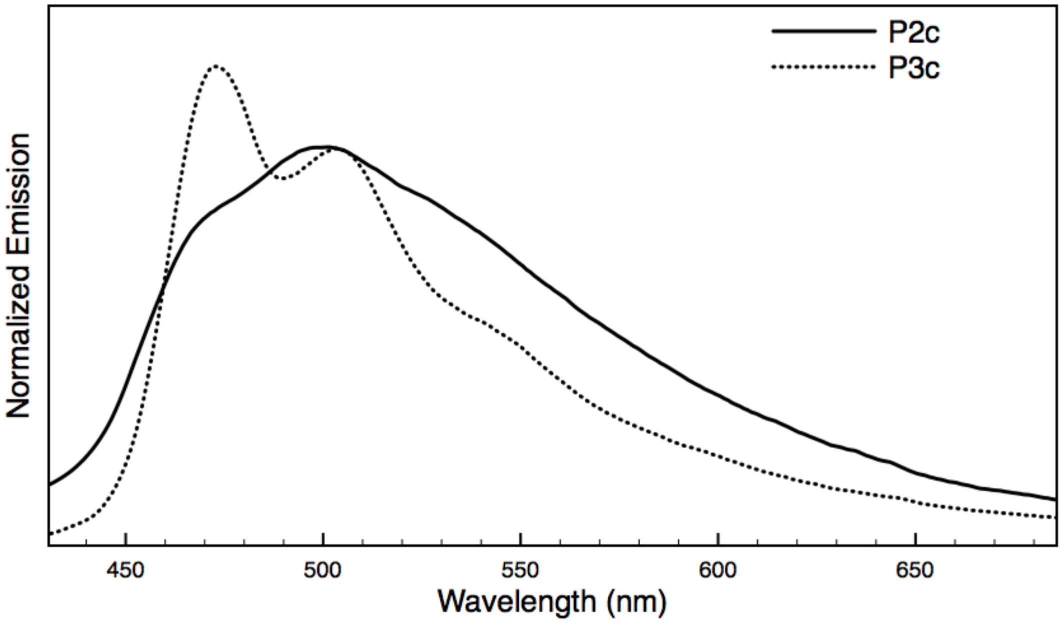

Figure 4.62. Fluorescence spectrum overlay of **P2c** and **P3c** in THF. Excitation at 400 nm and 420 nm, respectively.

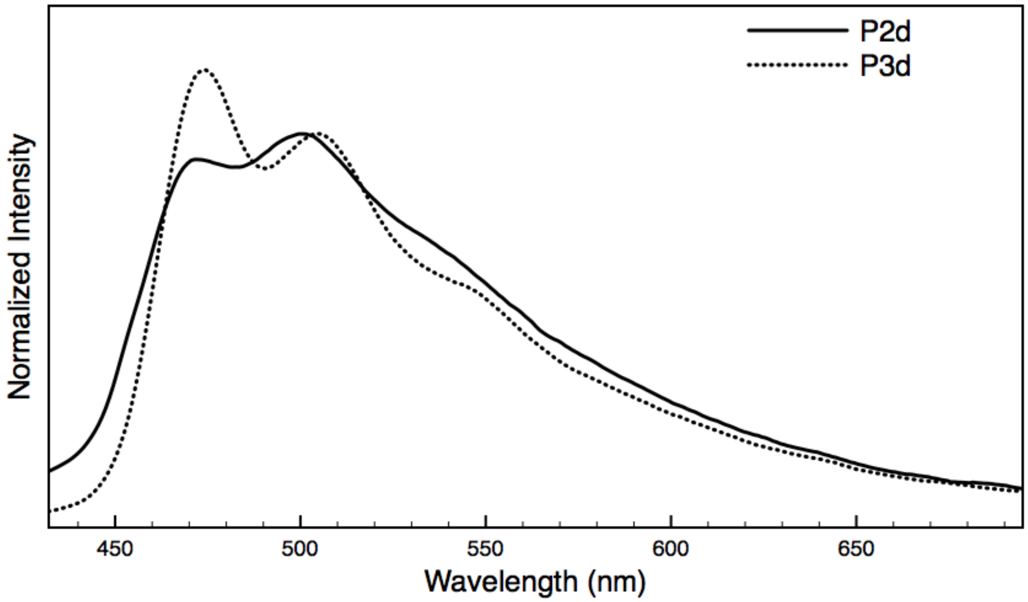

Figure 4.63. Fluorescence spectrum overlay of **P2d** and **P3d** in THF. Excitation at 400 nm and 420 nm, respectively.

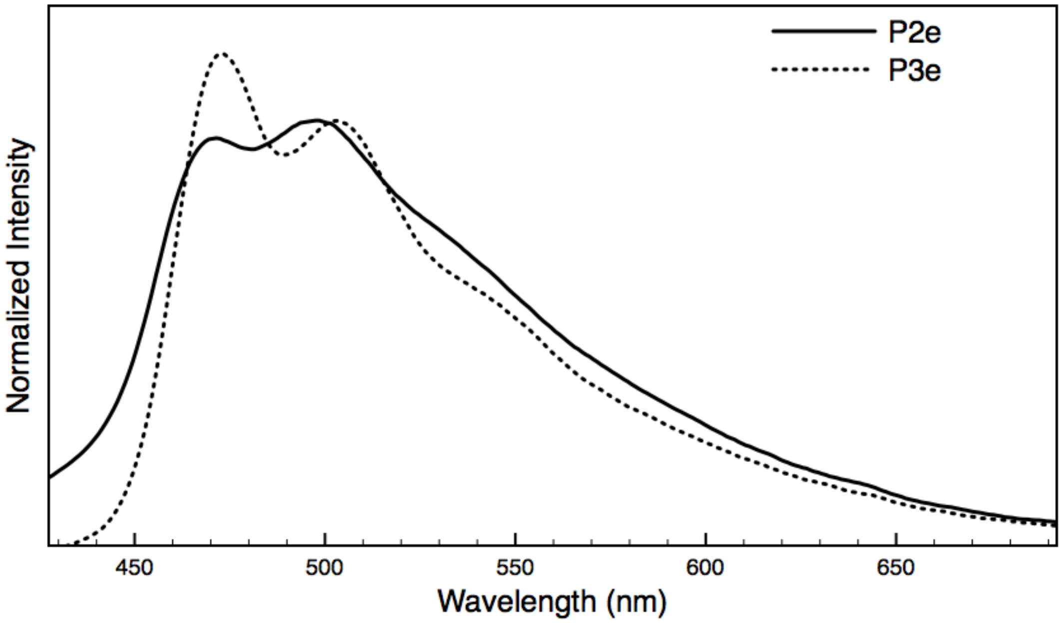

Figure 4.64. Fluorescence spectrum overlay of **P2e** and **P3e** in THF. Excitation at 400 nm and 420 nm, respectively.

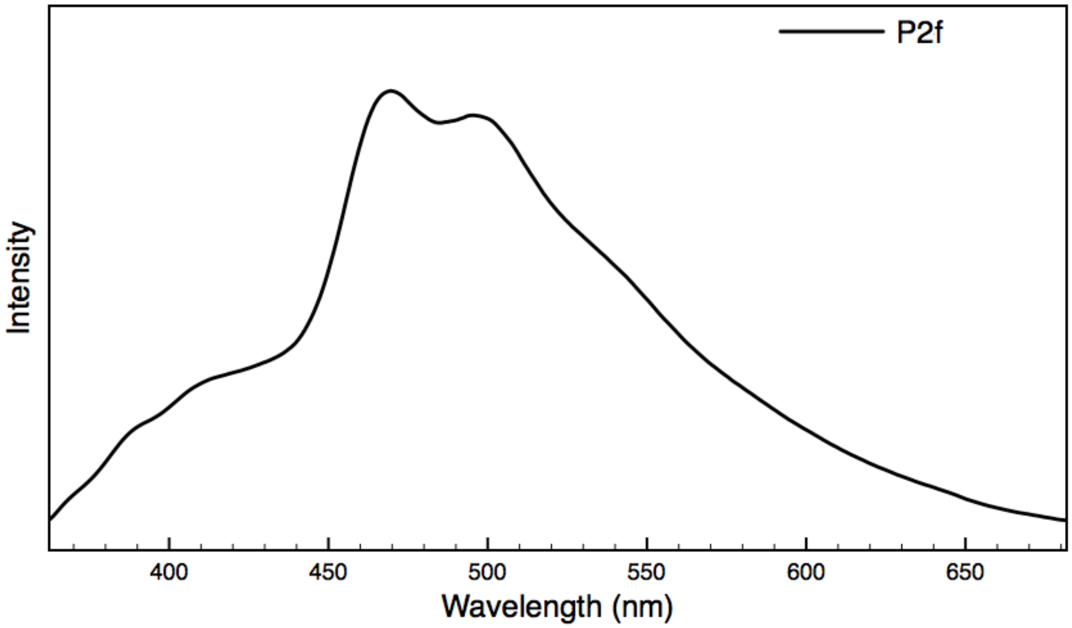

Figure 4.65. Fluorescence spectrum of **P2f** in THF. Excitation at 340 nm.

4.4.9. TGA Thermograms

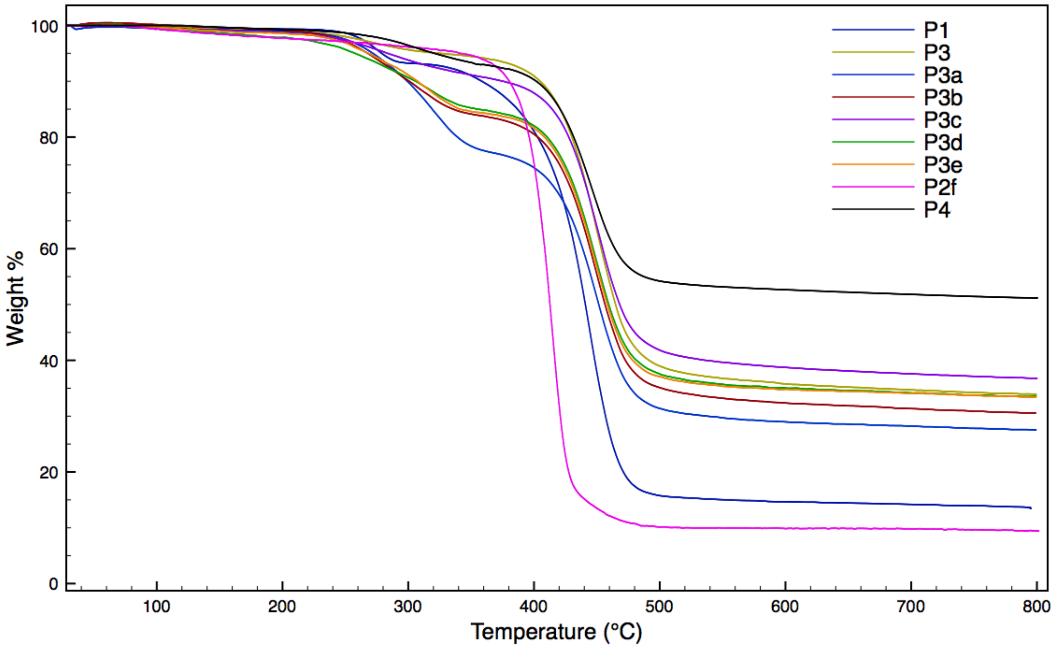

Figure 4.66. TGA thermogram overlay of **P1**, **P3**, **P3a**, **P3b**, **P3c**, **P3d**, **P3e**, **P2f**, and **P4.**

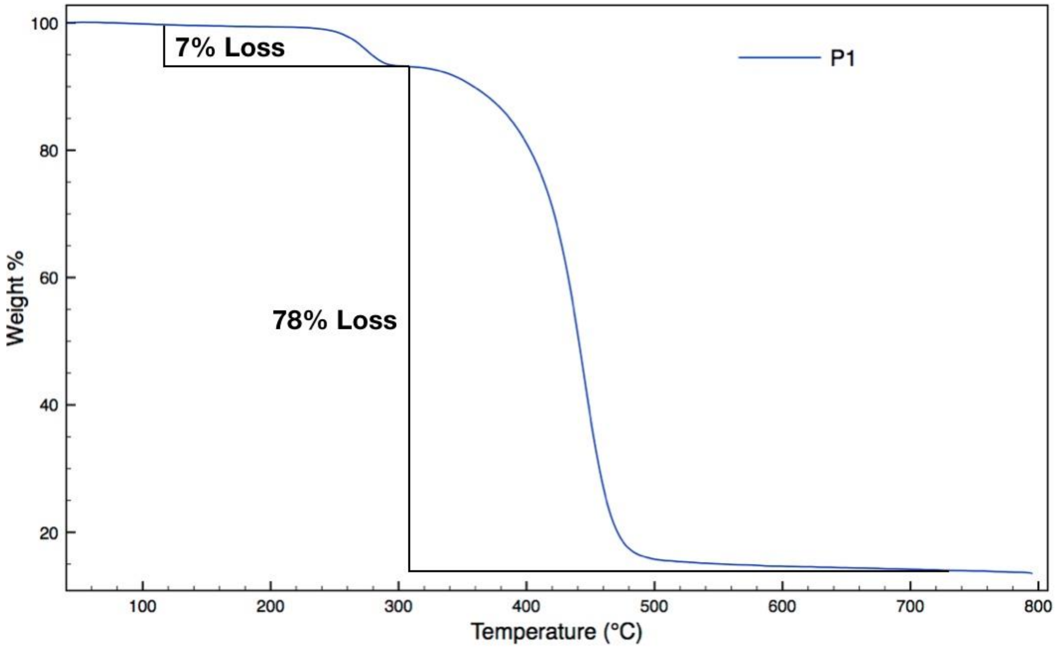

Figure 4.67. TGA thermogram of **P1.**

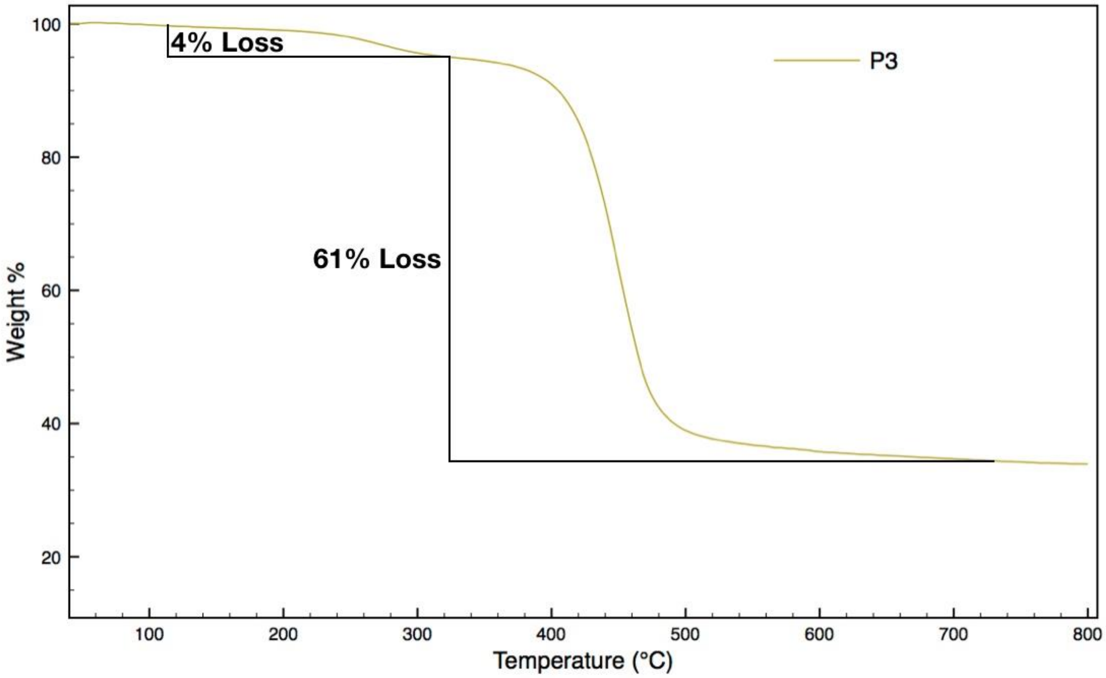

Figure 4.68. TGA thermogram of **P3.**

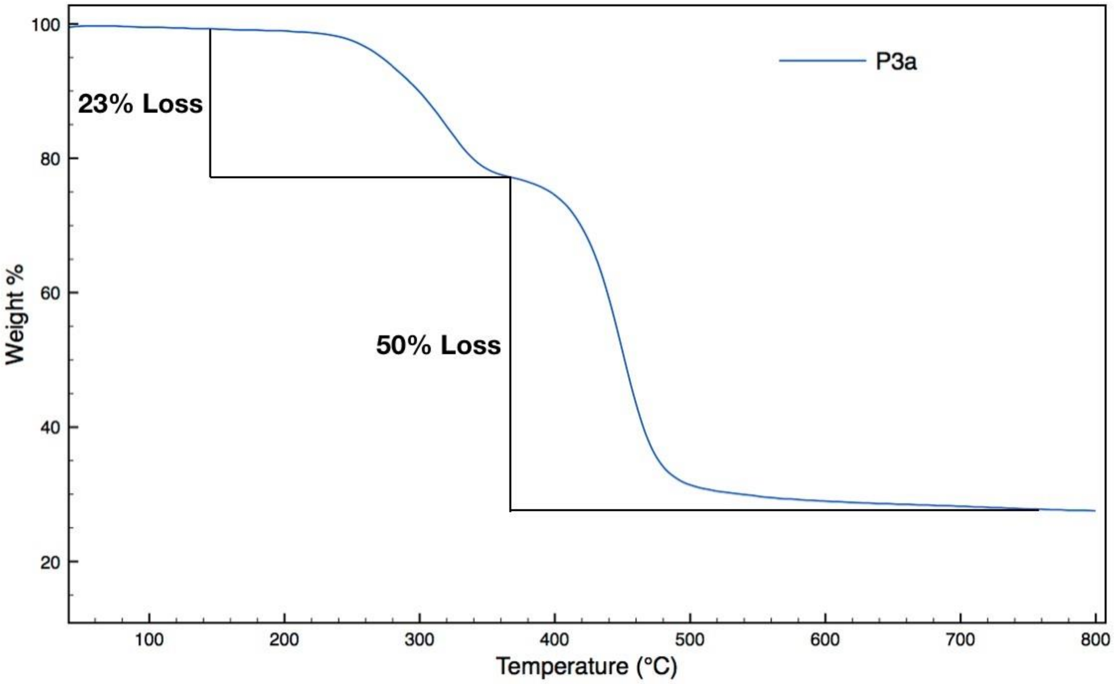

Figure 4.69. TGA thermogram of **P3a.**

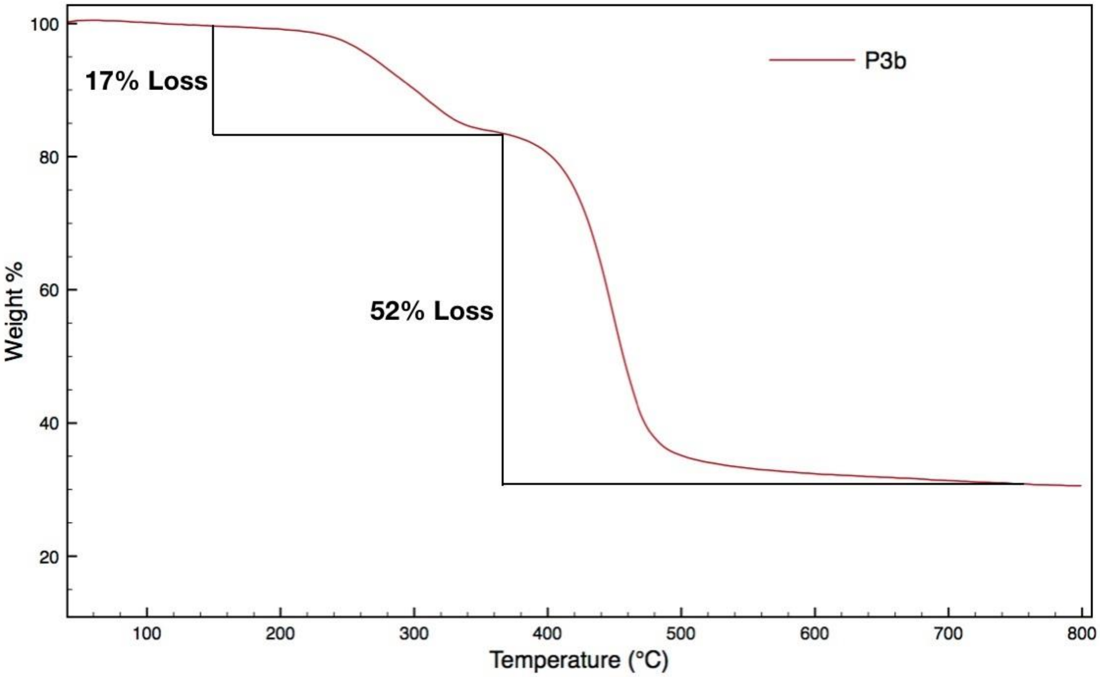

Figure 4.70. TGA thermogram of **P3b.**

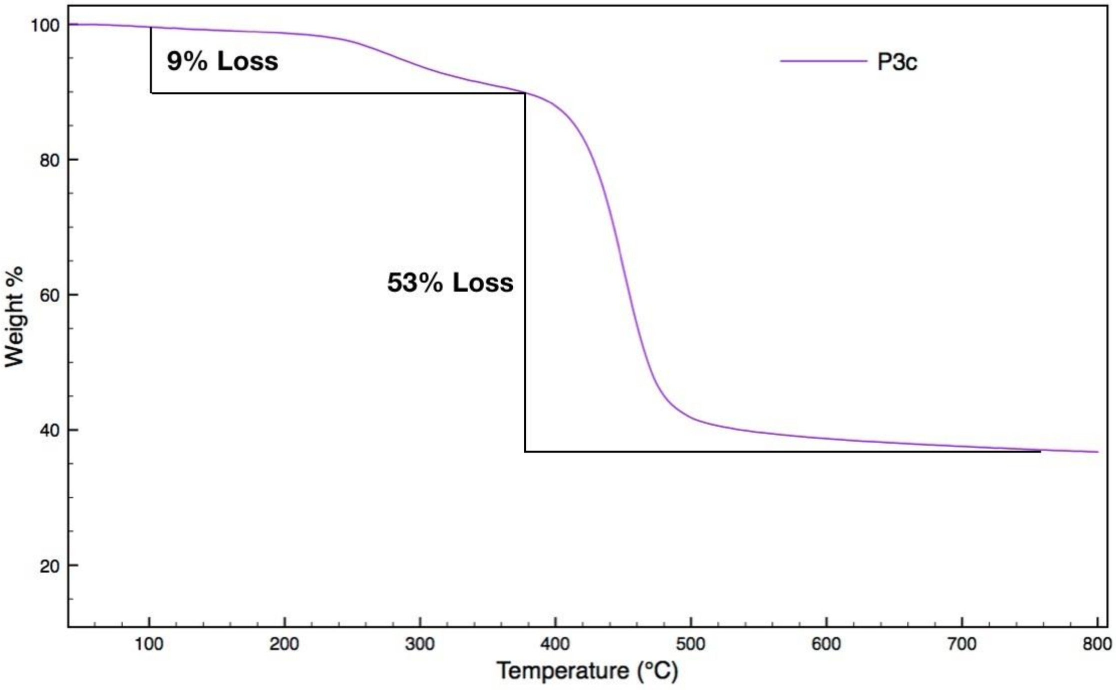

Figure 4.71. TGA thermogram of **P3c.**

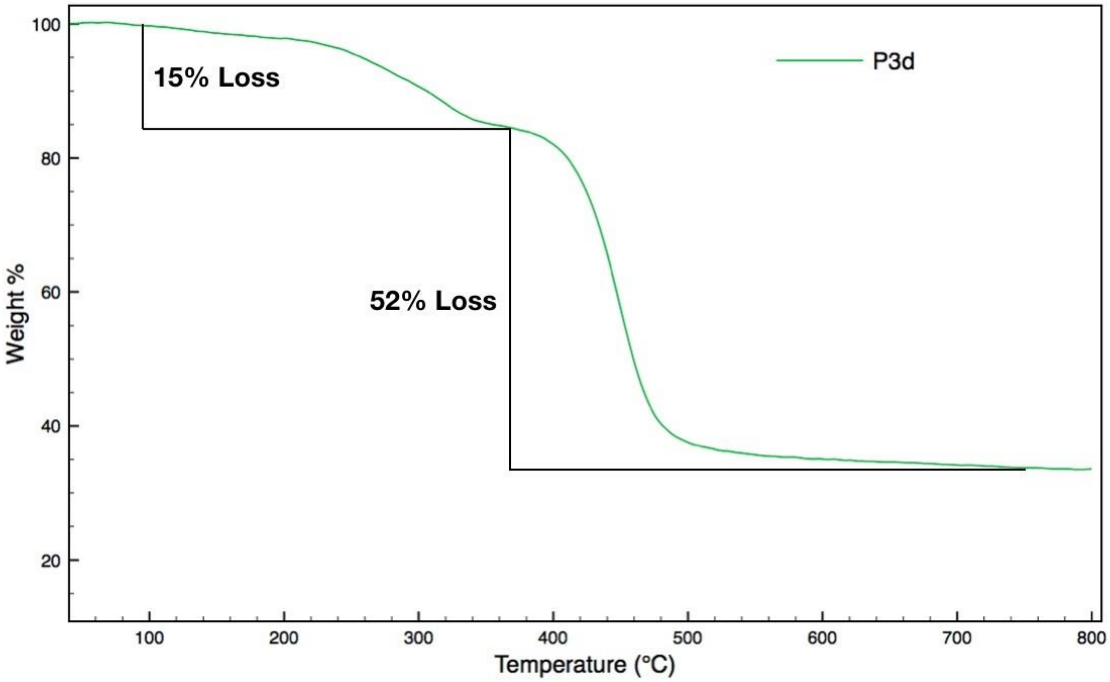

Figure 4.72. TGA thermogram of **P3d.**

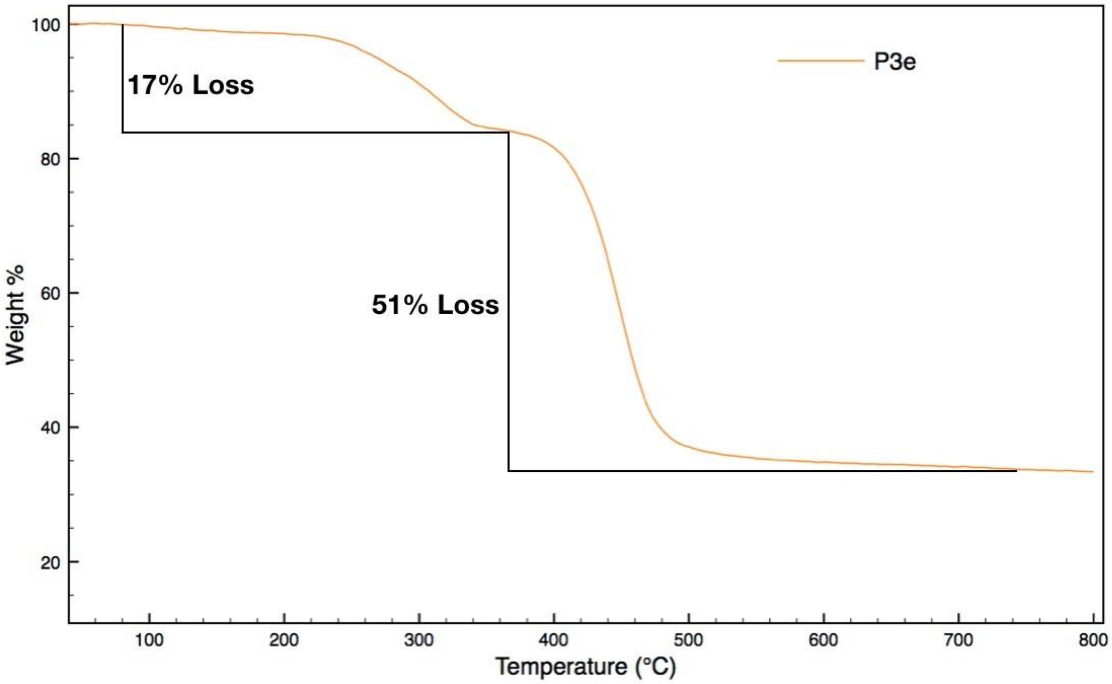

Figure 4.73. TGA thermogram of **P3e.**

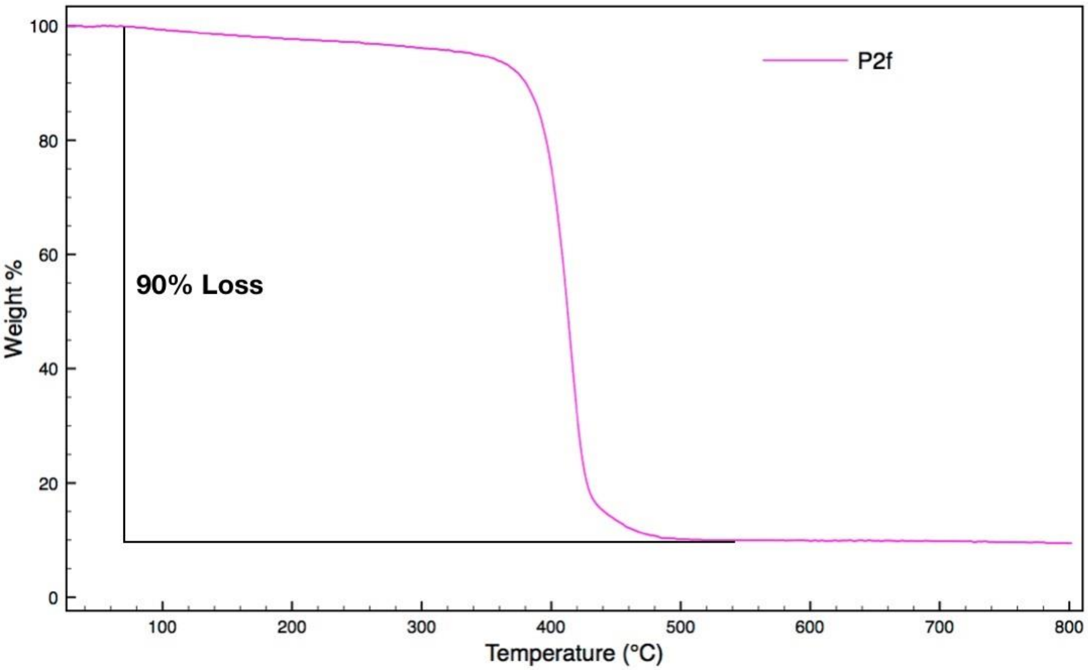

Figure 4.74. TGA thermogram of **P2f.**

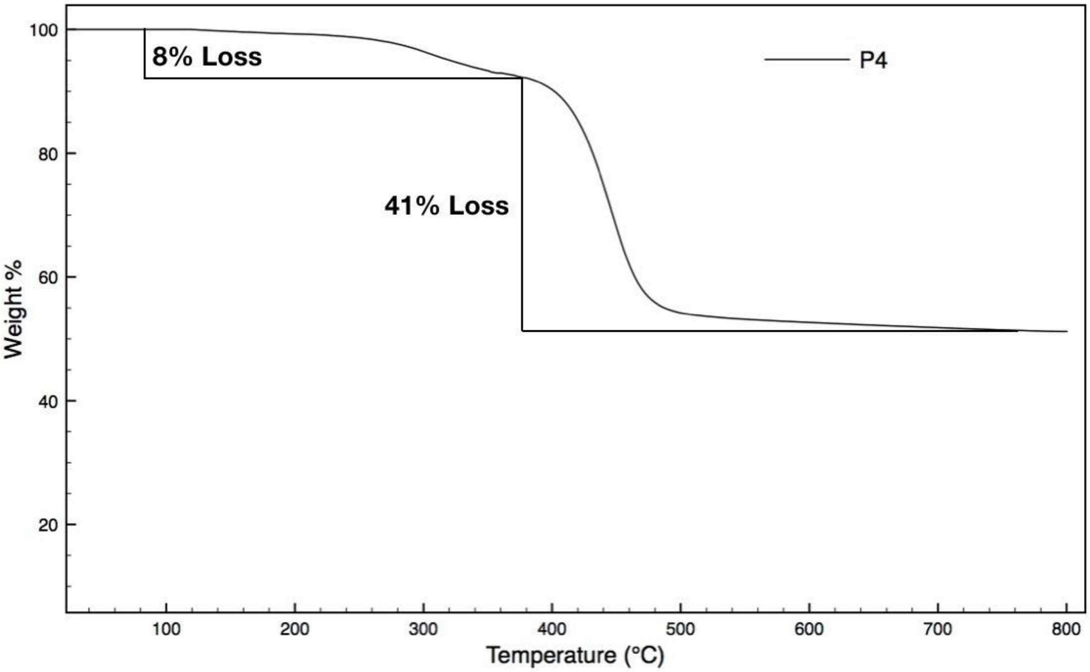

Figure 4.75. TGA thermogram of **P4b.**

4.4.10. GPC Traces

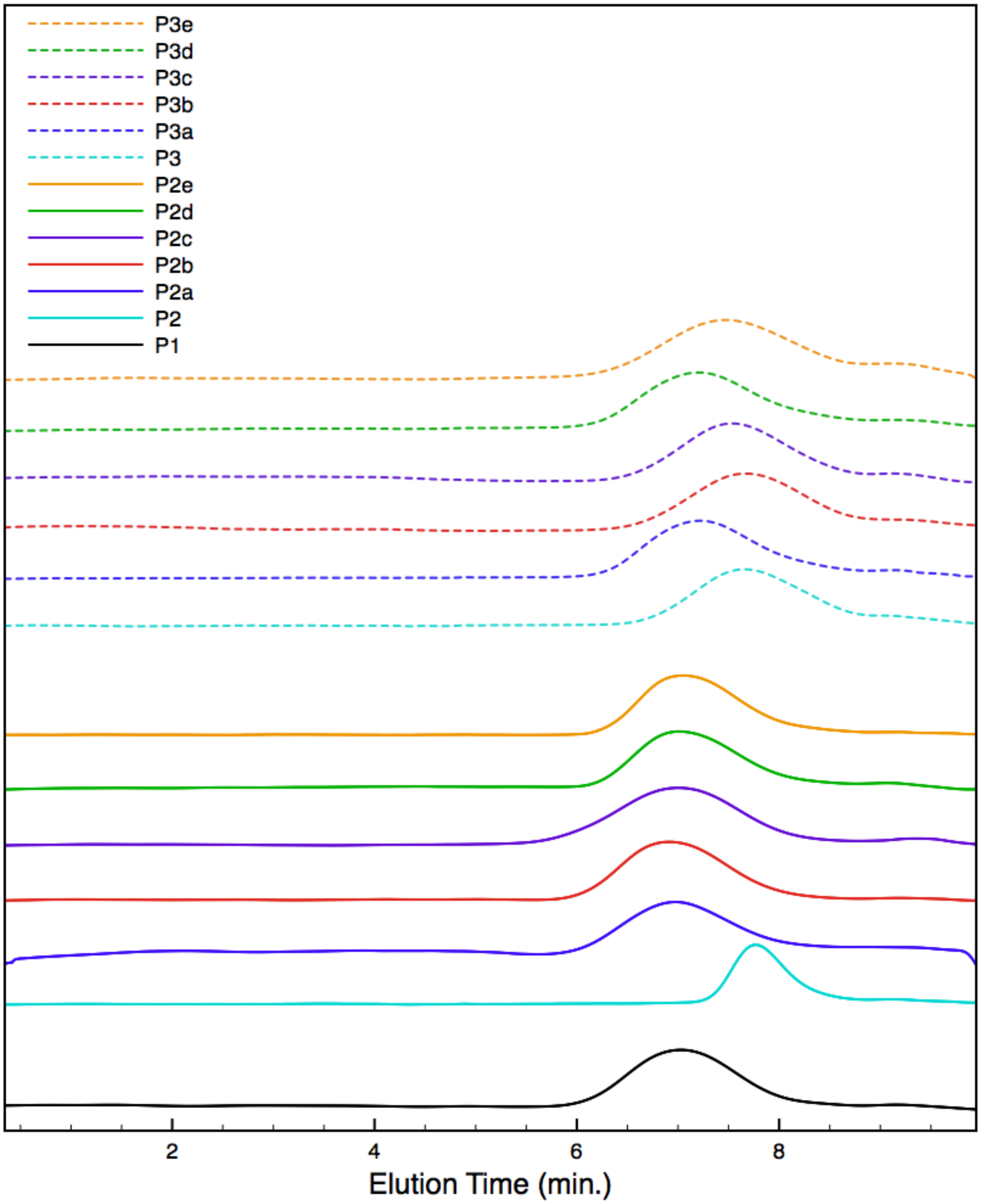

Figure 4.76. GPC trace overlay of **P1** with “clicked” polymers.

4.4.11.IR Spectra

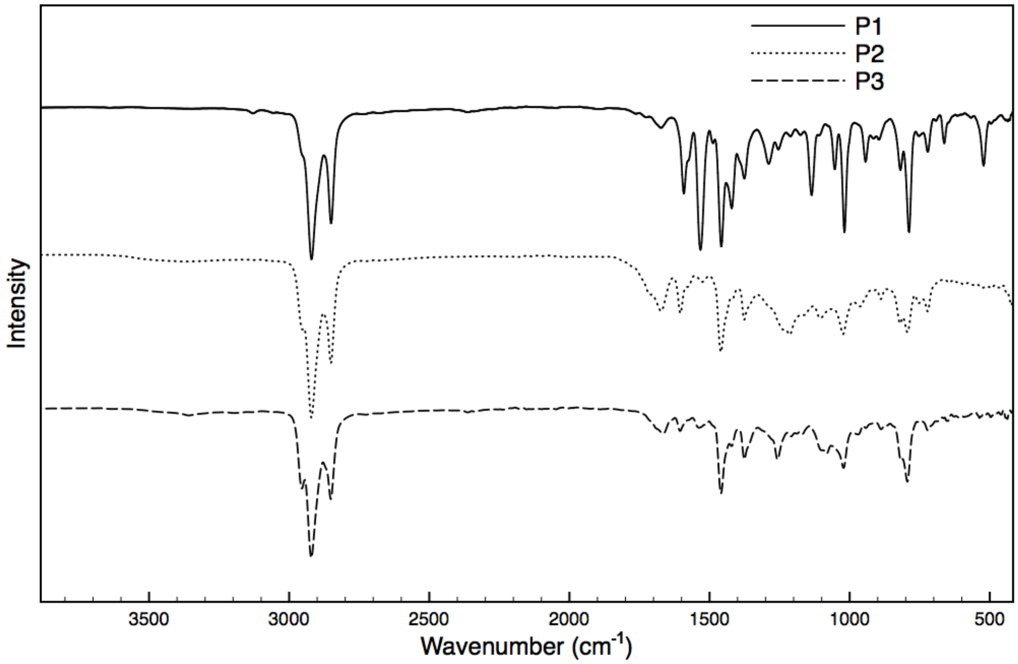

Figure 4.77. FTIR spectrum overlay of **P1**, **P2**, and **P3.**

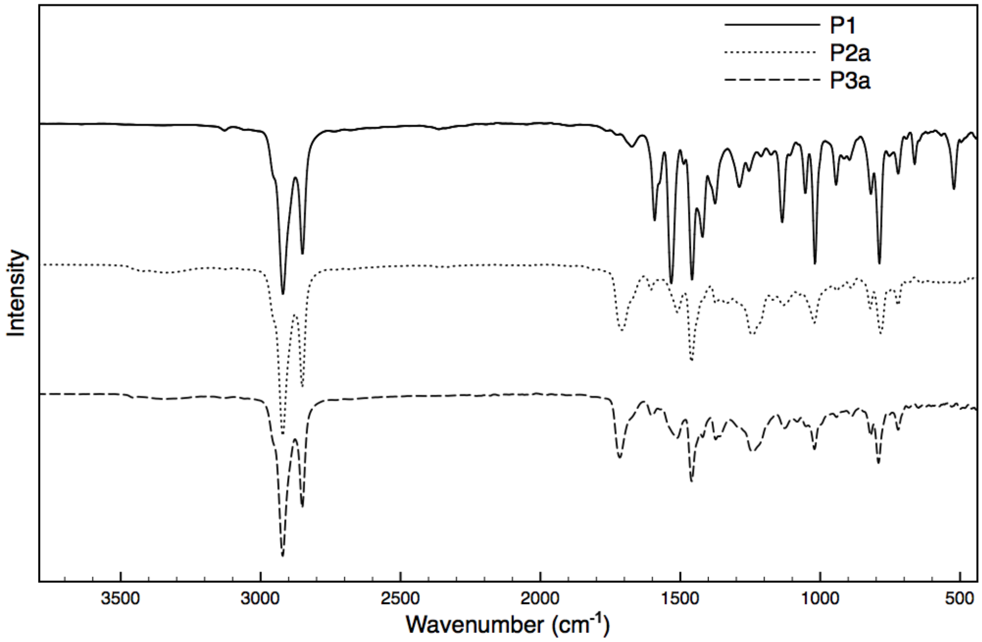

Figure 4.78. FTIR spectrum overlay of **P1**, **P2a**, and **P3a**.

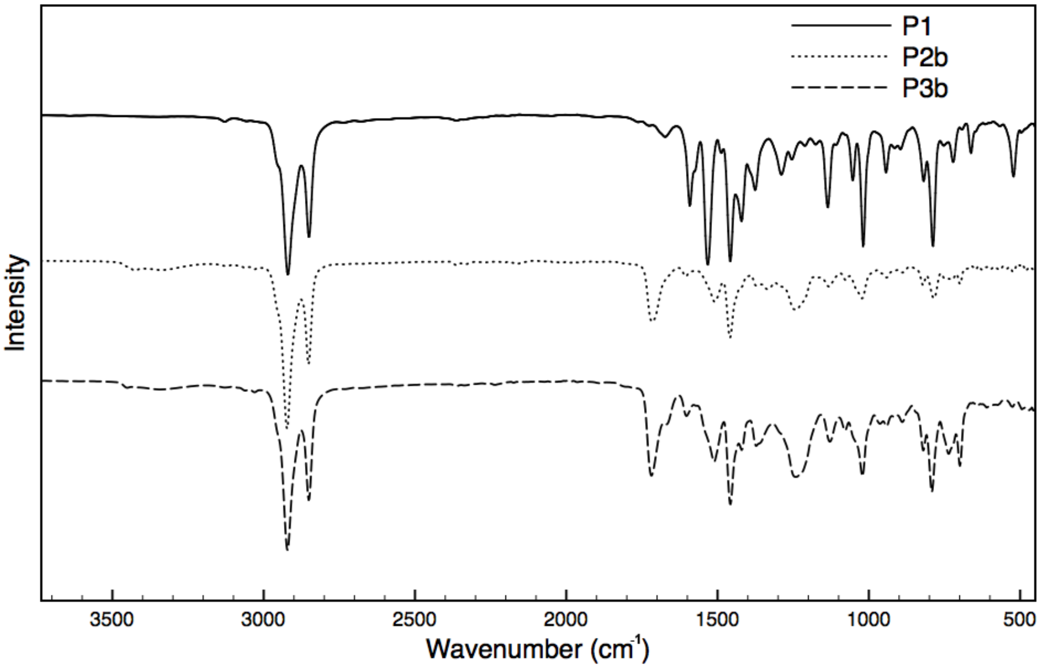

Figure 4.79. FTIR spectrum overlay of **P1**, **P2b**, and **P3b**.

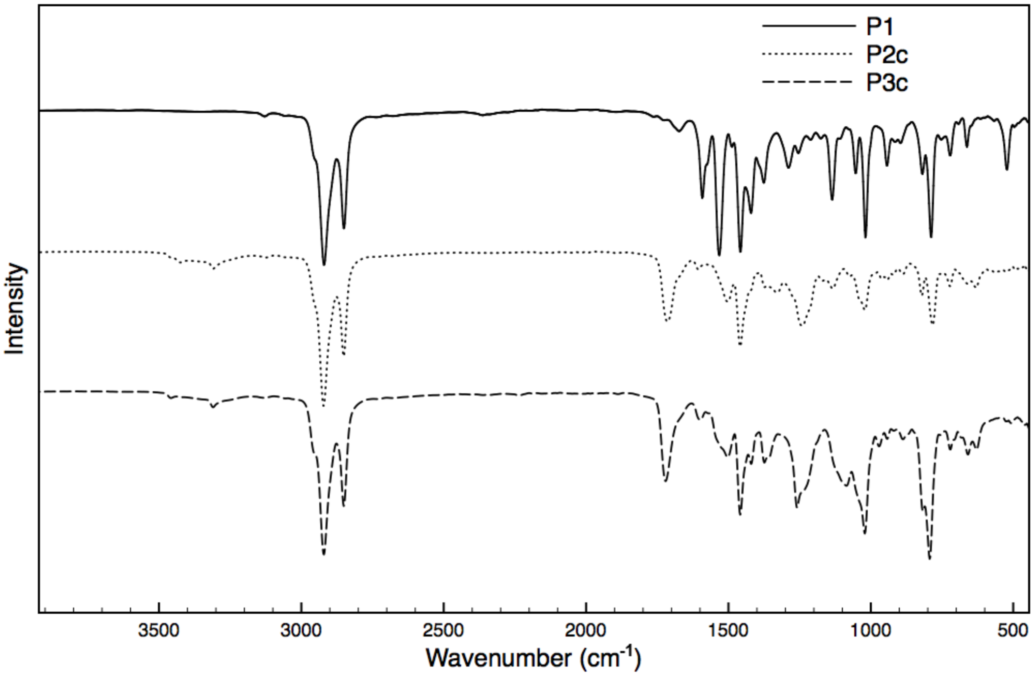

Figure 4.80. FTIR spectrum overlay of **P1**, **P2c**, and **P3c**.

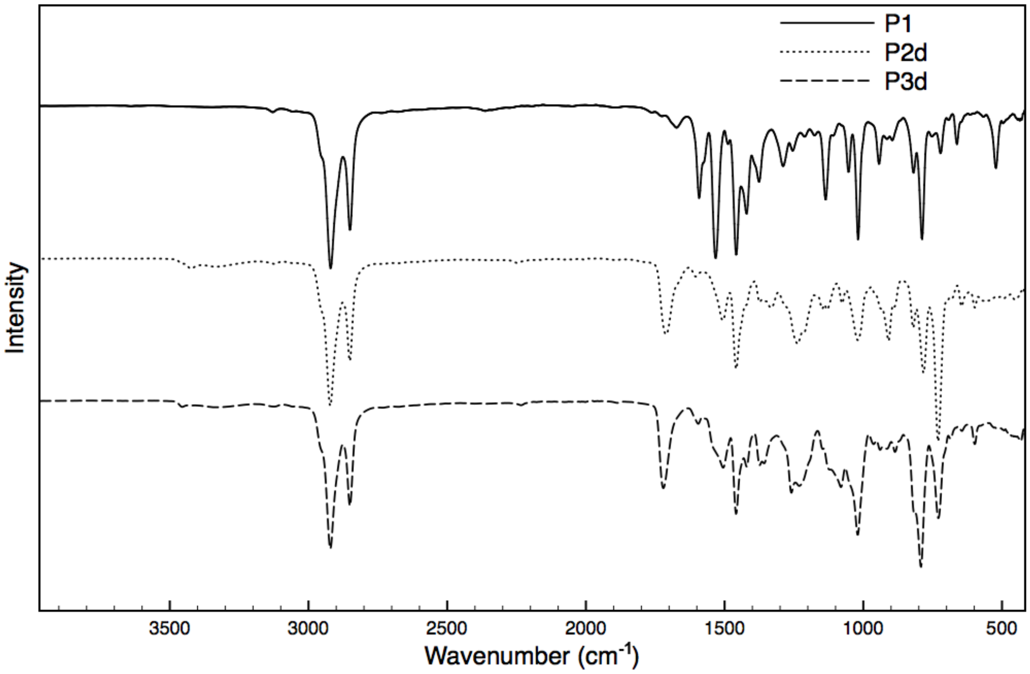

Figure 4.81. FTIR spectrum overlay of **P1**, **P2d**, and **P3d**.

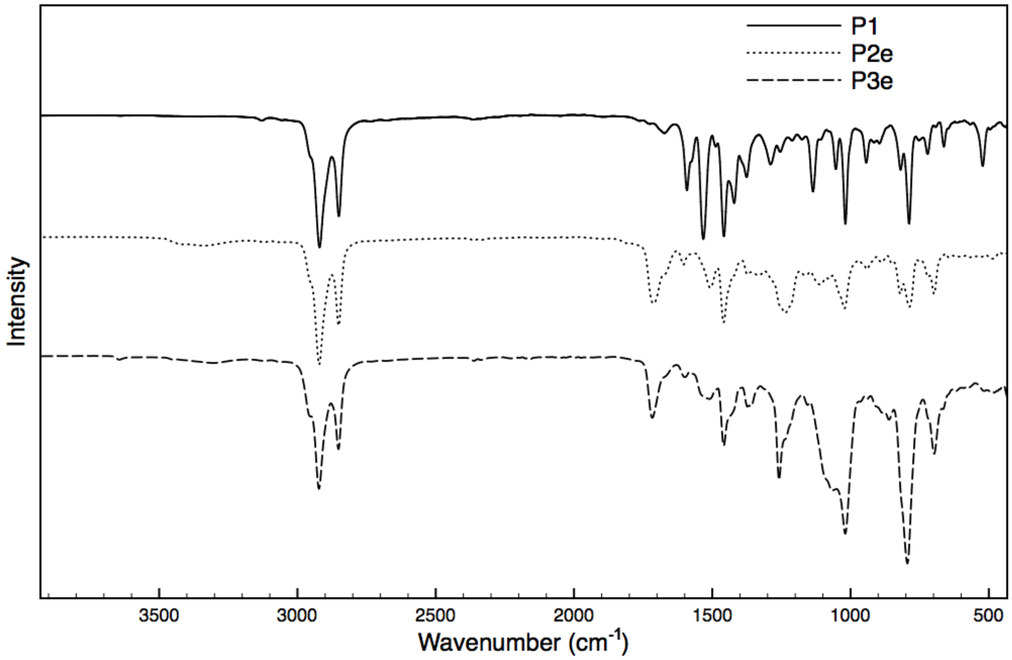

Figure 4.82. FTIR spectrum overlay of **P1**, **P2e**, and **P3e**.

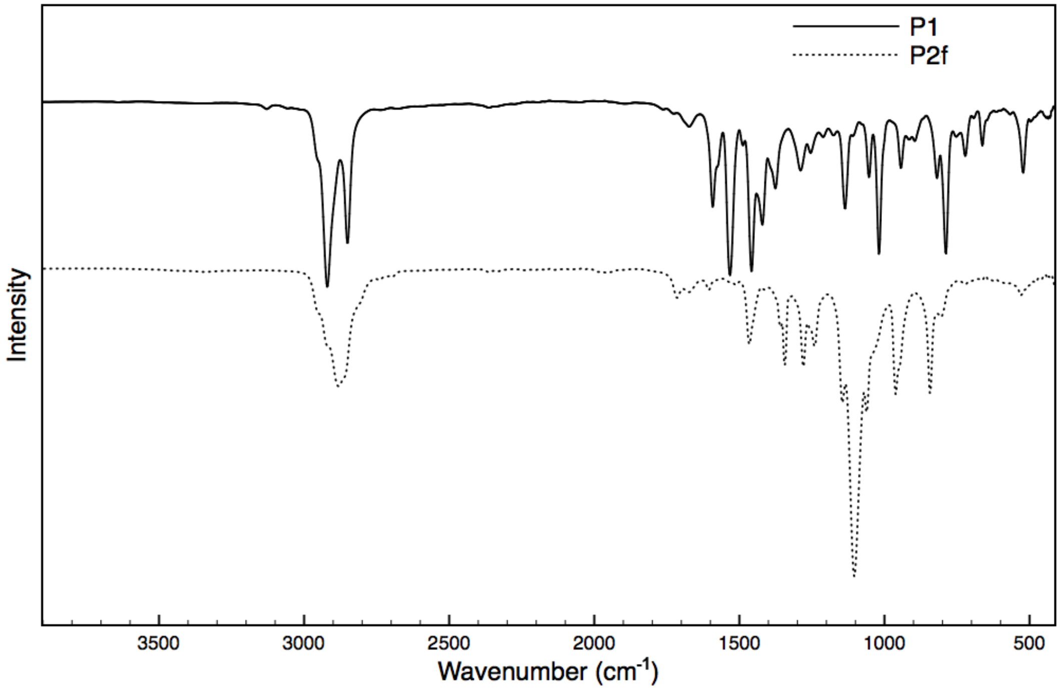

Figure 4.83. FTIR spectrum overlay of **P1** and **P2f**.

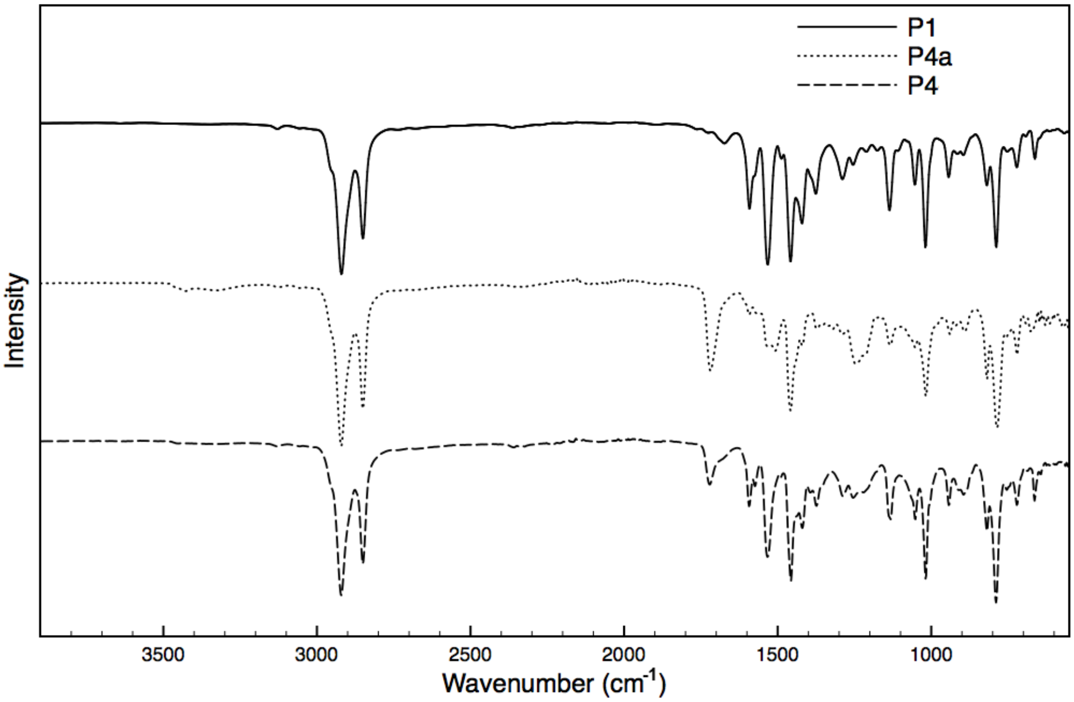

Figure 4.84. FTIR spectrum overlay of **P1**, **P4a**, and **P4b**.

4.4.12.Raman Spectra

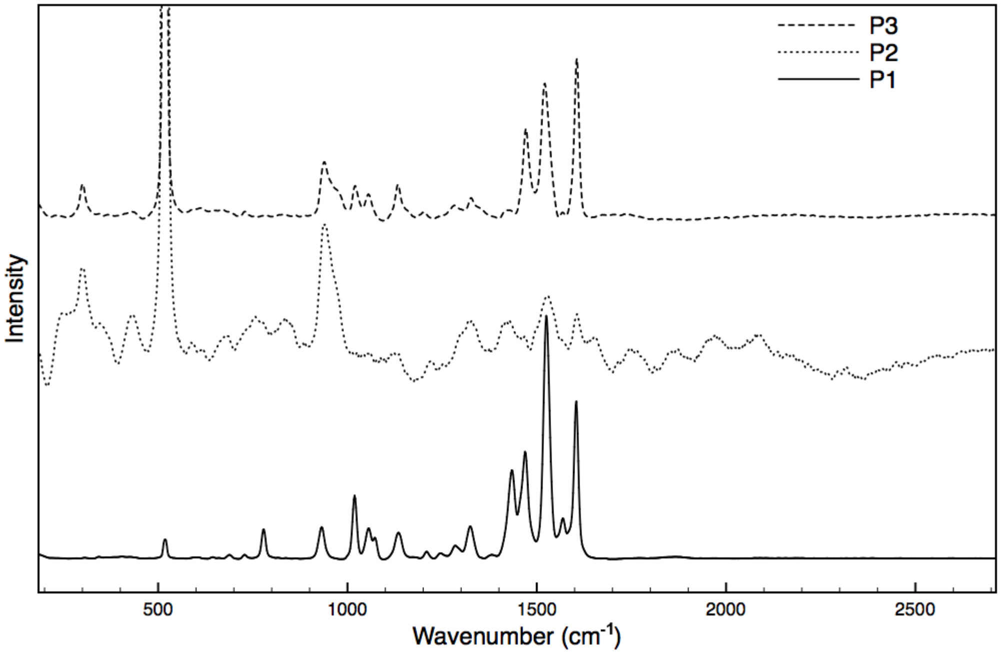

Figure 4.85. Raman spectrum overlay of **P1**, **P2**, **P3**. 785 nm excitation.

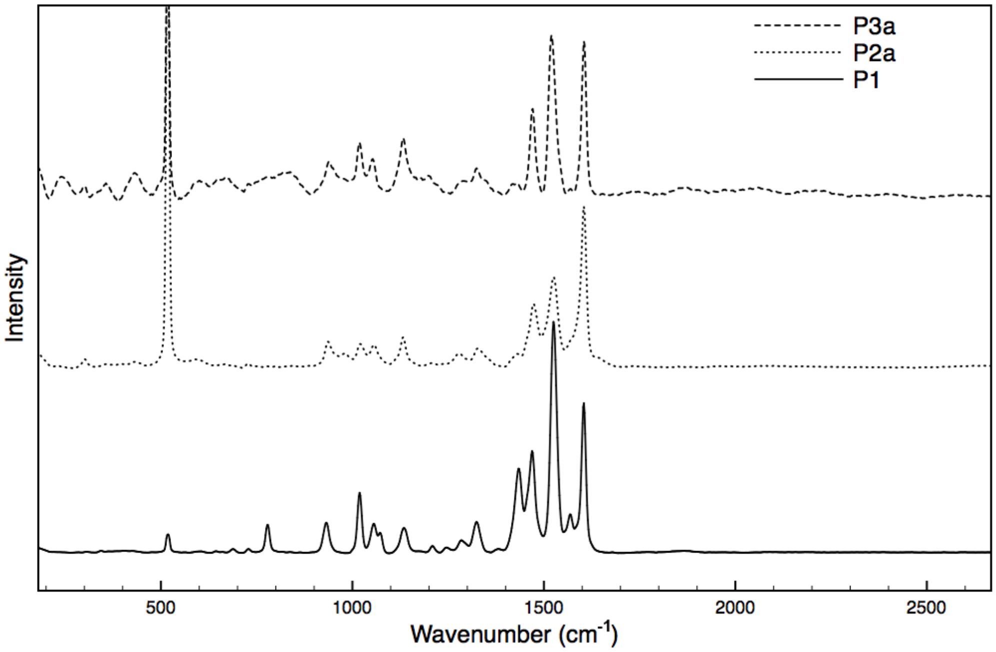

Figure S4.86. Raman spectrum overlay of **P1**, **P2a**, **P3a**. 785 nm excitation.

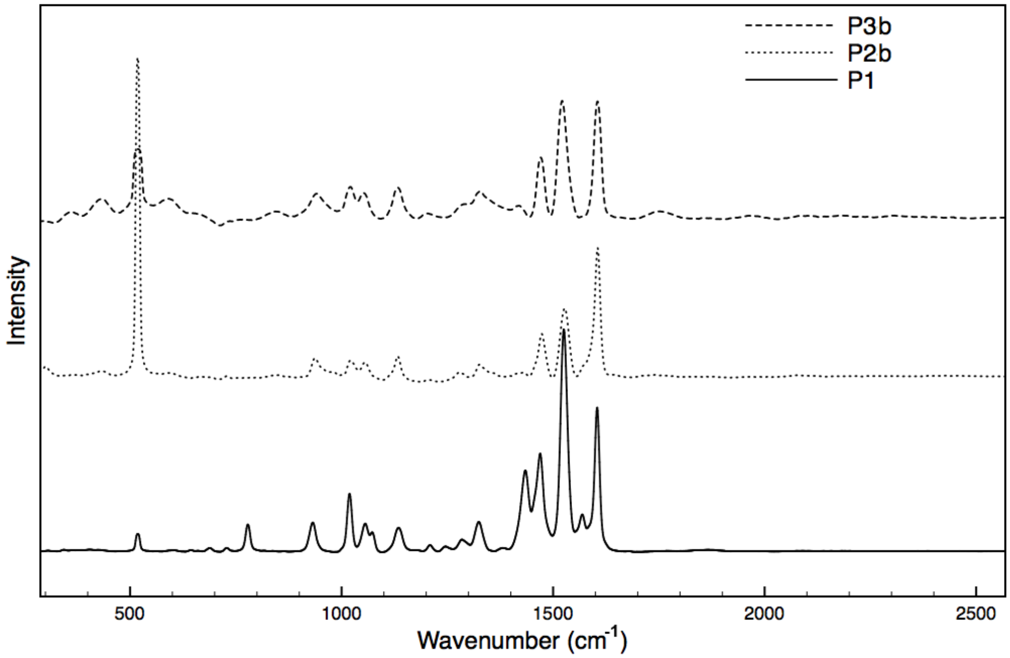

Figure S4.87. Raman spectrum overlay of **P1**, **P2b**, **P3b**. 785 nm excitation.

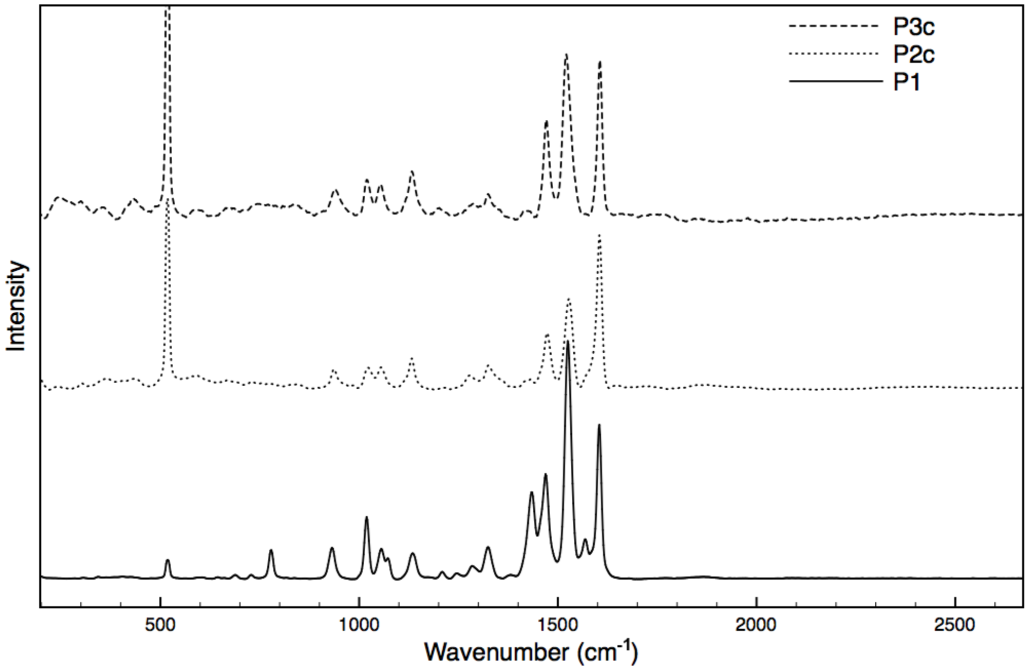

Figure S4.88. Raman spectrum overlay of **P1**, **P2c**, **P3c**. 785 nm excitation.

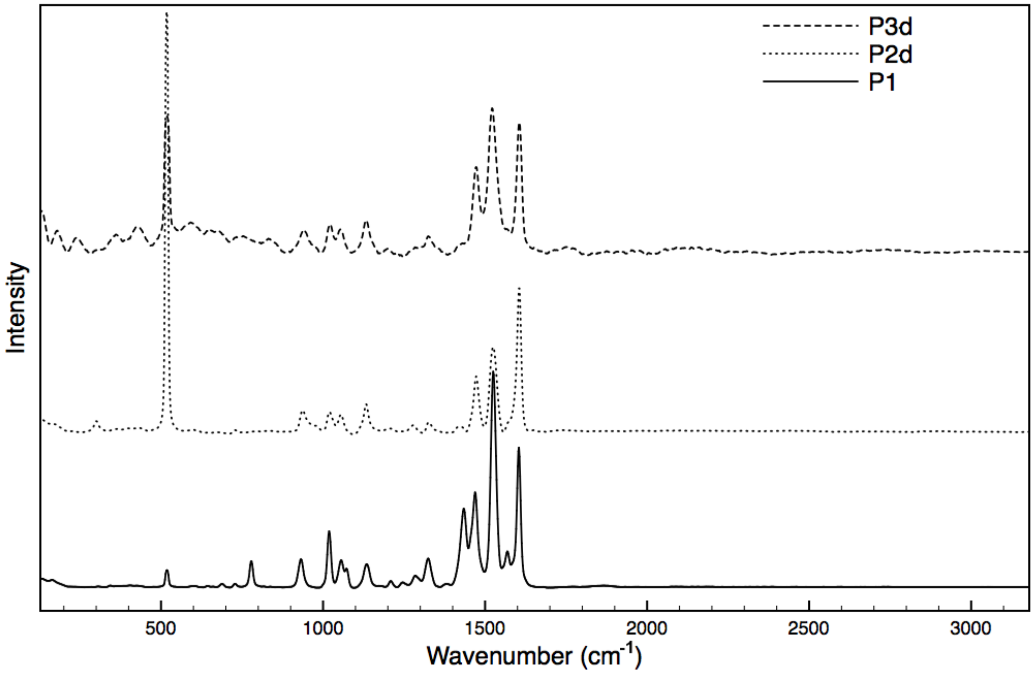

Figure S4.89. Raman spectrum overlay of **P1**, **P2d**, **P3d**. 785 nm excitation.

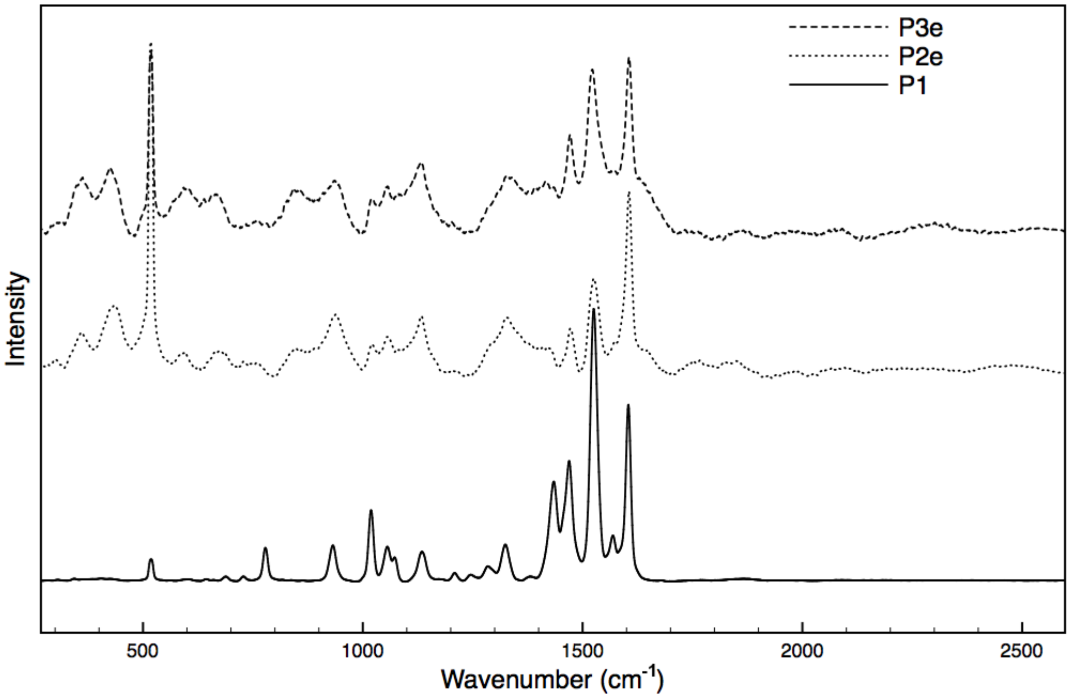

Figure S4.90. Raman spectrum overlay of **P1**, **P2e**, **P3e**. 785 nm excitation.

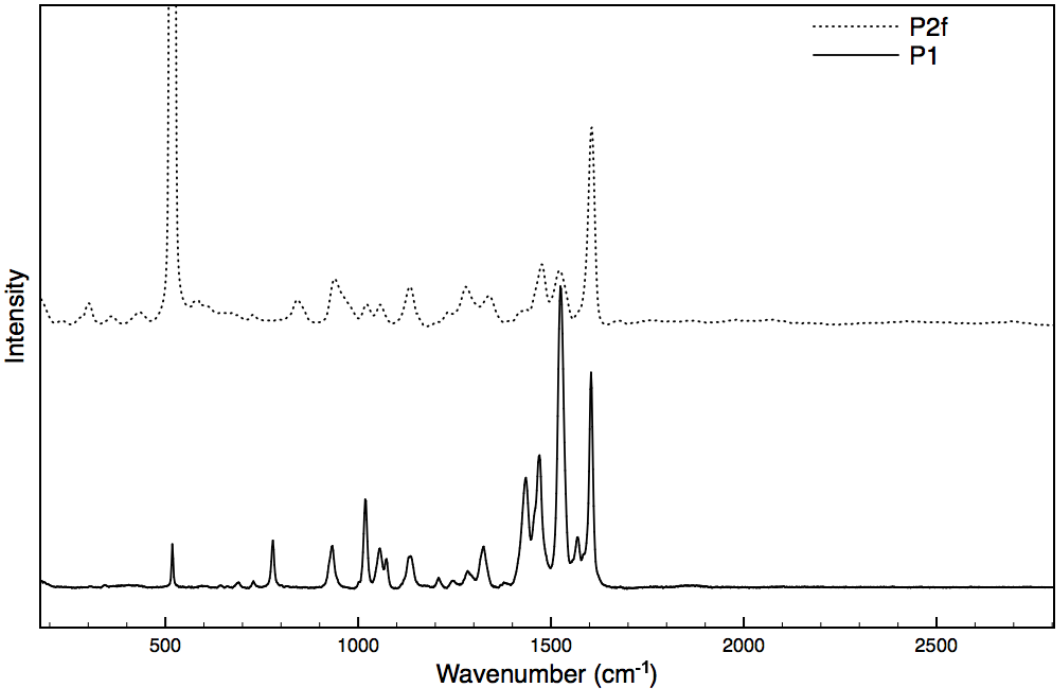

Figure S4.91. Raman spectrum overlay of **P1** and **P2f**. 785 nm excitation.

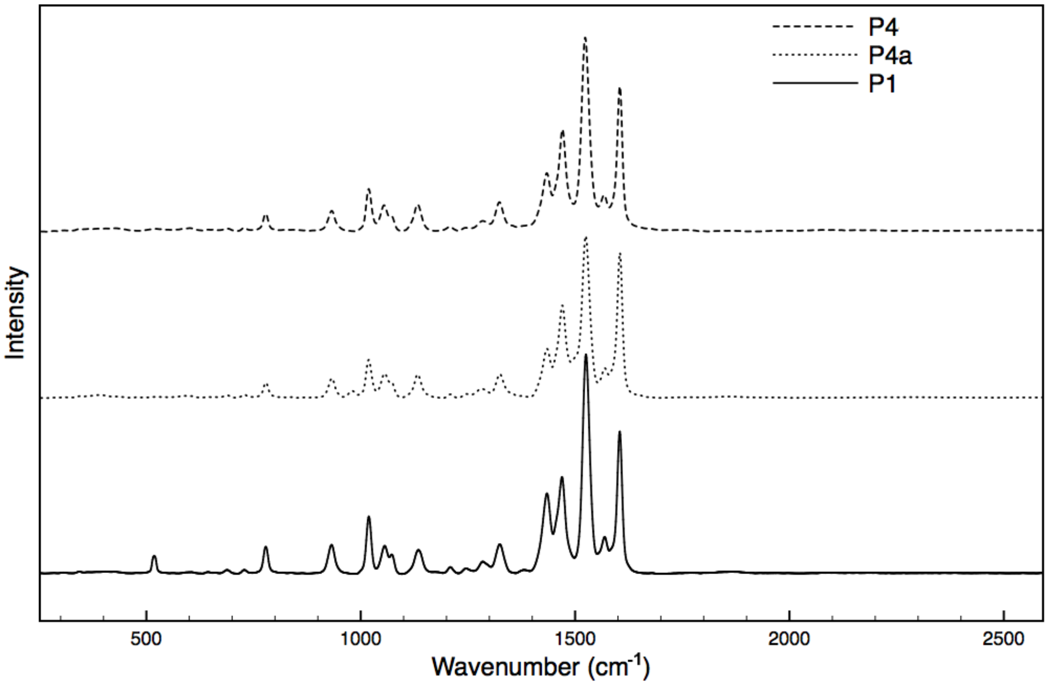

Figure S4.92. Raman spectrum overlay of **P1**, **P4a**, **P4b**. 785 nm excitation.

IEDDA Reaction Image

Figure S4.93. IEDDA reaction mixture of **5** with **P1** in THF. Taken 20 seconds after the addition of **5**.

4.5. References

(1) *Polymers for Light-Emitting Devices and Displays*; Inamuddin, Boddula, R., Ahamed, M. I., Asiri, A. M., Eds.; Wiley-Scrivener: Hoboken, NJ, USA, 2020.

(2) Wang, G.; Melkonyan, F. S.; Facchetti, A.; Marks, T. J. All-Polymer Solar Cells: Recent Progress, Challenges, and Prospects. *Angew. Chemie - Int. Ed.* **2019**, *58* (13), 4129–4142.

(3) Taylor, D.; Dalgarno, S. J.; Xu, Z.; Vilela, F. Conjugated Porous Polymers: Incredibly Versatile Materials with Far-Reaching Applications. *Chemical Society Reviews*. Royal Society of Chemistry June 21, 2020, pp 3981–4042.

(4) Swager, T. M. Sensor Technologies Empowered by Materials and Molecular Innovations. *Angew. Chemie - Int. Ed.* **2018**, *57* (16), 4248–4257.

(5) Tyler McQuade, D.; Pullen, A. E.; Swager, T. M. Conjugated Polymer-Based Chemical Sensors. *Chem. Rev.* **2000**, *100* (7), 2537–2574.

(6) Kimpel, J.; Michinobu, T. Conjugated Polymers for Functional Applications: Lifetime and Performance of Polymeric Organic Semiconductors in Organic Field-Effect Transistors. *Polym. Int.* **2020**, No. February.

(7) Wakim, S.; Blouin, N.; Gingras, E.; Tao, Y.; Leclerc, M. Poly(2,7-Carbazole) Derivatives as Semiconductors for Organic Thin-Film Transistors. *Macromol. Rapid Commun.* **2007**, *28* (17), 1798–1803.

(8) Liu, S.; Chen, X.; Liu, G. Conjugated Polymers for Information Storage and Neuromorphic Computing. *Polym. Int.* **2020**, No. March.

(9) *Conjugated Polymers: Theory, Synthesis, Properties, and Characterization*, 3rd ed.; Skotheim, T. A., Reynolds, J., Eds.; CRC Press: Boca Raton, 2006.

(10) Blouin, N.; Leclerc, M. Poly(2,7-Carbazole)s: Structure−Property Relationships. *Acc. Chem. Res.* **2008**, *41* (9), 1110–1119.

(11) Morin, J.-F.; Leclerc, M. 2,7-Carbazole-Based Conjugated Polymers for Blue, Green, and Red Light Emission. *Macromolecules* **2002**, *35* (22), 8413–8417.

(12) *Design and Synthesis of Conjugated Polymers*; Leclerc, M., Morin, J.-F., Eds.; Wiley-VCH Verlag GmbH & Co.: Weinheim, 2010.

(13) Morin, J.-F.; Leclerc, M.; Adès, D.; Siove, A. Polycarbazoles: 25 Years of Progress. *Macromol. Rapid Commun.* **2005**, *26*, 761–778.

(14) Boudreault, P.-L. T.; Blouin, N.; Leclerc, M. Poly(2,7-Carbazole)s and Related Polymers. *Adv. Polym. Sci.* **2008**, *212* (1), 99–124.

(15) Sheina, E. E.; Liu, J.; Lovu, M. C.; Laird, D. W.; McCullough, R. D. Chain Growth Mechanism for Regioregular Nickel-Initiated Cross-Coupling Polymerizations. *Macromolecules* **2004**, *37*, 3526–3528.

(16) Javier, A. E.; Varshney, S. R.; McCullough, R. D. Chain-Growth Synthesis of Polyfluorenes with Low Polydispersities, Block Copolymers of Fluorene, and End-Capped Polyfluorenes: Toward New Optoelectronic Materials. *Macromolecules* **2010**, *43*, 3233–3237.

(17) Stefan, M. C.; Javier, A. E.; Osaka, I.; McCullough, R. D. Grignard Metathesis Method (GRIM): Toward a Universal Method for the Synthesis of Conjugated Polymers. *Macromolecules* **2009**, *42*, 30–32.

(18) Bryan, Z. J.; McNeil, A. J. Conjugated Polymer Synthesis via Catalyst-Transfer Polycondensation (CTP): Mechanism, Scope, and Applications. *Macromolecules* **2013**, *46* (21), 8395–8405.

(19) Yokozawa, T.; Ohta, Y. Transformation of Step-Growth Polymerization into Living Chain-Growth Polymerization. *Chem. Rev.* **2016**, *116* (4), 1950–1958.

(20) Baker, M. A.; Tsai, C. H.; Noonan, K. J. T. Diversifying Cross-Coupling Strategies, Catalysts and Monomers for the Controlled Synthesis of Conjugated Polymers. *Chem. - A Eur. J.* **2018**, *24* (50), 13078–13088.

(21) Ye, S.; Cheng, S.; Pollit, A. A.; Forbes, M. W.; Seferos, D. S. Isolation of Living Conjugated Polymer Chains. *J. Am. Chem. Soc.* **2020**, *142* (25), 11244–11251.

(22) Arslan, H.; Saathoff, J. D.; Bunck, D. N.; Clancy, P.; Dichtel, W. R. Highly Efficient Benzannulation of Poly(Phenylene Ethynylene)S. *Angew. Chemie - Int. Ed.* **2012**, *51* (48), 12051–12054.

(23) Creamer, A.; Wood, C. S.; Howes, P. D.; Casey, A.; Cong, S.; Marsh, A. V.; Godin, R.; Panidi, J.; Anthopoulos, T. D.; Burgess, C. H.; Wu, T.; Fei, Z.; Hamilton, I.; McLachlan, M. A.; Stevens, M. M.; Heeney, M. Post-Polymerisation Functionalisation of Conjugated Polymer Backbones and Its Application in Multi-Functional Emissive Nanoparticles. *Nat. Commun.* **2018**, *9* (1).

(24) Kardelis, V.; Chadwick, R. C.; Adronov, A. Click Functionalization of a Dibenzocyclooctyne-Containing Conjugated Polyimine. *Angew. Chemie - Int. Ed.* **2016**, *55* (3), 945–949.

(25) Kardelis, V.; Li, K.; Nierengarten, I.; Holler, M.; Nierengarten, J.-F. J. F.; Adronov, A. Supramolecular Organogels Prepared from Pillar[5]Arene-Functionalized Conjugated Polymers. *Macromolecules* **2017**, *50* (23), 9144–9150.

(26) Li, K.; Kardelis, V.; Adronov, A. "Click" Generation of a Conjugated Polymer Library for SWNT Dispersion. *J. Polym. Sci. Part A-Polymer Chem.* **2018**, *56* (18), 2053–2058.

(27) Li, K.; McNelles, S. A.; Adronov, A. Preparation and Properties of a Hydrolytically Stable Cyclooctyne-Containing Polymer. *Synlett* **2018**, *29* (19), 2535–2541.

(28) Oliveira, B. L.; Guo, Z.; Bernardes, G. J. L. Inverse Electron Demand Diels-Alder Reactions in Chemical Biology. *Chemical Society Reviews*. 2017, pp 4895–4950.

(29) Ye, Q.; Neo, W. T.; Cho, C. M.; Yang, S. W.; Lin, T.; Zhou, H.; Yan, H.; Lu, X.; Chi, C.; Xu, J. Synthesis of Ultrahighly Electron-Deficient Pyrrolo[3,4- d]Pyridazine-5,7-Dione by Inverse Electron Demand Diels-Alder Reaction and Its Application as Electrochromic Materials. *Org. Lett.* **2014**, *16* (24), 6386–6389.

(30) McCulloch, I.; Cacialli, F.; Clarke, T. M.; Friend, R. H.; Freeman, D. M. E.; Bronstein, H.; Frost, J. M.; Rapidis, A. G.; Musser, A. J.; Stern, H. L.; Forster, A. K.; Fallon, K. J. Synthesis and Exciton Dynamics of Donor-Orthogonal Acceptor Conjugated Polymers: Reducing the Singlet–Triplet Energy Gap. *J. Am. Chem. Soc.* **2017**, *139* (32), 11073–11080.

(31) Royzen, M.; Yap, G. P. A.; Fox, J. M. A Photochemical Synthesis of Functionalized Trans-Cyclooctenes Driven by Metal Complexation. *J. Am. Chem. Soc.* **2008**, *130* (12), 3760–3761.

(32) Gordon, C. G.; MacKey, J. L.; Jewett, J. C.; Sletten, E. M.; Houk, K. N.; Bertozzi, C. R. Reactivity of Biarylazacyclooctynones in Copper-Free Click Chemistry. *J. Am. Chem. Soc.* **2012**, *134* (22), 9199–9208.

(33) Arrington, K. J.; Murray, C. B.; Smith, E. C.; Marand, H.; Matson, J. B. Precision Polyketones by Ring-Opening Metathesis Polymerization: Effects of Regular and Irregular Ketone Spacing. *Macromolecules* **2016**, *49* (10), 3655–3662.

(34) Bhatthula, B. kumar goud; Kanchani, J. reddy; Arava, V. reddy; Subha, M. C. S. Total Synthesis of Carbazole Alkaloids. *Tetrahedron* **2019**, *75* (7), 874–887.

(35) Ting, A. Y.; Fox, J. M.; Tangpeerachaikul, A.; Selvaraj, R.; Liu, D. S.; Taylor, M. T. Diels–Alder Cycloaddition for Fluorophore Targeting to Specific Proteins inside

Living Cells. *J. Am. Chem. Soc.* **2011**, *134* (2), 792–795.

(36) Schmidt, M. W.; Baldridge, K. K.; Boatz, J. A.; Elbert, S. T.; Gordon, M. S.; Jensen, J. H.; Koseki, S.; Matsunaga, N.; Nguyen, K. A.; Su, S.; Windus, T. L.; Dupuis, M.; Montgomery, J. A. General Atomic and Molecular Electronic Structure System. *J. Comput. Chem.* **1993**, *14* (11), 1347–1363.

(37) Stewart, J. J. P. Optimization of Parameters for Semiempirical Methods I. Method. *J. Comput. Chem.* **1989**, *10* (2), 209–220.

Chapter 5

Overall Conclusions and Recommendations for Future Work

5.1. General Conclusions

The previous chapters have illustrated how conjugated polymers can be efficiently tailored for different applications based on a post-polymerization functionalization approach compared to a *de novo* approach whereby the monomer is functionalized pre-polymerization. While a suitable monomer scaffold for functionalization can be more readily synthesized, this strategy falls short whenever a larger library of homologous polymers is desired. More often than not, functionalizing a di-halogenated monomer with a large or bulky group has a substantial impact on the degrees of polymerization (DP) and dispersity (Đ) of the resultant cross-coupled polymer. Thus, a large coefficient of variation in polymer molecular weights is expected whenever building up a conjugated polymer library using this approach. These variations in the degrees of polymerization between polymers in a homologous series can introduce unwanted differences in polymer morphologies and greatly impact the validity of any comparison study.

An example of one such study involves the observation of conjugated polymer supramolecular interactions with single-walled carbon nanotubes (SWNTs). In an ongoing effort to purify SWNTs, these supramolecular complexes offer one possible route; however, the exact principles behind the CPs' selectivity for certain nanotubes over others requires more intricate study. Because CP molecular weights have been shown to greatly impact the efficiency of interactions with SWNTs, a polymer library generated *de novo* would lack control over chain lengths and dispersity, and as such would make any comparison between CP-SWNT interactions flawed. Conversely, synthesizing libraries of CPs via post-polymerization functionalization has eliminated any variations in degrees of polymerization and dispersity between polymer chains.

Upon conceptualization of the first reactive conjugated polymer (dibenzocyclooctyne-containing polyimine), we demonstrated its synthesis was possible to a high molecular weight (M_n > 30 kDa) despite the polymer containing highly strained cyclooctyne moieties. This CP exhibited high solubility in many common organic solvents, an ideal property when performing subsequent reactions in solution phase. Additionally, each cyclooctyne sub-unit within the polymer backbone could be reacted quantitatively with aliphatic and aryl azides at a second order rate constant of 0.03 $M^{-1}s^{-1}$, a rate that is consistent with that of small molecule analogues. From the single progenitor cyclooctyne-containing CP, we prepared a series of homologous polymers via SPAAC, a reaction that converted the cyclooctyne backbone to substituted triazoles. Accordingly, we also demonstrated the high-efficiency of these click reactions via coupling with three different chain lengths of azide-terminated polystyrene (4kDa, 9 kDa, and 24 kDa) in addition to azide-terminated polyethylene glycol. Despite the longer chain lengths of the polystyrenes, these grafting 'onto' reactions were rapid and quantitative, generating novel CPs with compositions containing up to 97% PS graft in under 12 hours at modest temperatures.

Amongst the numerous advantages to using a reactive polyimine scaffold for post-polymerization functionalization, a glaring drawback hindered its utilization in certain applications. Like small molecule Schiff bases, the dibenzocyclooctyne-containing polyimine is prone to hydrolysis in aqueous acidic conditions, the slightest of which will dramatically impact its average DP and dispersity. This issue was ultimately resolved by replacing the CP's reactive cyclooctyne moieties with that of *s*-tetrazine, which provided the reactive polymer backbone with far more robust C-C linkages.

As with the dibenzocyclooctyne-containing polymer, we demonstrated the fully conjugated poly(tetrazine) could be reproducibly synthesized to a high molecular weight ($M_n > 35$ kDa), while preserving the reactive *s*-tetrazine moieties throughout the backbone. As observed with the cyclooctyne-containing polyimine, the poly(tetrazine) also exhibited good solubility in less polar organic solvents. The progenitor poly(tetrazine) was successfully functionalized via IEDDA using a series of TCO derivatives to generate a library of dihydropyridazine polymers, which could be further oxidized to produce the corresponding conjugated poly(pyridazine) series. Interestingly, the product polymers, both the dihydropyridazines and pyridazines, exhibited substantial hypsochromic shifts in absorption spectra, and an increased emission intensity, relative to poly(tetrazine) progenitor. In contrast to the cyclooctyne-containing polyimine, molecular modeling studies illustrated that, upon undergoing "click", the pyridazine rings along the polymer backbone do not exhibit a significant change in conformation, remaining relatively planar. In conjunction with GPC, NMR analysis reaffirmed that the "click" reaction and oxidation did not alter the degree of polymerization of the polymers. Exploration of IEDDA reaction kinetics on the backbone of the poly(tetrazine) revealed the "clicks" occur at rates comparable to those of small molecule *s*-tetrazines with TCO (1.25 $M^{-1}s^{-1}$), and considerably faster than SPAAC. Subsequently, we demonstrated the high efficiency of the

IEDDA reaction by grafting on a 5 kDa poly(ethylene glycol)-TCO chain. This reaction that resulted in a rapid, quantitative functionalization over the course of 8 hours at 40 °C to generate a water-soluble poly(pyridazine) graft copolymer.

Following the synthesis of reactive CPs, we initiated the exploration of new applications, which led to the synthesis of supramolecular polymer gels based on pillar[5]arenes. Here, we demonstrated the cyclooctyne-containing polyimine can be functionalized with a mono-azide derivative of pillar[5]arene via SPAAC. The resulting poly(pillar[5]arene) structure consequently undergoes host-guest chemistry with dicyanohexane, in addition to cyanohexane-terminated PEG chains. We observed relatively unstable organogel formation upon mixing the poly(pillar[5]arene) structure with cyanohexane-terminated PEG_{600}. However, the reaction of the polyimine with 11-azidoundecanenitrile produced a polymeric guest that assembles with poly(pillar[5]arene) to generate a significantly more crosslinked, stiffer gel that is stable over extended periods of time. Interestingly, acid-catalyzed hydrolysis of the gels can be carried out by exposure to acid vapor in the presence of moisture, leading to cleavage of the imine linkages. However, the degraded gel can then be re-formed via dehydration with molecular sieves. A more noteworthy feature of having supramolecular crosslinks is that this gel exhibits self-healing properties if severed and re-joined.

We have but scratched the surface of potential applications for these novel reactive conjugated polymers. Now, with the current CP scaffolds in hand, the road to synthesizing the desired polymer for any given applications can be accelerated.

5.2. Recommendations for Future Work

The majority of work discussed in this thesis focused on the synthesis of various reactive conjugated polymers and their resultant functionalization reactions. While we were able to synthesize these "clickable" polymers in appreciable quantities and thus, achieve one of the main goals of the thesis, many subsequently formed questions regarding their chemical properties and applications remain unanswered. In greater detail, we want to explore how changing the structure of the comonomer (e.g.: *s*-tetrazine) will impact the resultant polymer's solubility and reactivity toward TCO derivatives and other cycloalkenes/cycloalkynes. Additionally, large exploratory studies regarding the aforementioned CP's effects in the dispersion of SWNT remain incomplete. This work represents a potential research direction for any future chemists.

The changes made to the reactive CP structure as we transitioned from the polyimine to the poly(tetrazine) demonstrates the capacity for several critical improvements. These improvements include improved stability toward acids and bases, increased backbone planarity upon "clicking", and significantly faster second-order rate constants (1.25 $M^{-1}s^{-1}$ compared to 0.03 $M^{-1}s^{-1}$). However, in order to make the poly(tetrazine) polymer series more amenable to applications requiring solution processibility at higher concentrations further modifications on the progenitor polymer are required. These modifications should be achievable via alkylation of the *s*-tetrazine comonomer, pre-polymerization. Compared to the fluorene comonomer, *s*-tetrazines are intrinsically less soluble in most solvents due to their propensity toward π-π staking. The substitution of a dodecyl or ethyl-hexyl group onto the furyl rings should mitigate this intermolecular interaction and result in greater overall solubility pre- and post-polymerization.

Additional exploration into the use of poly(tetrazine) and its derivatized polymers for supramolecular functionalization of SWNTs is required to fully exploit this reactive polymer platform. In undertaking this study, the library of poly(pyridazines) can be further expanded with the synthesis of new TCO-derivatives in addition to functionalized cyclooctynes and norbornenes, all of which undergo IEDDA with the progenitor polymer. This would afford three different libraries of conjugated polymers differing in their backbone functionality while maintaining the average chain lengths. The impact of the backbone variations on the resultant SWNT-CP dispersions should then be evaluated through a combination of absorption spectroscopy (UV-Vis-NIR) and fluorescence mapping. With the improvements we made toward post-polymerization functionalization of CPs thus far, future researchers should have a substantial pool of derivatized polymers to experiment with.